MEDICINE BALLS AND SMASHING CRYSTALS: FROM NEW MECHANOCHEMICAL C-N COUPLING REACTIONS TO THERMOSALIENT CRYSTALS

Davin Tan

Department of Chemistry

McGill University

Thesis Supervisor: Associate Professor Dr. Tomislav Friščić

April 2017

A thesis submitted to McGill University in partial fulfilment

of the requirements of the degree of

Doctor of Philosophy

TABLE OF CONTENTS

ABSTRACT

Solid-state reactions are vast and have great importance in synthetic chemistry. In particular, solid-solid reactions using mechanical force *i.e.* mechanochemical reactions, are advantageous as they are normally conducted at ambient temperature and pressure, do not require bulk solvents, which are often hazardous, and can rapidly transform inexpensive and readily accessible starting materials into products of high value. Whilst mechanochemistry has been widely used for the synthesis and investigation of new forms of pharmaceutical solids, such as salts, solvates, polymorphs and cocrystals, its use for the synthesis of molecules of actual active pharmaceutical ingredients (APIs) *via* covalent bond formation has not really been well established. In recent years, this emergent field of "medicinal mechanochemistry" has started to gain momentum, as evidenced by a shift in research focus towards developing mechanochemical strategies for the synthesis of API molecules. This Dissertation contribute to this growing field by studying transition metal-catalyzed coupling reactions to furnish pharmaceutically-important molecules and motifs using mechanochemical means. This is in coherence with the explicit call from pharmaceutical industries to develop cleaner, more efficient and less solvent demanding synthetic procedures. Whilst mechanochemistry can be seen as greener alternative to conventional solution methodologies, it can also allow synthetic chemist to access molecules or compounds that are normally inaccessible through traditional solution techniques. Herein described is the development of new C-N bond coupling reactions, specifically coupling of sulfonamides, sulfonimides, isatins, benzamides and imides with isocyanates and carbodiimides, which is largely enabled by ball milling techniques.

The use of copper-catalyzed mechanochemical C-N bond formation has allowed for the creation of a library of arylfulsonylguanidines, of which eight members have been found to form a surprisingly large family of isostructural single-component crystals. Using robust and reliable supramolecular design principles, a new family of thermosalient crystals that exhibit "jumping" motion upon heating, based on Etter-type *N*,*N*'-bis(aryl)ureas was serendipitously discovered. Sonochemistry enabled the gram-scale synthesis of these compounds. This, in turn, allowed for the systematic investigation of how the functional group placement affects thermosalient behaviour in these methoxy-substituted bis(aryl)ureas. The combined use of X-ray diffraction techniques, hot-stage microscopy and differential scanning calorimetry facilitated the discovery and characterization of a new thermosalient compound that exhibited pronounced thermosalient behaviour with high reversibility.

RÉSUMÉ

Les réactions à l'état solide sont vastes et ont une grande importance dans la chimie synthétique. En particulier, des réactions entre les solides utilisant une force mécanique, c'est-à-dire des réactions mécanochimiques, sont avantageuses car elles sont normalement effectuées à température et pression ambiantes, ne nécessitent pas de solvants dangereux, et peuvent rapidement effectuer la transformationdes matériaux de départ peu coûteux et facilement accessibles en produits de grande valeur. Bien que la mécanochimie est largement utilisée pour la synthèse et l'investigation de nouvelles formes pharmaceutiques solides tels que les sels, les solvates, les polymorphes et les co-cristaux, son utilisation pour la synthèse des ingrédients pharmaceutiques actifs est mal établie. Ces dernières années, le domaine émergent de “mécanochimie médicinale” a commencé à prendre une plus grande importance, appuyé par un la recherche axé sur le développement de stratégies mécanochimiques pour la synthèse de molécules API. Cette thèse contribue à ce domaine croissant en étudiant les réactions de couplage catalysées par des métaux de transition pour fournir des molécules et des motifs d’importance pharmaceutique en utilisant des moyens mécanochimiques. Ceci est en cohérence avec l'appel explicite des industries pharmaceutiques pour développer des procédures de synthèse plus propres, plus efficaces et moins exigeantes en solvants. Bien que la mécanochimie puisse être considérée comme une alternative plus verte aux méthodologies de solutions classiques, elle peut également permettre aux chimistes synthétiques d'accéder à des molécules ou des produits à l’état solide qui sont normalement inaccessibles par les techniques de solutions traditionnelles. La présente invention concerne le développement de nouvelles réactions de couplage de liaison C-N, en particulier le couplage de sulfonamides, de sulfonimides, d'isatines, de benzamides et d'imides avec des isocyanates et des carbodiimides, qui est largement permise par des techniques de broyage à billes.

L'utilisation d'une formation de liaison C-N mécanochimique catalysée par du cuivre a permis la création d'une bibliothèque d'arylfulsonylguanidines, dont huit membres se sont révélés former une famille étonnamment grande de cristaux de composant unique isostructurales. En utilisant des principes de design supramoléculaires robustes et fiables, on a découvert une nouvelle famille de cristaux thermosalents à base de *N*, *N*'-bis(aryl)urées de type Etter qui présentent un mouvement de "saut" lors du chauffage. La sonochimie a permis la synthèse à l'échelle des grammes de ces composés. Ceci, à son tour, a permis l'étude systématique de la façon dont le placement de groupe fonctionnel affecte le comportement thermosalient dans ces bis (aryl) urées methoxy-substituées. La combination des techniques

d’analyse à l’état solide, dont la diffraction des rayons X, de la microscopie à l'étape chaude et de la calorimétrie différentielle à balayage a facilité la découverte et la caractérisation d'un nouveau composé thermosalient qui a manifesté un comportement thermosensible prononcé avec un degré élevé de réversibilité.

ACKNOWLEDGEMENTS

First and foremost, I would like to express my sincere gratitude and thank my PhD supervisor, Prof. Tomislav Friščić, who has inspired me, guided me, and was always there to encourage me, throughout my PhD study and in the completion of this thesis. Your boundless enthusiasm towards chemistry and research is infectious, and I am forever grateful for allowing me to present my work in numerous conferences. I have learnt so much about solid-state chemistry, writing, and about life from you, and I am glad to have called you my Boss.

I would also like to thank my PhD Advisory Committee, Prof. Chao-Jun Li, Prof. Jean-Philip Lumb, Prof. Audrey Moores, Prof. James Gleason and Prof. Nicolas Moitessier, for their valuable feedback regarding my research during my yearly review presentations.

My sincere thanks also go to Prof. Scott Bohle and Prof. Robin Rogers at McGill University, and Prof. Xavier Ottenwaelder from Concordia University, for their help in obtaining single crystal X-ray diffraction data. I would also like to thank Mr Nadim Saadé and Dr. Alexander Wahba for their assistance in obtaining mass spectroscopy data for all my compounds, Dr. Robin Stein and Dr. Frederick Morin for their expertise in running all the nuclear magnetic resonance spectroscopy experiments, and Dr. Petr Fiurasek for teaching me how to use the differential scanning calorimeter in the Centre for Self-Assembly of Chemical Structures. Ms Jacqueline Farrell is acknowledged for being a wonderful coordinator and organizing the various CREATE in Green Chemistry workshops, Ms Chantal Marotte for being a great administrator for the Chemistry Graduate Program, and Ms Jennifer Marleau and Ms Karen Turner for her help in all finance-related administrative matters.

To my colleagues and friends in the Friščić group and in the Department of Chemistry, many of whom I have had the absolute pleasure to work with, thank you for making my PhD experience a fulfilling and enjoyable one. In particular, special thanks go to Dr. Cristina Mottillo, Mr. Louis Do, Dr. José Gregorio Hernández, Ms. Karen Ardila-Fierro, Dr. Athanassios D. Katsenis, Ms. Athena Fidelli, Ms. Ghada Ayoub, Dr. Dayaker Gandrath, Prof. Ivani Malvestiti, Prof. Ricardo Longo, Dr. Leigh Loots, and Dr. Oleksandr Bushuyev for all the brainstorming sessions about chemistry, for all the fun times we had during our travels, for all the frustrations we had shared together, and most importantly, for being wonderful friends. A special shout-out also goes to Mr. Mahdi Roohnikan, Mr. Michael Landry, Dr. Violeta Toader, Dr. Petr Fiurasek, Ms Yu-Chen Wang, Dr. Haining Wang and Dr. Inna Perepichka for being great lab neighbours and for being such friendly and helpful people. I would also like to acknowledge Ms. Naomi Biggins and Mr. Richard von Celsing

for being great undergraduate students. I enjoyed being your mentor and guiding you guys in the lab in the summer.

To Dr. Richmond Lee and Ms. Xiaozhi Lim, I am grateful for you two being excellent friends and thank you for all your support. I always cherish the times we spent together in our travels. To Dr. Susan Lauw, Dr. Matthias Lee, Dr. Xiaohe Miao and Dr. Yihan Zhu, I would also show my gratitude for the friendship and all the mutual support, since the days in Saudi Arabia and beyond. To my great friends Mr. Wootien Ang, Mr. Choon-Meng Tan, Mr. Aik-Heng Yap, Ms. Eunice Phua, Ms. Geck-Woon Ng, Ms Wanjun Lock, I thank you all for your understanding and words of encouragement during my PhD study. To my oldest friends, Dr. Junrong Tan and Mr. Licheng Tay, I would like to thank you for keeping in contact with me during my graduate studies and for your kind heartening words.

I would also like to show appreciation to my previous supervisors, Prof. Andy Huang, Prof. Wee-Shong Chin and Prof. Wang Jian for all that they have taught me whilst I was working in their research laboratories.

Last but not least, I would like to show my deepest gratitude to my family, especially my mother, Ms. Elsie Ng, and my father, Mr. Jimmy Tan, for their unconditional love, support, understanding and upbringing that has led me to where I am today. I would also like to thank my sister, Ms. Colleen Tan, and my brother, Mr. Damien Tan, for their support and for taking care of my parents in Singapore during my pursuit of graduate studies over the last 6 years.

PREFACE AND CONTRIBUTION OF AUTHORS

This Dissertation entitled, "Medicine balls and smashing crystals: from new mechanochemical C-N coupling reactions to thermosalient crystals", describes research conducted and published by myself, Davin Tan, from January 2013 to January 2017. Prof. Tomislav Friščić provided guidance in all aspects of this Dissertation and the research described herein, in addition to editing and revision of all manuscripts included here.

Chapter 1 consists of a literature review, covering the brief history of mechanochemistry, the development of liquid-assisted grinding techniques for the synthesis of organic and inorganic solid materials, the advancement of *ex situ* and *in situ* analytical methods used to monitor and understand mechanochemical reactions, evolution of organic transformation reactions in mechanochemistry including recent advancements and trends, and lastly, a brief introduction to the various aspects of mechanochemistry. These topics discussed are relevant to all chapters in this Dissertation. *Section 1.4* of *Chapter 1* consists of texts which has already been published, specifically as a recent review on development of mechanochemistry for medicinal and pharmaceutical purposes, and as a chapter dedicated to organic mechanochemistry in the book "Sustainable Catalysis-Energy-Efficient Reactions and Applications", which was written by D. Tan and edited by Prof. Tomislav Friščić. The chapter, which has been formatted and modified for inclusion in this Thesis, describes the recent advancements of the use of metal catalysts and new frontiers of mechanochemistry for organic transformation reactions.

Chapter 2 consists of work that is part of a published paper entitled "Mechanosynthesis of pharmaceutically relevant sulfonyl-(thio)ureas", discussing the mechanochemical synthesis of anti-diabetic sulfonylurea APIs using base-mediated and copper-catalyzed strategies. This article is co-authored by Davin Tan, Dr. Vjekoslav Štrukil, Dr. Cristina Mottillo and Prof. Tomislav Friščić. The paper was written by D. Tan with guidance and editing contributions from Prof. T. Friščić. Dr. V. Štrukil and Dr. C. Mottillo aided in the collection of the single crystal X-ray diffraction data. All experimental results and analysis, including screening, synthesis and instrumental characterization (FTIR, NMR, MS) of the various compounds were performed by D. Tan. This work has been re-written for inclusion in this chapter with additional results included.

Chapter 3 describes the work that is a part of a published paper entitled "Development of C-N coupling using mechanochemistry: catalytic coupling of sulfonamide and carbodiimide", discussing the use of mechanochemistry as a powerful tool for new

reaction discovery. This article is co-authored by Davin Tan, Dr. Athanassios D. Katsenis, Dr. Cristina Mottillo, Dr. Vjekoslav Štrukil, and Prof. Tomislav Friščić. The paper was written by D. Tan with guidance and editing contributions from Prof. T. Friščić. The text has been formatted and re-written for inclusion in this Dissertation. All experimental results, including screening, synthesis and instrumental characterization (FTIR, NMR, MS) of the various compounds were performed by D. Tan, with help from Dr. C. Mottillo. Dr. A. D. Katsenis and Dr. V. Štrukil for the collection of the SCXRD data. This work has been re-written for inclusion in this chapter with additional results included.

Chapter 4 describes the work that is part of a recently published paper entitled "Carbodiimide insertion into sulfonimides: one-step route to azepine derivatives by a two-atom saccharin ring expansion", describing a previously not known insertion reaction of carbodiimides into sulfonimides, enabling the first one-step, two-atom expansion of the 5-membered ring of saccharin into a 7-membered benzo[1,2,4]thiadiazepine, and a two-atom chain extension of a non-cyclic sulfonimide. This article is co-authored by Davin Tan and Prof. Tomislav Friščić, and is based on the continuation of the research concept from *Chapter 3*, of using mechanochemistry as a powerful tool to discover new reactions. The paper was written by D. Tan with guidance and editing contributions from Prof. Tomislav Friščić, The text has been formatted and re-written for inclusion in this Dissertation. All described experimental work and results, including screening, synthesis and instrumental characterization (FTIR, NMR, MS, XRD) of the various compounds were performed by D. Tan.

Chapter 5 describes work that is a part of a manuscript in preparation entitled "Base-free mechanochemical copper-catalyzed amide coupling of isatins, benzamides and imides with isocyanates", discussing the rapid base-free coupling reaction between poorly nucleophilic isatins, benzamides and imides to access a variety of biologically active carbamoyl-isatins, -benzamides and –imides. Similar to *Chapter 4*, results discussed in this chapter are based on the continuation of the research concept from *Chapter 3*: using mechanochemistry to discover new C-N coupling reactions. This manuscript is co-authored by Davin Tan, Ms. Naomi Biggins and Prof. Tomislav Friščić. The contribution of Ms. Naomi Biggins, a summer undergraduate exchange student from University of Nottingham, consists of performing selected reactions, reaction screening and optimizations, and conducting NMR analyses under the direct guidance and supervision of D. Tan. All other experimental results, including screening, synthesis and instrumental characterization (FTIR, NMR, MS, SCXRD) of the various compounds were collected and analyzed by D. Tan.

Chapter 6 consists of a not yet published draft manuscript entitled "A family of isostructural crystals from conformationally flexible ortho-substituted *N*,*N*'-bis(cyclohexyl)-arylsulfonylguanidines", discussing a series of *N*,*N*'-bis(cyclohexyl)-arylsulfonylguanidines, with particular *ortho*-substituents on the aryl ring. Eight of these achiral compounds, which were synthesized using the mechanochemical methods as discussed in *Chapter 3*, assembled isostructurally through classical intermolecular S=O···H-N hydrogen bonds, forming one-dimensional helical chains, containing a three-fold rotation axis. This manuscript is co-authored by Davin Tan, Mr. Richard von Celsing, Dr. Athanassiso D. Katsenis and Prof. Tomislav Friščić, The paper was written by D. Tan with guidance and editing contributions from Prof. Tomislav Friščić. Contributions of Dr. Athanassios D. Katsenis include making two of the images used in Fig. 6.2, and Mr. Richard von Celsing, an undergraduate summer student from McGill University, who contributed to the synthesis of two of the isostructural compounds, and performed FTIR-ATR and NMR analyses under the direct guidance and supervision of D. Tan. The text has been formatted and written for inclusion in this Dissertation. All other experimental results, including screening, synthesis and instrumental characterization (FTIR, NMR, MS, PXRD, SCXRD) of the various compounds were performed by D. Tan.

Chapter 7 comprises of part of a not yet published manuscript entitled "Evolution through design: a serendipitous discovery, systematic investigation and design of a new thermosalient crystal based on Etter-type *N*,*N*'-bis(aryl)ureas", discussing the discovery and development of a family of organic thermosalient crystals, through systematic positional functionalization of *N*,*N*'-bisarylureas. This article is co-authored by Davin Tan, Dr. José G. Hernández and Prof. T. Friščić. The manuscript was written by D. Tan with guidance and editing contributions from Prof. T. Friščić. Dr. José G. Hernández contributed to the discussion and brainstorming process. The text has been formatted and written for inclusion in this Dissertation. All experimental results, including synthesis and instrumental characterization (FTIR, NMR, MS, XRD, TGA, DSC, HSM) of the various compounds were performed by Davin Tan.

LIST OF ABBREVIATIONS

ACN: acetonitrile

API: active pharmaceutical ingredient

AFM: atomic force microscopy

BPU: benzomoylphenylureas

BSS: bismuth(III) subsalicylate

caf: caffeine

$CF_3SO_2NH_2$: trifluoromethylsulfonamide

CH_3NO_2: nitromethane

CM: cross metathesis

Cp*: pentamethylcyclopentadienide

CP-MAS: cross polarization magic angle spinning

cnge: cyanoguanidine

CSD: Cambridge Structural Database

CyNCO: cyclohexylisocyanate

DABCO: 1,4-diazabicyclo[2.2.2]octane

DCC: dicyclohexylcarbodiimide

DIC: di(*iso*-propyl)carbodiimide

DMF: *N*,*N*-dimethylformamide

DMSO: dimethylsulfoxide

DPTC: di(*p*-tolyl)carbodiimide

DSC: differential scanning calorimetry

DTBC: di-*tert*-butylcarbodiimide

DTMSC: di(trimethylsilyl)carbodiimide

EtOAc: ethylacetate

EMK: ethylmethylketone

EDC: 1-ethyl-3-(3-dimethylaminopropyl)carbodiimide

FTIR: Fourier-transform infrared

FTIR-ATR: Fourier-transform infrared attenuated total reflectance

HMBC: heteronuclear multiple bond correlation

HR-MS: high resolution mass spectroscopy

HSM: hot-stage microscopy

IBX: 2-iodoxybenzoic acid

ILAG: ion- and liquid-assisted grinding

IUPAC: International Union of Pure and Applied Chemistry

KI: Knoop Index

KOCN: potassium isocynate

L-ta: L-tartaric acid

LAG: liquid-assisted grinding

MeOH: methanol

MOF: metal-organic frameworks

mRNA: messenger ribonucleic acid

MS: mass spectroscopy

NDC: 2,3-naphthylenedicarboximide

Na_2H_2EDTA: sodium ethylenediaminetetraacetate

NHC: *N*-heterocyclic carbene

NHS: *N*-hydroxysuccinimidyl

NMR: nuclear magnetic resonance

PEG: polyethylene glycol

Ph-NCO: phenylisocyanate

PMMA: polymethylmetacrylate

POLAG: polymer-assisted grinding

PXRD: powder X-ray diffraction

RCM: ring closing metathesis

SC-SC: single-crystal-to-single-crystal

SCXRD: single crystal X-ray diffraction

SDG: solvent-drop grinding

SEM: scanning electron microscopy

ssNMR: solid-state nuclear magnetic resonance

TBEC: 1-tert-buyl-3-ethyl-carbodiimide

TCT: 2,4,6-trichloro-1,3,5-triazine

TGA: thermogravimetric analysis

THF: tetrahydrofuran

THz-TDS: Terahertz time-domain-spectroscopy

WC: tungsten carbide

XRD: X-ray diffraction

ZIF: zeolitic imidazole framework

LIST OF FIGURES

LIST OF TABLES

INTRODUCTION

This Dissertation will introduce mechanochemistry, and its use as a powerful tool for discovering new carbon-nitrogen (C-N) coupling reactions, for the covalent synthesis of molecules of active pharmaceutical ingredients (APIs), as well as other pharmaceutically-relevant organic compounds. *Chapter 1* provides a general overview of the historical developments and recent advances in mechanochemistry. In *Chapter 2*, the mechanosynthesis of anti-diabetic sulfonylureas is discussed, demonstrating a new method of making these drug molecules in a rapid, solvent-free manner. The reactions were conducted in a ball mill, and utilize either a base-mediated or a copper-catalyzed coupling reaction between sulfonamides and isocyanates. Subsequently, in *Chapter 3*, the discovery and development of a novel C-N coupling reaction, which is only enabled by mechanochemistry, is presented. The reaction involves the coupling of arylsulfonamides with carbodiimides to afford arylsulfonylguanidines, a structural subunit that can be found in many biologically-active compounds. Furthermore, *Chapters 4* and *5* will outline the extension of this philosophy of investigating solid-state reactivities of other poorly nucleophilic reactants, such as amides, using mechanochemical techniques only. This exploration, which is the topic of *Chapter 4*, led to the discovery of a new two-atom C-N insertion of carbodiimides into the sulfonimide moiety of saccharin, yielding various azepine derivatives. In *Chapter 5*, a new base- and solvent-free copper-catalyzed mechanochemical coupling of isatins, benzamides and imides with isocyanates is discussed. Many of these compounds exhibited highly interesting molecular self-assembly motifs in the solid state. The efficient mechanosynthesis enabled a family of arylsulfonylguanidines to be synthesized in gram-scale amounts, facilitating the growth of high-quality single crystals. In *Chapter 6*, X-ray diffraction analysis of those crystals is discussed, revealing a surprisingly large set of eight isostructural single-component crystals. In addition, *Chapter 7* discusses the discovery and systematic development of a family of thermosalient crystals, based on Etter-type *N*,*N*'-bis(aryl)ureas. This chapter focused on investigating the relationship between the functional group positioning on such molecules and their observed thermosalient behaviour.

CHAPTER 1

LITERATURE REVIEW

"I am always excited for the new changes in how we do chemistry" -David Macmillan, McGill Chemical Society Seminar, 2016.

1.1 Definitions and historical overview of organic and supramolecular mechanochemistry

In this introductory chapter, I will delineate the most significant aspects of topics that are relevant for this thesis, notably mechanochemical reactions, their mechanism and use in synthesis and discovery of pharmaceutical solids, as well as the use of mechanochemistry and solvent-free synthesis in making active pharmaceutical ingredients (APIs). This introduction is not aimed to be a detailed, exhaustive overview of mechanochemistry, as these can be found in a number of recently published reviews and books, and provide a highly detailed analysis of the current state of the art of mechanochemistry in the areas of organic, inorganic and organometallic synthesis, as well as in the synthesis and development of advanced metal-organic materials, nanomaterials and inorganic solids. A significant fraction of this introductory section has already been published, specifically as a review on development of mechanochemistry for medicinal and pharmaceutical purposes, and as a chapter dedicated to organic mechanochemistry in the book "Sustainable Catalysis-Energy-Efficient Reactions and Applications" edited by Rafael Luque and Frank Lam. In order to improve the overall readability of this introduction, the text adopted from these publications has been expanded and modified from its original published form.

A "mechano-chemical reaction", according to the International Union of Pure and Applied Chemistry (IUPAC) compendium of chemical terminology (the Gold Book), is defined as "a chemical reaction that is induced by the direct absorption of mechanical energy."[1a] The input of mechanical energy can take place through different mechanisms, such as shearing, stretching, compression, friction or other types of mechanical action. Such mechanical action is generally thought to create sites or mechanisms of activation that lead to chemical reactions. There are conflicting views on what in fact takes place during a mechanochemical reaction. On one hand, most chemists can readily associate mechanochemistry with a process in which solids are brought together to react through mechanical activity, *e.g.* grinding in a mortar and pestle. On the other hand, an often encountered view is that mechanochemical reactions must somehow involve a liquefaction of the reactants, for example, through formation of a eutectic phase or by melting due to frictional heating. The view that mechanochemical reactions must involve a liquid intermediate has been observed to perpetuate a general view that no transformation can take place without a solvent or a liquid phase. This view can be traced back to a quote ascribed to Aristotle ""*corpora non agunt nisi fluida (or liquida) seu solute*" which, when translated, means "*compounds do not react unless fluid or if dissolved"*.[1b] The literature shows that

mechanochemical reactions can indeed be mediated by eutectic liquids or melts,[1g] but also that they can proceed through the solid state, or even be mediated by gas-phase transfer of molecules.[1c-e, 4a, 17] Therefore, assigning a particular gas-, liquid- or a solid-state mechanism to mechanochemical reactions does not seem justified, as the reactivity is complex, most likely varies from case to case and, in the current state, is still very poorly understood.

Such poor level of understanding may come as a surprise for a methodology that has been in use, in one form or another, since the Stone Age. Early beginnings of mechanochemistry are likely to find their roots in primitive Stone Age technologies, used to obtain fire, make tools or grind wheat.[1f, 2] According to Takacs,[3a] the so far earliest written record of a mechanochemical reaction appears to be a description of a metallurgical process. Namely, in 315 B.C.E, Theophrastus of Eresus in his book *De Lapidibus* (*On Stones*)[3c] described a method to obtain mercury by grinding cinnabar, an ore of mercury(II) sulfide (HgS), in a copper or bronze mortar. As explained by Takacs,[3a, 3b] this process is most likely a galvanic reduction of HgS (equation 1) with the material of the mortar and pestle, which yields liquid Hg and cupric sulfide (CuS). The process was conducted with the addition of a small amount of vinegar,[3b] thought to serve as a lubricant. In that way, this early report also foreshadows the modern technique of liquid-assisted grinding (LAG)[4] which will be discussed in later sections.

$$HgS(s) + Cu(s) \rightarrow Hg(l) + CuS(s) \text{ --- (equation 1)}$$

Coincidentally, it appears that this first written record of mechanochemistry may also be the first written record of an inorganic chemical reaction. This method of mechanical grinding or milling was then extended to the processing of minerals, grains, building materials *etc.,* mostly without a systematic written record.[3d] From *ca.* 300 B.C.E to 18th century, records of using mechanochemical grinding to induce chemical reactions are scarce in contrast to its use for transformations associated with metal mining, alloying, and metallurgical operations in general.[3d, 5] It is possible that some sort of mechanochemical reaction could have taken place in the grinding vessel when people experimented with manual grinding of two or more different solids together, but without proper scientific documentation, it is difficult to conclude that any sort of organized mechanochemistry or mechanochemical research occurred during this period. The mortar and pestle continued to be the primary tools for mechanical treatment of compounds and medicinal preparations. It was only in 1820, with Faraday's report that grinding of silver chloride (AgCl) with zinc, tin, iron and copper leads

to displacement reactions (equation 2), that systematic scientific studies of mechanochemistry began.[6] Among other systematic studies of mechanochemistry in the 19th century, notable contributions were those by Spring in 1880s,[7] who studied the salt metathesis reaction between barium sulfate ($BaSO_4$) and sodium carbonate (equation 3), conducted with a mortar and pestle. Importantly, this salt metathesis reaction is an early example of a process that is very difficult or even impossible to achieve in aqueous solution, in this case due to the extremely poor solubility of $BaSO_4$.

$$AgCl(s) + M(s) \rightarrow Ag(s) + MCl(s) \text{ --- (equation 2)}$$

$$BaSO_4(s) + Na_2CO_3(s) \rightarrow BaCO_3(s) + Na_2SO_4(s) \text{ --- (equation 3)}$$

$$2AgCl(s) \rightarrow 2Ag(s) + Cl_2(g) \text{ --- (equation 4)}$$

$$HgCl_2(s) \rightarrow Hg(l) + Cl_2(g) \text{ --- (equation 5)}$$

A major contributor to the early systematic development of mechanochemistry was Carey Lea (Fig. 1.1a), whose work on colloidal silver and its reduction aided the development of film photography.[8] Carey Lea examined the behaviour of silver halides under static pressure (compaction) and during trituration (grinding) in a mortar, and discovered that shearing forces during grinding led to more significant chemical outcome compared to compression. He also established that mechanical grinding can induce reactions that are different from thermal heating of the same system. For example, he observed that mercuric chloride ($HgCl_2$) sublimes upon heating, while silver chloride (AgCl) melts at elevated temperature. However, both of these inorganic salts decompose upon trituration at room temperature (equation 4,5). [9] This work is often noted as one of the first, and perhaps the most significant demonstration of differences between thermochemical and mechanochemical processes, earning him the mantle of being "the father of mechanochemistry".[10] However, the term mechanochemistry was not officially coined until thirty years later, when Ostwald (Fig. 1.1b) included it in his terminology of chemical science, along with photochemistry, thermochemistry, electrochemistry and other types of chemical transformations.[11]

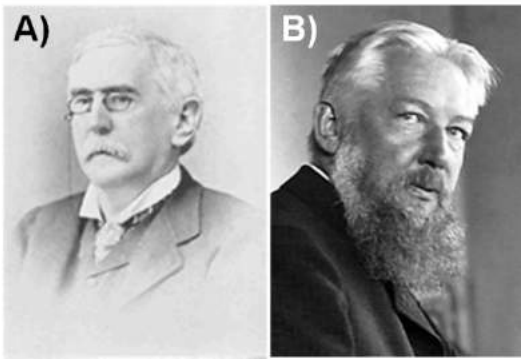

Fig 1.1. Pictures of the "father of mechanochemistry" (a) Matthew Carey Lea, and Nobel laureate in chemistry 1909 (b) Wilhelm Ostwald, who coined the term mechanochemistry. Adapted with permission from ref. 3a and 3b.

In the same way that thermal, sonochemical, microwave and photochemical reactions are often designated by generally accepted symbols, the Hanusa group[13] has recently proposed a symbol to represent mechanochemical reactions, in the form of three circles, reminiscent of grinding media used in ball milling (Fig. 1.2). However, it must be noted that this symbol for mechanochemical treatment includes not only the use of mechanical electrical mills, but also encompasses other techniques, such as manual grinding by a mortar and pestle.

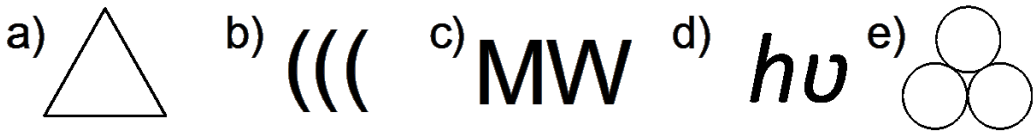

Fig 1.2. Symbolic representation of a) solvothermal, b) sonochemical, c) microwave irradiation, d) photochemical and e) mechanochemical reactions.

1.1.1 Early development of organic mechanochemistry

Although historical examples noted in the preceding section focused on transformations of inorganic materials, the history of organic mechanochemical reactions has begun to develop almost at the same time. Along with traditional solution chemistry, milling and grinding have been of considerable interest as synthetic techniques to organic chemists of the 19th century. Notably, in 1844, Wöhler described an early example of making a cocrystal of quinhydrone by grinding.[12] Later, in 1893, Ling and Baker reported a similar mechanochemical cocrystallization reaction of *meta*-dichloroquinone and *meta*-dichloroquinol.[15] As explained by Jones *et al.*,[14] mechanochemical formation of the cocrystal was significantly superior to attempted solution synthesis, where redox self-isomerization

tend to lower the efficiency of complex formation. This cocrystal formation by simple grinding is now considered to be the first synthesis of a quinhydrone charge-transfer complex which was synthesized mechanochemically in the solid state. Almost a century later, in 1983, this work was revisited by Paul and Curtin, whereby they cocrystallized benzoquinone with other hydroquinones using a mortar and pestle. It is important to reiterate the point that these charge-transfer molecular complexes are difficult to synthesize in solution due to redox self-isomerization but were easily achieved through mechanochemical means (Fig. 1.3).[16] Similarly, Kuroda *et al.* also demonstrated that neat grinding of related benzoquinone and *bis*-naphthol system can afford crystal forms that could not be obtained by other methods, such as by crystallization from solution or by melting.[17]

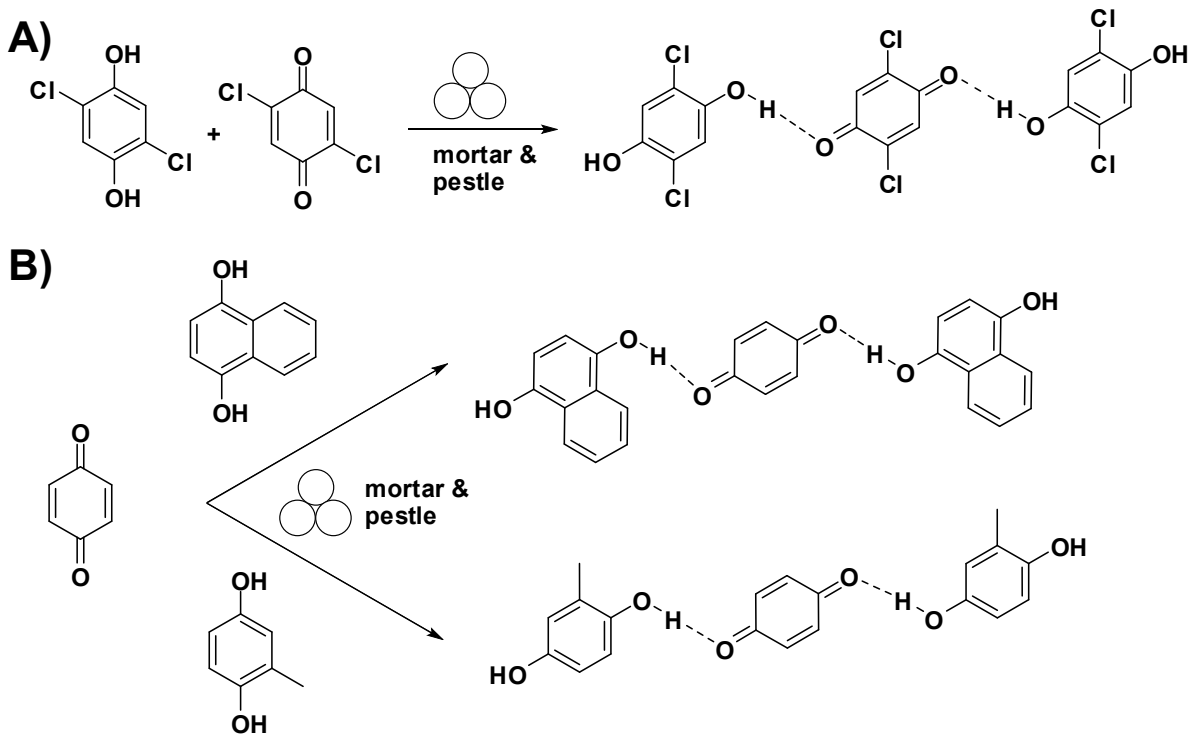

Fig 1.3. a) Cocrystallization of *meta*-dichloroquinone and *meta*-dichloroquinol by grinding; b) charge-transfer complex formation of benzoquinone and different hydroquinones by grinding.

For most of the 20th century, mechanochemical reactions were largely in the domain of inorganic chemists and metallurgists.[3d] It was only in the late 1980s that the research fervour of mechanochemical organic reactions started to gain momentum again. Most notable contributions in that context came from the pioneering work of Toda and coworkers,[18] who demonstrated the versatility of solvent-free chemistry for a wide range of organic transformations, as well as for complexation and separation of organic molecules in the solid

state. In that work,[18a] they successfully synthesized several host-guest inclusion complexes of different compounds, such as *N,N,N,N′*-tetra(*iso*-propyl)oxamide with *p*-cresol, by use of an agate mortar and pestle or a mechanical test tube shaker. They have also demonstrated stoichiometric control over the mechanochemical product formed by simply controlling the amount of reactants used, performed enantioselective complexation reactions between cyanohydrins and brucine,[18a] investigated concomitant solid-state grinding and stereoselective photochemical reactions,[18a] as well as conducted low temperature grinding reactions, which removes frictional heating effects normally associated with mechanical grinding.[18b] The latter observation is especially important, as it shows the ability to conduct mechanochemical self-assembly processes at conditions under which melting is not expected. In doing so, they have shown that organic reactions and formation of these inclusion complexes can take place mechanochemically in the absence of bulk solvent, and also yield products that are inaccessible by conventional solution syntheses. Around the same time, the Etter group investigated solid-state grinding as a synthetic methodology to prepare cocrystals based on supramolecular hydrogen-bonding synthons.[19] This work, and also results reported by Caira[20b] on hydrogen-bonded self-assembly in the solid state, laid the foundations for the extensive employment of mechanochemistry in pharmaceutical materials science, notably the solvent-free neat grinding and ball milling as techniques for the synthesis and discovery of cocrystals, salts and polymorphs of APIs.

1.1.2 Evolution of mechanochemical reactions: from mortar and pestle to ball mills

Section 1.1.1 gave a brief overview of the historical development of mechanochemistry, which also revealed three main advantages of this technique over conventional routes in organic and inorganic synthesis. First, mechanochemical reactions eliminate the need for bulk solvents and thus have the potential to be more environmentally-friendly by generating less solvent waste. Neat grinding or milling reactions can also be conducted at mild temperatures, which further highlights the "green" and easily accessible aspect of the methodology. Second, without the need for bulk solvents, the issues of solubility and solvolysis of reagents can sometimes be completely circumvented, thus abolishing the need to search for suitable but often toxic solvents. Such reactivity independent of solubility has the potential to make a plethora of alternative starting materials accessible to the synthetic chemist. This in turn can reduce reaction times and cost, increase product yields and allow for improved stoichiometric control. Third, while a case can be made for using mechanochemical synthesis to augment existing synthetic protocols, there is

also a growing body of evidence that demonstrates mechanochemical reactions can enable the formation of products, molecules as well as materials that are normally unattainable through solution-based methods.[60, 68, 121] Specific examples will be discussed in detail later.

The Braga group has pioneered mechanochemical reactions by kneading,[21] *i.e.* by manually grinding powdered reactants in a mortar and pestle in the presence of small amounts of solvent. The solvent additive in kneading has been suggested to improve mechanochemical reactivity by effectively acting as a lubricant for molecular diffusion. While kneading is a powerful and also simple methodology, its dependence on using a mortar and pestle also leads to limitations. Whereas such equipment is simple and readily available, its use is far from ideal. Principal disadvantages of using a mortar and pestle for conducting reactions are: 1) inherent difficulty in controlling a number of parameters such as force or pressure exerted by the experimenter, the composition of the material and hardness of the mortar and pestle, the surface area and radius of the curvature of the mortar and pestle, and also exposure to ambient factors such as humidity and temperature. The inability to track and control these important parameters can lead to poor reproducibility and incorrect interpretation of experimental results. For example, Cinčić *et al.* have shown that grinding and aging aromatic aldehydes with anilines in dry air can provide very different results to grinding in the presence of moisture or organic solvent vapours. Grinding in the presence of air that is moist or saturated with organic vapour led to facile formation of Schiff base products, whereas grinding in dry air gave little or no result.[24a] 2) Limited duration of the reaction: manual grinding is mostly limited to 30-60 minutes due to practical reasons. 3) Limitation of reaction scale: it is difficult to manually conduct large-scale reactions and most laboratory experiments are limited to milligram amounts. Even though these problems can be alleviated by the development of mechanical mortar grinders (Fig.1.4a), mechanochemical synthesis so far has mostly been dominated by the use of ball mills. Shaker (or vibrational, mixer) mills are commonly used for reactions in milligram to gram scale (Fig. 1.4b), while larger scale operations (gram to kilogram) are mostly performed in planetary or attrition mills (Fig.1.4c). Continuous flow mechanochemical reactions can also be achieved by the use of co-rotatory twin screw extruders. The use of these modern electrical mills, in comparison to manual techniques, allows for greater reproducibility through better control of duration of milling, frequency of shaking (or speed of rotation), ratio of the reactant weight to the reaction vessel volume and other mechanochemical parameters, which in turn can improve the efficacy of the mechanochemical reactions.

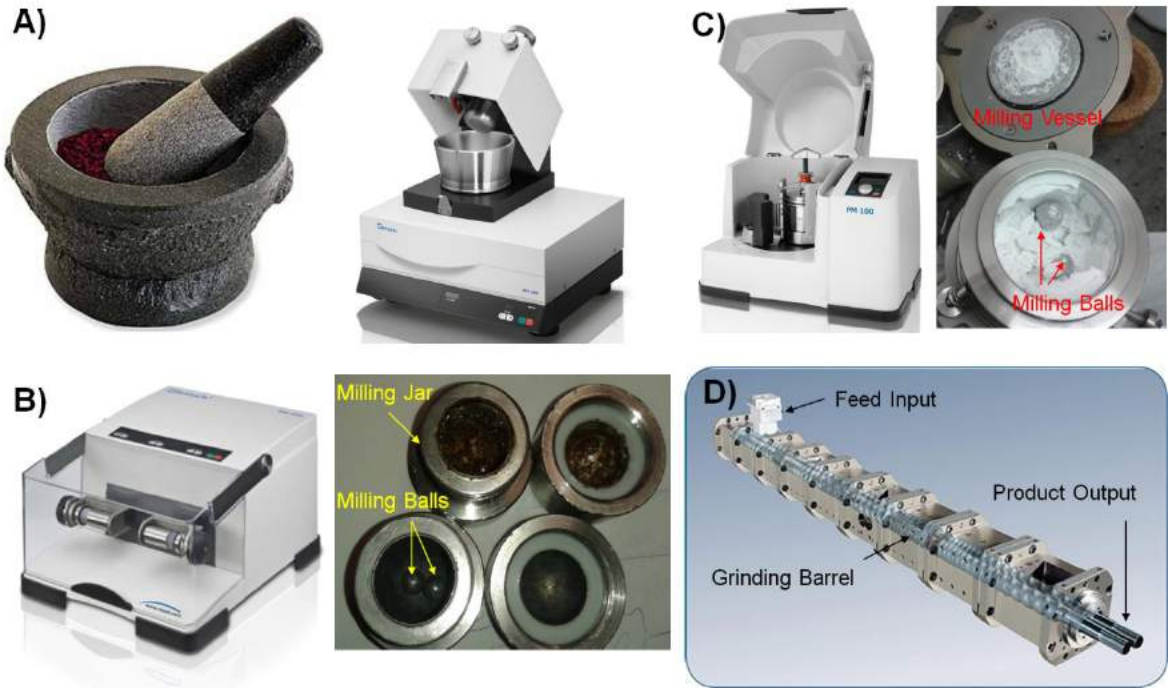

Fig 1.4. a) traditional (left) and automated (right, Retsch RM200) mortar and pestle, b) shaker or vibrational mill (Retsch MM200) using jars and ball bearings, c) planetary mill (Retsch PM100) for multigram scale synthesis and d) twin screw extruders (Plastic Technology) for continuous flow mechanochemical synthesis. Images are taken from the websites of the respective manufacturers (Retsch and Plastic Technology).

However, it must be noted that there is a significant difference from using a mortar and pestle *versus* using an electrical ball mill. It is often assumed that during ball milling reactions, the milling media *i.e.* ball bearings, hit the ends of the moving milling vessel (Fig. 1.5).[159, 160] However, there is a wide range of ball mills, each with a different mode of operation, including shaker (mixer) mills, planetary mills, attritors, roller, gravity or magnetic mills *etc*. In the context of organic, organometallic and supramolecular chemistry, the most significant ones are shaker and planetary mills. Each of these different types of milling devices is characterized by a different type of mechanical motion exerted by the milling media. The type of mechanical motion can have a strong, and yet not fully understood effect on reactivity and energy transfer.[79, 160] For example, Boldyreva's group has demonstrated how different regimes or modes of mechanical motion can have a profound effect on the cocrystallization reaction of glycine and malonic acid, [22] leading to differences in reaction kinetics and even the formation of different products. Specifically, milling of α-glycine with β-malonic acid in a 1:1 stoichiometric ratio led to the formation of a glycinium semimalonate salt, which was followed by the appearance of another phase, proposed to be a cocrystal of glycine and malonic acid. However, depending on which section of the milling vessel was

sampled, the analysis of the reaction mixture gave different results. Samples taken from the central part of the milling jar, where the sliding motion of the balls resulted in a more pronounced shearing regime, contained a significant amount of the semimalonate salt rather than cocrystal. On the other hand, samples taken from the ends of the milling jar, where the motion of the balls tends to result in mostly impact and compression forces, revealed a higher proportion of the cocrystal. While the differences in reactivity arising from the type of mechanical force are still poorly understood, this example illustrates how outcomes of a mechanochemical reaction can be affected by the different mechanical regimes in the milling vessel.

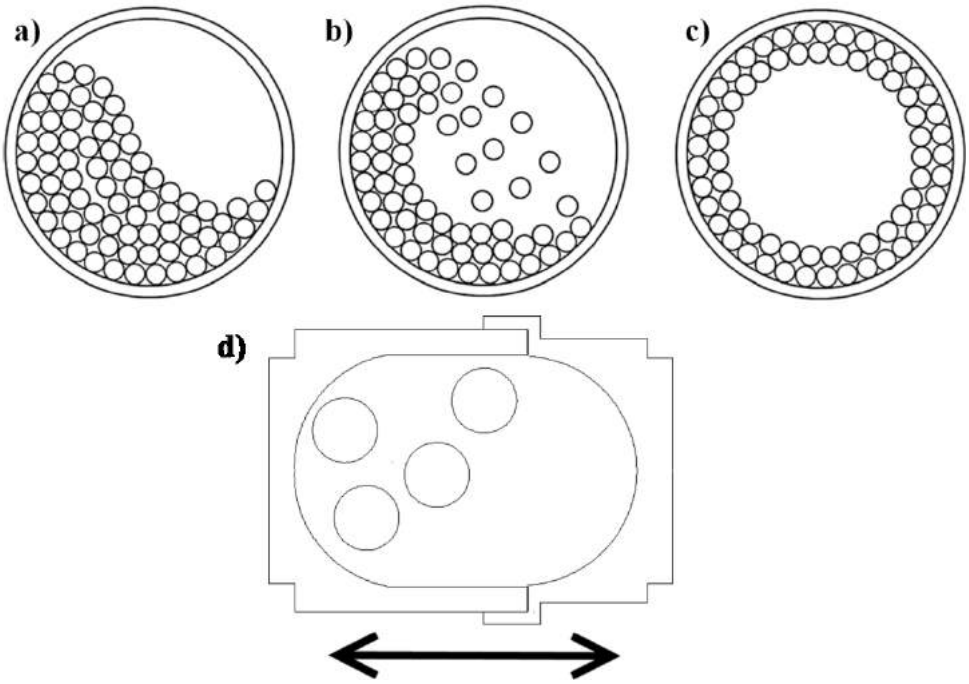

Fig 1.5. Scheme depicting the ball motion in a milling vessel of a planetary ball mill (*a-c*) showing: a) cascading, b) cataracting and c) rolling motion; d) movement and motion of the shaker mill jar and balls. Adapted from ref. 160a and 160b.

Mechanochemical reactions can also be modulated by varying the size and number of milling media, as well as the material from which the milling assembly (*i.e.* the media and the milling container) are made of, by simply changing the density and hardness of the material. A useful guide in selecting the material of the milling assembly is the Knoop index (KI),[23] which is a measure for the mechanical hardness of the material. A selection of material of milling media such as stainless steel (density = 7.7 g/cm^3, KI = 138), zirconia (density = 4.5 g/cm^3, KI =1160), copper (density = 8.96 g/cm^3, KI = 163), alumina (density = 3.95 g/cm^3, KI = 2100) and tungsten carbide (density = 15.63 g/cm^3, KI = 1880) can be employed. In

addition to the strategy of changing the milling media and material of the milling assembly to vary mechanochemical conditions, ball milling reactions can also be modified by input of other types of energy, such as light and heat, in order for these solid-state reactions to take place. It was recently demonstrated that concomitant photochemical and thermochemical reactions can be conducted in tandem with mechanochemical treatment by using a vortex mixer[24b] or a lysis[24c] mills respectively.

1.2 Advancing mechanochemical techniques: liquid-assisted grinding (LAG)

Solvent-free mechanochemical grinding has been highly successful in the synthesis of multi-component organic solids, specifically solvates, salts and cocrystals.[38, 122, 123] This has proven to be of particular value for the screening and synthesis of new solid forms of model, as well as active pharmaceutical ingredients (APIs). The landmark contribution by Shan and coworkers has demonstrated that the scope of mechanochemical cocrystallization can be further expanded through the addition of small amounts of a liquid.[25] The authors were investigating the cocrystallization of 1,3,5-cyclohexanetricarboxylic acid with hydrogen bond acceptors such as hexamethylenetetraamine, 4,4'-bipyridine and 4,7-phenanthroline *via* grinding. It was observed that the addition of a small amount of a liquid (1 or 2 drops of methanol) drastically enhanced the kinetic rate of cocrystal formation and significantly reduced the grinding time needed for quantitative conversion, from 1 hr to 10 min. Such acceleration of cocrystallization reaction, through what was termed as solvent-drop grinding (SDG) technique, was observed for polar liquid additives such as acetonitrile, ethyl acetate and water, but not for non-polar liquids such as cyclohexane. The addition of a grinding liquid is somewhat similar to and reminiscent of the previously described technique of using vinegar in the processing of cinnabar in a copper mortar, as highlighted by Takacs.[3b]

A subsequent report by Trask *et al.* explored the use of SDG for the selective mechanochemical synthesis of two polymorphs of the cocrystal of caffeine and glutaric acid in a 1:1 stoichiometric ratio, the monoclinic Form I and the triclinic Form II.[26] Neat grinding or SDG with non-polar solvents such as hexane, heptanes and cyclohexane was found to predominantly yield Form I, as characterized by powder X-ray diffraction (PXRD). On the other hand, SDG using polar additives such as acetonitrile, water, chloroform or dichloromethane gave only Form II. This remarkable control over the polymorphic outcome of the mechanochemical cocrystallization may be considered a milestone in the development of mechanochemical reactivity of organic solids. Trask and coworkers have also described a

similar method to control the polymorphism of anthranilic acid by using SDG.[29c] Anthranilic acid is known to exist in at least three polymorphs, known as Forms I, II and III. It was observed that milling anthranilic acid Form I with heptane leads to the selective formation of the polymorphic Form II. On the other hand, milling Form II with chloroform led to tautomerization and formation of the zwitterionic form III. The addition of a liquid in milling not only improves reaction kinetics, but also affords highly crystalline products in quantitative yields and mitigates the problem of amorphization usually associated with neat grinding of organic solids.[27-28]

In 2006, the term was redefined from SDG to LAG,[29] in an effort to more accurately describe the role of the added liquid during grinding, as the term solvent led to unjustified assumptions that mechanochemical reactivity is related to reactant solubility in the liquid additive. That such an assumption is not necessarily correct was shown in a systematic exploration of the synthesis of a three-component cocrystal by reacting caffeine, succinic acid and a small guest molecule. The reactions were expected to yield inclusion compounds based on hydrogen-bonded framework of caffeine and succinic acid, with the small molecules taking the role of space-filling guest. This study revealed the formation of the targeted three-component cocrystals in 4 out of 25 cases when using solution methods. Direct milling of caffeine, succinic acid and the tentative guest molecule gave, in contrast, 15 out of 25 positive results. Importantly, the efficiency of mechanochemical cocrystallization was further improved by the addition of another liquid phase. Such LAG improved the cocrystallization efficiently, leading to the formation of the three-component cocrystal in 18 out of 25 cases. Most importantly, as some of the guest molecules are liquids, the work illustrated that the role of the liquid additive in LAG is more than just a physical "lubricant".

Although the mechanism of LAG reactivity remains largely unknown, the role of the liquid encompasses not only the improvements in reaction kinetics but also permitting reactions to take place even with poorly soluble solid reagents. This was demonstrated in a systematic study which also established a quantitative descriptor of LAG reaction conditions. Focusing on cocrystallization of model APIs caffeine and theophylline with L-tartaric and L-malic acids (Fig. 1.6),[30] this study introduced the parameter η, defined as the ratio of the added liquid (in μL) to the total weight of the solid reactants (in mg). The parameter η provides a more accurate descriptor for comparing mechanochemical reactions, replacing vague terms such as "one or two drops of liquid" or "a small amount of liquid". The investigation of the same model reaction at different η values allows for the comparison of how LAG reactivity is affected by the amount of liquid used. Specifically, η = 0 μL/mg refers

to neat reactions, whilst η = 0-1 μL/mg has been empirically established as the range in which the mechanochemical reactions are not affected by differences in solubilities of the reactants. Higher η values, roughly between 1-12 μL/mg denote reactions in a slurry wherein the effects of solubility on reactivity begin to be noticeable. Finally, η > 12 μL/mg corresponds roughly to reactions in homogenous solution, where the reactivity is controlled by thermodynamic solubilities of the reactants and products. The results (Fig.1.6d) show that LAG reactivity is, at best, only slightly dependent on solubility as cocrystallization was achieved in most liquids except cyclohexane. Most notable are the use of highly non-polar benzene and di-*iso*-propyl ether as grinding liquids, in which the reactants, caffeine and L-tartaric acid, exhibit very poor solubility, yet actually enabled the formation of the cocrystal. It is important to note that the assessment of η is very much based on this one systematic study and that the definitions of LAG and η could, therefore, be of very limited scope. Unfortunately, at this point there are only a handful of systematic studies of LAG reaction conditions.[29-30] Despite a poor understanding of underlying mechanism, LAG represents a significant improvement from manual kneading as it provides access to a much higher level of control over reaction parameters. It is also important to note that LAG refers to enclosed ball milling systems.[30b]

There are several other mechanochemical methods that have evolved from LAG, therefore further expanding the toolbox of milling mechanochemistry. Ion- and liquid-assisted grinding (ILAG) was developed in the context of the mechanochemical synthesis of metal-organic frameworks (MOFs). In particular, the use of ILAG enables the quantitative conversion of simple metal oxides into metal-organic materials, including not only MOFs but also metallodrugs.[33a, 35] The development of ILAG was initiated in 2010,[33a-b] by the discovery that the addition of a catalytic quantity of an inorganic salt, like potassium nitrate or ammonium sulfate (in parts per million amounts), can have a profound effect on the kinetics and control of the polymorphic outcome of mechanosynthesis of pillared MOFs (Fig. 1.7). Specifically, ILAG of zinc oxide, terephthalic acid and 1,4-diazabicyclo[2.2.2]octane (DABCO) led to the formation of a popular pillared MOF, originally developed by the Kim and the Hupp groups in early 2000s.[33c-d] This work revealed that nitrate salts induced the formation of a tetragonal polymorph of the MOF, while sulfates formed a much less known hexagonal structure based on Kagome topology zinc terepthalate layers bridged by DABCO pillars. The observed selectivity in the formation of different MOF topologies highlights the use of ionic additives in ILAG not only as a means to accelerate reactivity of metal oxides, but also to screen for different MOF topologies. Although the mechanisms of ILAG reactions are still not clear, the authors proposed an anion templating effect for the observed selectivity.

A)

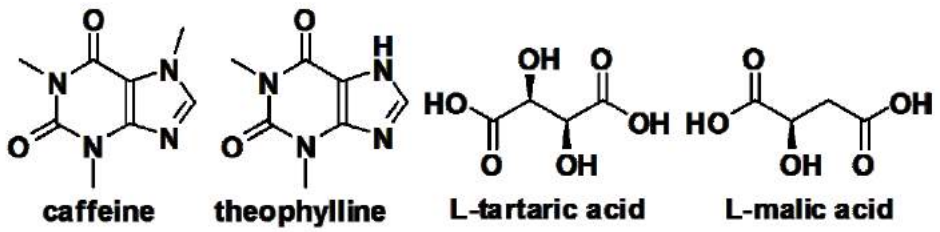

B)

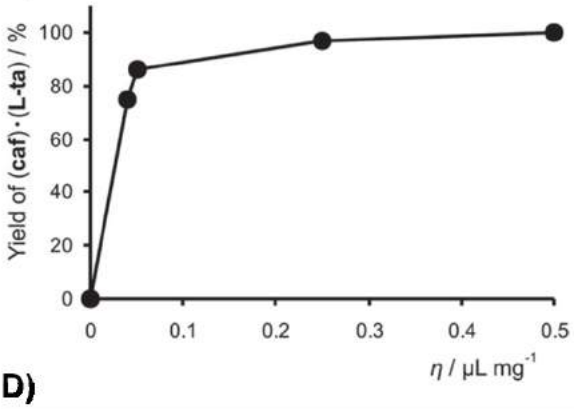

C)

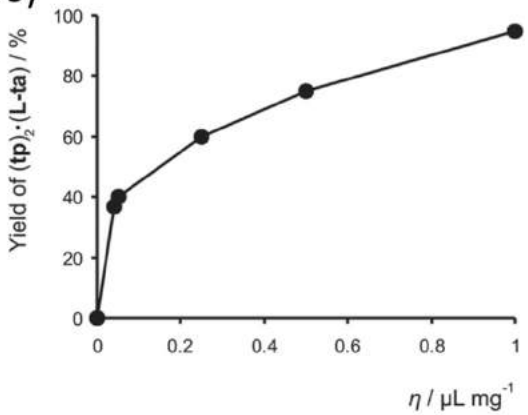

D)

Grinding liquid	Solubility caf	Solubility L-ta	Product
None (neat grinding)	—	—	No reaction
Water	15	400	caf hydrate
MeOH	10	170	Cocrystal
EtOH	6	72	Cocrystal
i-Propanol	3	27	Cocrystal
n-Butanol	3	16	Cocrystal
TFE	450	2	Cocrystal + caf
Benzene	<2	<2	Cocrystal + caf
Fluorobenzene	15	<2	Cocrystal + caf
ACN	21	13	Cocrystal
NMe	45	<2	Cocrystal
CHL	135	<2	Cocrystal
Ethyl acetate	7	9	Cocrystal
di-*i*-Propyl ether	<2	<2	Cocrystal
Ethyl methyl ketone	8	15	Cocrystal
Cyclohexane	<2	<2	No reaction

Fig 1.6. a) Model API and reagents used in the work by Friščić and coworkers. Yield of the mechanochemical cocrystallization of b) caffeine and L-tartaric acid in a 1:1 ratio, and c) theophylline and L-tartaric acid in a 2:1 ratio, as a function of η (µL/mg) parameter; d) table showing the solubility of caffeine (caf) and L-tartaric acid (L-ta) and results of LAG in a 1:1 ratio in various grinding liquids. Adapted from ref. 30a.

The use of ILAG was subsequently extended towards pharmaceutical solids by demonstrating the first mechanochemical synthesis of an API. Notably, ILAG was used in the one-step synthesis of bismuth(III) subsalicylate (BSS), the active component in the popular anti-ulcer drug Pepto-Bismol®. An early attempt of mechanochemical synthesis of BSS was reported by Andrews *et al.*[34] who utilized manual grinding to synthesize a bismuth(III) trisalicylate compound from salicylic acid and triphenylbismuth. This work, however, did not yield the BSS metallodrug, but instead afforded a new material that, upon recrystallization from acetone, gave complex bismuth oxo-clusters decorated with salicylate ions. The first successful synthesis of BSS by mechanochemical route was reported by André and coworkers, who obtained the API directly from bismuth oxide (Bi_2O_3) by ILAG with one equivalent of salicylic acid.[35] Furthermore, by varying the stoichiometric ratio of Bi_2O_3 to salicylic acid (1:2 or 1:4 or 1:6), it was also possible to selectively synthesize bismuth disalicylate monohydrate and bismuth trisalicyate (Fig 1.8a). Importantly, the obtained bulk bismuth disalicylate monohydrate was structurally characterized through the use of high resolution synchrotron PXRD data, revealing a two-dimensional coordination polymer. This is the thus far only known structure of a bismuth salicylate without any auxiliary organic ligands (Fig 1.8b) and is likely the best possible model for the still unknown structure of BSS.

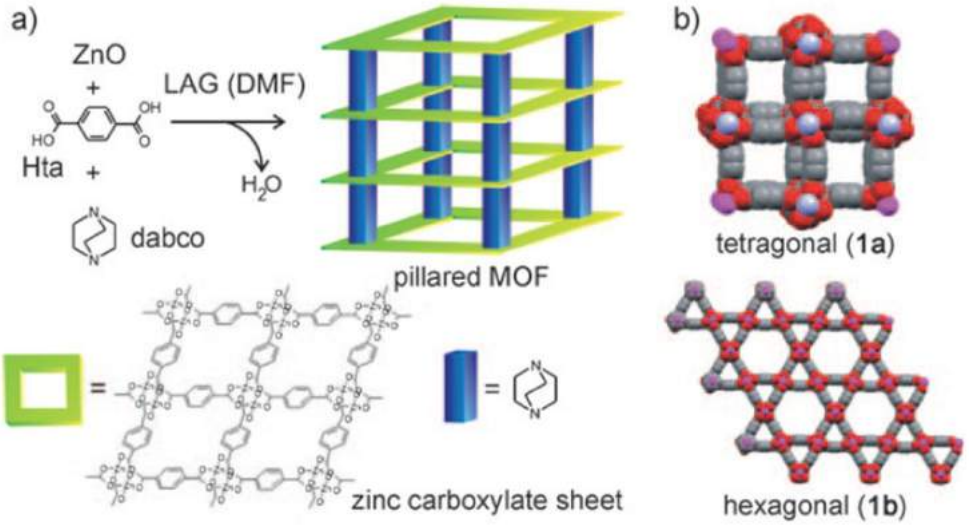

Fig 1.7. (a) ILAG synthesis of a zinc-terephthalate pillared MOF; (b) nitrate and sulfate salts led to formation of a tetragonal and hexagonal topology respectively. Adapted from ref. 33a.

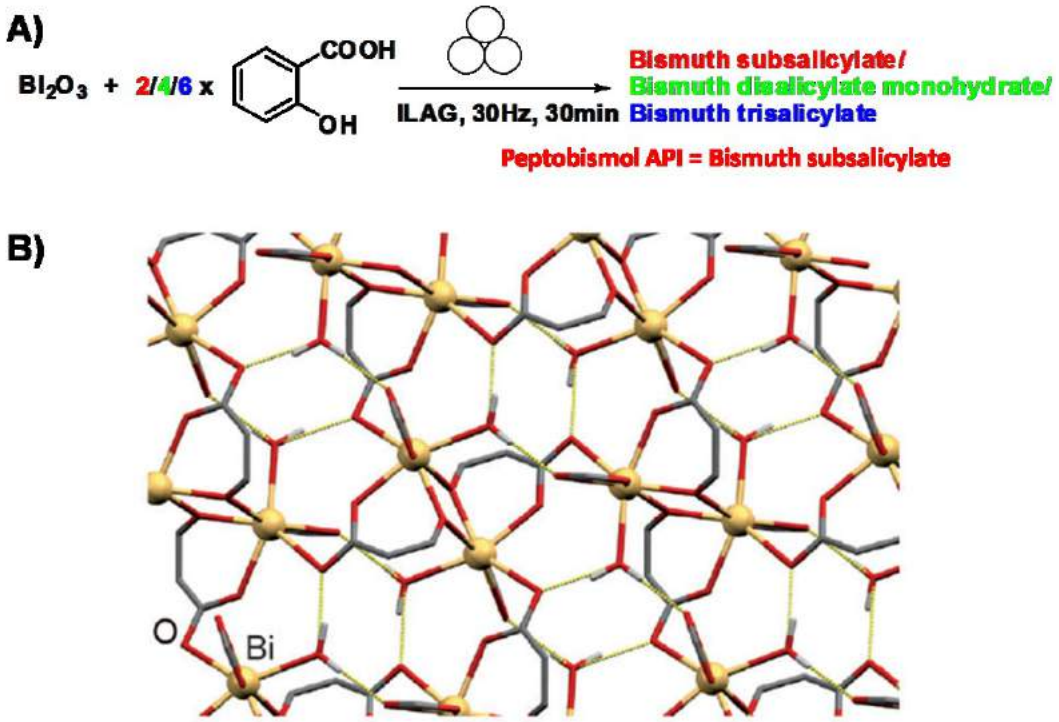

Fig 1.8. a) Scheme of the ILAG synthesis of metallodrug bismuth salicylates, including the API bismuth subsalicylate (BSS). b) fragment of the mechanochemically obtained coordination polymer bismuth disalicylate monohydrate determined from high-resolution PXRD. Adapted from ref. 35.

The ionic (salt) additives in ILAG are used in small, substoichiometic amounts, as catalysts. However, simple salts, such as sodium chloride (NaCl), potassium sulfate (K_2SO_4) *etc* can also be used in larger amounts as inert additives and abrasives that allow the modification of the mechanochemical reaction environment. Such use of salts as abrasive auxiliaries typically utilizes amounts that are comparable, or significantly higher than the amount of reactants. Other milling auxiliaries such as silica (SiO_2) and alumina (Al_2O_3) solids can also be used for the same purpose. However, using simple salts has the advantage of their high solubility in water, which is an important factor in simplifying their removal from organic[36a] or organometallic[37a] mechanochemical reaction systems. In effect, these additives can also act as diluents, effectively reducing the solid-state concentration of reagents. This was exploited by Štrukil *et al.*, who used NaCl as a diluent in the 1:1 reaction system of *p*-phenylenediamine and different isothiocyanates, in order to achieve selective functionalization of only one amino group.[106a] This allowed for the efficient desymmetrization of *p*-phenylenediamine, without resorting to any excess reagents, yielding amino-substituted thioureas.

Another example of using simple salts as abrasives was reported by Do and coworkers in 2015, who described the first generally applicable mechanochemical strategy for ruthenium-catalyzed olefin metathesis (Fig. 1.9a).[36] In this work, the introduction of inert salts such as sodium chloride (NaCl) into the milling vessel (approximately 150% of total reactant weight) was used to significantly improve the reproducibility of the mechanochemical reaction. The salt acted as an abrasive medium that improved the mixing of the reactants and, therefore, enabled reproducible and high yields of reactions. Importantly, screening of various salt abrasives gave similar results, indicating that the improvements in reactivity were not due to any specific cation or anion effects. The use of water-soluble salts also meant they could be easily removed from the system during the product isolation step.

In an analogous report, for an inorganic transformation reaction, García and coworkers recently described the use of lithium chloride (LiCl) as a milling auxiliary for the rapid mechanochemical transformation of a bicyclic phosphazane into a sterically encumbered adamantoid conformer through a rearrangement reaction (Fig. 1.9b).[37] This adamantoid phosphazane was thought to be impossible to synthesize for almost fifty years. The authors initially attempted a number of mechanochemical conditions, eventually discovering that lithium salts such as LiCl, enabled the formation of the target compound in 20% yield. The mechanochemical reaction was subsequently optimized to qualitative formation within 90 min. In particular, the authors established there is a "sweet spot" of LiCl amount used for enhancing the reactivity, whereby the highest reaction yields was always achieved with 20 wt% of lithium chloride. Lower salt loadings resulted in sluggish reactivity, which was explained by a lower concentration of the salt and, therefore poor mixing. Similarly, higher salt loadings also led to reduced yield, which were now explained due to less efficient mechanical impact and dilution of reactants. This work, while illustrating the power of using milling auxiliaries for expanding the scope of mechanochemistry, also demonstrates a major obstacle for the systematic development of mechanochemical techniques, as the choice and the amount of the reaction-enhancing salt additive had to be established by extensive trial-and-error screening.

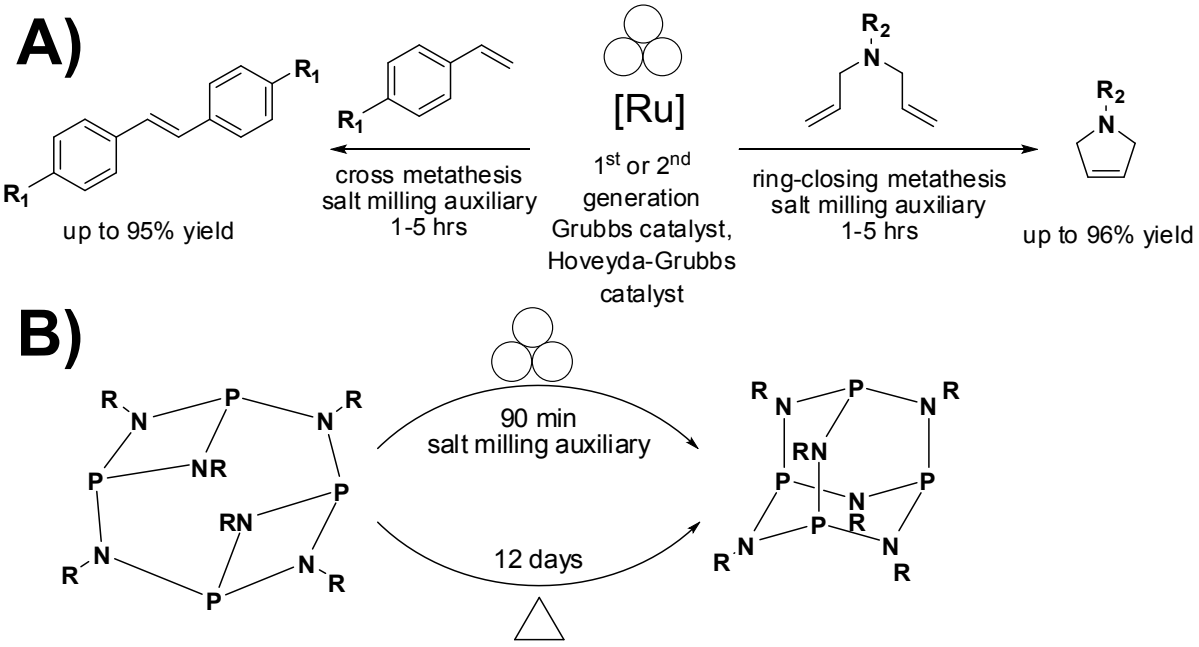

Fig 1.9. Salt milling auxiliaries used as inert abrasive media in mechanochemical a) organic ruthenium catalyzed metathesis reaction and b) inorganic rearrangement of phosphazanes.

A most recent contribution to the toolbox of mechanochemical techniques is the use of polymers as milling auxiliaries, that was reported by the Jones group. While the use of LAG, as discussed earlier, can be beneficial in expediting reaction kinetics and improve mixing in mechanochemical cocrystal formation, in some cases it can afford undesired solvates and inclusion complexes. This prompted the authors to investigate the use of long chain polyethylene glycol (PEG) additives with different molecular weight (200-10000) for the cocrystallization of the model API caffeine with citric acid. This novel treatment was named polymer-assisted-grinding (POLAG).[38a] The authors reported that the use of POLAG permitted control over polymorphic composition of the cocrystal product. It was observed that neat milling of reactants in a 1:1 stoichiometric ratio gave the thermodynamically favoured polymorph Form I, while POLAG with either a liquid (PEG-200) or a solid (PEG-10000) polymer led to the formation of the metastable Form II. However, the presence of the polymer additive did affect the particle size of the cocrystals formed, as determined by scanning electron microscopy (SEM), which was rationalized by active participation of the polymer in cocrystal nucleation and growth. In subsequent work, [38b] the authors performed an extensive systematic study of POLAG cocrystallization of caffeine and glutaric acid. This study revealed that the polymorphic outcome of the product can effectively be controlled by varying the length and polarity of the polymer used during grinding. POLAG was also

recently utilized by Konnert *et al.* for the mechanochemical synthesis of Ethotoin, an anti-convulsant drug.[136c]

Overall, over the last three decades there has been a noticeable evolution and improvement in mechanochemical techniques useful to organic and supramolecular chemists. At the beginning, grinding reactions were performed under solvent-free neat conditions but were later developed to include small amounts of liquids, such as SGD or LAG that can catalyze and improve the rates and selectivity of the solid-state reactions. Subsequently, the LAG technique for ball milling reactions then evolved to include the addition of salts in catalytic amounts (as in ILAG) or in weight equivalent as milling auxiliary, as well as the recently developed inclusion of polymer additives (as in POLAG). These various techniques are part of the toolbox of mechanochemical grinding conditions that can be utilized by synthetic chemists to create new solid compounds and can also enable reactions that were previously inaccessible using solution-based methods. The use and development of these techniques is a corner stone in the recent development of mechanochemistry research. Another growing area of mechanochemistry research is the use of different analytical methods for monitoring mechanochemical reactions.

1.3 Recent advances in mechanochemistry: *ex situ* and *in situ* measurements

While *Section 1.2* has covered the evolution and recent development of the different liquid-assisted mechanochemical techniques, in this section, we will discuss the toolbox of solid-state methods that can be employed to monitor mechanochemical reactions. Different solid-state techniques can be either used individually, or employed in combination, to observe such reactions. When dealing with solid-state chemistry and mechanochemical reactions, PXRD is very often the first choice of analytical tool used for characterization of powder compounds. Although this analytical technique is mostly confined to traditional inorganic materials, solid organic compounds are also amenable to PXRD analysis.[57] PXRD can be a fast qualitative tool for analysis of powdered reaction mixtures, by simply comparing the diffraction patterns (diffractograms) of the reagents and products (similar to monitoring of solution-based reactions using thin layer chromatography) with those simulated from known crystal structures found in databases such as the Cambridge Structural Database (CSD). However, PXRD alone cannot be used to fully understand mechanochemical reactions, as this technique is sensitive mostly to transformations of highly crystalline materials. This creates a serious limitation in evaluating milling reactions of soft materials, typically organic solids, wherein grinding or milling often leads to complete or partial amorphization, which results in

loss of diffraction signal and reduction in overall quality of the data obtained. On the other side, PXRD has an important advantage that it can also be used for structure determination of reaction products or even intermediates without the need to grow diffraction-quality single crystals.[58] With regards to pharmaceutical cocrystallization of APIs with small organic molecules as cocrystal formers (coformers), structure determination from PXRD data has been demonstrated as an invaluable tool.[59a,b] In addition, Byrn and coworkers have also demonstrated that PXRD can be used for quantitative investigation of spontaneous API salt formation *via* acid-base reaction taking place upon gentle mixing and aging of flufenamic acid and magnesium oxide.[59c] With that in mind, PXRD is particularly useful for the structural characterization of compounds that are too sensitive to solvents to be characterized by conventional solvent-dependent techniques. For example, Štrukil and coworkers recently reported the mechanochemical synthesis and isolation of aryl *N*-thiocarbamoylbenzotriazoles, once thought to be unisolatable intermediates in the synthesis of thioureas using bis(benzotriazolyl)methanethione reagent.[60] The mechanochemically prepared aryl N-thiocarbamoylbenzotriazoles are bench-top stable solids that rapidly decompose in solution, hence employment of solid-state characterization techniques such as PXRD was quintessential for their identification and characterization. Structures of these compounds were determined, for the first time, from high resolution synchrotron PXRD data collected on mechanochemically prepared powders (Fig. 1.10).

Another analytical technique, that can directly address the chemical composition rather than crystallinity of the sample is Fourier-transform infrared spectroscopy (FTIR). This technique is especially useful for monitoring organic solid-state chemistry as functional groups with characteristic FTIR stretching bands can easily be identified, such as C=O, C=N, O-H stretching frequencies *etc*. Traditionally, preparation of samples for FTIR studies involves the formation of pellets by manual grinding with potassium bromide (KBr), followed by compression in a dye press. However, it was reported by Braga and coworkers such preparation of pellets for FTIR analysis can actually cause a mechanochemical reaction between the analyte and KBr, for example leading to ionic cocrystals.[61] A more convenient approach of attenuated total reflectance spectroscopy (FTIR-ATR) enables rapid qualitative analysis of samples from mechanochemical reactions as it is much faster, simpler, requires less sample and removes the need for using solid KBr as a support. For example, Tan *et al.* recently reported the mechanochemical coupling reaction between sulfonamides and carbodiimides to furnish pharmarceutically relevant sulfonylguanidines.[121a] This reaction can easily be monitored using FTIR-ATR spectroscopy as the disappearance of the characteristic

C=N stretching band of carbodiimides at 2200-2000 cm^{-1} aided in the determining whether the reaction has achieved full conversion.

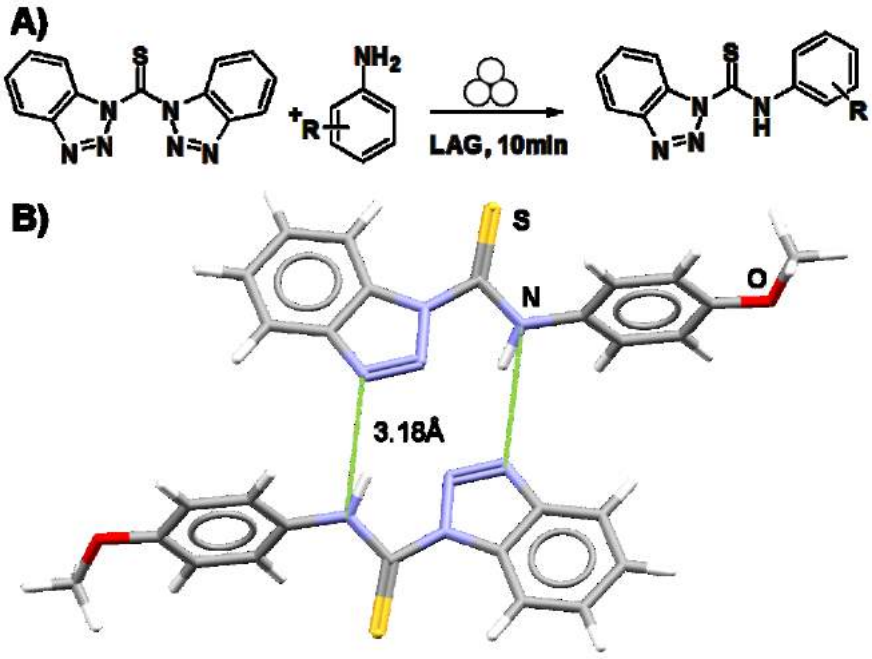

Fig 1.10. a) Mechanochemical LAG reaction for the formation of thiocarbamoyl benzotriazoles. b) Molecular structure of *p*-methoxythiocarbamoyl benzotriazole as determined from PXRD.

Terahertz time-domain-spectroscopy (THz-TDS) is an emerging and versatile spectroscopic technique that can be seen as an alternative to PXRD for the characterization of crystalline solids.[62a] THz-TDS is a vibrational spectroscopic technique that can be used to probe the intermolecular interactions throughout the crystal lattice *via* infrared active vibrational modes in the far-infrared region by using short pulses of non-ionizing and non-destructive terahertz radiation (0.1-4 THz = 3-133 cm^{-1}). This technique is complementary to IR and Raman spectroscopy and can be used for "fingerprinting" crystal structures.[62a] Nguyen *et al.* reported the use of THz-TDS for the monitoring of mechanochemical cocrystallization of phenazine and mesaconic acid in a 1:1 ratio (Fig. 1.11a). They observed from THz-TDS analysis that the cocrystallization followed a first-order reaction kinetics, as well as that the reaction levelled off at 70% conversion after 60 minutes of grinding. In a separate experiment, THz-TDS analysis revealed that grinding of pure cocrystals, separately grown from solution, led to the apparent reduction in cocrystal content to approximately 70%. At the same time, no new reflections were observed in the PXRD pattern of the material. The difference between PXRD and THz-TDS analysis was accounted for by particle

size effect and partial amorphization of the sample. The Zhao group utilized THz-TDS to quantitatively monitor the mechanochemical reaction between L-tartaric acid and sodium carbonate monohydrate to form sodium L-tartrate dehydrate salt. THz-TDS analysis clearly shows distinct characteristic peaks for both reactants as well the product, allowing for quantitative characterization (Fig. 1.11b).

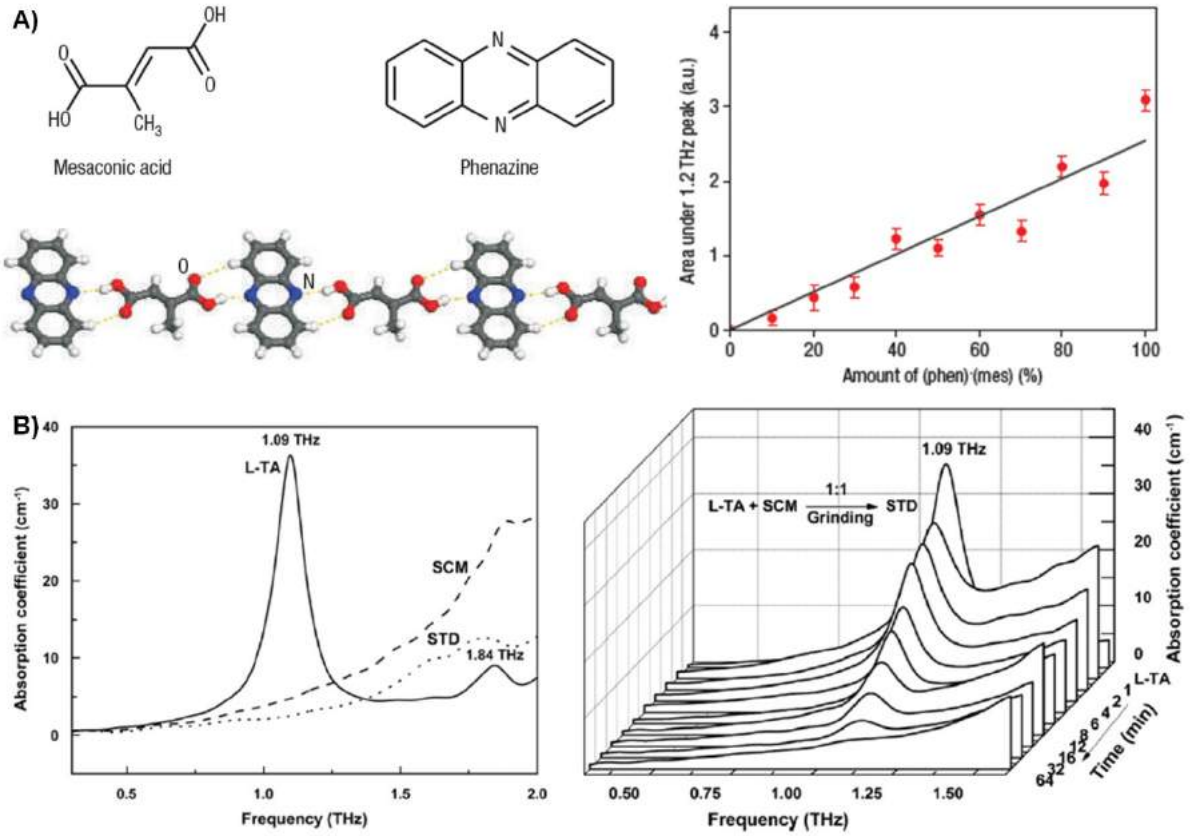

Fig 1.11. a) (*left*) Mechanochemical cocrystallization between mesaconic acid and phenazine (1:1) forming an infinite chain by Nguyen *et al.* (right) Monitoring of the reaction by THz-TDS. Adapted from ref 62b; b) Monitoring of the mechanochemical reaction of L-tartaric acid (L-ta) with sodium carbonate monohydrate (SCM) to form sodium L-tartrate dehydrate (STD). Adapted from ref 62c.

Another popular technique for characterization of mechanochemical reactions and products is solid-state nuclear magnetic resonance spectroscopy (ssNMR). This is a powerful analytical technique, mostly applied in the characterization of crystalline materials as a means to support XRD structural analyses by providing additional information on the number of molecules in the asymmetric unit or symmetry of the occupied positions within the unit cell. This technique is also helpful for amorphous solids where XRD data cannot be obtained. Whereas interactions that affect nuclear spin are averaged out due to random motion of molecules in solution NMR, in ssNMR line broadening resulting from anisotropic shielding,

dipole-dipole coupling and quadrapole coupling (spin, $I > ½$) can be an issue. There are methods to circumvent this problem such as the employment of cross-polarization magic angle spinning (CP-MAS). For example, Balema *et al.* reported the mechanochemical synthesis of various phosphonium[63b] salts and phosphorus ylides for Wittig reactions,[93a] in each case analysing the products by means of CP-MAS ^{31}P-ssNMR spectroscopy. Similarly, Fernandes *et al.*[63a] recently reported an extensive characterization of the LAG between model API theophylline with 4-aminobenzoic acid in a 1:1 ratio using CP-MAS ^{13}C-ssNMR along with XRD data.

It is also important to note that the type of analytical method used for monitoring mechanochemical reactions is also dependent on the time frame in which the data needs to be collected. For example, Raman, FTIR-ATR and THz-TDS spectroscopy measurements can be performed within seconds. On the other hand, PXRD acquisition requires several minutes and a ssNMR experiment might require several hours for good resolution and data. This in turn limits the type of *ex situ* measurement techniques employed for monitoring mechanochemical reactions.

1.3.1 *Ex situ* monitoring

Despite the rapid growth of mechanochemical reactions for synthetic applications, there has been general lack of insight into the kinetics, thermodynamics and mechanism underlying these solid-state reactions. Until recently, analysis of mechanochemical reactions has been limited to stepwise, *ex situ* measurements, performed by intermittently interrupting the grinding or milling process and taking out a portion of the sample for solid-state analysis *via* PXRD, FTIR-ATR or Raman spectroscopy.[57-61] There are a number of examples of using X-ray powder diffraction to analyze the course of a mechanochemical reaction.[28a, 28b, 161, 123f, 158] An example of such analysis has been provided by Štrukil *et al.* who recently studied the mechanochemical synthesis of cadmium coordination polymers with the heteroditopic ligand cyanoguanidine (cnge) by utilizing time-resolved PXRD analysis (Fig. 1.12).[64a] In particular, the heteroditopic nature of cnge enables the formation of two stoichiometrically distinct complexes with $CdCl_2$: the 1:1 compound $Cd(cnge)Cl_2$ with a three-dimensional (3-D) framework structure, and the 1:2 compound $Cd(cnge)_2Cl_2$ with a one-dimensional (1-D) coordination polymer structure. The authors discovered that ball milling of cadmium chloride with cnge in a 1:2 respective stoichiometric ratio, using 7 mm stainless steel balls, only gave

the $Cd(cnge)Cl_2$ coordination polymer, along with trace amounts of the $Cd(cnge)_2Cl_2$ product and unreacted cnge. However, by conducting the same reaction using heavier 10 mm stainless steel balls, the authors were able to obtain the $Cd(cnge)_2Cl_2$ product. The authors then attempted to monitor the mechanochemical formation of $Cd(cnge)_2Cl_2$ coordination polymer using *ex situ* PXRD analysis, conducted at 5 min intervals. They were able to observe that the mechanochemical reaction first formed $Cd(cnge)Cl_2$, which then gradually transformed into $Cd(cnge)_2Cl_2$ as the milling reaction progresses. This shows how topology can be related to mechanochemical kinetic stability, which explains the formation of the 1:1 3-D framework structure rather than the 1:2 1-D coordination polymer.

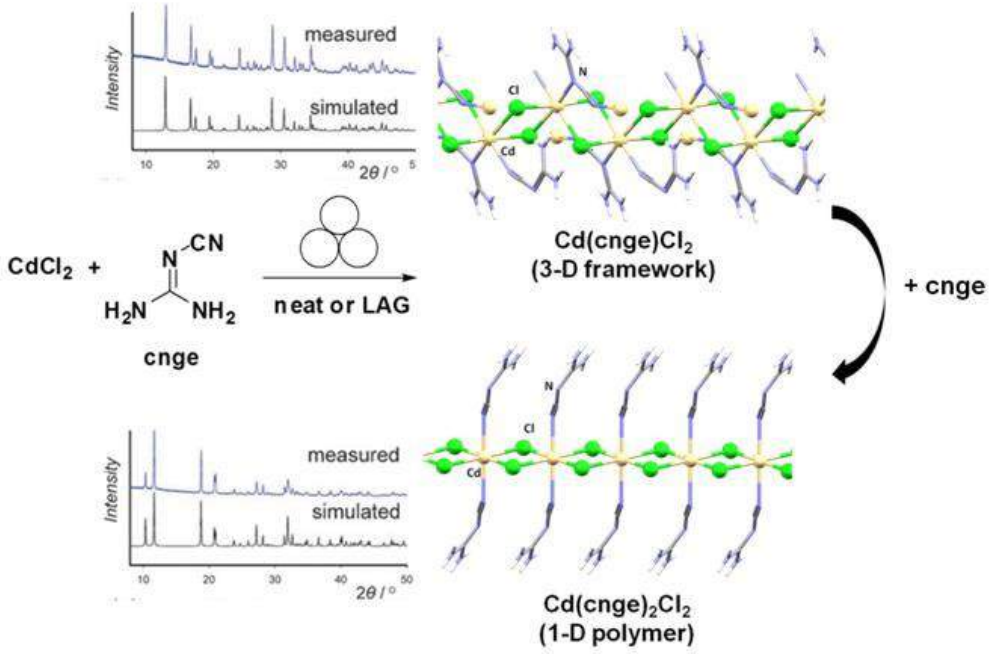

Fig 1.12. Mechanochemical synthesis of cadmium cyanoguanidine coordination polymers. PXRD figures adapted from ref. 64a.

Similarly, *ex situ* measurements can also be performed using FTIR-ATR techniques, which can be particularly helpful for organic compounds with characteristic functional group stretching frequencies. Recently, Stolle *et al.* reported on the hydroamination of alkynes with *o*-substituted anilines in the planetary mill in order to afford benzannulated *N*-heterocyclic benzoxazine (Fig. 1.13).[64b] They employed fast FTIR-ATR technique by *ex situ* monitoring of the changes in the characteristic absorption band of 1) reactant ester carbonyl stretching vibration at 1720 cm^{-1}, 2) product lactone carbonyl vibration at 1762 cm^{-1} and 3) the aromatic bending at 750 cm^{-1}, in order to observe the hydroamination reaction. Full conversion to the

desired product was indicated by the disappearance of the ester vibration peak and increased intensity of adsorption bands associated with lactone group and ring stretching.

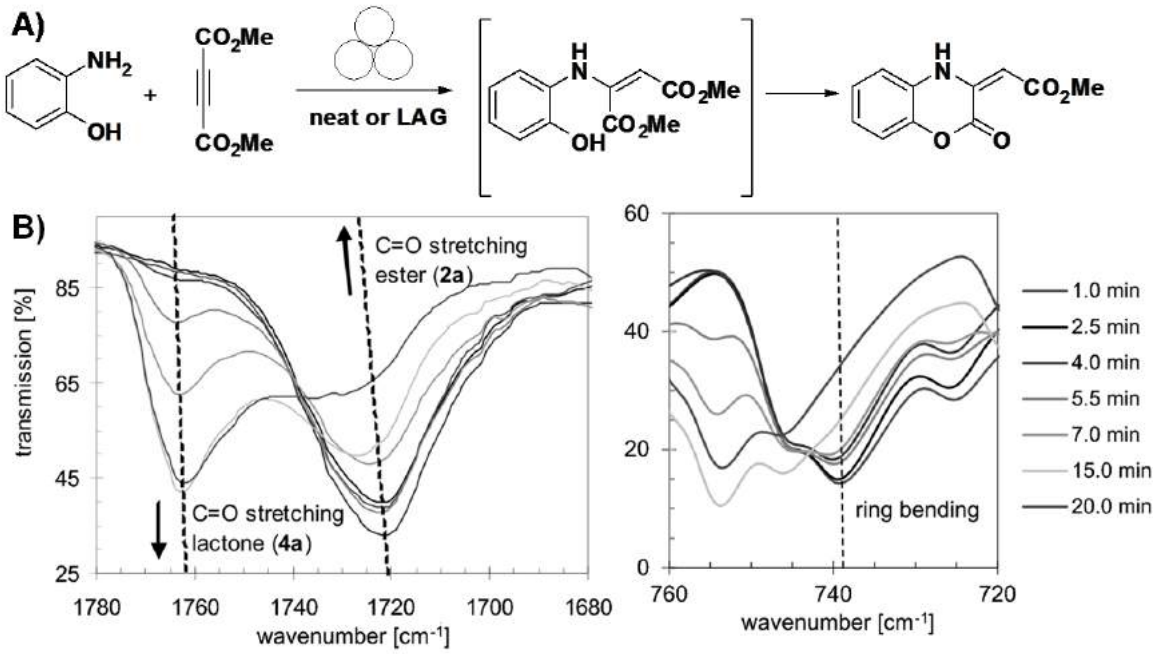

Fig 1.13. a) Mechanochemical hydroamination cyclization reaction. b) Time resolved IR spectrum of the reaction. Adapted from ref. 64b.

Another useful technique for characterization of mechanochemical reactions is Raman spectroscopy. A notable example of using Raman spectroscopy for not only qualitative but quantitative analysis of mechanochemical reaction kinetics was conducted by the James group,[64c] who explored the mechanochemical synthesis of zeolitic imidazole framework ZIF-6 from zinc oxide and imidazole. For this purpose, the ball milling process was periodically interrupted (20-1800 s intervals) and samples were taken out for Raman spectroscopic analysis. Importantly, the authors verified that the reaction did not continue, at least not detectably, when milling was stopped. This allowed for the first quantitative analysis of the kinetics of a mechanochemical assembly of ZIFs. More specifically, the authors observed that the solid-state mechanochemical reaction behaved similar to a second-order solution- or gas-phase reaction. In addition, the rate of the mechanochemical reaction was found to be related to the frequency of milling, which was explained by a higher number of potentially reactive encounters between reactant particles caused by more intense milling. In most mechanochemical ball milling reactions, prolonged milling can lead to a slight increase in the

temperature of the reaction vessel. However, in this system, the authors reported that the reaction rates at different frequencies, especially at higher frequencies, are not affected by the temperature of the reaction. Most importantly, utilizing these data, the authors proposed a pseudo-fluid model for the description of the mechanochemical reaction (Fig. 1.14). In that model, they proposed the reaction mixture can be seen as having fluid-like character due to the mobility of the particles induced by mechanical agitation, with reactivity possibly assisted through a high-energy amorphous phase. The key factor which determines the overall kinetics of the mechanochemical reaction is the rate of contact formation between the reactant particles, which in turn is affected by the milling frequency.

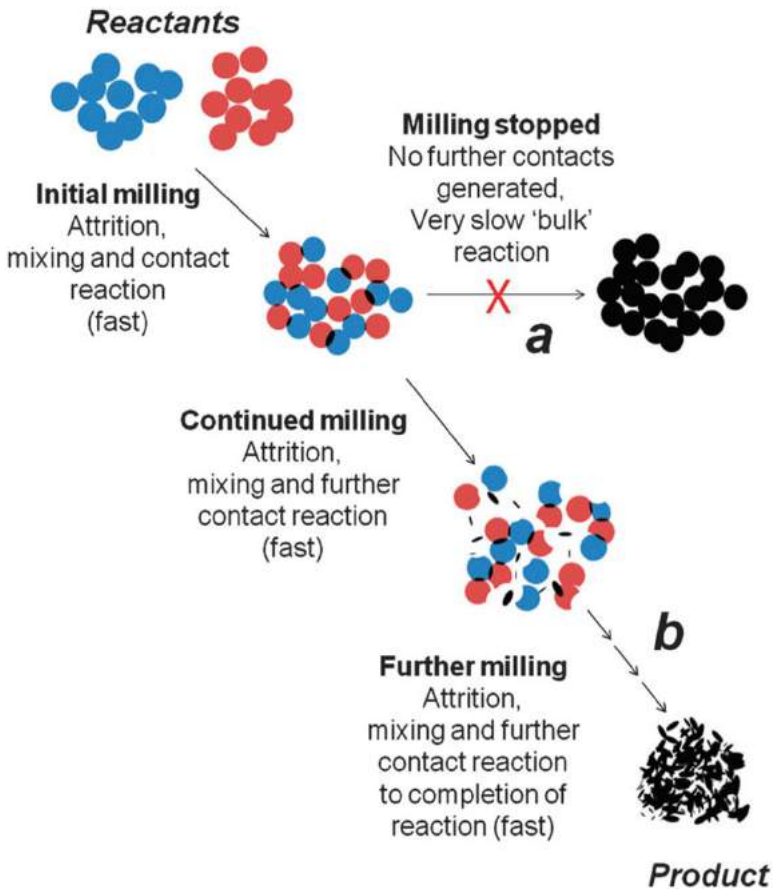

Fig. 1.14. Representation of the pseudo-fluid model proposed by James *et al.* Adapted from ref. 64c.

1.3.2 *In situ* measurements

Whereas *ex situ* monitoring has notable advantages in studying mechanochemical reactions, such as simplicity and ease of implementation in diverse laboratories, it also has significant limitations. First, mechanochemical reactions may still continue to occur even after the milling process has been ended, illustrating the phenomenon of mechanical

activation. This can lead to inconsistencies between the measurements, and lead to misinterpretation of reaction mechanism and kinetics. Second, some mechanochemical reactions may proceed too rapidly for *ex situ* monitoring, as reaction intermediates and high energy phases, such as amorphous solids, can rapidly relax during sample extraction, preparation and even during analysis. Such activated phases are highly reactive and can easily transform upon sample extraction.[21a] Third, *ex situ* measurements are performed by exposure of the closed reaction vessel to the open atmosphere, and hence the state of the reaction can be subject to atmospheric interferences such as moisture, temperature and pressure.[24a]

A way to circumvent these inherent problems has been enabled by a recent breakthrough of conducting *in situ* monitoring of mechanochemical reactions. This technique was pioneered by Friščić *et al.*,[65a] who employed the use of high energy synchrotron X-ray radiation to study the time dependent diffraction of the synthesis of ZIFs from zinc oxide and imidazoles under ball milling conditions. In order to do that, plastic grinding jars made from transparent polymethylmethacrylate (PMMA) were used, because this material is amorphous and has a low of X-ray absorption coefficient.[65a] Steel and aluminium jars were also used when the plastic PMMA jars gradually deteriorated during neat milling, due to deformation of the soft material, and also during LAG reactions, as the liquid additive can react with the PMMA polymer.[65b, 75] In addition, *in situ* monitoring also allowed for the analysis of the kinetics of the reactions. It was discovered that the LAG reaction followed an Avrami-type nucleation and growth mechanism, which was identified by a sigmoidal curve in a time dependent diffraction plot. On the other hand, it was also discovered from quantitative *in situ* measurements that ILAG synthesis of ZIF-8, using ammonium nitrate as the salt catalyst, achieved maximum conversion of zinc oxide in only 4 minutes (Fig1.15). A further development of this *in situ* PXRD measurement technique was the use of microcrystalline silicon as an internal X-ray scattering standard. This provided the first quantitative, real-time evaluation of the course of a ball milling synthesis.[65c] In particular, by using ZIF synthesis as a model reaction, it was observed that time-dependent conversion of zinc oxide starting reagent resembles the 1st order reaction kinetics rate law. The results obtained were consistent with the previously described *ex situ* measurements and the pseudo-fluid mechanochemical reaction model proposed by the James group.[64] Most importantly, by introducing crystalline silicon as an inert internal diffraction standard, quantitative analysis of the amorphous content of the reaction was also obtained. *In situ* data indicated that the amount of amorphous content in the LAG and ILAG reactions was approximately 30% by weight. *Ex situ* measurements, in

comparison, showed only 7% by weight. This provides strong evidence that rapid relaxation of the high energy amorphous phase into a more stable crystalline phase can occur during sample preparation for *ex situ* analysis, further highlighting the importance of being able to monitor mechanochemical transformations *in situ*.

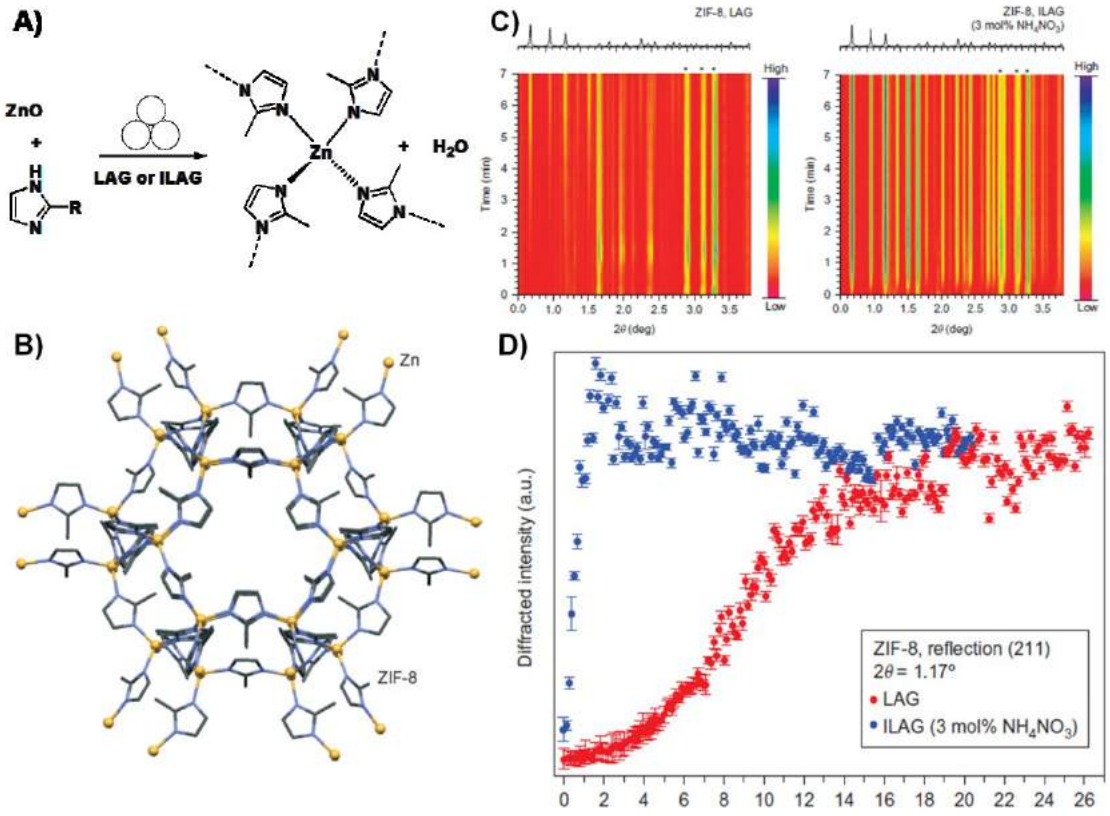

Fig 1.15. a) Mechanochemical synthesis of zeolitic imidazole frameworks, b) fragment of the microporous crystal structure of ZIF-8, c) illustration of time-resolved diffraction plots for the LAG and ILAG synthesis of the ZIF-8 framework, d) plot of the change in diffraction intensity versus milling time for the LAG and ILAG syntheses of ZIF-8, illustrating the sigmoidal behavior indicative of an Avrami-type mechanism. Adapted from ref 65a.

In situ monitoring can also be performed using a benchtop Raman spectrometer, since access to a high power synchrotron radiation source can be limited and costly. The recent report by Užarević and coworkers demonstrated the *in situ* monitoring of the previously described mechanochemical synthesis of the cadmium cyanoguanidine complex by use of a modified Raman probe.[66] Further extrapolation of this technique was reported by the Emmerling group,[67] who combined Raman and synchrotron X-ray diffraction monitoring, for the mechanochemical synthesis of different metal-organic compounds involving zinc, bismuth and cobalt ions. Simultaneous monitoring of mechanochemical reactions using two different analytical techniques is possible as both Raman and XRD techniques are

orthogonally compatible with each other. A combination of two *in situ* techniques allows for a more detailed study and provides a more reliable and complete picture for the mechanistic investigation of mechanochemical reactions.[67]

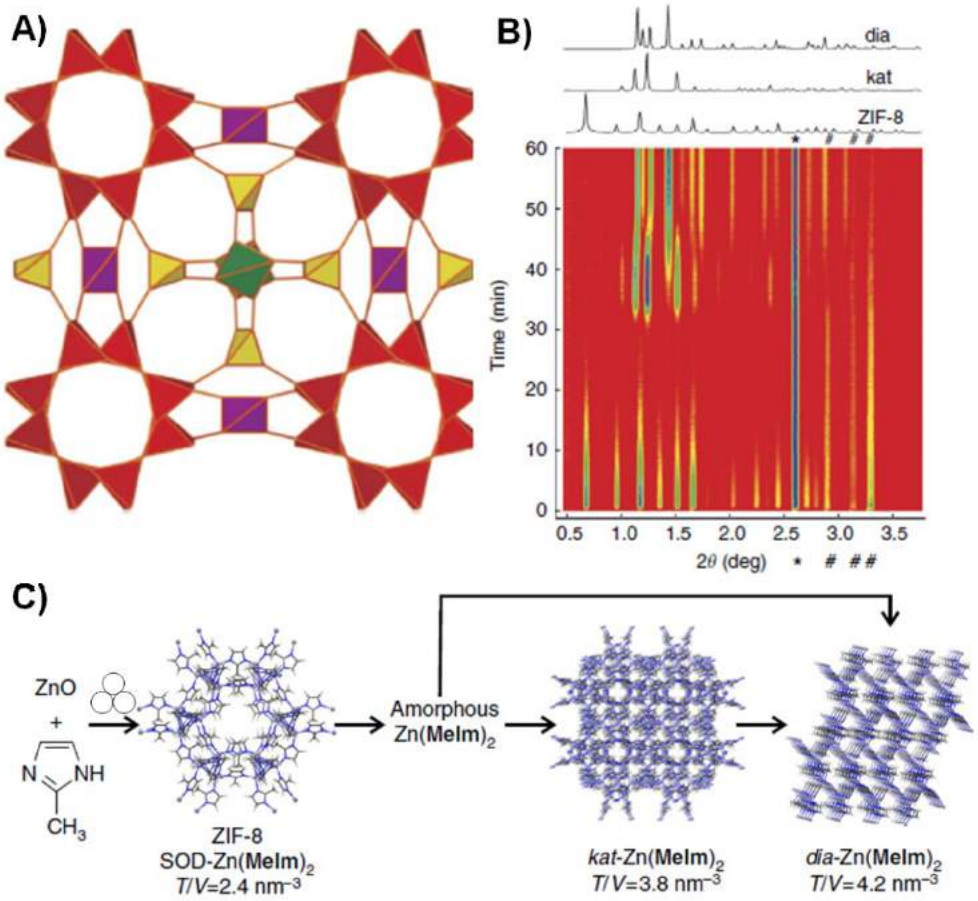

Fig 1.16. a) Structure of the katsenite framework in a colored vertex figure, b) time-resolved diffraction plots for the same reaction, c) Sequential transformation of topologically different structures during milling reaction of ZnO and 2-methylimidazole in the presence of an aqueous milling liquid. Adapted from ref 68.

Another advantage of *in situ* measurements is the possible real time observation of transient unknown phases in mechanochemical reactions. A recent work by Katsenis *et al.* who reported an *in situ* PXRD study of acetic acid induced amorphization of ZIF-8. This study led to the discovery of a previously unknown topology, which the authors named *katsenite*.[68a] Mechanochemical reaction involving zinc oxide with 2-methylimidazole initially formed the open packed ZIF-8 *sodalite* topology. Continued milling then resulted in an amorphous phase, which subsequently crystallized into a topologically novel *katsenite* phase, and finally transforming into a close packed *diamondoid* topology. This step-wise

transformation of phases is consistent with Ostwald's rule of stages, wherein the system in a high energy state relaxes in a stepwise manner, through the formation of several intermediate, metastable phases[68b] (Fig. 1.16). More importantly, the transient *katsenite* phase cannot be produced using solution methods, as it readily rearranges upon exposure to solvents, and can only be achieved by mechanochemical treatment after prolonged milling, further proving the importance of mechanochemistry in obtaining products normally inaccessible by traditional solution techniques.

The *in situ* measurement technique can also be employed for cocrystallization reactions. Real-time *in situ* synchrotron PXRD monitoring was conducted for the cocrystallization of APIs carbamazepine and nicotinamide, with saccharin and suberic acid respectively.[69] *In situ* analysis revealed that milling of carbamazepine and saccharin in a 1:1 stoichiometric ratio quickly formed an amorphous product, which was consistent with earlier cryomilling studies that indicated amorphization by milling,[78d] while LAG of the reactants at ambient temperature rapidly afforded the desired cocrystal. For the nicotinamide-suberic acid system (in a 2:1 substoichiometric ratio), *ex situ* PXRD analysis revealed that the reaction occurred in a stepwise manner, which involved the formation of a 1:1 intermediate complex that preceded the formation of the 2:1 product. However, *in situ* PXRD monitoring revealed a previously unknown metastable phase prior to the formation of the 1:1 intermediate.

Monitoring of solid-state organic and organometallic reactions using *in situ* techniques have also been studied. Recently, the Ćurić group reported the *in situ* Raman monitoring of the mechanochemical formation of a tetracyclopalladated complex from azobenzene, palladium acetate and acetic acid.[70] This complex is formed by multiple sp^2 C-H bond activations of the phenyl rings of the azobenzene by palladium ions (Fig. 1.17). Formation of this complex was only accessible by mechanochemical treatment, through a stepwise formation of a dimeric palladacycle complex. This palladazycle complex was first observed by *in situ* Raman spectroscopy. The same group also investigated the mechanochemical reaction of *p*-nitrobenzoylazide with *p*-phenylenediamine and monitored the changes of the carbonyl C=O vibrational stretching frequencies of the acylazide functional group using *in situ* Raman spectroscopy.[71] The authors postulated that the amine can react with the acylazide functional group *via* two possible pathways, namely 1) nucleophilic substitution on the carbonyl group of the acylazide forming an amide product, or 2) Curtius rearrangement of the acylazide to form an isocyanate intermediate which then reacts with the amine to form a urea product. Time-resolved Raman *in situ* monitoring of the

mechanochemical reaction revealed that the characteristic isocyanate intermediate and urea C=O vibration band did not form. This data along with corroborated nuclear magnetic resonance (NMR) results, supported the nucleophilic substitution pathway instead.

All in all, this section has briefly discussed various *in situ* techniques for monitoring mechanochemical reactions. The examples included a range of metal-organic coordination polymers, organometallic, cocrystal formation and organic transformation reactions. For a more comprehensive discussion, a recent review by Užarević *et al.* is recommended.[72]

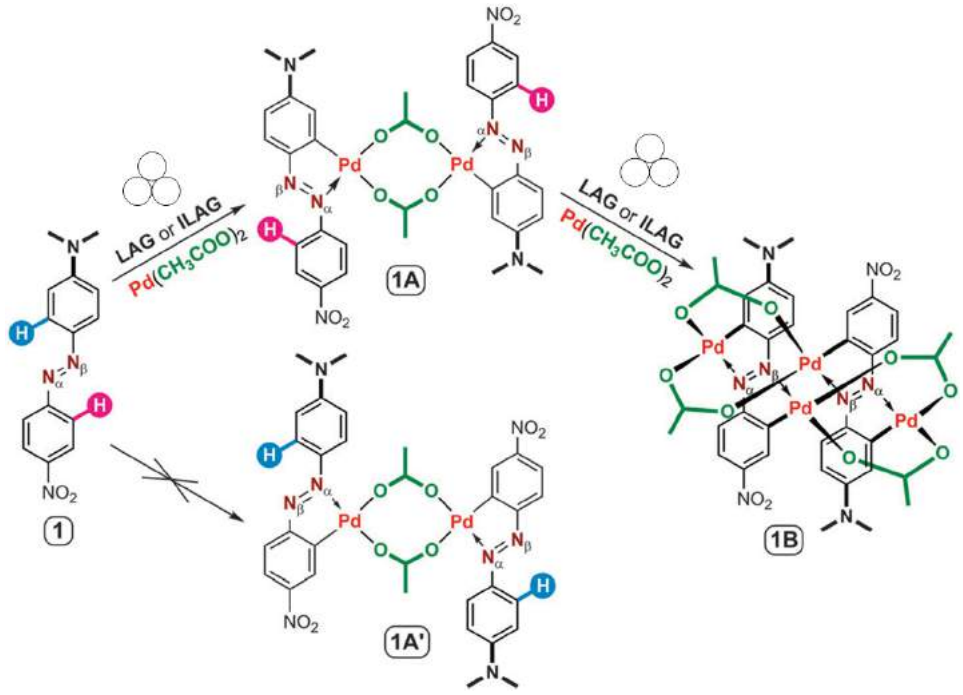

Fig 1.17. Mechanochemical C-H activation of azobenzene. Adapted from ref 70.

1.4 Organic transformation reactions in mechanochemistry: an evolution.

In this section, we will highlight the recent works of the use of mechanochemistry for organic and organometallic transformation reactions. There are several excellent authoritative reviews and books published on the topic of utilizing mechanochemistry for organic covalent bond formation reactions.[13, 73, 74, 75] Similarly, Bowmaker has also argued for the wider use of mechanochemical methods, notably liquid-assisted techniques by synthetic chemists,[32] especially for organic and organometallic transformations. An example of the use of mechanochemistry for functionalization of complex molecules was demonstrated by Aakeröy and coworkers.[31] The authors reported the fucntionalization of cavitands, by an organic

transformation of the peripheral aldehyde groups into oximes *via* a mechanochemical condensation reaction. This was achieved by simple grinding of a tetraaldehyde cavitand precursor with hydroxylammonium hydrochloride, sodium hydroxide pellets and few drops of a liquid additive, specifically dichloromethane and methanol. This reaction serves well to illustrate the simplicity and potential of kneading for functionalization of complex, multi-functional molecules. The reaction was completed in a short amount of time (5 min), afforded excellent yields (up to 95% yield), gave no by-products, and thus a significant reduction of solvent use when compared to solution synthesis, as it avoided tedious purification procedures. A related work on the use of mechanochemistry for the facile synthesis of supramolecular calixarenes was reported by the Atwood group.[42b] In particular, they performed simple kneading of isovaleraldehyde and pyrogallol, in the presence of catalytic amounts of *p*-toluenesulfonic acid to furnish pyrogallol[4]arenes *via* a condensation reaction. The reaction was monitored by thin layer chromatography and NMR techniques, and was found to reach completion within 5 minutes of grinding in a mortar and pestle. This mechanochemical method of synthesizing the desired calix[4]pyrogallolarene was significantly faster than its solvent-based counterparts.[42b] In this case, mechanochemistry not only reduced reaction times, but also eliminated the energy required for heating and the need of finding suitable solvents, and its subsequent waste-related issues. These are all important factors that are in compliance with performing efficient organic synthesis in a green manner. Even more remarkable is that the pyrogallol[4]arene product obtained from grinding, was able to spontaneously self-assemble to form a hexameric nano-capsule, which was held together by an extended network of hydrogen-bonds (Fig. 1.18). This nano-capsule, comprised of six pyrogallol-[4]arene macrocycles, was found to enclose an internal molecular volume of over 1300 $Å^3$.

This following section will briefly discuss proposed reaction models, energy considerations and particle size effects pertinent to mechanochemical transformations of and leading to organic molecules. We will also discuss new frontiers in metal-catalyzed mechanochemical organic reactions as well as the shift of focus of using mechanochemistry in making pharmaceutical cocrystals, solvates and salts to synthesizing API molecules.

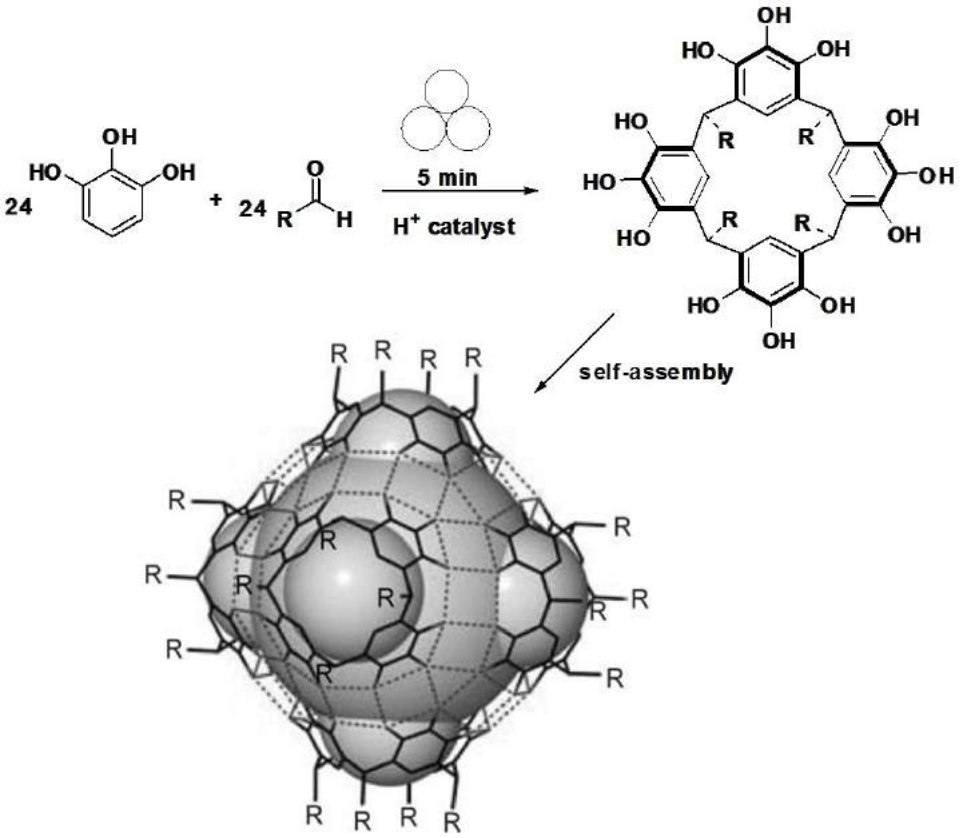

Fig 1.18. Mechanochemical synthesis of pyrogallol-[4]arene, which spontaneously self-assembles to form a hexameric nano-capsule structure. Adapted from ref 42b.

1.4.1 What happens in solid-state mechanochemical reactions: proposed models

According to Kaupp, mechanochemical transformations of organic molecules can be described by a three-stage model,[76] which first involves surface activation of the solid reactants, then combination of the reactant particles, which then enables the reaction to occur on the surface, product formation and nucleation, and lastly removal of the product from the reactant to expose new surfaces (Fig. 1.19). Based on this model, mass transfer proceeds through a mobile medium, be it a gas, a liquid, a solid (amorphous) phase or a combination of all these. Mechanochemical reactivity is sometimes explained through a hot-spot model, whereby ball impact during milling causes brief localized areas of high temperature.[77] The hot-spot model is perhaps more relevant for milling of hard and abrasive inorganic materials than for softer organic compounds. Arguments against general validity of the hot-spot model were suggested recently by studies of thermally reversible Diels-Alder reaction, conducted by the Mack and the Blair groups, who found that mechanochemical reactions may be taking place under conditions analogous to conventional heating at *ca.* 80°C.[78a] A recent report by

the Stolle group also suggests a temperature dependence for the reaction rate of a Knoevanagel condensation conducted in a planetary mill.[78b] Temperature dependence of reaction rates implies that hot-spots do not necessarily play a major role in determining mechanochemical reactivity. This is also corroborated by similar results in a recent study by Užarević and coworkers for the *in situ* temperature monitoring of metal-organic reactions in a vibrational mill.[78c]

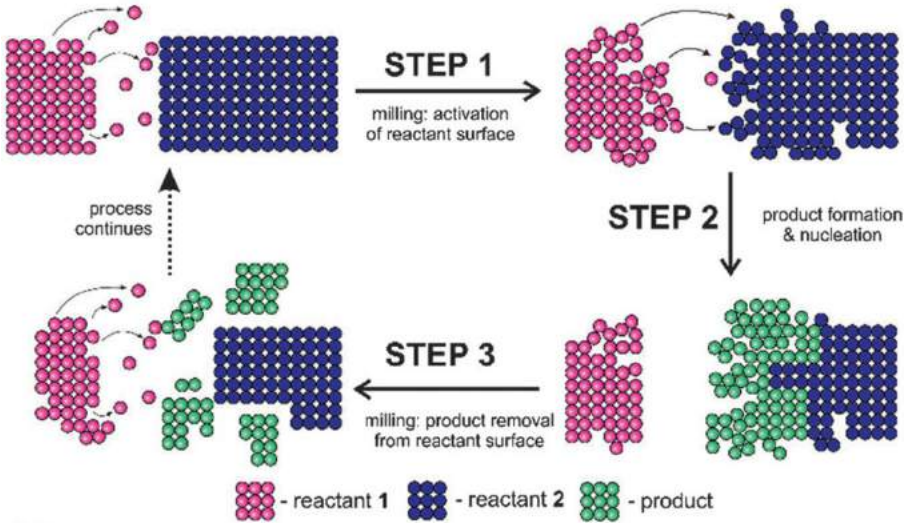

Fig 1.19. The three-step model for mechanochemical reactions. Adapted from ref 76.

Mechanochemical transformations of soft organic solids can also be mediated by an amorphous phase. However, these amorphous intermediate phases can be unstable and rapidly crystallize upon exposure to air or during *ex situ* characterization.[65] However, observation of the amorphous phase can be observed by milling under cryogenic temperatures. This was demonstrated by Rodríguez-Hornedo and coworkers,[78d] who reported that cryomilling of carbamazepine and saccharin in a 1:1 stoichiometric ratio produced an amorphous material, that upon heating or storage, led to recrystallization into the cocrystal. This amorphous intermediate was also observed for room temperature neat milling as evidenced by *in situ* X-ray monitoring experiments.[69]

Another important parameter in enabling mechanochemical reactivity is particle size. In relation to pharmaceutical compounds, the relationship between mechanochemical reactivity and reactant particle size was addressed by Blagden and coworkers.[82] The authors established that for model API cocrystallization reactions involving caffeine with urea and malonic acid with 2-methoxybenzamide, spontaneous cocrystallization was observed if

particle size fell below a certain experimentally determined threshold of 20-45 μm, without formation of amorphous or eutectic states. On the other hand, spontaneous cocrystallization of theophylline and nicotinamide was observed by Ervasti *et al.* upon mixing powdered reactants together,[83] without a firm correlation of reactivity to particle size. This demonstrates the complexity of solid-solid reactions conducted under mechanochemical conditions and suggests that each organic system can be uniquely different from one another and each of them require different considerations.

1.4.2 Energy comparison

Energy efficiency and energy consumption of mechanochemical transformation reactions are another important aspect to consider for industrial scale applications. Recent studies by the Stolle group, performed on Suzuki-Miyaura coupling reaction[79a] as well as potassium permanganate mediated oxidation of *p*-toluidine,[79b] has shown compelling evidence that at least on laboratory scales, energy consumption for organic transformation reactions performed in ball mills are a fraction of that used in other synthetic methodologies such as microwave and conventional heating (Fig. 1.20). This observation can be explained by the fact that the energy imparted from the instrument is directly absorbed by the reactants in solvent-free methods. In comparison, for solution-based reactions, most of the energy is dissipated into the solvent. By removing the presence of solvent from the reaction vessel, mechanochemical reactions can thus be considered more efficient and greener. Furthermore, the high energy efficiency for mechanochemical reactions of organic compounds is not surprising when considering the three-step mechanism proposed by Kaupp.[76] In such a mechanism, mechanochemical reactivity is largely due to surface activation, which has a lower energy requirement (*ca.* 0.05–0.5 kJ/mol) when compared to processes that are based on particle fragmentation and breakdown (*ca.* 5–500 kJ/mol).[81] This lowered energy requirement and energy consumption when performing mechanochemical organic transformation reactions is in agreement with the demands of pharmaceutical industries' call for greener and more efficient approaches to chemical synthesis and processing.[80]

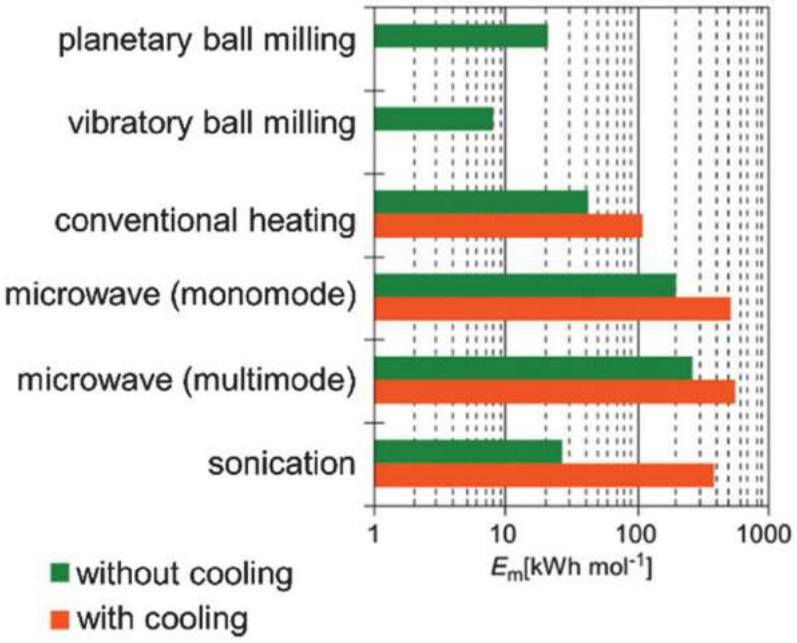

Fig 1.20. Comparison of energy usage for different synthetic methods for the potassium permanganate mediated oxidation of *p*-toluidine. Adapted from ref 79b.

1.4.3 Metal-catalyzed mechanochemical organic transformation reactions

In the context of organic transformation reactions, many C-C bond formation reactions have been performed mechanochemically either by manual grinding or by ball milling. This include classical Michael reactions,[84] in particular organocatalytic asymmetric Michael additions,[85] Aldol reactions,[86] including asymmetric Aldol variant,[87] Morita-Baylis-Hillman,[88] Knoevanagel condensation,[89] Barbier reaction,[90] Pinacol,[91] Grignard reaction,[92] Wittig and Horner-Wadsworth-Emmons reactions,[93] assymetric alkylations,[94] Reformatsky reaction,[95] Biginelli reaction[96] and various cyclization reactions[86b, 97] including Diels-Alder reaction.[78a,98] Template assisted [2+2] photodimerization reactions has also been performed mechanochemically to synthesize stereochemically selective cyclobutane products[101a] as well as synthetically challenging ladderanes.[101b] Vortex milling,[24a] conducted in a transparent test tube with a vortex mixer, was also developed to conduct tandem photochemical and solvent-free mechanochemical milling. In addition, mechanochemical reactions using stable and environmentally friendly oxone has also gained popularity as an oxidant for organic oxidation reactions[99] as well as for the recovery of 2-iodoxybenzoic acid (IBX).[99g] In addition, reduction of carbonyl compounds,[100] including the novel *in situ* salt metathesis formation of $LiBH_4$ as a reductant, was also conducted mechanochemically.[100c] Other classical reactions that were adapted to mechanochemical techniques include condensation type imine

synthesis,[24a, 102] formation of ethers and epixodation,[103] esterification,[104] transesterification[105] and thiourea synthesis.[106]

Organic transformations enabled by transition metal-catalysts[107] are ubiquitous in academic research and industrial chemical manufacturing. In recent years, there has been a sharp increase in developing mechanochemical protocols that would adapt these important reactions to a solvent-free or a solvent-limited environment. As a result, a number of important catalytic transformations are now accessible by milling or manual grinding, including Suzuki-Miyaura[108], Heck-Mizoroki[109], Sonogashira[110] and Glaser[111] coupling reactions. This section provides an overview of the most recent contributions to this young and rapidly evolving area of transition metal catalyzed mechanochemical organic synthesis, while a detailed overview can be found in a recent comprehensive reviews. [13, 73, 74]

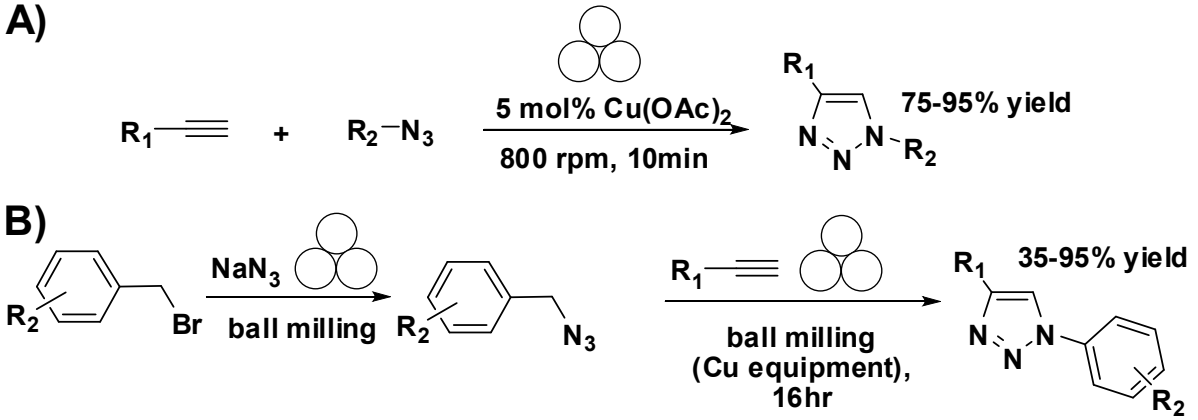

Fig 1.21. Examples of mechanochemically conducted copper-catalyzed azide-alkyne Huisgen "click" reactions achieved by using: (a) external copper(II) acetate as the catalyst and (b) copper milling equipment as the catalyst source.[113b]

The copper-catalyzed azide-alkyne [2+3] cycloaddition reaction, also known as the Huisgen coupling, is the central transformation of click chemistry, an area of synthesis oriented towards rapid assembly of molecular fragments *via* highly thermodynamically-driven reactions.[112] In contrast to its importance in conventional synthesis, the Huisgen coupling has hardly been explored in mechanochemistry. The first solvent-free protocol for this important reaction was reported by the Stolle group (Fig. 1.21a), who utilized copper(II) acetate to enable coupling of terminal azides and alkynes[113a] within 10 min, with yields ranging from 75%-95%. An important development was reported by the Mack group in 2012,[113b] who demonstrated that the reaction can be conducted without an additional copper-based catalyst, simply by using a completely copper-based milling assembly (Fig. 1.21b). This work also demonstrated how the handling of hazardous organic azide reactants can be circumvented by conducting the reaction in a two-step one-pot manner, wherein the first step

was *in situ* formation of the organic azide *via* nucleophilic substitution of benzyl bromide and sodium azide, followed by the click reaction. In a further advance, the recyclability of the catalyst was greatly improved by the Ranu group, who demonstrated the use of a copper-embedded alumina as the catalyst.[113c]

Another important reaction is olefin metathesis. Olefin metathesis is a powerful synthetic tool, effectively permitting the shuffling of functional groups across carbon-carbon double bonds. Whereas the use of well-defined ruthenium-based catalysts for olefin metathesis reactions of neat liquid olefins is known, such transformations have been almost completely unexplored in the solid state.[114] The first mechanochemical protocol[36a] for cross metathesis (CM) and ring closing metathesis (RCM) reactions of solid and liquid olefins using 1st- and 2nd-generation Grubbs and Hoveyda-Grubbs catalysts were reported in 2015 by Do and coworkers (Fig. 1.7), as described in *Section 1.2*. In addition, a recent work by Scott and coworkers reported the mechanochemical immobilization of Zhan and 2nd-generation Hoveyda-Grubbs catalysts in MOFs.[36b] The resulting protocols led to excellent yields of mechanochemical CM and RCM reactions (>95%). Importantly, the RCM of 3,5-dinitrophenyl-methanone-dihydropyrrole was conducted in 92% yield, whereas previous attempts at solvent-free thermal reactivity gave *ca.* 3% yields.[115]

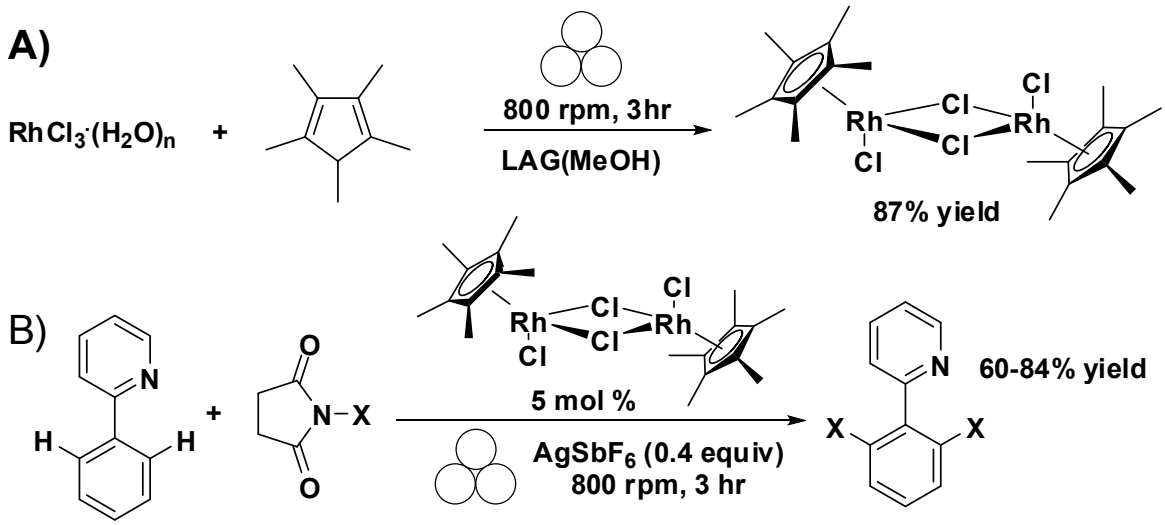

Fig 1.22. (a) Mechanochemical synthesis of $[Cp^*RhCl_2]_2$, the organometallic catalyst used for (b) the mechanochemical C-H activation and halogenation of *o*-phenylpyridine conducted in the planetary mill.[117]

One of the most exciting topics in organic chemistry in recent years is functional group-directed C-H bond activation.[115,116] As mentioned earlier, the first entry of mechanochemistry into this type of transformations was reported by Juribašić and coworkers,

who performed the palladium-mediated regioselective activation of sp^2 C-H bonds in azobenzenes by ball milling.[70] Recently, Hernandez and Bolm reported a C-H bond activation and dihalogenation of an *o*-phenylpyridine derivative in a planetary mill using a Cp*Rh (Cp*=pentamethylcyclopentadienide) catalyst (Fig. 1.22b).[117] Mechanistically, it is rationalized that the rhodium catalyst binds initially onto the nitrogen atom of the pyridine group and is therefore brought into close proximity of the *o*-phenyl C-H moiety for activation and insertion. Remarkably, the organometallic bis-rhodium catalyst $[Cp^*RhCl_2]_2$ used in this work was first synthesized mechanochemically from the less expensive and more readily accessible $RhCl_3$ and HCp* (Fig. 1.22a).[118]

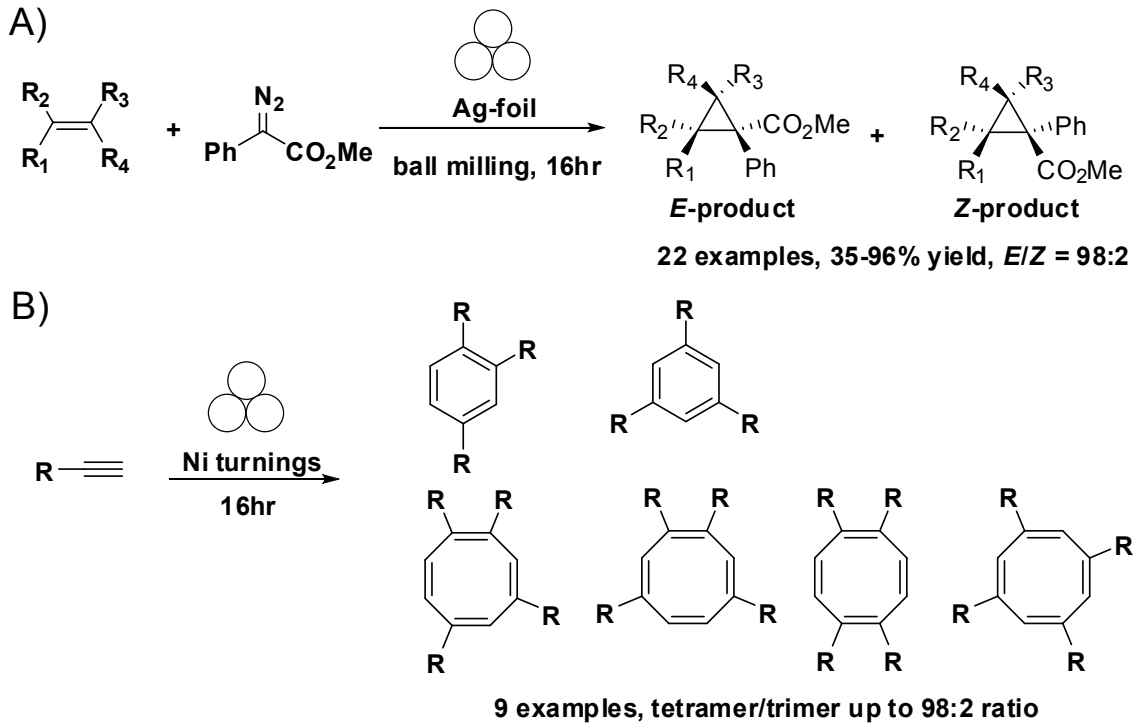

Fig 1.23.Mechanochemical ball milling a) cyclopropanation of alkenes with diazoacetates using a silver metal foil as a source of silver catalyst,[119a] b) recyclable Ni catalyst for synthesizing cyclooctatetraene compounds.[119b]

Ball milling also provides an attractive opportunity for the design of metal-catalyzed reactions, by using elementary metals as a source of catalytic metal species formed by impact and collision of milling media. As mentioned earlier, the Mack group demonstrated the possibility to avoid external copper salts as catalysts and cocatalysts in Huisgen and Sonogashira reactions, respectively, by using milling equipment made entirely out of copper. However, a potential limitation to this design of reactivity is the unavailability of milling equipment made from materials other than brass, copper, steel, tungsten carbide (WC),

zirconia (ZrO_2) or alumina, hindering the exploration of catalytically highly attractive but also costly metals, such as silver, gold, platinum, palladium or ruthenium. An elegant and, very likely, general solution to this problem was recently delineated by the Mack group who utilized a silver foil, inserted into the milling assembly, as a source of catalyst for the first reported mechanochemical stereoselective formation iof cyclopropanes by silver-catalyzed reaction of alkenes with diazoacetates (Fig. 1.23a).[119a] The use of a foil allowed for the recyclability of the catalyst and easy removal from the solid reaction mixture, suggesting a surprisingly simple means to utilize rare earth and transition metals as catalysts. The Mack group later extended this methodology for the nickel-catalyzed mechanochemical synthesis of cyclooctatetraene from terminal alkynes (Fig. 1.23b).[119b] Simple use of a neodymium magnet to easily remove the nickel turnings from the reaction mixture allowed for recyclability of the catalyst for subsequent mechanochemical reactions.

1.4.4 New frontiers in organic synthesis enabled by mechanochemistry.

An often encountered criticism of organic mechanochemistry is that its use is limited to developing solvent-free protocols for otherwise well known transformations. It is, however, becoming increasingly clear that mechanochemistry can be utilized to discover new reactions or reach molecular structures that have previously not been achievable or have been considered too unstable to isolate from solution. This section is dedicated to highlighting several instances in which mechanochemical reactions have been utilized for the synthesis of complex molecular targets, or in which the exploration of mechanochemical reactions led to unexpected discovery and progress in organic synthesis. Examples of such reactions, that are likely to become more abundant with the increased interest of synthetic organic chemists in ball milling, reveal mechanochemistry is not only a means of "greening" existing chemical transformation, but is also a powerful standalone approach to reaction discovery.

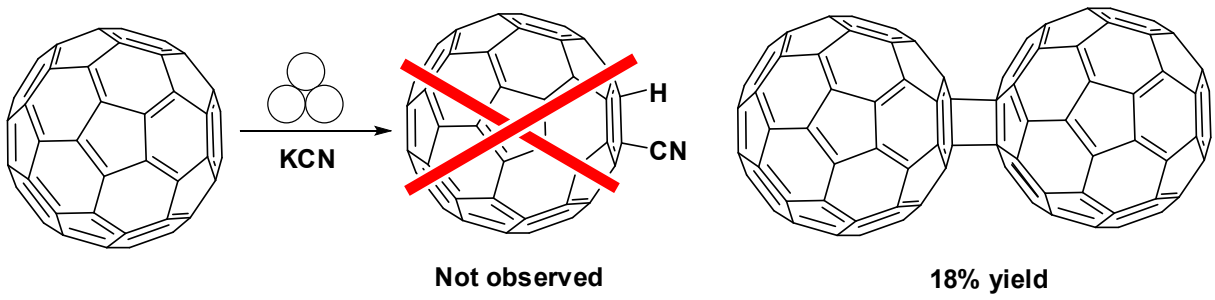

Fig.1.24. The mechanochemically-enabled synthesis of dumbbell C_{120} molecule from C_{60} using KCN, discovered by Wang *et al.*[120]

A pioneering example of a new transformation, discovered and enabled by mechanochemistry is the [2+2] coupling reaction of fullerenes, serendipitously discovered in 1997 by Wang and coworkers upon isolation of the dumb-bell-shaped fullerene dimer C_{120} (Fig. 1.24).[120] The work was initially directed towards hydrocyanation of the fullerene C_{60} using potassium cyanide. However, after ball milling the unexpected dimer C_{120} was obtain in low yields (18% yield), with 70% recovery of the C_{60} starting material. Careful isolation of the compound using flash chromatography provided the dark brown product whose structure was subsequently elucidated using single crystal X-ray diffraction. The formation of C_{120} was explained through a proposed stepwise mechanism in which the solid-state reactivity of the cyanide ion was as crucial, functioning first as a nucleophilic activator of C_{60} and then acting as a good leaving group.

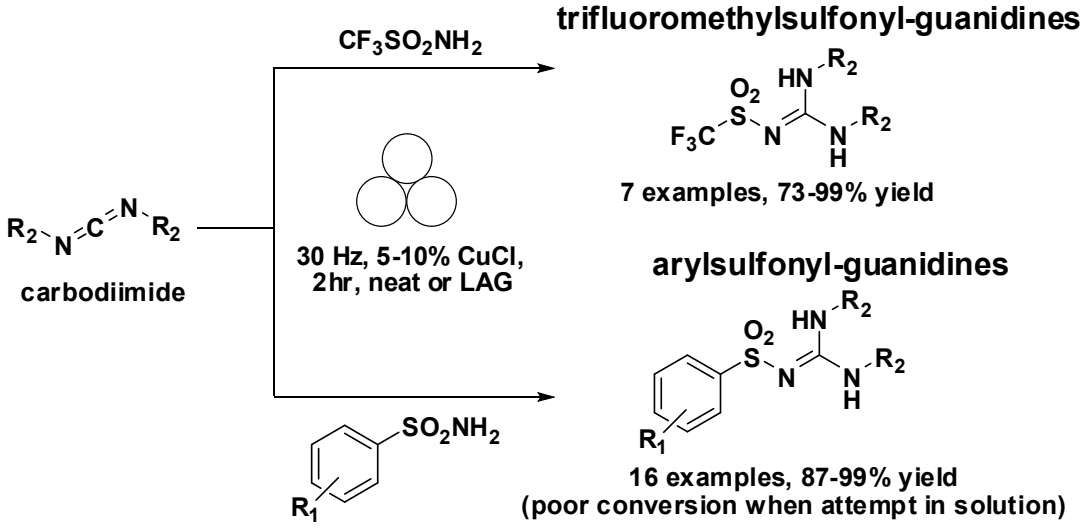

Fig. 1.25. Mechanochemically-enabled synthesis of sulfonyl-guanidines by copper-catalyzed coupling of carbodiimides and aryl sulfonamides, reported by Tan *et al*.[121a]

A more recent example of using mechanochemistry to enable a reaction strategy not readily accessible in solution was provided in 2014 by Tan *et al.* who reported the first coupling of aryl sulfonamides with carbodiimides, by using a copper catayst (CuCl) under mechanochemical conditions (Fig. 1.25).[121a] Milling of differently substituted arylsulfonamides with a handful of commercially available carbodiimides led to rapid (2-4 hours) and efficient (largely >95% yield) formation of sulfonylguanidines, molecular fragments of relevance in pharmaceuticals and herbicides. This scalable procedure was readily adaptable for at least 15 different targets, requiring only minor optimization of the

LAG strategy. In contrast, attempts to conduct some of the highest yielding examples of this novel transformation in solution led to either no reaction or conversions below 15% over two days (*see Chapter 3 for more details)*. Consequently, this work illustrates how chemical transformations that are not readily accessible in solution can be discovered and developed using mechanochemistry.

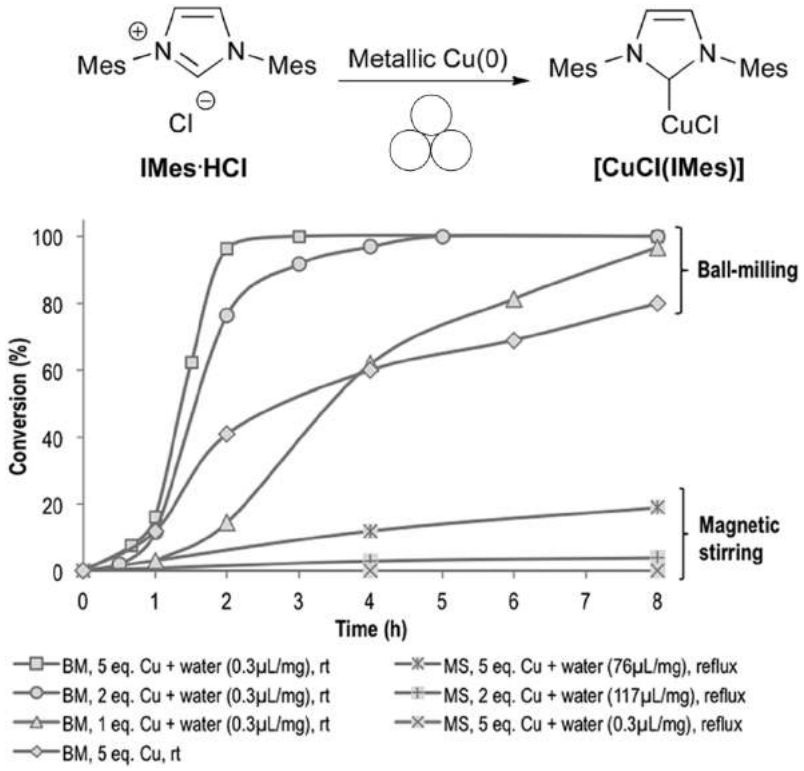

Fig. 1.26. Comparison of conversion for the mechanochemical synthesis of Cu(NHC) complex with solution synthesis. Adapted from ref. 121b.

Another good example of mechanochemistry that can enable reactivity of reagents that exist in different physical states was recently demonstrated by Métro *et al.*[121b] In this report, the use of ball mills to promote multi-step reactions involving solid reactants with gaseous reagents, specifically molecular oxygen, at ambient temperature was demonstrated. The authors performed the mechanochemical synthesis of copper *N*-heterocyclic carbene (NHC) complexes by grinding metallic copper, imidazolium chloride (a NHC precursor) and water (as the LAG liquid) in a planetary mill filled with molecular oxygen as the oxidant. This work revealed a uniquely novel technique of grinding of solids, liquid and gaseous reactants to synthesize an organometallic complex (Fig. 1.26). Under refluxing conditions (in

water) continuously for 8 hr, the reaction only achieved 19% conversion. On the other hand, conducting the same reaction under ball milling conditions, the authors were able to achieve >95% conversion after 3 hours, using only 1.0 equivalent of Cu(0). Again, this demonstrates how mechanochemistry can be used to enable reactivity between reagents that are not achievable by traditional solution methods.

1.4.5 Evolution of mechanochemistry

A recently discussed concept in mechanochemistry of organic compounds is "medicinal mechanochemistry",[122] which embodies the paradigm of a solvent-free research laboratory in the context of making and modifying active pharmaceutical ingredients. The goal of medicinal mechanochemistry is to replace solution-based procedures for making pharmaceutically relevant compounds with mechanochemical, solvent-free ones. The development of medicinal mechanochemistry can be traced from early uses of mechanochemical ball milling to screen for and synthesize new solid forms of pharmaceuticals, specifically polymorphs, cocrystals, salts and salt cocrystals, leading to a now emerging area in which mechanochemical techniques are used for the covalent synthesis and derivatization of drugs. The concept of medicinal mechanochemistry has been a strong inspiration for the title of this Thesis. The term "medicine balls" is a double entendre: it can be used to describe an exercise equipment, but also encompass the concept of applying mechanochemical ball milling for making APIs and new forms of pharmaceutical solids.

1.4.5.1 Mechanochemistry and API polymorphs, cocrystals and salts.

The use of mechanochemistry in the synthesis and discovery of new solid forms of APIs is well established.[122,123] The list of APIs whose polymorphs, solvates, cocrystal and salt forms have been prepared using LAG is already extensive and continuously growing (Fig. 1.27). Although several examples illustrating the use of mechanochemistry for making pharmaceutical solids have already been discussed, other notable works deserves a more in depth discussion. Specifically, the ability to conduct cocrystal and polymorphic screening was largely enabled by mechanochemistry and not by other means of energy input. In addition, the screening of cocrystals of APIs using mechanochemistry has also enabled the investigation of molecular recognition of biomolecules in the solid-state.

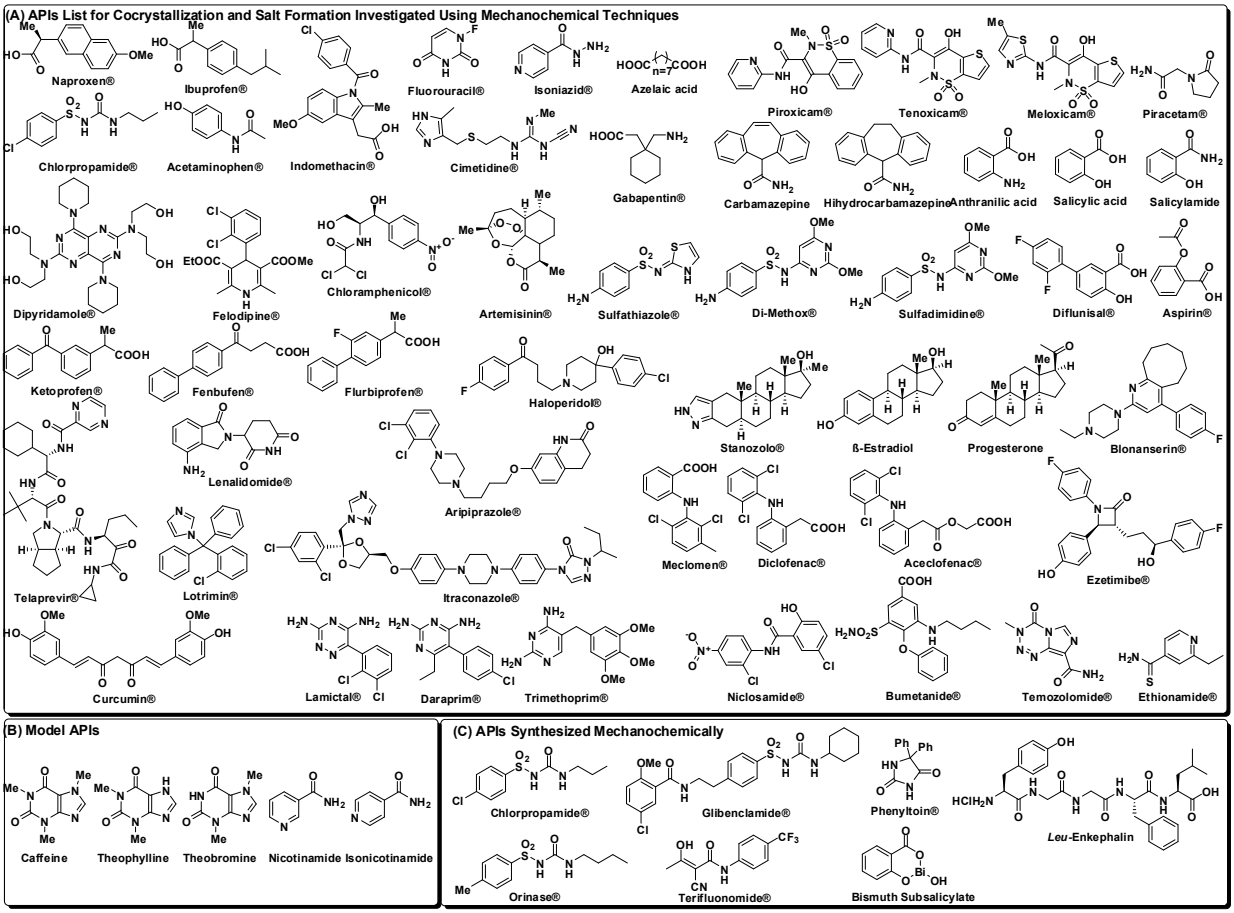

Fig. 1.27. Non-exhaustive list of: (A) APIs and (B) model APIs utilised in mechanochemical solid form screening and (C) mechanochemically synthesized APIs.

The ability to control polymorphism of API solids is critical to pharmaceutical industries. Thermal and mechanical treatment of pharmaceutical solids can lead to different polymorphic outcomes. Recently, the Boldyreva group[124] described an unusual effect of neat milling of chlorpropamide, an early 1st generation anti-diabetic drug. It was reported that milling of the α-polymorph of chlorpropamide at room temperature was found to lead to formation of minor amounts of the other known ε-polymorph, while no particular change was observed upon milling of pure ε-polymorph. Upon cryomilling at 77 K, the α-form underwent complete amorphisation, but the ε-polymorph reverted to the α-polymorph. The authors proposed that interconversion was due to the formation of a low temperature ε'-form, which has structural similarity to the α-polymorph. Cooling to 77 K induced a temperature dependent transformation of the ε-polymorph to the ε'-form, and then milling induced the transformation to the α-polymorph (Fig. 1.28). This process, is analogous to the Hedvall effect[125] in which there is a clear difference between thermal and mechanical treatment:

milling induces ε' → α transformation while heating or warming leads to ε' → ε transformation.

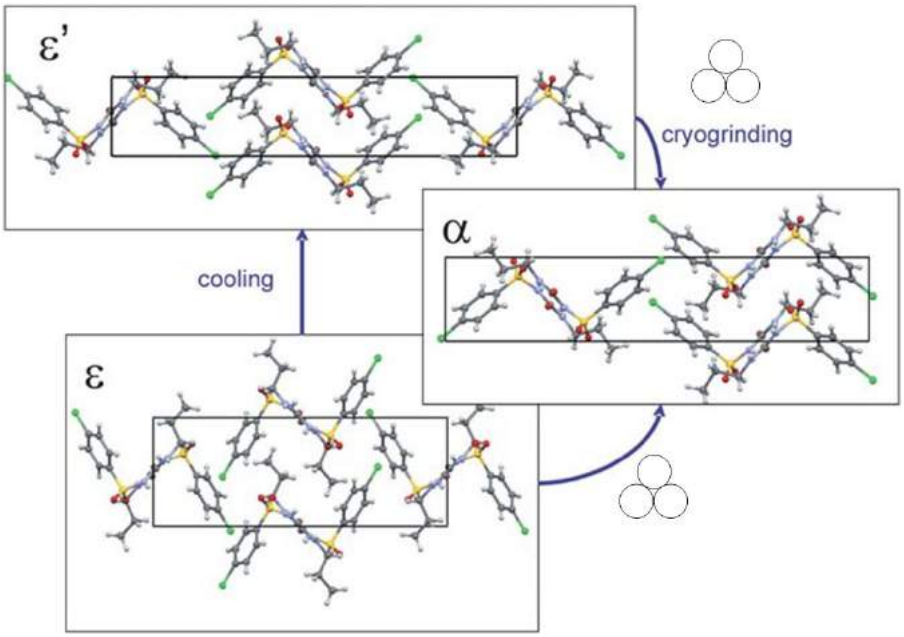

Fig. 1.28. Crystal packing of the α, ε' and ε-forms of chlorpropamide. Adapted from ref. 124.

Another technique commonly used for polymorphic control of APIs is seeding. This technique has been transferred from solution to mechanochemistry for the synthesis of organic Schiff bases, as demonstrated by the Cinčić group.[102] With regards to API polymorphic control, Bučar and coworkers has spearheaded an international team investigating the formation of the cocrystals of model API caffeine and benzoic acid.[126] In that study, attempts over decades of experimentation to obtain a cocrystal of caffeine and benzoic acid were unsuccessful using neat grinding, LAG and other types of solvent-mediated phase transformations,[127] despite computational calculations suggesting its stability. However, exposure of the reaction mixture to cocrystal seeds of the easily obtained caffeine-pentafluorobenzoic acid led to rapid formation of the elusive caffeine-benzoic acid cocrystal.

Mechanochemistry can also be used to improve the efficiency of screening of API salts. In particular, LAG of magnesium oxide with salicyclic acid, naproxen or with enantiomerically pure R-Ibuprofen or as a racemic mixture, led to the formation of their respective magnesium coordination polymer and salts.[129] The use of magnesium oxide is two-fold, as not only is magnesium as an excipient considered non-toxic in contrast to most metals, it can also be used under LAG conditions to generate new solid forms of APIs. Similarly, Galcera and coworkers demonstrated the use of ball milling for the systematic

synthesis of an impressive library of 34 isostructural salt solvates based on the anti-convulsant API drug lamotrigine.[130] LAG of lamotrigine with twelve different dicarboxylic acids with dimethylsulfoxide (DMSO), acetone, tetrahydrofuran (THF) and acrolein, gave a family of isostructural three-component inclusion complexes, based on a robust hydrogen-bonded lamotriginium carboxylate host network structure (Fig. 1.29). For such large quantity screening experiments, Bysouth and coworkers had separately developed a high throughput mechanochemical cocrystal screening device, based on a modified planetary mill, in which 48 grinding experiments can be performed simultaneously.[131]

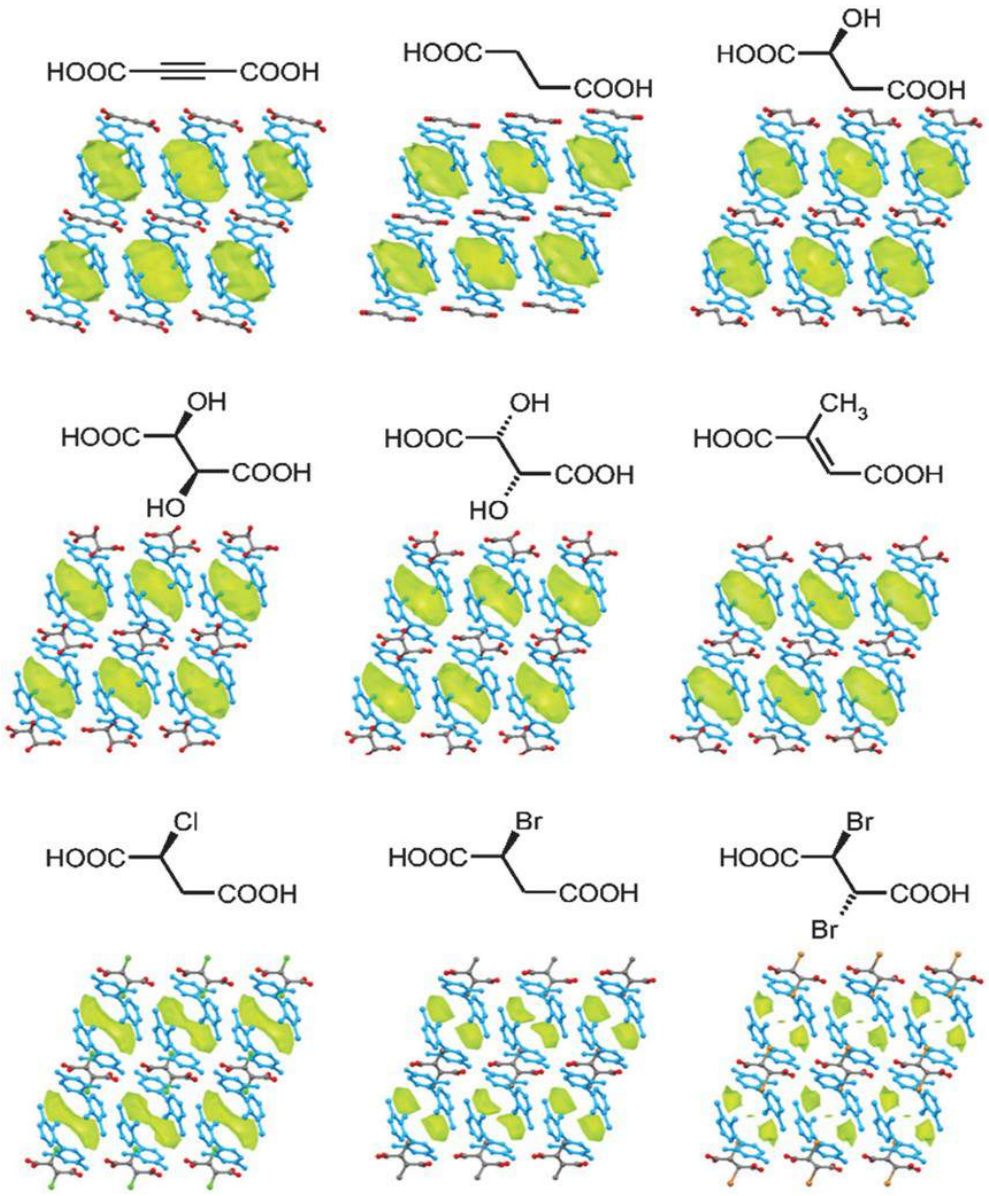

Fig. 1.29. Crystal structures of robust network structure for the three-component isostructural solvate salts of lamotrigine with dicarboxylic acid salt coformer shown for each structure. The guest-containing cavity is outlined in green. Adapted from ref. 130.

Similarly, mechanochemical cocrystallization can lead to the discovery and understanding of molecular recognition of biomolecules in the solid-state. For example, Friščić and coworkers[132] performed the mechanochemical cocrystal screening of four female sex hormone steroids, namely progesterone, pregnenolone, estrone and β-estradiol, with various extended aromatic compounds. This led to the discovery of a previously unknown steroid recognition interaction, which the authors designated as the α···π interaction (Fig. 1.30). Without classical hydrogen-bond acceptors and donors, cocrystals of progesterone with extended aromatic compounds forms layered complex formation held by the α···π interaction. For β-estradiol cocrystals, mechanochemical screening revealed a possible templating effect of the cocrystal former to allow for the assembly of the steroid molecules to form square-grid hydrogen-bonded host framework structures.

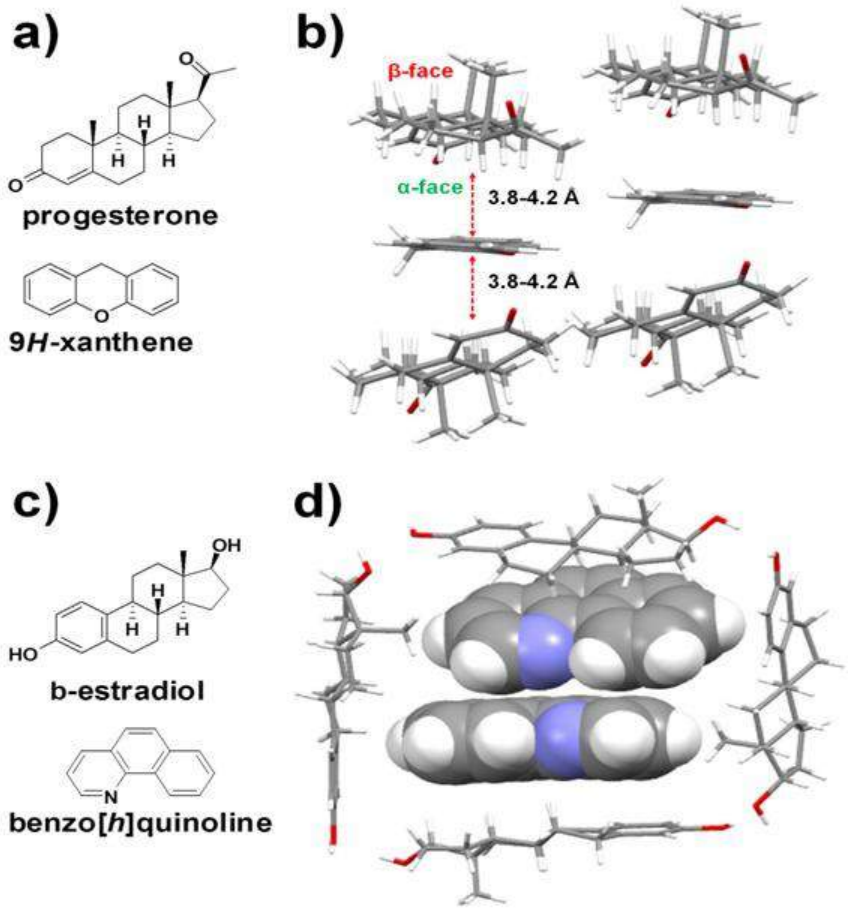

Fig. 1.30. a) Molecular structure of progesterone and 9*H*-xanthene; b) Fragment of the crystal structure of the cocrystal of progesterone with 9*H*-xanthene, showing the α···π interaction; c) Molecular structure of β-estradiol and benzo[*h*]quinoline; d) Fragment of the crystal structure of the cocrystal of β-estradiol and benzo[*h*]quinoline, forming a square-grid framework topology. Unpublished results.

1.4.5.2 Mechanochemistry and API molecule synthesis.

The actual covalent bond formation of pharmaceutically active ingredient (API) using mechanochemical techniques is now emerging and being recognized as a clean and greener alternative to solution synthesis. A major contribution to this area was the development of a mechanochemical protocol, reported by the Lamaty group,[133] to conduct peptide coupling reactions using benzyl-protected amino acids in the presence of a mild base $NaHCO_3$, enabling the mechanochemical syntheses of dipeptides, tripeptides, tetrapeptides and pentapeptides. The power of this synthetic procedure was demonstrated by incorporation into a seven-step, completely solvent-free procedure for making the covalent backbone of Leu-enkephalin (Fig. 1.31).[134] This *tour de force* example of solvent-free synthesis, based on consecutive mechanochemical coupling and thermochemical deprotection steps clearly demonstrates the ability to synthesize complex targets using solvent-free reaction steps only.

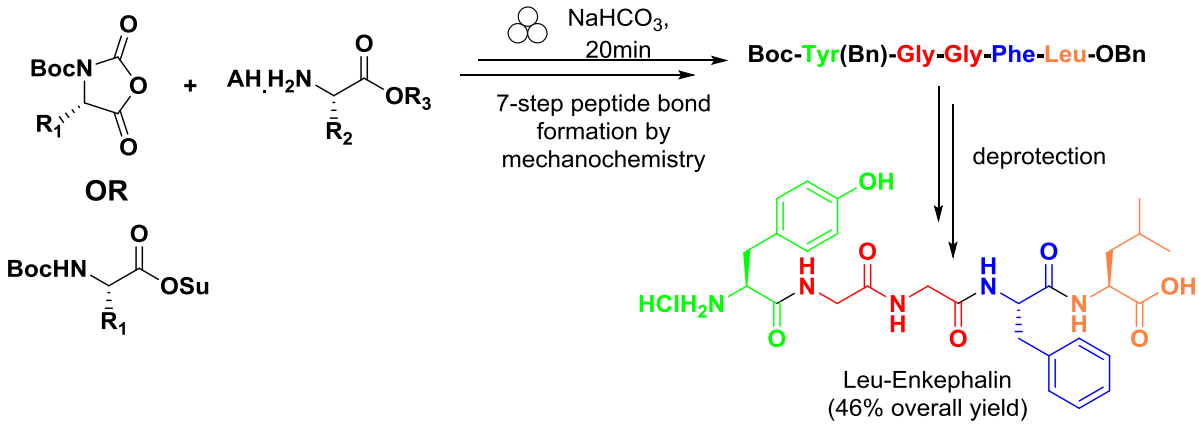

Fig. 1.31. Mechanochemical synthesis of the natural product Leu-Enkephalin through a 7-step sequence of solvent-free mechanochemical coupling and thermochemical deprotection steps.[134]

In a further application of this procedure, Konnert *et al.*[136a] utilised a biphenyl-based aminoacid in a one-pot two-step mechanosynthesis of the antiepileptic drug Phenytoin,[136b] (Phenytek). The use of a significantly less toxic trimethylsilylisocyanate instead of potassium isocyanate (KOCN), conducted in the presence of water, enabled the activation of the methyl-protected biphenyl aminoacid salt to form the N-urea moiety. Subsequent cyclisation was achieved by grinding with Cs_2CO_3, giving the desired API in good yield (Fig. 1.32). Extending this methodology further, the authors utilized a POLAG with PEG for the synthesis of the anti-convulsant drug Ethotoin.[136c]

In 2014, Tan and coworkers[137a] presented two mechanochemical synthetic routes for making anti-diabetic sulfonyl-urea[137b] APIs (*see Chapter 2 for more details*). Conventional

and protected synthetic procedures for sulfonyl-ureas utilise sulfonamides and isocyanate reagents in a two-step process in which the first step is the activation of the poorly nucleophilic sulfonamide by stoichiometric base, followed by reaction with the isocyanate.[137b] This two-step procedure was readily adapted into a one-pot milling process, using K_2CO_3 as the stoichiometric base, to give 1st generation APIs tolbutamide and chlorpropamide. However, this work also provided a novel, and shorter, route to both APIs, by a one-step mechanochemical procedure involving the direct copper-catalyzed coupling of the sulfonamide and isocyanate, effectively eliminating one synthetic step and need for stoichiometric base.[137c] The copper-catalyzed procedure was readily combined with a mechanochemical approach for carbodiimide-mediated amide synthesis,[137d] to yield the more complex 2nd generation drug molecule, Glibenclamide® in a two-step mechanochemical process. In all cases, the copper catalyst was readily removed by brief milling of the organic product with aqueous solution of sodium ethylenediaminetetraacetate ($Na_2H_2EDTA{\cdot}2H_2O$), followed by washing with water. A variety of copper catalysts were explored with success, including simple milling with brass balls, echoing the work of the Mack group in using a copper-based milling assembly to conduct Huisgen- and Sonogashira-type coupling reactions without a discrete copper catalyst added to the reaction mixture.[113b]

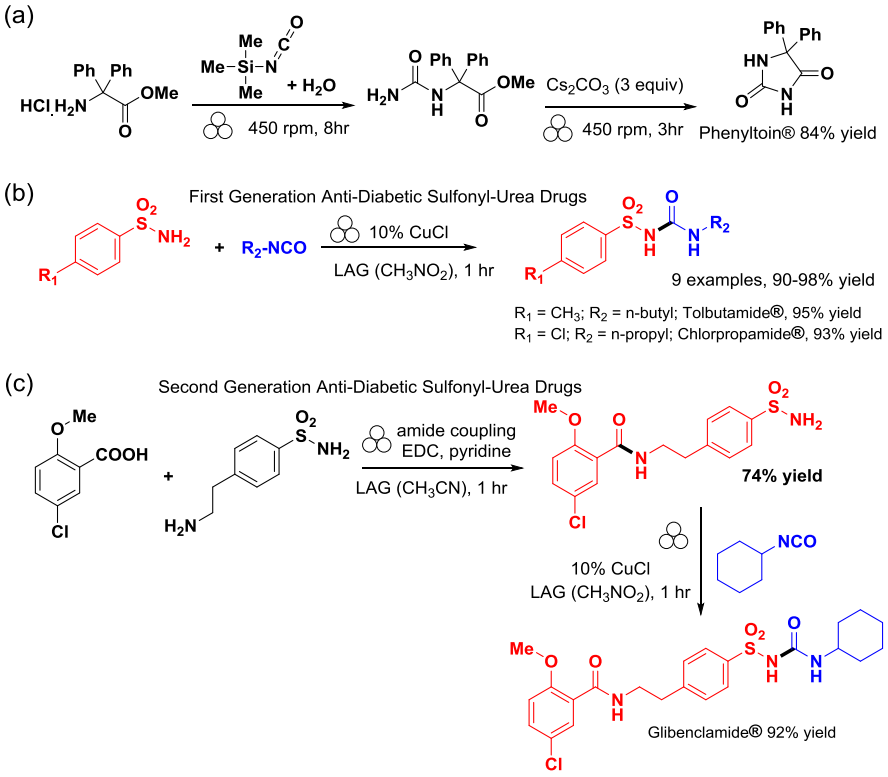

Fig. 1.32. Reported mechanochemical syntheses of APIs: a) Phenyltoin®,[136b] (b) Chlorpropamide® and Tolbutamide® and (c) Glibenclamide®.[137a] For clarity, sulphonamide- and isocyanate-based fragments in (b) and (c) are shown in red and blue, respectively.

1.4.5.3 Mechanosynthesis of pharmaceutically-relevant functional groups and fragments

A number of recent contributions have demonstrated the use of mechanochemistry for solvent-free and rapid assembly of molecular fragments important in API design. Of these, one of the simplest and the most important ones is certainly the amide group.[138] Mechanochemical, solvent-free protocols for amide bond formation and peptide synthesis have been provided by several groups, including those of Métro and Lamaty,[139a] Juaristi[139b] and Štrukil.[137d] Most recently, Pattarawarapan and coworkers[140] demonstrated the mechanochemical synthesis of amide and peptide bonds by using the inexpensive and highly versatile 2,4,6-trichloro-1,3,5-triazine (TCT) as a reagent in combination with substoichiometric triphenylphosphine to activate carboxylic acids in presence of amine bases (Fig. 1.33). This coupling reaction, conducted in a simple mortar and pestle, gave good to excellent yields within 20 minutes. In this process, triphenylphosphine acts as a catalyst which first forms a highly activated phosphonium salt with TCT, then subsequently activates the carboxylic acid into an ester capable of reacting with a secondary amine, forming the desired amide and regenerating the phosphine catalyst.

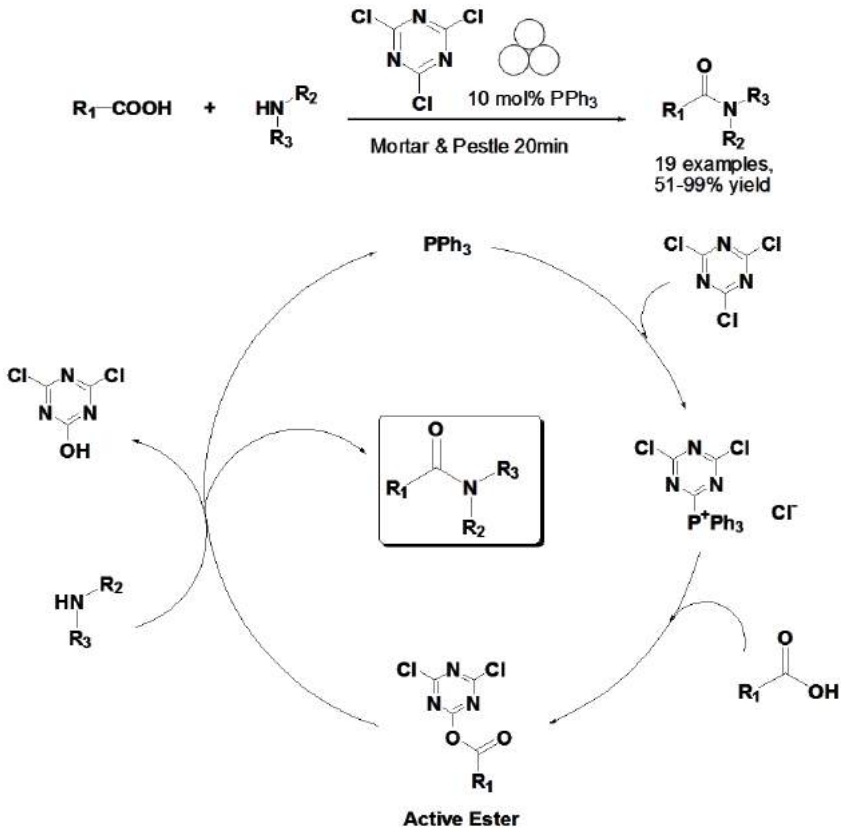

Fig. 1.33. Mechanosynthesis of amides using trichlorotriazine (TCT) as coupling agent and PPh_3 as a catalyst.

The hydrazone functionality, relevant for vasodilators in treatment of hypertension, anti-oxidants against sepsis and tuberculosis, as well as anti-tumour agents, is another important moiety in drug development.[141] The synthesis of hydrazones by mechanochemical condensation reactions of hydrazides with solid aldehydes has been reported by the Baltas group,[142] leading to quantitative conversions in contrast to poor reactivity of hydrazides that normally require long reaction times (up to 48 h) under conventional refluxing solution conditions (Fig. 1.34a).

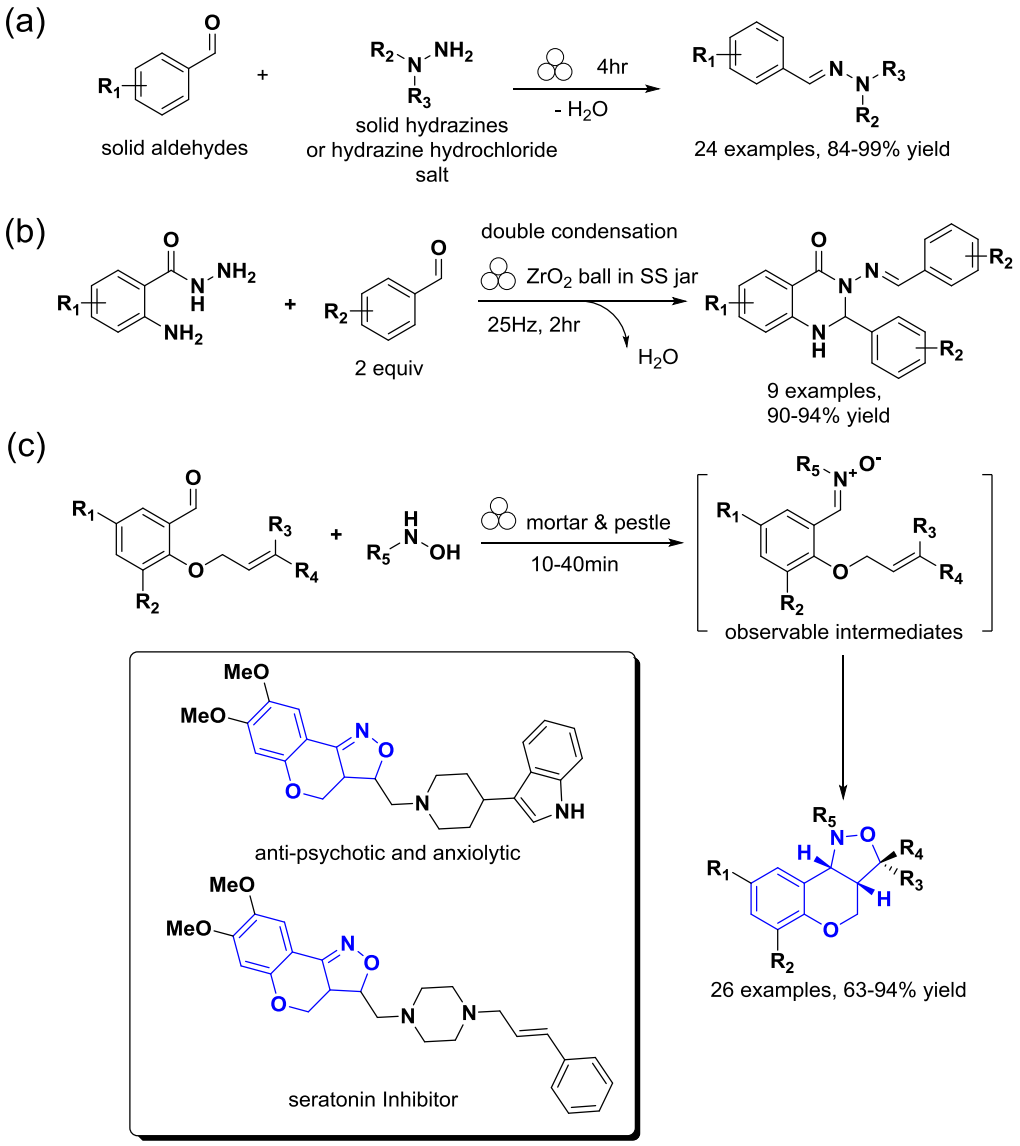

Fig. 1.34. (a) Single[142] and (b) double[143] Schiff base condensation reactions performed mechanochemically. (c) Mechanosynthesis of a fused chromano[4,3-c]isoxazole.[145]

Fülöp and coworkers[143] reported the double condensation reaction of anthranilic hydrazides (Fig. 1.34b) with aromatic aldehydes to give 4-quinazolinones, another set of biologically active compounds. Fused isoxazolidines with a chromano moiety are pharmaceutically important in the context of antidepressant, antipsychotic and antianxiolytic medications.[144] Bhutia *et al.* reported an efficient, catalyst-free mechanochemical synthesis of *cis*-fused chromano[4,3-c]isoxazoles *via* intramolecular 1,3-dipolar nitrone cycloaddition.[145] The mechanosynthesis is based on a two-step solvent-free reaction, involving the formation of a nitrone intermediate by kneading, followed by subsequent thermal treatment to afford the target chromano[4,3-c] isoxazoles in good to excellent yields, without extensive purification (Fig. 1.34c).

Benzimidazole and benzothiazole fragments are common scaffolds in various biologically active compounds and natural products, including clinical medicines such as Riluzole,[146a] for motor neurone disease treatment, Esomerprazole,[146b] an anti-ulcerative drug, and Astimazole,[146c] a 2nd generation anti-histamine drug. In 2014, Banerjee *et al.* demonstrated how mechanochemistry can be used to synthesise various benzimidazoles and benzothiazoles, from aromatic aldehydes and *o*-diaminobenzenes and *o*-thiol-anilines, respectively.[147] After screening of different kneading conditions, including the choice of liquid additive and duration of grinding, good to excellent yields (60-90%) were achieved.

Functionalisation of nucleosides is a traditionally challenging area of organic synthesis, typically requiring strongly polar and toxic solvents such as dimethylformamide, dimethylsulfoxide and pyridine.[148] Moreover, the use of highly moisture-sensitive chlorosilane reagents requires extensive drying of the solvents (*e.g.* over CaH_2 or P_2O_5) and distillation. The Vyle group demonstrated that solvent-free mechanochemistry provides an excellent means to circumvent these challenges and achieve a rapid, quantitative route to nucleoside and phenolic analogues (Fig. 1.35a).[149] The protocol was subsequently expanded to enable a fast and chemoselective acylation using *N*-hydroxysuccinimidyl (NHS) esters, leading to azobenzene-grafted propargylamides for use as chromophore-functionalised nucleoside and nucleotide mimetics (Fig. 1.35b).[150] Investigation of the formation of nucleotide pyrophosphate linkages in the ball mill[151] revealed that quantitative conversions and excellent yields of nucleoside polyphosphates are achievable in the presence of additives such as $MgCl_2 \cdot 6H_2O$, 1*H*-tetrazole and water, which suppressed the formation of side products (Fig. 1.35c).

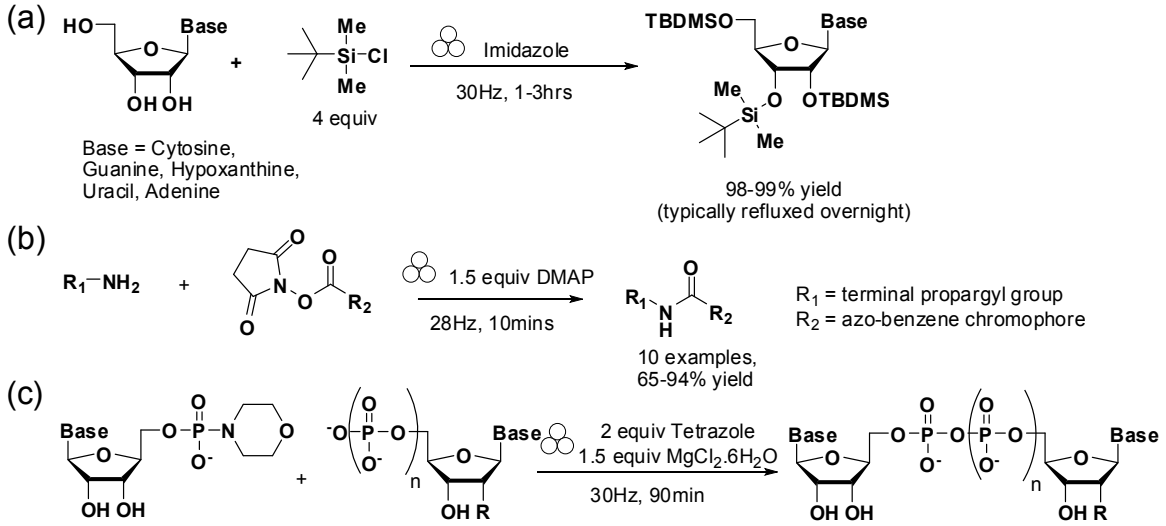

Fig. 1.35. a) Rapid mechanochemical protection of nucleosides,[149] b) mechanosynthesis of propargylamides containing azobenzene chromophores using *N*-hydroxysuccinimidyl esters[150] and c) mechanosynthesis of nucleotide pyrophosphates.[151]

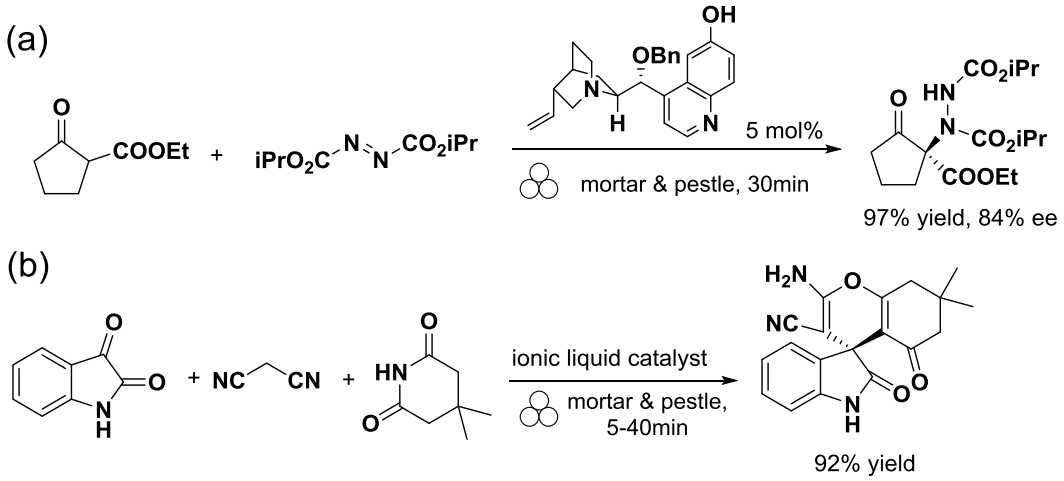

Fig. 1.36. Enantioselective organocatalytic reactions that generate a quartenary stereogenic carbon a) with an amino group[152] and b) spiro-oxindole moiety,[153] performed using gentle grinding on mortar and pestle.

A number of recent developments in organic mechanochemistry have targeted catalytic transformations and assembly of molecular fragments relevant to APIs, strongly indicating that mechanochemical synthesis of pharmaceutically- and medicinally-interesting targets will continue to gain momentum. In a recent example of a mechanochemical formation of C-N bonds relevant in the pharmaceutical context, Chauhan and Chimni[152] reported solvent-free organocatalytic, enantioselective amination of a β-ketoester to generate an amino-substituted quaternary stereocentre (Fig. 1.36a). Similarly, the Singh group[153]

reported on the mechanochemical formation of a quartenary stereocentre by domino Knoevenagel-condensation between isatin, malononitrile and a 1,3-diketone (Fig. 1.36b), affording a spiro-oxindole moiety, pharmaceutically attractive for anti-malarial, anti-tumour and anti-bacterial properties.[154]

1.5 Many faces of mechanochemistry.

While *Sections 1.1* to *1.4* covered the synthetic aspect of mechanochemistry, it is important to acknowledge that the umbrella of mechanochemistry encompasses not only synthetic chemistry, but also extends to other diverse areas in which mechanical action can bring about chemical consequences (Fig. 1.36). These other areas include lithography,[39] bond cleavage using mechanical induction *e.g.* in atomic force microscopy (AFM),[40] surface friction induced charge separation effects,[41a, 41b] rapid amorphisation under impact or pressure,[41c] supramolecular cages and rotaxanes,[42] and sonochemistry.[43] The aim of this section is not to explore in detail the various types of processes surrounding mechanochemistry, but to illustrate mechanochemistry as a broad area which encompasses different types of research. Whereas the term mechanosynthesis is often used to describe the synthesis of compounds achieved *via* introduction of mechanical energy, one of several alternative uses of this term is as an idealized molecular nanotechnology approach to manufacturing or manipulating molecules. In such a context, mechanosynthesis designates a process whereby the manipulation of the positions and orientations of individual molecules *via* the use of "molecular cranes", *e.g.* the tip of an AFM, can be used to bring molecules together in order to create new bonds in a precise and controlled manner.[44] Whereas such mechanosynthesis still remains largely a dream, the concept has been extensively used to probe mechanical properties of molecules and even individual covalent bonds through AFM based force spectroscopy. In general, one end of a single polymer chains can be tethered to the cantilever of the AFM probe and the other end anchored unto a support substrate. The AFM lever then slowly pulls the polymer chain apart until a specific covalent bond is broken (Fig. 1.37).

Another view of mechanochemistry, that is rapidly gaining momentum, is its use in the area of polymers.[45] A hallmark of this research area is the use of mechanophores *i.e.* functional groups that can respond to mechanical force or perturbation and can, therefore, be used to translate mechanical into chemical energy.[46] Such mechanophore groups are carefully engineered into polymer chains that can normally withstand a range of tensile stresses. The

presence of mechanophores enables the transformation or even cleavage of polymers in a precisely controlled location along the polymer chain upon ultrasonic irradiation. Such transformations can include, but are not limited to, bond breakage, isomerizations, cycloreversions, ring opening reactions and even catalytic bond scissions.[46] A number of reports and reviews have been published in recent years by the Craig group,[47] the Moore group,[48] Boydston group,[49] and the Beyer group.[40] Mechanistic studies of the mechanophore behaviour have also been reported by the Makarov group.[50]

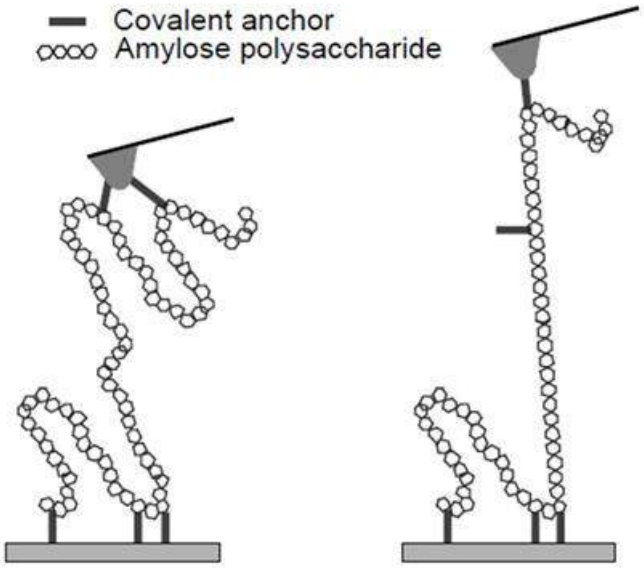

Fig. 1.37. Stretching of a single polysaccharide chain that is covalently linked to an AFM tip and a substrate surface. Adapted from ref. 40b.

An integrated view of different views of mechanochemistry, including ball milling, polymer sonochemistry and single molecule stretching, was recently given by Suslick[51] (Fig. 1.38), who addressed four distinct, but related areas of mechanochemistry, ranging from tribochemistry (surface friction), to trituration (grinding, milling and synthesis) to macromolecular and lastly sonochemistry. More importantly, he also suggests a connection between sonochemistry and mechanochemistry, as the physical effects of ultrasonic irradiation might be similar to the frictional effects of grinding forces in mechanochemical reactions. Sonochemical reactions are induced by the mechanical effects of sound on liquids, which is caused by acoustic cavitation, the rapid formation and collapse of bubbles in the media being exposed to ultrasonic irradiation.[52] The collapse of the bubbles creates immense implosive forces that can generate hot spot temperatures that exceed 5000 K, high pressures

of 1000 atmospheres, and extreme rapid temperature changes of 1010 K/s.[53] This in turn can be used to not only break bonds by stretching molecules apart as seen in polymer mechanochemistry,[45] but also used to induce formation of chemical bonds.[54]

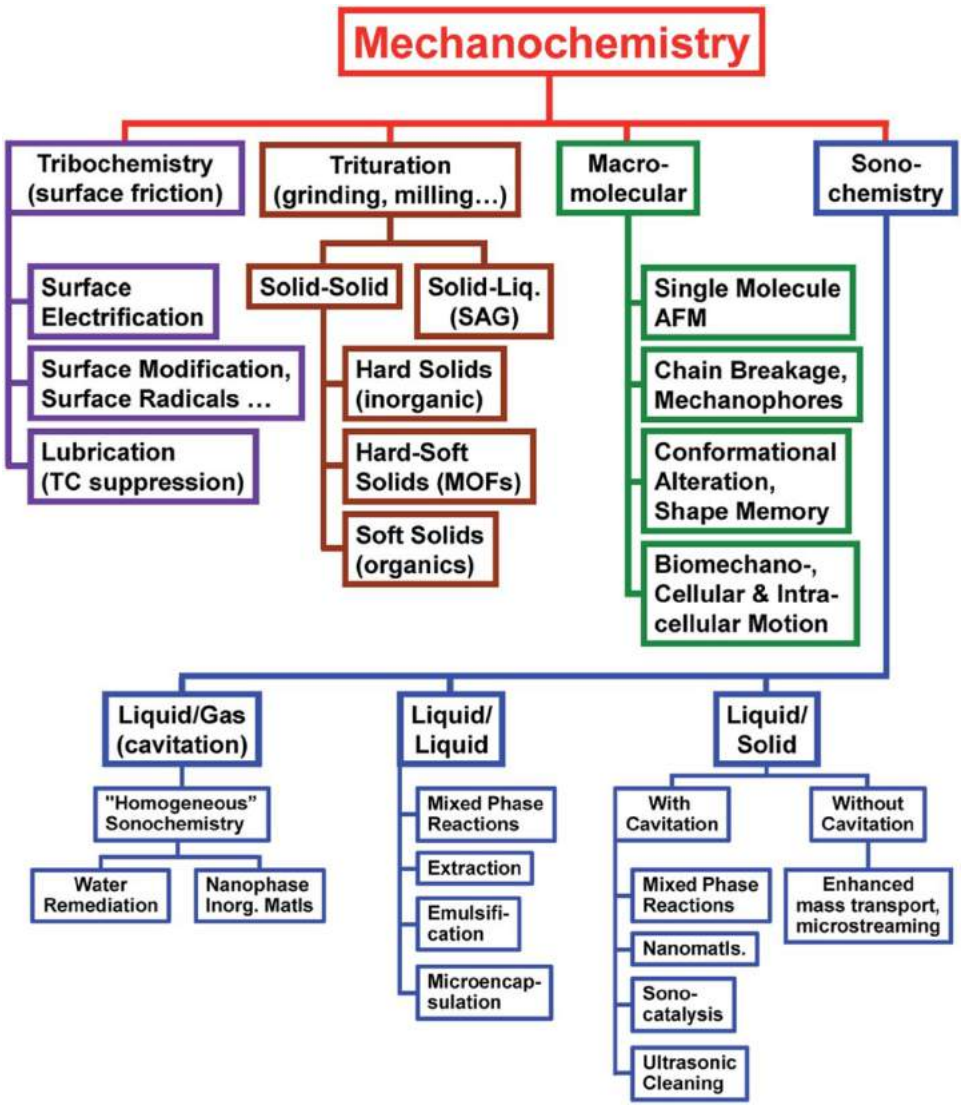

Fig 1.38. Overview of the different aspects of mechanochemistry, as described by Suslick Adapted from ref. 51.

Another recent, emerging area of mechanochemistry pertains to bio-mechanical systems, whereby cells and bacteria use biological processes to transform a mechanical force into a biochemical response, a process known as mechanotransduction. These are low energy demand processes that occur in biochemical systems and are collectively designated “soft mechanochemistry”.[55] However, it is worth noting that this term was initially introduced to describe mechanochemical reactions that involve participation of highly reactive compounds.[1c,56] An example of such soft mechanochemistry was provided by Senna,[56b] who

reported incipient chemical interaction by milling fine particles of PMMA, silica and $Mg(OH)_2$ together. This treatment produced composite materials consisting of core spheres of the PMMA polymer coated by a layer of silica and $Mg(OH)_2$. The demonstrated lack of clarity surrounding the term "soft mechanochemistry" also serves as an excellent illustration of the differences in interpretation and lack of consensus that affect modern mechanochemistry. This, however, is not unusual for a dynamic field, such as modern mechanochemistry and also should be taken as a reflection of the rapid progress and growth in popularity of mechanochemistry and mechanosynthesis over the past couple of decades.

Whereas most definitions of mechanochemistry address processes through which mechanical energy is translated to chemical reactivity (*e.g.* bond breaking or formation), this view has recently undergone a significant transformation. Modern mechanochemistry no longer focuses only on changes to polymeric chains or inorganic framework structures, but has already tacitly embraced transformations involving rearrangements of low energy, non-covalent interactions, *e.g.* during polymorphic transformations or cocrystal formation by milling. As a part of this ongoing evolution of definitions of mechanochemistry, it does not seem incongruous to also include in this field other types of processes, specifically those that convert chemical transformations into mechanical effects. These processes include the behaviour of thermosalient and photosalient compounds, as well as the activity of motor proteins and proton pumps. Thus, in this Thesis I have also included studies of thermosalient behavior, *i.e.* mechanical motion that is trigerred through polymorphic transformations of crystalline solids (*Chapter 7*).

The term thermosalient effect was first coined by Gigg to describe the observed thermally-induced jumping motion of (±)-3,4-di-*O*-acetyl-1,2,5,6-tetra-*O*-benzyl-*myo*-inositol crystals.[157] Thermosalient behavior or the "jumping crystal effect" is the result of a thermally-induced martensitic-type transition,[158] *i.e.* a first-order polymorphic transition that proceeds *via* homogenous lattice deformation without relocation of atoms or molecules by diffusion. This transition is characterized by sharp and quick anisotropic changes in the volume of the crystallographic unit cell, reflected in a macroscopic change in the bulk material, which is ultimately manifested as motion of single crystals, for example flipping, twisting, bending, exploding and jumping. Importantly, thermosalient behavior is due to solid-solid polymorphic transformation, and not a result of a thermochemical reaction such as decomposition. Thererfore, it seems reasonable for thermosalient compounds to be considered as under the field of mechanochemistry, which can be viewed as a discipline that investigates the interplay between chemical reactivity and mechanical motion (Fig. 1.39).

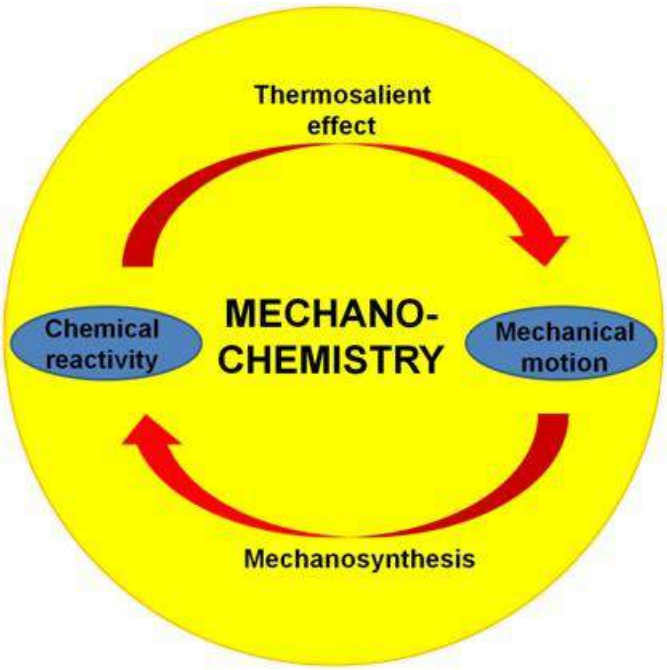

Fig. 1.39. Proposed concept of mechanochemistry as a discipline that investigates the interplay of mechanical motion and chemical reactivity.

1.6 Conclusion

This chapter has covered the various aspects of mechanochemistry: from its historical beginnings, to the evolution and development of its tools and techniques in recent decades, to understanding mechanochemical reactions through *ex situ* and *in situ* monitoring, to its application for medicinal chemistry and organic synthesis, and lastly, a brief discussion on the many changing faces of mechanochemistry. All in all, the points covered in this chapter indicate that the field of mechanochemistry is ever-growing and ever-evolving. In particular, the research interest of using mechanochemistry for the synthesis of API molecules, as well as other pharmaceutically-relevant compounds is slowly gaining momentum. The next few chapters in this Dissertation are novel contributions to this emergent area of medicinal mechanochemistry. Specifically, *Chapters 2-5* investigate how mechanochemistry can be used as a powerful tool for discovering new C-N bond coupling reactions for the synthesis of pharmaceutically relevant molecules. Furthermore, mechanochemistry can also enable synthetic chemists to access compounds that exhibit fascinating structural and physicochemical properties. In particular, an unprecedented degree of isostructurality among eight related compounds will be covered in *Chapter 6*, and discovery and systematic studies of thermosalient compounds will be discussed in *Chapter 7*.

1.7 References

1 a) IUPAC. *Compendium of Chemical Terminology*, 2nd ed. (the "Gold Book"). Compiled by A. D. McNaught, A. Wilkinson. Blackwell, **1997** Scientific Publications, Oxford; b) C. Reichardt, T. Welton, *Solvents and solvent effects in organic chemistry*, fourth ed., **2011** Wiley-VCH Verlag GmbH & Co. KGaA; c) R. P. Rastogi, P. S. Bassi, L. S. Chadha, *J. Phys. Chem.*, **1963**, *67*, 2569; d) R. P. Rastogi, N. B. Singh, *J. Phys. Chem.*, **1968**, *72*, 4446; e) R. P. Rastogi, N. B.Singh, *J. Phys. Chem*., **1966**, *70*, 3315; f) E. Avvakumov, M. Senna, N. Kosova, *Soft Mechanochemistry: A Basis for New Chemical Technologies*, **2001**, Kluwer Academic Publischers, Dordrecht; g) G. Rothenberg, A. P. Downie, C. L. Raston, J. L. Scott, *J. Am. Chem. Soc.,* **2001**, *123*, 8701.

2 A. J. Lynch, C. A. Rowland, *The History of Grinding*, Society of Mining, **2005**, Metallurgy and Exploration, Inc., Littleton, CO.

3 a) L. Takacs, *Chem. Soc. Rev*., **2013**, *42*, 7649. b) L. Takacs, *J. Met*., **2000**, *52*, 12; c) Theoprhastus, *On Stones* (De Lapidibus), **1965**, translated by D. E. Eichholtz, Oxford University Press; d) C. Suryanarayana, *Prog. Mat. Sci*., **2001**, *46*, 1.

4 a) T. Friščić, W. Jones, *Cryst. Growth Des.*, **2009**, *9* ,1621; b) A. V. Trask, N. Shan, W. D. S. Motherwell, W. Jones, S. Feng, R. B. H. Tan, K. J. Carpenter, *Chem. Commun.*, 2005, 880.

5 a) P. Baláž, *Extractive Metallurgy of Activated Minerals*, **2000**, Elsevier, Amsterdam; b) P. Baláž, *Mechanochemistry in Nanoscience and Minerals Engineering*, **2008**, Springer-Verlag, Berlin Heidelberg.

6 a) L. Takacs, *J. Therm. Anal. Calorim*., **2007**, *90*, 81. b) J. Johnston, L. H. Adams, *Am. J. Sci.*, **1913**, *35*, 205.

7 a) W. Spring, *Bull. Acad. R. Med. Belg*., **1880**, *49*, 323. b) W. Spring, *Bull. Soc. Chim. Fr.*, **1883**, *39*, 641. c) W. Spring, *Bull. Soc. Chim. Fr*., **1885**, *44*, 166.

8 M. C. Lea, *Am. J. Sci*., **1892**, *43*, 527.

9 M. C. Lea, *Am. J. Sci.*, **1893**, *46*, 413.

10 a) L. Takacs, *Bull. Hist. Chem*., **2003**, *28*, 26; b) V. Šepelák, A. Důvel, M. Wilkening, K.-D. Becker, P. Heitjans, *Chem. Soc. Rev.*, **2013**, *42*, 7507-7520.

11 W. Ostwald, *Die chemische Literatur und die Organisation der Wissenschaft*, in Handbuch der allgemeinen Chemie, ed. W. Ostwald and C. Drucker, Akademische Verlagsge-sellschaft m. b. H., Leipzig, **1919**, 70.

12 F. Wöhler, *Justus Liebigs Ann. Chem.*, **1844**, *51*, 145

13 N. R. Rightmire, T. P. Hanusa, *Dalton Trans.*, **2016**, *45*, 2352-236

14 W. Jones, M. D. Eddleston, *Faraday Discuss.,* **2014**, *170*, 9.

15 A. R. Ling, J. L Baker, *J. Chem. Soc. Trans*., **1893**, *63*, 1314.

16 A. O. Patil, D. Y. Curtin, I. C. Paul, *J. Am. Chem. Soc*., **1984**, *106*, 348.

17 a) R. Kuroda, Y. Imai, N. Tajima, *Chem. Commun*., **2002**, *37*, 2848; b) R. Kuroda, K. Higashiguchi, S. Hasebe, Y. Imai, *CrystEngComm*, **2004**, *6*, 463

18 a) F. Toda, K. Tanaka, A. Sekikawa, *J. Chem. Soc. Chem. Commun*., **1987**, 279; b) F. Toda, *Acc. Chem. Res.*, **1995**, *28*, 480.

19 M. C. Etter, G. M. Frankenbach, *Chem. Mater*., **1989**, *1*, 10.

20 a) M. C. Etter, S. M Reutzel, C. G Choo, *J. Am. Chem. Soc.*, **1993**, *115*, 4411; b) M. R. Caira, L. R. Nassibeni, A. F. Wildervanck, *J. Chem. Soc. Perkin Trans*., **1995**, *2*, 2213.

21 a) D. Braga, S. L. Giaffreda, F. Grepioni, A. Pettersen, L. Maini, M. Curzi, M. Polito, *Dalton Trans*., **2006**, 1249; b) D. Braga, F. Grepioni, L. Maini, *Chem. Commun.*, **2010**, *46*, 6232.

22 a) A. A. Michalchuk, I. A. Tumanov, E. V. Boldyreva, *CrystEngComm*, **2013**, *15*, 6403; b) A. A. Michalchuk, I. A. Tumanov, V. A. Drebushchak, E. V. Boldyreva, *Faraday Discuss*., **2014**, *170*, 311.

23 F. Knoop, C.G. Peters, W.B. Emerson, *J. Res. Nat. Bureau Standards*, **1939**, *23*, 39.

24 a) D. Cinčić, I. Brekalo, B. Kaitner, *Chem. Commun*., **2012**, *48*, 11683; b) J. Stojaković, B. S. Farris, L. R. MacGillivray, *Chem. Commun.*, **2012**, *48,* 7958; c) Y. Fang, N. Salamé, S. Woo, D. S. Bohle, T. Friščić, L. A. Cuccia, *CrystEngComm*, **2014**, *16*, 7180.

25 N. Shan, F.Toda, W. Jones, *Chem. Commun*., **2002**, *37*, 2372.

26 A. V. Trask, W. D. S. Motherwell, W. Jones, *Chem. Commun*., **2004**, *39*, 890.

27 K. L. Nguyen, T. Friščić , G. M. Day, L. F. Gladden, W. Jones, *Nat. Mater*., **2007**, *6*, 206.

28 a) S. Karki, T. Friščić, W. Jones, *CrystEngComm*, **2009**, *11*, 470; b) D. Cinčić, T. Friščić, W. Jones, *J. Am. Chem. Soc*., **2008**, *130*, 7524; c) A. V. Trask, W. D. S. Motherwell, W. Jones, *Chem. Commun*., **2004**, 890.

29 T. Friščić, A. V. Trask, W. Jones, W. D. S. Motherwell, *Angew. Chem. Int. Ed.,* **2006**, *45*, 7546.

30 a) T. Friščić, S. L. Childs, S. A. A. Rizvi, W. Jones, *CrystEngComm*, **2009**, *3*, 418; b) T. Friščić, W. Jones, *Faraday Discuss*., **2007**, *136*, 167; c) F. Fischer, G. Scholz, S. Benemann, K. Rademann, F. Emmerling, *CrystEngComm*, **2014**, *16*, 8272.

31 C. B. Aakeröy, P. D. Chopade, *Org. Lett.*, **2011**, *13*, 1.

32 G. A. Bowmaker, *Chem. Commun.*, **2013**, *49*, 334.

33 a) T. Friščić, D. G. Reid, I. Halasz, R. S. Stein, R. E. Dinnebier, M. J. Duer, *Angew. Chem. Int. Ed*., **2010**, *49*, 712; b) T. Friščić, *J. Mat. Chem.*, **2010**, *20*, 7599; c) D. N. Dybtsev, H. Chun, K. Kim, *Angew. Chem. Int. Ed.*, **2004**, *43*, 5033; d) B.-Q. Ma, K. L. Mulfort, J. T. Hupp, *Inorg. Chem*., **2005**, *44*, 4912.

34 P. C Andrews, G. B. Deacon, C. M. Forsyth, P. C. Junk, I. Kumar, M. Maguire, *Angew. Chem. Int. Ed.,* **2006**, *45*, 5638.

35 V. André, A. Hardeman, I. Halasz, R. S. Stein, G. J. Jackson, D. G. Reid, M. J. Duer, C. Curfs, M. T. Duarte, T. Friščić, *Angew. Chem. Int. Ed.*, **2011**, *50*, 7858.

36 a) J.-L. Do, C. Mottillo, D. Tan, V. Štrukil, T. Friščić, *J. Am. Chem. Soc.,* **2015**, *137*, 2476; b) J. Spekreijse, L. Őhrström, J. P. M. Sanders, J. H. Bitter, E. K. Scott, *Chem. Eur. J.,* **2016**, *22*, 15437.

37 a) G. J. Hernández, I. S. Butler, T. Friščić, *Chem. Sci*., **2014**, *5*, 3576; b) Y. X. Shi, K. Xu, J. K. Clegg, R. Ganguly, H. Hirao, T. Friščić, F. García, *Angew.Chem. Int.Ed.,* **2016**, *55* , 12736.

38 a) D. Hasa, R. G. Schneider, D. Voinovich, W. Jones, *Angew. Chem. Int. Ed*., **2015**, *54*, 7371; b) D. Hasa, E. Carlino, W. Jones, *Cryst. Growth Des*., **2016**, *16*, 1772.

39 J. R. Felts, A. J. Oyer, S. C. Hernández, K. E. Whitener Jr., J. T. Robinson, S. G. Walton, P. E. Sheehan, *Nat. Commun*., **2015**, *6*, 6467.

40 a) S. W. Schmidt, M. F. Pill, A. Kersch, H. Clausen-Schaumann, M. K. Beyer, *FaradayDiscuss.,* **2014***, 170, 357*; b) M. Grandbois, M. Beyer, M. Rief, H. Clausen-Schaumann, H. E. Gaub, *Science*, **1999**, *283*, 1727.

41 a) G. Kaupp, *CrystEngComm*, **2009**, *11*, 388; b) L. Beraldo da Silveira Balestrin, D. Del Dugue, D. S. da Silva, F. Galembeck, *Faraday Discuss.,* **2014***, 170, 369;* c) b) M. Jörres, J. L. Acena, V. A. Soloshonok, C. Bolm, *Chem. Cat. Chem.*, **2015**, *7*, 1265.

42 a) T. Friščić, *Chem. Soc. Rev.*, **2012**, *41*, 3493; b) J. Antesberger, G. W. V. Cave, M. C. Ferrarelli, M. W. Heaven, C. L. Raston, J. L. Atwood, *Chem. Commun.*, **2005**, 892.

43 S. You, M.-W. Chen, D. D. Dlott, K. S. Suslick, *Nat. Commun.*, 2015, **6**, 6581

44 a) K. E. Drexler, *Nanosystems: molecular machinery, manufacturing, and computation*, **1992**, John Wiley & Sons, Inc. New York, NY, USA; b) M. F. L. De Volder, S. H. Tawfick, R. H. Baughman, A. J. Hart, *Science*, **2013**, *339*, 535.

45 R. Boulatov, *Polymer Mechanochemistry*, *Top. Curr. Chem.*, **2015**, *369*, Springer International Publishing, Switzerland.

46 J. N. Brantley, K. M. Wiggins, C. J. Bielawski, *Polymer Int*., **2013**, *1*, 2.

47 a) S. L. Craig, *Nature*, **2012**, *487*, 176; b) J. Wang, T. B. Kouznetsova, Z. Niu, M. T. Ong, H. M. Klukovich, A. L. Rheingold, T. J. Martínez, S. L. Craig, *Nat. Chem.*, **2015**, *7*, 323; c) J. Wang, T. B. Kouznetsova, Z. S. Kean, L. Fan, B. D. Mar, T. J. Martínez, S. L. Craig, *J. Am. Chem. Soc*., **2014**, *136*, 15162; d) A. L. Black, J. A. Orlicki, S. L. Craig, *J. Mater. Chem*., **2011**, *21*, 8460; e) C. L. Brown, S. L. Craig, *Chem. Sci*., **2015**, *6*, 2158; f) J. Wang, I. Piskun, S. L. Craig, *ACS Macro Lett*., **2015**, *4*, 834.

48 a) J. Li, C. Nagamani, J. S. Moore, *Acc. Chem. Res*., **2015**, *48*, 2181; b) S. L. Potisek, D. A. Davis, N. R. Sottos, S. R. White, J. S. Moore, *J. Am. Chem. Soc*., **2007**, *129*, 13808; c) M. J. Kryger, M.T. Ong, S. A. Odom, N. R. Sottos, S. R. White, T. J. Martínez, J. S. Moore, *J. Am. Chem. Soc*., **2010**, *132*, 4558; d) J. Li, T. Shiraki, B. Hu, R. A. E. Wright, B. Zhao, J.

S. Moore, *J. Am. Chem. Soc.,* **2014**, *136*, 15925; e) M. J. Robb, J. S. Moore, *J. Am. Chem. Soc*., **2015**, *137*, 10946; f) T. Shiraki, C. E. Diesendruck, J. S. Moore, *Faraday Discuss.*, **2014**, ***170***, 385.

49 M. B. Larsen, A. J. Boydston, *J. Am. Chem. Soc*., **2013**, *135*, 8189.

50 S. M. Avdoshenko, D. E. Makarov, *J. Phys. Chem. B*, **2016**, *120*, 1537.

51 K. S. Suslick, *Faraday Discuss.*, **2014**, *170*, 411.

52 a) K. S. Suslick, *Science*, **1990**, *247*, 1439; b) H. Xu, B. W. Zeiger, K. S. Suslick, *Chem. Soc. Rev*., **2013**, *42*, 2555; c) K. S. Suslick, D. J. Flannigan, *Annu. Rev. Phys. Chem*., **2008**, *59*, 659.

53 a) D. J. Flannigan, K. S. Suslick, *Nature,* **2005**, *434*, 52–55; b) D. J. Flannigan, K. S. Suslick, *Nat. Phys*., **2010**, *6*, 598; c) W. B. McNamara, Y. T. Didenko, K. S. Suslick, *Nature*, **1999**, *401*, 772; d) Y. T. Didenko, K. S. Suslick, *Nature*, **2002**, *418*, 394.

54 G. Cravotto, E. C. Gaudinoa, P. Cintas, *Chem. Soc. Rev.,* **2013**, *42*, 7521.

55 P. Lavalle, F. Boulmedais, P. Schaaf, L. Jerry, *Langmuir*, **2016**, *32*, 7265.

56 P. Baláž, M. Achimovičová, M. Baláž, P. Billik, Z. Cherkezova-Zheleva, J. M. Criado, F. Delogu, E. Dutková, E. Gaffet, F. J. Gotor, R. Kumar, I. Mitov, T. Rojac, M. Senna, A. Streletskii, K. Wieczorek-Ciurowa, *Chem. Soc. Rev*., **2013**, *42*, 7571.

57 S. Karki, L. Fábián, T. Friščić, W. Jones, *Org. Lett*., **2007**, *9*, 3133.

58 a) K. D. M. Harris, *Top. Curr. Chem*., **2012**, *315*, 133; b) E. Y. Cheung, S. J. Kitchin, K. D. M. Harris, Y. Imai, N. Tajima, R. Kuroda, *J. Am. Chem. Soc*., **2003**, *125*, 14658.

59 a) M. U. Schmidt, J. Brűning, *J. Pharm. Pharmacol*., **2015**, *67*, 773; b) A. V. Trask, J. van de Streek, W. D. S. Motherwell, W. Jones, *Cryst Growth Des*., **2005**, *5*, 2233; c) X. Chen, J. G. Stowell, K. R. Morris, S. R. Bryn, *J. Pharm. Biomed. Anal*., **2010**, *51*, 866.

60 V. Štrukil, D. Gracin, O. V. Magdysyuk, R. E. Dinnebier, T. Friščić, *Angew. Chem. Int. Ed.*, **2015**, *54*, 8440.

61 D. Braga, L. Maini, M. Polito, F. Grepioni, *Chem. Commun*., **2002**, *37*, 2302.

62 a) E. P. J. Parrott, J. A. Zeitler, T. Friščić, M. Pepper, W. Jones, G. M. Day, L. F. Gladden, *Cryst. Growth Des*., **2009**, *9*, 1452 b) K. L. Nguyen, T. Friščić, G. M. Day, L. F. Gladden, W. Jones, *Nat. Mater*., **2007**, *6*, 206; c) X. Liu, G. Liu, H. Zhao, Z. Zhang, Y. Wei, M. Liu, W. Wen, X. Zhou, *J. Phys. Chem. Solids*, **2011**, *72*, 1245.

63 a) J. A. Fernandes, M. Sardo, L. Mafra, D. Choquesillo-Lazarte D, N. Masciocchi, *Cryst. Growth Des*., **2015**, *15*, 3674; b) V. P. Balema, J. W. Wiench, M. Pruski, V. K. Pecharsky, *Chem. Commun*., **2002**, *37*, 724;

64 a) V. Štrukil, L. Fábián, D. G. Reid, M. J. Duer, G. J. Jackson, M. Eckert-Maksić, T. Friščić, *Chem. Commun.*, **2010**, *46*, 9191; b) M. Weiße, M. Zille, K. Jacob, R. Schmidt, A. Stolle, *Chem. Eur. J.*, **2015**, *21*, 6511; c)X. Ma, W. Yuan, S. E. J. Bell, S. L. James, *Chem. Commun*., **2014**, *50*, 1585.

65 a) T. Friščić, I. Halasz, P. J. Beldon, A. M. Belenguer, F. Adams, S. A. J. Kimber, V. Honkimäki, R. E. Dinnebier, *Nat. Chem*., **2013**, *5*, 66; b) I. Halasz, S. A. J. Kimber, P. J. Beldon, A. M. Belenguer, F. Adams, V. Honkimäki, R. C. Nightingale, R. E. Dinnebier, T. Friščić, *Nat. Protoc*., **2013**, *8*, 1718; c) I. Halasz, T. Friščić, S. A. J. Kimber, K. Užarević, A. Puškarić, C. Mottillo, P. Julien, V. Štrukil, V. Honkimäki, R. E. Dinnebier*, Faraday Discuss*., **2014**, *170*, 203.

66 D. Gracin, V. Štrukil, T. Friščić, I. Halasz, K. Užarević, *Angew. Chem. Int. Ed*., **2014**, *53*, 6193.

67 L. Batzdorf, F. Fischer, M. Wilke, K.-J. Wenzel, F. Emmerling, *Angew. Chem. Int. Ed.*, 2015, **54**, 1799.

68 a) A. D. Katsenis, A. Puškarić, V. Štrukil, C. Mottillo, P. A. Julien, K. Užarević, M.-H. Pham, T.-O. Do, S. A. J. Kimber, P. Lazić, O. Magdysyuk, R. E. Dinnebier, I. Halasz, T. Friščić, *Nat Commun.,* **2015**, *6*, 6662; b) J. Nývlt, *Cryst. Res. Tech*., **1995**, *30*, 443.

69 a) I. Halasz, A. Puškarić, S. A. J. Kimber, P. J. Beldon, A. M. Belenguer, F. Adams, V. Honkimäki,R. E. Dinnebier, B. Patel, W. Jones, V. Štrukil, T. Friščić, *Angew. Chem. Int. Ed.*, **2013**, *52*, 11538; b) I. Halasz, S. A. J. Kimber, P. J. Beldon, A. M. Belenguer, F. Adams, V. Honkima¨ki, R. C. Nightingale, R. E. Dinnebier and T. Friščić, *Nat. Protoc*., **2013**, *8*, 1718.

70 M. Juribašić, K. Užarević, D. Gracin, M. Ćurić, *Chem. Commun*., **2014**, *50*, 10287

71 M. Tireli, M. Juribašić, N. Cindro, D. Gracin, N. Biliškov, M. Borovina, M. Ćurić, *Chem. Commun*., **2015**, *51*, 8058.

72 K. Užarević, I. Halasz, T. Friščić, *J. Phys. Chem. Lett.*, **2015**, *6*, 4129.

73 a) G.-W. Wang, *Chem. Soc. Rev*., **2013**, *42*, 7668; b) J. G. Hernández, T. Friščić, *Tetrahedron Lett*., **2015**, *56*, 4253; c) B. Rodríguez, T. Rantanen, C. Bolm, *Angew. Chem., Int. Ed*., **2006**, *45*, 6924; b) B. Rodríguez, A. Bruckmann, T. Rantanen, C. Bolm*, Adv. Synth. Catal*., **2007**, *349*, 2213; c) B. Rodríguez, A. Bruckmann, C. Bolm, *Chem. Eur. J.,* **2007**, *13*, 4710.

74 S. L. James, C. J. Adams, C. Bolm, D. Braga, P. Collier, T. Friščić, F. Grepioni, K. D. M. Harris, G. Hyett, W. Jones, A. Krebs, J. Mack, L. Maini, A. G. Orpen, I. P. Parkin, W. C. Shearouse, J. W. Steed, D. C. Waddell, *Chem. Soc. Rev*., **2012**, *41*, 413.

75 D. Margetić, V. Štrukil, *Mechanochemical Organic Synthesis*, 1st ed., **2016**, Elsevier Inc., Amsterdam, Netherlands.

76 a) G. Kaupp, *CrystEngComm*, **2003**, *5*, 117; b) G. Kaupp, J. Schmeyers, U. D. Hangen, *J. Phys. Org. Chem*., **2002**, *15*, 307; c) G. Kaupp, *CrystEngComm*, **2006**, *8*, 794.

77 F. K. Urukaev, V. V. Boldyrev, *Powder Technol.*, **2000**, *107*, 197.

78 a) K. S. McKissic, J. T. Caruso, R. G. Blair, J. Mack, Green Chem., 2014, 16, 1628; b) R. Schmidt, C. F. Burmeister, M. Baláž, A. Kwade, A. Stolle, *Org. Process Res. Dev.*, **2015**, *19*, 427; c) K. Užarevic´, V. Štrukil, C. Mottillo, P. A. Julien, A. Puškarić, T. Friščić, I. Halasz, *Cryst. Growth Des*., **2016**, *16*, 2342; d) A. Jayasankar, A. Somwangthanaroj, Z. J. Shao and N. Rodríguez-Hornedo, *Pharm. Res*., **2006**, *23*, 2381.

79 a) F. Schneider, T. Szuppa, A. Stolle, B. Ondruschka, H. Hopf, *Green Chem*., **2009**, *11*, 1894; b) A. Stolle, *Technical Implications of Organic Synthesis in Ball Mills, in Ball Milling Towards Green Synthesis – Applications, Projects, Challenges*, ed. A. Stolle and B. C. Ranu, RSC Green Chemistry, **2014**.

80 a) W. J.W.Watson, *Green Chem*., **2012**, *14*, 251; b) J. Rantanen, J. Khinast, *J. Pharm. Sci*., **2015**, *104*, 3612; c) C. Jiménez-González, D. J. C. Constable, C. S. Ponder, *Chem. Soc. Rev*., **2012**, *41*, 1485; d) D. J. C. Constable, A. D. Curzons, L. M. Freitas dos Santos, G. R. Geen, R. E. Hannah, J. D. Hayler, J. Kitteringham, M. A. McGuire, J. E. Richardson, P.

Smith, R. L. Webb, M. Yu, *Green Chem*., **2001**, *3*, 7; e) P. J. Dunn, *Chem. Soc. Rev*., **2012**, *41*, 1452.

81 P. Baláž, *Mechanochemistry in Nanoscience and Minerals Engineering*, **2008**, Springer-Verlag, Berlin.

82 A. Y. Ibrahim, R. T. Forbes, N. Blagden, *CrystEngComm*, **2011**, *13*, 1141.

83 T. Ervasti, J. Aaltonen, J. Ketolainen, *Int. J. Pharm.*, **2015**, *486*, 121.

84 a) Z. Zhang, Y.-W. Dong, G.-W. Wang, K. Komatsu, *Chem. Lett*., **2004**, *33*, 168; b) Z. Zhang, Y.-W. Dong, G.-W. Wang, K. Komatsu, *Synlett*., **2004**, 61.

85 a) C. Jia, D. Chen, C. Zhang, Q. Zhang, B. Cao, Z. Zhao, *Tetrahedron*, **2013**, *69*, 7320; b) E. Veverková, V. Poláčková, L. Liptaková, E. Kázmerová, M. Mečiarová, Š. Toma, R. Šebesta, *ChemCatChem*, **2012**, *4*, 1013; c) Y.-F. Wang, R.-X. Chen, K. Wang, B.-B. Zhang, Z.-B. Li, D.-Q. Xu, *Green Chem*., **2012**, *14*, 893; d) M. Jörres, S. Mersmann, G. Raabe, C. Bolm, *Green Chem*., **2013**, *15*, 612; e) M. Hestericovà, R. Šebesta, *Tetrahedron*, **2014**, *70*, 901.

86 a) C. L. Raston, J. L. Scott, *Green. Chem*., **2000**, *2*, 49; b) G. Kaupp, M. R. Naimi-Jamal, J. Schmeyers, *Chem. Eur. J*., **2002**, *8*, 594; c) A. S. Heintz, J. E. Gonzales, M. J. Fink, B.S. Mitchell, *J. Mol. Catal. A Chem*., **2009**, *304*, 117.

87 a) G. Guillena, M. del Carmen Hita, C. Nájera, S. F. Viózquez, *Tetrahedron Asymm*., **2007**, *18*, 2300; b) G. Guillena, M. del Carmen Hita, C. Nájera C, S. F. Viózquez, *Org. Chem*., **2008**, *73*, 5933; c) D. Almaşi, D. A. Alonso, C. Nájera, *Adv. Synth. Catal*., **2008**, *350*, 2467; d) J. Hernández, E. Juaristi, *J. Org. Chem*., **2011**, *76*, 1464; e) J. G. Hernández, E. Juaristi, *Tetrahedron*, **2011**, *67*, 6953; f) J. G. Hernández, V. García-López, E. Juaristi, *Tetrahedron*, **2012**, *68*, 92; g) E. Machuca, Y. Rojas, E. Juaristi, *Asian J. Org. Chem*., **2015**, *4*, 46; h) B. Rodríguez, A. Bruckmann, C. Bolm, *Chem. Eur. J*., **2007**, *13*, 4710; i) B. Rodríguez, T. Rantanen, C. Bolm, *Angew. Chem. Int. Ed*., **2006**, *45*, 6924.

88 J. Mack, M. Shumba, *Green. Chem*., **2007**, *9*, 328.

89 a) S. Wada, H. Suzuki, *Tetrahedron Lett*., **2003**, *44*, 399; b) G. Kaupp, M. R. Naimi-Jamal, J. Schmeyers, *Tetrahedron*, **2003**, *59*, 3753; c) C. F. Burmeister, A. Stolle, R.

Schmidt, K. Jacob, S. Breitung-Faes, A. Kwade, *Chem. Eng. Technol*., **2014**, *37*, 857; d) R. Trotzki, M. M. Hoffmann, B. Ondruschka, *Green Chem*., **2008**, *10*, 767.

90 S. Wada, N. Hayashi, H. Suzuki, *Org. Biomol. Chem*., **2003**, *1*, 2160.

91 a) G.-W. Wang, L. Liu, Chin. Chem. Lett., 2004, 15, 587; b) K. Tanaka, S. Kishigimi, F. Toda, *J. Org. Chem.*, **1990**, *55*, 2981.

92 J. M. Harrowfield, R. J. Hart, C. R. Whitaker, *Aust. J. Chem*., **2001**, *54*, 423

93 a) V. P. Balema, J. W. Wiench, M. Pruski, V. K. Pecharsky, *J. Am. Chem. Soc*., **2002**, *124*, 6244; b) W. C. Shearouse, J. Mack, *Green Chem*., **2012**, *14*, 2771; c) A. Baron, J. Martinez, F. Lamaty, *Tetrahedron Lett*., **2010**, *51*, 6246.

94 a) M. Jörres, J. L. Aceña, V. A. Soloshonok, C. Bolm, *ChemCatChem*, **2015**, *7*, 1265; b) P. Nun P, V. Pérez, M. Calmès, J. Martinez, F. Lamaty, *Chem. Eur. J*., **2012**, *18*, 3773.

95 C. Falenczyk, B. Pölloth, P. Hilgers, B. König, *Synth. Commun*., **2014**, *45*, 348.

96 M. O. M'hamed, O. K. Alduaij, *Phosph. Sulfur Silicon*, **2014**, *189*, 235.

97 a) T. Shy, P. Mackin, A. S. Orvieto, D. Gharbharan, G. R. Peterson, N. Bampos, T. D. Hamilton, *Faraday Discuss*., **2014**, *170*, 59; b) G. Kaupp, J. Schmeyers, J. Boy, *J. Prakt. Chem*., **2000**, *342*, 269; c) Y.-W. Dong, G.-W. Wang, L. Wang, *Tetrahedron*, **2008**, *64*, 10148.

98 a) Z. Zhang, Z.-W. Peng, M.-F. Hao, J.-G. Gao*, Synlett*., **2010**, *19,* 2895; b) H. Watanabe, M. Senna, *Tetrahedron Lett*., **2005**, *46*, 6815; H. Watanabe, R. Hiraoka, M. Senna, *Tetrahedron Lett*., **2006**, *47*, 4481; c) Y.-J. Tan, Z. Zhang, F.-J. Wang, H.-H. Wu, Q.-H. Li, *RSC Adv*., **2014**, *4*, 35635; d) Y. Murata, B. Kato, K. Fujiwara, K. Komatsu, *J. Org. Chem.* **1999**, *64*, 3483.

99 a) P. T. Lang, A. M. Harned, J. E. Wissinger, *J. Chem. Educ*., **2011**, *88*, 652; b) R. Thorwirth, F. Bernhardt, A. Stolle, B. Ondruschka, J. Asghari, *Chem. Eur. J*., **2010**, *16*, 13236; c) I. Huskić, I. Halasz, T. Friščić, H. Vančik, *Green Chem*., **2012**, *14*, 1597; d) S. L. Collom, P. T. Anastas, E. S. Beach, R. H. Crabtree, N. Hazari, T. J. Sommer, *Tetrahedron Lett*., **2013**, *54*, 2344; e) W. C. Shearouse, C. M. Korte, J. Mack, *Green Chem.*, **2011**, *13*, 598; f) G. Cravotto, D. Garella, D. Carnaroglio, E. Calcio Gaudino, O. Rosati, *Chem. Commun*., **2012**, *48*, 11632; g) T. K. Achar, S. Maiti, P. Mal, *RSC Adv*., **2014**, *14*, 12834.

100 a) F. Toda, K. Kiyoshige, M. Yagi, *Angew. Chem. Int. Ed. Engl*., **1989**, *28*, 320; b) M. R. Naimi-Jamal, J. Mokhtari, M. G. Dekamin, G. Kaupp, *Eur. J. Org. Chem*., **2009**, 3567; c) J. Mack, D. Fulmer, S. Stofel, N. Santos, *Green Chem*., **2007**, 1041.

101 a) T. Friščić, L. R. MacGillivray, *Chem. Commun*., **2005**, 5748; b) T. Friščić, L. R. MacGillivray, *Supramol. Chem*., **2005**, *17*, 47.

102 a) V. Stilinović, D. Cinčić, M. Zbačnik, B. Kaitner, *Croat. Chem. Acta*., **2012**, *85*, 485; b) M. Zbačnik, I. Nogalo, D. Cinčić, B. Kaitner, *CrystEngComm*, **2015**, *17*, 7870; c) T. Friščić, W. Jones, *Cryst. Growth Des*., **2009**, *9*, 1621; d) D. Cinčić, I. Brekalo, B. Kaitner, *Cryst. Growth Des*., **2012**, *12*, 44.

103 a) M. Tyagi, D. Khurana, K. P. R. Kartha, *Carbohydr Res*., **2013**, *379*, 55; b) X. Zhu, Z. Li, Q. Shu, C. Zhou, W. Su, *Synth. Commun.*, **2009**, *39*, 4199; c) S. Menuel, B. Doumert, S. Saitzek, A. Ponchel, L. Delevoye, E. Monflier, F. Hapiot, *J. Org. Chem*., **2015**, *80*, 6259.

104 a) W. C. Waddell, I. Thiel, A. Bunger, D. Nkata, A. Maloney, T. Clark, B. Smith B, J. Mack, *Green Chem*., **2011**, *13*, 3156; b) L. Konnert, A. Gauliard, F. Lamaty, J. Martinez, E. Colacino, *ACS Sustain Chem. Eng*., **2013**, *1*, 1186.

105 T. Chatterjee, D. Saha, B. C. Ranu, *Tetrahedron Lett*., **2012**, *53*, 4142.

106 a) V. Štrukil, M. D. Igrc, M. Eckert-Maksić, T. Friščić, *Chem. Commun.,* **2012**, *48*, 9705; b) V. Štrukil, M. D. Igrc, L. Fábián, M. Eckert-Maksić, S. L. Childs, D. G. Reid, M. J. Duer, I. Halasz, C. Mottillo, T. Friščić, *Green Chem*., **2012**, *14*, 2462; c) V. Štrukil, M. D. Igrc, M. Eckert-Maksić, T. Friščić, *Chem. Eur. J*., **2012**, *18*, 8464; d) M. Đud, O. V. Magdysyuk, D. Margetić, V. Štrukil, *Green Chem.*, **2016**, *18*, 2666.

107 R. Bates, *Organic Synthesis Using Transition Metals*, 2nd Ed., **2012**, John Wiley & Sons Ltd.

108 a) D. Braga, D. D'Addario, M. Polito, *Organometallics*, **2004**, *23*, 2810; b) S. F. Nielsen, D. Peters, O. Axelsson, *Synth. Commun.*, **2000**, *30*, 3501; c) L. M. Klingensmith, N. E. Leadbeater, *Tetrahedron Lett*., **2003**, *44*, 765.

109 a) E. Tullberg, D. Peters, T. Frejd, *J. Organomet. Chem*., **2004**, *689*, 3778; b) E. Tullberg, F. Schacher, D. Peters, T. Frejd, *Synthesis*, **2006**, *7*, 1183; c) X. Zhu, J. Liu, T.

Chen, W. Su, *Appl. Organometal. Chem.*, **2012**, *26*, 145; d) V. Declerck, E. Colacino, X. Bantreil, J. Martinez, F. Lamaty, *Chem. Commun*., **2012**, *48*, 11778.

110 a) D. A. Fulmer, W. C. Shearouse, S. T. Mendoza, J. Mack, *Green Chem*., **2009**, *11*, 1821; b) R. Thorwirth, A. Stolle, B. Ondruschka, *Green Chem*., **2010**, *12*, 985; c) A. Stolle, B. Ondruschka, *Pure. Appl. Chem*., **2011**, *83*, 1343.

111 a) R. Schmidt, R. Thorwirth, T. Szuppa, A. Stolle, B. Ondruschka, H. Hopf, *Chem. Eur. J.*, **2011**, *17*, 8129; b) L. Chen, B. E. Lemma, J. S. Rich, J. Mack, *Green Chem*., **2014**, *16*, 1101.

112 a) P. L. Golas, K. Matyjaszewski, *Chem. Soc. Rev*., **2010**, *39*, 1338; b) L. Liang, D. Astruc, *Coord. Chem. Rev*., **2011**, *255*, 2933.

113 a) R. Thorwirth, A. Stolle, B. Ondruschka, A. Wild, U. S. Schubert, *Chem. Commun*., **2011**, *47*, 4370; b) T. L. Cook, J. A. Walker Jr, J. Mack, *Green Chem*., **2013**, *15*,617; c) N. Mukherjee, S. Ahammed, S. Bhadra, B. C. Ranu, *Green Chem*., **2013**, *15*, 389.

114 a) G. W. Oakley, K. B. Wagener, *Macromol. Chem. Phys*., **2005**, *206*, 15; b) M. D. Watson, K. B. Wagener, *Macromolecules*, **2000**, *33*, 1494.

115 A. McNally, B. Haffemayer, B. S. L. Collins, M. J. Gaunt, *Nature*, **2014**, *510*, 129.

116 a) K. Godula, D. Sames, *Science*, **2006**, *312*, 67; b) T. W. Lyons, M. S. Sanford, *Chem. Rev*., **2010**, *110*, 1147; c) L. Ackermann, *Chem. Rev*., **2011**, *111*, 1315; d) J. Yamaguchi, A. D. Yamaguchi, K. Itami, *Angew. Chem. Int. Ed*., **2012**, *51*, 8960.

117 J. G. Hernández, C. Bolm, *Chem. Commun*., **2015**, *51*, 12582.

118 V. D. Makhaev, A. P. Borisov, L. A. Petrova, *J. Organomet. Chem*., **1999**, 590, 222.

119 a) L. Chen, M. O. Bovee, B. E. Lemma, K. S. M. Keithley, S. L. Pilson, M. G. Coleman, J. Mack, *Angew. Chem. Int. Ed*., **2015**, *54*, 11084; b) R. A. Haley, A. R. Zellner, J. A. Krause, H. Guan, J. Mack, *ACS Sustainable Chem. Eng*., **2016**, *4*, 246.

120 G.-W. Wang, K. Komatsu, Y. Murata, M. Shiro, *Nature*, **1997**, *387*, 583.

121 a) D. Tan, C. Mottillo, A. D. Katsenis, V. Štrukil, T. Friščić, *Angew. Chem. Int. Ed*., **2014**, *53*, 9321; b) A. Beillard, T.-X. Métro, X. Bantreil, J. Martinez, *Chem. Sci.,* **2017**, *DOI: 10.1039/c6sc03182j*.

122 D. Tan, L. Loots, T. Friščić, *Chem. Commun*., **2016**, *52*, 7760.

123 a) A. Delori, T. Friščić, W. Jones, *CrystEngComm*, **2012**, *14*, 2350; b) D. R. Weyna, T. Shattock, P. Vishweshwar, M. J. Zaworotko, *Cryst. Growth Des.* **2009**, *9*, 1106; c) N. Shan, M. L. Perry, D. R. Weyna, M. J. Zaworotko, *Exp. Opinion Drug Met. Tox*., **2014**, *10*, 1255; d) S. Karki, T. Friščić, W. Jones, W. D. S. Motherwell, *Mol. Pharm.,* **2007**, *4*, 347; e) S. Domingosa, V.Andréa, S. Quaresmaa, I. C. B. Martinsa, M. Fátima Minas da Piedadea, M. T. Duarte, *J. Pharma. Pharma*., **2015**, *67*, 830; f) L. Trőbs, F. Emmerling*, Faraday Discuss*., **2014**, *170*, 109.

124 T. N. Drebuschak, A. A. Ogienko, E. V. Boldyreva, *CrystEngComm*, **2011**, *13*, 4405.

125 P. D. Garn, T. S. Habash, *J. Phys. Chem.*, **1979**, *83*, 229.

126 D.-K. Bučar, G. M. Day, I. Halasz, G. G. Z. Zhang, J. R. G. Sander, D. G. Reid, L. R. MacGillivray, M. J. Duer, W. Jones, *Chem. Sci.*, **2013**, *4*, 4417.

127 D.-K. Bučar, R. F. Henry, C. Lou, T. B. Borchardt, G. G. Z. Zhang, *Chem. Commun*., **2007**, 525.

128 D.-K. Bučar, R. W. Lancaster, J. Bernstein, *Angew. Chem., Int . Ed.*, **2015**, *54*, 6972.

129 a) E. H. H. Chow, F. Strobridge, T. Friščić, *Chem. Commun.*, **2010**, *46*, 6368; b) J. Parojčić, O. I. Corrigan, *Eur. J. Pharm. Biopharm.*, **2008**, *69*, 640.

130 J. Galcera, T. Friščić, K. Hejczyk, L. Fábián, S. M. Clarke, G. M. Day, E. Molins, W. Jones, *CrystEngComm*, **2012**, *14*, 7898.

131 S. R. Bysouth, J. A. Bis, D. Igo, *Int. J. Pharm.*, **2011**, *411*, 169.

132 a) T. Friščić, R.W. Lancaster, L. Fábián, P. G. Karamertzanis, *Proc. Natl. Acad. Sci. U. S. A*., **2010**, *107*, 13216; b) K. J. Ardila-Fierro, V. André, D. Tan, M. T. Duarte, R. W. Lancaster, P. G. Karamertzanis, T. Friščić, *Cryst. Growth Des.*, **2015**, *15*, 1492.

133 J. Bonnamour, T.-X. Métro, J. Martinez, F. Lamaty, *Green Chem.*, **2013**, *15*, 1116.

134 W. J. Lukiw, *Cell. Mol. Neurobiol.*, **2006**, *26*, 1003.

135 L. Konnert, B. Reneaud, R. M. Figueiredo, J.-M. Campagne, F. Lamaty, J. Martinez, E. Colacino, *J. Org. Chem.*, **2014**, *79*, 10132.

136 a) L. Konnert, B. Reneaud, R. M. Figueiredo, J.-M. Campagne, F. Lamaty, J. Martinez and E. Colacino, *J. Org. Chem.*, **2014**, *79*, 10132; b) M. Dhanawat, A. G. Banerjee, S. K. Shrivastava, *Med. Chem. Res.*, **2011**, *21*, 2807; c) L. Konnert, M. Dimassi, L. Gonnet, F. Lamaty, J. Martinez and E. Colacino, *RSC Adv*., **2016**, *6*, 36978.

137 a) D. Tan, V. Štrukil, C. Mottillo, T. Friščić, *Chem. Commun.,* **2014**, ***50***, 5248; b) R. Heinrich, A. Walter, K. Gerhard, W. Hans, S. Josef, B. Alfred, *US Patent*, **1961**, *US2968158A*; c) J. Cervello, T. Sastre, *Synthesis*, **1990**, 221; d) V. Štrukil, B. Bartolec, T. Portada, I. Dilović, I. Halasz and D. Margetic, *Chem. Commun.,* **2012**, *48*, 12100.

138 a) V. R. Pattabiramen, J. W. Bode, *Nature,* **2011**, *480*, 471; b) R. M. Lanigan, T. D. Sheppard, *Eur. J. Org. Chem.,* **2013**, *33*, 7453.

139 a) T.-X. Métro, J. Bonnamour, T. Reidon, J. Sarpoulet, J. Martinez, F. Lamaty, *Chem. Commun.,* **2012**, *48*, 11781; b) J. G. Hernández and E. Juriasti, *J. Org. Chem.,* **2010**, *75,* 7107.

140 Duangkamol, S. Jaita, S. Wangngae, W. Phakhodee, M. Pattawarapan, *RSC Adv.*, **2015**, *5*, 52624.

141 a) A. G. Silva, G. Zapata-Suto, A. E. Kummerle, C. A. M. Fraga, E. J. Barreiro, R. T. Sudo, *Bioorg. Med. Chem.,* **2005**, *13*, 3431-3437; b) D. R. Dabideen, K. F. Cheng, B. Aljabari, E. J. Miller, V. A. Pavlov, Y. Al-Abed, *J. Med. Chem.,* **2007**, *50*, 1993-1997; c) N. Belkheri, B. Bougerne, F. Bedos-Beval, H. Duran, C. Bernis, R. Salvayre, A. Négre-Salvayre, M. Baltas, *Eur. J. Med. Chem.,* **2010**, *45*, 3019.

142 P. F. M. Oliveira, M. Baron, A. Chamayou, C. André-Barrés, B. Guidetti, M. Baltas, *RSC Adv.,* **2014**, *4*, 56736.

143 T. Magyar, F. Miklós, L. Lázár, F. Fülöp, *Chem. Heterocyclic Compd.,* **2015**, *50*, 1463.

144 S. Singh, A. Chopra, G. Singh, A. K. Saxena, M. Paul, S. Ishar, *J. Pharmacol. Res.*, **2013**, *7*, 337.

145 Z. T. Bhutia, G. P., A. Malik, V. Kumar, A. Chatterjee, B. G. Roy, M. Banerjee, *RSC Adv.,* **2015**, ***5***, 99566.

146 a) P. Jimonet, F. Audiau, M. Barreau, J.-C. Blanchard, A. Boireau, Y. Bour, M.-A. Coléno, A. Doble, G. Doerflinger, C. D. Huu, M.-H. Donat, J. M. Duchesne, P. Ganil, C. Guérémy, E. Honoré, B. Just, R. Kerphirique, S. Gontier, P. Hubert, P. M. Laduron, J. L. Blevec, M. Meunier, J.-M. Miquet, C. Nemecek, M. Pasquet, O. Piot, J. Pratt, J. Rataud, M. Reibaud, J.-M. Stutzmann, S. Mignani, *J. Med. Chem.,* **1999**, *42*, 2828; b) L. J. Scott, C. J. Dunn, G. Mallarkey, M. Sharpe, *Drugs,* **2002**, *62*, 1503; c) H. Al Muhaimeed, *J. Int. Med. Res.,* **1997**, ***25***, 175.

147 M. Banerjee, A. Chatterjee, V. Kumar, Z. T. Bhutia, D. G. Khandare, M. S. Majik, B. G. Roy, *RSC Adv.,* **2014**, *4*, 39606.

148 a) K.K. Ogilvie,M. J. Nemer, J.Mona, G. H. Hakimelahi, Z. A. Zbigniew, M. Lucas, *Tetrahedron Lett.,* **1982**, *26*, 2615; b) G. H. Hakimelahi, Z. A. Proba, K. K. Ogilvie, *Can. J. Chem.,* **1982**, *60*, 1106.

149 N. Giri, C. Bowen, J. S. Vyle, S. L. James, *Green Chem.,* **2008**, *10*, 627.

150 F. Ravalico, S. L. James, J. S. Vyle, *Green Chem.,* **2011**, *13*, 1778.

151 F. Ravalico, I. Messina, M. V. Berberian, S. L. James, M. E. Migaud, J. S. Vyle, *Org. Biomol. Chem.,* **2011**, *9*, 6496.

152 a) P. Chauhan and S. S. Chimni, *Beilstein J. Org. Chem.,* **2012**, *8,* 2132; b) P. Chauhan and S. S. Chimni, *Asian J. Org. Chem.,* **2012**, *1*, 138.

153 M. Srivastava, P. Rai, J. Singh and J. Singh, *RSC Adv.,* **2014**, *4*, 30592.

154 a) B. K. S. Yeung, B. Zou, M. Rottmann, S. B. Lakshminarayana, S.-H. Ang, S. Y. J. Tan, J. Wong, S. Keller-Maerki, C. Fischli, A. Goh, E. K. Schmitt, P. Krastel, E. Francotte, K. Kuhen, D. Plouffe, K. Henson, T. Wagner, E. A. Winzeler, F. Petersen, B. Reto, V. Dartois, T. T. Diagana, T. H. Keller, *J. Med. Chem.,* **2010**, ***53***, 5155; b) K. Ding, Y.-P. Lu, Z. Nikolovska-Coleska, G.-P. Wang, S. Qiu, S. Shangary, W. Gao, D.-G. Qin, J. Stuckey, K.

Krajewski, P. P. Roller, S.-M. Wang, *J. Med. Chem.,* **2006**, *49*, 3432; c) A. Nandakumar, P. Thirumurugan, P. T. Perumal, P. Vembu, M. N. Ponnuswamy, P. Ramesh, *Bioorg. Med. Chem. Lett.,* **2010**, *20*, 4252.

155 a) P. Calvert, *Chem. Mater.*, **1996**, *8*, 1715; b) H. M.Wache, D. J. Tartakowska, A.Hentrich, M. H.Wagner, *J. Mater. Sci.: Mater. Med.*, **2003**, *14*, 109; c) I. Bellin, S. Kelch, R. Langer, A. Lendlein, *Proc. Natl. Acad. Sci. U. S. A.*, **2006**, *103*, 18043; d) A. Metcalfe, A.-C. Desfaits, I. Salazkin, L. Yahia, W. M. Sokolowski, J. Raymond, *Biomaterials*, **2003**, *24*, 491.

156 a) N. Spencer, J. F. Stoddart, *J. Am. Chem. Soc.*, **1991**, *113*, 5131; b) R. A. Bissell, E. Cordova, A. E. Kaifer, J. F. Stoddart, *Nature*, **1994**, *369*, 133; c) L. Fang, M. Hmadeh, J. Wu, M. A. Olson, J. M. Spruell, A. Trabolsi, Y.-W. Yang, M. Elhabiri, A.-M. Albrecht-Gary, J. F. Stoddart, *J. Am. Chem. Soc.*, **2009**, *131*, 7126; d) D. A. Leigh, J. K. Y. Wong, F. Dehez, F. Zerbetto, *Nature*, **2003**, *424*, 174.

157 J. Gigg, R. Gigg, S. Payne, R. Conant, *J. Chem. Soc., Perkin Trans.* 1, **1987**, 2411.

158 M. –X. Zhang, P. M. Kelly, *Prog. Mater. Sci.*, **2009**, 54, 1101; b) C. M. Wayman, H. K. D. H. Bhadeshia, *Physical Metallurgy*, 4th ed.; Cahn, R. W., Haasen, P., Eds., Elsevier Science BV: New York, **1996**, 1507.

159 a) P. Radziszewski, *Wear*, **1933**, *169*, 77; b) P. Radziszewski, S. Tarasiewicz, *Wear*, **1933**, *169*, 309; c) A. K. Gangopadhyay, *Wear*, **1987**, *144*, 249; d) I. Iwasaki, R. L. Pozzo, K. A. Natarajan, K. Adam, J. N. Orlich, *Int. J. Mineral Proc.*, **1988**, *22*, 345; e) D. Gavrilov, O. Vinogradov, W. J. D. Shaw, *Powder Tech.*, **1999**, *101*, 63; f) A. Concas, N. Lai, M. Pisu, G. Cao, *Chem. Eng. Sci*., **2006**, *61*, 3746.

160 a) C. F. Burmeister, A. Kwade, *Chem. Soc. Rev.,* **2013**, *42*, 7660; b) R.Schmidt, C. F. Burmeister, M. Baláž, A. Kwade, A. Stolle, *Org. Process Res. Dev*., **2015**, *19*, 427.

161 F. C. Stobridge, N. Judaš, T. Friščić, *Crystengcomm*, **2010**, *12*, 2409.

162 K. C. Neuman, A. Nagy, *Nature Methods*, **2008**, *5*, 491.

CHAPTER 2

MECHANOSYNTHESIS OF PHARMACEUTICALLY RELEVANT SULFONYL-(THIO)UREAS

"Chemistry is about telling a story." –Prof. Louis A. Cuccia, Centre for Self-Assembled Chemical Structures (CSACs) seminar, 2013.

2.1 Introduction and connecting text.

The work presented in this chapter is a part of a published paper entitled "Mechanosynthesis of pharmaceutically relevant sulfonyl-(thio)ureas", discussing the mechanochemical synthesis of anti-diabetic sulfonylurea APIs using a base-mediated, as well as a copper-catalyzed methodology. The paper was written by D. Tan with guidance and editing contributions from Prof. T. Friščić, and co-authored with Dr. V. Štrukil and Dr. C. Mottillo. The text has been formatted and re-written for inclusion in this Dissertation. All experimental results, including screening, synthesis and characterization (FTIR-ATR, NMR, MS) of the various compounds were performed by D. Tan, with help from Dr. V. Štrukil and Dr. C. Mottillo for the collection of the single crystal X-ray diffraction (SCXRD) data. This work has been re-written for inclusion in this chapter with additional results. In the previous chapter, the role of mechanochemistry for the synthesis of new solid forms of APIs by making salts, solvates, polymorphs and cocrystals were discussed. It was also mentioned that there is a growing field of research involving the use of mechanochemistry for the synthesis of API molecules through covalent bond formation. In this chapter, one of the contributions to this emerging field of medicinal mechanochemistry will be discussed.

Mechanochemical reactions,[1] *i.e.* chemical reactions induced or sustained by mechanical force, is one of the most successful modes of solvent-free synthesis. Whereas mechanochemistry has led to important improvements in diverse areas of chemical synthesis (*e.g.* pharmaceutical materials, metallodrugs,[2] metal-organic frameworks,[3] nanoparticles[4]) one of the most important areas of its application and development remains organic chemistry.[5] Several research groups have recently demonstrated the potential of mechanochemistry in a number of important areas of organic chemistry, including organo-[6] and transition metal-catalyzed reactions,[7] (oligo)peptide synthesis[8] and enantioselective transformations.[9] Importantly, Lamaty and coworkers have recently demonstrated the ability to construct relatively complex molecular targets, such as Leu-enkephaline,[10] through a combination of several exclusively solvent-free synthetic steps. Although mechanosynthesis has been widely employed for the formation of hydrogen-bonded cocrystals of pharmaceutical drugs,[12a] including notable works on *in situ* monitoring of such reactions by use of a high power synchrotron radiation source,[12b] the use of mechanochemical synthesis for covalent synthesis of API molecules has not been explored. We have recently established mechanochemistry as a useful methodology to conduct click solvent-free (thio)urea synthesis by coupling of amines and iso(thio)cyanates, providing a simple means for the

desymmetrization of organic diamines and access to chiral organocatalysts.[11] Using this as a foundation to explore the mechanosynthesis of API molecules, we now describe two mechanochemical synthetic pathways to sulfonyl-ureas and sulfonyl-thioureas as targets structurally similar to (thio)ureas. A number of sulfonyl-ureas are known as highly potent commercial anti-diabetic drugs[12] (Fig. 2.1a), providing an additional impetus to develop cleaner and more efficient solvent-free methodologies for their synthesis. Indeed, the development of solvent-free synthetic procedures is one of the most heavily expected developments in environmentally-friendly pharmaceutical chemistry.[13]

2.2 One-pot two-step base-assisted synthesis of 1st generation sulfonylurea APIs

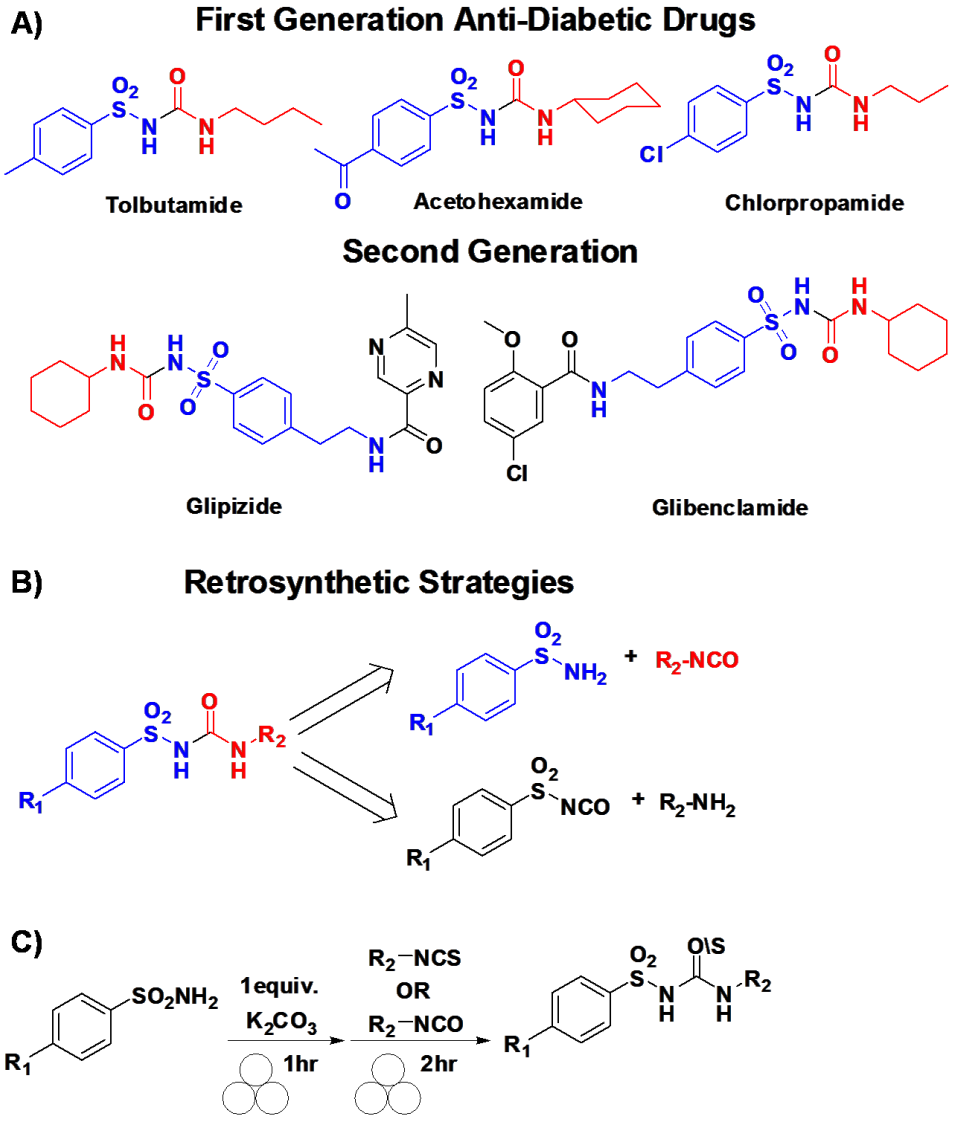

Fig 2.1. a) Examples of first and second generation anti-diabetic sulfonyl-urea APIs. b) Retrosynthetic analysis for the formation of sulfonyl-urea moiety. c) Two step mechanosynthesis by first activation of the poorly nucleophilic sulfonamide using a base and subsequent coupling with isocyanates.

We first considered two possible retrosynthetic pathways (Fig. 2.1b) for developing a mechanochemical approach to sulfonyl-ureas: the coupling of sulfonamides with isocyanates or the coupling of sulfonyl-isocyanates with organic amines. The highly reactive and corrosive nature of sulfonyl-isocyanates[14] led us to opt for the former pathway as the one more compatible with the logic of green and sustainable chemistry.[15] As our first entry into the mechanosynthesis of sulfonyl-ureas we explored the reaction of toluylsulfonamide with *n*-butyl isocyanate, expected to generate the anti-diabetic tolbutamide (**1a**) (Fig. 2.1a). Simple milling of the two reagents did not lead to a reaction, most likely due to the poorly nucleophylic nature of sulfonamides, caused by the highly electron-withdrawing sulphonyl group.[16] To activate the sulfonylamide NH_2 group, we explored a two-step mechanochemical approach in which the sulfonamide was first deprotonated by milling with one equivalent of K_2CO_3 and then, in the same pot, with one equivalent of *n*-butyl isocyanate (Fig. 2.1c).

Such procedure gave **1a** in 88% yield after acidic aqueous workup. Next, we expanded this base-assisted mechanochemical protocol to aromatic isocyanates and thioisocyanates (Table 2.1). Reactions yielded respective sulfonyl-(thio)ureas in 80%-90% isolated yields. The formation of *N*-tolylsulfonyl-*N*'-phenylthiourea **1d** (Fig. 2.2a) was confirmed by X-ray structure determination from single crystals obtained after work-up. Also, recrystallization of the crude reaction mixture (prior to acid workup) from the synthesis of *N*-tolylsulfonyl-*N*'-(4-nitrophenyl)thiourea **1e** gave single crystals of its potassium salt with acetone solvate (Fig. 2.2b), whose structure revealed the deprotonation of the sulfonyl-thiourea nitrogen atom, confirming the role of K_2CO_3 in deprotonating the sulfonamide group (Fig 2.2). The relevant XRD crystallographic details can be found in *Appendix A*. An alternative reaction pathway to form **1a** using *p*-tolylsulfonyl-isocyanate and *n*-butylamine was also performed mechanochemically. This reaction yielded **1a** in 93% yield. However, the high reactivity and moisture sensitive nature of *p*-toluenesulfonyl-isocyanate meant that prior to the reaction, preparation had to be done in a glovebox. Thus sulfonyl-isocyanates (mostly liquids) in general are less ideal, in terms of ease of handling, as compared to sulfonamides (mostly solids). For further experimental details, please refer to *Chapter 8, Section 8.1.3.*

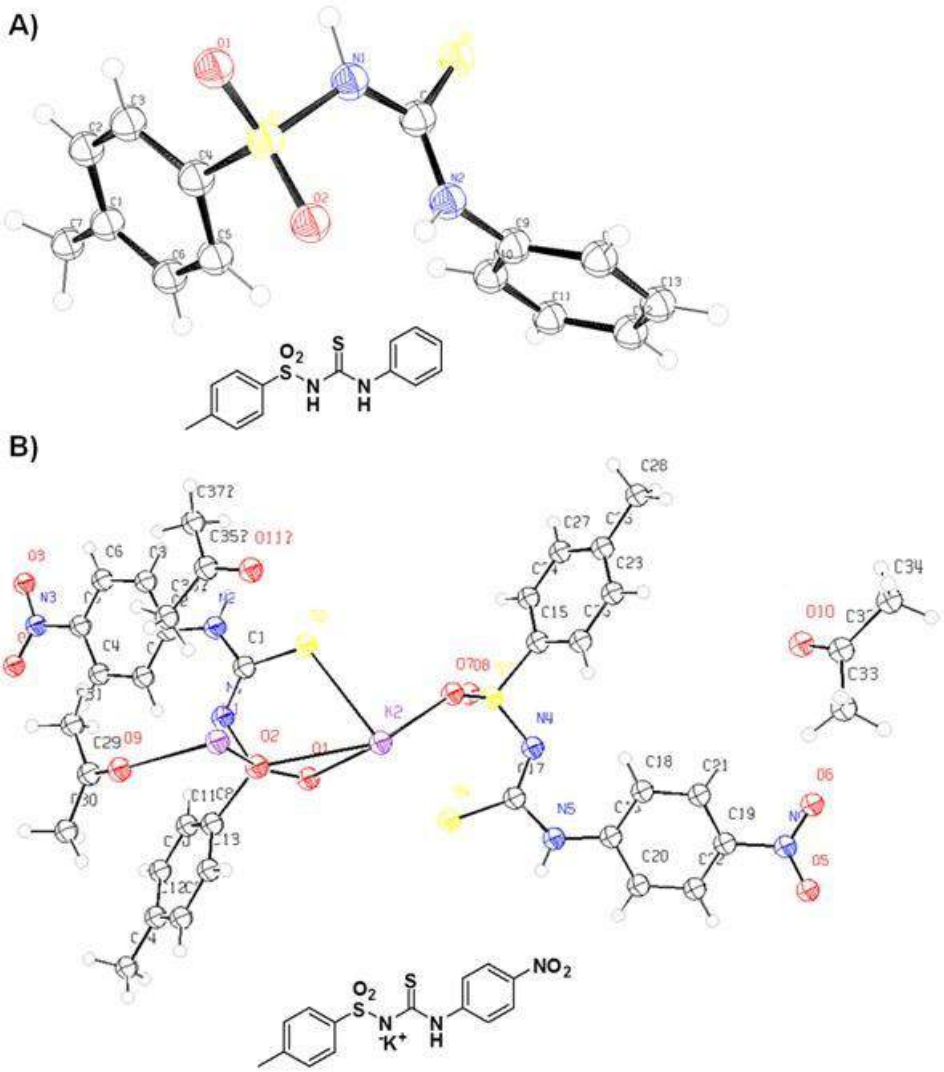

Fig 2.2. Molecular structure of (a) **1d** and (b) potassium salt of **1e** with acetone, visualized using ORTEP-3 with thermal ellipsoids at 50% probability as determined by SCXRD, along with Chemdraw images of the compound. Detailed crystallographic information can be found in *Appendix A*.

Table 2.1. Results of optimized two-step mechanosyntheses of sulfonyl-(thio)ureas using K_2CO_3.

Compound	R_1	R_2-NCO or R_2-NCS	Yield (%)[a]
1d	Me	phenyl-NCS	91
1e	Me	4-NO_2-phenyl-NCS	80
1f	Me	phenyl-NCO	93

[a]Isolated yield after aqueous workup.

2.3 Copper-catalyzed direct coupling.

Despite the demonstrated potential in the synthesis of sulfonyl-(thio)ureas, the so far developed mechanochemical protocol still depended on using a stoichiometric amount of sacrificial base. Consequently, we decided to explore further modes of mechanochemical reactivity that would avoid using a stoichiometric base. In 1990, Cervello and Sastre reported the direct coupling of 4-methylbenzenesulfonamide with various isocyanates using CuCl as a catalyst.[17] The reactions used *N*,*N*-dimethylformamide (DMF) as a solvent, and the reactant mixture was stirred at ambient temperature for 21 hours, affording desired sulfonylureas in good to excellent yields (46-98%). Intrigued by this report, we explored if **1a** could be synthesized in a catalytic mechanochemical process from 4-methylbenzenesulfonamide and *n*-butylisocyanate, using CuCl as a catalyst (Fig. 2.3).

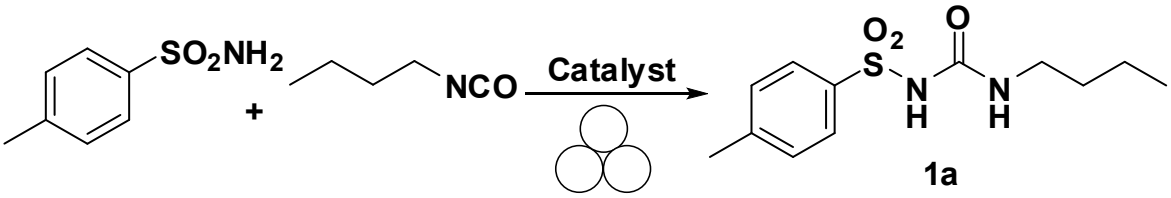

Fig 2.3. Direct coupling of sulfonamide and isocyanate to synthesize tolbutamide **1a** mechanochemically.

To our delight, the reaction readily provided a good yield (68%) of **1a** after only 2 hours milling with 5 mol% CuCl (Table 2.2, entry 1). Experimental details on conducting the CuCl-catalyzed reaction can be found in *Chapter 8 Section 8.1.2* and the details of characterization of the product **1a** can be found in *Appendix A*. The yield was further improved to 91% by using a larger amount (20 mol%) of CuCl (Table 2.2, Entry 2). To further optimize the reaction conditions we conducted several liquid-assisted grinding (LAG)[18] experiments using different catalytic liquid additives (Table 2.2, Entries 1-7). It was previously proposed that adding a catalytic amount of a liquid to a mechanochemical reaction could enable its modification and optimisation in a manner similar to switching bulk solvents in conventional synthesis.[19] Although there is no observable trend in the type of LAG liquid used, CH_3NO_2 was found to the best LAG liquid and allowed the reaction to be rapidly optimized to 90% isolated yield (Table 2.2, Entry 5).

Table 2.2. Results of mechanochemical syntheses of tolbutamide (**1a**) by CuCl-catalyzed coupling of 4-methylbenzenesulfonamide and *n*-butylisocyanate

Entry	Catalyst loading (mol%)	Time (hr)	Grinding liquid	Yield (%)
1	5	2	-	68
2	20	2	-	91
4	5	2	CH_3CN	54
3	5	2	DMF	79
6	5	2	toluene	85
7	5	2	acetone	86
5	5	2	CH_3NO_2	90

[a]LAG with η = 0.25 μL/mg

We found that coupling was catalyzed not only by Cu(I) but also by Cu(II) additives and even elemental copper as powder or pellets (Table 2.3). The reaction also proceeded without additional copper reagents, simply by using milling balls made of copper or brass (Table 2.3, Entries 18, 19). In addition, a copper ethylenediaminetetraacetate complex, Cu-EDTA (Table 2.3, Entry 17) was synthesized by reacting $CuCl_2 \cdot 2H_2O$ with disodium ethylenediaminetetraacetate ($Na_2H_2EDTA \cdot 2H_2O$) in a 1:1 stoichiometric ratio in water. However, the use of the Cu-EDTA complex as a catalyst did not afford **1a**, which is reasonable as the Cu(II) is coordinatively saturated and encapsulated by the EDTA ligand, which prevents it from activating the starting materials. Potential catalytic activity of salts of other transition metals was explored by using chloride salts of Zn(II), Mg(II), Ni(II), Ag(I), Fe(II) and Fe(III) (Entries 6, 7, 11, 13, 14). The reactions were sluggish for Zn(II) and Ni(II) (18% and 10% yields, respectively) chlorides, while chlorides of Mg(II), Ag(I), Fe(II) and Fe(III) gave no reaction at all.

Several analytical techniques were employed to prove that product formation is due to mechanochemical treatment and not a result of the workup step. Powder X-ray diffraction analysis was not useful as patterns of the milled reaction mixtures exhibited no sharp features, indicating their amorphous nature. Next, infra-red spectroscopy was used to determine whether the mechanochemical coupling reaction, using either base mediated or CuCl catalysis, has achieved qualitative conversion. Comparison of the FTIR-ATR spectra of the crude mechanochemical reaction mixtures clearly showed the absence of characteristic isocyanate C=O stretching bands in the 2000-2200 cm^{-1} region, which denotes that all of the *n*-butylisocyanate had reacted (Fig. 2.4). In addition, ^{1}H-NMR spectroscopy was also used to

determine whether the mechanochemical reaction afforded the desired product **1a** (Fig. 2.5). Deuterated dimethylsulfoxide (DMSO) was used as the NMR solvent. In the absence of a base or CuCl, the milled reaction mixture contained only the starting reagents, *p*-tolylsulfonamide and *n*-butylisocyanate, with the characteristic $–NH_2$ protons of the sulfonamide at 6.82-6.85ppm. When milling was performed using one equivalent of K_2CO_3 or 5 mol% of CuCl, after simple workup, ^{1}H-NMR spectra of the solids obtained showed disappearance of the sulfonamide proton peaks and the formation of the two distinctive sulfonyl-urea –NH proton peaks at 10.49 ppm and 6.48 ppm. These results showed that the coupling reaction to form **1a** indeed took place mechanochemically rather than during workup.

Table 2.3. Selected results of screening for transition metal-catalyzed coupling of 4-methylbenzenesulfonamide and n-butylisocyanate.

Entry	Catalyst	Loading (%mol)	Time (hr)[a]	Grinding liquid[b]	Yield (%)[c]
1	CuBr	5	2	Neat	36
2	$CuBr_2$	5	2	Neat	19
3	Cu powder	10	2	Neat	88
4	Cu_2O	5	2	Neat	75
5	$CuCl_2.2H_2O$	5	2	Neat	84
6	$NiCl_2$	5	2	Neat	18
7	$ZnCl_2$	5	2	Neat	10
8	$MgCl_2$	5	2	Neat	NR
9	$MgCl_2.6H_2O$	5	2	Neat	NR
10	Cu pellets	5	2	Neat	71
11	AgCl	5	2	Neat	NR
12	$CuCl_2$	5	2	Neat	86
13	$FeCl_2.2H_2O$	5	2	Neat	NR
14	$FeCl_3.6H_2O$	5	2	Neat	NR
15	$Cu(acetate)_2 \cdot H_2O$	5	2	Neat	83
16	-	-	2	Neat	0
17	Cu-EDTA	10	2	LAG	0
18[d]	-	-	2	CH_3NO_2	37
19[e]	-	-	2	CH_3NO_2	87

a) unless noted otherwise, milling was using standard‡ conditions; b) LAG with η = 0.25 mL/mg; c) isolated yield after acid workup; d) using ten 3 mm diameter copper balls in a 10 mL stainless steel jar; e) using one 10 mm diameter brass ball in a 10 mL stainless steel jar.

Next, the CuCl catalyzed mechanochemical coupling protocol was further extended to other sulfonamides and isocyanates, affording other tolbutamide analogues (Table 2.4), including the anti-diabetic drug chlorpropamide (**2a**), in 80%-92% yields (please see *Appendix A* for details). The CuCl catalyzed coupling was, however, not applicable to aromatic isocyanates.

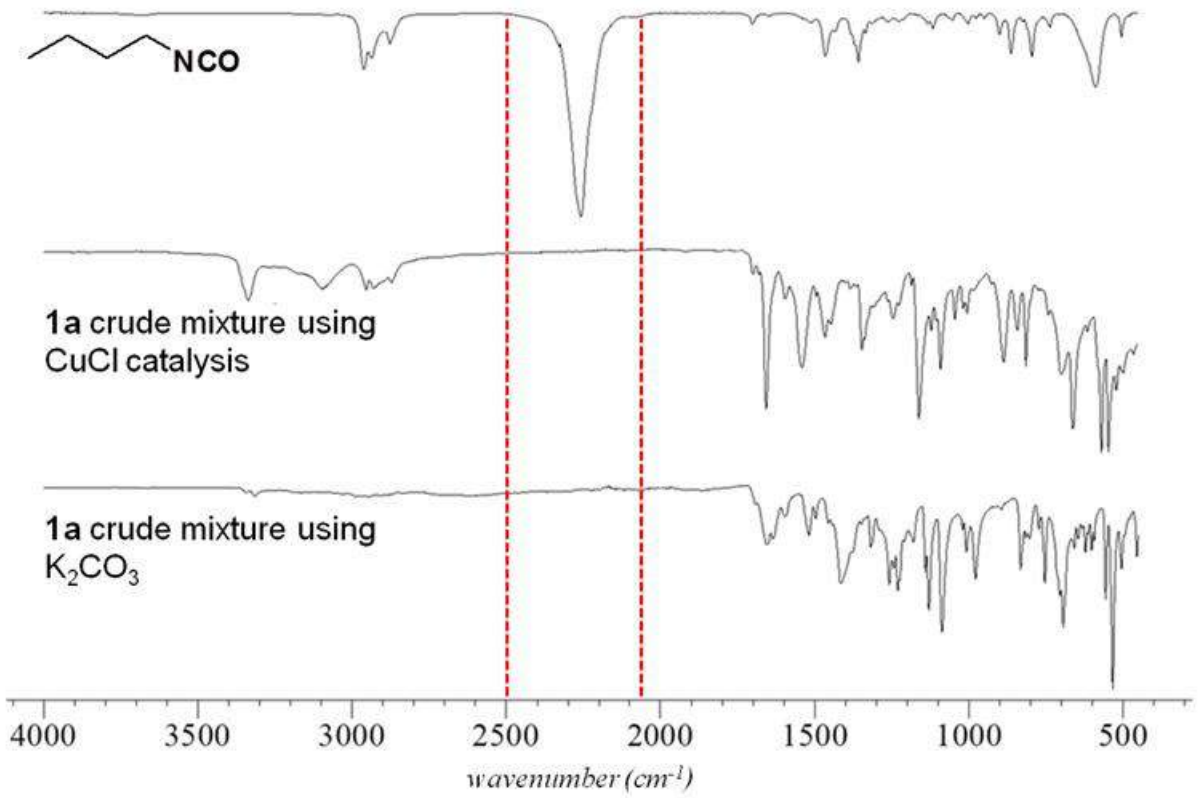

Fig 2.4. FTIR-ATR spectra of the crude reaction mixture for the mechanochemical synthesis of tolbutamide **1a** (either by CuCl catalysis or base mediated reaction).

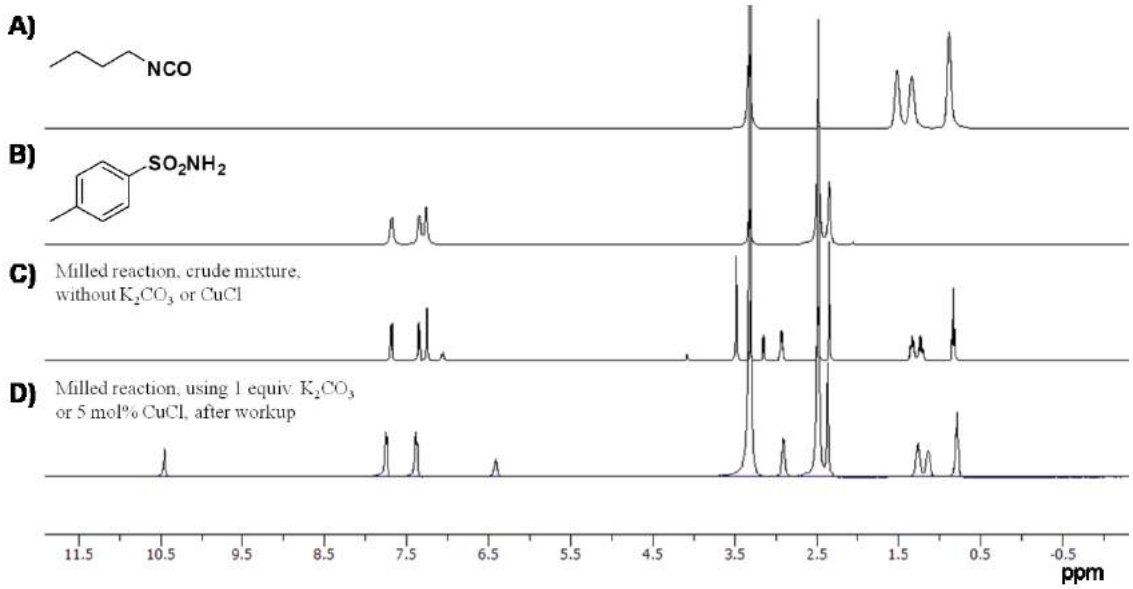

Fig 2.5. Comparison of the ^{1}H-NMR spectra of the starting reagents, a) *n*-butylisocyanate, b) *p*-tolylsulfonamide, c) milled crude reaction mixture without additive and d) milled reaction after workup for the mechanochemical synthesis of tolbutamide **1a** (either by CuCl catalysis or base mediated reaction). DMSO-d_6 was used as the NMR solvent.

Table 2.4. Results of mechanosynthesis of tolbutamide analogues using CuCl catalyst (5 mol%) and LAG with nitromethane (η = 0.25 µL/mg)

Compound	R_1	R_2	Yield (%)[a]
1b	Me	Cy	88
1c	Me	n-Pr	86
2a	Cl	n-Pr	80
2b	Cl	n-Bu	92
2c	Cl	Cy	91

[a]isolated yields after aqueous workup.

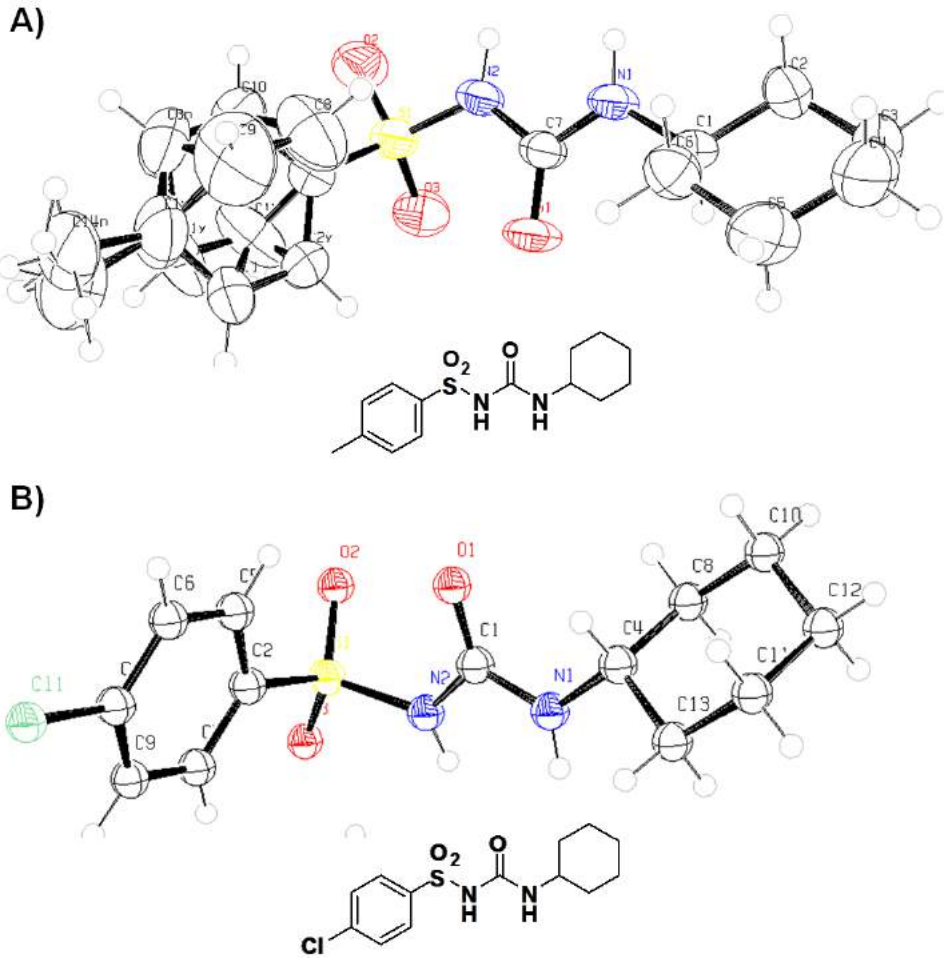

Fig 2.6. Molecular structure of (a) **1b** and (b) **2c**, visualized using ORTEP-3 with thermal ellipsoids at 50% probability as determined by SCXRD, along with Chemdraw images of the compounds. Detailed crystallographic information can be found in *Appendix A*.

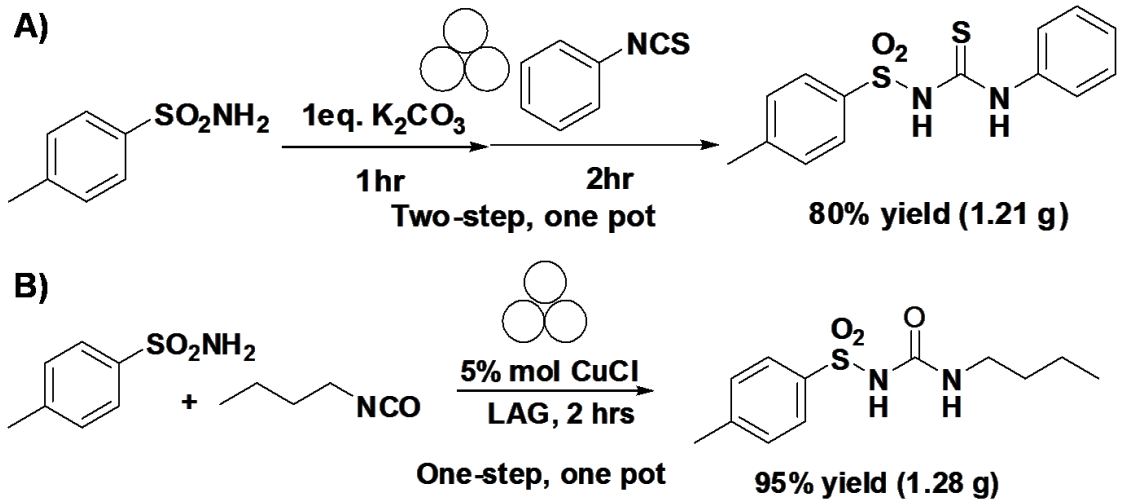

Fig 2.7. Gram-scale synthesis of **1b** and **1a** using a) base-mediated and b) copper-catalyzed methods.

In addition, XRD quality single crystals were also obtained for **1b** and **2c** (Fig 2.6), further proving the formation of the desired products using this mechanochemical direct coupling tactic. Detailed XRD crystallographic data can be found in *Appendix A*. The synthetic protocol was readily scaled-up to gram amounts, using the syntheses of **1a** and **1d** as model reactions for CuCl-catalysis and base-assisted grinding, respectively. The two compounds were obtained in > 1 gram amount with up to 95% yields (Fig. 2.7). For experimental details of the gram scale reactions, please see *Chapter 8, Section 8.1*.

2.4 Mechanochemical synthesis of 2nd generation sulfonylurea glibenclamide

Lastly, we set our sights on the 2nd generation anti-diabetic drug glibenclamide (**3b**, Fig. 2.1), which could be obtained from the simple starting material *p*-(2-aminoethyl)benzenesulfonamide in a sequence of two mechanochemical steps. First, a previously described[20] mechanochemical amide coupling protocol was used to form the sulfonamide precursor **3a** in a yield comparable to solution synthesis (Fig. 2.8a). Crystal structure of **3a** was also obtained (Fig. 2.8b) using XRD. Detailed crystallographic information can be found in *Appendix A*. Next, **3b** was formed by the mechanochemical CuCl-catalyzed coupling of **3a** with cyclohexylisocyanate. Although extensive screening of various LAG liquids was not performed, CH_3NO_2 was generally chosen as the main liquid additive for further reaction optimization as it gave the highest conversion (Table 2.5, entries 5, 9-15). Quantitative conversion of **3a** (92% yield) was only achieved with slight excess of

isocyanate (Table 2.5, entry 10-12), due to a side-reaction forming dicyclohexylurea (**dcu**), the use of only 5 mol% catalyst loading demonstrates the applicability of this new mechanochemical procedure for glibenclamide synthesis (Table 2.5, Entry 12). All in all, glibenclamide can be synthesized in a two-step manner in which both steps can be performed using mechanochemical methods.

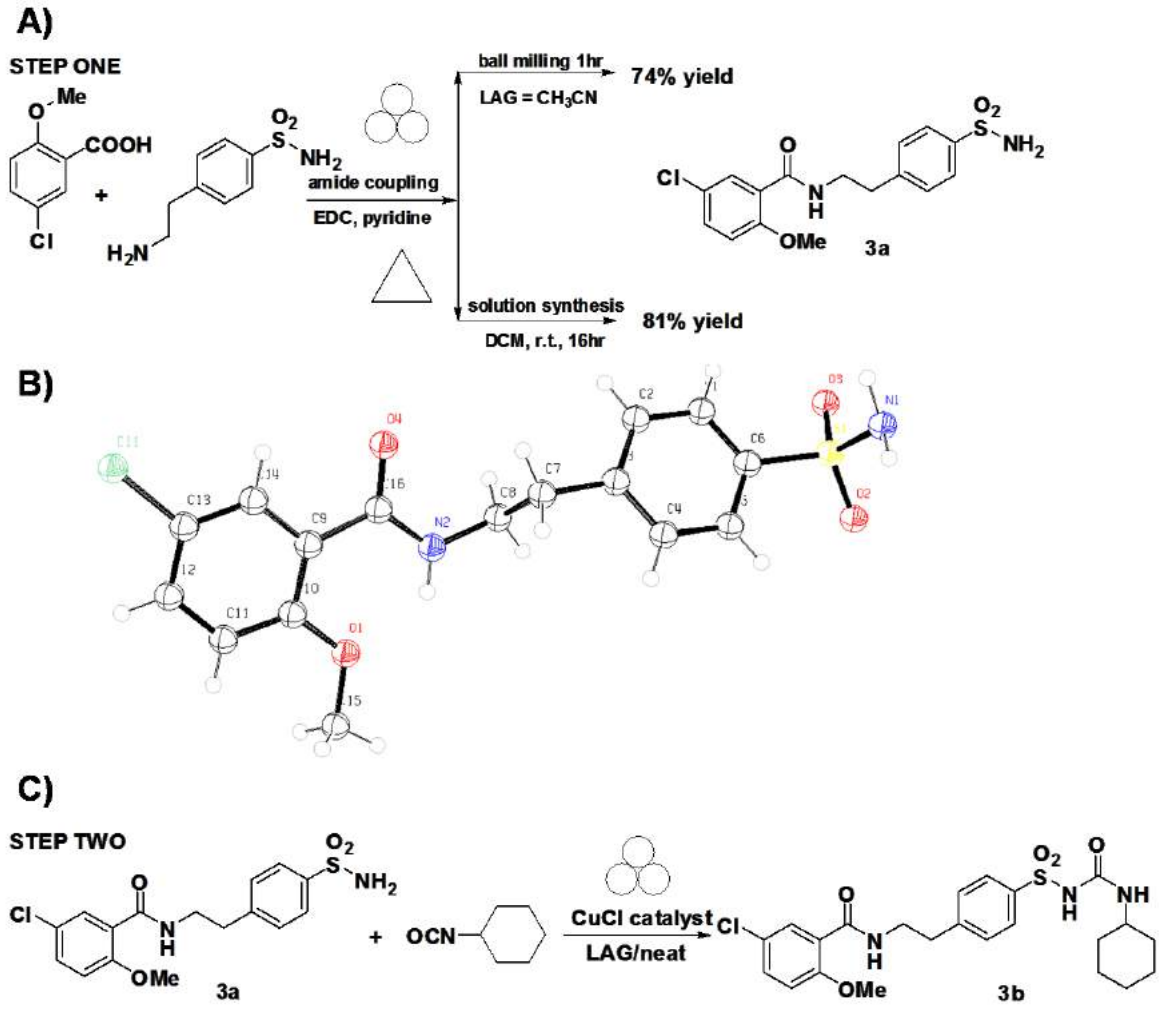

Fig 2.8. a) Schematic diagram of the solution and ball milling synthesis of **3a**. b) Molecular structure of **3a** visualized using ORTEP-3 with thermal ellipsoids at 50% probability as determined by SCXRD. Detailed crystallographic information can be found in *Appendix A*. c) Schematic diagram of the coupling of **3a** with cyclohexylisocyanate to furnish glibenclamide **3b**.

Table 2.5. Results of the second, copper-catalyzed mechanochemical step in the synthesis of glibenclamide (**3b**).

Entry	Catalyst	Amount of Isocyanate	Loading (% mol)	Time (hr)	LAG or neat[a]	Conversion (%)[b]
1	CuCl	1.0 eq	5	2	Neat	54
2	CuCl	1.0 eq	5	2	DMF	60
3	CuCl	1.0 eq	20	2	Neat	43
4	Cu powder	1.0 eq	20	2	Neat	38
5	CuCl	1.0 eq	20	2	CH_3NO_2	83
6	Cu_2O	1.0 eq	20	2	Neat	50
7	$CuCl_2.2H_2O$	1.0 eq	20	2	Neat	30
8	$CuCl_2$	1.0 eq	20	2	Neat	48
9	CuCl	1.0 eq	20	4	CH_3NO_2	87
10	CuCl	1.2 eq	20	4	CH_3NO_2	100
11	CuCl	1.2 eq	20	2	CH_3NO_2	100
12	CuCl	1.2 eq	5	2	CH_3NO_2	100
13	CuCl	1.1 eq	5	2	CH_3NO_2	68
14	CuCl	1.0 eq	5	2	CH_3NO_2	66
15	-	1.0 eq	-	2	CH_3NO_2	0

[a]LAG with η = 0.25 μL/mg; [b]determined using ^{1}H-NMR.

2.5 Possible Mechanism

Although Cervello and Sastre did not mention the mechanistic role of the CuCl catalyst in their report,[17] it is reasonable to envision a plausible mechanism for the sulfonamide-isocyanate coupling reaction to form the sulfonyl-urea **1a** (Fig. 2.9). The CuCl can act as a bifunctional catalyst in which it can coordinate to both the polar sulfonamide nucleophile, as well as the isocyanate electrophile, and bring the two molecules in close proximity to one another. When coordinated to the π-system of the isocyanate, the CuCl can act as a Lewis acid catalyst which activates the electrophile and makes the central carbon of the isocyanate more electrophilic. Next, C-N bond formation occurs and forms a zwitterionic intermediate, which is still coordinated to the catalyst. Subsequently, intramolecular proton transfer between the nitrogen atoms forms the desired sulfonyl-urea product **1a**. Lastly, removal of the catalyst from the product **1a** regenerates the CuCl thus completing the catalytic cycle. However, attempts to experimentally obtain the intermediate complexes, in particular the complexation of CuCl with **1a**, either from solution or mechanochemically has so far been unsuccessful.

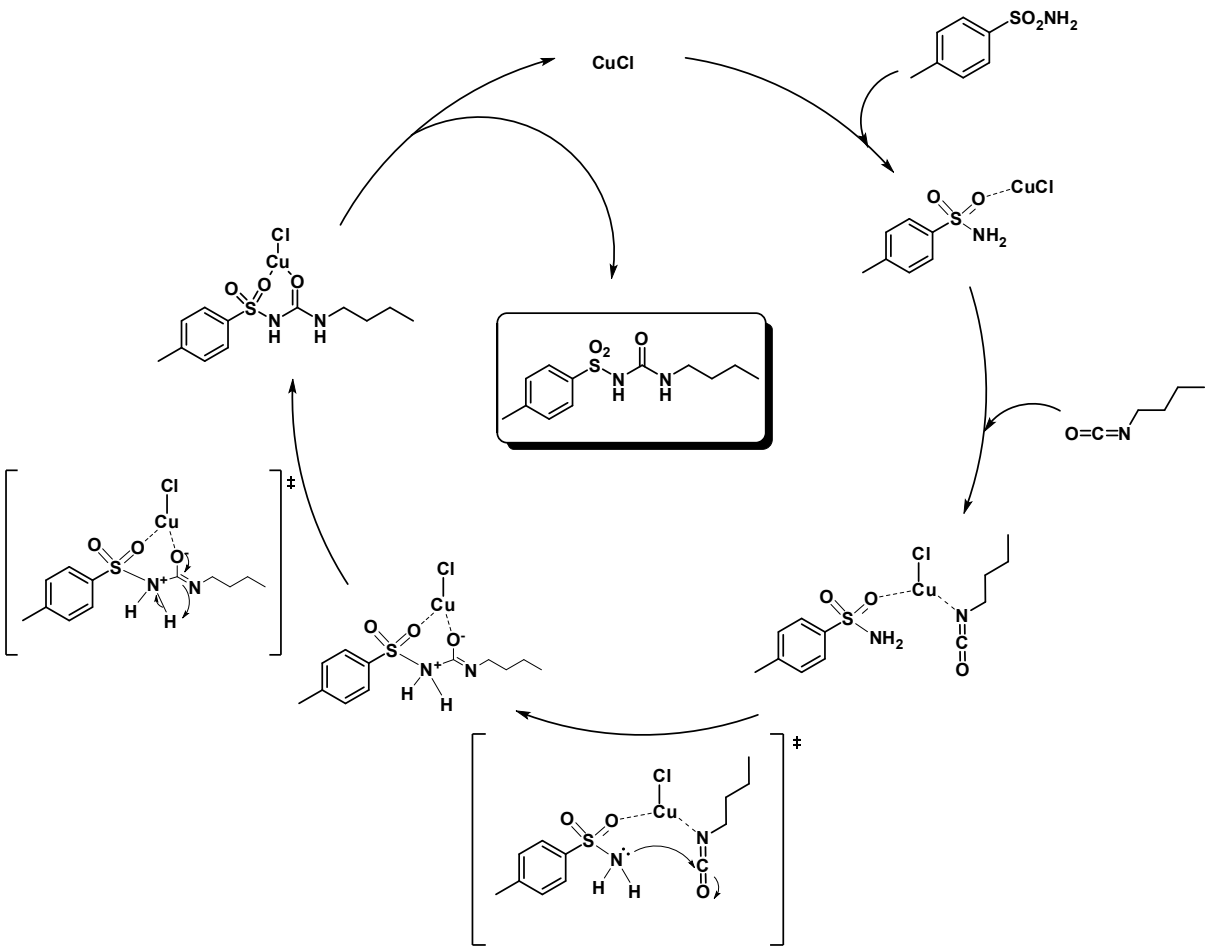

Fig 2.9. Proposed catalytic cycle for the CuCl-catalyzed formation of Tolbutamide **1a** from 4-methylbenzenesulfonamide and n-butylisocyanate.

2.6 Conclusion

In conclusion, we have demonstrated two completely new protocols for the synthesis of sulfonyl-(thio)ureas, an important family of pharmaceutically relevant molecules, using mechanochemistry. Simple targets, including known anti-diabetic drugs tolbutamide and chlorpropamide were obtained in excellent yields. By using a two-step protocol combining previously reported mechanochemical amide synthesis and the novel mechanochemical copper-catalyzed sulfonyl-urea synthesis, we prepared a more complex target glibenclamide in overall 70% yield. Both copper-catalyzed and base-assisted protocols can be scaled up to at least one gram. A total of 11 compounds and five crystal structures were obtained. Whereas our results open possibilities in solvent-free synthesis of medicinal targets, we are now exploring further potential of metal-catalyzed solvent-free coupling sulfonamides and

isocyanates. Results of these new CuCl-catalyzed coupling reactions will be covered in subsequent chapters in this Thesis.

2.6 References

1 S. L. James, C. J. Adams, C. Bolm, D. Braga, P. Collier, T. Friščić, F. Grepioni, K. D. M. Harris, G. Hyett, W. Jones, A. Krebs, J. Mack, L. Maini, A. G. Orpen, I. P. Parkin, W. C. Shearouse, J. W. Steed, D. C. Waddell, *Chem. Soc. Rev*, **2012**, *41*, 413.

2 V. André, A. Hardeman, I. Halasz., R. S. Stein., G. J. Jackson, D. G. Reid, M. J. Duer1, C. Curfs, M. T. Duarte, T. Friščić, *Angew. Chem. Int. Ed.*, **2011**, *50*, 7858.

3 T. Friščić, D. G. Reid, I. Halasz, R. S. Stein, R. E. Dinnebier, M. J. Duer *Angew. Chem. Int. Ed.,* **2010**, *49*, 712.

4 P. Baláž, M. Achimovičová, M. Baláž, P. Billik, Z. Cherkezova-Zheleva, J. M. Criado, F. Delogu, E. Dutková, E. Gaffet, F. José Gotor, R. Kumar, I. Mitov, T. Rojac, M. Senna, A. Streletskiikl, K. Wieczorek-Ciurowam, *Chem. Soc. Rev.*, **2013**, *42*, 7571.

5 a) A. Stolle, T. Szuppa, S. E. S. Leonhardt, B. Ondruschka *Chem. Soc. Rev.,* **2011**, *40*, 2317; b) G.-W. Wang, *Chem. Soc. Rev.*, **2013**, *42*, 7668.

6 J. G. Hernández, E. Juaristi, *Chem. Commun.*, **2012**, *48*, 5396.

7 D. A. Fulmer. W. C. Shearouse, S. T. Medonza, J. Mack, *Green Chem.*, **2009**, *11*, 1821.

8 a) J. G. Hernánde, E. Juaristi, *J. Org. Chem.*, **2010**, *75*, 7107; b) F. Lamaty, J. Martinez, P. Nun, V.Declerck, *Angew. Chem. Int. Ed.,* **2009**, *48*, 9318.

9 a) A. M. Flock, C. M. M. Reucher, C. Bolm, *Chem. Eur. J.*, **2010**, *16*, 3918; b) B. Rodríguez, T. Rantanen, C. Bolm, *Angew. Chem. Int. Ed.*, **2006**, *41*, 7078.

10 J. Bonnamour, T.-X. Métro, J. Martinez, F. Lamaty, *Green Chem.*, **2013**, *15*, 1116.

11 a) V. Štrukil, D. Margetić, M. D. Igrc, M. Eckert-Maksić, T. Friščić, *Chem. Commun.*, **2012**, *48*, 9705; b) V. Štrukil, M. D. Igrc, M. Eckert-Maksić, T. Friščić, *Chem. Eur. J.*, **2012**, *18*, 8464.

12 H. Schmid-Antomarchi, J. D. Weille, M. Fosset, M. Lazdunski, *J. Bio. Chem.*, **1987**, *33*, 15840.

13 a) C. Jiménez-González, D. J. C. Constable, C. S. Ponder, *Chem. Soc. Rev.*, **2012**, *41*, 1485; b) W. C. Shearouse, D. C. Waddell, J. Mack, *Curr. Opin. Drug Discov. Develop.* **2009**, *12*, 772.

14 H. Ulrich, *Chem. Rev.*, **1965**, *3*, 369.

15 P. Anastas, N. Eghbali, *Chem. Soc. Rev.*, **2010**, *39*, 301.

16 A. Martínez-Asencio, D. J. Ramón, M. Yus, *Tetrahedron Lett.*, **2010**, *51*, 325.

17 J. Cervello, T. Sastre *Synthesis*, **1990**, 221.

18 The amount of liquid is expressed as η, the ratio of the liquid volume (in μL) to the weight of reaction mixture (in mg): T. Friščić, S. L. Childs, S. A. A. Rizvi, W. Jones, *CrystEngComm*, **2009**, *11*, 418.

19 T. Friščić, A. V. Trask, W. Jones, W. D. S. Motherwell, *Angew. Chem. Int. Ed.*, **2006**, *45*, 7708.

20 V. Štrukil, B. Bartolec, T. Portada, I. Đilović, I. Halasz, D. Margetić, *Chem. Commun.*, **2012**, *48*, 12100.

CHAPTER 3

DEVELOPMENT OF C-N COUPLING USING MECHANOCHEMISTRY: CATALYTIC COUPLING OF SULFONAMIDES AND CARBODIIMIDE

"It is important to have original idea. Original idea." – Prof. Akira Suzuki, McGill public lecture, 2014.

3.1 Introduction and connecting text.

The work presented in this chapter is a part of a published paper entitled "Development of C-N coupling using mechanochemistry: catalytic coupling of sulfonamide and carbodiimide", discussing the use of mechanochemistry as a powerful tool for new reaction discovery. The paper was written by D. Tan with guidance and editing contributions from Prof. T. Friščić, and co-authored with Dr. C. Mottillo, Dr. A. D. Katsenis and Dr. V. Štrukil. The text has been formatted and re-written for inclusion in this dissertation. All experimental results, including screening, synthesis and characterization (FTIR, NMR, MS) of the various compounds was performed by D. Tan, with help from Dr. C. Mottillo. Dr. A. D. Katsenis and Dr. V. Štrukil for the collection of the single crystal XRD data. This work has been re-written for inclusion in this chapter with additional results included from the supporting information. In *Chapter 2*, the mechanochemical coupling between poorly nucleophilic arysulfonamides with iso(thio)cyanates were discussed. This reaction can either be base-mediated using stoichiometric amounts of K_2CO_3 in a one-pot two-step manner, or copper-catalyzed direct coupling in a one-pot one-step manner. The use of copper as a catalyst is attractive in the synthetic methodology as it negates the use of a base for activation which then removes the need for a subsequent acid neutralization step during the workup procedure. In this chapter, we will explore the mechanochemical copper-catalyzed coupling of sulfonamides with another class of electrophiles, namely carbodiimides. This idea encompasses the philosophy of using mechanochemistry for discovering new coupling reactions as well as for the mechanosynthesis of pharmaceutically-relevant compounds.

Mechanosynthesis,[1] or the synthesis of compounds *via* mechanical force (grinding, shearing, stretching), is rapidly becoming popular in the development of environmentally-friendly and solvent-free synthetic procedures, including organic[2] and inorganic[3] transformations, as well as the synthesis and screening for functional materials, including pharmaceutical cocrystals[4] as well as metal-organic and covalent organic frameworks.[5] Recent years have witnessed an explosion of research fervor in using mechanochemistry to conduct organocatalytic[6] and transition metal-catalyzed[7] organic transformations, including numerous examples of asymmetric synthesis.[8] Importantly, mechanochemical methodologies of neat and liquid-assisted grinding (LAG),[9] which are conducted in either a completely solvent-free environment or using catalytic amounts of a liquid phase, respectively, provide an exciting opportunity to avoid the use of bulk solvents in chemical synthesis. Besides improving the atom-efficiency of synthesis, mechanochemical reactions significantly

improve the efficiency of energy consumption[10] and widen the scope of synthesis by allowing room-temperature synthesis independent[11] of reactant solubility. The excellent selectivity and stoichiometric control demonstrated in supramolecular,[12] metal-organic[13] and organic mechanochemical reactions offers an attractive opportunity for either efficient derivatization of multi-functional molecules[14] or the desymmetrization[15] of small molecules by site-selective derivatization. In particular, there have been rapid developments in the area of mechanochemical organic synthesis,[2,16] with several recent reports[17] describing multi-step or multi-component ball milling procedures of relatively complex targets. Of these, particularly notable are the completely solvent-free multi-step synthesis of Leu-enkephalin, demonstrated by the Lamaty group,[18] as well as the one-pot assembly of a boronate ester and imine based molecular cage composed of altogether 11 components.[19] Mechanochemistry is on a clear path to provide solvent-free organic synthesis with access to synthetic freedoms akin to those of conventional synthetic organic chemistry: for example, interconversions of all nitrogen-based organic functionalities are now accessible through solvent-free routes.[20]

3.2 Sulfonylguanidine moiety in pharmaceuticals

We have recently demonstrated the efficient base- or copper-catalyzed mechanochemical coupling of sulfonamides with isocyanates and isothiocyanates[21] to form pharmaceutically relevant sulfonyl-(thio)ureas, including 1st generation anti-diabetic drugs Tolbutamide and Chlorpropamide in gram amounts. Coupling of this catalytic procedure with mechanochemical amide synthesis[22] enabled the solvent-free synthesis of the 2nd generation drug Glibenclamide. By chemical analogy we speculated that a similar coupling procedure might be applicable using carbodiimides, instead of isocyanates, leading to pharmaceutically attractive arylsulfoguanidine units. The guanidine moiety can be found in many biologically active compounds and natural products.[23] Guanidines are also known to be organic superbases[24] and have been used as catalysts for organic reactions.[25] Similarly, the related sulfonylguanidine moiety can also be found in many biologically active molecules and are important to pharmaceutical industries. In particular, the marketed racemic anti-ulcer drug Osutidine®,[26] the anti-obesity agent Ibipinabant®[27a], the anti-bacterial drug Sulfaguanidine®,[27b] and the compound *N*-(2-biphenylylsulfonyl)*N*'-(4-methoxy-6-methyl-pyrimidin-*Z*-yl)-guanidine, which is patented as a herbicide[28] (Fig. 3.1), all contain the sulfonylguanidine functional group. Recently, Lange *et al.* reported the solution synthesis of unsymmetrical sulfonyl-guanidines from amines and thioureas in a five step process.[29]

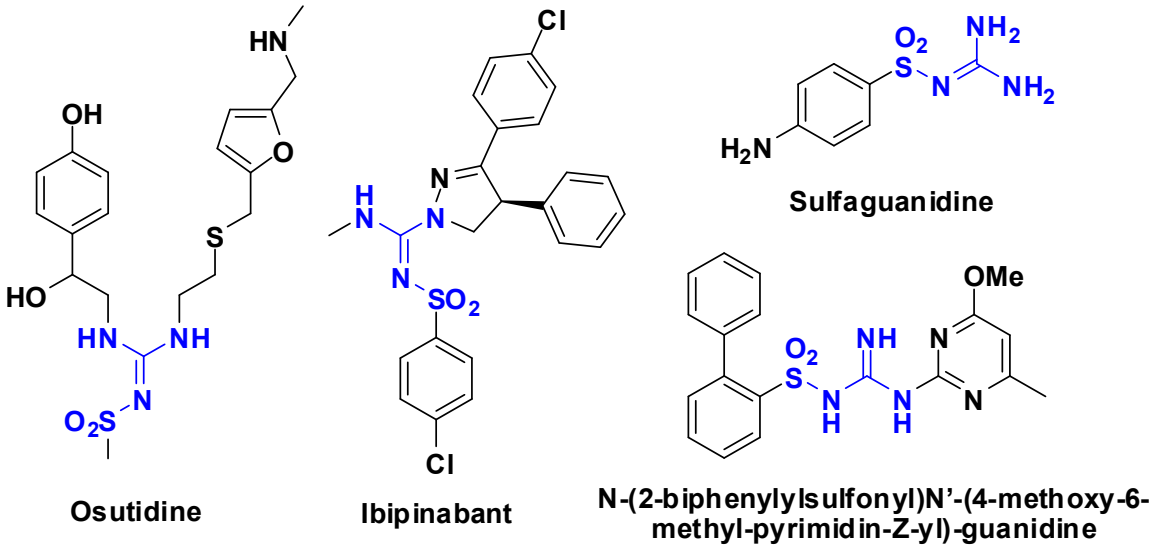

Fig. 3.1 Various pharmaceutical and biologically active compounds containing sulfonylguanidine moiety.

We now demonstrate the use of mechanochemistry for the synthesis of arylsulfoguanidines by a never previously demonstrated copper-catalyzed coupling of arylsulfonamides with carbodiimides. Whereas the present work opens a simple and clean route to this type of molecular target, the systematic exploration of this novel synthetic strategy has been conducted using exclusively mechanochemical reaction screening. To the best of our knowledge, this is the first time that a novel synthetic strategy is introduced and explored through mechanochemistry only.

3.3 Initial reactions :trifluoromethylsulfonamide coupling with carbodiimides

Our study was inspired by the recent discovery of Shaiyan and coworkers that trifluoromethanesulfonamide ($CF_3SO_2NH_2$) undergoes direct coupling with either dicyclohexylcarbodiimide (DCC) or di(*iso*-propyl)carbodiimide (DIC), to give trifluoromethylsulfonylguanidines **1a** and **1b**, respectively.[30] Compounds **1a** and **1b** were reported to form in excellent yields by stirring for 6 hours in dichloromethane solution. We readily performed the synthesis of **1a** and **1b** by mechanochemical milling, within 2 hr, in high yields (95% and 96%). The mechanosynthesis was further improved by using LAG,[9] a technique which utilizes sub-stoichiometric amounts of a liquid to enhance milling reactivity. Addition of catalytic[31] amounts of nitromethane gave **1a** and **1b** in 98% and 96% yields, respectively (Fig. 3.2b), *i.e.* in yields comparable to solution synthesis but in a fraction of the time.

We expected that the reaction of *p*-tolylsulfonamide and DCC should proceed in a similarly straightforward fashion to yield 4-methylphenylsulfonyl-N-di(cyclohexyl)guanidine (**2a**). In contrast to our expectations, however, attempts to synthesize **2a** failed, both in solution, by neat milling and by LAG (Fig. 3.2c).

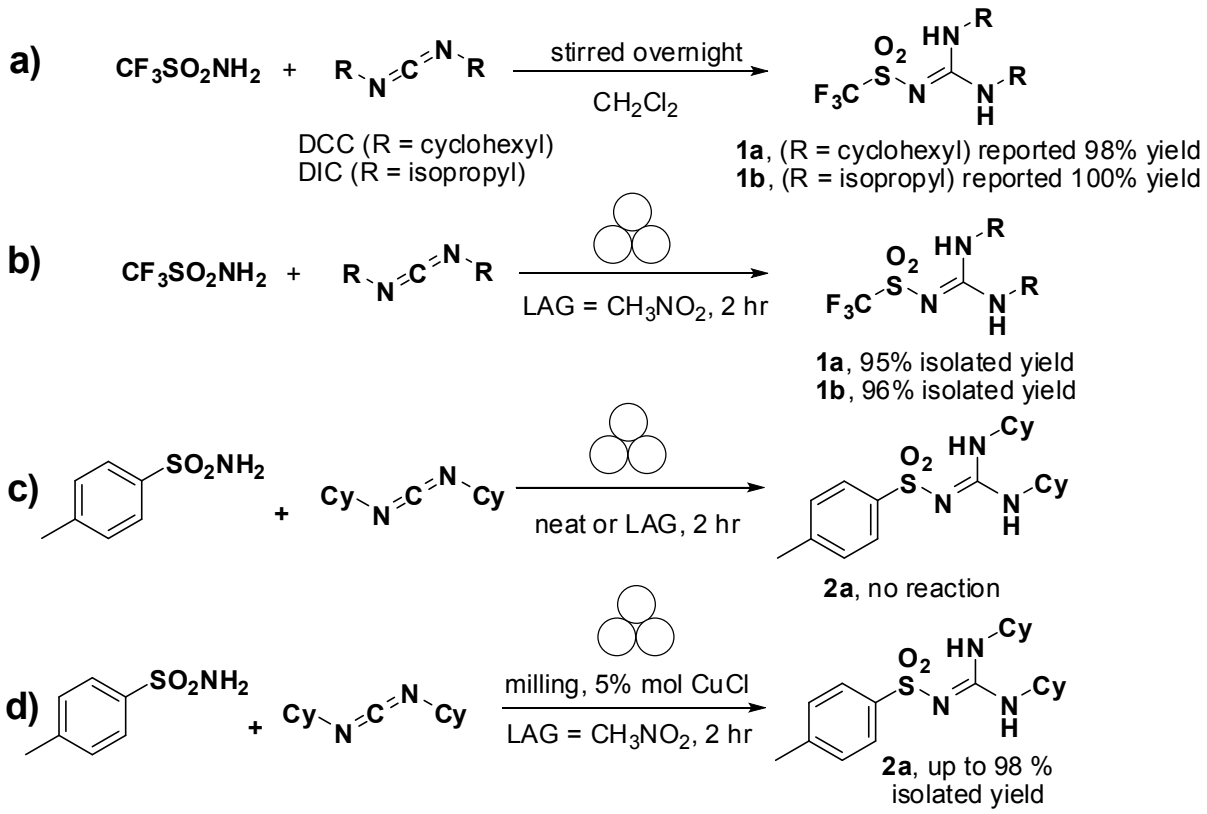

Fig. 3.2. Synthesis of **1a**, a) as reported by Shainyan *et al.*,[30] or b) mechanochemical synthesis of **1a**. Mechanochemical reaction for the synthesis of **2a** c) without copper catalyst and d) with catalyst.

Next, we explored the possibility to achieve the coupling of *p*-tolylsulfonamide and DCC by milling in the presence of catalytic amounts of CuCl. Namely, we recently established that CuCl is an efficient catalyst for the mechanochemical coupling of phenylsulfonamides with isocyanates.[21] Indeed, addition of 5 mol% of CuCl to the reaction mixture resulted in 81% conversion to **2a** after 2 hours of neat milling (Fig. 3.2d), as established by ^{1}H-NMR. Performing the reaction by LAG (η = 0.25 μL/mg)[31] for 2 hours provided **2a** in excellent (99%) isolated yield. The product was isolated *via* our previously developed protocol,[21] in which the crude mixture is briefly (5 min) milled with an aqueous solution of the sodium salt of ethylenediaminetetraacetic acid, which quenched the reaction

and removed the metal catalyst by complexation. The water insoluble **2a** is then isolated by simple filtration as white solid. Spectroscopic details of the compounds can be found in *Appendix B*.

To the best of our knowledge, the demonstrated syntheses of **1a** and **2a** are first examples of mechanochemically performed syntheses of sulfonylguanidines. More importantly, the copper-catalyzed synthesis of **2a** is the first case of a direct coupling between a carbodiimide and an arylsulfonamide. We have also attempted to conduct the copper-catalyzed coupling of DCC with *p*-tolylsulfonamide in solution, in refluxing CH_2Cl_2 or acetone. After overnight reflux, however, no trace of **2a** was observed in any of the reactions. The sulfonamide starting material was readily retrieved from these attempts at solution synthesis, highlighting the importance of mechanochemical treatment for conducting the copper-catalyzed coupling. Therefore, the novelty of this catalytic reaction and the inability to readily reproduce it in bulk solution, provides a unique opportunity to demonstrate and explore the synthetic potentials of a novel chemical reaction using only mechanochemical methods. In particular, trifluoromethylsulfonamide readily underwent mechanochemical coupling with all explored aliphatic carbodiimides (Fig. 3.3), except the most sterically hindered di(trimethylsilyl)carbodiimide (DTMSC). Crude reaction mixture of the 1:1 stoichiometric reaction between $CF_3SO_2NH_2$ and DTMSC were subjected to ^{1}H-NMR and FTIR-ATR analysis (Fig. 3.4). FTIR-ATR spectrum showed the presence of the characteristic carbodiimide peak at at 2180 cm^{-1} in the FTIR spectrum, which indicates the presence of unreacted DTMSC. Similarly, ^{1}H-NMR of the same crude reaction mixture revealed the presence of a $–NH_2$ proton peak at 8.9 ppm, indicating unreacted sulfonamide. The proton NMR peaks are also slightly broad, which is due to metal iron contaminants caused by milling of soft organic solids. Based on both NMR and IR spectroscopy, the reaction did not take place at all, recovering back both starting materials.

Single crystal X-ray diffraction (SCXRD) structures of the previously unknown coupling products **1c** and **1d** were also obtained (Fig. 3.5). $CF_3SO_2NH_2$ also did not react with the aromatic di(*p*-tolyl)carbodiimide (DPTC) in the absence of catalyst. In contrast, the copper-catalyzed reaction of *p*-tolylsulfonamide readily proceeded with DCC, DIC and the aromatic DPTC. However, copper-catalyzed coupling did not take place with carbodiimides involving sterically demanding *tert*-butyl (DTBC) and trimethylsilyl (DTMSC) groups, even with prior addition of K_2CO_3 base.

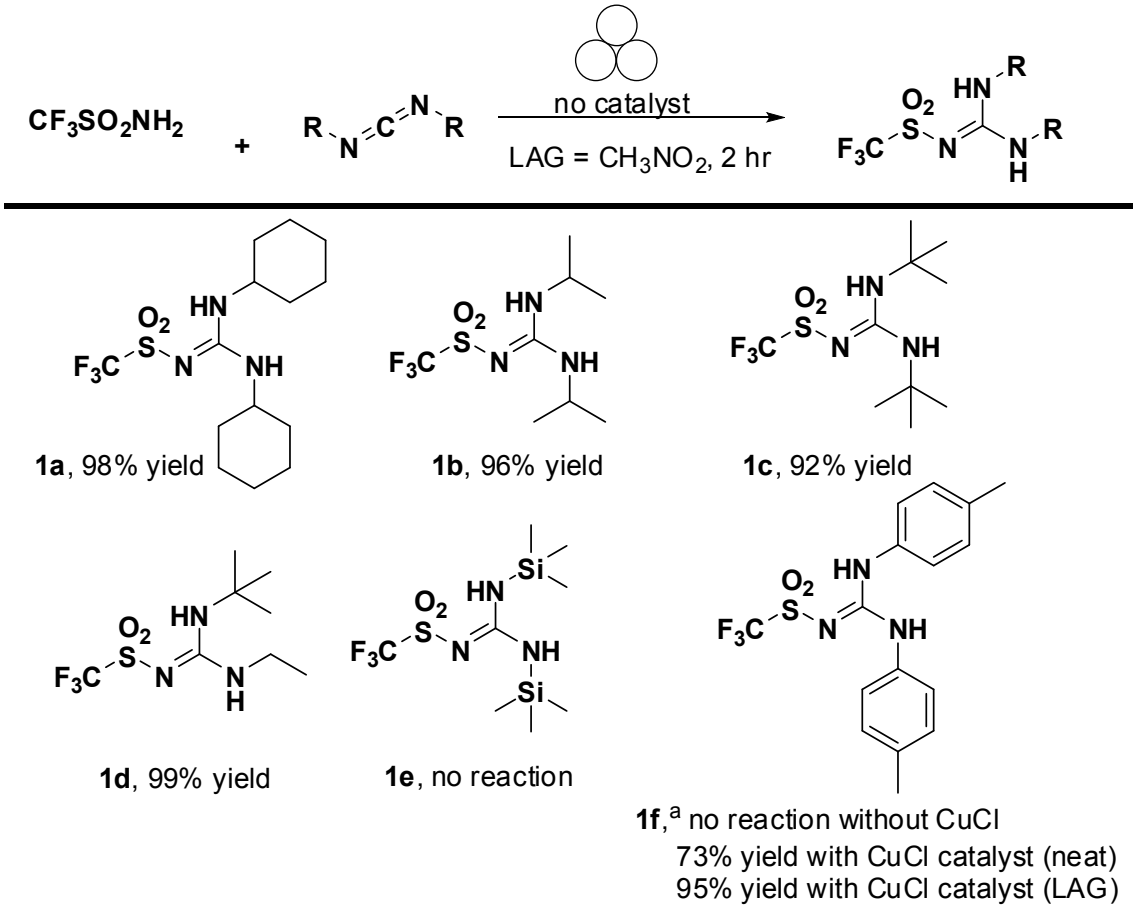

Fig. 3.3. Catalyst-free coupling of trifluoromethylsulfonamide with different carbodiimides. One 10 mm diameter stainless steel ball in a 10 mL stainless steel jar was used at a frequency of 30 Hz in the presence of nitromethane (η = 0.25 mL/mg). [a]Synthesis of **1f** was only possible after the addition of CuCl catalyst (10 mol%).

These preliminary comparisons indicate that $CF_3SO_2NH_2$ is unique in its ease of reaction with carbodiimides and that such reactivity might be limited to aliphatic substrates only. In contrast, copper-catalyzed coupling appears to be more general in sulfonamide choice and, while limited by the steric requirements of the carbodiimide, it allows reactions of aliphatic and aromatic carbodiimides. Indeed, the addition of 10 mol% CuCl subsequently also enabled the coupling of $CF_3SO_2NH_2$ with di(*p*-tolyl)carbodiimide, previously not achievable either in solution[33] or mechanochemically (Fig. 3.3). The conversion to **1f** upon neat milling was 73%, and LAG gave 95% isolated yield. Whereas the mechanism of the copper-based coupling is still unknown, this suggests that it is distinct to the catalyst-free reactivity seen with $CF_3SO_2NH_2$ and that CuCl is relevant most likely for activating the

carbodiimide. Similarly, the mechanochemical coupling of $CF_3SO_2NH_2$ with di-(*o*-tolyl)carbodiimide (DOTC) was also investigated using two experiments with similar results, due to a forbidding cost of this commercial reagent (please see *Chapter 8, Section 8.2.3*).

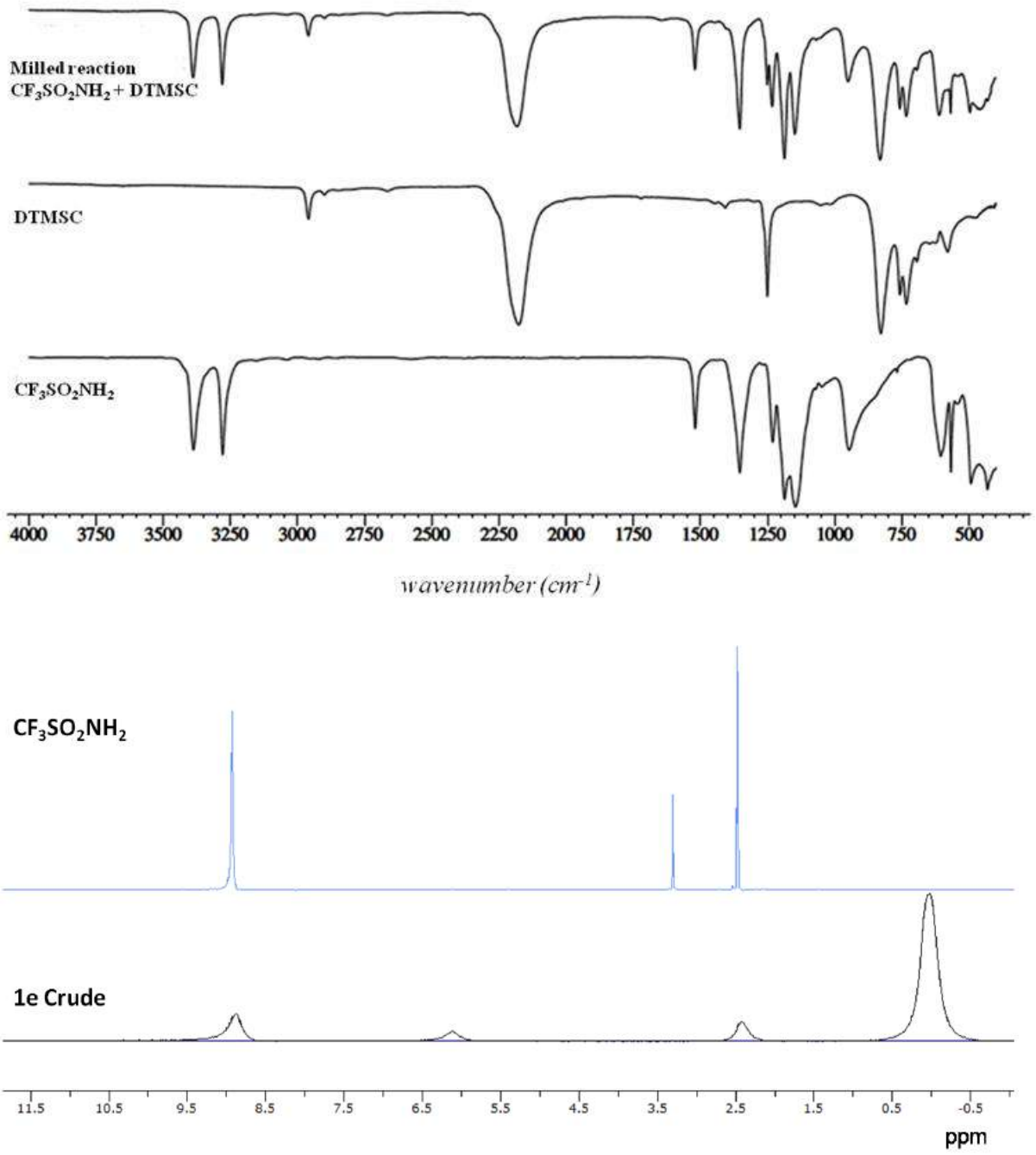

Fig 3.4. Comparison of the FTIR-ATR spectra (top) of the crude ball milling reaction mixture between $CF_3SO_2NH_2$ and DTMSC, and ^{1}H-NMR spectra (bottom) of the same reaction mixture. DMSO-d_6 was used as the NMR solvent.

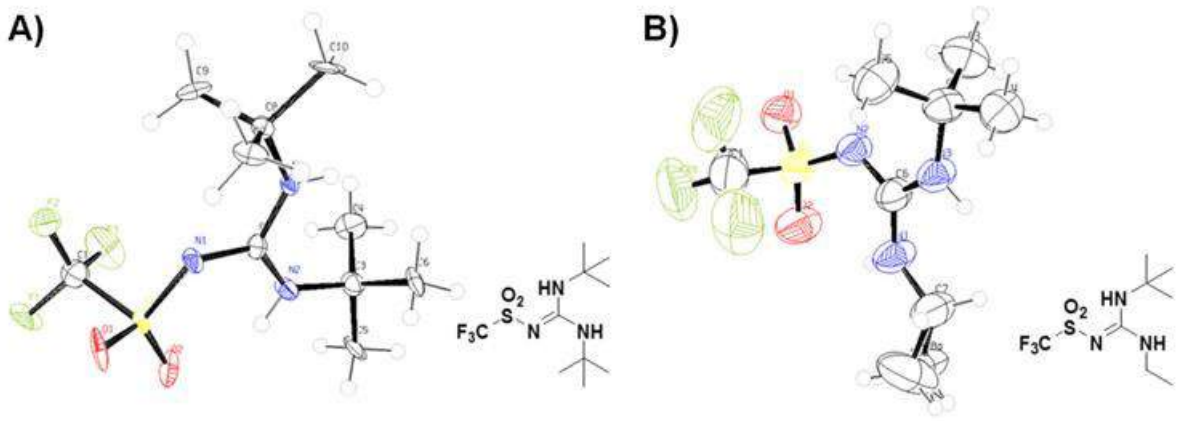

Fig 3.5. Molecular structures of a) **1c** and b) **1d** visualized using ORTEP-3 with thermal ellipsoids at 50% probability level, as determined by SCXRD, along with Chemdraw images of the compounds. Refer to *Appendix B* for crystallographic details.

3.4 Arylsulfonamides coupling with carbodiimides

Initially, we considered that the difference in reactivity of trifluoromethylsulfonamide and *p*-tolylsulfonamide might be simply a result of the ease of deprotonation of trifluoromethylsulfonamide, which would make the more reactive sulfonamidate species available for attack on the carbodiimide. Therefore, we attempted to achieve catalyst-free synthesis of **2a** by milling *p*-tolylsulfonamide first with K_2CO_3 to deprotonate the sulfonamide moiety, followed by further milling with DCC. Notably, a similar base-assisted two-step mechanochemical approach was previously successful in generating sulfonylthioureas from sulfonamides and non-reactive thiocyanates.[21] However, no reaction was observed for *p*-tolylsulfonamide, either with DCC or with DIC. An identical pattern of reactivity as for *p*-tolylsulfonamide was observed for *p*-chlorophenylsulfonamide (Fig. 3.6), which exhibited no reactivity in the absence of CuCl but upon addition of this metal catalyst readily yielded the *p*-chlorophenylsulfoguanidines **2a-c** with sterically less hindered carbodiimides DCC, DIC and DPTC.

Sterically bulky carbodiimides, however, did not react to form the desired coupling product. This was evidenced by FTIR-ATR spectroscopy (Fig. 3.7) which showed unreacted carbodiimides.

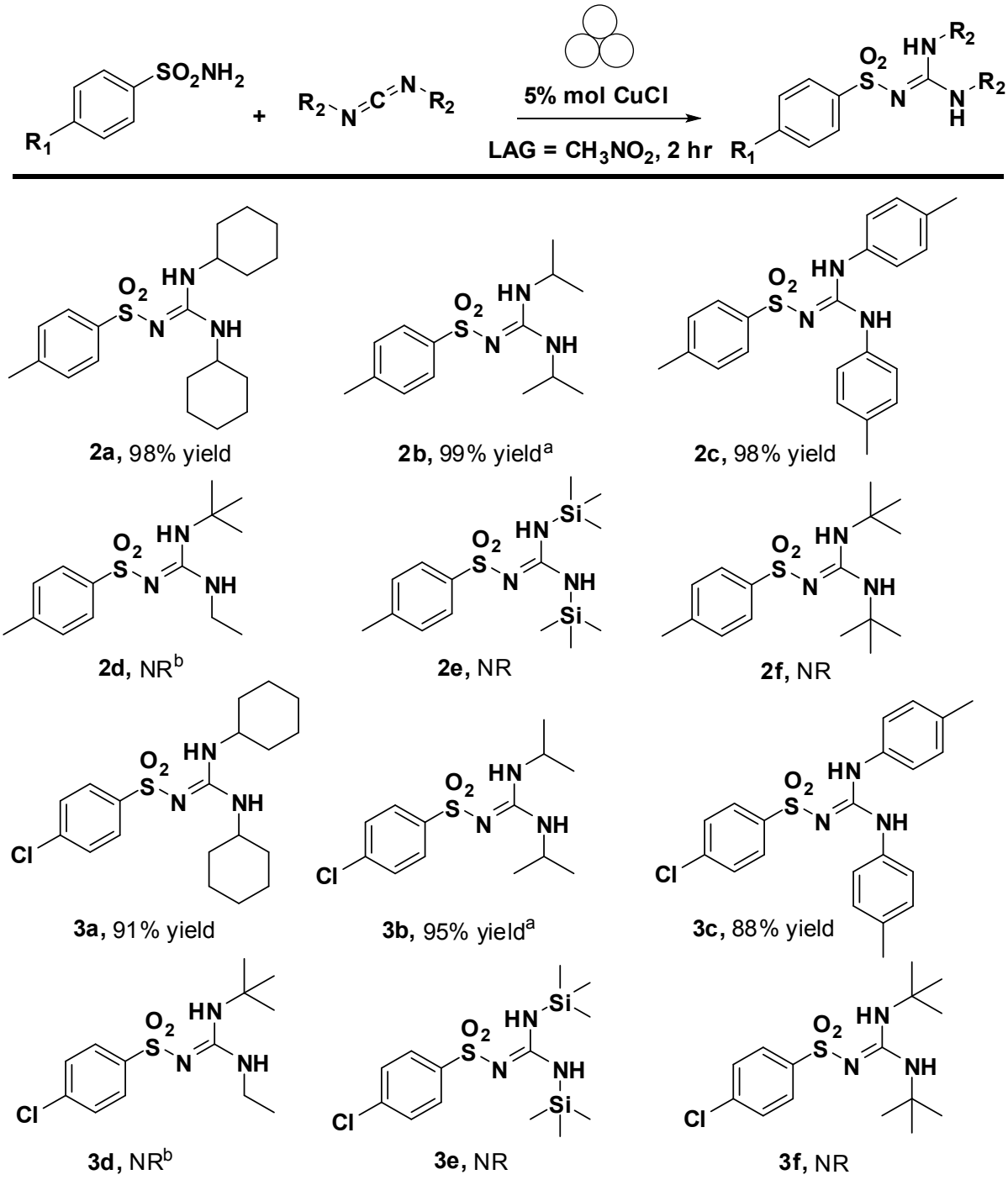

Fig. 3.6. CuCl-catalyzed coupling of *p*-tolyl- and *p*-chlorophenylsulfonamides with different carbodiimides. CuCl-catalyzed coupling of *p*-tolyl- and *p*-chlorophenylsulfonamides with different carbodiimides. One 10 mm diameter stainless steel ball in a 10 mL stainless steel jar was used, at a frequency of 30 Hz, using nitromethane a grinding liquid (η = 0.25 mL/mg). Unless otherwise noted, 5 mol% of CuCl catalyst was used. [a]10% CuCl was used. [b]The reaction did not proceed even when the sulfonamide was first milled with K_2CO_3.

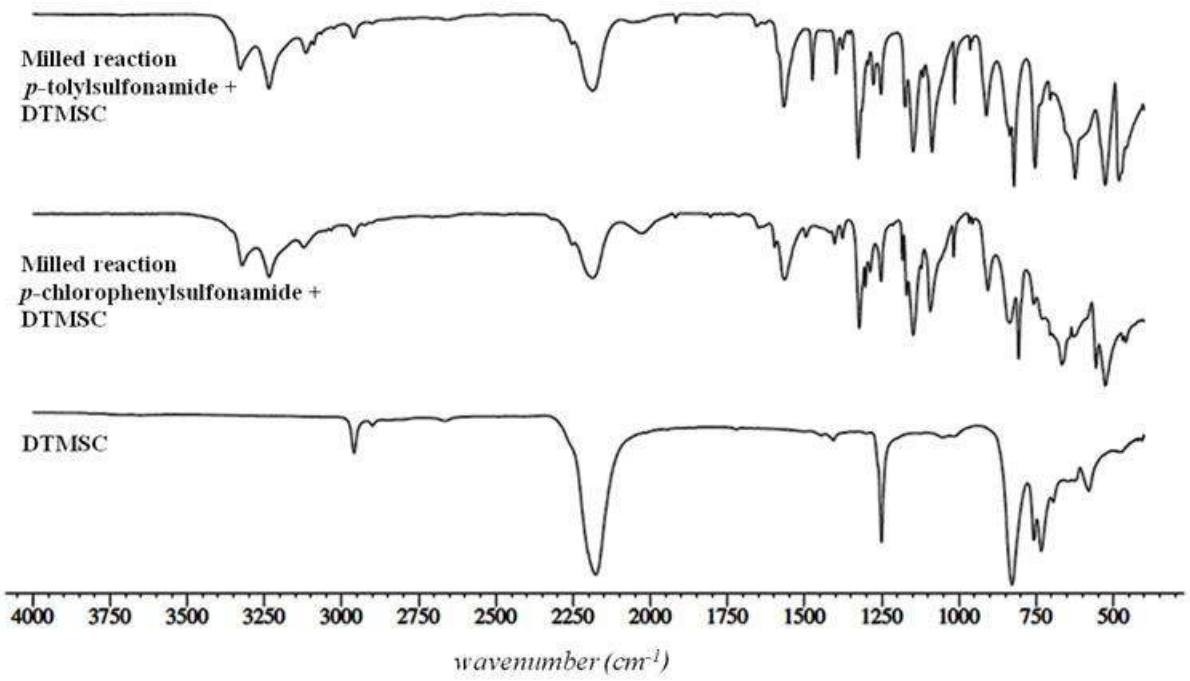

Fig. 3.7. Comparison of the FTIR-ATR spectra of the crude reaction mixtures of *p*-tolylsulfonamide (top) and *p*-chlorophenylsulfonamide (middle) with DTMSC.

Next, the scope of mechanochemical copper-catalyzed coupling was expanded to other commercially accessible aromatic sulfonamides (Fig. 3.8), focusing only on the sterically less hindered DCC, DIC and DPTC. No reactivity was observed in the absence of CuCl. With the copper catalyst present, the reaction readily took place in almost all cases, affording the expected sulfonylguanidines in excellent yields after simple optimization of reaction conditions. Optimization typically included switching between neat and LAG reactions, varying the amount of CuCl between 5 mol% and 10 mol%, as well as varying the reaction time between two hours and four hours. Detailed spectroscopic characterization of the various compounds can be found in *Appendix B*.

Poorer reactivity was observed for *p*-nitrophenyl- and 2-naphthylsulfonamides, even with catalyst loadings of up to 20 mol%. Consequently, we resorted to further modification of the mechanochemical reaction environment by varying the liquid additive for LAG. In principle, LAG should enable the optimization of mechanochemical reactions by switching the catalytic liquid additive, in a similar way that switching between bulk solvents is used to affect conventional solution synthesis.

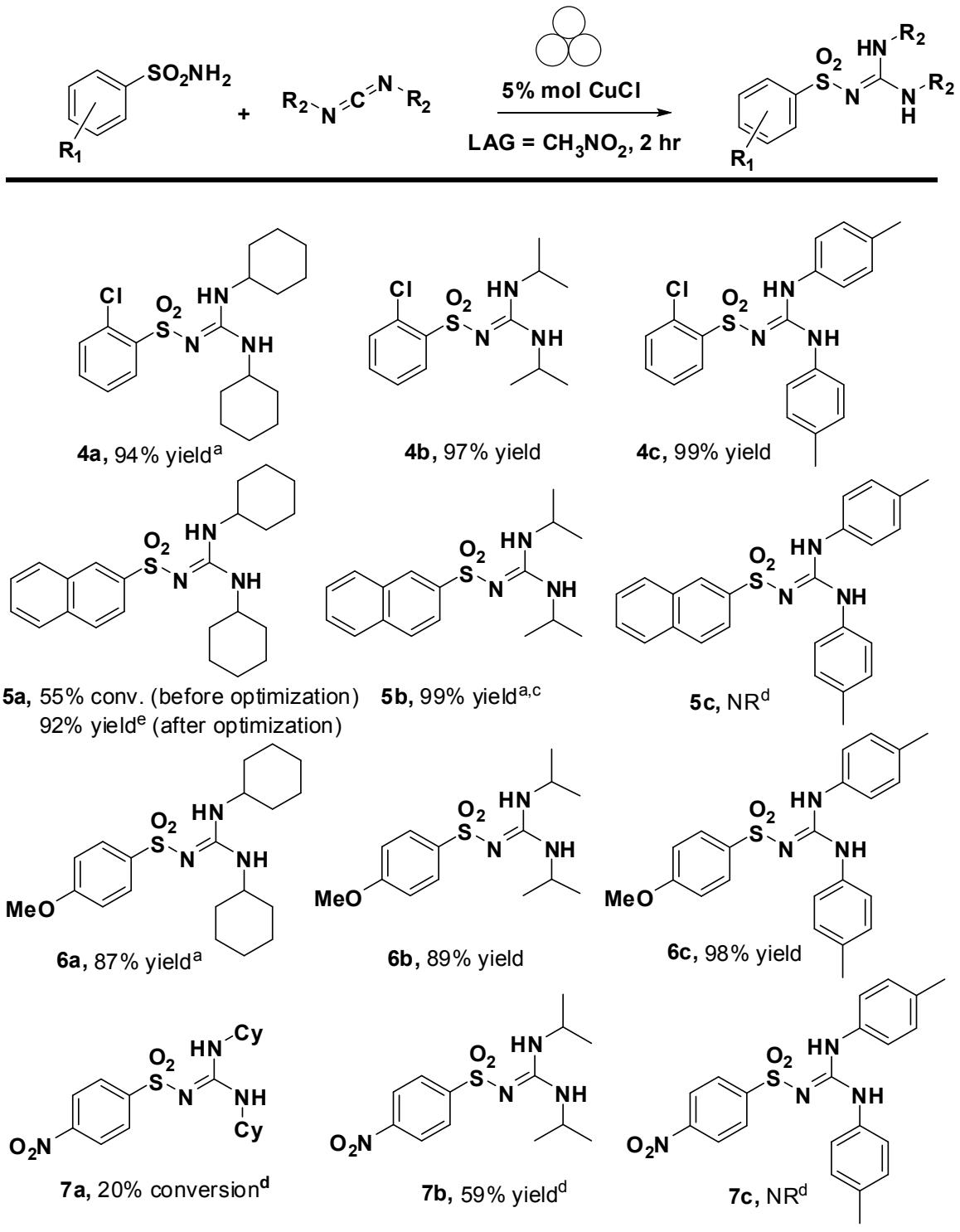

Fig. 3.8. CuCl-catalyzed coupling of *o*-chloro-, *2*-naphthyl-, *p*-methoxy- and *p*-nitro-phenylsulfonamides with different carbodiimides. One 10 mm diameter stainless steel ball in a 10 mL stainless steel jar was used, at a frequency of 30 Hz, in the presence of a grinding liquid (η = 0.25 mL/mg). All reported yields are isolated yields after workup. Unless otherwise noted, all reactions were performed with 5 mol% CuCl catalyst. [a]10% CuCl was used. [b]The reaction did not proceed even with prior milling of the sulfonamide with K_2CO_3. [c]using 1.1 equiv.alents carbodiimide. [d]using 20 mol% CuCl. [e]Optimized conditions: 10 mol% CuCl, acetone as the grinding liquid, 4 hr milling.

3.5 Optimization using only mechanochemical techniques

Table 3.1. Optimization of LAG synthesis of **4a**

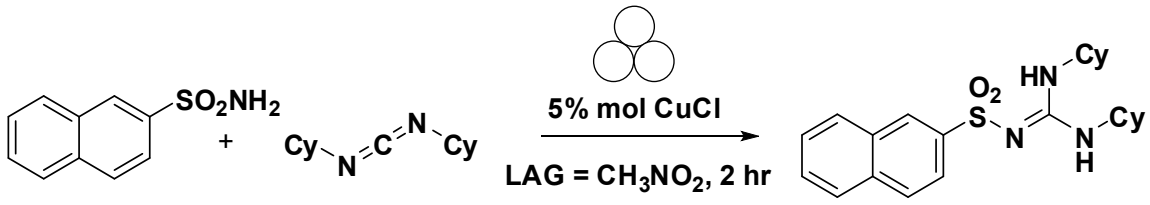

Entry	CuCl (% mol)	time (hr)	LAG	Conversion (%)[a]
1	5	2	CH_3NO_2	36
2	10	2	CH_3NO_2	55
3	10	4	CH_3NO_2	75
4	20	2	CH_3NO_2	50
5	20	2	acetone	84
6	10	4	acetone	100[b]
7	10	2	EMK	79
8	10	2	CH_3CN	43
9	10	2	cyclohexanone	61
10	10	2	DMF	47
11	10	2	neat	58

[a]based on ^{1}H-NMR; [b] 92% isolated yield.

To investigate whether a poorly performing coupling reaction can be enhanced and optimized by varying the liquid additive, we focused on the reaction of 2-naphthylsulfonamide and DCC. Optimization parameters included increasing the catalyst amount, reaction time, and conducting milling in the presence of different catalytic liquids (η=0.25 μL/mg): acetonitrile, *N*,*N*-dimethylformamide (DMF), acetone, ethylmethylketone (EMK), cyclohexanone (Table 3.1). Increasing the reaction time to 4 hours or catalyst content to 20 mol% improved the yield of **5a** from 50% to 75% yield, respectively. However, a significantly higher isolated yield of 84% was obtained using acetone as the grinding liquid in combination with 20 mol% CuCl. Further optimization of this reaction systems led to a quantitative conversion (based on ^{1}H-NMR analysis in solution and solid-state FTIR-ATR spectrum of the crude reaction mixture after milling) and 92% isolated yield of the desired 2-naphthylsulfonylguanidine **5a** at 10 mol% catalyst loading. We believe that the described optimization of the mechanosynthesis of **5a** strongly suggests that the initially poorer reactivity of 2-naphthyl- and *p*-nitrophenylsulfonamides is not associated to effects of solid-

state structure (*e.g.* high melting point[16b]), but is more likely a result of conventional molecular-level factors (*i.e.* steric hindrance, electronic effects). The presented work suggests that this copper-catalyzed coupling can be enhanced by certain mechanochemical reaction environments. At a first glance, it appears that ketone-based liquid additives represent a "sweet spot" of reactivity for the combination of 2-naphthylsulfonamide with DCC.

3.6 Infra-red spectroscopy, single crystal X-ray diffraction analysis and gram scale synthesis

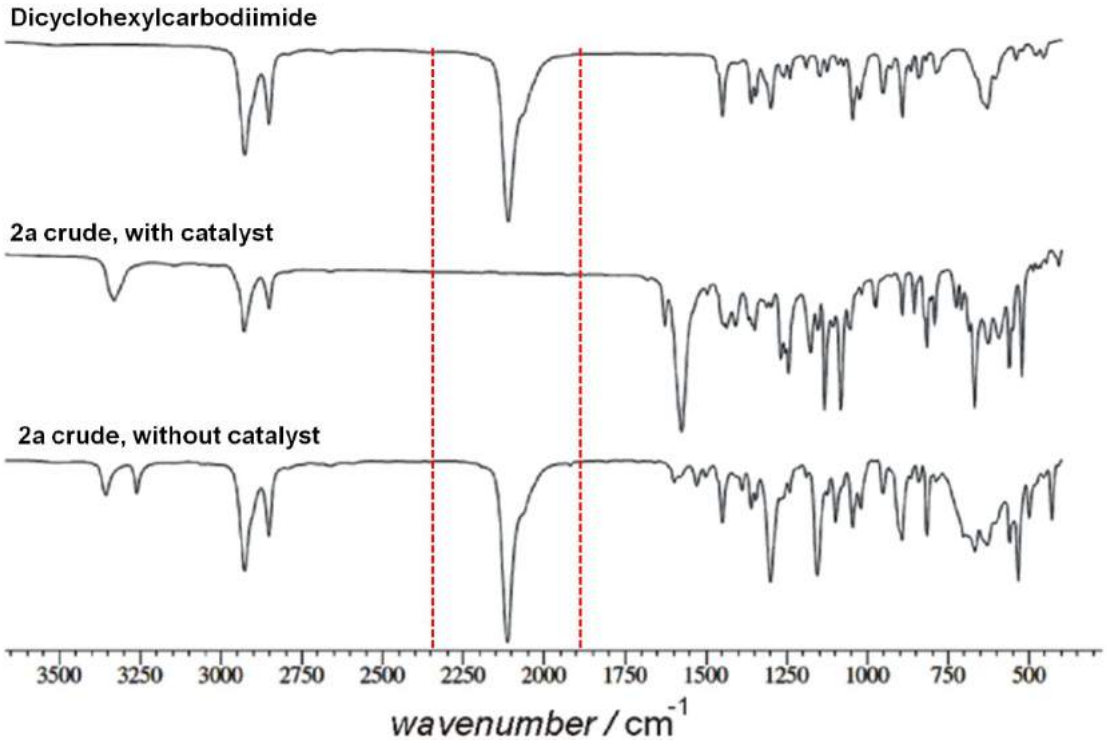

Fig. 3.9. Comparison of FTIR-ATR spectra for the mechanosynthesis of **2a**: reactant DCC (top); freshly milled reaction mixture containing 5 mol% CuCl (middle) and freshly milled mixture of DCC and p-tolylsulfonamide without CuCl (bottom). The overlay clearly shows that the coupling reaction takes place during milling and requires CuCl catalyst.

That the formation of **2a** indeed took place by a mechanochemical copper-catalyzed coupling, rather than during work-up, is supported by Fourier-transform attenuated total reflectance (FTIR-ATR) spectroscopy. Spectroscopic analysis (Fig. 3.9) clearly revealed the absence of the characteristic carbodiimide vibration band at 2120 cm^{-1} immediately after milling, consistent with the coupling taking place mechanochemically. In contrast, if the

milling was performed in the absence of CuCl, the carbodiimide signal was clearly visible, confirming that the milling reaction does not proceed without a copper catalyst. Similar spectra were also observed for the crude mixture for the reaction of trifluoromethylsulfonamide, *p*-tolylsulfonamide and *p*-chlorophenylsulfonamide with DTMSC, in attempts to form **1e**, **2e** and **3e** respectively (please see *Chapter 8, Section 8.2.4*). However, the peaks at 2180 cm^{-1} in the FTIR-ATR spectrum indicated the presence of unreacted DTMSC, which is also corroborated by ^{1}H-NMR spectroscopic analysis.

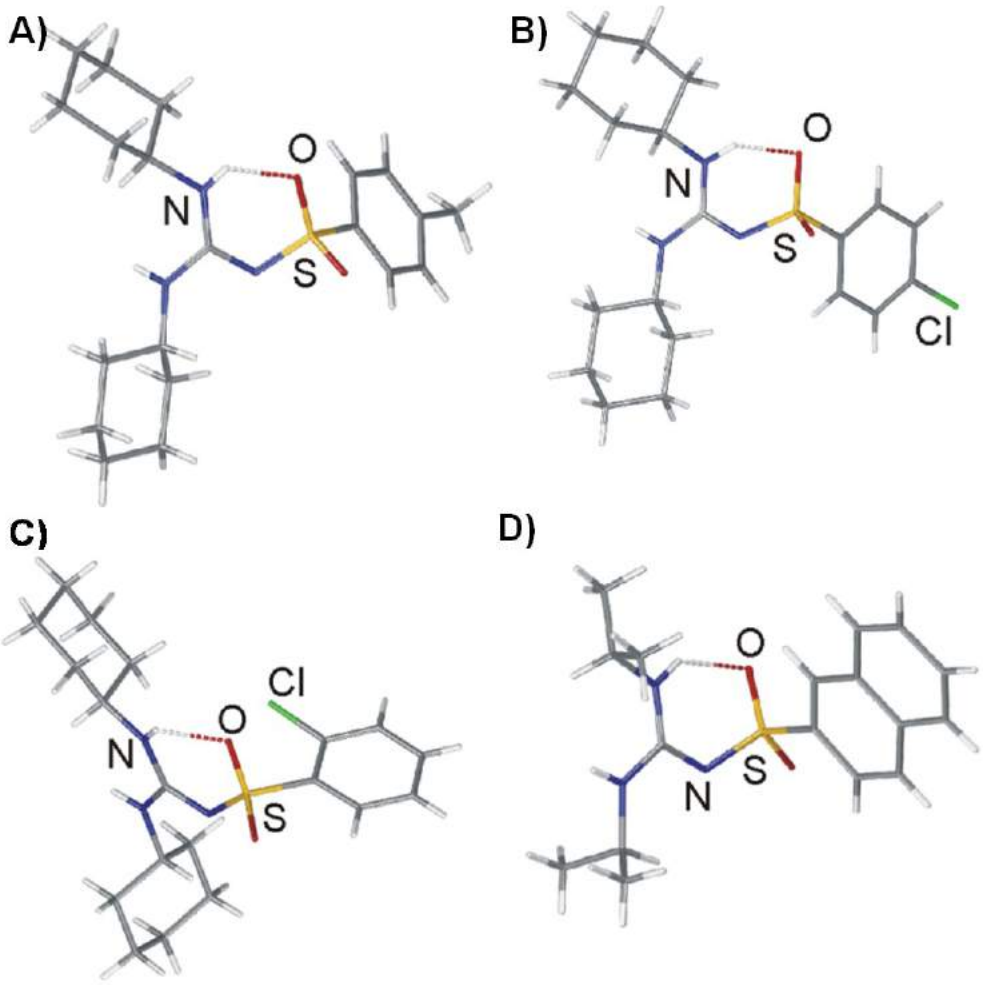

Fig. 3.10. Molecular structures of mechanochemical products: a) **2a**, b) **3a**, c) **4a** and d) **5b** as determined by single crystal X-ray diffraction analysis. Detailed crystallographic data can be found in *Appendix B*.

The formation of selected products was also confirmed by X-ray crystallography on single crystals grown after work-up (Fig. 3.10). Crystal structures of **2a**, **4a**, **5b** and **6a** obtained from XRD data clearly confirmed the presence of sulfoguanidine moieties, and the

expected formation of an intramolecular N-H···O hydrogen-bond.[30] Detailed crystallographic data can be found in *Appendix B*.

In addition, similar to **2a**, model synthesis of **3b**, **4c** and **6b** were performed under conventional refluxing methods using acetone as the solvent and was compared to their mechanochemical counterpart. After 18 hours at reflux in acetone, using 10 mol% CuCl, the conversion into **3b** and **6b** was only 8% and 5%, respectively, whereas no conversion was observed for **4c**. This presents a very unique system whereby the synthesis of the arylsulfonylguanidine moiety through direct coupling of arylsulfonamides with carbodiimides was only possible using mechanochemistry, but not possible using traditional solution methods.

Finally, we explored the possibility of scaling up the mechanochemical procedure to >1 gram (Fig. 3.11). As model reactions, we used the syntheses of **2a** and **2b** and obtained the desired products in 96% and 87% yields, respectively, denoting the feasibility of adapting the mechanosynthetic protocols to larger scales. Experimental details for the mechanochemical gram scale reaction can be found in *Chapter 8, Section 8.2*.

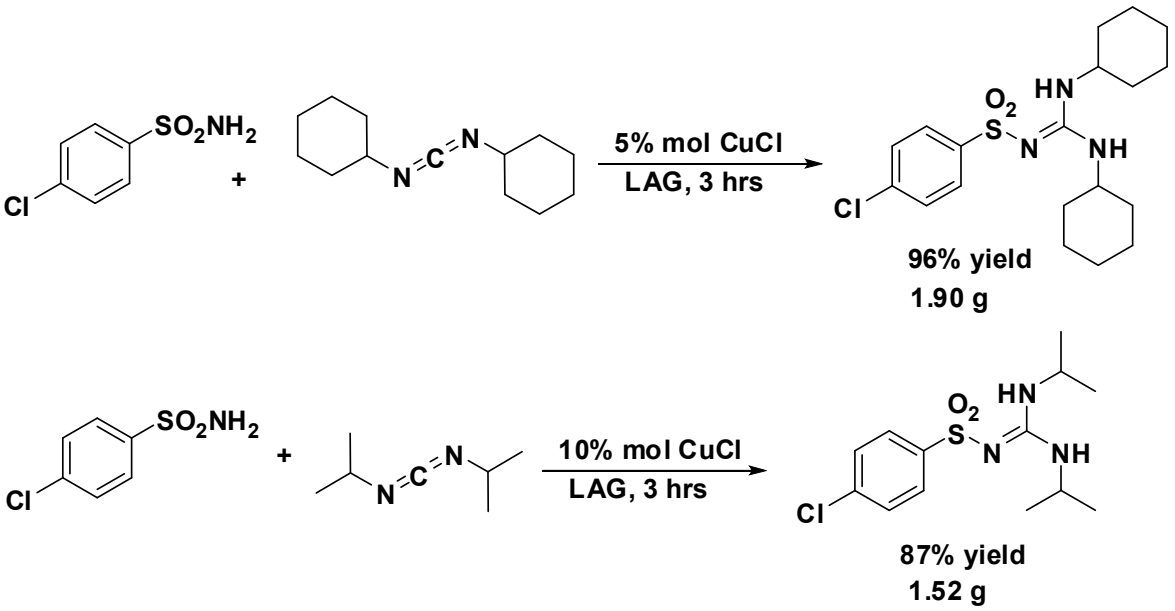

Fig. 3.11. Mechanochemical coupling on gram scale. One 10 mm diameter stainless steel ball in a 10 mL stainless steel jar was used, at a frequency of 30 Hz, in the presence of nitromethane (η = 0.25 μL/mg).

3.7 Conclusion

In summary, we have demonstrated the use of mechanochemical synthesis to establish a novel synthetic strategy for the synthesis of arylsulfonylguanidines, in excellent isolated yields, by direct copper-catalyzed coupling of various sulfonamides with aromatic or aliphatic carbodiimides. The synthesis is attractive, having in mind the interest in sulfonylguanidines as pharmaceutical targets, as well as the demands[32] of pharmaceutical industries for the development of cleaner and more efficient synthesis. A total of 22 compounds were synthesized and 10 crystal structures were obtained. However, the most important aspect of the presented work is the first exploration of a novel synthetic strategy by using exclusively mechanochemical synthetic procedures. Indeed, attempts to conduct the reaction using conventional solution chemistry were unsuccessful. Consequently, we believe that the presented work demonstrates the use of mechanochemical synthesis and ball milling not only as a tool to make existing synthetic procedures cleaner, but to pursue the discovery and the development of new synthetic pathways. We are now performing extensive reaction screens and initiating computational studies that would allow us to elucidate the mechanism and aid in the rational optimization of this, and related, mechanosynthetic coupling procedures.

3.8 References

1 S. L. James, C. J. Adams, C. Bolm, D. Braga, P. Collier, T. Friščić, F. Grepioni, K. D. M. Harris, G. Hyett, W. Jones, A. Krebs, J. Mack, L. Maini, A. G. Orpen, I. P. Parkin, W. C. Shearouse, J. W. Steed, D. C Waddell, *Chem. Soc. Rev.,* **2012**, *41*, 413; b) A. Bruckmann, A. Krebs, C. Bolm, *Green Chem.,* **2008**, *10*, 1131.

2 a) A. Stolle, T. Szuppa, S. E. S. Leonhardt, B. Ondruschka, *Chem. Soc. Rev.,* **2011**, *40*, 2317; b) G.-W. Wang, *Chem. Soc. Rev.,* **2013**, *42*, 7668; c) E. Boldyreva, *Chem. Soc. Rev.,* **2013**, *42*, 7719.

3 a) P. Baláž, M. Achimovičová, M. Baláž, P. Billik, Z. Cherkezova-Zheleva, J. M. Criado, F. Delogu, E. Dutková, E. Gaffet, F. J. Gotor, R. Kumar, I. Mitov, T. Rojac, M. Senna, A. Streletskii, K. Wieczorek-Ciurowa, *Chem. Soc. Rev.,* **2013**, *42*, 7571; b) V. Šepelák, S. Bégin-Colin, G. Le Caër, *Dalton Trans.,* **2012**, *41*, 11927.

4 a) D. Braga, L. Maini, F. Grepioni, *Chem. Soc. Rev,* **2013**, *42*, 7638; b) D. R. Weyna, T. Shattock, P. Vishweshwar, M. J. Zaworotko, *Cryst. Growth Des.* **2009**, *9*, 1106; c) D. J.

Berry, C. C. Seaton, W. Clegg, R. W. Harrington, S. J. Coles, P. N. Horton, M. B. Hursthouse, R. Storey, W. Jones, T. Friščić, N. Blagden, *Cryst. Growth Des.,* **2008**, *8*, 1697.

5 a) T. Friščić, D. G. Reid, I. Halasz, R. S. Stein, R. E. Dinnebier, M. J. Duer, *Angew. Chem. Int. Ed.,* **2010**, *49*, 712; b) B. P. Biswal, S. Chandra, S. Kandambeth, B. Lukose, T. Heine, R. Banerjee, *J. Am. Chem. Soc.,* **2013**, *135*, 5328.

6 a) J. G. Hernández, E. Juaristi, *Chem. Commun.*, **2012**, *48*, 5396; b) B. Rodríguez, T. Rantanen, C. Bolm, *Angew. Chem. Int. Ed.,* **2006**, *118*, 7078; c) B. Rodríguez, A. Bruckmann, C. Bolm, *Chem. Eur. J.,* **2007**, *13*, 4710; d) Y.-F. Wang, R.-X. Chen, K. Wang, B.-B. Zhang, Z.-B. Li, D.-Q. Xu, *Green Chem.,* **2012**, *14*, 893.

7 a) T. L. Cook, J. A. Walker, J. Mack, *Green Chem.*, **2013**, *15*, 617; b) R. Thorwirth, A. Stolle, B. Ondruschka, *Green Chem.*, **2010**, *12*, 985; c) D. A. Fulmer, W. C. Shearouse, S. T. Medonza, J. Mack, *Green Chem.,* **2009**, *11,* 1821; d) R. Thorwirth, A Stolle, B. Ondruschka, A. Wild, U. S. Schubert, *Chem. Commun.,* **2011**, *47*, 4370; e) G.-W. Wang, Y.-W. Dong, T.-T. Yuan, Y.-B. Shen, *J. Org. Chem.,* **2008**, *73*, 7088; f) E. Tullberg, F. Schacher, D. Peters, T. Frejd, *Synthesis,* **2006**, *7*, 1183.

8 a) A. M. Flock, C. M. M. Reucher, C. Bolm, *Chem.-Eur. J.,* **2010**, *16*, 3918; b) B. Rodríguez, T. Rantanen, C. Bolm, *Angew. Chem. Int. Ed.,* **2006**, *118*, 7078; c) J. Hernández, E. Juaristi, *J. Org. Chem.,* **2011**, *76*, 1464; d) P. Nun, V. Pérez, M. Calmès, J. Martinez, F. Lamaty, *Chem. Eur. J.,* **2012**, *18*, 3773.

9 a) T. Friščić, A. V. Trask, W. Jones, W. D. S. Motherwell, *Angew. Chem. Int. Ed.,* **2006**, *45*, 7546; b) T. Friščić, W. Jones, *Cryst. Growth Des.,* **2009**, *9*, 1621; c) R. Schmidt, A. Stolle, B. Ondruschka, *Green Chem.,* **2012**, *14*, 1673; d) G. A. Bowmaker, *Chem. Commun.,* **2013**, *49*, 334; e) K. L. Nguyen, T. Friščić, G. M. Day, L. F. Gladden, W. Jones, *Nature Mater.,* **2007**, *6*, 206.

10 a) F. Schneider, T. Szuppa, A. Stolle, B. Ondruschka, H. Hopf, *Green Chem.,* **2009**, *11*, 1894; b) R. B. N. Baig, R. S. Varma, *Chem. Soc. Rev.,* **2012**, *41*, 1559.

11 a) T. Friščić, S. L. Childs, S. A. A. Rizvi, W. Jones, *CrystEngComm,* **2009**, *11*, 418; b) T. Friščić, *Chem. Soc. Rev.,* **2012**, *41*, 3493.

12 a) K.-D. Wu, Y.-H. Lin, C.-C. Lai, S.-H. Chiu, *Org. Lett.* **2014**, *16*, 1068; b) D. Cinčić, T. Friščić, W. Jones, *J. Am. Chem. Soc.,* **2008**, *130*, 7524; c) I. Halasz, A. Puškarić, S.

A. J. Kimber, P. J. Beldon, A. M. Belenguer, F. Adams, V. Honkimäki, R. E. Dinnebier, B. Patel, W. Jones, V. Štrukil, T. Friščić, *Angew. Chem. Int. Ed.,* **2013,** *52*, 11538.

13 a) V. Štrukil, L. Fábián, D. G. Reid, M. J. Duer, G. J. Jackson, M. Eckert-Maksić, T. Friščić, *Chem. Commun.,* **2010**, *46*, 9191; b) G. A. Bowmaker, N. Chaichit, C. Pakawatchai, B. W. Skelton, A. H. White, *Chem. Commun.,* **2008**, 2926.

14 a) C. B. Aakeröy, P. D. Chopade, *Org. Lett.,* **2011**, 1*3*, 1; b) C. B. Aakeröy, A. S. Sinha, K. N. Epa, C. L. Spartz, J. Desper, *Chem. Commun.,* **2012**, *48*, 11289.

15 a) V. Štrukil, D. Margetić, M. D. Igrc, M. Eckert-Maksić, T. Friščić, *Chem. Commun.,* **2012**, *48*, 9705; b) M. Ferguson, N. Giri, X. Huang, D. Apperley, S. L. James, *Green Chem.,* **2014**, *16*, 1374; c) V. Štrukil, M. D. Igrc, M. Eckert-Maksić, T. Friščić, *Chem. Eur. J.,* **2012**, *18*, 8464.

16 a) B. Rodríguez, A. Bruckmann, T. Rantanen, C. Bolm, *Adv. Synth. Catal.,* **2007**, *349*, 2213; b) G. Rothenberg, A. P. Downie, C. L. Raston, J. L. Scott, *J. Am. Chem. Soc.,* **2001**, *123*, 8701; c) K. Tanaka, F. Toda, *Chem. Rev.,* **2000**, *100*, 1025; d) F. Ravalico, S. L. James, J. S. Vyle, *Green Chem.,* **2011**, *13*, 1778; e) J. G. Hernández, E. Juaristi, *J. Org. Chem.,* **2010**, *75*, 7107; f) A. Baron, J. Martinez, F. Lamaty, *Tetrahedron,* **2010**, *51*, 6246.

17 a) M. Pascu, A. Ruggi, R. Scopelliti, K. Severin, *Chem. Commun.,* **2013**, *49*, 45; b) P.-N. Chen, C.-C. Lai, S.-H. Chiu, *Org. Lett.,* **2011**, *13*, 4660; c) V. P. Balema, J. W. Wiench, M. Pruski, V. K. Pecharski, *J. Am. Chem. Soc.,* **2002**, *124*, 6244.

18 J. Bonnamour, T.-X. Métro, J. Martinez, F. Lamaty, *Green Chem.,* **2013**, *15*, 1116.

19 B. Içli, N. Christinat, J. Tönneman, C. Schüttler, R. Scopelliti, K. Severin, *J. Am. Chem. Soc.,* **2009**, *131*, 3154.

20 a) J. Schmeyers, F. Toda, J. Boy, G. Kaupp, *Perkin Trans. 2,* **1998**, 989; b) P. Nun, C. Martin, J. Martinez, F. Lamaty, *Tetrahedron,* **2011**, *67*, 8187; c) D. S. Bose, A. V. Narsaiah, *Tetrahedron Lett.,* **1998**, *39*, 6533; d) E. Colacino, P. Nun, F. M. Colacino, J. Martinez, F. Lamaty, *Tetrahedron,* **2008**, *64*, 5569; e) R. Thorwirth, F. Bernhardt, A. Stolle, B. Ondruschka, J. Asghari, *Chem. Eur. J.,* **2010**, *16*, 13236.

21 D. Tan, V. Štrukil, C. Mottillo, T. Friščić, *Chem. Commun.,* **2014**, *50*, 5248.

22 a) V. Štrukil, B. Bartolec, T. Portada, I. Đilović, I. Halasz, D. Margetić, *Chem. Commun.,* **2012**, *48*, 12100; b) T.-X. Métro, J. Bonnamour, T. Reidon, J. Sarpoulet, J. Martinez, F. Lamaty, *Chem. Commun.,* **2012**, *48*, 11781.

23 R. G. S. Berlinck, A. E. Trindade-Silva, M. F. C. Santos, *Nat. Prod. Rep.,* **2012**, *29*, 1382.

24 T. Isobe, K. Fukuda, T. Ishikawa, T. *J. Org. Chem.,* **2000**, *65*, 7770.

25 a) C. Uyeda, E. N. Jacobsen, *J. Am. Chem. Soc.* **2011**, *133*, 5062; b) T. Ishikawa, T. Isobe, *Chem. Eur. J.,* **2002**, *8*, 553; c) D. Leow, C.-H. Tan, *Chem. Asian. J.,* **2009**, *4*, 488.

26 S. Tsuji, S. Kawano, M. Tsujii, N. Kawai, E. S. Gunawan, W. H. Sun, M. Hori, *Arzneimittelforschung,* **2001**, *51*, 46.

27 a) J. H. M. Lange, H. K. A. C. Coolen, H. H. van Stuivenberg, J. A. R. Dijksman, A. H. J. Herremans, E. Ronken, H. G. Keizer, K. Tipker, A. C. McCreary, W. Veerman, H. C. Wals, B. Stork, P. C. Verveer, A. P. den Hartog, N. M. J. de Jong, T. J. P. Adolfs, J. Hoogendoorn, C. G. J. Kruse, *Med. Chem.,* **2004**, *47*, 627; b) A. Ishikawa, M. Matsuoka, T. Tsuchida, F. Yoshinaga, *Biosci. Biotech. Biochem.*, **1995**, *59*, 2259.

28 K. Shiokawa, M. Koichi, T. Goto, A. Kamochi, S. Kohama, *United States Patent*, **1985**, *USP No. 4559079*.

29 J. H. M. Lange. S. Verhoog, H. J. Sanders, A. Loevezijn, C. G. Kruse, *Tetrahedron Lett.,* **2011**, *51*, 3198.

30 a) B. A. Shainyan, L. L. Tolstikova, U. Schilde, *J. Fluor. Chem.,* **2012**, *135*, 261; b) L. L. Tolstikova; N. N. Chipanina, L. P. Oznobikhina, B. A. Shainyan, *Russ. J. Org. Chem.,* **2011**, *47*, 1278.

31 LAG reactions are described using the η parameter: the ratio of added liquid (in μL) per mass of the solid reaction mixture (in mg), which typically ranges from 0.1-1 μL/mg, see: T. Friščić, S. L. Childs, S. A. A. Rizvi, W. Jones, *CrystEngComm,* **2009**, *11*, 418.

32 a) P. J. Dunn, *Chem. Soc. Rev.,* **2012**, *41*, 1452; b) C. Jiménez-González, D. J. C. Constable, C. S. Ponder, C. S. *Chem. Soc. Rev.,* **2012**, *41*, 1485; c) H.-J. Federsel, *Green Chem.,* **2013**, *15*, 3105; d) W. J. W. Watson, *Green Chem.* **2012**, *14*, 251.

CHAPTER 4

CARBODIIMIDE INSERTION INTO SULFONIMIDES: ONE-STEP ROUTE TO AZEPINE DERIVATIVES BY A TWO-ATOM SACCHARIN RING EXPANSION

"It is great to see young, energetic scientists caring about how to conduct chemistry in a greener way." -Rajender S. Varma, Pacifichem, 2015.

4.1 Introduction and connecting text.

The work presented in this chapter is part of a recently published paper entitled "Carbodiimide insertion into sulfonimides: one-step route to azepine derivatives by a two-atom saccharin ring expansion", which describes a previously unknown insertion reaction of carbodiimides into sulfonimides, enabling the first one-step, two-atom expansion of the 5-membered ring of saccharin into a 7-membered benzo[1,2,4]thiadiazepine, and a two-atom chain extension of a non-cyclic sulfonimide. The paper was written by D. Tan with guidance and editing contributions from Prof. T. Friščić, The text has been formatted and re-written for inclusion in this Dissertation. All experimental results, including screening, synthesis and instrumental characterization (FTIR, NMR, MS, XRD) of the various compounds were performed by D. Tan. This work has been re-written for inclusion in this chapter with additional results included from the supporting information. In *Chapters 2* and *3* of this Dissertation, the roles of mechanochemistry in affording APIs in a clean and rapid manner, as well as a powerful tool for reaction discovery to access pharmaceutically relevant compounds were discussed. The reactions performed were mostly focused and based on copper-catalyzed mechanochemical coupling between sulfonamides with isocyanates and carbodiimides. As an extension of the substrate scope, in this Chapter, the coupling reaction is extended from acyclic arylsulfonamides to cyclic sulfonamide, namely saccharin, in order to use mechanochemistry for the discovery of new coupling reactions.

The development of coupling reactions is central to modern organic synthesis, leading to simpler, cleaner and often faster chemical transformations that are of particular value in the context of modern pharmaceutical manufacturing.[1,2] With our interest in clean and solvent-free synthesis by mechanochemistry, i.e. reactions induced or sustained by mechanical milling or grinding,[3] we recently demonstrated rapid, high-yielding copper-catalyzed carbon-nitrogen (C-N) coupling reactions of sulfonamides, leading to improved syntheses of anti-diabetic sulfonyl-urea drugs.[4] This led to the discovery of a new route to sulfonylguanidines by direct, copper-catalyzed coupling of sulfonamides and carbodiimides.[5] Using mechanochemistry as a tool for reaction discovery, we attempted to screen various poorly nucleophilic substrates, similar to sulfonamides, to see if they can form C-N bonds with isocyanates or carbodiimides (Fig. 4.1). These substrates include saccharin, isatins, terminal amides such as benzamides, imides such as phthalimide, thymine, ureas and amino acids *etc*. This chapter will discuss specifically the reactions with saccharin and other sulfonimide compounds.

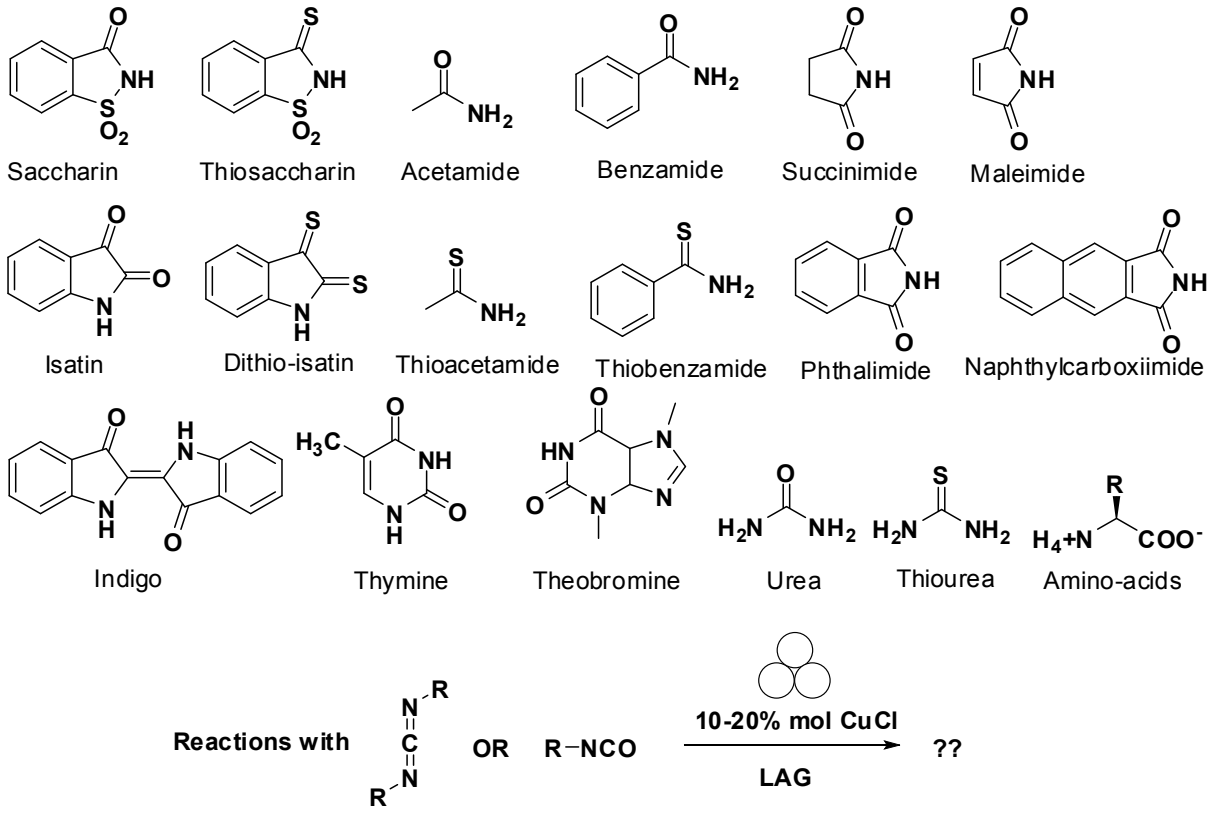

Fig 4.1 Brief overview of mechanochemical screening of various possible C-N coupling reactions between poorly nucleophilic substrates with isocyantes and carbodiimides.

4.2. Saccharin-carbodiimide reaction

As part of the ongoing research program of discovering new C-N coupling reactions, in this chapter, we will discuss the solution and mechanochemical coupling of saccharin and other sulfonimide compounds with carbodiimides and isocyanates. We discovered a previously unknown carbodiimide insertion reaction which enables the direct two-atom expansion of the saccharin imide ring into a seven-membered azepine system. The synthesis of azepines is an active research areas due to their well-established roles in medicinal and pharmaceutical chemistry,[6] with different thiadiazepines being investigated in the treatment of Alzheimer's disease, different varieties of cancer, and diabetes mellitus.[7] While the syntheses of thiadiazepines have mostly focused on benzo[1,2,5]-,[8] benzo[1,3,4]-[9] and, more recently, benzo[1,4,5]thiadiazepines,[10] there have been only a few reports on the herein addressed benzo[1,2,4]thiadiazepine systems.[11] As ring expansion reactions on saccharin are rare, and normally require prior derivatization and stoichiometric auxiliary reagents,[12,13] the

herein presented work is unique as the first report of a one-step expansion of saccharin into a benzothiadiazepine (Fig 4.2).

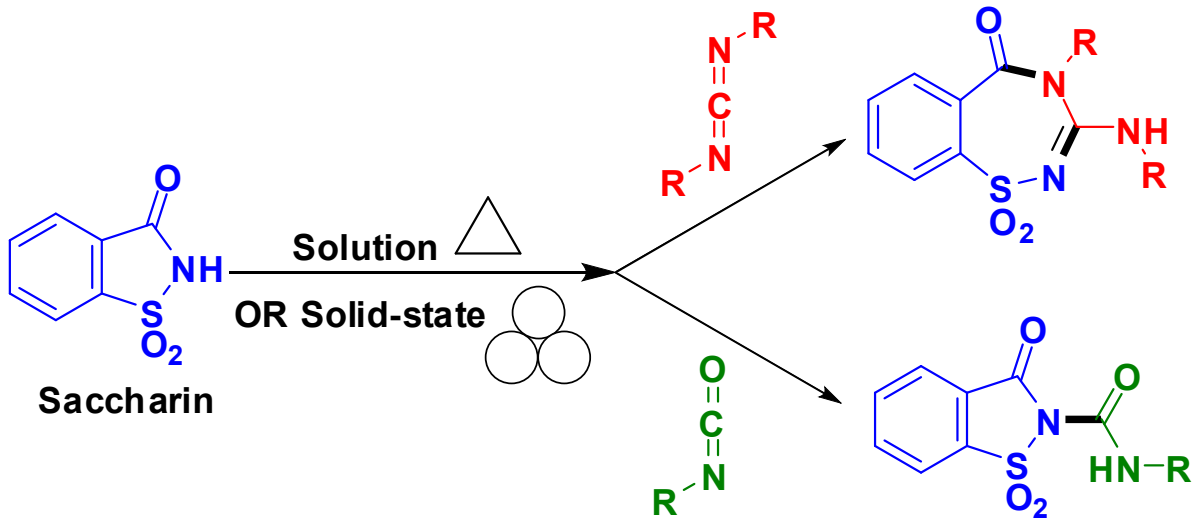

Fig. 4.2. Herein described reactions of saccharin with carbodiimides or isocyanates, yielding benzo[1,2,4]thiadiazepines and saccharyl-ureas, respectively. For clarity, the carbodiimide moiety undergoing insertion is shown in red, and isocyanate fragment undergoing C-N coupling in green. The symbol for mechanochemical reactions has been adopted from the work of Hanusa group.[4h]

This work was inspired by the 1971 report of Lerch and Moffatt,[14] who described the formation of a 1:1 adduct of saccharin with di(cyclohexyl)carbodiimide (DCC) in different solvents. The adduct was never fully characterized, and was proposed to be a saccharyl-guanidine produced by the addition of the saccharin N-H group onto DCC (Fig. 4.3a). As such reactivity would be in contrast to our previous work,[5] which demonstrated that C-N coupling of arylsulfonamides and carbodiimides proceeds efficiently only with a copper catalyst, we decided to reinvestigate this work. Consistent with the published report, room temperature stirring or refluxing of saccharin and DCC in ethyl acetate (EtOAc), acetone, or acetonitrile (Fig 4.3c) produced a white crystalline powder (**1**), characterized by ^{1}H and ^{13}C nuclear magnetic resonance (NMR) spectroscopy, as well as high-resolution mass spectrometry (HRMS) and powder X-ray diffraction (PXRD). Diffraction-quality single crystals of **1** were obtained from acetone and from EtOAc. Whereas ^{1}H-NMR data was consistent with that reported by Lerch and Moffatt, crystal structure determination from SCXRD data revealed **1** is in fact a benzo[1,2,4]thiadiazepine with cyclohexyl groups flanked

in the 2- and 4-positions (Fig 4.3b). Structure of **1** reveals a so far unprecedented one-step expansion of the saccharine ring by insertion of the carbodiimide C-N moiety.

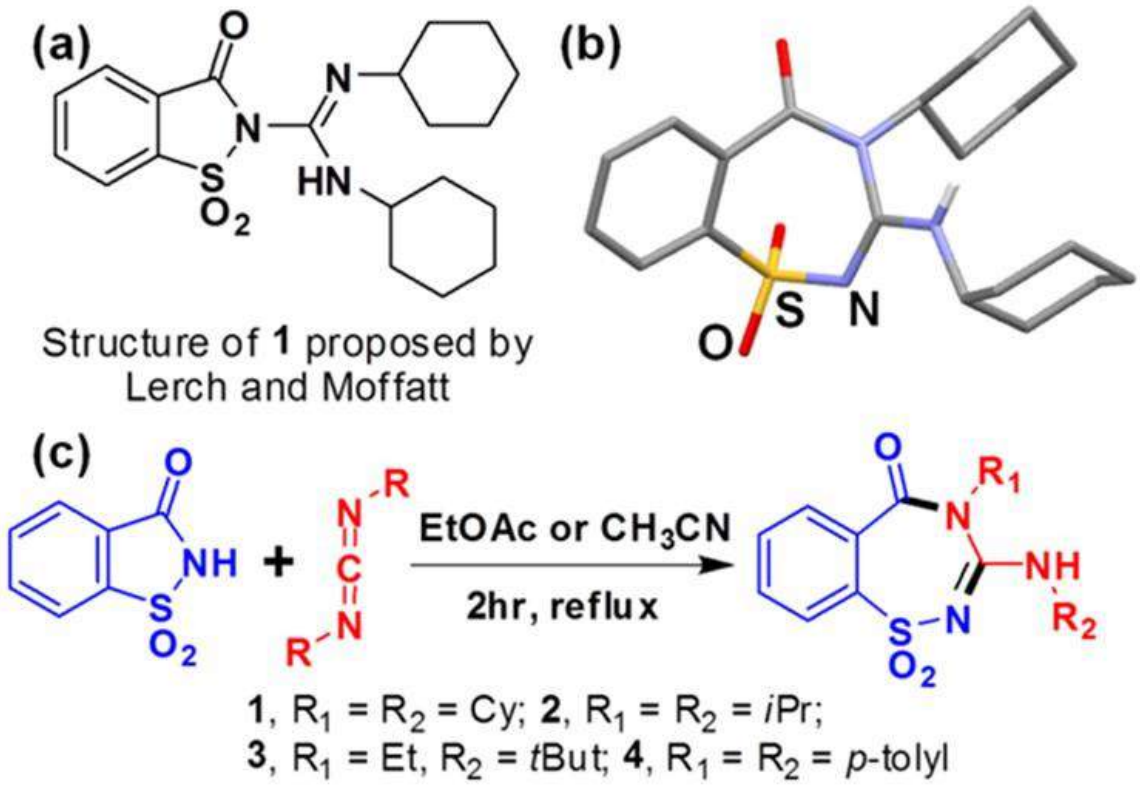

Fig. 4.3. (a) Structure of **1**, as proposed by Lerch and Moffatt and (b) a molecule of **1**, as established by X-ray single crystal diffraction, with hydrogen atoms bonded to carbon omitted for clarity. (c) Reactions of saccharin with commercially available carbodiimides.

Next, we explored reactivity of saccharin with other commercially available carbodiimides (Fig 4.4). Reactions with di(isopropyl)- (DIC), 1-tert-buyl-3-ethyl- (TBEC), or di(p-tolyl)carbodiimide (DPTC) proceeded readily to give **2** (96% yield), **3** (98% yield) and **4** (95% yield), respectively. However, no reaction was observed with more sterically demanding di(tert-butyl)- (DTBC) and di(trimethylsilyl)-carbodiimide (DTMSC). Lack of reactivity with DTBC and DTMSC was evidenced by FTIR-ATR spectra of reaction mixtures after solvent removal, which all exhibited the characteristic carbodiimide band in the 2000-2200 cm^{-1} region (Fig 1d). Compounds **2-4** were fully characterized by NMR, MS, FTIR-ATR and PXRD.

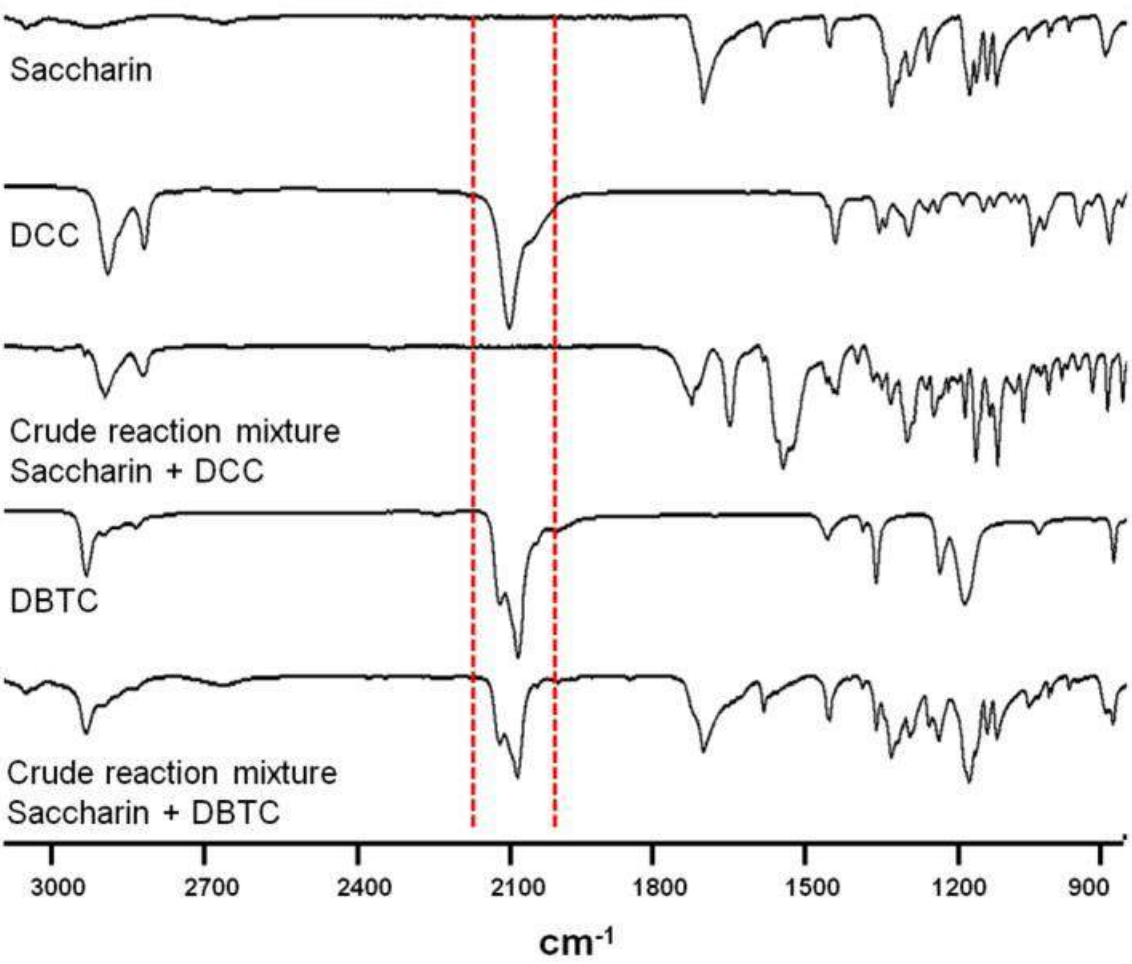

Fig. 4.4. Comparison of FTIR-ATR spectra of reactants and crude reaction mixtures for attempted reactions of saccharin with DCC and DTBC, evidencing complete conversion with DCC, and no reaction with DTBC.

Single crystal X-ray structure determination confirmed **2-4** are all benzo[1,2,4]thiadiazepines resulting from carbodiimide insertion into the saccharin 5-membered ring. Whereas the non-symmetrical TBEC can potentially yield two isomeric ring insertion products, all data so far revealed the formation of only one product, resulting from the insertion of the less sterically-hindered ethyl-substituted side of the TBEC molecule (Fig 4.5).

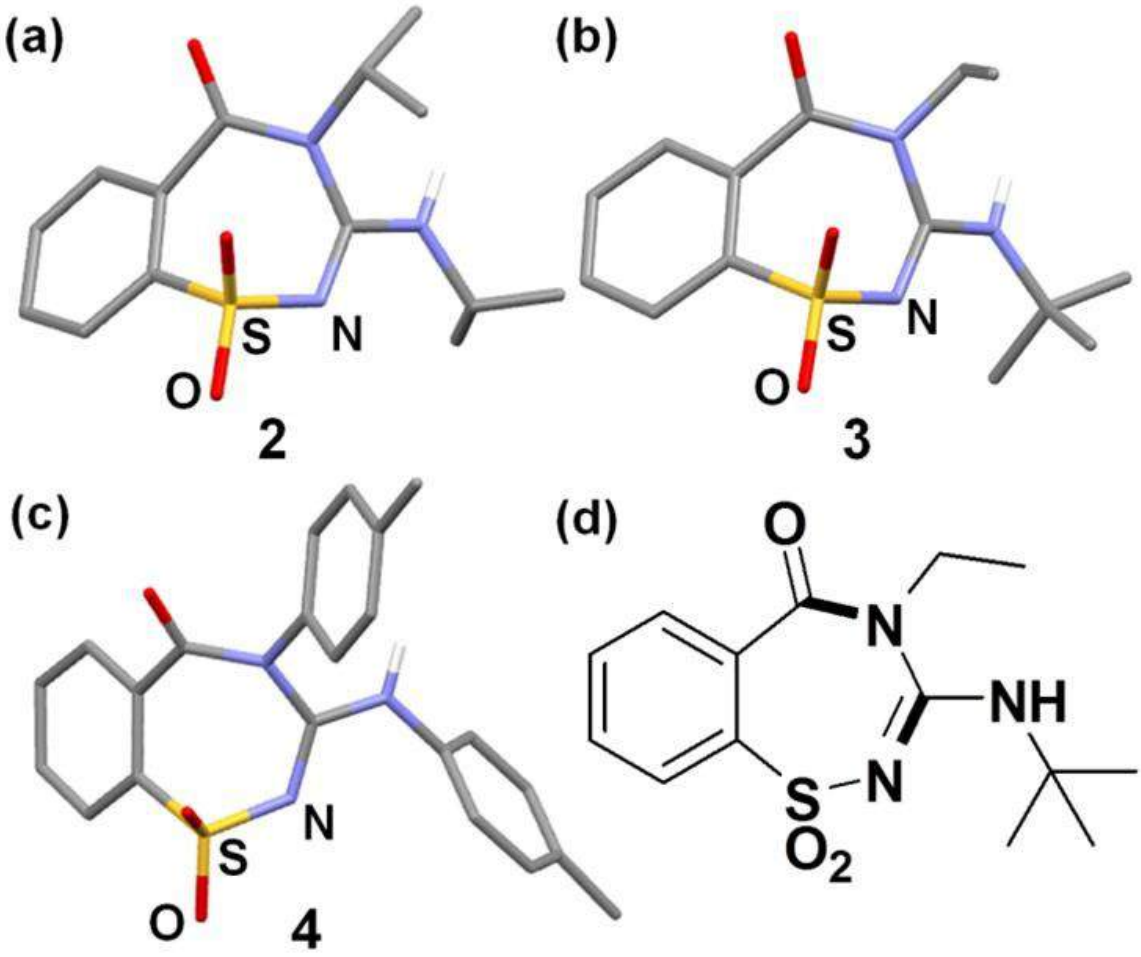

Fig. 4.5. Molecular structures of benzo[1,2,4]thiadiazepines: (a) **2**; (b) **3** and (c) **4**, based on respective single crystal X-ray structures. Hydrogen atoms bonded to carbon atoms are omitted for clarity. (d) Molecular scheme of the only so far observed isomer of **3.**

4.3 From solution to mechanochemistry

With our interest in developing solvent-free reactivity of potential use in pharmaceutical synthesis,[4,5,15] we attempted the C-N insertion by mechanochemistry. No reaction was observed by milling of saccharin and DIC, either neat, or by liquid-assisted grinding (LAG)[16] in the presence of catalytic amounts of EtOAc or nitromethane (50 μL per 200 mg of solid reaction mixture, corresponding to η = 0.25 μL/mg[17]). Next, we explored the use of catalytic CuCl, a strategy that previously enabled the coupling of carbodiimides with sufonamides. Indeed, LAG with 10 mol% of CuCl led to the quantitative formation of **2**, obtained as a white powder after a simple isolation protocol involving brief milling with aqueous Na_2EDTA and washing with deionized water. Formation of **2** by LAG, rather than

during work-up, was confirmed by the FTIR-ATR spectrum of the crude reaction mixture, which showed the complete disappearance of DIC (Fig. 4.6).

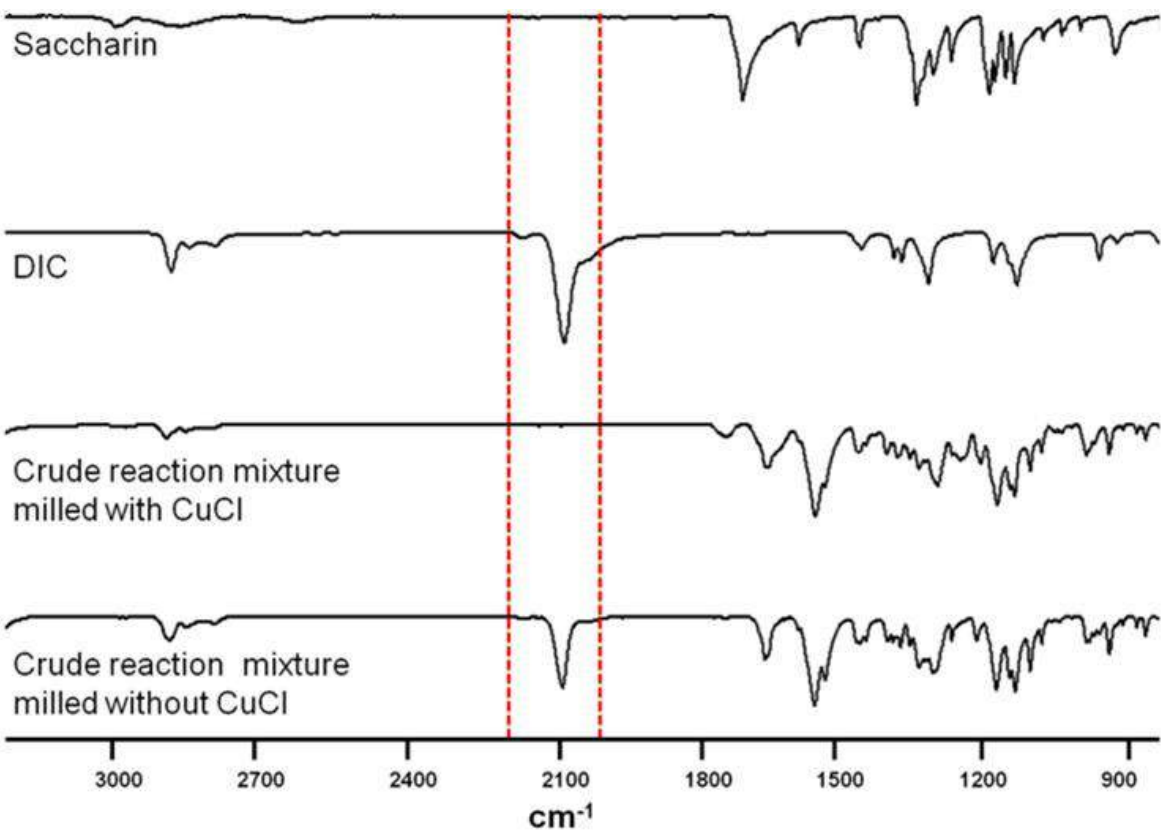

Fig. 4.6 Comparison of FTIR-ATR spectra of DIC and saccharin to that of their crude mechanochemical reaction mixtures with and without CuCl. FTIR-ATR spectra and PXRD patterns confirm the formation of **2** by LAG in presence of CuCl.

That DIC insertion took place by milling is also confirmed by the PXRD pattern of the crude reaction mixture, revealing an excellent fit to that simulated for the obtained single crystal structure of **2** (Fig. 4.7).

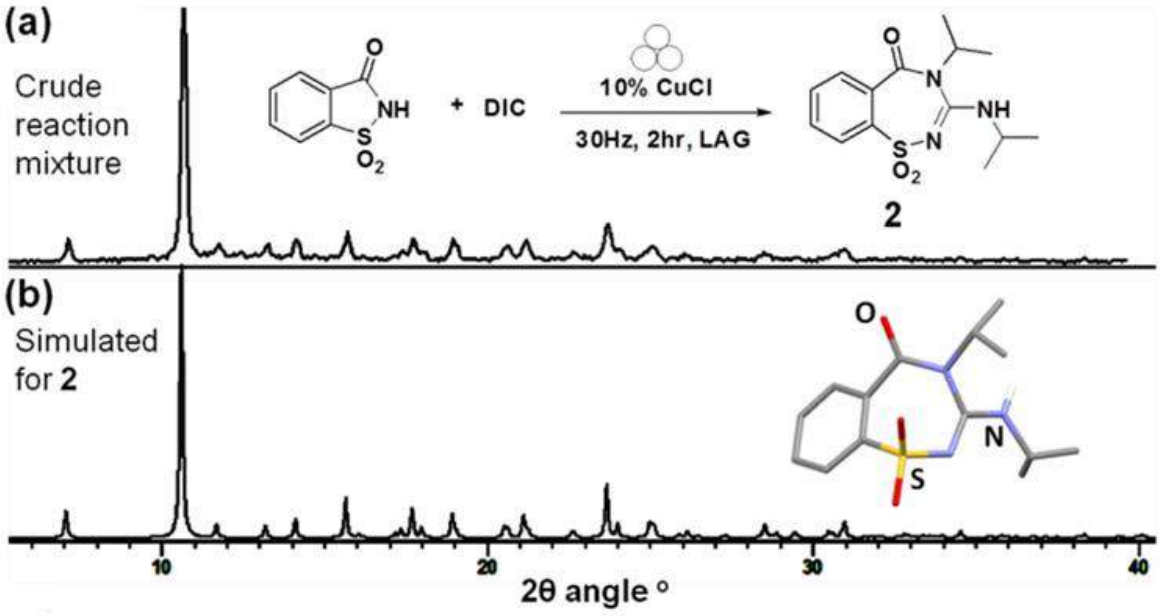

Fig. 4.7 Comparison of PXRD patterns for: (a) crude LAG reaction mixture of DIC and saccharin in presence of CuCl, and (b) the simulated pattern for **2.**

Screening for reactivity of other carbodiimides using copper-catalyzed LAG gave results identical to those seen in solution: DCC, DIC, TBEC and DPTC readily yielded compounds **1-4**, while no transformation was observed with either DTBC or DTBSC, which is consistent with the results obtained from solution. Spectroscopic (FTIR-ATR, NMR, MS) and diffraction (XRD) data of compounds **1-4** can be found in *Appendix C*.

Comparison of the ^{1}H-NMR (Fig. 4.8) and the ^{15}N heteronuclear multiple bond correlation (^{15}N-HMBC) (Fig. 4.9) of the mechanochemical synthesis and solution synthesis of **1** also revealed an excellent match, proving that the product **1** obtained by mechanochemical methods is the same as from solution synthesis. The inconsistency of the ^{1}H-NMR spectra between solution and mechanochemical syntheses, as clearly seen in extra peaks, specifically the triplet at 1.27 ppm and singlet at 2.07 ppm, are due to residual ethyl acetate solvent that was used during the purification for the solution synthesis of **1**.

Table 4.1. Reactions of saccharin with carbodiimides in solution without a catalyst, and by LAG (CH_3NO_2, η = 0.25 mL/mg) with 10 mol% CuCl

Reactant carbodiimide	Product	Solution yield (%)	Mechanochemistry yield (%)
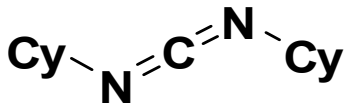	**1**	95	78[a]
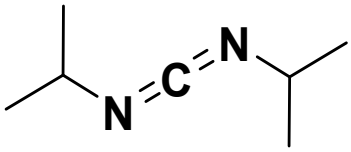	**2**	96	95
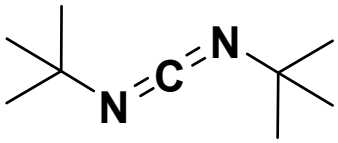	-[b]	-[b]	-[b]
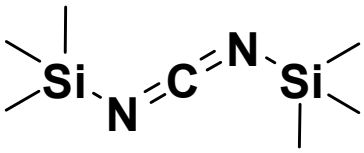	-[b]	-[b]	-[bs]
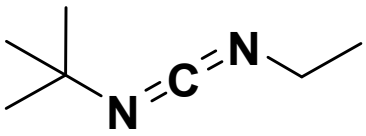	**3**	95	85[a]
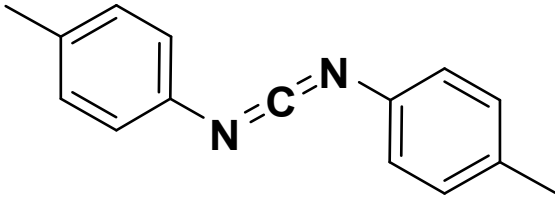	**4**	98	80[a]

[a]Isolated yields after column purification; [b]No reaction was observed with either DTBC or DTMSC.

Similarly, PXRD data of the crude mixture for the mechanochemical synthesis of **1** matches the simulated pattern obtained from single crystal XRD data (Fig. 4.10). This means that **1** is indeed the benzo[1,2,4]thiadiazepine ring-expanded compound and not the previously reported adduct.

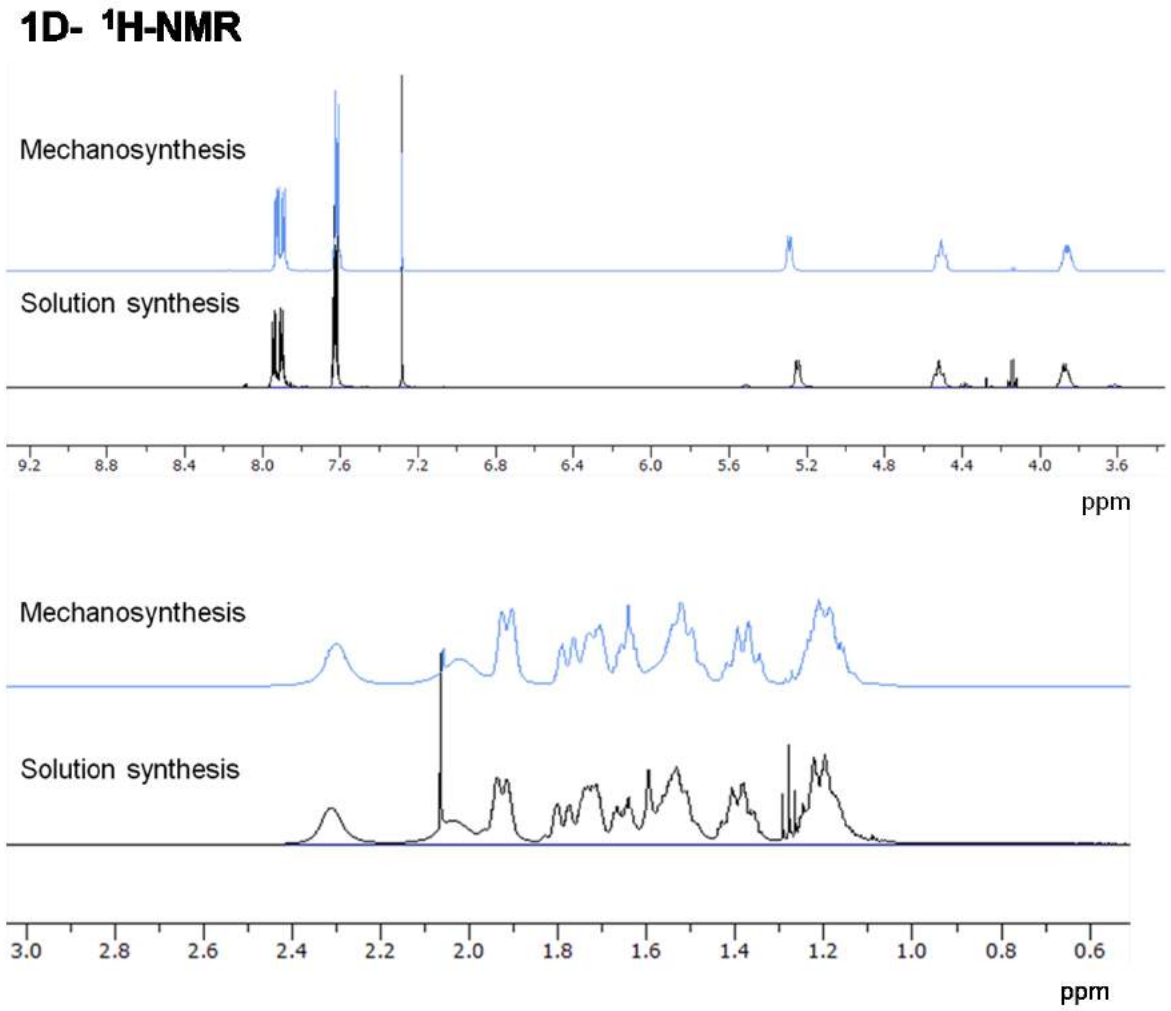

Fig. 4.8 Comparison of ^{1}H-NMR for the mechanosynthesis and solution synthesis of **1.** Deuterated chloroform was used as the NMR solvent.

To further demonstrate the scalability of this novel transformation, syntheses of **1** and **3** were also conducted on 5 mmol scale mechanochemically (by LAG over 4 hours, with 10% mol CuCl), as well as in solution (in refluxing acetone overnight, without catalyst). Compound **1** was obtained in 1.3 g (85% mechanochemically) and 1.4 g (92% in solution) amounts, and **3** in 1.4 g (88% mechanochemically) and 1.3 g (85% in solution) amounts. Experimental details of the gram scale reactions can be found in *Chapter 8, Section 8.4*.

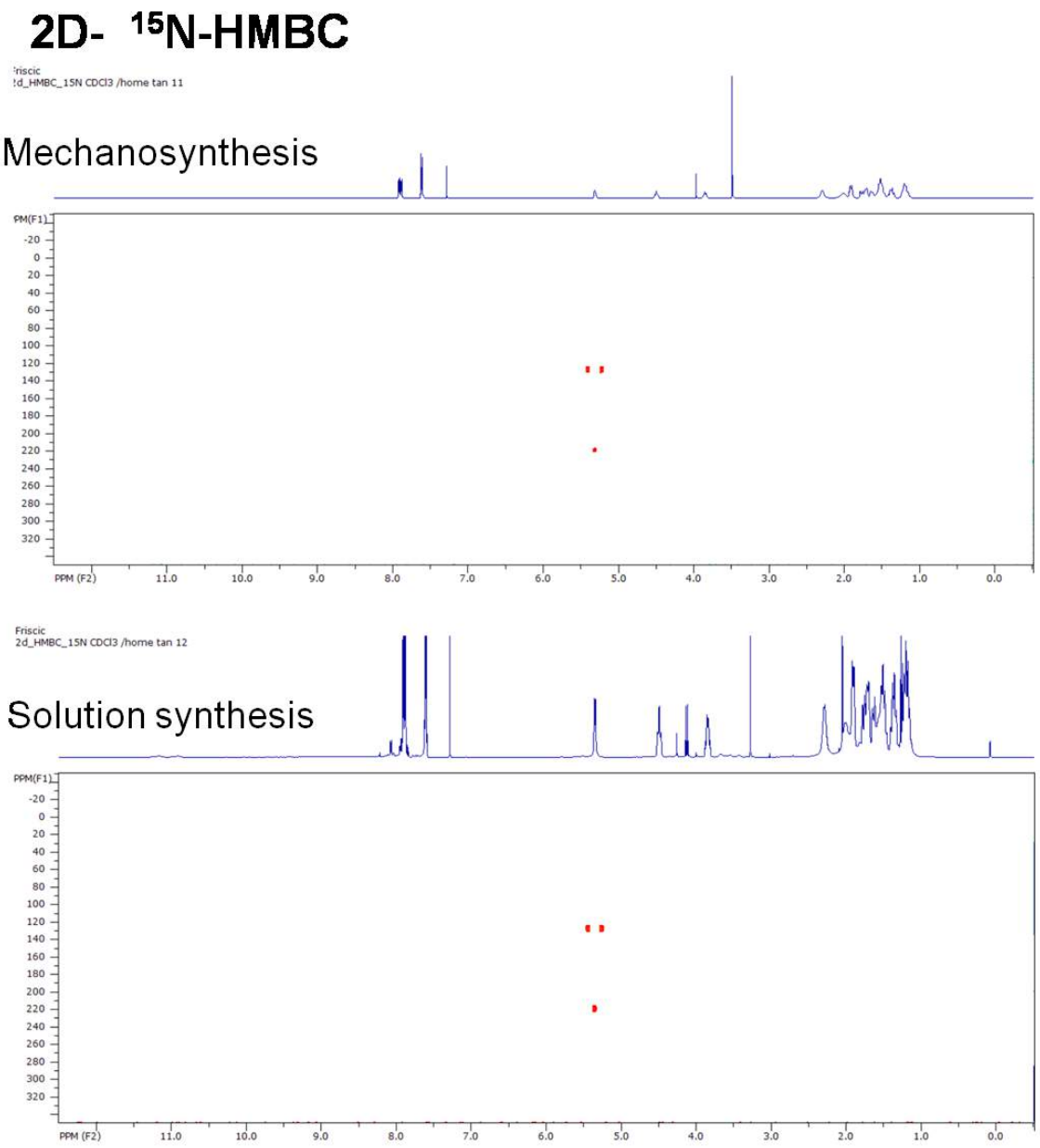

Fig. 4.9. Comparison of ^{15}N-HMBC for the mechanosynthesis and solution synthesis of compound **1**. Deuterated chloroform was used as the NMR solvent.

The catalytic expansion of saccharin is particularly remarkable considering that examples of saccharin ring expansion in the literature are rare and have so far been based on multi-step reactions involving stoichiometric auxiliary reagents. Such transformations include, for example, the formation of an 8-membered ring through N-alkylation with Leakadine and intramolecular nucleophilic ring expansion, reported by Žalubovskis,[18] and the Gabriel-Colman rearrangement[19] in presence of stoichiometric strong base.[20]

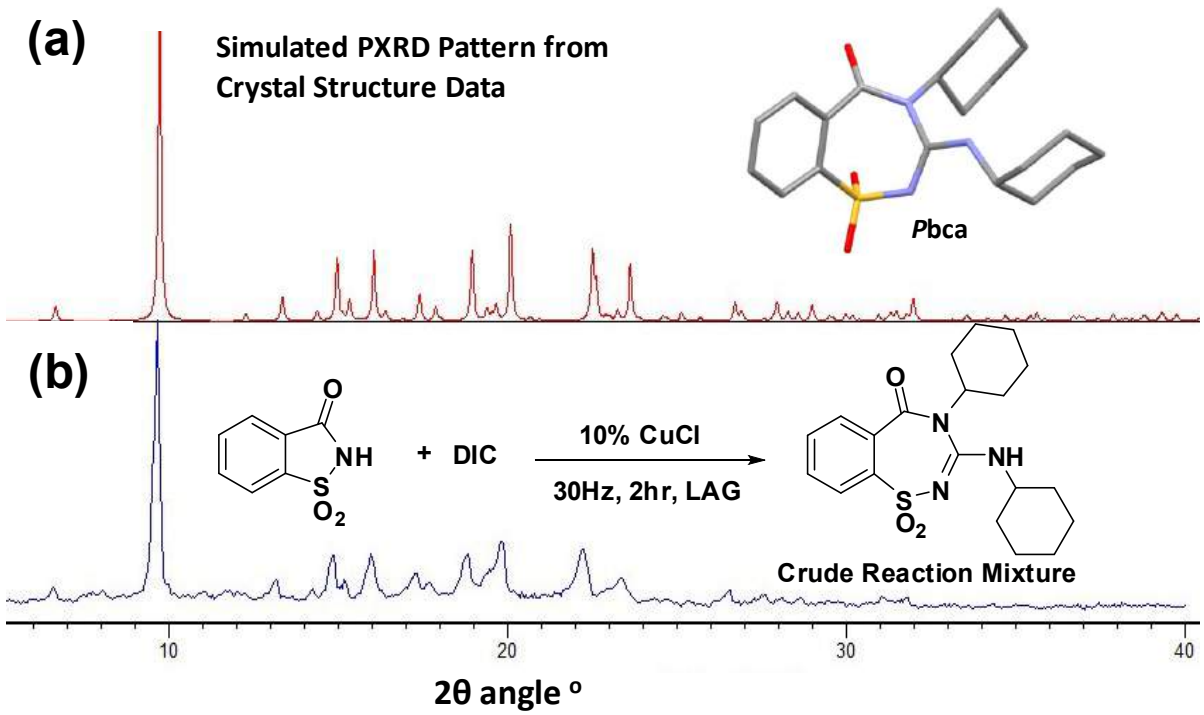

Fig. 4.10. Comparison of the PXRD patterns from (a) the crude mixture of the mechanochemical reaction and (b) the simulated pattern of **1**. The peaks of the crude mixture shows a good fit with the simulated pattern.

4.4 Linear analogue of saccharin

To explore if the facile carbodiimide insertion may be due to the strained nature of the saccharin 5-membered ring, we explored the reactivity of an acyclic analogue of saccharin, 4-methyl-N-tosylbenzamide (**5**), prepared by a Steiglich coupling reaction of p-tolylsulfonamide and toluic acid (Fig. 4.11a). Milling of **5** with DIC in presence of CuCl over two hours gave 30% conversion to a new compound, **6**. The same product was also obtained in 55% conversion by overnight solution reaction in acetone. Eventually, **6** was obtained in quantitative conversion by overnight reflux in acetonitrile in the presence of 20% mol CuCl, as evidenced by 1H-NMR spectroscopy. Compound **6** was characterized by ^{1}H-NMR, MS and FTIR-ATR, as well as by X-ray diffraction on single crystals grown from either methanol or acetone. Crystal structure analysis revealed **6** is the product of carbodiimide insertion into the C-N bond of the sulfonimide moiety of **5** (Fig. 4.11c), which extended the length of the molecule by two atoms. Similar results were also obtained with DCC, yielding the insertion product **7** (Figure 4.11d). Formation of **6** and **7** demonstrates that the saccharin ring is not crucial for the carbodiimide insertion, and that this reaction can be more generally applicable

for chain extension. Spectroscopic (FTIR-ATR, NMR, MS) and diffraction (XRD) data of compounds **5-7** can be found in *Appendix C*.

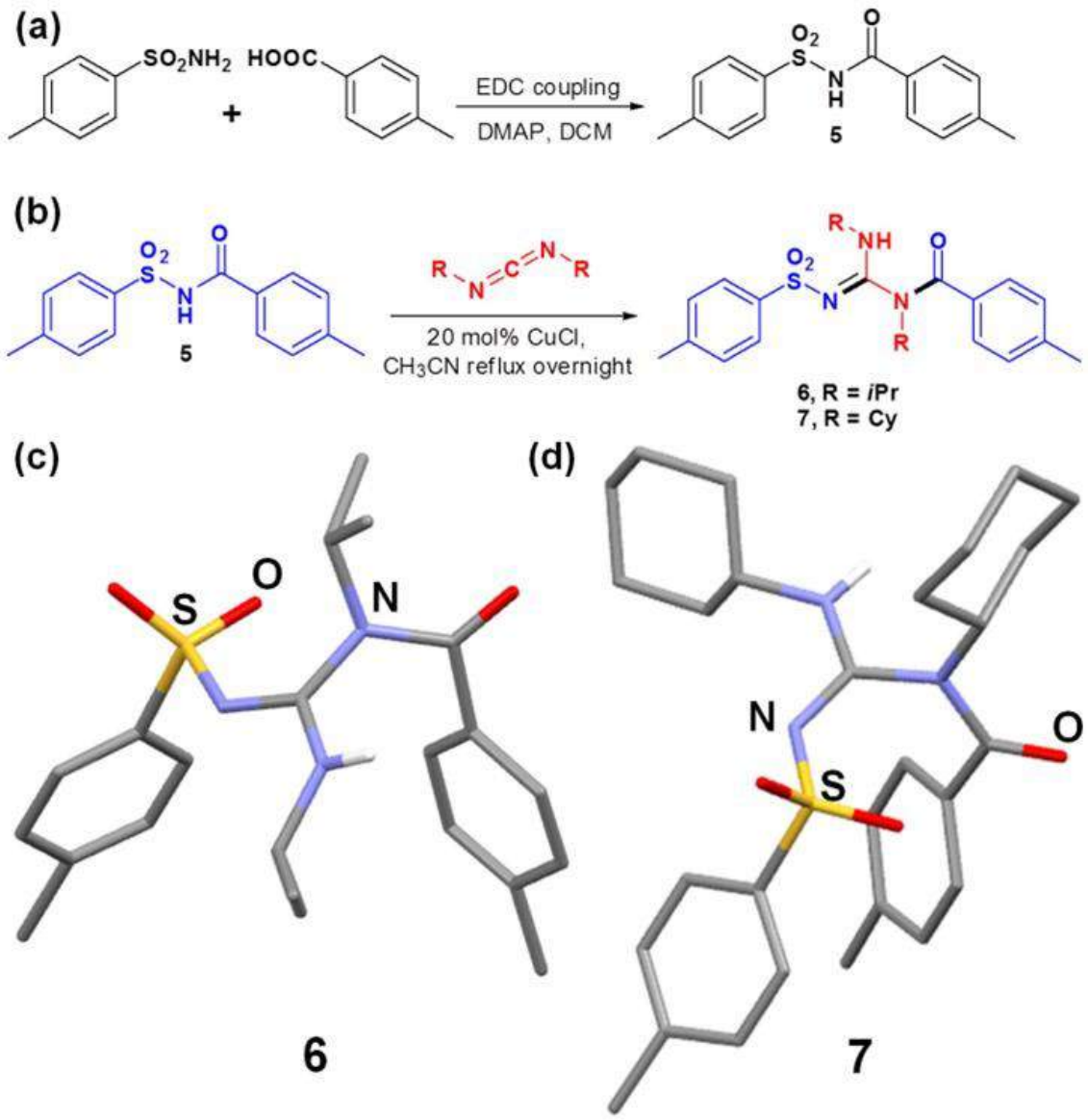

Fig. 4.11. (a) Synthesis of a linear saccharin analogue **5** by Steiglich coupling of p-tolylsulfonamide and *p*-toluic acid in the presence of 1-ethyl-3-(3-dimethyl aminopropyl)carbodiimide (EDC). (b) Insertion reaction of 5 with carbodiimides. Molecular structures of: (c) **6** and (d) **7**, established by single crystal X-ray diffraction.

4.5 Saccharin-isocyanate reaction

Finally, we explored if the ring expansion can be applied to other electrophiles, such as isocyanates. Attempts to conduct a reaction between saccharin and cyclohexylisocyanate, either in solution or by milling were not successful. However, LAG of saccharin and cyclohexylisocyanate (Cy-NCO) in presence of 10 mol% CuCl led to quantitative formation of a new product (**8**), characterized by NMR, MS and FTIR-ATR. Crystal structure analysis (Fig. 4.12b) revealed **8** is a saccharyl-urea that would be expected from a copper-catalyzed C-N coupling analogous to that seen with sulfonamides.[4] Similar results were observed with n-butyl, 2-chloroethyl, and phenylisocyanates, which yielded coupling products **9**, **10**, and **11**, respectively (Table 4.2), all characterized by spectroscopy (please see *Appendix C*).

Table 4.2. Reactivity of saccharin with isocyanates upon LAG (CH_3NO_2, η = 0.25 μL/mg) with 10 mol% CuCl.

Compound	R-NCO	Yield (%)
8	Cy-NCO	95[a]
9	n-butyl-NCO	71[a]
10	2-Cl-ethyl-NCO	80[a]
11	Ph-NCO	65[b]

[a]isolated yield after workup; [b]conversion.

Compounds **8**, **10** and **11** (Fig. 4.12b-d) were also characterized by single crystal X-ray diffraction, confirming the formation of saccharyl-ureas. Consequently, reactivity of saccharin towards isocyanates is consistent with that of sulfonamides.

In addition, several control experiments were performed mechanochemically in order to understand the mechanism of the reaction. No reaction was observed with DIC when sodium or potassium saccharinate was used (Fig. 4.13a). Similar lack of reactivity was also observed between saccharin and DIC or Cy-NCO (Fig. 4.13b-c), as evidenced by thin-layer-chromatography, FTIR-ATR and ^{1}H-NMR. Likewise, attempts to achieve a reaction between N-methylsaccharin and DIC have also been unsuccessful (Fig. 4.13d), even with 20 mol% loading of CuCl, suggesting that the sulfonimide N-H moiety is important for the insertion.

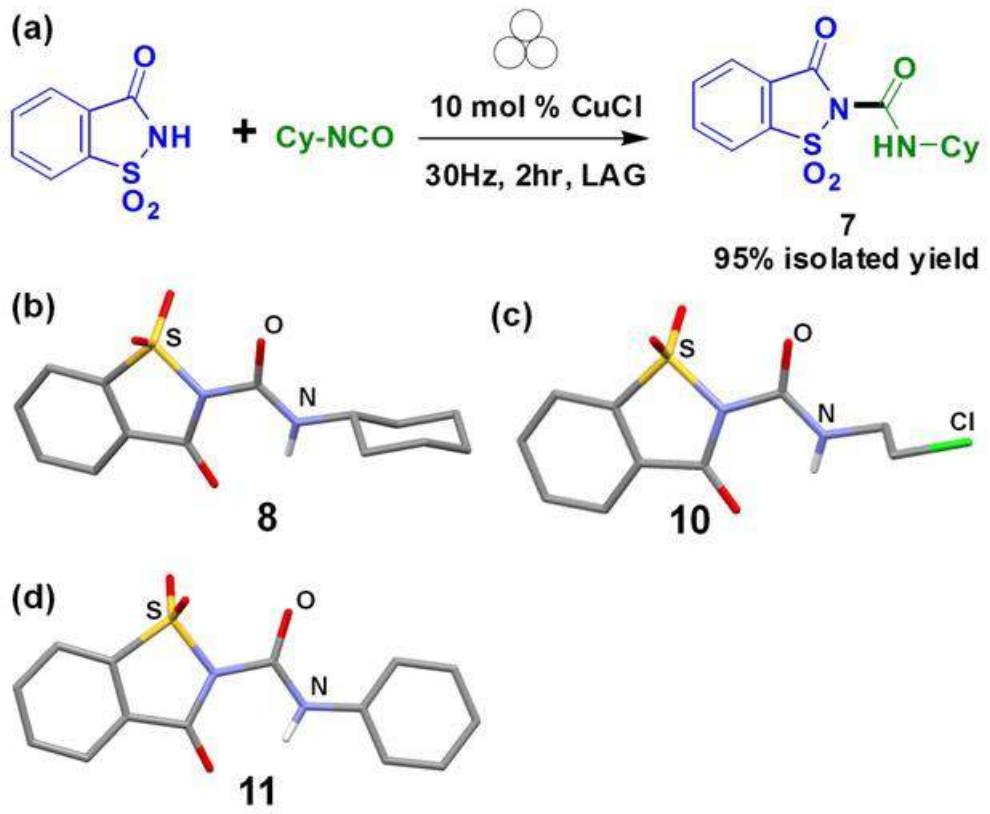

Fig. 4.12. (a): Coupling between saccharin and CyNCO to form the saccharyl urea **8**. Molecular structures of: (b) **8**, (c) **10** and (d) **11** as determined SCXRD. Hydrogen atoms bonded to carbons are omitted for clarity.

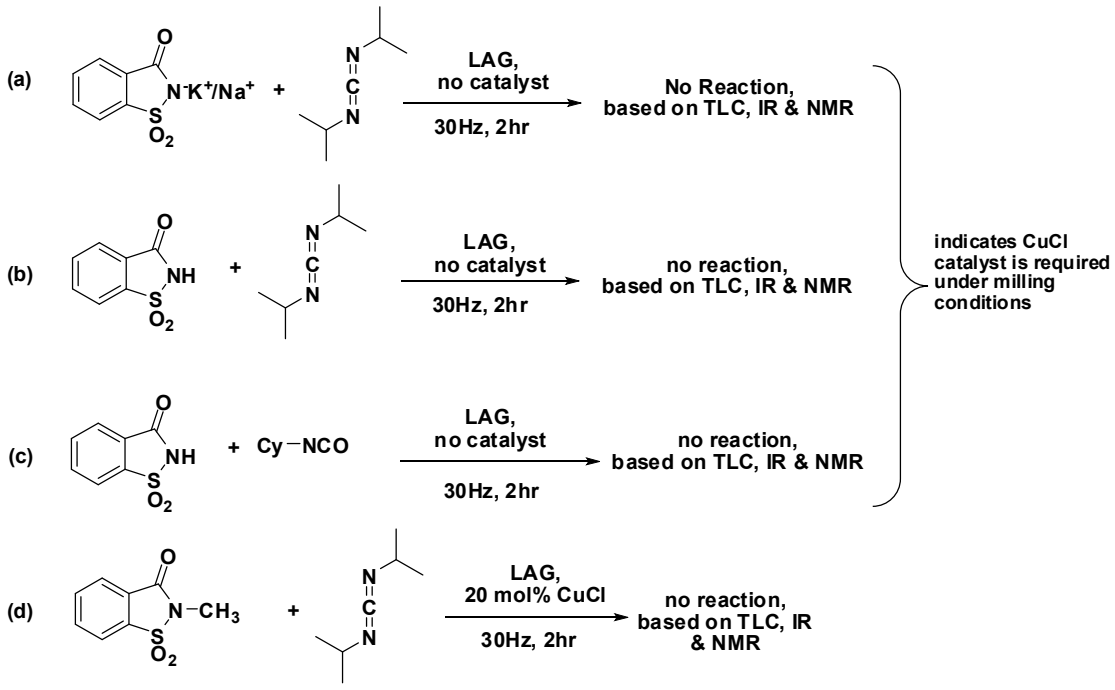

Fig. 4.13. Various control reactions performed mechanochemically. Reactions were conducted using a 10 mL stainless steel jar with one 10 mm diameter stainless steel ball (weight *ca.* 4 grams).

4.6 Mechanistic considerations

Based on all these results, we hypothesized two plausible mechanisms for the insertion of carbodiimides into sulfonimide moiety without the use of copper catalyst (Fig. 4.14). First, the saccharin forms an unisolatable intermediate adduct with carbodiimide. This short-lived intermediate then rapidly undergoes a rearrangement to form the two atom insertion product. The second mechanism involves a concerted pathway, whereby the carbodiimide approaches the sulfonimide moiety of the saccharin ring and rapidly undergoes a rearrangement that inserts into the C-N bond. We believe that for the concerted mechanistic pathway, the CuCl can act as a bifunctional Lewis acid catalyst, in which it activates the electrophile (carbodiimide and isocyanate) and through electrostatic coordination brings the sulfonimide moiety and electrophile together in close proximity for the reaction to occur. We initially speculated that the insertion might proceed *via* a guanidine adduct intermediate formed by such a C-N coupling. However, *in situ* infrared spectroscopy monitoring (using the ReactIR setup) of the reaction of saccharin and DIC in solution so far gave no evidence for such an intermediate, suggesting that the carbodiimide insertion proceeds *via* a different route.

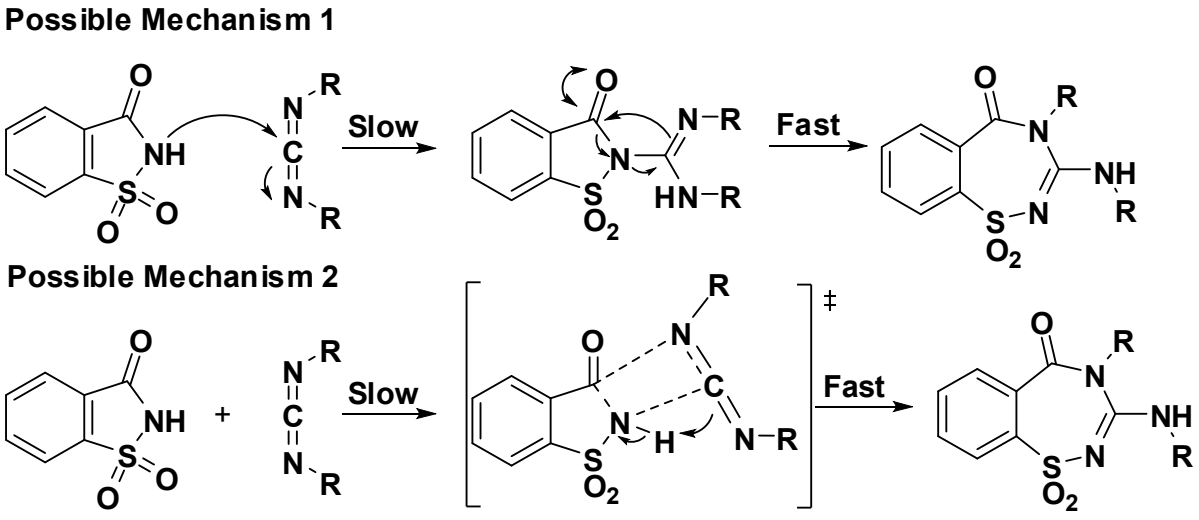

Fig. 4.14. Two possible mechanism, a) step-wise and b) concerted mechanism, for the ring expansion reaction of saccharin with carbodiimide.

4.7 Conclusion

In summary, we have demonstrated a previously unknown carbodiimide transformation, allowing the insertion of a two-atom C-N fragment into a sulfonimide. The transformation allows a simple, one-step transformation of saccharin into thiadiazepine systems of potential pharmaceutical relevance and, at least in two cases, a two-atom chain extension of a linear sulfonimide. A total of 12 compounds were synthesized and nine crystal structures were obtained. We believe that the ability to simply, in a single step, assemble a thiadiazepine ring from saccharin can make this transformation of particular interest in context of green pharmaceutical synthesis and medicinal chemistry. It is unclear why sulfonimides, even in the presence of a copper-based catalyst, undergo a carbodiimide insertion reaction instead of the simple C-N coupling seen with sulfonamides. We are currently exploring the use of density functional theory calculations to elucidate the mechanism of this reaction.

4.8 References

1 a) J. Ding, T. Rybak, D. G. Hall, *Nat. Commun.*, **2014**, *5*, 5474; b) N. A. Weires, E. L. Baker, N. K Garg, *Nat. Chem.*, **2016**, *8*, 75; c) L. Zhang, G. J. Lovinger, E. K. Edelstein, A. A. Szymaniak, M. P. Chierchia, J. P. Morken, *Science*, **2016**, *351*, 70; d) S. Xu, A. Oda, H. Kamada, E.-I. Negishi, *Proc. Nat. Acad. Sci.*, **2014**, *111*, 8368, e) N. Rodríguez, L. J. Goossen, *Chem. Soc. Rev.*, **2011**, *40*, 5030; f) S. Z. Tasker, E. A. Standley, T. E. Jamison, *Nature*, **2014**, *509*, 299; g) T. Qin, J. Cornella, C. Li, L. R. Malins, J. T. Edwards, S. Kawamura, B. D. Maxwell, M. D. Eastgate, P. S. Baran, *Science*, **2016**, *352*, 801; h) E. B. Pinxterhuis, M. Giannerini, V. Hornillos, B. L. Feringa, *Nat. Commun.*, **2016**, 7, DOI: 10.1038/ncomms11698; i) C. M. Crudden, C. Ziebenhaus, J. P. G. Rygus, K. Ghozati, P. J. Unsworth, M. Nambo, S. Voth, M. Hutchison, V. S. Laberge, Y. Maekawa, D. Imao, *Nat. Commun.*, **2015**, *7*, 11065; j) S. A. Girard, T. Knauber, C.-J. Li, *Angew. Chem. Int. Ed.*, **2014**, *53*, 74; k) Y. Yamashita, J. C. Tellis, G. A. Molander, *Proc. Nat. Acad. Sci.*, **2015**, *112*, 12026; l) M. H. Shaw, V. W. Shurtleff, J. A. Terrett, J. D. Cuthbertson, D. W. C. Macmillan, *Science*, **2016**, *352*, 1304; m) S. Z Tasker, E. A. Standley, T. F. Jamison, *Nature*, **2014**, *509*, 299; n) L. Chen, M. O. Bovee, B. E. Lemma, K. S. M. Keithley, S. L. Pilson, M. G. Colman, J. Mack, *Angew. Chem.*, **2015**, *127*, 11236; o) B. Xu, J.-P. Lumb, B. A. Arndtsen, *Angew. Chem. Int. Ed.*, **2015**, *54*, 4208.

2 For examples and reviews focusing on C-N coupling reactions, see: a) D. S. Surry S. L. Buchwald, *Angew. Chem. Int. Ed.*, **2008**, *47*, 6338; b) J. F. Hartwig, *Acc. Chem. Res.*, **2008**, *41*, 1534; c) J. Bariwal, E. Van der Eycken, *Chem. Soc. Rev.*, **2013**, *42*, 9283; (d) M.-L. Louillat, F. W. Patureau, *Chem. Soc. Rev.*, **2014**, *43*, 901; e) M. Baumann, I. R. Baxendale, *Beilstein J. Org. Chem.*, **2013**, *9*, 2265; f) S. L. Zultanski, J. Zhao, S. S. Stahl, *J. Am. Chem. Soc.*, **2016**, *138*, 6416; g) Q. M. Kainz, C. D. Matier, A. Bartoszewicz, S. L. Zultanski, J. C. Peters, G. C. Fu, *Science*, **2016**, *351*, 681; h) N. M. Camasso, M. S. Sanford, *Science*, **2015**, *347*, 1218.

3 a) P. Anastas, N. Eghbali, *Chem. Soc. Rev.*, **2010**, *39*, 301; b) P. J. Dunn, *Chem. Soc. Rev.*, **2012**, *41*, 1452; c) C. Jiménez-González, D. J. C. Constable, C. S. Ponder, *Chem. Soc. Rev.*, **2012**, *41*, 1485; d) H.-J. Federsel, *Green Chem.*, **2013**, *15*, 3105.

4 a) S. L. James, C. J. Adams, C. Bolm, D. Braga, P. Collier, T. Friščić, F. Grepioni, K. D. M. Harris, G. Hyett, W. Jones, A. Krebs, J. Mack, L. Maini, A. G. Orpen, I. P. Parkin, W. C. Shearouse, J. W. Steed, D. C. Waddell, *Chem. Soc. Rev.*, **2012**, *41*, 413; b) A. Stolle, T. Szuppa, S. E. S. Leonhardt, B. Ondruschka, *Chem. Soc. Rev.*, **2011**, *40*, 2317; c) G.-W. Wang, *Chem. Soc. Rev.*, **2013**, *42*, 7668; d) J. G. Hernández, E. Juaristi, *Chem. Commun.*, **2012**, *48*, 5396; e) B. P. Biswal, S. Chandra, S. Kandambeth, B. Lukose, T. Heine, R. Banerjee, *J. Am. Chem. Soc.*, **2013**, *135*, 5328; f) T. L. Cook, J. A. Walker, J. Mack, *Green Chem.*, **2013**, *15*, 617; g) V. Declerck, E. Colacino, X. Bantreil, J. Martinez, F. Lamaty, *Chem. Commun.*, **2012**, *48*, 11778; h) N. R. Rightmire, T. P. Hanusa, *Dalton Trans.*, **2016**, *45*, 2352.

5 a) D. Tan, V. Štrukil, C. Mottillo, T. Friščić, *Chem. Commun.*, **2014**, *50*, 5248; b) J. G. Hernández, T. Friščić, *Tetrahedron Lett.*, **2015**, *56*, 4253.

6 D. Tan, C. Mottillo, A. D. Katsenis, V. Štrukil, T. Friščić, *Angew. Chem. Int. Ed.*, **2014**, *53*, 9321.

7 a) A. Romero ,J. Egea, G. C. González-Muñoz, M. D. Martín de Saavedra, L. del Barrio, M. I. Rodríguez-Franco, S. Conde, M. G. López, M. Villarroya, C. de los Ríos, *ACS Chem Neurosci*., **2014**, *5*, 770; b) G. C. González-Muñoz, M. P. Arce, C. Pérez, A. Romero, M. Villarroya, M. G. López , S. Conde, M. I. Rodríguez-Franco, *Eur. J. Med. Chem*., **2014**, *81*, 350; c) N. Lebegue, S. Gallet, N. Flouquet, P. Carato, B. Pfeiffer, P. Renard, St. Léonce, A. Pierré, P. Chavatte, P. Berthelot, *J. Med. Chem*., **2005**, *48*, 7363; d) R. J. Cherney, J. J.-W. Duan, M. E. Voss, L. Chen, L. Wang, D. T. Meyer, Z. R. Wasserman, K. D. Hardman, R.-Q.

Liu, M. B. Covington, M. Qian, S. Mandlekar, D. C. Christ, J. M. Trzaskos, R. C. Newton, R. L. Magolda, R. R. Wexler, C. P, Decicco, *J. Med. Chem*., **2003**, *46*, 1811; e) S. Conde-Ruzafa, A. Garcia-Garcia, M. Garcia-Lopez, G. C. Gonzalez-Munoz, M. I. Rodriguez-Franco, M. Villarroya-Sanchez, *WO Patent WO2010063862-A3*, **2010**; f) S. Gallet, P Berthelot, N. Lebegue, N. Flouquet, P. Carato, J. Hickman, A. Pierre, B. Pfeiffer, P. Renard, *US Patent US2006079677-A1*, **2005**; g) P. Gillberg, I. Starke, H. Graffner, A. Lindqvist, B. Angelin, P. G. Gilbereu, A. M. Rindeukeubiseuteu, *WO Patent WO2012064268-A1*, **2012**; h) H,-B. Zhou, H. Alper *J. Org. Chem.*, **2003**, *68*, 3439.

8 a) T. M. Krűlle, J. C. H. M. Wijkmans, *Tetrahedron*, **2001**, *57*, 7021; b) V. Fülöpová, A. Krchňáková, E. Schütznerová, J. Zajíček, V. Krchňák, *J. Org. Chem*., **2015**, *80*, 1795; c) V. Fülöpová, V. Krchňák, *ACS Comb. Sci*., **2014**, *16*, 412.

9 a) N. N. Volkova, E. V. Tarasov, M. I. Kodess, W. Dehaen, V. A. Bakulev, *Mendeleev Commun*., **2002**, *12*, 131; b) T. E. Glotova, A. S. Nakhmanovich, L. S. Romanenko, M. V. Sigalov, *Chem. Heterocyclic Comp*., **1991**, *27*, 795; c) M. Kidwai, P. Sapra, P. Misra, R. K. Saxena, M. Singh, *Bioorg. Med. Chem*., **2001**, *9*, 217; d) V. M. Reddy, K. R. Reddy, *Chem. Pharm. Bull*., **2010**, *58*, 1081; e) T. A. Kalinina, D. V. Shatunova, T. V. Glukhareva, Yu. Yu. Morzherin, *Chem. Heterocyclic Comp*., **2013**, *49*, 350.

10 H. H. Szmant, Y. L. Chow, *J. Org. Chem.*, **1971**, *36*, 2887.

11 a) H. J. Diehr, R. Kisten, J. Kluth, K. H. Muller, T. Peister, U. Priesnitz, H. J. Riebel , W. Roy, *US Patent US4645528-A*, **1986**; b) Warner-Lambert Co., *US Patent US3803131-A*, **1973**; c) S. Plescia, P. Agozzino, I. Fabra, *J. Heterocyclic Chem*., **1977**, *14*, 1431; d) J. B. Wright, *J. Heterocyclic Chem*., **1968**, *5*, 719; e) P. V. Ramana, A. R. Reddy, *J. Sulphur Chem*., **2010**, *31*, 71; f) G. Palmisano, B. Danieli, G. Lesma, G. Fiori, *Tetrahedron*, **1988**, *44*, 1545; g) J. Daniel, D. N. Dhar, *Syn. Commun.*, **1993**, *23*, 121; h) H. A. Luts, *J. Org. Chem.*, **1968**, *33*, 4528; i) S. Harikrishna, L. K. Ravindranath, *Der Pharma Chemica*, **2015**, *7*, 62; j) S. Harikrishna, L. K. Ravindranath, *World J. Pharm. Pharm. Sci.*, **2015**, *4*, 1284.

12 E. J. Kantorowski, M. J. Kurth, *Tetrahedron*, **2000**, *56*, 4317.

13 a) H. Zinnes, R. A. Comes, J. Shavel, *J. Org. Chem.*, **1964**, *29*, 2068; b) J. C. Grivas, *J. Org. Chem.*, **1976**, *41*, 1325; c) J. R. Proudfoot, U. R. Patel, A. B. Dyatkin, *J. Org. Chem.*, **1997**, *62*, 1851.

14 U. Lerch, J. G. Moffatt, *J. Org. Chem.*, **1971**, *36*, 3686.

15 a) D. Tan, L. Loots, T. Friščić, *Chem. Commun.*, **2016**, *52*, 7760; b) J. Bonnamour, T.-X. Métro, J. Martinez, F. Lamaty, *Green. Chem.*, **2013**, *15*, 1116; c) L. Konnert, B. Reneaud, R. M. Figueiredo, J.-M. Campagne, F. Lamaty, J. Martinez, E. Colacino, *J. Org, Chem.*, **2014**, *79*, 10132; d) L. Konnert, M. Dimassi, L. Gonnet, F. Lamaty, J. Martinez, E. Colacino, *RSC Adv.*, **2016**, *6*, 36978.

16 a) T. Friščić, W. Jones, *Cryst. Growth Des.*, **2009**, *9* ,1621; b) G. A Bowmaker, *Chem. Commun.*, **2013**, *49*, 334.

17 The *η*-parameter describes mechanochemical LAG conditions in terms of the ratio of liquid additive volume and the weight of the reactants, see: T. Friščić, S. L. Childs, S. A. A. Rizvi, W. Jones, *CrystEngComm*, **2009**, *11*, 418.

18 G. Kiselev , A. F. Mishnev , E. M. Ivanova1 , I. V. Vozny, R. Žalubovskis, *Chem. Heterocyclic Comp.*, **2012**, *48*, 1412.

19 a) S. Gabriel and J. Colman, J. Ber., 1900, 33, 980; b) S. Gabriel, J. Colman, *J. Ber.*, **1900**, *33*, 2630; c) S. Gabriel, J. Colman, *J. Ber.*, **1902**, *35*, 1358.

20 a) C. F. H. Allen, *Chem. Rev.*, **1950**, *47*, 275; b) J. H. M. Hill, *J. Org. Chem.*, **1965**, *30*, 620; c) J. G. Lombardino, E. H. Wiseman, W. M. McLamore, *J. Med. Chem.*, **1971**, *14*, 1171; d) C. B. Schapira, I. A. Perillo, S. Lamdan, *J. Heterocycl. Chem.*, **1980**, *17*, 1281.

21 H. Ulrich, *Chemistry and Technology of Carbodiimides*, **2007**, John Wiley & Sons, Chichester, United Kingdom.

22 For examples of 3- and 4-membered ring expansion with carbodiimides, see: a) K. Gulbins, K. Hamann, *Chem. Ber.*, **1961**, *94*, 3287; b) A. Baba, I. Shibata, K. Masuda, H. Matsuda, *Synthesis*, **1985**, 1144; c) J.-O. Baeg, H. Alper, *J. Org. Chem.*, **1992**, *57*, 157; d) J.-O. Baeg, C. Bensimon, H. Alper, *J. Org. Chem.*, **1995**, *60*, 253; e) C. Larksarp, H. Alper, *J. Am. Chem. Soc.*, **1997**, *119*, 3709; f) C. Larksarp, H. Alper, *J. Org. Chem.*, **1998**, *63*, 6229; g) D. C. D. Butler, G. A. Inman, H. Alper, *J. Org. Chem.*, **2000**, *65*, 5888; h) R. N. Lacey, W. R. Ward, *J. Chem. Soc.*, **1958**, 2134.

23 a) F. Chériou, G. Süss-Fink, *Tetrahedron Lett.*, **2002**, *43*, 6653; b) H. A. Abd El-Nabi, G. Kollenz, *Monats. Chem.*, **1997**, *128*, 381; c) H.-B. Zhou, H. Alper, *Tetrahedron*, **2004**, *60*, 73.

CHAPTER 5

BASE-FREE MECHANOCHEMICAL COPPER-CATALYZED AMIDE COUPLING OF ISATINS, BENZAMIDES AND IMIDES WITH ISOCYANATES

"Research is like walking on a field of snow. It is most difficult for the first person to create the path in the snow, and once the path is created, it becomes easier for others to walk on it." –Elena Boldyreva, International Symposium on Mechanochemistry (Mech'cheM), Montpellier, France, 2015.

5.1 Introduction and connecting text.

The work presented in this chapter is a part of a not yet published manuscript entitled "Base-free mechanochemical copper-catalyzed amide coupling of isatins, benzamides and imides with isocyanates", which addresses the discovery and development of a novel and rapid base-free coupling reaction between poorly nucleophilic isatins, benzamides or imides with isocyanates to access a variety of potentially biologically active carbamoyl-isatins, -benzamides and -imides. This development is based on mechanochemistry, carried out under ball milling conditions, with the use of substoichiometric amounts of CuCl as a catalyst. This is the first mechanochemical strategy for catalytic derivatization of amides and imides. The respective products were purified without requiring bulk organic solvents, and have all been isolated with good to excellent yields. The paper was written by D. Tan with guidance and editing contributions from Prof. T. Friščić, and co-authored with N. Biggins, a summer undergraduate exchange student from University of Nottingham, who contributed to the screening and optimization reactions. The text of the manuscript has been formatted and re-written for inclusion in this Dissertation. All experimental results, including reactivity screening, crystal growth, synthesis and instrumental characterization (FTIR, NMR, MS, SCXRD) of the various compounds were obtained by D. Tan. In *Chapter 4* of this Dissertation, it was described how various poorly nucleophilic substrates were screened for participating in the copper-catalyzed mechanochemical coupling reactions with isocyanates or carbodiimides. The presented chapter extends this concept of using mechanochemistry as a tool for discovering new carbon-nitrogen (C-N) bond formation reactions, without bulk solvents or stoichiometric auxiliaries, for the functionalization of cyclic and non-cyclic amides with isocyanates to form carbamoyl-amides will be discussed.

The amide linkage is certainly one of the most important bonds in organic chemistry, with structural significance across a wide range of areas, from peptide linkage in protein biochemistry, to synthetic polymer chemistry, and can be found in many natural and synthetic biologically active compounds.[1] Many synthetic strategies have been developed to synthesize amide bonds and/or further functionalization of amides. These strategies include the use of metal catalysts,[2] acyl derivatives,[3-4] peroxide- reactions,[5] boron- reactions,[6] *N*,*N*'-carbonyldiimidazole-mediated reactions,[7] the use of functionalized protecting groups,[8] carbene-catalyzed reactions,[9] classical Steglich-type couplings using carbodiimides and hydroxybenzotriazole,[10] dehydrogenative amidation,[11] Pd-catalyzed oxidative Buchwald-Hartwig coupling[12] and Cu-catalyzed Ulmann-type reactions[13] *etc*. All these existing methods

typically require the use of sacrificial reagents such as bases in stoichiometric amounts, or highly expensive second- and third-row transition metal catalysts.[14] For such reasons, these synthetic strategies raise concerns of atom efficiency and the amount of waste being generated. Although there have been recent efforts to address these problems by formulating improved synthetic strategies,[15] most of the current methodologies are still tethered by traditional solution protocols which require extensive use of solvents both in the reaction, as well as workup procedures.

Mechanochemistry,[16-18] on the other hand, is a rapidly developing synthetic technique that allows conducting chemical reactions in the solid state by using shearing, grinding, stretching and impact force to provide energy to chemical reactions. Such mechanosynthesis does not require the use of any bulk solvent or elevated temperatures, and is thus considered a much greener alternative to solution-based methodologies. Although the use of transition metal catalysts for organic transformations using mechanochemistry is a well-established[19] area, recent developments showed that mechanochemistry can not only be used to augment existing reactions in a greener fashion,[20] it can also serve as a tool for reaction discovery. Specifically, mechanochemistry has been used to synthesize compounds that are unstable in solution,[21] and thus impossible to synthesize and isolate using traditional methods. A number of recent publications[8,22] have highlighted how mechanosynthesis can be used to efficiently afford the amide moiety, as well as other types of functionalities involving C-N bonds, in a green solvent-free manner. However, functionalization of the amide bond using mechanochemistry is a highly underdeveloped area. Our group recently reported the mechanosynthesis of various anti-diabetic sulfonylurea drugs[23] by a direct C-N bond formation between terminal sulfonamides and isocyanates, using CuCl as a catalyst. Mechanochemistry was also used to discover the first direct route to arylsulfonylguanidines,[24] *via* a direct coupling reaction between arylsulfonamides with carbodiimides. This new type of C-N bond formation proceeds very poorly in solution, even at elevated temperatures, which indicates mechanochemistry as a quintessential strategy for the synthesis of sulfonylguanidine units. Extending this philosophy of using mechanochemistry as a means to access other not yet known coupling reactions, we decided to explore the solid-state functionalization of amides with isocyanates to form carbamoyl-amide targets (Fig. 5.1).

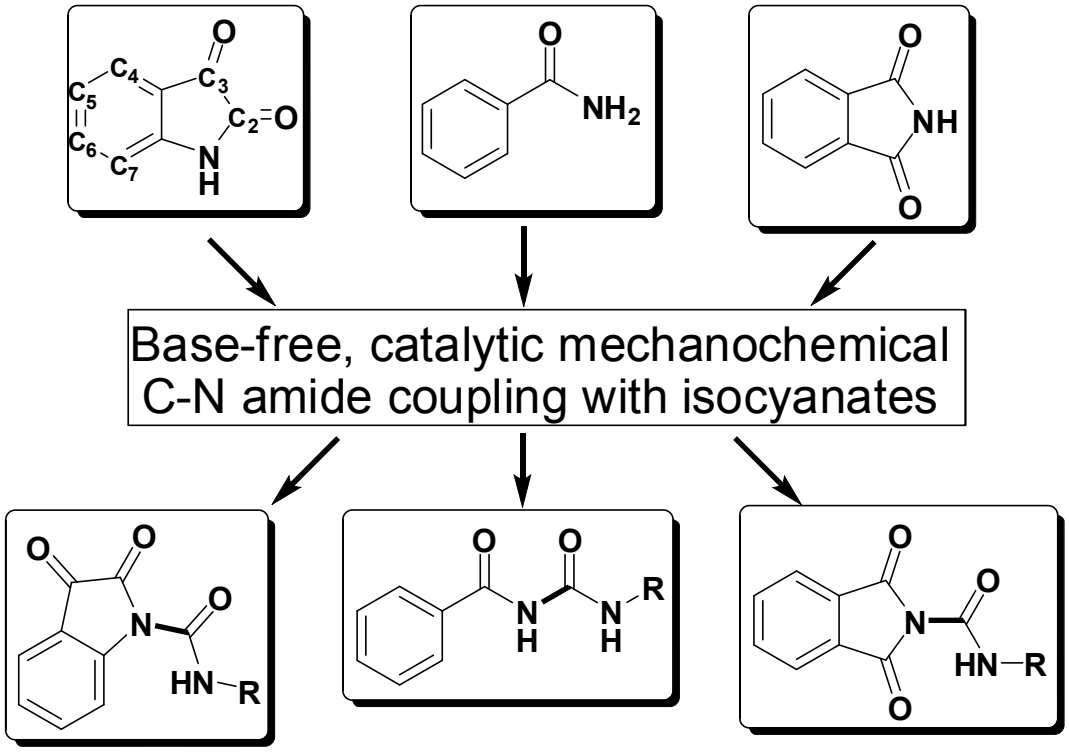

Fig. 5.1 The catalytic, base-free mechanochemical coupling reaction of isatins, benzamides and imides with isocyanates (R-NCO) to form carbamoyl-isatins, -benzamides and -imides respectively. The carbonyl carbons of isatins have been labelled as C3 (keto) and C2 (amide) for clarity.

2.2 Carbamoyl-amide in biologically active molecules

The carbamoyl-amide moiety is present in many biologically active synthetic compounds (Fig. 5.2), such as Flucycloxuron® and Triflumuron®, which belong to a class of benzomoylphenylureas (BPUs), known to be potent insecticides.[25] Carbamoyl-amides are also present in many pharmaceutical drugs, including Cefoperazone® and Piperacillin®,[26] which are used in combination as anti-bacterial drugs to combat *pseudomonas* infections. In addition, the carbamoyl-amide moiety can also be found in Cabergoline®,[27] which is a dopamine agonist and prolactin inhibitor, and in Glimepiride®, a second generation anti-diabetic drug.[28] Hence, it is anticipated that the synthetic functionalization of amides to form carbamoyl-amides *via* a direct one-step reaction should be an attractive strategy in the context of insecticide and pharmaceutical manufacturing. With this in mind, we conducted the initial trial reactions of how mechanochemistry can be used in the amide derivatization, using as a model substrate the biologically active heterocyclic amide isatin. Isatins were first discovered in 1800s by Laurent and Erdmann as oxidation products of indigo dyes.[29] Since then, isatins

have transcended their original use as dyes and recently, derivatives of isatin have become of interest for pharmaceutical properties, including anti-convulsant, anti-inflammatory and anti-bacterial activities.[30] It is important to note (Fig. 5.1) that the isatin moiety offers only one reactive carbonyl group (C3), as the other one (C2) is a part of an amide moiety and hence, less reactive. Although functionalization of the C3 keto-carbonyl moiety of isatins to form new biologically active molecular scaffolds has been well-studied,[31] derivatization of the amido N-H group to form the carbamoyl moiety is less developed.[32]

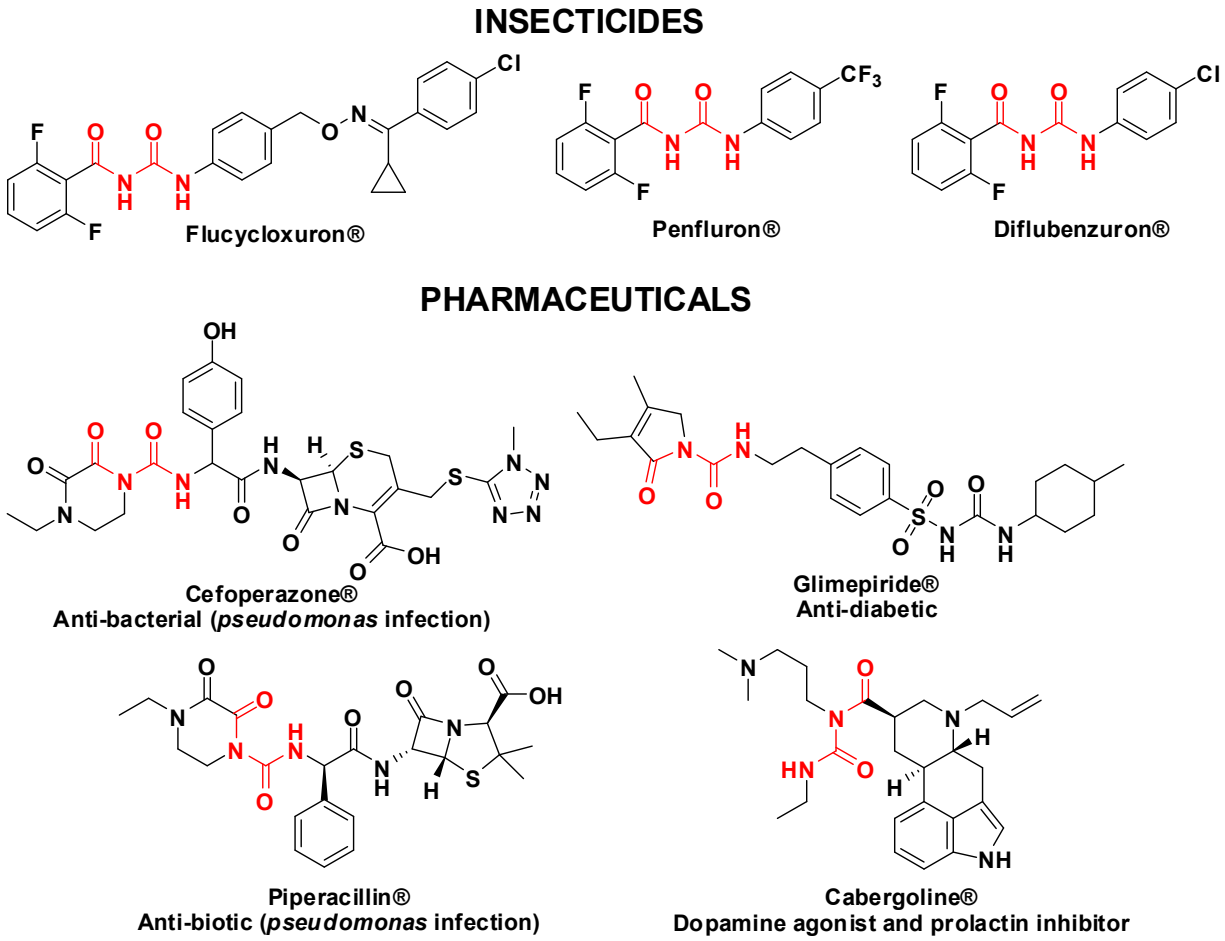

Fig 5.2 Carbomoyl-amide moiety present in various insecticidal and pharmaceutical compounds.

5.3 Isatin-isocyanate coupling by grinding

As the initial foray in this study, we first attempted the mechanochemical coupling reaction between isatin and cyclohexylisocyanate (CyNCO) by ball milling in a 1:1 stoichiometric ratio. No reaction was observed either by neat milling or by liquid-assisted grinding (LAG)[33] in the presence of catalytic amounts of acetone or nitromethane as the liquid additive (50 μL per 200 mg of reaction mixture, η = 0.25μL/mg)[33c]. However, when a catalytic amount (10 mol %) of CuCl was used, a strategy that previously enabled coupling of sulfonamides with isocyanates,[23] the targeted product **1a** was obtained in excellent yield (95%), following a simple isolation procedure involving brief milling with aqueous solution of disodiumethylenediaminetetraacetate ($Na_2H_2EDTA{\cdot}2H_2O$) and deionized water (Fig. 5.3a). After milling, the resulting suspension was washed with more water, filtered and dried over vacuum. Following such simple purification, the product obtained was an orange solid. For experimental details, please refer to *Chapter 8, Section 8.4*. Subsequently, the analogous product of coupling isatin with phenylisocyanate (PhNCO) **2a** (Fig. 5.3b) was also obtained with almost complete conversion of the isatin as evidenced by ^{1}H-NMR, along with a small amount of bisphenylurea byproduct using this protocol. The presence of bisphenylurea might be due to the higher reactivity and more moisture sensitive nature of the PhNCO reagent, which had to be stored below room temperature. For further details of synthesis and characterization including NMR, FTIR-ATR and MS data for all compounds, please see *Appendix D*.

As evidenced by FTIR-ATR spectroscopy, the formation of **1a** indeed took place mechanochemically, rather than by subsequent work-up. Specifically, spectroscopic analysis (Fig. 5.3c) of the crude reaction mixture clearly depicts the absence of the characteristic isocyanate C=N stretching band at 2200-2300 cm^{-1}, which is consistent with the coupling reaction taking place during milling. In contrast, if the milling reaction was not complete or did not take place at all, such as in the absence of the catalyst, the characteristic isocyanate signal could be clearly observed. In addition, the formation of the target **1a** can also be observed by comparison of the carbonyl C=O stretching frequencies of the starting material to those of the product in the 1650-1800 cm^{-1} region.

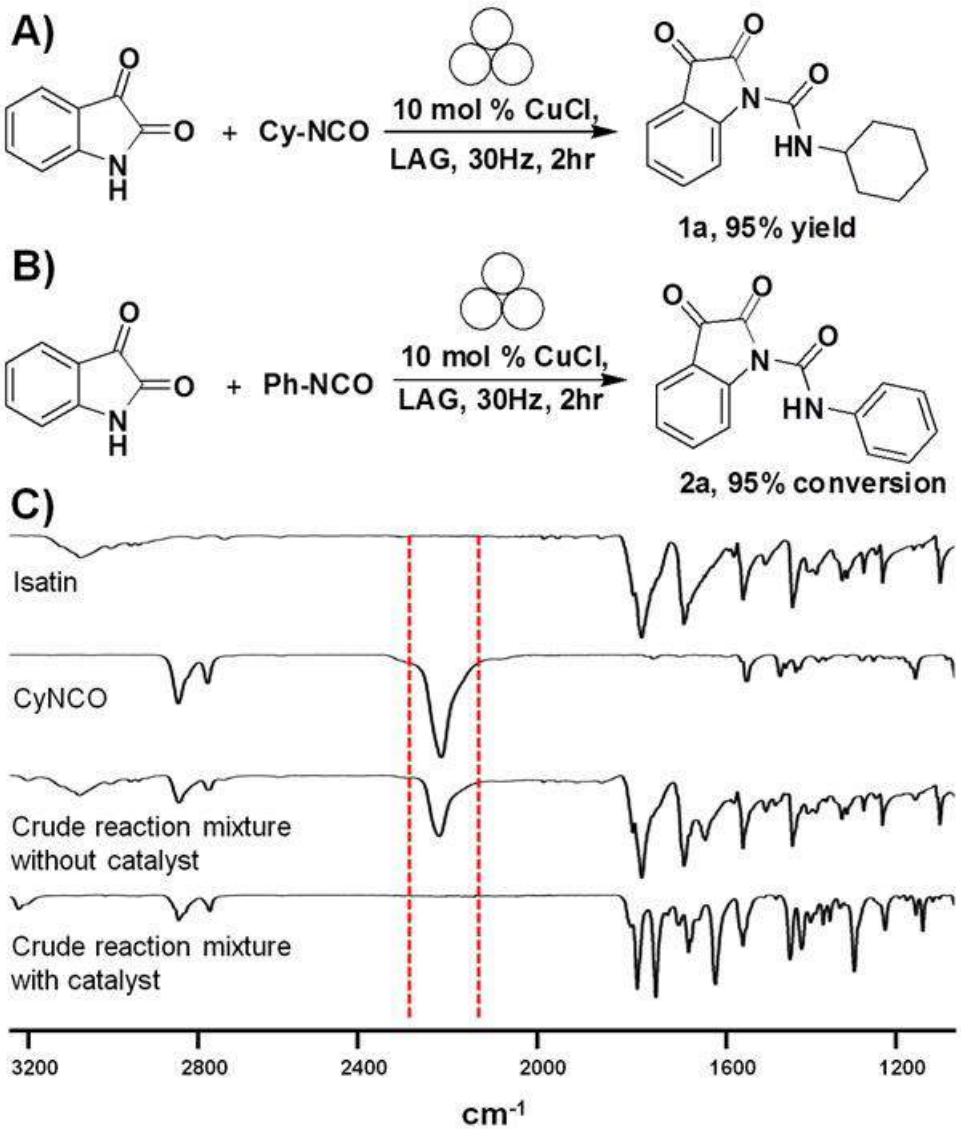

Fig. 5.3. Mechanochemical coupling reactions between isatin and, (a) cyclohexylisocyanate and (b) phenylisocyanate; (c) comparison of FTIR-ATR spectra for the mechanochemical synthesis of **1a** with and without CuCl catalyst added.

Using the coupling between isatin and CyNCO to form **1a** as the model reaction, we next attempted to screen different LAG liquid additives (Table 5.1, Entry 1-7), as well as various potential copper-based catalysts (Table 5.1, Entry 8-23) to further optimize the mechanochemical coupling reaction (Table 5.1). In general, the reaction worked for both polar and non-polar LAG liquids, with toluene affording the highest yield (99% isolated yield). Although there are no observable trend on how the type of LAG liquid affects the reaction, CH_3NO_2 was subsequently preferred over toluene for further optimization reactions as the former is easier to remove during workup. Amongst the screened catalysts, with the

exception of CuCl and $Cu(CH_3CN)_4BF_4$, most did not lead to complete conversion of reactants, or did not show any reactivity at all. The coupling reaction also worked when copper catalysts of varying oxidation states were used, namely elemental Cu^0 powder (Table 5.1, Entry 8, 56% conversion) and Cu^{2+} salts (Table 5.1, Entries 11, 16-19, ranging from 28-91% conversion). Using Cu^0 or Cu^{2+} based catalysts led to poorer conversions than CuCl. In addition, limited reactivity was also observed when poorly soluble copper compounds were explored as catalysts, notably oxides of copper, such as Cu_2O (Table 5.1, Entry 14-15, 32% conversion) and CuO (Table 5.1, Entry 13, 8% conversion), and copper carbonates, such azurite ($Cu_3(CO_3)_2(OH)_2$, Table 5.1, Entry 21, 13% conversion) and malachite ($Cu_2CO_3(OH)_2$, Table 5.1, Entry 22, 17% conversion). Inspired by the work of Mack and coworkers,[34] we also tested the coupling reaction using a brass ball (Entry 23) whereby the source of the copper catalyst came from the milling environment itself. The reaction achieved up to 61% conversion, demonstrating how the coupling reaction can be conducted without any catalyst additives.

Next, a series of various isatin and isocyanate derivatives were explored to expand the substrate scope for the coupling reaction (Fig 5.4). In general, the reactions proceeded excellently, with good yields for both electron-rich (**1b**, 99% yield) and electron-deficient isatins (**1e-h**, 91-97% yield). However, isatins containing substituents in the C7-position (Fig. 5.1), namely 5,7-dimethylisatin and 5,7-dichloroisatin, did not show any reactivity to form the respective expected products **1c** and **1d**. This could be attributed to the steric hindrance in the C7-position that might be impeding the catalytic formation of the C-N bond. When 3-oxime-isatin was used as the reactant, the CyNCO reacted with the oxime N=OH moiety instead of forming a carbamoyl-oxime **1i**. This nucleophilic addition reaction readily takes place in the absence of the CuCl catalyst, in up to 95% isolated yield. However, when two equivalents of CyNCO were used, in the presence of CuCl catalyst, the *N*-carbamoyl-*O*-carbamoyl-oxime product **1j** was formed in 68% yield. Compound **1j** was also formed telescopically *i.e.* in a one-pot two-step reaction, by reacting 3-oxime-isatin with two sequential additions of CyNCO. Subsequently, different isatin-benzoyl compounds were synthesized using aromatic isocyanates (**2a-c**), in up to 83% isolated yield. Overall, this novel isatin-isocyanate coupling reaction worked for both aliphatic and aromatic isocyanates, but was not applicable to more sterically demanding adamantylisocyanate (**2g**). Although most of the isocyante reactants are liquids at room temperature, it is important to note that some of them are also solids, such as the *p*-biphenylylisocyanate and *p*-bromophenylisocyanate,

further highlighting the fact that this copper-catalyzed coupling reaction does not require liquid reagents. All relevant details of experimental procedures can be found in *Chapter 8, Section 8.4*, and spectroscopic characterization of the various compounds can be found in *Appendix D*.

Table 5.1. Optimization and screening of LAG liquids and catalysts for isatin-isocyanate coupling

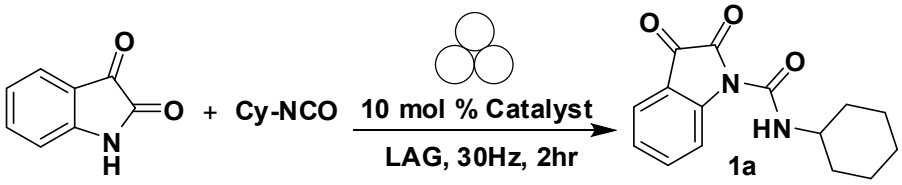

Entry	LAG	Catalyst	Yield (%)
1	CH_3NO_2	CuCl	95
2	Ethylmethylketone (EMK)	CuCl	93
3	Acetone	CuCl	87
4	Ethylacetate (EtOAc)	CuCl	85
5	Toluene	CuCl	99
6	Acetonitrile (CH_3CN)	CuCl	87*
7	Dichloromethane (DCM)	CuCl	84
8	CH_3NO_2	Cu	56*
9	CH_3NO_2	CuBr	NR
10	CH_3NO_2	CuI	NR
11	CH_3NO_2	$CuCl_2$	91*
12	CH_3NO_2	$CuBr_2$	NR
13	CH_3NO_2	CuO	8*
14	CH_3NO_2	Cu_2O	32*[a]
15	CH_3NO_2	Cu_2O	8*
16	CH_3NO_2	$CuSO_4$	28*
17	CH_3NO_2	$Cu(BF_4)_2$	NR
18	CH_3NO_2	$Cu(OAc)_2 \cdot H_2O$	83*
19	CH_3NO_2	$Cu(NO_3)_2 \cdot 3H_2O$	NR
20	CH_3NO_2	$Cu(ACN)_4BF_4$	77
21	CH_3NO_2	Azurite	13*
22	CH_3NO_2	Malachite	17*
23	CH_3NO_2	Brass Ball	61*

*Percent conversion based on ^{1}H-NMR spectroscopy. [a]20 mol % catalyst loading was used. One 10 mm diameter stainless steel ball in a 10 mL stainless steel jar was used at a frequency of 30 Hz in the presence of a grinding liquid (η = 0.25 μL/mg).

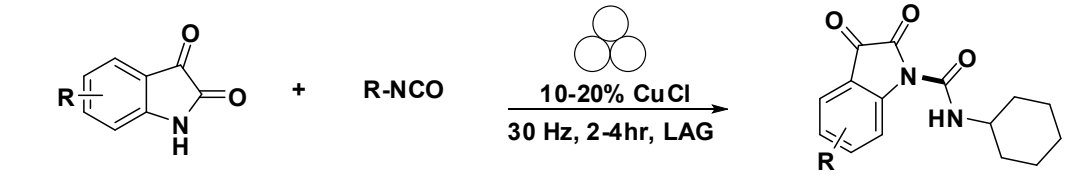

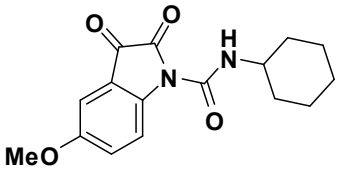

1b, 99% yield

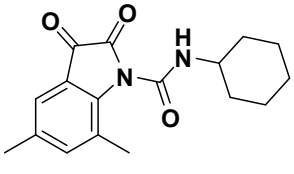

1c, NR

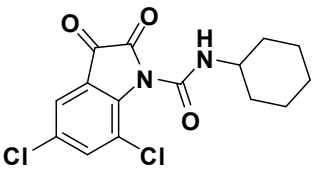

1d, NR

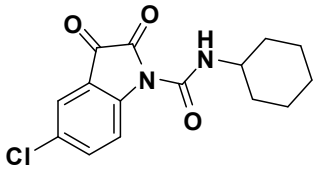

1e, 99% yield

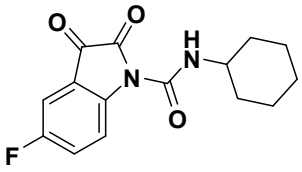

1f, 99% yield

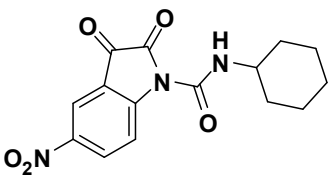

1g, 97% yield

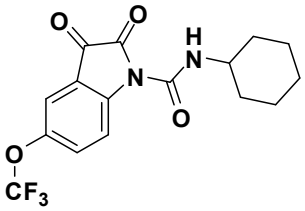

1h, 91% yield

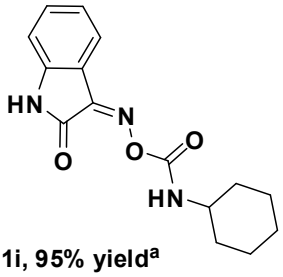

1i, 95% yield[a]

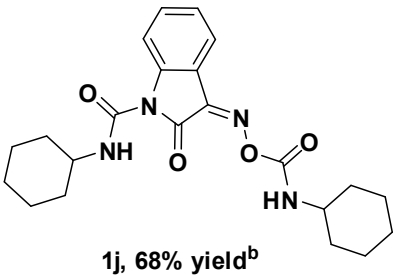

1j, 68% yield[b]

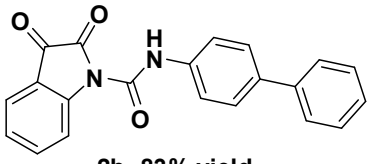

2b, 83% yield

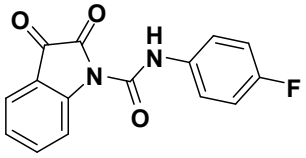

2c, 58% yield

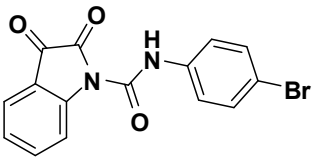

2d, 83% yield

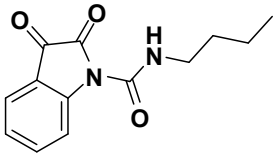

2e, 56% yield

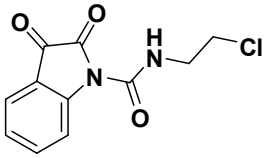

2f, 83% yield

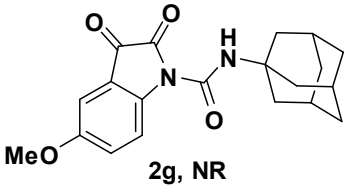

2g, NR

Fig. 5.4. Expanding the substrate scope of the mechanochemical isatin-isocyanate coupling reaction. One 10 mm diameter stainless steel ball in a 10 mL stainless steel jar was used at a frequency of 30 Hz in the presence of nitromethane as the grinding liquid (η = 0.25 µL/mg).[a]No catalyst was added; [b]2 equivalent of CyNCO used.

Using the synthesis of **1b** as an example, it is possible to compare the ^{1}H-NMR spectrum of the starting material 5-methoxyisatin with the product of its coupling with CyNCO, in order to determine whether the reaction is successful, and if it achieved complete conversion (Fig. 5.5). Generally, isatins exhibit a characteristic, highly deshielded N-H

proton signal at *ca.* 10-11ppm. Upon successful coupling with an isocyanate to form a carbamoyl-isatin product, this signal disappears and a new, more shielded N-H resonance appears at *ca.* 6.8-7.3ppm. This chemical shift is characteristic of the carbamoyl moiety of the product.

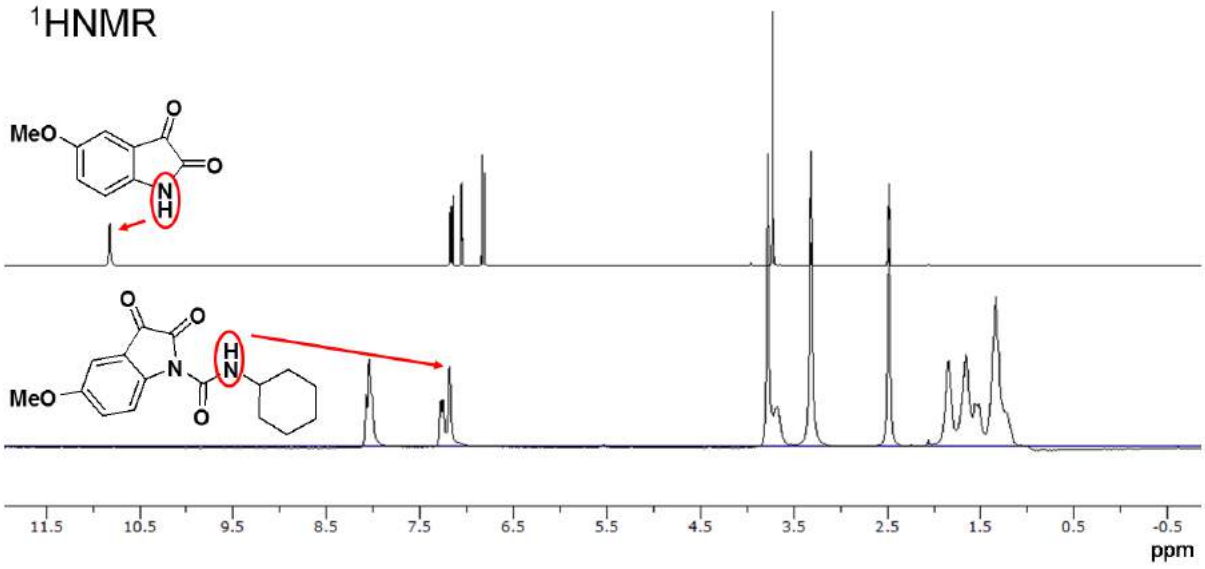

Fig. 5.5. ^{1}H-NMR comparison of the 5-methoxyisatin starting material and its isocyanate coupled product **1b**, using DMSO-d_6 as the NMR solvent.

The physical appearances of all products are in stark contrast with the appearance of their respective starting materials. As mentioned earlier, isatins have been originally used in the textile industry as synthetic dyes, because their derivatives exhibit a strong deep coloration, both in the solid state, as well as in solution. Although 5-methoxyisatin is a dark maroon solid, the product of its coupling with CyNCO (**1b**) has a bright orange appearance (Fig. 5.6). Similarly, unsubstituted isatin has a deep red color, but the products of its coupling with aromatic isocyanates (**2a-c**) are all dark green solids (Fig. 5.6). In addition to visual observation, as well as spectroscopic evidence (^{1}H-NMR, ^{13}C-NMR, FTIR-ATR, HRMS) for the mechanochemical isatin-isocyanate adduct formation, X-ray diffraction (XRD) data was also obtained from single crystals of **1b** grown by slow evaporation of a solution in acetone (Fig. 5.7). Crystal structure analysis of **1b** revealed that apart from the bulky cyclohexyl group, the carbamoyl-isatin structure is planar. Such a planar conformation is most likely due to the formation of an intramolecular C=O···H-N hydrogen-bond between the isatin carbonyl

group and the carbamoyl moiety. Each molecule of **1b** in the crystal structure is then connected to neighbouring molecules *via* a network of intermolecular C-H···O type hydrogen bonds (C···O distances ranging from 3.385(3) to 3.471(3)Å). Further details of structural studies are given in *Appendix D*.

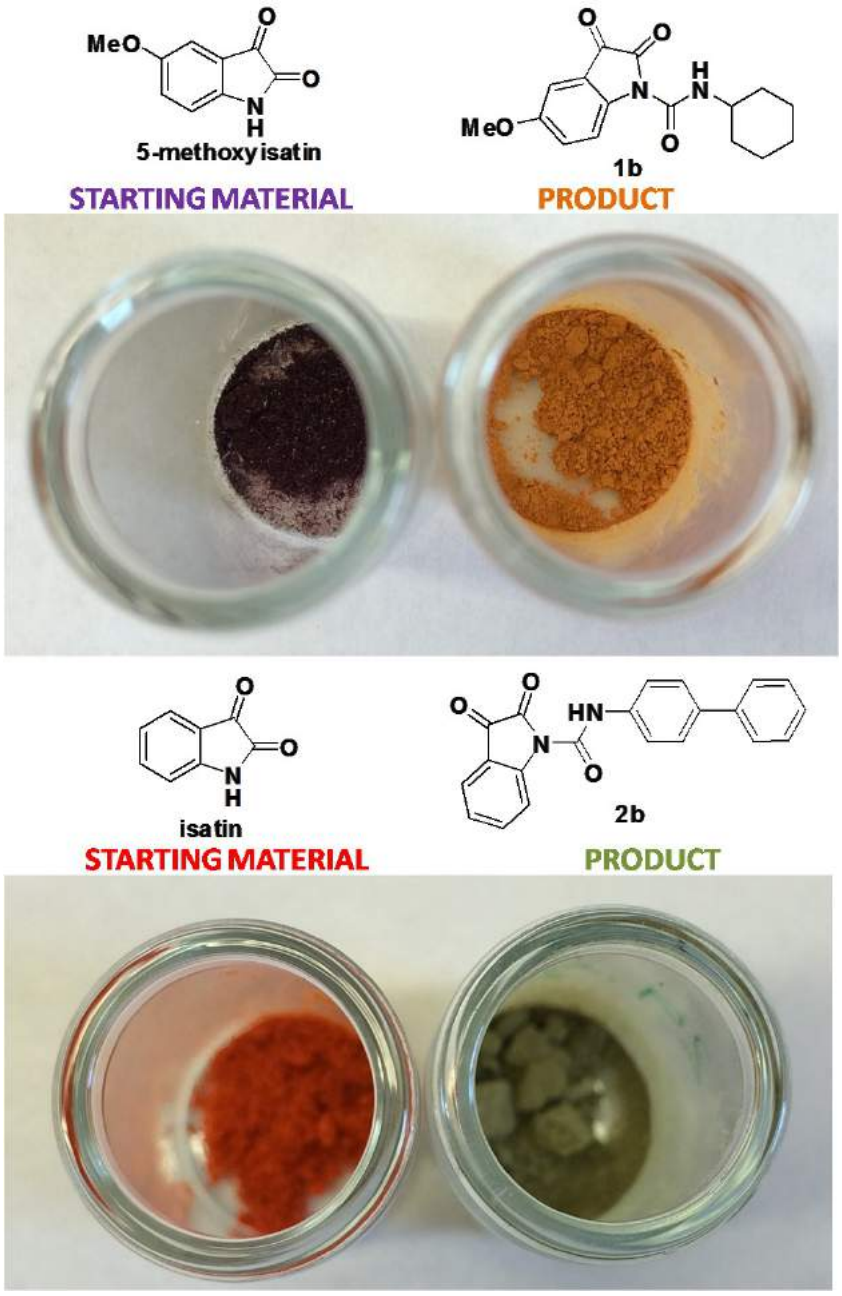

Fig. 5.6. Illustration of color changes upon mechanochemical coupling of isatin and its derivatives with isocyanates. (*Top*): Significant change in color of the 5-methoxyisatin (purple) and its carbamoyl-isatin product **1b** (orange). (*Bottom*): Significant change in color of the isatin (red) and its carbamoyl-isatin product **2h** (green).

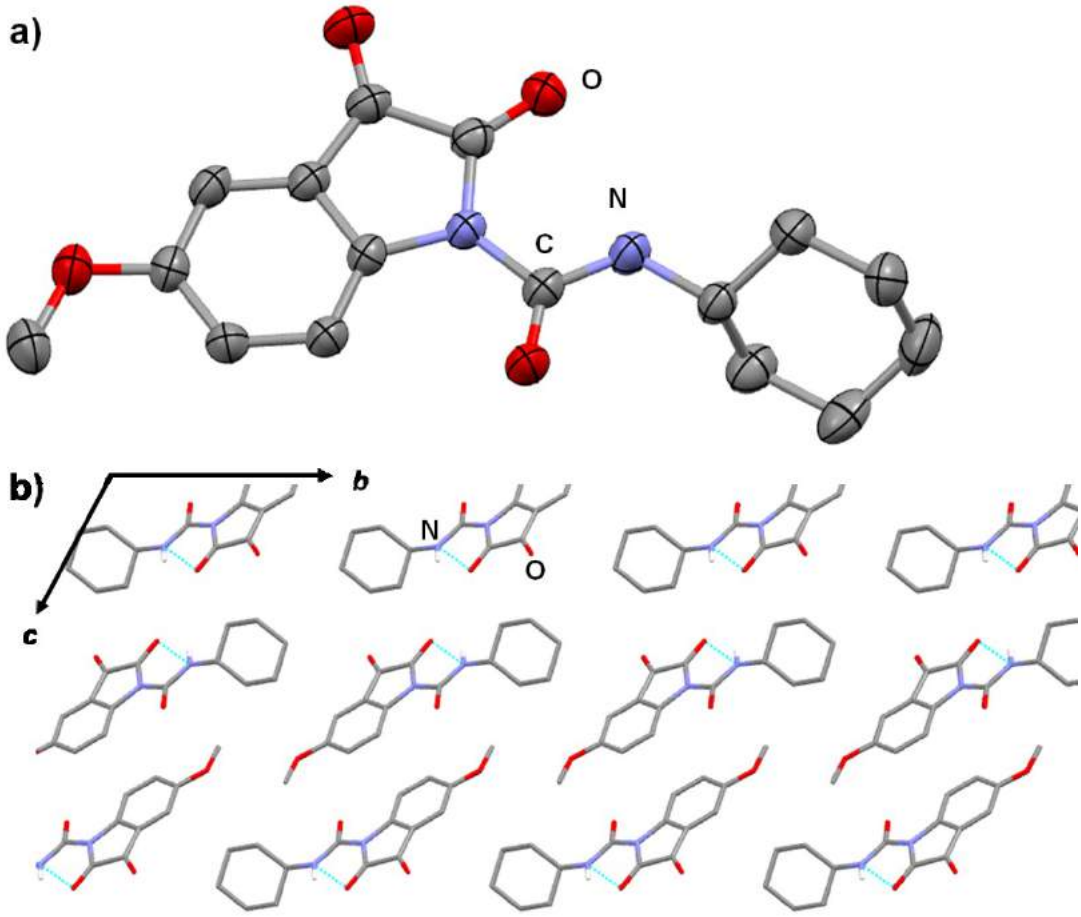

Fig. 5.7. a) Molecular structure of **1b**, visualized using Mercury with thermal ellipsoids shown at 50% probability level, as determined by SCXRD. Hydrogen atoms are omitted for clarity. b) Fragment of the crystal structure of **1b**, as viewed along the crystallographic *bc*-plane, showing the intramolecular hydrogen bonds. Crystallographic details can be found in *Appendix D*.

5.4 Benzamide-isocyanate coupling by grinding

Another class of poorly nucleophilic amides are benzamides, which are important molecules, ubiquitous in research and industry.[35] Retro-synthetic analysis of the above mentioned insecticides, would lead to the direct coupling reaction between functionalized benzamides and iscoyanates to form the necessary carbamoyl-benzamide moiety. In fact, the reaction between acylic amides and isocyanates was first discovered in 1884 by Kühn,[36a-b] and subsequently also by Wiley in 1949,[36c] who showed that the coupling can take place in dry toluene solvent under refluxing conditions for 24 hrs (95% yield). In general, stoichiometric amounts of a base such as triethylamine and/or sacrificial activators are required to generate a more nucleophilic reactant from the amide, [37] albeit at the loss of atom

economy. Using these examples as an inspiration, the base-free rapid mechanochemical benzamide-isocyanate coupling reaction was investigated, focusing only on one isocyanate, Cy-NCO, as a proof-of-concept (Table 5.2). The mechanochemical coupling reaction between unsubstituted benzamide with Cy-NCO, in the presence of 10% mol CuCl and LAG, gave the desired compound **3a** in moderate conversions (Table 5.2, Entry 1, 50% conversion). Through thorough screening of various LAG liquids and potential copper catalysts, complete conversion of the benzamide to **3a** was achieved, in up to 98% isolated yield, within 2 hrs. Entries 1-5 in Table 5.2 show that the reaction works best by using carbonyl-containing liquid additives such as 2-butanone (63% yield) and acetone (70% yield), but proceeded poorly using toluene (12% conversion) and protic methanol (no conversion). Experimental details can be found in *Chapter 8, Section 8.4*.

Table 5.2. Outcomes of optimization reactions for the mechanochemical copper-catalyzed benzamide-isocyanate coupling.

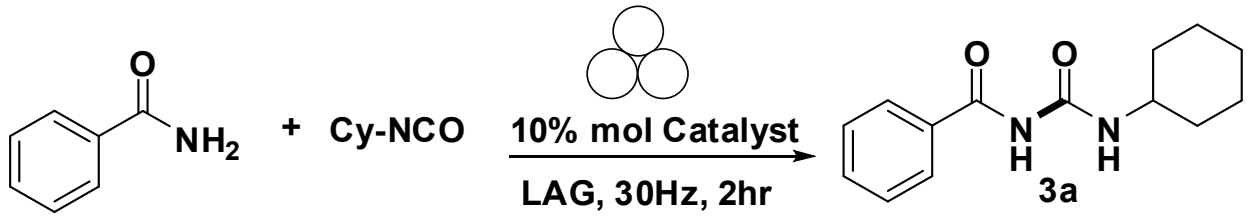

Entry	LAG	Catalyst	Yield (%)
1	CH_3NO_2	CuCl	50*
2	2-Butanone	CuCl	63
3	Acetone	CuCl	70
4	MeOH	CuCl	NR
5	Toluene	CuCl	12*
6	CH_3NO_2	$Cu(OAc)_2$	98
7	CH_3NO_2	$Cu(acetonitrile)_2BF_4$	8*
8	CH_3NO_2	$Cu(L^b)ClOH$	32*

*Percent conversion based on ^{1}H-NMR. ^{b}Tetramethylethylenediamine was used as a ligand to augment the catalyst.

Next, the reactivity of various other benzamide reagents was explored (Fig. 5.8). All reactions were optimized by using either CuCl or $Cu(OAc)_2 \cdot H_2O$ as catalysts, with catalyst loading of up to 20% mol, increased milling time (4 hr), and nitromethane, 2-butanone or acetone as milling liquid additives. The choice of the LAG liquid additive was based on results from optimization of **3a** synthesis. It was observed that benzamides with electron-

withdrawing substituents like bis-trifluoromethyl (**3b-c**) and nitro (**3d**) groups led to poorer reactivity (**3d**, 35% conversion), compared to their electron-rich counterparts with electron donating groups (**3e-f**, leading up to 73% isolated yield). Single crystals of **3c**, obtained by slow evaporation of a solution in acetone, allowed for X-ray diffraction data to be collected. Crystal structure of **3c** reveals similarities to that of the carbamoyl-isatin **1b**. Again, apart from the bulky cyclohexyl group, the carbamoyl-benzamide molecular structure is planar, which is most likely caused by the intramolecular C=O···H-N hydrogen bond between the benzamide carbonyl group and the carbamoyl moiety. Molecules of **3c** then assemble to form $R^2_2(8)$ type dimers *via* intermolecular hydrogen bonds. These dimeric pairs of molecules then connected to the neighbouring molecules *via* a network of intermolecular hydrogen bonds of the C-H···O type. In addition, mechanochemical coupling of *N*-methylbenzamide with CyNCO was also successful, affording compound **3g** in 76% yield, which demonstrates that this mechanochemical C-N coupling reaction can also work for secondary amides. Detailed spectroscopic data and XRD crystallographic data for the various compounds can be found in *Appendix D*.

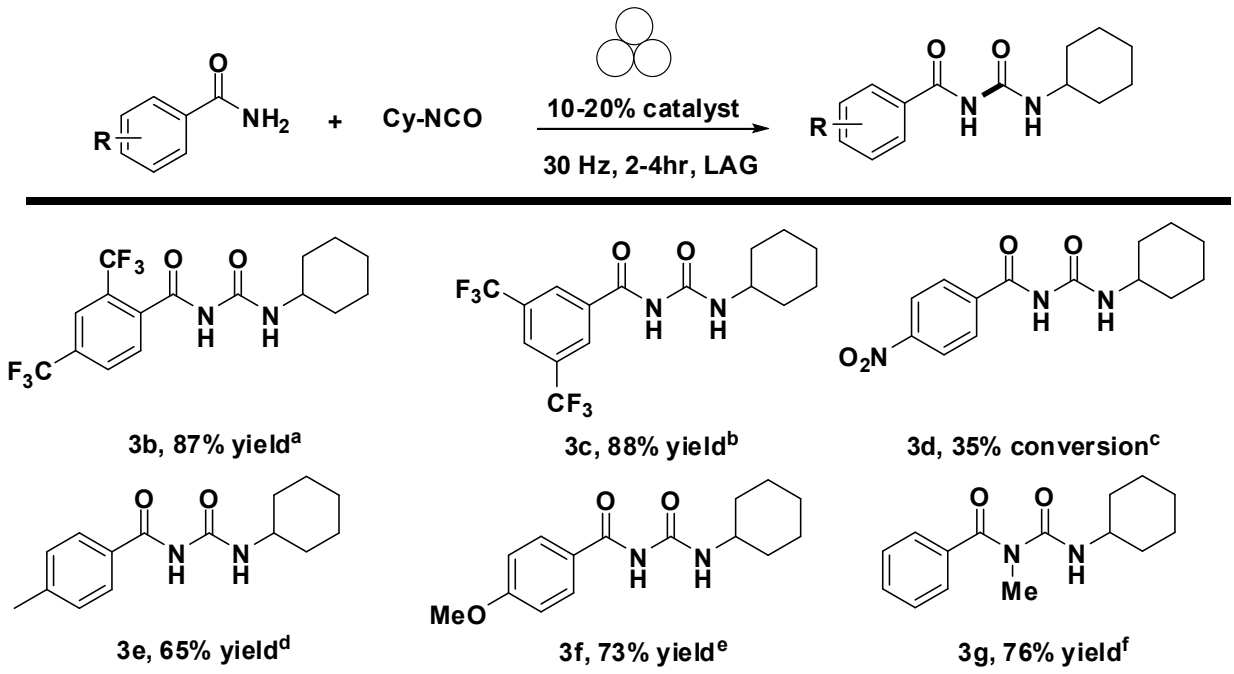

Fig. 5.8. Expanding the substrate scope of the mechanochemical benzamide-isocyanate coupling reaction. One 10 mm diameter stainless steel ball in a 10 mL stainless steel jar was used, at a frequency of 30 Hz, using a grinding liquid for LAG (η = 0.25 μL/mg). [a]1.2 eq. CyNCO, LAG = EMK, 4 hr, 20% CuCl; [b]1.2 eq. CyNCO, LAG = EMK, 4 hr, 20% CuCl, no reaction when $Cu(OAc)_2 \cdot H_2O$ was used as catalyst; [c]LAG = CH_3NO_2, 2 hr, 10% $Cu(OAc)_2 \cdot H_2O$ as catalyst; [d]1.2 eq. CyNCO, LAG = CH_3NO_2, 4 hr, 20% CuCl; [e]1.2 eq. CyNCO, LAG = CH_3NO_2, 4 hr, 20% CuCl; [f]LAG = CH_3NO_2, 2 hr, 20% CuCl.

Using the synthesis of **3g** as an illustrative example, it is possible to compare the ^{1}H-NMR spectrum of the starting material *N*-methylbenzamide with that of the product of its coupling with CyNCO, to determine whether the reaction is successful, and if it achieved complete conversion (Fig. 5.9). Unlike with isatins, the shift of the proton N-H signals between the starting material and the product is not distinct (from 8.41 to 8.32 ppm). However, for **3g**, there is a significant shift in the signal of the *N*-methyl group, from 2.76 to 3.06 ppm.

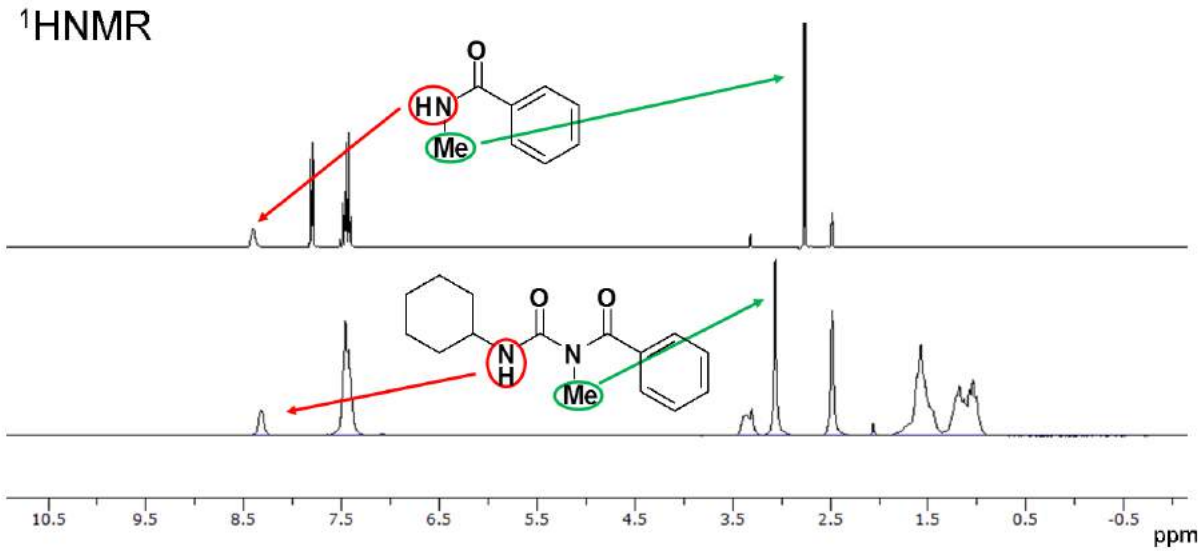

Fig. 5.9. ^{1}H-NMR comparison of the 5-methoxyisatin starting material and its isocyanate coupled product **3g**, using DMSO-d_6 as the NMR solvent.

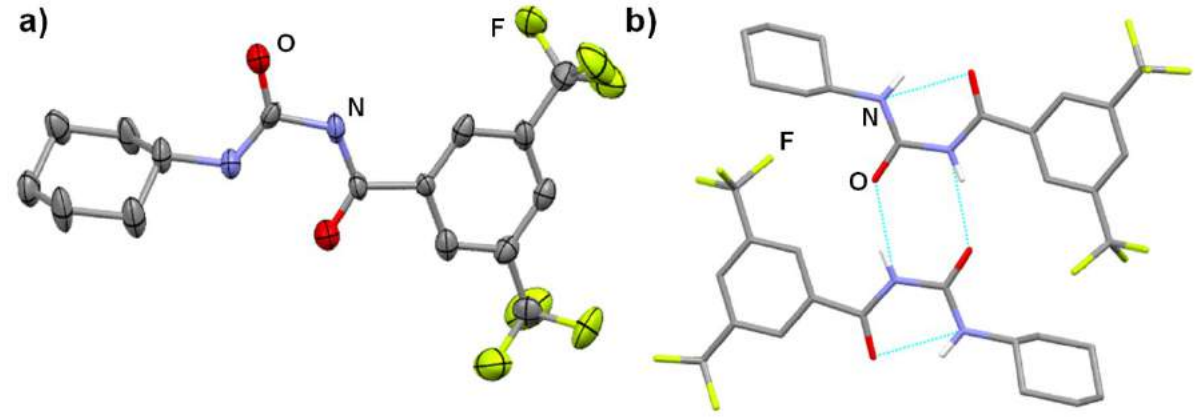

Fig. 5.10. a) Molecular structure of **3c**, visualized using Mercury with thermal ellipsoids shown at 50% probability level, as determined by SCXRD. Hydrogen atoms are omitted for clarity. b) Fragment of the crystal structure of **3c**, depicting a dimeric hydrogen-bonded pair of molecules. Crystallographic details can be found in *Appendix D*. Hydrogen bonds are shown as blue dotted lines.

5.5 Imide-isocyanate coupling by grinding

Lastly, the possibility of conducting the coupling reaction between cyclic imides and isocyanates was investigated. It was anticipated that imides would have similar reactivities[38] to isatin; as the principal structural difference between isatin and phthalimide is the position of the NH group, it was expected that cyclic imides would also undergo coupling with isocyanates to form analogous carbamoyl-imido compounds. Again, the proof-of-concept mechanochemical coupling reaction was tested using Cy-NCO and four commercially available imides as starting materials, namely 2,3-naphthylenedicarboximide (NDC), succinimide, maleimide and phthalimide (Table 3). The result of mechanochemical reactivity screening (Table 5.3, entries 1-8) showed that the copper-catalyzed coupling reaction with NDC did not take place at all (no conversion), even with presence of stoichiometric base such as Cs_2CO_3 (Table 5.3, Entry 9). Reactions with succinimide and maleimide also did not take place. However, the coupling reaction with phthalimide to form **4** was successful, and proceeded in good conversions (Table 5.3, Entry 14, 89% conversion) using 20% mol CuCl or 10% $Cu(OAc)_2 \cdot H_2O$ (Table 5.3, Entry 15, 79% conversion). Last, but not least, the coupling reaction with oxazolidin-2-one substrate to form **5** was also successful (Table 5.3, Entry 16, 92% isolated yield). Spectroscopic details for **4** and **5** can be found in *Appendix D*. We did not observe any particular pattern that might explain the lack of reactivity for all reactions involving imides. However, to the best of our knowledge, this work has provided the first examples of a base- and solvent-free catalytic functionalization of cyclic imides to furnish carbamoyl-imido compounds. Importantly, attempted solvothermal reactions in a pressurized autoclave at elevated temperatures led to comparable or poorer reactivity for all coupling reactions of isatins, benzamides or imides with isocyanates.

Table 5.3. Optimization and screening of LAG liquids and potential catalysts for imide-isocyanate coupling

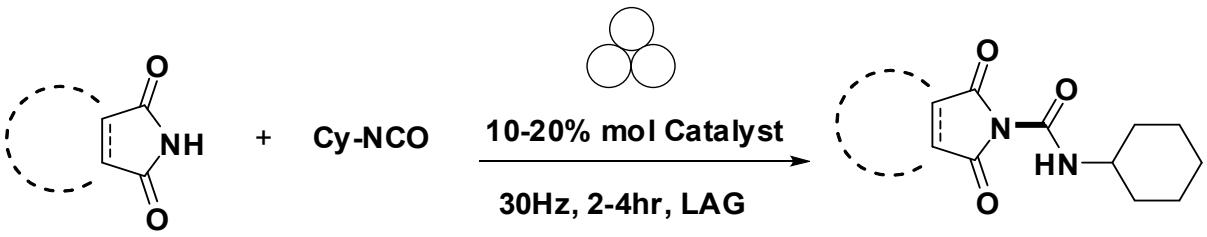

Entry	Imide	Catalyst	Load(%)	Conv.(%)
1	NDC	CuCl	10	NR
2	NDC	CuCl	10	NR
3	NDC	$Cu(OAc)_2 \cdot 2H_2O$	10	NR
4	NDC	$Cu(OAc)_2 \cdot 2H_2O$	10	NR
5	NDC	$Cu(L^a)ClOH$	10	NR
6	NDC	$Cu(acetonitrile)_2BF_4$	10	NR
7	NDC	CuCl	20	NR
8	NDC	CuCl	20	NR
9	NDC	Cs_2CO_3	100	NR
10	NDC	$AgNO_3$	10	NR
11	Succinimide	CuCl	10	NR
12	Maleimide	CuCl	10	NR
13	Phthalimide	CuCl	10	74
14	Phthalimide	CuCl	20	89[b]
15	Phthalimide	$Cu(OAc)_2 \cdot 2H_2O$	10	79
16	Oxazolidin-2-one	CuCl	10	100[c]

*Percent conversion based on NMR. [a]Tetramethylethylenediamine was used as a ligand to augment the catalyst. [b]60% isolated yield after column chromatography. [c]92% isolated yield.

5.6 Conclusion

In conclusion, we have demonstrated the use of mechanochemistry to establish a novel synthetic methodology for the functionalization of amides to form carbamoylamides by direct, copper-catalyzed coupling between cyclic (isatin and phthalimide) and acylic (benzamide) amides with isocyanates. This synthetic strategy is appealing as it involves a direct C-N coupling conducted in a solvent-free and base-free manner. A total of 23 compounds were synthesized and two crystal structures were obtained. Another important aspect of the presented work is the exploration and optimization of a novel synthetic route

using exclusively mechanochemical procedures. Consequently, we believe that the presented work further buttresses the view of mechanochemistry not only for augmenting the existing synthetic procedures, by making them greener and more environmentally-friendly, but it can also be used as a tool to discover and develop new reactions.

5.7 References

1 A. Greenberg, C. M. Breneman, J. F. Liebman, *The Amide Linkage: Structural Significance in Chemistry, Biochemistry, and Materials Science*, **2000**, Wiley & Sons, Inc, New York.

2 C. L. Allen, J. M. J. Williams, *Chem. Soc. Rev*., **2011**, *40*, 3405.

3 C. A. G. N. Montalbetti, V. Falque, *Tetrahedron*, **2005**, *61*, 10827.

4 F. Albericio, *Curr. Opin. Chem. Bio.*, **2004**, *8*, 211.

5 F. Xiao, Y. Liu, C. Tang, G.-J. Deng, *Org. Lett*., **2012**, *14*, 984.

6 H. Charville, D. Jackson, G. Hodges, A. Whiting, *Chem. Commun*., **2010**, *46*, 1813.

7 S. K. Verma, R. Ghorpade, A. Pratap, M. P. Kaushik,. *Tetrahedron Lett.*, **2013**, *53*, 2373.

8 V. Declerck, P. Nun, J. Martinez, F. Lamaty, *Angew. Chem. Int. Ed.*, **2009**, *48*, 9318 .

9 T. Rovis, H. U. Vora, *J. Am. Chem. Soc.*, **2007**, *129*, 13796.

10 a) G. P. Hess, J. C. Sheehan, *J. Am. Chem. Soc.*, **1955**, *77*, 1067; b) W. Kőnig.; R. Geiger, *Chem. Ber.*, **1970**, *103*, 788.

11 H. Liu, N. Yan, P. J. Dyson, *Chem. Commun*., **2014**, *50*, 7848.

12 a) J. F. Hartwig, Acc. Chem. Res., 2008, 41, 1534; b) M.-L. Louillat, F. W. Patureau, *Chem. Soc. Rev.*, **2014**, *43*, 901.

13 C. Sambiagio, S. P. Marsden, A. J. Blacker, P. C. McGowan, *Chem. Soc. Rev*., **2014**, *43*, 3525.

14 Y. Sunesson, E. Limé, S. O. N. Lill, R. E. Meadows, P.-O. Norrby, *J. Org. Chem*., **2014**, *79*, 11961.

15 V. R. Pattabiraman J. W. Bode, *Nature*, **2011**, *480*, 471.

16 a) James, S. L.; Adams, C. J.; Bolm, C.; Braga, D.; Collier, P.; Friščić, T.; Grepioni, F.; Harris, K. D. M.; Hyett, G.; Jones, W.; Krebs, A.; Mack, J.; Maini, L.; Orpen, A. G.; Parkin, I. P.; Shearouse, W. C.; Steed J. W.; Waddell, D. C. *Chem. Soc. Rev.* **2012**, *41*, 413; b) R. B. N. Baig, R. S. Varma, *Chem. Soc. Rev*., **2012**, *41*, 1559.

17 G. -W. Wang, *Chem. Soc. Rev.*, **2013**, *42*, 7668.

18 a) A. Bruckmann, A. Krebs, C. Bolm, *Green Chem*., **2008**, *10*, 1131; b) B. Rodríguez, A. Bruckmann, T. Rantanen, C. Bolm, *Adv. Synth. Catal.*, **2007**, *349*, 2213.

19 a) J. G. Hernández, T. Friščić, *Tetrahedron Lett.*, **2015**, *56*, 4253; b) N. R. Rightmire, T. P. Hanusa, *Dalton Trans.*, **2016**, *45*, 2352.

20 a) J. –L. Do, C. Mottillo, D. Tan, V. Štrukil, T. Friščić, *J. Am. Chem. Soc.*, **2015**, *137*, 2476; b) L. Chen, M. O. Bovee, B. E. Lemma, K. S. M. Keithley, S. L. Pilson, M. G. Coleman, J. Mack, *Angew. Chem. Int. Ed.*, **2015**, *38*, 11236; c) G. N. Hermann, P. Becker, C Bolm, *Angew. Chem. Int. Ed.*, **2015**, *54*, 7414; d) J. G. Hernández, C Bolm, *Chem. Commun*., **2015**, *51*, 12582.

21 V. Štrukil, D. Gracin, O. V. Magdysyuk, R. E. Dinnebier, T. Friščić, *Angew. Chem. Int. Ed*., **2015**, *54*, 8440.

22 a) V. Štrukil, B. Bartolec, T. Portada, I. Dilović, I. Halasz, D. Margetic, *Chem. Commun*., **2012**, *48*, 12100; b) J. G. Hernández, E. Juriasti, *J. Org. Chem*., **2010**, *75*, 7107; c) T. X. Métro, J. Bonnamour, T. Reidon, J. Sarpoulet, J. Martinez, F. Lamaty, *Chem. Commun.*, **2012**, *48*, 11781; d) J. Bonnamour, T. X. Métro, J. Martinez, F. Lamaty, *Green Chem.*, **2013**, *15*, 1116; e) L. Konnert, B. Reneaud, R. M. Figueiredo, J.-M. Campagne, F. Lamaty, J. Martinez, E. Colacino, *J. Org. Chem*., **2014**, *79*, 10132; f) C. Duangkamol, S. Jaita, S. Wangngae, W. Phakhodee, M. Pattawarapan, *RSC Adv*., **2015**, *5*, 52624; g) L. Konnert, M. Dimassi, L. Gonnet, F. Lamaty, J. Martinez, E. Colacino, *RSC Adv*., **2016**, *6*, 36978; h) D. Tan, L. Loots, T. Friščić, *Chem. Commun*., **2016**, *52*, 7760.

23 D. Tan, V. Štrukil, C. Mottillo, T. Friščić, *Chem. Commun*., **2014**, *50*, 5248.

24 D. Tan, C Mottillo, A. D. Katsenis, V. Štrukil, T. Friščić, *Angew. Chem. Int. Ed*., **2014**, *35*, 9475.

25 a) N. P. Haijar, J. E. Casida, **Science**, **1978**, *200*, 1499; b) H. Oberlander, D. L. Silhacek, E. Leach, I. Ishaaya, E. Shaaya, *Arch. Insect Biochem. Physio*., **1991**, *18*, 219.

26 a) R. L. Jones, A. L. Barry, *Rev. Infect. Dis.*, **1983**, *5*, 108; b) T. P. Jr. Lodise, B. Lomaestro, G. L. Drusano, *Clin. Infect. Dis.*, **2007**, *44*, 357.

27 B. M. Biller, M. E. Molitch, M. L. Vance, K. B. Cannistraro, K. R. Davis, J. A. Simons, J. R. Schoenfelder, A. J. Klisbanski, *Clin. Endocrinol. Metab.*, **1996**, *81*, 2338.

28 F. Becić, E. Kapić, E. Becić, Med. Arh., 2003, 57, 125.

29 a) O. L. Erdmann, *J. für Praktische Chem.*, **1840**, *19*, 321–362; b) A. Laurent, *Annal. Chim. Phys.*, **1840**, *3*, 393.

30 a) D. A. Horne, R. Jove, C. Lincoln, S. Nam, L. Overman, J. Xie, *US Patent*, **2013**, *US2013225637-A1*; b) B. Bhrigua, D. Pathak, N. Siddiqui, M. S. Alam, W. Ahsan, *Int. J. Pharm. Sci. Drug. Res.*, **2010**, *2*, 229; c) D. Ray, B. K. Paul, N. J. Guchhait, *Photochem. Photobio.*, **2013**, *127*, 18.

31 a) W. C. Sumpter, Chem. Rev., 1944, 34, 393; b) F. D. Popp, *Adv. Heterocyc. Chem*., **1975**, *18*, 1; c) J. F. M. da Silva, S. J. Garden, A. C. Pinto, *J. Braz. Chem. Soc*., **2001**, *12*, 273; d) J. Azizian, M. K. Mohammadi, O. Firuzi, N. Razzaghiasl, R. Miri, *Med. Chem. Res*., **2012**, *21*, 3730; e) G. Cerchiaro, K. Aquilano, G. Filomeni, G. Rotilio, M. R. Ciriolo, A. M. D. C. Ferreira, *J. Inorg. Biochem*., **2005**, *99*, 1433; f) S. Rehn, J. Bergman, B. Stensland, *Eur. J. Org. Chem*., **2004**, *413*; g) M. Yamagishi, K.-I. Ozaki, Y. Yamada, T. Da-Te, K. Okamura, M. Suzuki, *Chem. Pharm. Bull.*, **1991**, *39*, 1694; h) M. Yamagishi, Y. Yamada, K.-I. Ozaki, J. Tani, M. Suzuki, *Chem. Pharm. Bull*., **1991**, *39*, 626.

32 a) B. Tan, N. R. Candeias, C. F. Barbas, *J. Am. Chem. Soc.*, **2011**, *133*, 4672; b) A. D. Mamuye, S. Monticelli, L. Castoldi, W. Holzer, V. Pace, *Green Chem*., **2015**, *17*, 4194.

33 a) T. Friščić, W. Jones, *Cryst. Growth Des.*, **2009**, *9*, 1621; b) G. A. Bowmaker, *Chem. Commun.*, **2013**, *49*, 334; c) The η-parameter describes mechanochemical LAG conditions in terms of the ratio of liquid additive volume and the weight of the reactants, see: T. Friščić, S. L. Childs, S. A. A. Rizvi, W. Jones, *CrystEngComm*, **2009**, *11*, 418.

34 T. L. Cook, J. A. Walker Jr, J. Mack, *Green Chem.*, **2013**, *15*, 617.

35 P. Jenner, C. D. Marsden, *Life Sci.*, **1979**, *25*, 479.

36 a) Kühn, *Bcr.,* **1884**, *17*, 2880; b) Kühn, *Bcr.*, **1885**, *18*, 1478; c) P. F. Wiley, *J. Am. Chem. Soc.*, **1949**, *71*, 1310.

37 a) H. G. Schwein, *Arch. Pharm*., **1986**, *319*, 814; b) A. K. Singh, R. Chawla, L. D. S. Yadav, *Tetrahedron Lett.*, **2013**, *54*, 5099; c) Y. H. Chang, F.-T. Chiu, G. Zon, *J. Org. Chem.*, **1981**, *46*, 342; d) S. Stokes, N. G. Martin, *Tetrahedron Lett*., **2012**, *53*, 4802; e) D. –Q. Song, Y. –M. Wang, N. –N. Du, W.-Y. He, K.-L. Chen, G.-F. Wang, P. Yang, L.-Z. Wu, X.-B. Zhang, J.-D. Jiang, *Bioorg. Med. Chem. Lett.*, **2009**, *19*, 755; f) I. A. Atanassova, J. S. Petrov, N. M. Mollov, *Synthesis*, **1987**, *8*, 734.

38 a) T. Sengoku, Y. Murata, Y. Aso, A. Kawakami, T. Inuzuka, M Sakamoto, M. Takahashi, H. Yoda, *Org. Lett*., **2015**, *17*, 5846; b) N. Fotouhi, N. Kong, E. A. Liu, A. J. Lovey, J. G. Jr. Mullin, *World I. P. O. Patent*, **2001**, *WO01/27106A1*.

CHAPTER 6

A FAMILY OF ISOSTRUCTURAL CRYSTALS FROM CONFORMATIONALLY FLEXIBLE ORTHO-SUBSTITUTED N,N'-BIS(CYCLOHEXYL)-ARYLSULFONYLGUANIDINES

"To organic synthetic chemists, crystallography is the end. To supramolecular synthetic chemists, crystallography is the beginning." – Prof. Joel Bernstein, Gordon Research Conference (GRC), 2014.

6.1 Introduction and connecting text.

The work presented in this chapter is part of not yet published manuscript entitled "A family of isostructural crystals from conformationally flexible *ortho*-substituted *N*,*N*'-bis(cyclohexyl)-arylsulfonylguanidines", which discusses a series of various *N*,*N*'-bis(cyclohexyl)-arylsulfonylguanidines that were synthesized mechanochemically and solvothermally, bearing different substituents in the *ortho*-position of the aryl ring. These compounds crystallize in the enantiomorphic $P3_2$ or $P3_1$ space groups, with molecules assembled through intermolecular S=O···H-N hydrogen bonds in one dimensional (1-D) helical chains parallel to three-fold helical axes of rotation. These structures represent a surprising case of isostructurality in a family of eight single-component crystals of molecules with significantly diverse functional groups. To the best of our knowledge, isostructurality of such scope has not been achieved before in single-component crystals. The draft manuscript was written by D. Tan with guidance and editing contributions from Prof. T. Friščić, and co-authored with Dr. A. D. Katsenis and R. von Celsing, an undergraduate summer student from McGill University who contributed to the synthesis of two of the isostructural crystals. The text has been formatted and re-written for inclusion in this Dissertation. All experimental results, including screening, synthesis and instrumental characterization (FTIR, NMR, MS, PXRD, SCXRD) of the various compounds were performed by D. Tan. In *Chapter 3*, a new copper-catalyzed mechanochemical coupling reaction between arylsulfonamides and carbodiimides to furnish arylsulfonylguanidines was discussed. As an extension of that study, in this chapter, the library of the arylsulfonylguanidine products has been extended even further in order to investigate a series of single-component isostructural compounds.

The ability to control the solid-state assembly of molecules into crystal structures based on periodic lattices, with specific and desired properties, is a hallmark of crystal engineering, a discipline that pertains to the design and synthesis of functional molecular solids.[1] The main challenge in accomplishing these goals of crystal engineering, however, is the difficulty in controlling crystal structures. This is evidenced, for example, by the phenomenon of polymorphism, *i.e.* the ability of a compound to exist in more than one crystalline form.[2] Polymorphism is of extreme importance in pharmaceutical industry,[3] as the way in which molecules assemble in the crystal can affect a range of physicochemical properties of the compound. On the other hand, the yin to the yang of polymorphism is the concept of isostructurality, whereby two or more compounds having similar functional groups, or similar functional group patterns, can adopt an identical crystalline arrangement of

molecules. Although polymorphism and isostructurality may appear to be intuitively viewed as opposing concepts, they can also be complementary to each other.[4] In principle, the control and understanding of isostructurality can be a useful tool in crystal engineering, and it can allow for the assembly of different molecules in the solid state by following a certain supramolecular guideline. Isostructurality is commonly observed in multi-component solids, *i.e.* crystals composed of more than one chemical species, such as cocrystals and salts,[5] molecular complexes[6] and solvent/guest inclusion compounds.[7] According to the principle of close packing established by Kitaigorodskii,[8] molecules with functional groups that have similar shape, size and structural role are likely to adopt the same crystal structure, *i.e.* such molecules are likely to be isostructural. One good example of this is the rule of chloro-methyl exchange, whereby structurally similar molecules bearing chloro and methyl groups in identical positions often crystallize isostructurally to each other.[9] Other examples of functional groups that are structurally equivalent and therefore, can lead to pairs of isostructural compounds are commonly the pair of Cl and Br substitutents,[10] as well as other related functionalities such as OH/NH, aromatic CH/N, CH/CF and Br/OH.[11] These different types of structurally equivalent groups can also be combined to produce sets of isostructural molecular solids. For example, Cinčić *et al.* have combined Br/I exchange and CH/N exchange to design a set of four isostructural halogen-bonded two-component cocrystals.[11f] This is a so far unique report in deliberately creating isostructural molecular solids.

Overall, for multi-component crystals (cocrystals), guidelines have been established to design relatively large sets of isostructural solids. However, isostructurality within single component molecular crystals is particularly rare,[12] and there are very few sets of isostructural compounds that include more than two members.[13] This is because minor changes in the molecular structure are very likely to lead to different molecular volumes and charge distribution. This changes the way the molecules pack in the solid state. In that context, the most challenging are conformationally flexible molecules, which exhibit high degrees of flexibility. For example, rotational freedom around single bonds may lead to different molecular conformations, as well as different hydrogen bonding motifs, subsequently leading to different molecular packing arrangement or polymorphism. Although there has been many reports on the synthesis and investigation of isostructurality in conformationally flexible compounds,[14] the diversity of the functional groups found in those isostructural sets is still limited to the pair-wise combinations mentioned in the previous paragraph. As a result, it has so far not been possible to create or study a family of more than

two or three single-component isostructural compounds. To the best of our knowledge, the largest set studied so far consists of six members.[14d] Herein, we report a serendipitous discovery of a family of eight arysulfonyguanidines, containing a variety of functional groups, that crystallize isostructurally.

6.2 Arylsulfonyl-guanidines.

Recently, we reported a new mechanochemical coupling reaction between poorly nucleophilic sulfonamides with carbodiimides to fashion arylsulfonylguanidines.[15] For one of our compounds, namely *N*,*N*'-bis(cyclohexyl)-2-chloro-arylsulfonylguanidine (compound **1**, Fig. 6.1), we were able to obtain X-ray diffraction (XRD) quality single crystals *via* slow evaporation of solvent from an acetone-methanol mixture, and discovered that **1** crystallized in the chiral $P3_2$ space group containing a three-fold screw axis. That compound **1** crystallized in a chiral helical manner in the solid state, even though it is an achiral molecule, is remarkable.[16]

The crystal structure of **1** consists of one-dimensional hydrogen-bonded helical chains of molecules. There are a total of three symmetrical molecules per unit cell and each molecule is connected to two nearby neighbours through a set of N-H···O bonds. These three molecules form a helix around a crystallographic 3_2 screw axis parallel to the crystallographic *b* direction (Fig 6.2). Each supramolecular helix in turn is surrounded by six neighboring helices that are held together through C─H···O2=S interactions. The helices are depicted as the green coils in Fig. 6.2b. Each molecule of **1** contains a $S^1_1(6)$ intramolecular hydrogen bonding motif based on atoms S=O1···H─N2, which locks the sulfonamide and the planar Y-shaped guanidine moieties into a rigid unit (Fig. 6.2a). The molecules are then connected *via* S=O1···H─N3 hydrogen bonds to form a supramolecular helical chain of the $C^1_1(6)$ type, as illustrated with the green ribbon in Fig. 6.2c, when viewed along the crystallographic *b*-axis. The S=O1 oxygen atom thus acts as a bifurcated hydrogen bond acceptor for both intramolecular and intermolecular hydrogen bonds. In addition, it is worth noting that there are no Cl···Cl interactions in this structure despite the presence of chloro-substituents on an aryl ring.

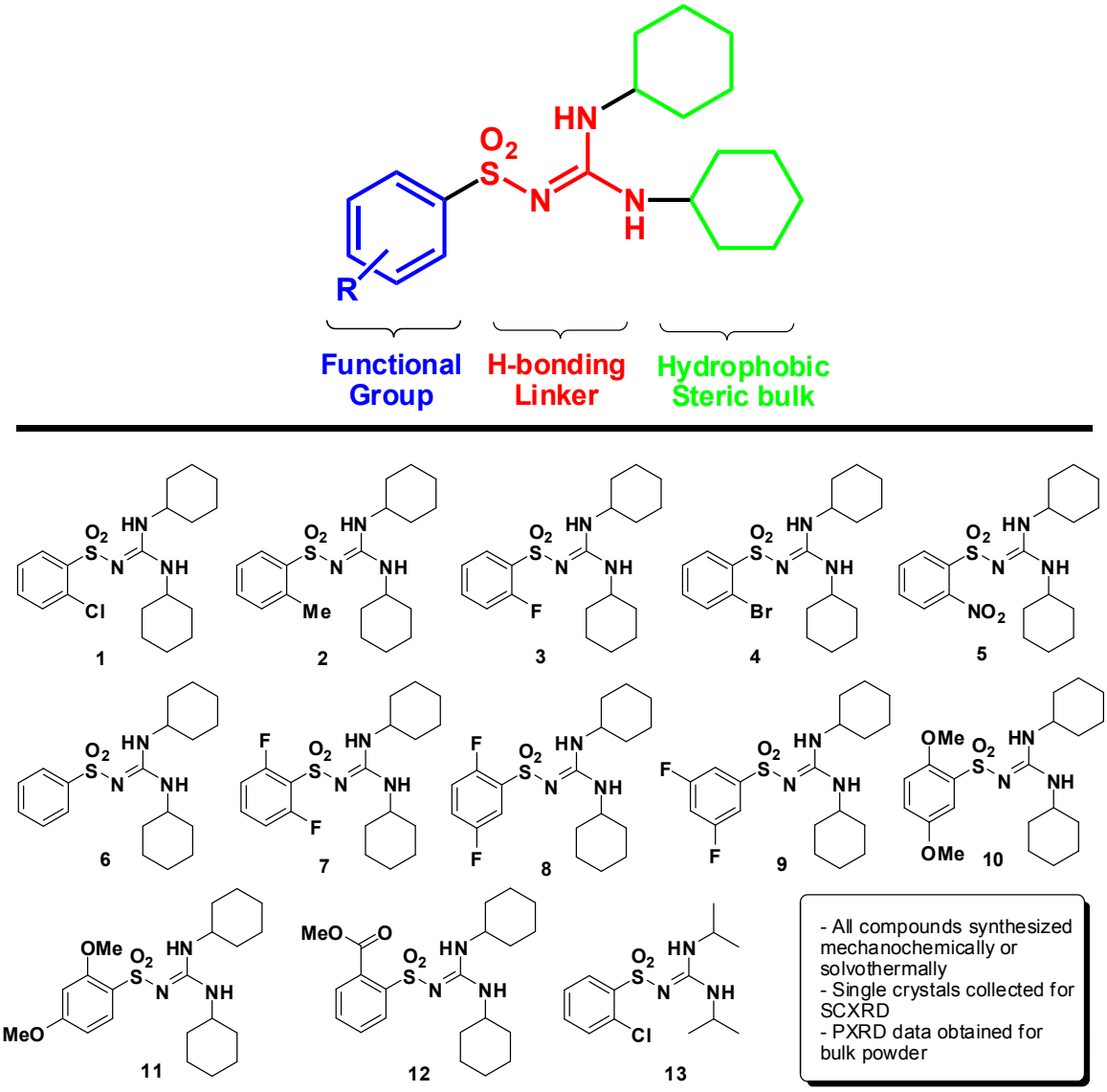

Fig. 6.1. List of arylsulfonylguanidines described in this work.

The formation of a chiral structure from the achiral compound **1** is particularly surprising, having in mind that there exist many degrees of freedom through single bond rotations throughout the molecule. This, in turn, allows for different possible motifs for molecules of **1** to associate in the solid state. It can be imagined that the arylsulfonylguanidine molecules could be connected by a specific "sulfonylguanidine synthon", *i.e.* a hydrogen-bonded S=O···H─N-C(N)N unit, in a wide diversity of ways. This might lead to discrete dimers, trimers and larger units, or forming different types of catemer chains. Within the catemer variant, the molecules can be packed in a homotopic manner, forming helices in which the hydrogen bonds formed between molecules in a bifurcated manner (Fig. 6.3a), similar to **1**, or in a hypothetical non-bifurcated manner (Fig. 6.3b). On the other hand, these sulfonylguanidine molecules can also form chains, linked by alternating

molecules flipped in opposite directions (Fig 6.3c). Importantly, non-helical chain structures could also potentially form, without the oxygen atom acting as a bifurcated hydrogen bond acceptor. Indeed, such supramolecular sulfonylguanidine chains have been observed in the structure of *N*,*N*'-bis(cyclohexyl)-4-methyl-arylsulfonylguanidine, which we have previously published.[15] In that structure, the sulfonylguanidine molecules alternatively adopt two different orientations along the chain (Fig. 6.3d). Thus, we believe that the chances of polymorphism in **1** are high due to the inherent conformational flexibility and different possible modes of self-assembly available for the molecule. Therefore, an extensive screen for potential polymorphs of **1** was conducted by both solution and mechanochemical (LAG)[17] methods. However, all these attempts so far yielded only the described chiral structure of **1**.

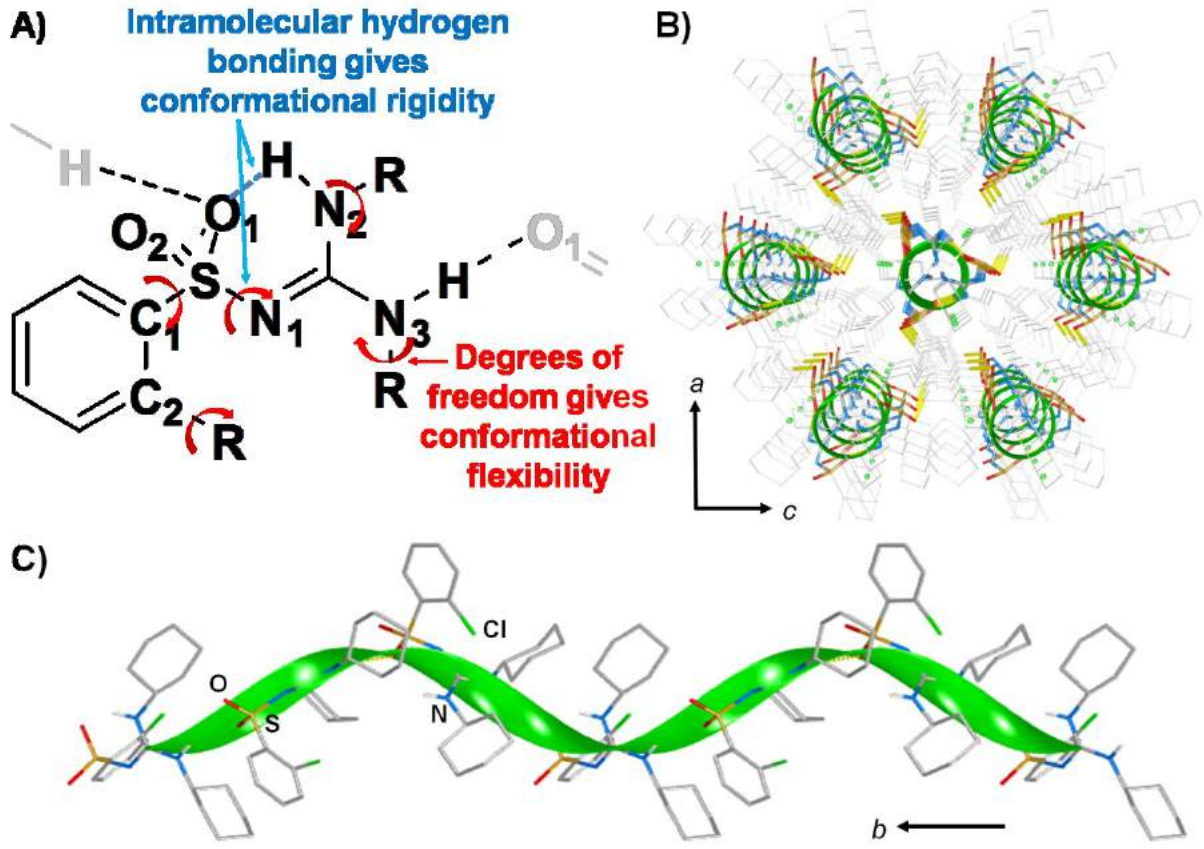

Fig. 6.2. (a) Molecular diagram depicting the intramolecular hydrogen bonding (blue arrow) and various degrees of freedom of bond rotations for the *ortho*-substituted arysulfonylguanidines. (b) Top to down view of the helical chain of **1** as viewed down the crystallographic *b*-axis. The green coils depict the helical chains (c) Side view of the helical chain of **1** as the hydrogen-bonded helix propagates along the crystallographic *b*-axis. The green ribbon depicts the hydrogen-bonded helical chain.

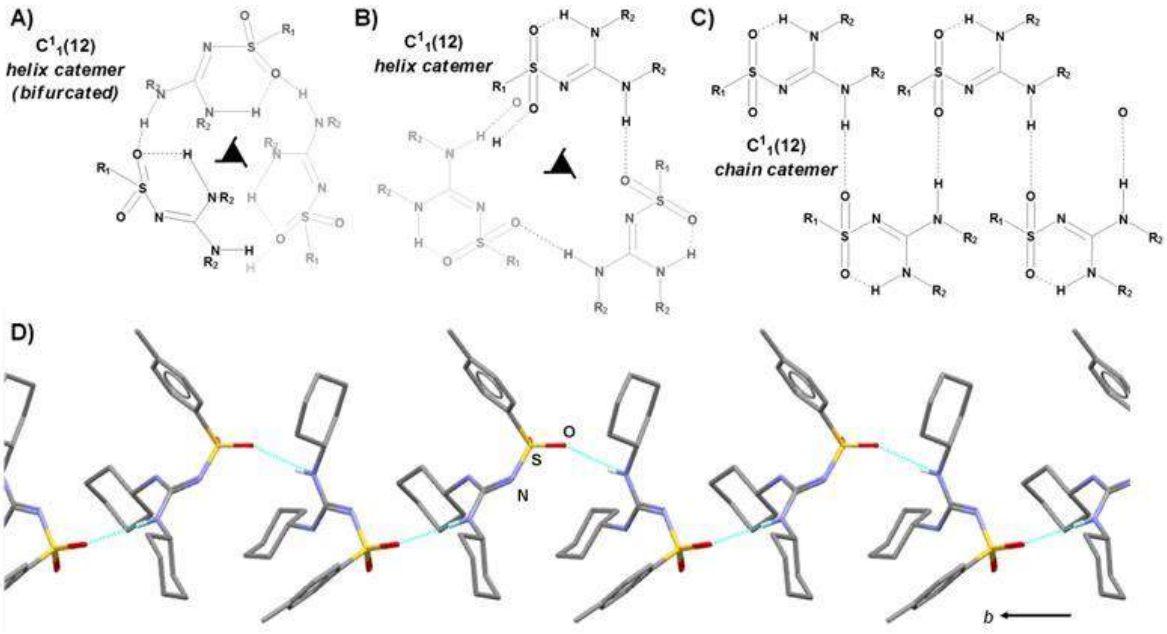

Fig. 6.3. Schematic illustration of catemers of sulfonylguanidine molecules forming a) a bifurcated $C^1_1(12)$ helix, b) a hypothetical non-bifurcated $C^1_1(12)$ helix or c) $C^1_1(12)$ chains comprised of alternating molecules flipped in opposite directions. d) Fragment of the crystal structure of *N*,*N*'-bis(cyclohexyl)-4-methyl-arylsulfonylguanidine,[15] depicting the chain catemer with alternating molecules flipped in opposite directions, and showing the hydrogen-bonded chain as it propagates along the crystallographic *b*-axis.

The unexpected formation of a helical self-assembly motif for compound **1** invites speculation that a similar structure could also be obtained for an analogous compound bearing a methyl group instead of the chloro substituent in the *ortho*-position. As previously discussed, this can be explained by the well-known, often encountered structural equivalence of chloro and methyl groups in solid-state organic chemistry. Achieving isostructurality in these arylsulfonylguanidines can be a challenge as it can be envisaged that the molecules can form a multitude of possible hydrogen-bonded arrangements. In order to explore this possibility, compound **2** was synthesized mechanochemically by milling together 2-methylbenzenesulfonamide and DCC, in the presence of 10 mol% CuCl catalyst. Diffraction-quality single crystals of **2** were then obtained by slow evaporation of a solution mixture using acetone and methanol as the solvents. Experimental details can be found in *Chapter 8, Section 8.5*. Crystal structure determination revealed that **2** is indeed isostructural to **1**, and they both exhibited similar unit cell parameters, and crystallized in the $P3_2$ space group. Specifically, comparison of unit cell parameters (Table 6.1) showed little variation, from 10.1292(7) Å to 9.975(2) Å and 17.234(1) Å to 17.291(4) Å (unit cell dimensions for *a*- and

c-axis) and 1531.7(2) Å^3 to 1489.9(7) Å^3 (unit cell volume) for **1** and **2**, respectively. The hydrogen-bonding patterns in **2** are almost identical to those in **1**, comprising of the bifurcated intramolecular $S^1_1(6)$ S=O1···H─N2 and intermolecular $C^1_1(6)$ S=O1···H─N3 hydrogen bonds, which again form the helical chains (Fig. 6.4). The lengths of intermolecular hydrogen bonds, namely O1···N3 distances, are also very similar, 2.922(5) Å and 2.89(1) Å for **1** and **2**, respectively (Table 6.2). The isostructurality of **1** and **2**, despite the known principle of chloro-methyl exchange, is still surprising. Namely, the chloro and methyl group substituents have very different electronic properties. Yet, the observed robustness of the crystal packing motif between **1** and **2** is interesting, and encourages us to perform a more extensive study. Using this as our inspiration, we attempted to design and synthesize a series of bis(cyclohexyl)-arylsulfonylguanidines that might also crystallize isostructurally to compound **1** and **2** (Fig. 6.1).

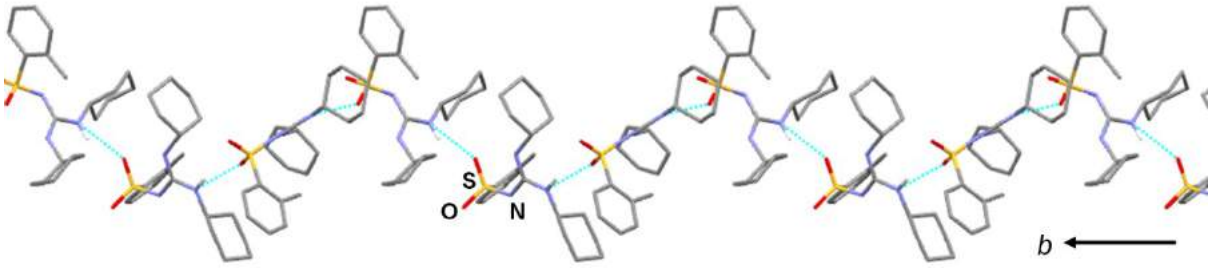

Fig. 6.4. Fragment of the crystal structure of **2** depicting the hydrogen-bonded helical chains, as viewed along the crystallographic *b*-axis.

6.3 Hypothesis and building a library of isostructural compounds.

Isostructurality of **1** and **2** suggests that the *ortho*-substitution of the aryl ring does not have a strong effect on the crystal packing of the molecules. Instead, the assembly of molecules in the solid state appears to be dominated by S=O1···H-N3 hydrogen-bonded chains that seem to be isolated from the rest of the crystal structure through bulky cyclohexyl groups on the guanidine moiety. Therefore, the structure of molecules of **1** and **2** can be described in terms of three segments: the cyclohexyl substituents, the hydrogen-bonding sulfonylguanidine unit and the substituted aryl system. Of these, the last one appears to have the least effect on the molecular assembly in the crystal (factoring only *ortho*-substitution). In such a scenario, it might be possible to extensively vary the aryl group substitution without

disturbing the molecular assembly encountered in compounds **1** and **2**. To test this hypothesis, we conducted the synthesis and systematic analysis of crystal structures of compounds **3-13** (Fig. 6.1). Crystals were obtained using the same crystallization solvent and method. Experimental details can be found in *Chapter 8, Section 8.5*. The compounds **2-12** were synthesized with the intention to explore the influence of the aryl group substituent on the sulfonylguanidine molecule crystal packing. Compound **13** was selected to evaluate the relevance of the guanidine *N*-substituent on the crystal structure. It was remarkable to find out that compounds **3-8** all crystallized in a way that is analogous to both **1** and **2**, therefore providing an unprecendented system of eight isostructural single-component crystals. The functional group on the aryl ring varies from a single halogen substituent (**1**, **3**, **4**), to non-substituted (**6**), methyl (**2**), bis-fluorinated (**7**, **8**) and even a structurally and electronically very different nitro (**5**) group, which might interfere with the hydrogen-bonding S=O···H-N motif.

6.4 X-ray diffraction analysis

Comparison of single crystal X-ray diffraction data reveals that all of the compounds **1-8** adopt almost the same crystal structure, with little variation in the unit cell parameters (Table 6.1). As all the compounds crystallized in a hexagonal space group, the only variations in the unit cell parameters are the dimensions along the crystallographic *a*- and *c*-axes, which vary from 9.745(1) Å to 10.1292(7) Å and 17.208(1) Å to 17.855(3) Å respectively. Similarly, the unit cell volumes of the eight isostructural compounds, ranging from 1462.7(7) $Å^3$ to 1531.7(2) $Å^3$, did not exhibit any significant de*via*tion. This is highly unusual, especially since compounds **1-8** have significantly different functional group substituents on the aryl ring. This means that the extent of isostructurality achieved in these so far unique compounds greatly exceeds the trends previously described.[9-11]

The relative size of the substituent groups, from a large Br atom in **4** to a small hydrogen atom on the unsubstituted phenyl ring in **6**, does not seem to affect the packing of the molecules. Similar to **1**, compound **4** also did not exhibit any Br···Br or Br···O interactions. Fluoro-substitution in the 5- and 6- position of the phenyl ring, in compounds **7** and **8** respectively, was also tolerated and did not disrupt the intermolecular hydrogen-bonding motifs or cause deviation from isostructurality. Even more remarkable is that the presence of a nitro group (**6**) also did not disrupt the sulfonylguanidine hydrogen bonding,

even though it can compete with the sulfonyl group as a hydrogen bond acceptor. Compounds **3-8** had similar analogous hydrogen-bonding motifs with **1** and **2**, and formed 1-D helical chains (Fig. 6.5).

Table 6.1. Crystallographic data for compounds **1-8**

Compound	(1)	(2)	(3)	(4)
Functional group	2-chloro	2-methyl	2-fluoro	2-bromo
Molecular formula	$C_{19}H_{28}N_3O_2SCl$	$C_{20}H_{31}N_3O_3S$	$C_{19}H_{28}N_3O_3SF$	$C_{19}H_{28}N_3O_2SBr$
M_r	397.95	378.76	309.11	442.41
Crystal System	Trigonal	Trigonal	Trigonal	Trigonal
Crystal colour	Colorless	Colorless	Colorless	Colorless
Space group	$P3_2$	$P3_2$	$P3_2$	$P3_2$
Temperature (K)	100K	150K	150K	100K
Unit cell dimensions (Å,°)				
a	10.1292(7)	9.975(2)	9.8042(8)	10.0051(6)
b	10.1292(7)	9.975(2)	9.8042(8)	10.0051(6)
c	17.2377(13)	17.291(4)	17.6800(15)	17.2075(10)
α	90	90	90	90
β	90	90	90	90
γ	120	120	120	120
Volume (Å^3)	1531.7(2)	1489.9(7)	1471.8(3)	1491.7(2)
Z	3	3	3	3
D_{calc} (g cm^{-3})	1.294	1.266	1.291	1.456
μ (mm^{-1}) (abs coeff)	0.307	0.182	0.192	2.189
***F*(000)**	636	614	612	677
Refl. collected/independent	16826/4148	8909/ 4201	17531/ 4494	37796 / 8009
No. observed refl. [$I>2\sigma(I)$]*	3174	3017	4139	5614
No. restraints/No. parameters	1/235	1/ 266	1/ 235	1/ 255
R [all/gt]	0.0670/ 0.0432	0.0963/ 0.0694	0.0388/ 0.0341	0.1372/ 0.0587
wR [ref/gt]	0.0971/ 0.0880	0.1854/ 0.1665	0.0782/ 0.0756	0.1661/ 0.1400
Goodness-of-fit on F^2	1.013	0.986	1.048	1.126
Peak and hole (e Å^{-3})	0.249, -0.396	0.346, -0.365	0.234, -0.294	0.983, -1.747

Compound	(5)	(6)	(7)	(8)
Functional group	2-nitro	phenyl	2,6-difluoro	2,5-difluoro
Molecular formula	$C_{19}H_{28}N_4O_4S$	$C_{19}H_{30}N_3O_2S$	$C_{19}H_{27}N_3O_2SF_2$	$C_{19}H_{27}N_3O_2SF_2$
M_r	309.11	363.51	399.49	399.49
Crystal System	Trigonal	Trigonal	Trigonal	Trigonal
Crystal colour	Colorless	Colorless	Colorless	Colorless
Space group	$P3_2$	$P3_2$	$P3_2$	$P3_2$
Temperature (K)	100K	150K	100K	100K
Unit cell dimensions (Å,°)				
a	10.0198(8)	9.7459(14)	9.7765(6)	9.9346(6)
b	10.0198(8)	9.7459(14)	9.7765(6)	9.9346(6)
c	17.3774(13)	17.855(3)	17.6713(11)	17.6480(11)
α	90	90	90	90
β	90	90	90	90
γ	120	120	120	120
Volume (Å^3)	1510.9(3)	1468.7(5)	1462.7(2)	1508.4(2)
Z	3	3	3	3
D_{calc} (g cm^{-3})	1.347	1.233	1.361	1.319
μ (mm^{-1}) (abs coeff)	0.194	0.182	0.204	0.198
***F*(000)**	654	588	636	636
Refl. collected/independent	57011/7082	17553/ 4551	40833/ 8690	32270 / 7205
No. observed refl. [$I>2\sigma(I)$]*	5702	4150	7732	6166
No. restraints/No. parameters	1/ 253	1/ 244	1/244	1/ 244
R [all/gt]	0.0723/ 0.0465	0.0385/ 0.0334	0.0476/ 0.0364	0.0566/ 0.0395
wR [ref/gt]	0.0993/ 0.0914	0.0822/ 0.0796	0.0770/ 0.0732	0.0824/ 0.0771
Goodness-of-fit on F^2	1.051	1.044	1.041	1.048
Peak and hole (e Å^{-3})	0.282,-0.338	0.192, -0.245	0.364, -0.297	0.289, -0.329

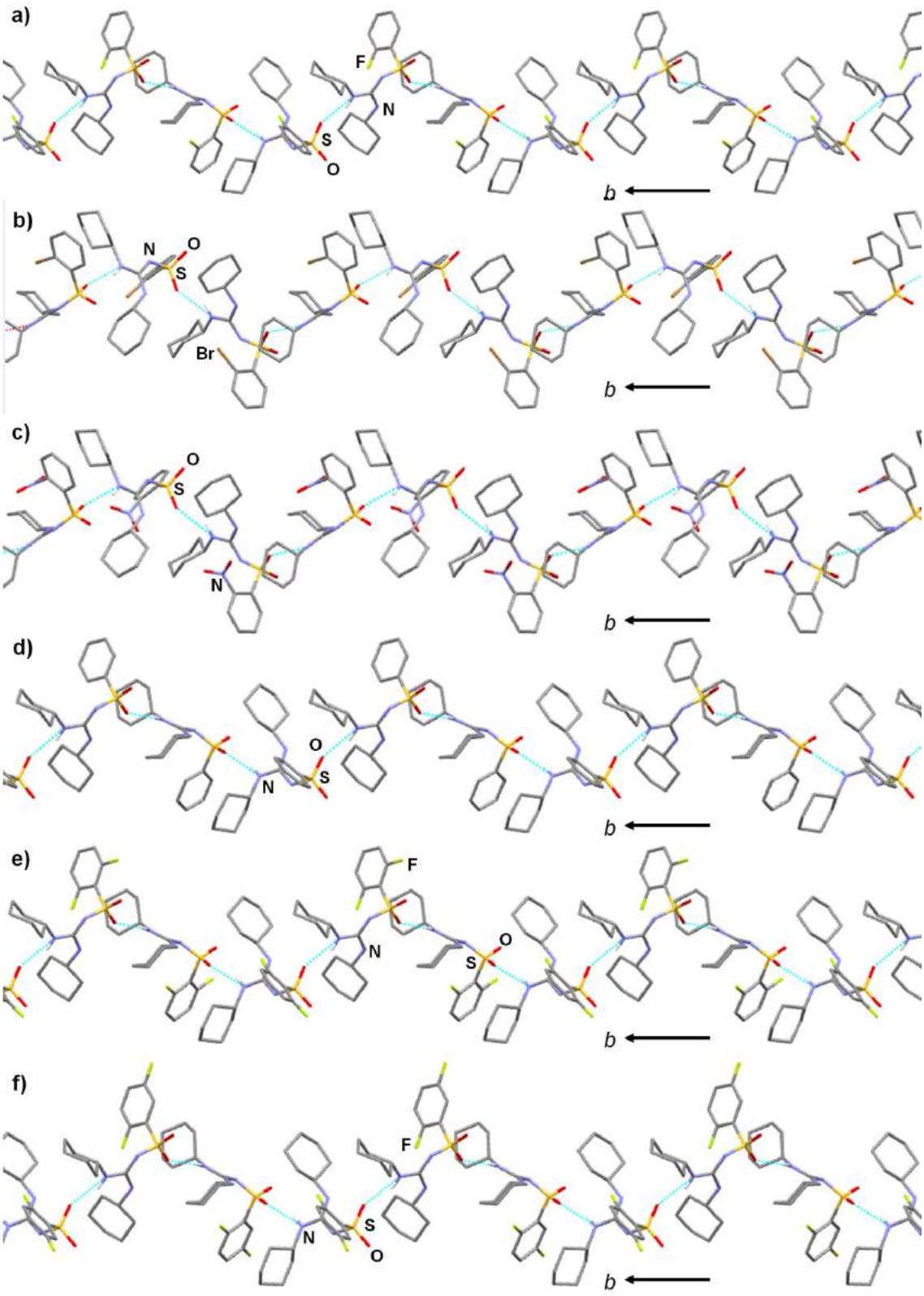

Fig. 6.5. Similarly oriented fragments of the crystal structures of compounds a) **3** (2-fluoro), b) **4** (2-bromo), c) **5** (2-nitro), d) **6** (phenyl), e) **7** (2,6-difluoro) and f) **8** (2,5-difluoro), depicting the one-dimensional hydrogen-bonded helical chains as, viewed along the crystallographic *b*-axis. These compounds are isostructural to one another, as well as to compounds **1** and **2**.

As molecules of compounds **1-8** are all highly conformationally flexible, it was important to check for potential polymorphic behaviour. The crude bulk solids **1-8**, prepared mechanochemically, were analyzed by PXRD. Comparison of the powder patterns reveals that the powdered forms of the bulk compounds of **1-8** are isostructural to one another. All of the experimentally obtained PXRD patterns were found to match to those simulated from the SCXRD of compounds **6** and **7**. This data confirms that the observed isostructurality is not an artefact of polymorphism caused by crystallization conditions (Fig 6.6) and that compounds **1-8** also are isostructural in the as prepared bulk powdered form.

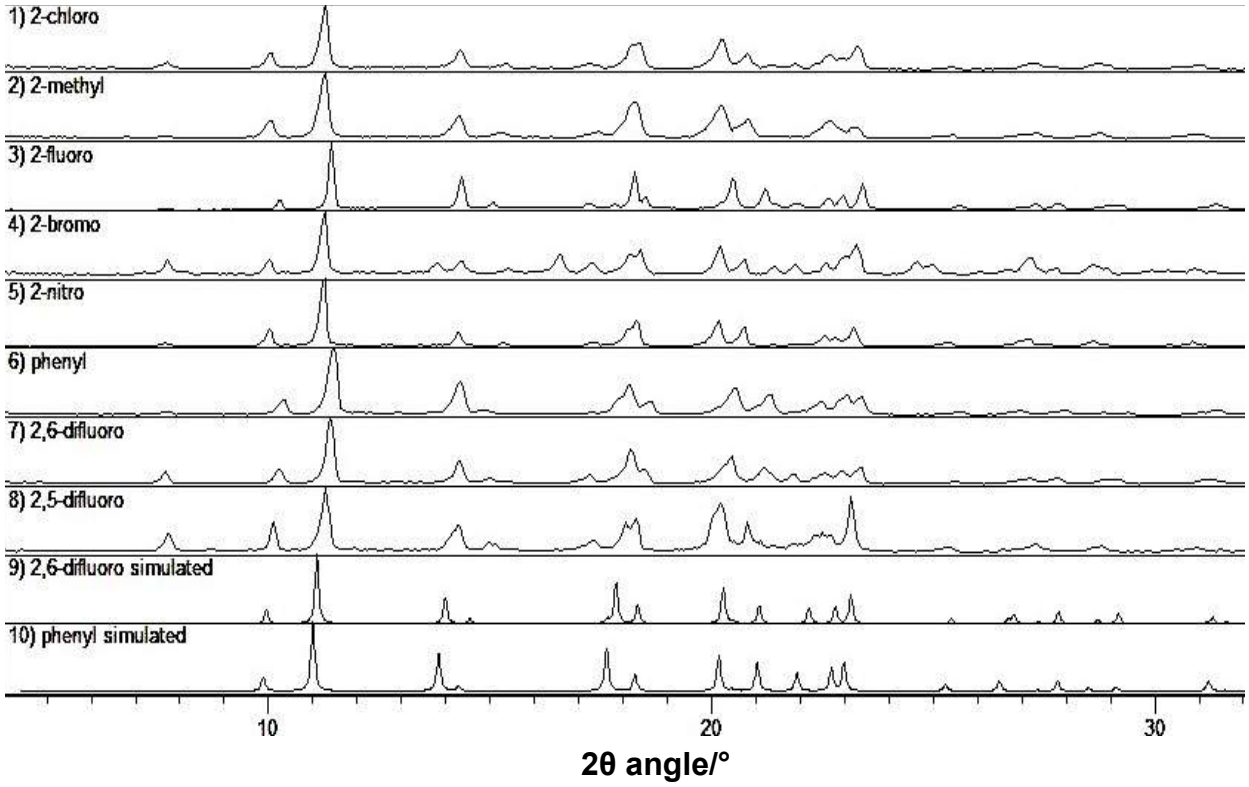

Fig. 6.6. Powder X-ray diffraction patterns of the bulk compounds **1-8** as synthesized mechanochemically. Comparison with the simulated patterns (bottom two patterns) from single crystal X-ray diffraction data of compounds **6** and **7** show that they are all isostructural.

Upon close inspection of the crystal structures of **1-8**, it was revealed that all of the functional group substituents in the 2-position of the aryl ring resided in a small spatial cleft within the molecule, just above the Y-shaped guanidine moiety (Fig. 6.7a). This cleft is surrounded, and possibly protected, by the exterior shell of hydrophobic groups, comprised of the two cyclohexyl and one phenyl rings. Twisting of the C1-S single bond orients the aryl

ring such that the functional group in the 2-position faces into this cleft, which isolates it and possibly prevents it from participating in intermolecular interactions with neighbouring molecules.

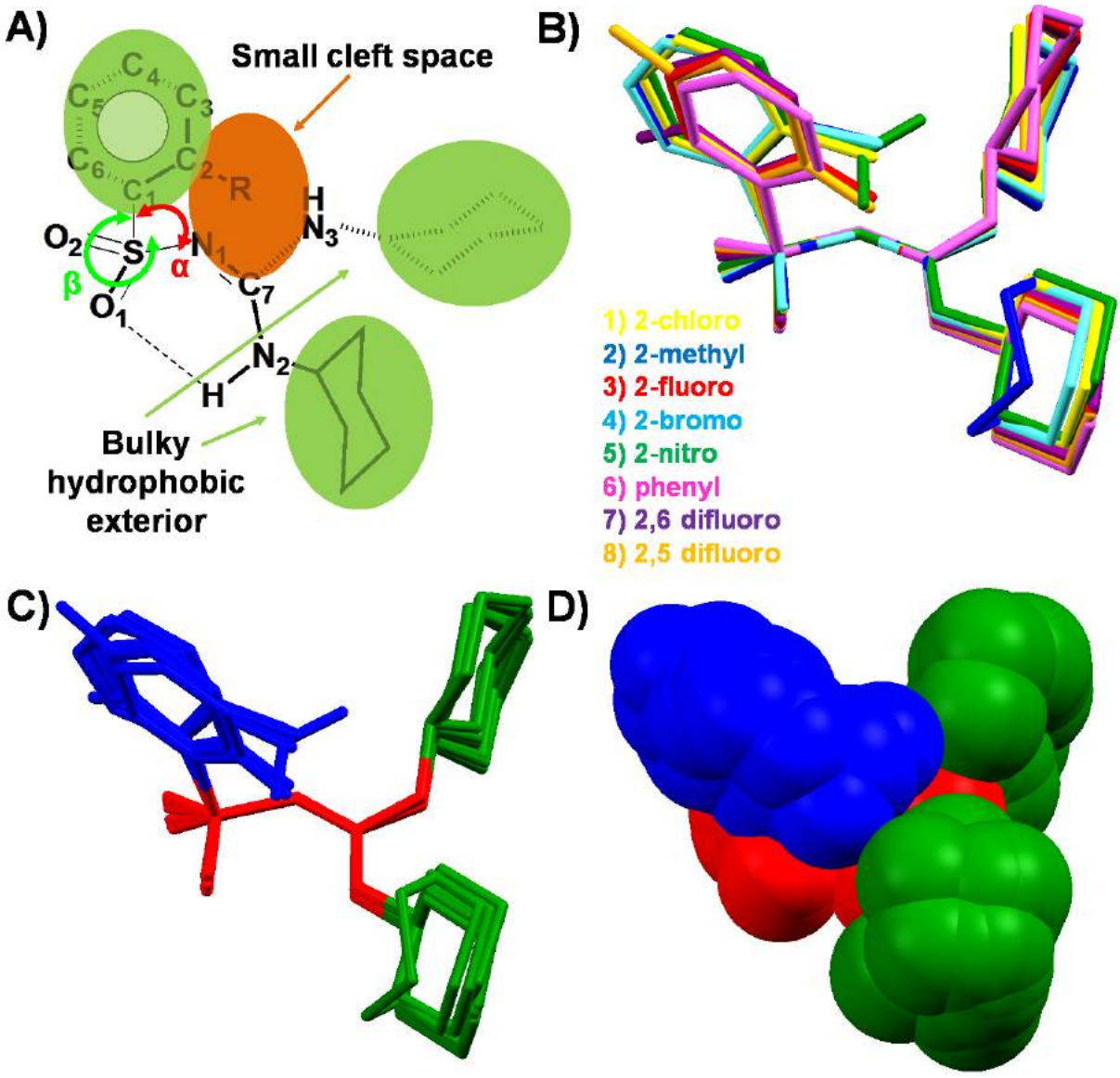

Fig. 6.7. (a) Molecular diagram depicting the small cleft space within the arylsulfonylguanidine that allows for the *ortho*-substituent (R) to reside, and illustrating molecular parameters α and β. The structure is surrounded and protected by sterically demanding cyclohexyl and phenyl rings. (b) Overlay of molecules in crystal structures of compounds **1-8**. Image is created by superimposing the S-N1=C7 atoms. Various compounds are color-coded accordingly. Hydrogen atoms are omitted for clarity. (c) Similar image to (b) but color-coded to show the bulky cyclohexyl group (green), the supramolecular hydrogen bonding unit (red) and the different substituted aromatic unit (blue). (d) Space-filling image of (c) depicting the volume accessible to a molecule crystallizing isostructurally to compounds **1-8**.

Superposition of the molecules in the crystal structures of all eight compounds show how they all adopt almost the same molecular conformation, with most of the atoms superimposed onto the same approximate space (Fig. 6.7b). Again, the 2-position functional groups are all tucked into the cleft of the molecule, with the exception of compounds **7** and **8**, whereby one of the fluorine atoms sticks outside of the molecule. In order to compare the conformational properties of molecules **1-8**, two parameters of the molecular geometry are defined. The first is the angle of incline between atoms C1-S-N1 (Table 6.2), defined as α, and the other one is the torsional dihedral angle between C2-C1-S-N1, defined as β. These parameters are illustrated on Fig. 6.7a. The range of α angles was found to be between 104.8(1)° and 107.5(4)°, smallest for **5** and largest for **4**. Similarly, the angle β was found to be smallest for **6** and largest for **8**, ranging from 54.1(3)° to 61.9(2)°. We believe that these two angles are important as they affect how the molecule orients and assembles in the solid state. As shown in Fig. 6.7c, again, the molecular structures of compounds **1-8** can be divided into three segments: the bulky cyclohexyl groups (green), the hydrogen-bonding sulfonylguanidine unit (red) and the substituted aryl system (blue). The space-filling representation of superimposed molecules of compounds **1-8** (Fig.6.7d) illustrates the spatial demand in the crystal structure which is shared between these compounds. The resulting image illustrates all of the space occupied by the combined van der Waals volumes of molecules of **1-8** located at a particular site in the crystallographic unit cell. Thus, this image can be considered to be a visualization of the "volumetric descriptor" proposed by Fábián *et al*.[18] Hence, it is plausible that other arylsulfonylguanidine compounds whose molecules can fit into this "shaped volume" should also be isostructural to **1-8**. Furthermore, the intermolecular hydrogen bond lengths for compounds **1-8**, in this case measured by the N3···O1 inter-atomic distances, are in the narrow range of 2.866(2) Å to 2.943(3) Å, the shortest being for **8** and the longest being for **5**. Such low degree of variability provides further proof of isostructurality between compounds **1-8**. From the superimposed structural models of molecules **1-8** in the solid state (Fig. 6.7c), we can also see that the rotational freedom of one of the cyclohexyl rings (**2**) does not seem to affect significantly the crystal packing of the compounds, further illustrating the robustness of their isostructurality.

Table 6.2. Values of angles α and β, and the intermolecular N···O hydrogen bond distances for compounds **1-13.**

Compound	Substituent	α (°)	β (°)	N···O distance (Å)
1	2-chloro	106.4(2)	60.8(5)	2.922(5)
2	2-methyl	105.9(6)	57.7(1)	2.891(1)
3	2-fluoro	105.9(1)	59.2(3)	2.883(3)
4	2-bromo	107.5(4)	58.8(7)	2.856(6)
5	2-nitro	104.8(1)	59.3(3)	2.943(3)
6	phenyl	105.5(1)	54.1(3)	2.887(3)
7	2,6-difluoro	104.96(8)	61.7(2)	2.871(2)
8	2,5-difluoro	105.94(9)	61.9(2)	2.866(2)
9	3,5-difluoro	103.5(2)	120.9(5)	2.982(3)
10	2,5-dimethoxy	103.28(9)	60.5(2)	3.120(2)
11	2,4-dimethoxy	106.89(8)	61.4(2)	3.144(2)
12	2-COOMe	107.3(1), 106.5(1)	128.2(2), 130.6(2)	2.848(2), 3.084(2)
13	Isopropyl	104.69(7), 105.83(9)	57.78(2), 65.5(0.2)	2.975(4), 3.019(2)

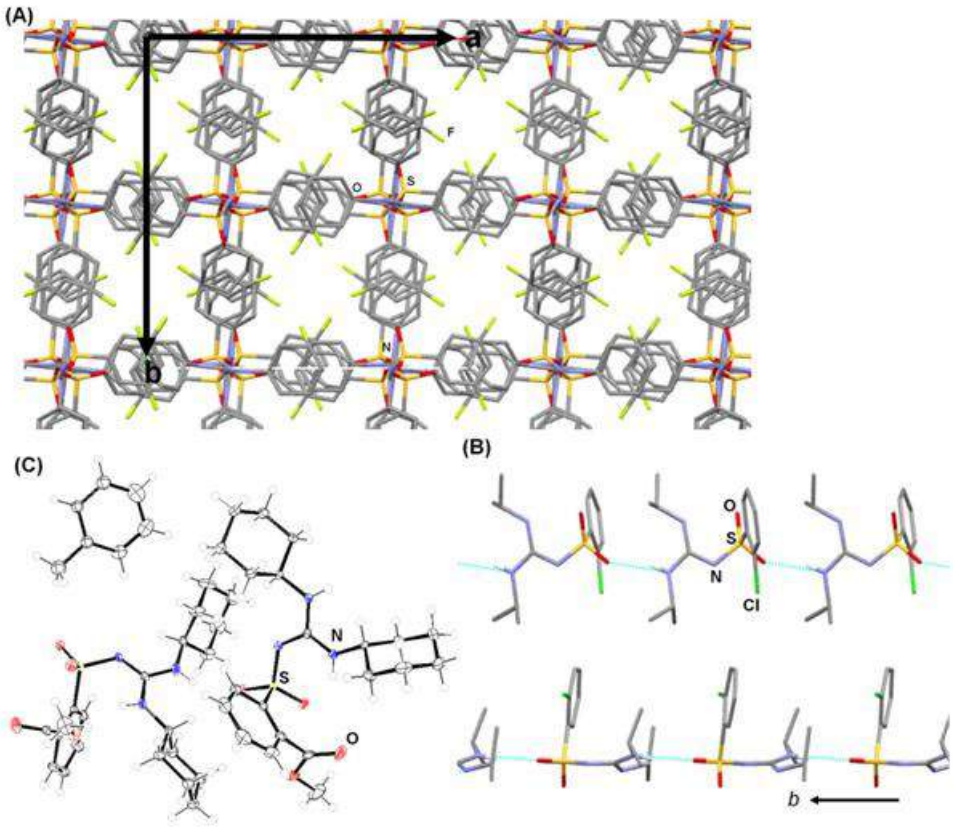

Fig. 6.8. (a) Fragment of the crystal structure of **9**, as viewed down the crystallographic *c*-axis, clearly illustrating four-fold symmetry. (b) The asymmetric unit of **12**, depicting two molecules of **12** and a molecule of toluene, $(\mathbf{12})_2$.(toluene), drawn using ORTEP-3 with thermal ellipsoids shown at 50% probability level, as determined by SCXRD. (c) Fragment of the crystal structure of **13**, depicting two anti-parallel one-dimensional chains propagating along the crystallographic *b*-axis.

On the other hand, compounds **9-13** did not crystallize in the same manner as the previous eight compounds. Compounds **9**, **10**, **11** and **13** were all synthesized mechanochemically[15] while compound **12** was synthesized by refluxing in toluene. Experimental details can be found in *Chapter 8, Section 8.5*. It was surprising that compound **9** (3,5-difluoro substituent) did not crystallize in the same manner as **7** and **8**, since the differences between compounds **7-9** are in the positioning of the fluoro substituents on the aryl ring. Instead, compound **9** assembled in the $I4_1/a$ tetragonal space group exhibiting a four-fold helical axis (Fig. 6.8a). Unlike compounds **1-8**, molecules of **9** are held together by non-bifurcated intermolecular S=O2···H-N2 hydrogen bonding interactions (Fig. 6.3). In addition, the β angle for **9** is 120.9(5)° which is significantly higher than seen among the isostructural series of compounds **1-8** (54.1(3)-61.9(2)°). This shows that subtle changes in the position of the functional group on the aryl ring, though small, can cause significant changes in the way these molecules assemble and pack. Attempts to obtain a potential polymorph of **9** that would be structurally similar to **6**, by seeding a hot saturated solution of **9** with small crystals of **6** were unsuccessful**.** Similarly, compounds **10-12** also did not crystallize in the same manner as **1-8**. Isostructurality was also not observed for **10** and **11**. This is probably because of the larger size and position of the methoxy groups on the 4- and 5-position of the aryl ring, which can significantly affect the molecular packing. Comparison of the N···O distances revealed that the intermolecular S=O···H-N hydrogen bonds are longer for **10** and **11** than for the other herein investigated compounds (Table 6.2), 3.120(2) Å and 3.144(2) Å for **10** and **11** respectively. Detailed X-ray crystallographic information can be found in *Appendix E*. The presence of methoxy substituents in **10** and **11** allowed for additional C-H···O hydrogen-bonding interactions between the methoxy oxygen atoms and neighbouring aryl and cyclohexyl groups. All these factors could have played a role in preventing **10** and **11** from being isostructural with **1-8**. For **12**, X-ray diffraction-quality single crystals were only obtained by using toluene as a solvent, and the resulting crystal structure of **12** was found to be a toluene solvate (Fig. 6.8b). However, desolvation of the crystals in vacuo gave crystalline powders, whose powder diffraction patterns that did not match those of **1-8**. In compound **13**, whereby the bulky cyclohexyl rings were replaced by smaller isopropyl groups, the molecules also did not crystallize to form a $P3_2$ helix, but adopted the monoclinic $P2_1/c$ space group instead. There are two molecules in the asymmetric unit of the crystal structure of **13**. These two molecules form hydrogen bonds with the neighbouring molecules, forming anti-parallel linear chains (Fig. 6.8c), with N···O distances of 2.975(4) Å and 3.019(2) Å. This further supports the view that the bulky

cyclohexyl groups may be "protecting" and "isolating" the hydrogen-bonded self-assembly motifs, and thus could be vital for maintaining the isostructurality in compounds **1-8**.

6.5 Multicomponent solid solution crystals

Discovery of an unprecedented set of eight isostructural single-component crystals opens up a very attractive opportunity to synthesize other isostructural materials containing the molecules of compounds **1-8**. Extrapolating the idea of robust isostructural compounds further, we wanted to investigate the possibility of constructing multi-component crystals by combining several of these bis(cyclohexyl)-arylsulfonylguanidines into a single, crystalline material. This would create a multi-component solid that would exhibit the same structural motifs as crystals of individual components, but comprising a random distribution of molecules *i.e.* a solid solution.[18] This would enable a creation of complex new solids by using isostructurality as a design element.

With that in mind, we took various bis(cyclohexyl)-arylsulfonylguanidines and tried to obtain multi-component solid solutions of their mixtures. This was done by first obtaining pure individual compounds and then dissolving them together in equimolar amounts, in acetone. Slow evaporation of such solutions, either on the benchtop or in a vacuum dessicator, yielded small single crystals, which were analyzed by SCXRD and, upon dissolution, high resolution mass spectroscopy (HRMS). Experimental details can be found in *Chapter 8, Section 8.5*. Compounds **2**, **4**, **5** and **6** were chosen for such studies, as they have significantly different functional groups, in terms of size and polarity, and thus would form isostructural solid solutions in which individual components would be distinguished by diffraction methods. Compounds **7** and **8** were also utilized due to having an additional fluorine functional group on the aryl ring, expected to aid in the identification and the refinement of crystal structures.

First, we obtained single crystals of two three-component solid solutions, namely **3CC-1** and **3CC-2**, containing compounds **2**, **4**, **8,** and compounds **2**, **6**, **8** respectively (Fig. 6.9). Subsequently, we also obtained single crystals of two four-component solid solutions, namely **4CC-1** and **4CC-2**, comprising compounds **4**, **5**, **7**, **8,** and **2**, **4**, **5**, **8** respectively. Analysis of the SCXRD data revealed that the various functional groups on the aryl ring were indeed all disordered over the same position for all four solid solutions. The unit cell

parameters for the solid solutions were also found to be almost identical to those of the corresponding single-component structures (Table 6.3). The refinement of the disorder for all the structures was not trivial and required several steps. Structure solution and refinement was performed using a combination of WinGX and X-Seed set of programs, utilizing SHELXS and SHELXL executables.[20] The structures of all the solid solutions are substitutionally disordered and are not related by symmetry or stoichiometry. Substitutional disorder of the *ortho*-position functional groups and the aryl ring can be seen during refinement from relative positions of the electron density maxima (the Q-peaks). As the rest of the molecule *i.e.* the sulfonyl-guanidine unit and the cyclohexyl rings, were not disordered, the focus was placed on refining those parts first. Once the relative positions and identities of the atoms comprised within the sulfonylguanidine and cyclohexyl moieties have been resolved through least-squares refinement, all those atoms were made isotropic before embarking on the refinement of the structural disorder of the aryl ring. In addition, the aromatic substituents on molecules of compounds **4**, **7**, and **8**, containing the bromine atom and fluorine atoms in the 2-, 5- and 6- positions of the aryl ring, respectively, could be easily identified during the refinement process due to the high electron density around those positions. Next, using the PART instruction in SHELXL, the disordered carbon atoms of the aryl ring were split into two groups *i.e.* PART1 and PART2, based on the electron density maxima around that region. Next, the second free variable of the refinement process was set at a reasonable arbitrary value of 0.6 (describing a 60–40% disorder) for all the carbon atoms. Subsequently, the site occupancy factor (*sof*) was assigned to refer to the second free variable of the refinement. For example, the value of the *sof* instruction was changed from 11.0000 to 21.0000 for all the atoms in PART1 and to −21.0000 for PART2. This means that the occupancy factors of atoms in the two refinement parts are being refined in a linked way, with their total sum being 1. Once the disorder around the aryl rings has been successfully resolved in this way, the disorder around the corresponding *ortho*-position atoms can then be fixed. Similar to the refinement of the aryl rings, each *ortho*-substituents in the three-component and four-component solid solution structures was assigned its own separate PART command, up to PART6. For example, for a four-component crystal, this means that there was a total of six structural PARTs that were being simultaneously refined *i.e.* four PARTs for each of the *ortho*-substituents of the molecular components and two PARTs for the disordered aryl rings. Similarly, the corresponding *sof* values were different for each individual PART unit. For solid solutions containing compounds **2** (2-methyl) and **6** (phenyl), the refinement was challenging as the electron density of the carbon and hydrogen atoms can

be overshadowed by that of the bromine atom in compound **4**. For structures containing compound **5** (2-nitro), it can be slightly easier to indentify the nitro group oxygen atoms during the refinement, as the $–NO_2$ group can be seen as a Y-shaped set of electron density peaks. Forced insertion and control over atomic coordinates for substituents in the *ortho*-position can also help during refinement. Once all the *ortho*-substituents have been identified and reasonably structurally refined, through several least squares refinement cycles, the PART instructions corresponding to the aryl rings and the *ortho*-groups can be combined, based on the known α- and β- angles for the individual molecular component structures. Lastly, all atoms were made anisotropic and the structure parameters refined again until no more major issues arose, such as atoms "flying apart" or not being in chemically sensible positions.

Table 6.3. Crystallographic data for the multi-component solid solution crystals.

Sample	**3CC-I**	**3CC-II**	**4CC-I**	**4CC-II**
Formula	$C_{19.52}H_{28.93}Br_{0.33}F_{0.62}N_3O_2S$	$C_{19.69}H_{29.32}F0_{.71}N_3O_2S$	$C_{18.97}H_{27.48}Br_{0.32}FN_{3.18}O_{2.36}S$	$C_{19.70}H_{29.27}Br_{0.17}F_{0.53}N_{3.15}O_{2.30}S$
Mr	407.94	385.57	414.17	402.79
Space group	$P3_2$	$P3_1$	$P3_2$	$P3_2$
Z	3	3	3	3
Wavelength (Å)	1.34139 (GaKα)	1.34139 (GaKα)	1.34139 (GaKα)	1.34139 (GaKα)
T (K)	100	100	100	100
***a* (Å)**	10.0280(3)	9.9168(4)	9.9816(3)	10.0294(3)
***b*(Å)**	10.0280(3)	9.9168(4)	9.9816(3)	10.0294(3)
***c* (Å)**	17.3301(5)	17.5313(7)	17.4468(6)	17.3525(5)
α	90	90	90	90
β	90	90	90	90
γ	120	120	120	120
***V* (Å^3)**	1509.25(10)	1493.10(13)	1505.38(10)	1511.62(10)
d_{calc} **gcm^{-3}**	1.346	1.286	1.371	1.327
***μ*(mm^{-1})**	1.579	1.084	1.597	1.339
***F*(000)**	649.0	620.0	656.0	644.0
Measured	56176	60767	54224	48785
Unique	4619	4577	4579	4585
Obs. [I > 2 σ (I)]	4575	4496	4574	4571
Parameters	262	271	310	296
Restraints	513	522	1034	1000
R_1 **[I > 2 σ (I)]**	0.0456	0.0441	0.0429	0.0409
wR_2 **[I > 2 σ (I)]**	0.1152	0.1128	0.1026	0.1033
R_1 **(all data)**	0.0460	0.0448	0.0429	0.0410
wR_2 **(all data)**	0.1155	0.1138	0.1026	0.1035
GoF	1.047	1.052	1.132	1.090

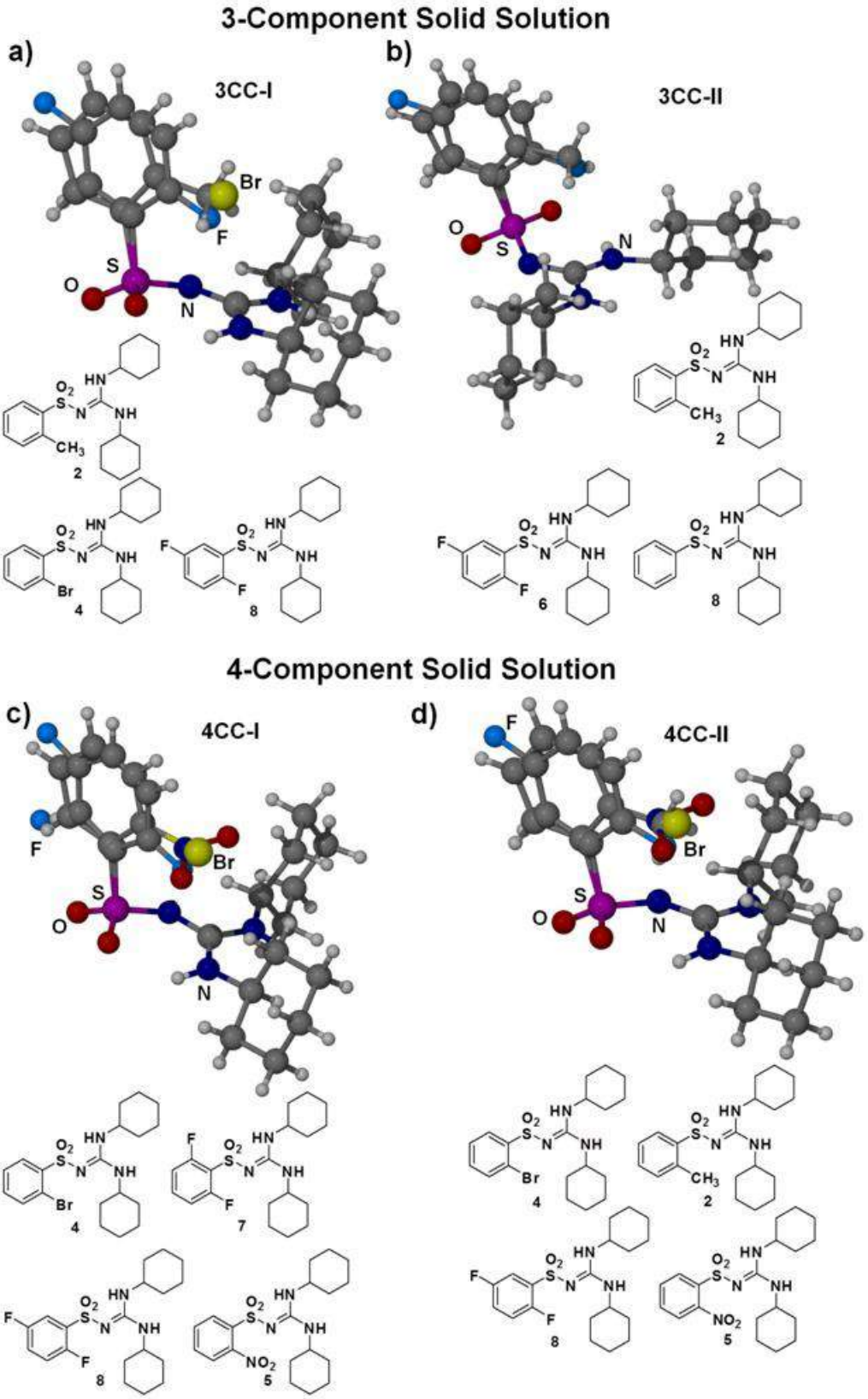

Fig. 6.9. Fragment of the crystal structures, as determined from single crystal X-ray diffraction, of the three-component solid solutions: (a) **3CC-I** comprising compounds **2**, **4**, **8** and (b) **3CC-II** comprising compounds **2**, **6**, **8**, and four-component solid solutions, namely (c) **4CC-I** comprising compounds **4**, **5**, **7**, **8** and (d) **4CC-II** comprising compounds **2**, **4**, **5**, **8.**

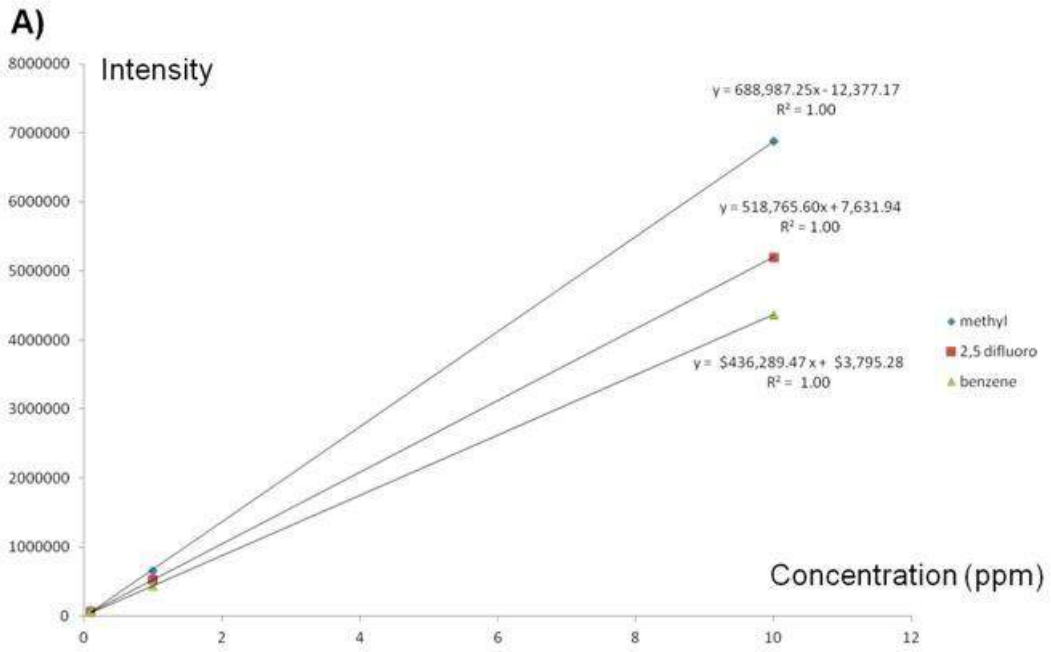

3CC-I	Benzene	2-Methyl	2,5-difluoro
Crystal Data s.o.f	0.299	0.394	0.356
Mass Spec Data	0.313925	0.309957	0.376118

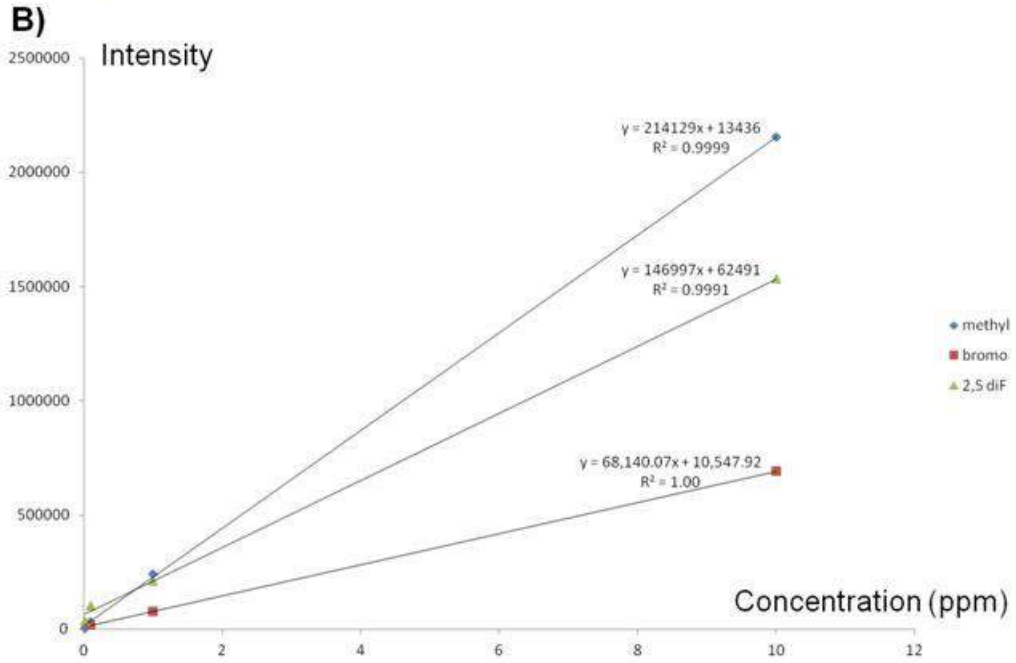

3CC-II	2-Bromo	2-Methyl	2,5-difluoro
Crystal Data s.o.f	0.322	0.381	0.311
Mass Spec Data	0.428541	0.277808	0.293651

Fig. 6.10. High resolution mass spectroscopy calibration curves and data obtained for each of the individual components of the solid solution crystal (a) **3CC-I** and (b) **3CC-II.**

A)

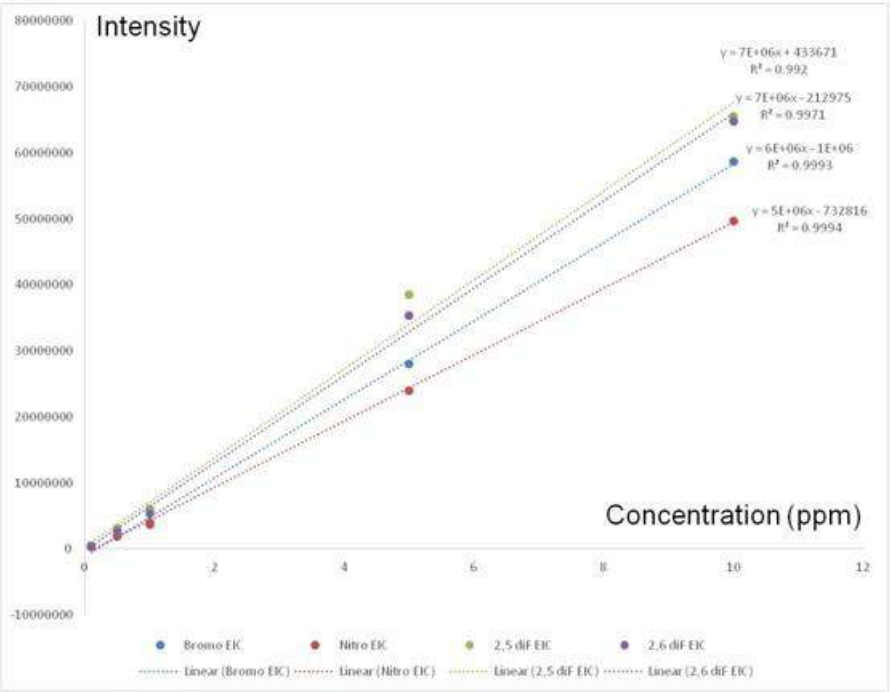

4CC-I	2-Bromo	2-nitro	2,5-difluoro	2,6-difluoro
Crystal Data s.o.f	0.316	0.178	0.256	0.245
Mass Spec Data	0.281931	0.072875	0.336642	0.308551

B)

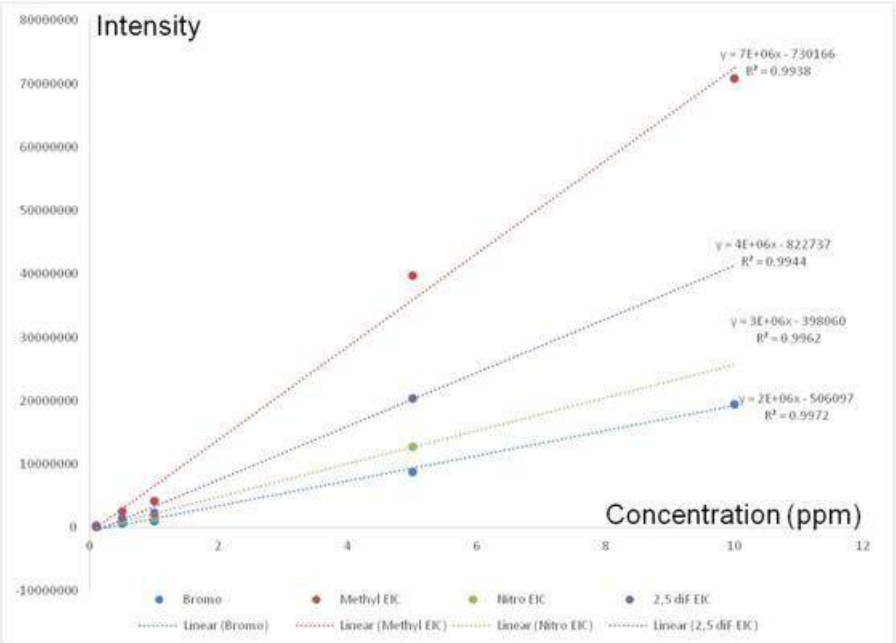

4CC-II	2-Bromo	2-Methyl	2,5-difluoro	2-nitro
Crystal Data s.o.f	0.170	0.457	0.265	0.150
Mass Spec Data	0.288141	0.334421	0.312994	0.06444

Fig. 6.11. High resolution mass spectroscopy calibration curves and data obtained for each of the individual components of the solid solution crystal (a) **4CC-I** and (b) **4CC-II.**

Analysis of the SCXRD structures of **3CC-I**, **3CC-II**, **4CC-I** and **4CC-II** revealed that these solid solutions, as anticipated, are mutually isostructural and that they consisted of molecules assembles into the same one-dimensional hydrogen-bonded helical motifs seen in compound **1**, through the same bifurcated hydrogen-bonding interactions. Except for **3CC-II**, the solid solutions all crystallized in the same helical chiral $P3_2$ space group. The solid solution **3CC-II** crystallized in the opposite chirality $P3_1$ space group. Similar to their individual components, the unit cell parameters of the solid solutions do not deviate much from each other, with unit cell lengths *a* and *c* ranging from 9.9168(3) Å to 10.0294(3) Å and from 17.3301(5) Å to 17.5313(7) Å respectively. The unit cell volumes also do not differ much, ranging from 1493.1(1) $Å^3$ to 1511.6(1) $Å^3$. In comparison to the individual components, the unit cell parameters of the solid solutions are between those of their respective individual components. For example, for **3CC-II** (compounds **2**, **6**, **8**) the unit cell edge *a* is 9.9168(4) Å, which is smaller than **2** (9.975(2) Å) but larger than **6** (9.746(2) Å). Similarly, the unit cell volume for **3CC-II** is 1493.1(1) $Å^3$, which is smaller than **8** (1508.4(2) $Å^3$) but larger than **6** (1468.7(5) $Å^3$).

Furthermore, as the sulfonylguanidine unit atoms, namely S, O1, O2, N1, N2, N3 and C7 are not disordered in the structures of the various solid solutions, it is possible to compare the hydrogen-bonding distances between the molecules to those in the respective individual component crystals. Refer to *Appendix E* for crystallographic details. The intermolecular hydrogen bond lengths based on the N3···O1 distance for **3CC-I**, **3CC-II**, **4CC-I** and **4CC-II** are 2.877(2) Å, 2.880(2) Å, 2.890(3) Å and 2.896(3) Å respectively. These values are very close to one another and also very similar to their respective individual components (Table 6.1).

In addition, for all solid solution crystals (**3CC-I**, **3CC-II**, **4CC-I** and **4CC-II**), high resolution mass spectroscopy (HRMS) was also performed, by dissolving the exact same single crystals that were used for XRD experiments. The relative stoichiometric ratio of the individual components for each solid solution were determined after measuring or obtaining a calibration curve of their respective solution mixtures at different concentrations, namely 10ppm, 0.5ppm, 1ppm, 0.5ppm and 0.1ppm. The resulting calibration curves (Fig. 6.10 and Fig. 6.11) were mostly linear. Based on the HRMS data, it was revealed that the relative ratio of the individual components were reasonably close to the refined *sof* values obtained by crystal structure refinement (Fig. 6.10 and 6.11). For example, for **3CC-II**, the *sof* values for the individual components are very similar to the values determined by HRMS. Specifically,

the values for the 2-bromo component *i.e.* compound **4** (*sof* = 0.299 *versus* HRMS = 0.314), the values for the 2-methyl component *i.e.* compound **2** (*sof* = 0.381 *versus* HRMS = 0.278) and the values for the 2,5-difluoro component *i.e.* compound **8** (*sof* = 0.311 *versus* HRMS = 0.293), are all reasonably close to one another. These results show that HRMS data obtained corroborates with the XRD data for the solid solution crystals.

6.6 Conclusion

We believe this is an exciting report on a family of eight conformationally flexible single-component bis(cyclohexyl)-arylsulfonylguanidine compounds, containing various functional groups, that exhibit isostructurality and crystallize in a chiral $P3_2$ space group. This was achieved through a combination of a previous serendipitous discovery of a new coupling reaction and subsequent structural exploration of a library of target molecules. Isostructurality of these compounds appears to be due to the strong hydrogen-bonding sulfonylguanidine synthons, as well as enclosure of the variable functional groups on the aryl ring into an inner spatial cleft of the molecule. The observed isostructurality in compounds **1-8** appears to be robust and does not seem to be limited by the common exchange rules of related atoms and functional groups seen in other types of molecules.[9-11,14] In addition, by using the robust isostructurality as a design element, we created four complex and different multi-component crystalline solid solutions that are made of the same structural motif as their individual components. The ability to form these isostructural multi-component solid solutions, comprising of these arylsulfonylguanidines, is novel and remarkable. We sincerely hope that this study might inspire others to take this idea further, and invent other sets of solid solutions and crystalline materials, that perhaps can be used for information storage in the future.

6.7 References

1 a) G. R. Desiraju, *Angew. Chem. Int. Ed*., **2007**, *46*, 8342; b) D. Braga, *Chem. Commun.*, **2003**, 2751; c) T. Friščić, W. Jones, *Faraday Discuss*., **2007**, *136*, 167; d) M. J. Zaworotko*, Cryst. Growth Des*., **2007**, *7*, 4; e) M. D. Ward, *Chem. Commun*., **2005**, 5838; f) D. Braga, *Chem. Commun.*, **2003**, 2751; g) C. B. Aakeröy, A. M. Beatty, B. A. Helfrich, *J. Am. Chem. Soc.*, **2002**, *124*, 14425; h) M. C. Etter, *J. Phys. Chem.*, **1991**, *95*, 4601.

2 a) J. Bernstein, R. J. Davey, J.-O. Henck, *Angew. Chem. Int. Ed.*, **1999**, *38*, 3440; b) J. D. Dunitz, J. Bernstein, *Acc. Chem. Res.*, **1995**, *28*, 193; c) A. Nangia, *Acc. Chem. Res.*, **2008**, *41*, 595; d) J. Bernstein, Nature Mater., 2005, 4, 427; e) D. Braga, L. Brammer, N. R. Champness, *CrystEngComm*, **2005**, *7*, 1.

3 a) S. L. Price, *Adv. Drug Delivery Rev*., **2004**, *56*, 301; b) R. J. Davey, *Chem. Commun.*, **2003**, 1463; c) S. R. Byrn, R. R. Pfeiffer, G. Stephenson, D. J. W. Grant, W. B. Gleason, *Chem. Mater.*, **1994**, *66*, 1148; d) R. W. Lancaster, P. G. Karamertzanis, A. T., Hulme, D. A. Tocher, T. C. Lewis, S. L. Price, *J. Pharm. Sci.*, **2007**, *96*, 3419.

4 a) L. Fábián A. Kálmán, *Acta Crystallogr. Sect. B: Struct. Sci.*, **2004**, *60*, 547; b) L. Fábián, G. Argay, A. Kálmán, M. Báthori, *Acta Crystallogr., Sect. B: Struct. Sci*., **2002**, *58*, 710; c) S. J. Coles, T. L. Threlfall, G. J. Tizzard, *Cryst. Growth Des*., **2014**, *14*, 1623.

5 a) S. Ebenezer, P. T. Muthiah, R. J. Butcher, *Cryst. Growth Des.*, **2011**, *11*, 3579; b) S. L. Childs, P. A. Wood, N. Rodríguez-Hornedo, L. S. Reddy, K. I. Hardcastle, *Cryst. Growth Des.*, **2009**, *9*, 1869; c) D. E. Braun, T. Gelbrich, V. Kahlenberg, R. Tessadri, J. Wieser and U. J. Griesser, *Cryst. Growth Des.*, **2009**, *9*, 1054; d) L. Fábián, A. Kálmán, G. Argay, G. Bernáth, Z. C. Gyarmati, *Cryst. Growth Des.*, **2005**, *5*, 773; e) J. B. Nanubolu, B. Sridhar, K. Ravikumar, S. Cherukuvada, *CrystEngComm*, **2013**, *15*, 4321; f) D. Cinčić, T. Friščić, W. Jones, *Chem. Eur. J*., **2008**, *14*, 747; g) P. A. Wood, M. A. Oliveira, A. Zin, M. B. Hickey, *CrystEngComm*, **2012**, *14*, 2413; h) G. Bolla, S. Mittapalli, A. Nangia, *IUCrJ*, **2015**, *2*, 389.

6 a) F. Topić, K. Rissanen, *J. Am. Chem. Soc*., **2016**, *138*, 6610; b) S. Bhattacharya, B. K. Saha, *Cryst. Growth Des*., **2012**, *12*, 169; c) J. Galcera, T. Friščić, K. E. Hejczyk, L. Fábián, S. M. Clarke, G. M. Day, E. Molins, W. Jones, *CrystEngComm*, **2012**, *14*, 7898; d) L. R. Nassimbeni, H. Sua, E. Weber, *New J. Chem*., **2008**, *32*, 1702; e) M. Rubčić, D. Milić, G. Pavlović and M. Cindrić, *Cryst. Growth Des*., **2011**, *11*, 5227; f) C.-K. Lam, T. C. W. Mak, *Cryst. Eng*., **2000**, *3*, 33.

7 a) I. Csöregh, S. Hirano, S. Toyota, P. Bombicz, F. Toda, *CrystEngComm*, **2004**, *6*, 60; b) S. Bhattacharya, J. Sameena, B. K. Saha, *Cryst. Growth Des.*, **2011**, *11*, 905; c) S. Bhattacharya, B. K. Saha, *Cryst. Growth Des.*, **2013**, *13*, 606; d) J. Galcera, T. Friščić, E. Molins, W. Jones, *CrystEngComm*, **2013**, *15*, 1332; e) R. Thakuria, A. Nangia, *Cryst. Growth Des*., **2013**, *13*, 3672; f) B. Stöger, P. Kautny, D. Lumpi, E. Zobetz, J. Fröhlich, *Acta*

Crystallogr. Sect. B: Struct. Sci., **2012**, *68*, 667; g) L. Rajput, K. Biradha, *New J. Chem*., **2010**, *34*, 2415; h) A. J. C. Cabeza, G. M. Day, W. D. S. Motherwell, W. Jones, *J. Am. Chem. Soc*., **2006**, *128*, 14466; i) T. Hosokawa, S. Datta, A. R. Sheth, N. R. Brooks, V. G. Young, Jr., D. J. W. Grant, *Cryst. Growth Des*., **2004**, *4*, 1195.

8 a) A. I. Kitaigorodskii, *Acta Cryst.*, **1965**, *18*, 585; b) A. I. Kitaigorodskii, *Organic Chemical Crystallography*, Consultant's Bureau, New York, **1961**.

9 a) N. N. L. Madhavi, A. K. Katz, H. L. Carrell, A. Nangia, G. R. Desiraju, *Chem. Commun*., **1997**, 1953; b) R. Banerjee, R. Mondal, J. A. K. Howard, G. R. Desiraju, *Cryst. Growth Des.*, **2006**, *6*, 999; c) M. Polito, E. D'Oria, L. Maini, P. G. Karamertzanis, F. Grepioni, D. Braga, S. L. Price, *CrystEngComm*, **2008**, *10*, 1848; d) J. V. de Streek and S. Motherwell, *J. Appl. Crystallogr.*, **2005**, *38*, 694; e) N. K. Nath, A. Nangia, *Cryst. Growth Des.*, **2012**, *12*, 5411.

10 a) D. Cinčić, T. Friščić, W. Jones, *Chem. Mater*., **2008**, *20*, 6623; b) A. Singh, A. Ramanan, D. Bandyopadhyay, *Cryst. Growth Des.*, **2011**, *11*, 2743; c) A. Dey, G. R. Desiraju, *CrystEngComm*, **2004**, *6*, 642; d) S. K. Chandran, R. Thakuria, A. Nangia, *CrystEngComm*, **2008**, *10*, 1891; e) R. K. R. Jetti, P. K. Thallapally, F. Xue, T. C. W. Mak, A. Nangia, *Tetrahedron*, **2000**, *56*, 6707; f) B. K. Saha, A. Nangia, *Heteroatom Chem.*, **2007**, *18*, 185.

11 a) A. Kálmán, L. Fábián, G. Argay*, Chem. Commun*., **2000**, 2255; b) T. Smolka, R. Boese, R. Sustmann, *Struct. Chem*., **1999**, *10*, 429; c) N. J. Babu, A. Nangia, *Cryst. Growth Des.*, **2006**, *6*, 1753; d) D. Cinčić, T. Friščić, W. Jones, *New J. Chem.*, **2008**, *32*, 1776; e) A. Nangia, *New J. Chem*., **2000**, *24*, 1049; f) S. Tothadi, S. Joseph, G. R. Desiraju, *Cryst. Growth Des.*, **2013**, *13*, 3242; g) D. Cinčić, T. Friščić, W. Jones, *Chem. Mater.*, **2008**, *20*, 6623.

12 a) C. M. Reddy, M. T. Kirchner, R. C. Gundakaram, K. A. Padmanabhan, G. R. Desiraju, *Chem. Eur. J.*, **2006**, *12*, 2222; b) T. Friščić, A. V. Trask, W. D. S. Motherwell, W. Jones, *Cryst. Growth Des.*, **2008**, *8*, 1605; c) B. R. Bhogala, S. Basavoju, A. Nangia, *Cryst. Growth. Des.*, **2005**, *5*, 1683; d) K. B. Landenberger, O. Bolton, A. J. Matzger, *Angew. Chem. Int. Ed.*, **2013**, *52*, 6468.

13 a) B. K. Saha, A. Nangia, *Heteroat. Chem*., **2007**, *18*, 185; b) A. Kálmán, L. Fábián, *Acta Crystallogr. Sect. B: Struct. Sci.*, **2007**, *63*, 411.

14 a) R. Thakuria, N. K. Nath, S. Roy, A. Nangia, *CrystEngComm*, **2014**, *16*, 4681; b) W. Jones, S. Ramdas, C. R. Theocharis, J. M. Thomas, G. R. Desiraju, *J. Chem. Soc. Chem. Commun.*, **1983**, 1443; c) A. Dey and G. R. Desiraju, *CrystEngComm*, **2004**, *6*, 642; d) N. K. Nath, A. Nangia, *Cryst. Growth Des.*, **2012**, *12*, 5411; e) R. G. Gonnade, M. M. Bhadbhade, M. S. Shashidhar, CrystEngComm, 2010, 12, 478; f) M. R. Caira, *Mol. Pharmaceutics*, **2007**, *4*, 310; g) T. Gelbrich, T. L. Threlfall, M. B. Hursthouse, *Acta Crystallogr. Sect. C: Cryst. Struct. Commun.*, **2012**, *68*, 6421; h) T. Gelbrich, D. S. Hughes, M. B. HursthouseT. L. Threlfall, *CrystEngComm*, **2008**, *10*, 1328; i) T. P. Mohan, U. Gangwar, R. Sankollid, D. Chopra, *CrystEngComm*, **2013**, *15*, 4549; j) D. Chopra, T. N. Guru Row, *CrystEngComm*, **2008**, *10*, 54.

15 D. Tan, C. Mottillo, A. D. Katsenis, V. Štrukil, T. Friščić, *Angew. Chem. Int. Ed*., **2014**, *53*, 9321.

16 a) T. Friščić, A. J. Lough, G. Ferguson, B. Kaitner, *Acta Cryst. C58*, **2002**, m313; b) P. S. M. Cheung, L. A. Cuccia, *Chem. Commun.*, **2009**, 1337; c) P. S. M. Cheung, J. Gagnon, J. Surprenant, Y. Tao, H. Xu, L. A. Cuccia, *Chem. Commun.*, **2008**, 987; d) S. Azeroual, J. Surprenant, T. D. Lazzara, M. Kocun, Y. Tao, L. A. Cuccia, J.-M. Lehn, *Chem. Commun.*, **2012**, *48*, 2292.

17 a) T. Friščić, W. Jones, *Cryst. Growth Des.*, **2009**, *9* ,1621; b) G. A Bowmaker, *Chem. Commun.*, **2013**, *49*, 334.

18 L. Fábián, A. Kálmán, *Acta Crystallogr. Sect. B: Struct. Sci.*, **1999**, *55*, 1099.

19 a) A. D. Burrows, *CrystEngComm*, **2011**, *13*, 3623; b) M. Dabros, P. R. Emry, V. R. Thalladi, *Angew. Chem.*, **2007**, *46*, 4132; c) M. L. Foo, S. Horike, T. Fukushima, Y. Hijikata, Y. Kubota, M. Takata, S. Kitagawa, *Dalton Trans.*, **2012**, *41*, 13791.

20 P. Mùller, R. Herbst-Irmer, A. L. Spek, T. R. Schneider, M. R. Sawaya, *Crystal Structure Refinement, A Crystallographer's Guide to SHELXL*, **2006**, Oxford Science Publications.

CHAPTER 7

EVOLUTION THROUGH DESIGN: A SERENDIPITOUS DISCOVERY, SYSTEMATIC INVESTIGATION AND DESIGN OF A NEW THERMOSALIENT CRYSTAL BASED ON ETTER-TYPE N,N'-BIS(ARYL)UREAS

"It is always fascinating to look at crystals under a microscope. You learn a lot from a microscope."– Prof. Michael D. Ward, McGill Chemical Society Seminar, 2016.

7.1 Introduction and connecting text.

The work presented in this chapter is a part of not yet published manuscript entitled "Evolution through design: a serendipitous discovery, systematic investigation and design of a new thermosalient crystal based on Etter-type *N*,*N*'-bis(aryl)ureas", discussing the discovery and development of a family of organic thermosalient crystals, through systematic positional functionalization of *N*,*N*'-bis(aryl)ureas. The draft manuscript was written by D. Tan with guidance and editing contributions from Prof. T. Friščić, and co-authored with Dr. J. G. Hernández, who contributed to the discussion and brainstorming process. The text has been formatted and re-written for inclusion in this Dissertation. All experimental results, including details of syntheses and instrumental characterization of the herein prepared compounds were performed by D. Tan. *Chapters 2* to *6* in this Dissertation have covered the discussion on how mechanochemistry had been used as a powerful tool for discovering new C-N coupling reactions to afford pharmaceutically-relevant products, as well as the formation of new isostructural compounds. In this chapter, we will focus on another small sub-discipline of mechanochemistry, in which thermal energy can be transformed into mechanical energy. In *Chapters 2* to *5*, X-ray diffraction (XRD) and crystallography have mostly been used as techniques to confirm the formation of mechanochemical coupling products. In particular, in *Chapter 4*, single crystal X-ray diffraction (SCXRD) was used in the identification of the ring-expanded benzo[1,2,4]thiadiazepine product between saccharin and DCC, rather than the saccharyl-guanidine adduct that was previously reported, almost 40 years ago. Similarly, in *Chapter 6*, XRD was central to the characterization and investigation of the solid-state assembly of eight isostructural arylsulfonyl-guanidine compounds. In this penultimate chapter of this Thesis, we will discuss the systematic investigation of a new family of crystals that show a propensity to undergo thermosalient behavior *i.e.* upon input of heat the crystals can "jump" or "move". In this case, SCXRD, differential scanning calorimetry (DSC) and hot-stage microscopy (HSM) were used as key techniques for the observation of the motion of the crystals, as well as for the characterization and understanding of the factors behind the "jumping" phenomenon.

The conversion of energy into motion or mechanical work is a common and naturally occurring process.[1a] Materials that can respond to external stimuli, such as heat, light, or changes in local magnetic or electric fields, by exhibiting changes to their appearance and properties, are of importance as sensors in natural and artificial systems. If such a reaction also involves a change in shape or size, these materials allow the conversion of external

stimuli into mechanical work, *e.g.* in the form of a photo-mechanical or a thermo-mechanical effect. Thus mechanically responsive materials have the potential to be used as components of a broad range of microscopic mechanical devices, such as medical biomimetic devices, electro- and thermo-mechanical actuators, photo- and heat-responsive sensors *etc*.[1b-e] Examples of such materials are elastic liquid-crystal gels and polymeric films that are capable of mechanical motion on the macroscopic scale.[2a-c] These materials are different from specially designed molecular mechanical systems, such as rotaxanes and catenanes,[2d-g] whereby mechanical actuation is constrained to the molecular-level motion. The mechanical response in crystalline materials, which are traditionally deemed as rigid bodies, are less intense and less observable than in the usually much softer, more flexible polymeric films and gels. In such crystalline materials, it is possible to imagine that small perturbations in the molecular conformation, as a result of external stimuli, can result in a buildup of localized stress within the crystal structure. Eventual sudden release of these localized stresses can be propagated throughout the bulk crystalline material, which can lead to breakage and/or motion of the material.

7.2 Thermosalient effect and previously reported thermosalient crystals

Recently, there has been a renaissance[3] of interest in thermal-, pressure- and photo-induced[4] mechanical behavior of crystalline materials, more specifically of molecular single crystals. The thermo-responsive phenomenon in a crystal appears[3b] to have been first described by Etter and coworkers in 1983,[5] as they observed tiny crystals of (phenylazophenyl)palladium hexafluoroacetylacetonate move upon heating. The term thermosalient effect appears to have been first coined by Gigg *et al.*,[6] to describe such thermally-induced jumping motion of crystals. Upon absorption of thermal energy, a thermosalient crystal undergoes a martensitic-type transition,[7] *i.e.* a first-order polymorphic transitions that happens *via* a homogenous structure deformation, without involving long-range rearrangement of atoms. Such transformations are often characterized by sharp and quick anisotropic changes in the crystallographic unit cell volume, leading to a macroscopic change in the bulk material which can manifest itself as a change in crystal appearance and/or as observable motion, such as flipping, twisting, bending, exploding and jumping of a single crystal.

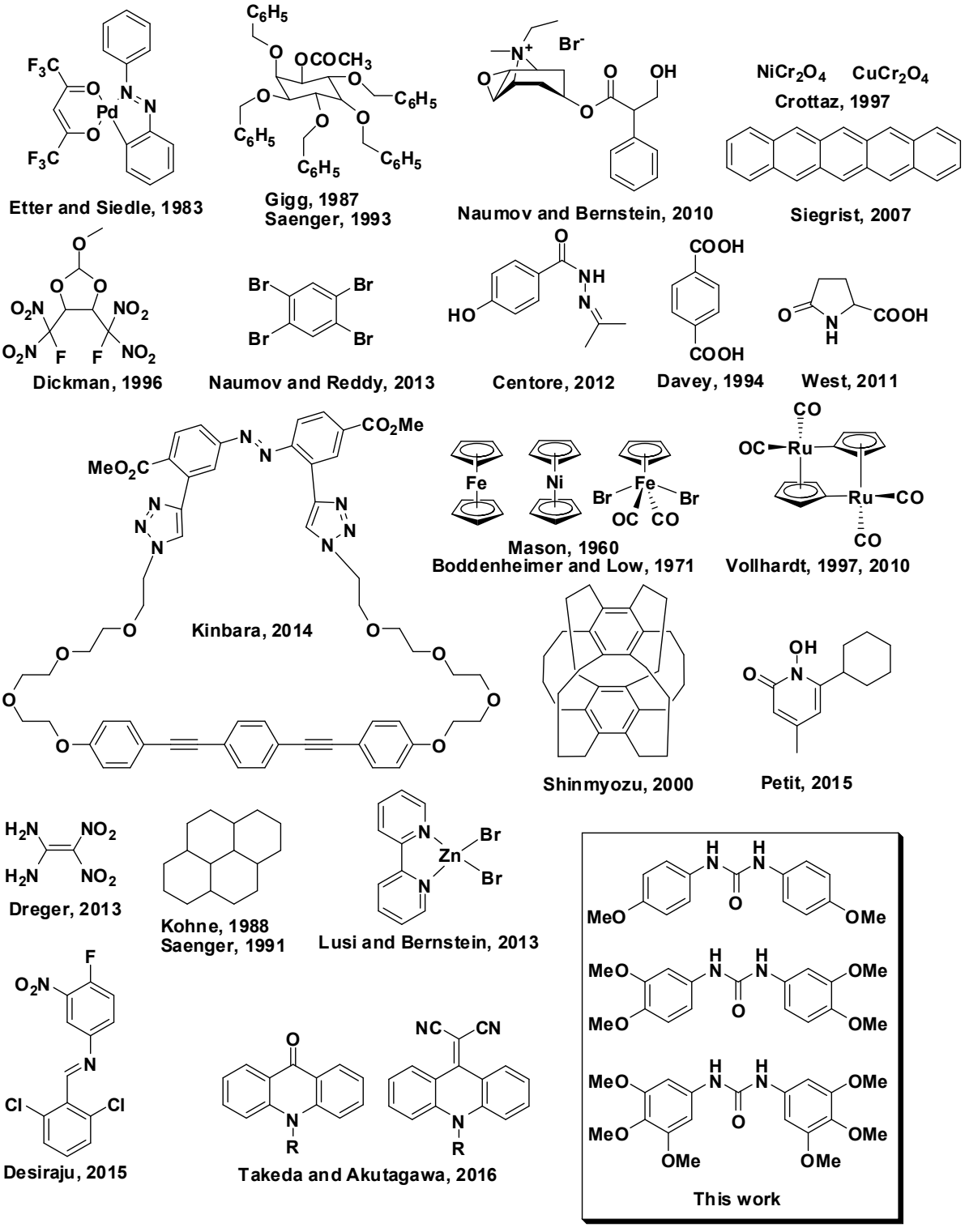

Fig. 7.1. An exhaustive schematic representation of so far reported thermosalient compounds, including the ones presented in this work.[3, 5, 6, 8]

Over the last 30 years, about 20 different thermosalient crystal systems have been discovered (Fig 7.1).[4m, 8] Each of these systems is a chemically highly unique case, as none of

them appear to be mutually related in terms of chemical composition, crystal structure or type of dominant intermolecular interactions in the solid state. With that in mind, Naumov and coworkers have elegantly pointed out the challenges not only in design but also in discovering new thermosalient compounds.[3] The same group has also performed pioneering, detailed studies of the mechanism of the thermosalient effect in a range of compounds, including pharmaceutically-relevant compounds oxitropium bromide[8a] and L-pyroglutamic acid,[8b] by utilizing high-speed camera recording to capture, observe and characterize structure-kinematic[7c] aspects of the thermosalient behavior. It was also claimed[8c] that thermosalient motion is only possible when there is accumulation of mechanical stress followed by an induction period as the crystal system absorbs heat. The relaxation of this stress after the induction period is then accompanied by a phase transformation, in which the movement of molecules (or atoms) causes rapid change in the shape of the crystal. Such rapid phase transformation is quintessential for causing a forceful motion. It is important to reiterate that the jumping motion is due to a solid-solid structural transformation and not due to a thermochemical reaction, for example the thermal decomposition of metal-nitroxide complexes, whereby the disintegration and motion of a crystal is due to gas evolution.[9]

It was recently proposed[3b] that there are three distinct categories of thermosalient behaviour, based on the type of the most significant supramolecular interaction that holds together molecules in the crystal. Class 1 thermosalient crystals do not contain strong hydrogen-bonding donor and acceptor groups, and the molecules are typically arranged in stacked layers. In Class 2 thermosalient crystals, there are weak intermolecular hydrogen-bonding motifs that form between sterically hindered functional groups. Finally, Class 3 thermosalient crystals contain functional groups that can form strong hydrogen bonds, leading to infinite chains or tapes in the solid state. Using this categorization as the basis of our study, we were interested in exploring a way to design and to create new Class 2 and/or Class 3 thermosalient compounds based on concepts of supramolecular synthons and crystal engineering.[10]

7.3 Etter-type ureas

This work was strongly inspired by the earlier reports of Etter and coworkers[11] on the polymorphism of extensively hydrogen-bonded bis(aryl)urea compounds with large dipole moments, such as derivatives of *p*-nitroaniline with potential nonlinear optical properties.[12] In the solid state, bis(aryl)ureas and some bis(aryl)thioureas bearing sterically non-hindering

groups tend to form infinite $C^2_1(4)$ linear chains, as well as zig-zag shaped chain catemers, respectively (Fig. 7.2), connected by NH···X hydrogen bonds (X=O,S).[13] This type of supramolecular arrangement is herein designated as a Type 1a catemer (Fig. 7.2). Bis(aryl)ureas with bulkier substituents can form the same type of $C^2_1(4)$ hydrogen-bonded chain, but in this case the aryl moieties of neighbouring molecules are often at 90° (orthogonal) to each other. This type of arrangement is designated as a Type 1b catemer (Fig. 7.2). In these two types of intermolecular arrangements, the aryl groups of the molecules are often coplanar with the urea moiety. On the other hand, sterically bulkier bis(aryl)thioureas and bis(aryl)selenoureas tend to form $R^2_2(8)$ dimers (Fig 7.2).[14] In molecular structures of bis(aryl)ureas, there is some degree of freedom of twisting between the aryl rings and the usually highly planar urea motif (Fig. 7.5). This ultimately affects how the molecules arrange in the crystal structure, and thus affects the propensity to form polymorphs. In a seminal report,[11a] the Etter group described a slight motion of tiny crystals of 1,3-bis(*o*-anisoyl)urea **1a** as they underwent a polymorphic transformation upon heating on a microscope stage. Following this lead, we decided to investigate how the position of the substituent on the aryl moiety (Fig. 7.3) might affect the polymorphic transformations in this, and other, related methoxy-substituted bis(aryl)ureas. Our studies were done using powder and SCXRD techniques, HSM along with thermal analysis by DSC.

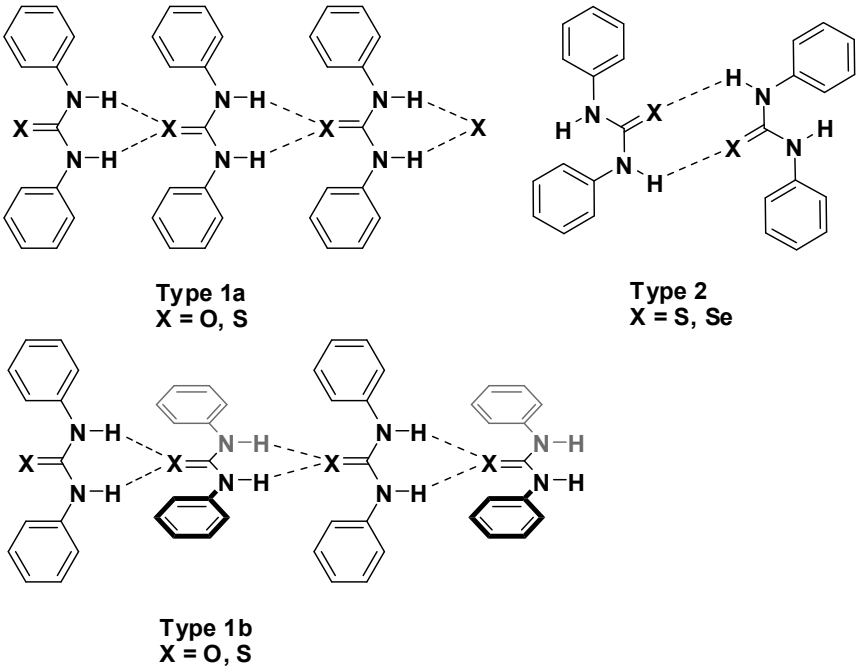

Fig. 7.2. Catemer and dimer motifs found in crystal structures of bis(aryl)ureas. The Type 1 catemer is mainly observed in (bis(aryl))ureas and thioureas, while type 2 dimers are more common in thioureas and selenoureas.

7.4 Sonochemical blowing reaction

The mono-substituted (methoxy) bis(aryl)urea compounds **1a-d** were synthesized using a newly developed sonochemical approach to the "blowing reaction".[15] To clarify, mono-substitution refers to having a single methoxy-substituent on each aryl ring of the symmetrical bis(aryl)ureas. This type of reaction involves two equivalents of an isocyanate, forming an diazetine-dione dimer intermediate which subsequently reacts with a molecule of water, and then undergoes a decarboxylation step to form a *N,N*-substituted urea. We discovered that conducting this reaction in an ultrasonic bath (Fig. 7.3) using water as both the reactant and the reaction medium, provides a rapid method (5-30 min) to synthesize symmetrical ureas. As most of the herein prepared *N,N*'-bis(aryl)urea products are not soluble in water, they immediately precipitate and can be easily purified by simple filtration, leading to high yields (95-99% isolated yields). Experimental details for such urea syntheses can be found in *Chapter 8, Section 8.6*. Spectroscopic data for the various compounds prepared in this way is provided in *Appendix F*.

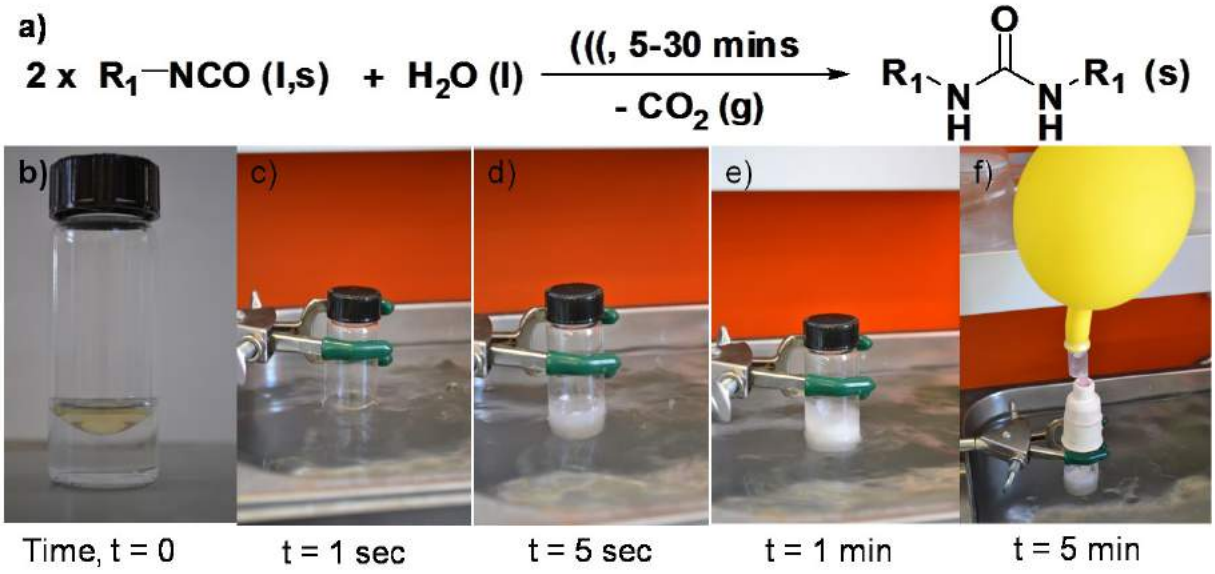

Fig. 7.3. (a) The blowing reaction involving isocyanates and water, conducted with the aid of ultrasonic irradiation, forming symmetrical *N,N*'-substituted ureas. Photographs of the blowing reaction of cyclohexylisocyanate and water, showing the sonochemical setup involving an ultrasonic bath, taken at varying time (t) intervals (b) t = 0, (c) t = 1 s, (d) t = 5 s, (e) t = 1 min and (f) t = 5 min. After the first minute, the reaction vessel becomes considerably pressurized (the pressurized vessel reaction was carried out behind a blast shield), as evidenced by the attached balloon being used to trap the CO_2 gas released during the reaction. The trapped gas was subsequently bubbled into a clear solution of $Ca(OH)_2$, leading to a white suspension of precipitated $CaCO_3$, confirming that the produced gas is indeed CO_2.

Next, we synthesized di-substituted (**2a-d**) and tri-substituted (**3a**) symmetrical *N*,*N*'-bis(aryl)ureas using the same sonochemical protocol (Fig. 7.5). Again, to clarify, di-substitution and tri-substitution refers to having two and three methoxy-substituents on each of the aryl rings, respectively. All products obtained were isolated in excellent yields (>95% yields). In addition, thiourea variants (**4a-c**) of some of the compounds were also synthesized using a previously reported click mechanochemical coupling reaction between isothiocyanates and amines (Fig. 7.4).[14a] The experimental details for these reactions are provided in *Chapter 8, Section 8.5*.

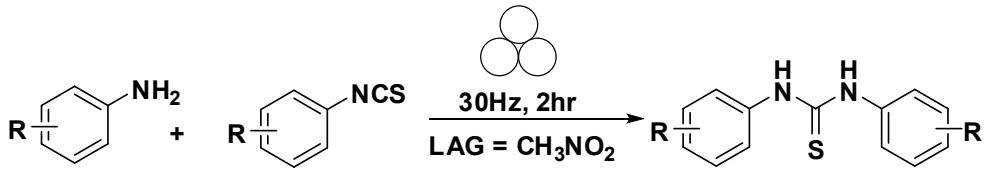

Fig. 7.4. Schematic representation of the click mechanochemical coupling between isothiocyanates and amines, used to synthesize thioureas.[14a]

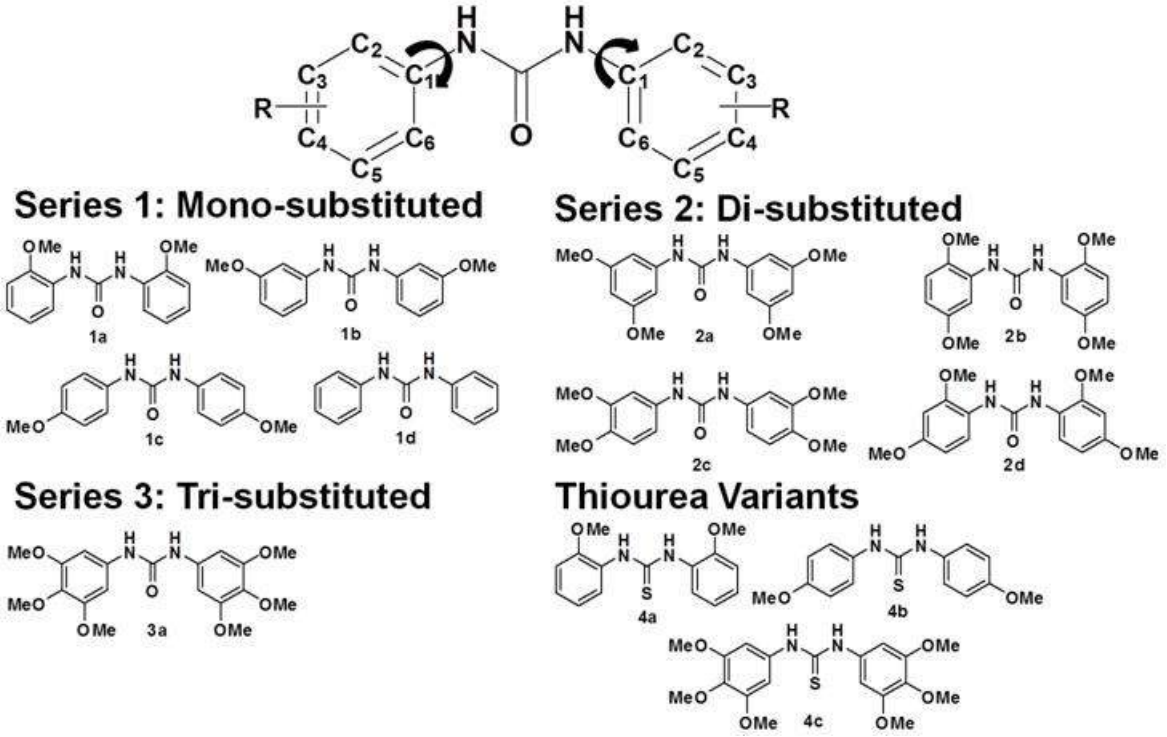

Fig. 7.5. Schematic representation of various members of the methoxy-substituted family of *N*,*N*'-bis(aryl)ureas and *N*,*N*'-bis(aryl)thioureas, that were prepared and investigated in this work.

7.5 Mono-substituted methoxy ureas

Crystals of all compounds were obtained *via* slow evaporation in various solvents and solvent combinations, including acetone, methanol, dimethylsulfoxide, ethyl acetate and acetonitrile. We first re-investigated the mono-substituted methoxy compounds (series 1) that were originally studied by Etter,[11] by heating the crystals while observing them using a hot-stage microscope. Similar to the previous report, crystals of **1a** underwent polymorphic transformation upon heating to 148.7 °C in a rather spectacular manner: the crystals wiggle and become opaque as they crack to form multiple daughter crystals that are still interconnected in the shape of the original mother crystal.[16] Data for both polymorphs of **1a** have already been published and can be found in the Cambridge Structural Database (CCDC codes SILTUC and SILTUC01). By using hot-stage microscopy, it is possible to observe the polymorphic transformation of **1a** in real time, from polymorph I to II, upon heating. Based on HSM videos, the polymorphic transformation of **1a** e starts from outside of the crystal and visibly propagates towards the centre of the crystal. Comparison of the crystal structure and how the molecules pack in the solid state also offers some insight into this polymorphic transformation. The change in the crystalline rearrangement of the molecules upon polymorphic transformation may be represented with a schematic diagram, shown in Fig 7.6a. In the structure of polymorph I of **1a**, the molecules are arranged in chains with alternating molecules adopting mutually orthogonal orientations. The compound crystallizes in the tetragonal $P4_2/n$ space group, with hydrogen-bonded chains propagating along a 4-fold helical axis (Fig. 7.6b and 7.6d). The polymorph II of **1a** crystallizes in the orthorhombic space group $P2_12_12_1$. In the crystal structure of polymorph II, the molecules still form the $C^2_1(4)$ supramolecular chains, but in this case, the molecules are more coplanar, and the chains are more linear. It is possible that upon heating, the alternating molecules along each chain in polymorph I twist at a ca. 90° angle, transforming the structure into that of polymorph II (Fig. 7.6c and 7.6e). The large changes in molecular orientation within the hydrogen-bonded chains in structures of **1a** polymorphs I and II could explain why the mother crystal internally fractures into a polycrystalline daughter sample. This change in the molecular arrangement in the crystal structure is also evident through modifications to the N-H¨¨O hydrogen-bonding motif in each chains, specifically the reduction of the N¨¨O distances from 3.144(2) Å to 2.996(2) Å upon transformation of polymorph I into II, respectively. Close inspection of both crystal structures also reveals that the aryl rings of each molecule in polymorph II are slightly twisted with respect to each other. In contrast, in polymorph I the

aryl rings were coplanar mutually, as well as with respect to the urea moiety. Although the two polymorphs of **1a** have already been reported 20 years ago, the polymorphic transition has not previously been characterized and observed using HSM and DSC. The transformation appears to be not reversible, which is indicated by DSC. Specifically, the DSC thermogram (Fig. 7.7a) shows that, upon heating to 148.7 °C, compound **1a** undergoes an endothermic event. As hot-stage microscopy (Fig. 7.7b) does not reveal any melting at that temperature, this endothermic event is most likely associated with the polymorphic transformation. However, no thermal event is observed upon cooling, all the way down to -50 °C. Also, the endotherm at 148.7 °C is no longer observed upon repeated heating. These observations are all consistent with **1a** not undergoing a reversible polymorphic transformation upon cooling.

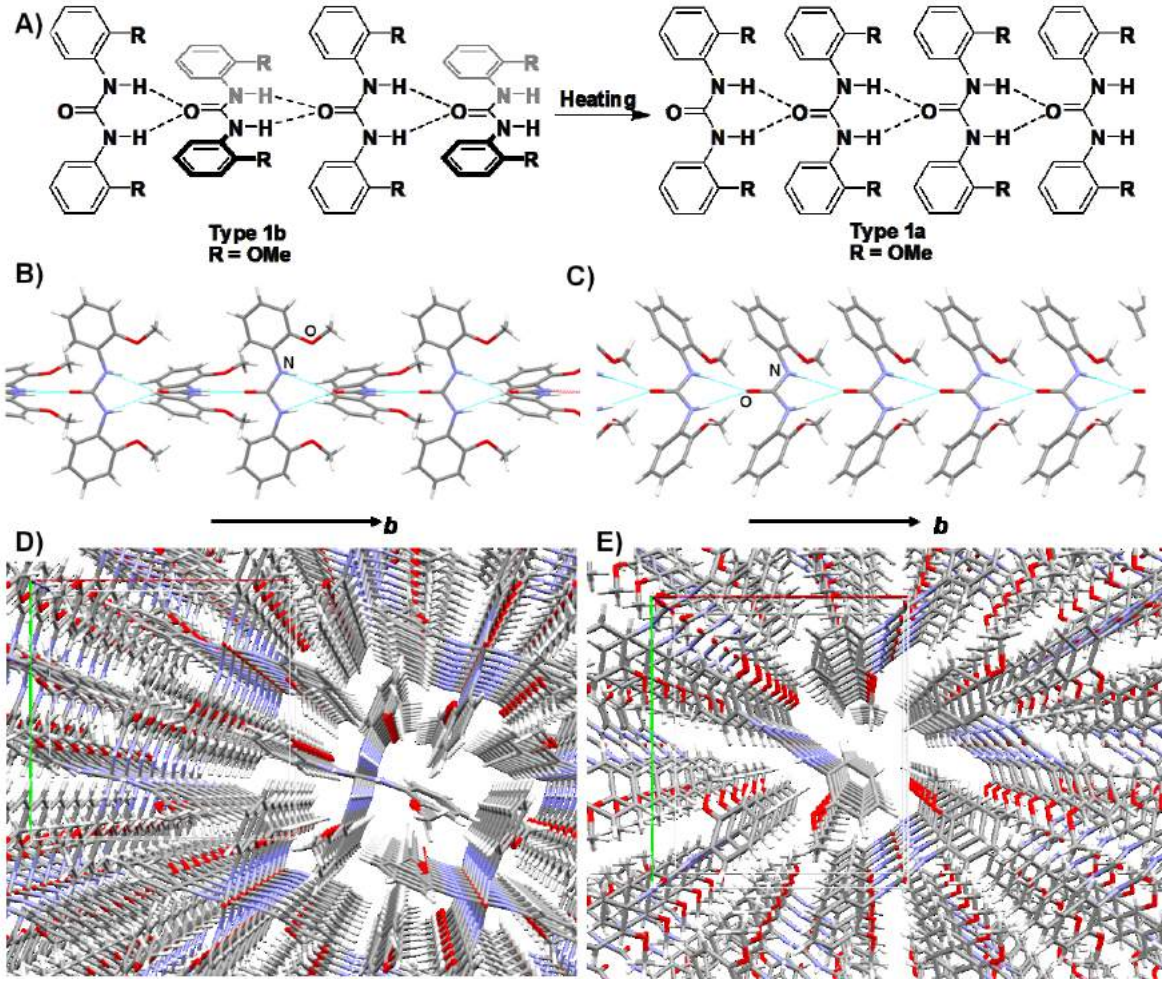

Fig. 7.6. a) Scheme showing the polymorphic transformation of 1,3-bis(*o*-anisoyl)urea **1a** upon heating, illustrating the change from a Type 1b chain catemer (polymorph I) to a Type 1a (polymorph II) one. Fragment of the crystal structure of: b) polymorph I and c) polymorph II of **1a**, depicting a hydrogen-bonded chain of molecules propagating along the crystallographic *b*-axis. Projection of the crystal structure, viewed down the crystallographic *b*-axis of: (d) polymorph I and (e) polymorph II of **1a**.

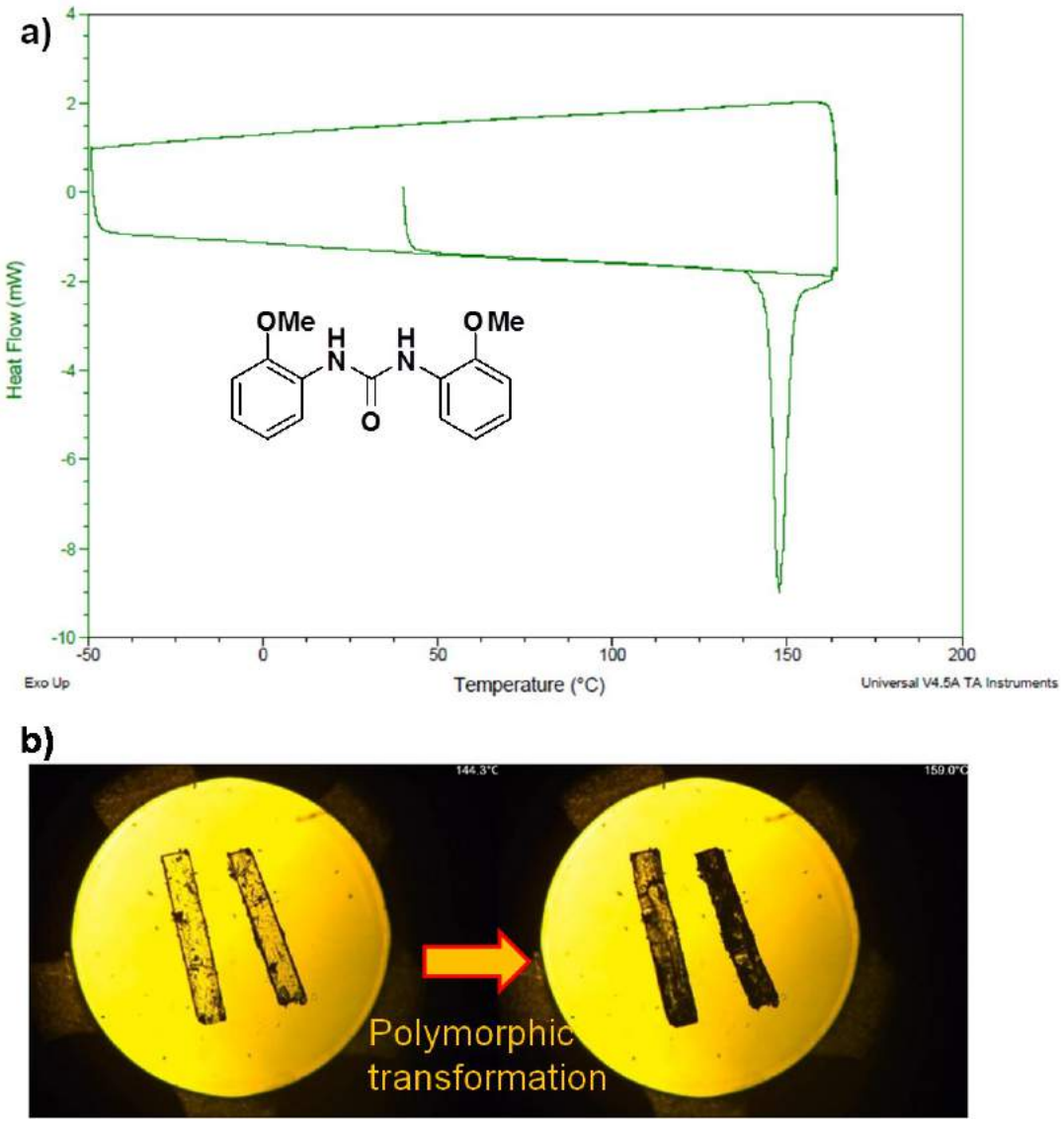

Fig. 7.7. (a) The cyclic DSC thermogram (two cycles of heating and cooling) appears to show an irreversible transition from polymorph I to polymorph II of 1,3-bis(*o*-anisoyl)urea (**1a**) upon heating. (b) Still images from hot-stage microscopy videos of two clear single crystals of **1a** (polymorph I), transforming into opaque fragmented polycrystals of polymorph II upon heating.

On the other hand, crystals obtained for compounds **1b** and **1d** did not undergo any apparent polymorphic transition upon heating, and just melted (Fig. 7.8). This suggests that substitution in the 3-position (**1b**) and the lack of substituents (**1d**) on the aryl ring do not readily lead to polymorphic behavior. However, further and more extensive polymorph screening would be needed to fully support this claim.

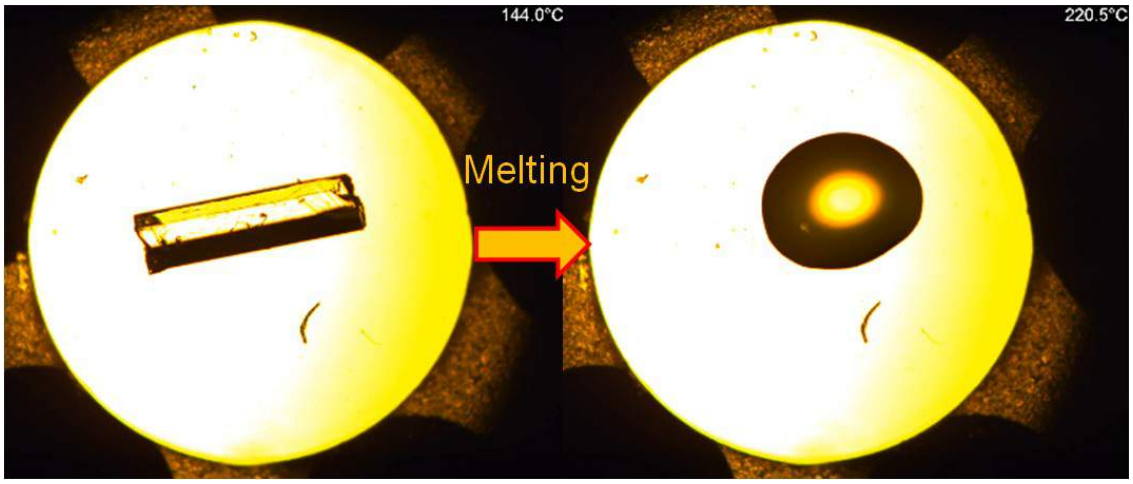

Fig. 7.8. Still images from a hot-stage microscopy study of crystals of **1b**, demonstrating melting of the crystal.

For compound **1c,** where the methoxy-substituent is in the 4-position on the aryl ring, hot-stage microscopy videos revealed that the clear block-like crystals undergo very slight movement when they were heated to 98 °C. Similar slight movement was again observed upon cooling of the crystals down to 87 °C. In both cases, the integrity of the crystal appeared to be intact on optical microscopy images (Fig. 7.9b), suggesting a single-crystal-to-single-crystal (SC-SC) transformation. The slight motion, without visible deterioration of the crystal, appears to be highly reversible and reproducible upon multiple heating and cooling cycles**,** as observed by HSM. We believe that the slight motions of the crystals are due to thermosalient effect that is difficult to observe. This involves a polymorphic transition between the low temperature phase I (triclinic $P\bar{1}$) and the herein discovered high temperature phase II (orthorhombic, $P2_12_12_1$) of **1c**. It is important to note that although the low temperature phase I of **1c** had been reported,[17] to the best of our knowledge, there has previously been no study conducted on the polymorphic behavior of **1c**. XRD quality crystals of phase II of **1c** were obtained *via* crystallization of the compound from different solvent mixtures. The reversibility of the polymorphic phase change of **1c** was also corroborated by DSC experiments. Based on the DSC thermogram (Fig. 7.9a), it appears that there is an endothermic and an exothermic process taking place at 98.4 °C and 88.1 °C, respectively, during the heating and cooling cycles. Again, hot-stage microscopy does not reveal any melting at 98.4 °C, indicating that the endothermic event is associated with a polymorphic transformation from phase I to phase II. Similarly, the observed exothermic process at 88.1 °C is also possibly associated with the reverse polymorphic transformation, from phase II to

phase I. Cyclic DSC experiments, with multiple heating/cooling cycles shown in Fig. 7.9a, are consistent with **1c** undergoing reversible polymorphic transformations. The polymorphic transformation of **1c** appears to be a martensitic type SC-SC phenomenon, as the entire crystal moves homogenously upon heating (or cooling) without any observable propagation of the polymorphic change.

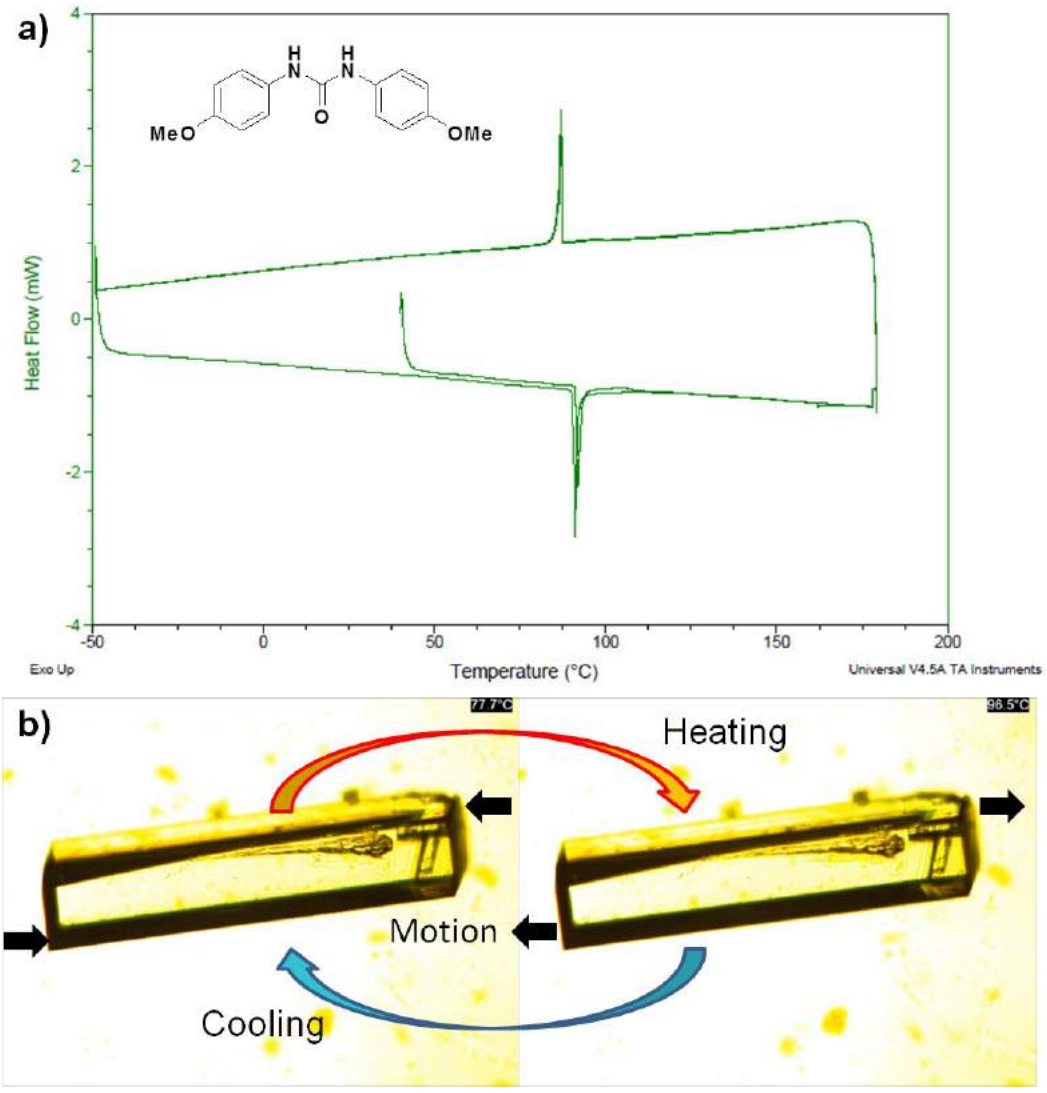

Fig. 7.9. (a) A cyclic DSC thermogram (two cycles of heating and cooling) showing a reversible transition from polymorph I to polymorph II of 1,3-bis(*p*-anisoyl)urea **1c** upon heating. (b) Still images from hot-stage microscopy videos of a clear crystal of **1c** and its reversible SC-SC transformation from one polymorph to another. The crystal moves very slightly (direction of motion is indicated by black arrows) during the polymorphic transformation, and this slight movement is more evident in the HSM videos.

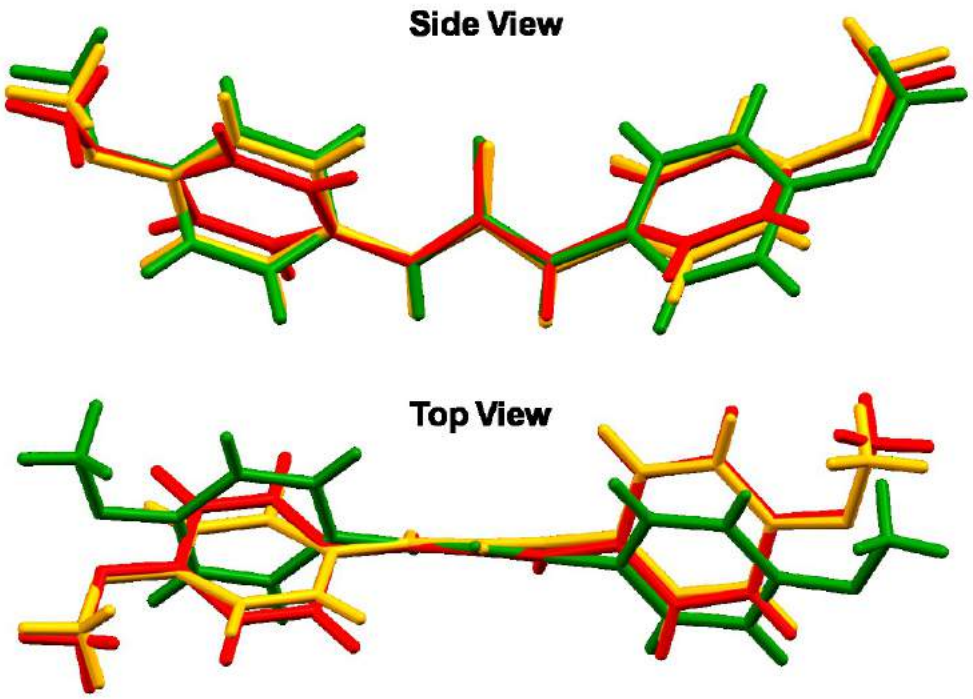

Fig. 7.10. Side and top views of the overlay of the molecules of polymorphs I and II of **1c**. Phase I contains two symmetrically independent molecules, shown in *red* and *orange*, while a molecule from the structure of phase II is shown in *green*. Crystallographic details for both polymorphs can be found in *Appendix F*.

Insight into this polymorphic transformation can be obtained by comparing the crystal structures, which were determined by SCXRD, of both polymorphs of **1c**. Based on the SCXRD data, it was revealed that phase I of **1c** contains two crystallographically non-equivalent molecules in the asymmetric unit, whilst phase II contains only one. From the overlay of the structures of the two polymorphs (Fig. 7.10), it is possible to imagine heating could have permitted the molecules of **1c** to move slightly and transform from polymorph I into polymorph II. Upon such heating, the aryl rings in phase I (*red* and *orange*) of **1c** are able to twist, in the opposite directions, to form the high temperature phase II (*green*), such that one of the aryl rings has twisted more out of the plane of the planar urea segment. It is possible that this twisting motion of the aryl groups led to a minor, but quick anisotropic change in the unit cell, which in turn resulted in a slight motion of the crystal. As both phases belong to different crystal systems (phase I is triclinic and phase II is orthorhombic), it is not possible to directly compare the changes in the unit cell parameters of both phases during the polymorphic transformation. The heat-induced polymorphic transformation in **1c** appears to be less evident than that in **1a**, as observed by the HSM videos whereby the structural

integrity of the crystals of **1c** during polymorphic transformation is maintained. This can be explained by the observation that the polymorphic transformation in **1c** involves mainly the twisting motion of the aryl rings, whilst in **1a**, polymorphic change is due to the twisting of alternating whole molecules, which involves large-scale changes to the molecular orientation of the hydrogen-bonding motif. Despite these observations, as the perceived polymorphic transformation of **1c** is much faster than **1a**, it is not possible to say with certainty if it proceeds *via* a similar mechanism to **1a**. The observation of thermosalient effect in **1c** prompted us to further explore other members of the methoxy-substituted family of symmetrical bis(aryl)ureas, including compounds that are di-substituted on each aryl ring. Based on the results observed thus far, we speculate that substituents in the 4-position might be relevant to thermosalient behaviour of such systems.

7.6 Di-substituted methoxy ureas

In the next step, we explored the thermal properties of the compounds **2a-d** (Fig. 7.5), bearing two methoxy groups per aryl ring. X-ray diffraction-quality crystals were obtained for **2a-c**, of which only **2b** and **2c** were found to undergo polymorphic transitions upon heating. Compound **2a** was found to just melt upon heating. The behavior of crystals of **2b** upon polymorphic transformation was similar to those of **1a** (Fig. 7.11), whereby, based on HSM videos, the irreversible and directional progression of the transition was observed. However, the phase transformation in **2b** occurred at a higher temperature, at 188 °C. Comparison of the crystal structures of the low temperature phase I for **1a** and **2b** (*I*4 space group) showed that they have very similar molecular packing arrangements, whereby alternate molecules in the hydrogen-bonded chains are arranged orthogonally, at 90° to each other, forming Type 1b chain catemers. Additionally, in the structures of **2b**, aside from the conventional N-H···O hydrogen bonds (N···O distance of 2.955(2)Å between the molecules, there are additional weaker C-H···O hydrogen bonding interactions with the 5-methoxy substituent (C···O interatomic distances of 3.266(3)Å and 3.458(3)Å). These additional intermolecular interactions might account for the higher temperature of the phase transition in **2b**, compared to **1a** (188 °C *versus* 148 °C respectively). Unfortunately, only PXRD data was available for phase II of **2b**, and the SCXRD data has yet to be acquired. However, it is suspected that the crystal structure for the phase II of **2b** might be similar to that of the phase II structure of **1a**, in which all the molecules along the hydrogen-bonded chains are no longer twisted at 90° and are mutually coplanar.

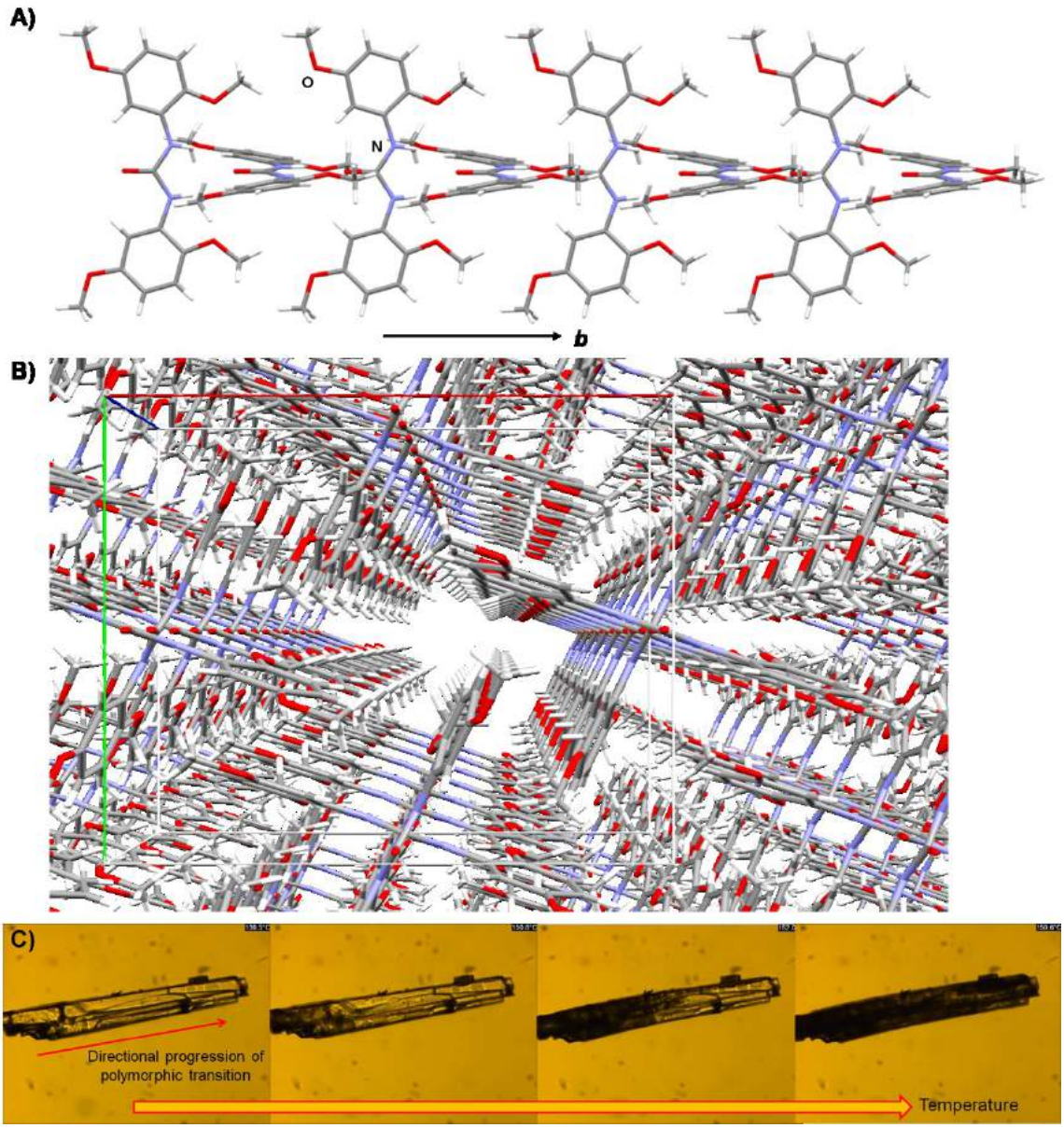

Fig. 7.11. (a) Fragment of a hydrogen-bonded chain of molecules propagating along the crystallographic *b*-axis in the polymorph I of **2c** and (b) projection of the crystal structure of polymorph I, viewed down the crystallographic *b*-axis; (c) Still images from hot-stage microscopy videos demonstrating the directional propagation of the polymorphic transformation of **2c** upon heating. Crystallographic details can be found in *Appendix F*.

For **2c**, thermosalient behaviour was observed by HSM. Upon heating to 103-106 °C, depending on the quality of the crystals, single crystals of **2c** exhibit some motion which varies from slight movement, to splitting along inherent cracks and defects, to sudden explosive jumps (Fig. 7.12). Examination of the crystal structures determined from SCXRD data (Table 7.1) for both polymorphs of **2c** revealed that the molecular packing arrangement in phase I of **2c** is similar to that found in **1c**, whereby it formed linear chains of highly

coplanar molecules. In addition, having an extra methoxy-substituent in the 3-position of each aryl ring permitted the formation of a more complex hydrogen-bonding network between molecules of **2c** belonging to neighbouring supramolecular chains. Specifically, the molecules of **2c** are packed in such a way that each C-H group of the methoxy substituent in the 3-position is able to form bifurcated C-H···O hydrogen bonding interaction with two oxygen atoms of methoxy groups in adjacent molecules (Fig. 7.12c). These interactions are characterized by C···O distances of 3.470(4) Å and 3.487(4) Å for polymorph I, and 3.438(4) Å and 3.461(4) Å for polymorph II. Comparison of the crystal structures for both the low temperature polymorph I and the high temperature polymorph II revealed that both phases adopted an identical space group (*C*2/c), as well as very similar unit cell parameters. Transitioning from phase I to phase II involves only a slight increase in the unit cell parameters (Table 7.1). For example, the unit cell volume for phase I is 1598(3) $Å^3$, and for phase II it is 1619.8(5) $Å^3$, which corresponds to a *ca.* 0.7-0.8% increase. This is accompanied by a slight increase in the lengths of intermolecular hydrogen bonds within the chains: the N···O distances in polymorphs I and II were found to be 2.929(2) Å and 2.935(2) Å, respectively. Furthermore, the DSC experiments conducted on crystals of **2c** suggest that the polymorphic transformation from phase I to phase II might be irreversible. The first endothermic event observed at 58.2 °C is most likely due to residual solvent on the surface of the crystals. Upon further heating of the crystals of phase I to 103.8 °C, the crystals undergo an endothermic event that does not correspond to melting, as corroborated by HSM videos. Upon cooling and subsequent heating, the endotherm at 103.8 °C is no longer observed. These observations are all consistent with **2c** not undergoing a reversible polymorphic transformation upon cooling.

Overlay of the molecular structures in phases I and II of **2c** (Fig. 7.13) reveals that the polymorphic transformation might involve twisting of both aryl rings on each molecule, in opposite directions. Unlike **1c**, where only one aryl ring per molecule has been significantly twisted upon heating, in **2c** the arrangement of both aryl rings in each molecule appears to have been changed notably. This might account for the more pronounced thermosalient behaviour in **2c**.

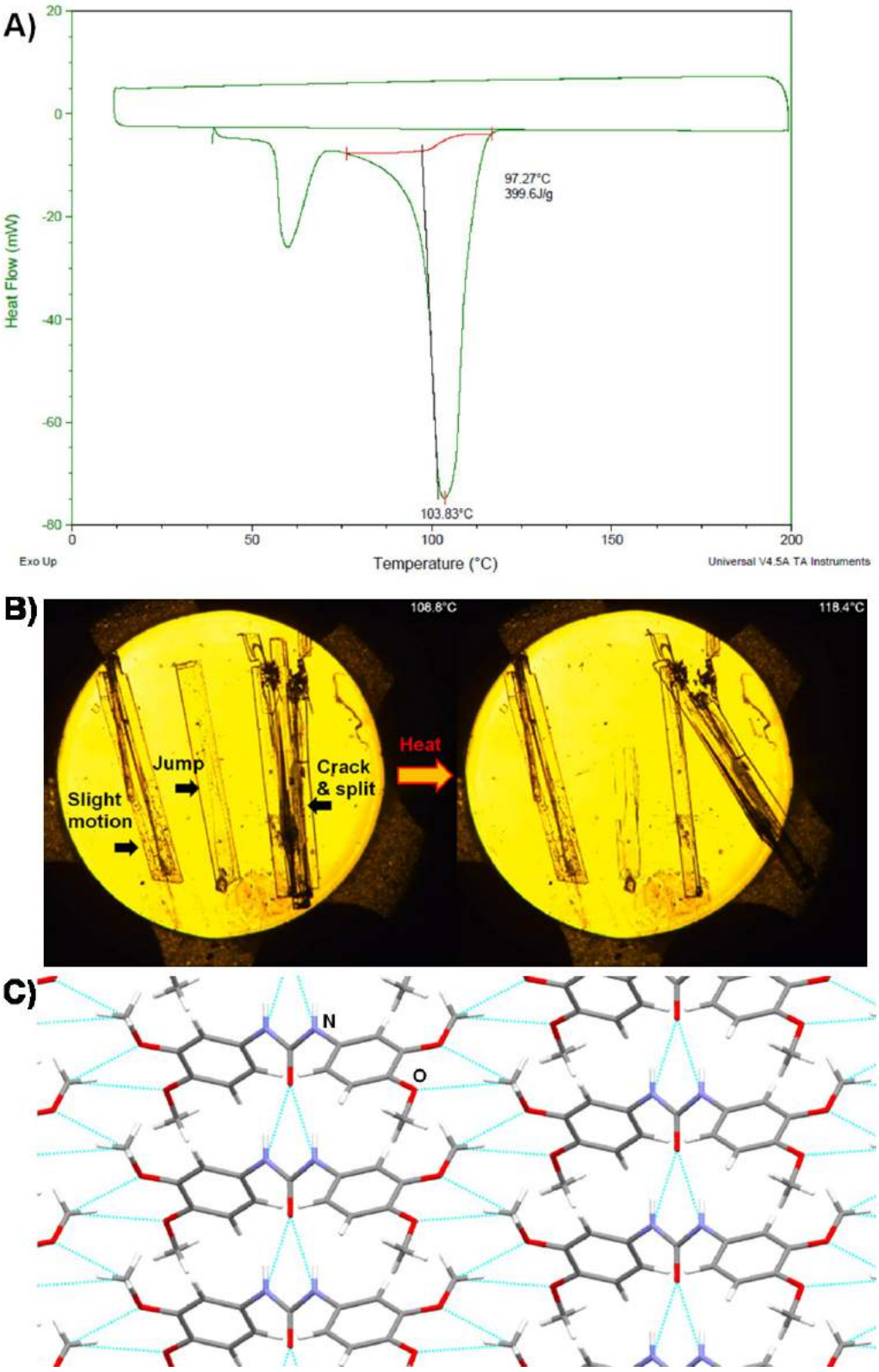

Fig. 7.12. (a) A cyclic DSC thermogram (two cycles of heating and cooling), showing an apparently irreversible transition from polymorph I to polymorph II of **2c** upon heating. (b) Still images from hot-stage microscopy videos of clear crystals of **2c** and their SC-SC transformation from one polymorph to another. (c) Fragment of the crystal structure of **2c**, depicting the intermolecular N-H···O and C-H···O hydrogen bonds (*blue* dotted lines).

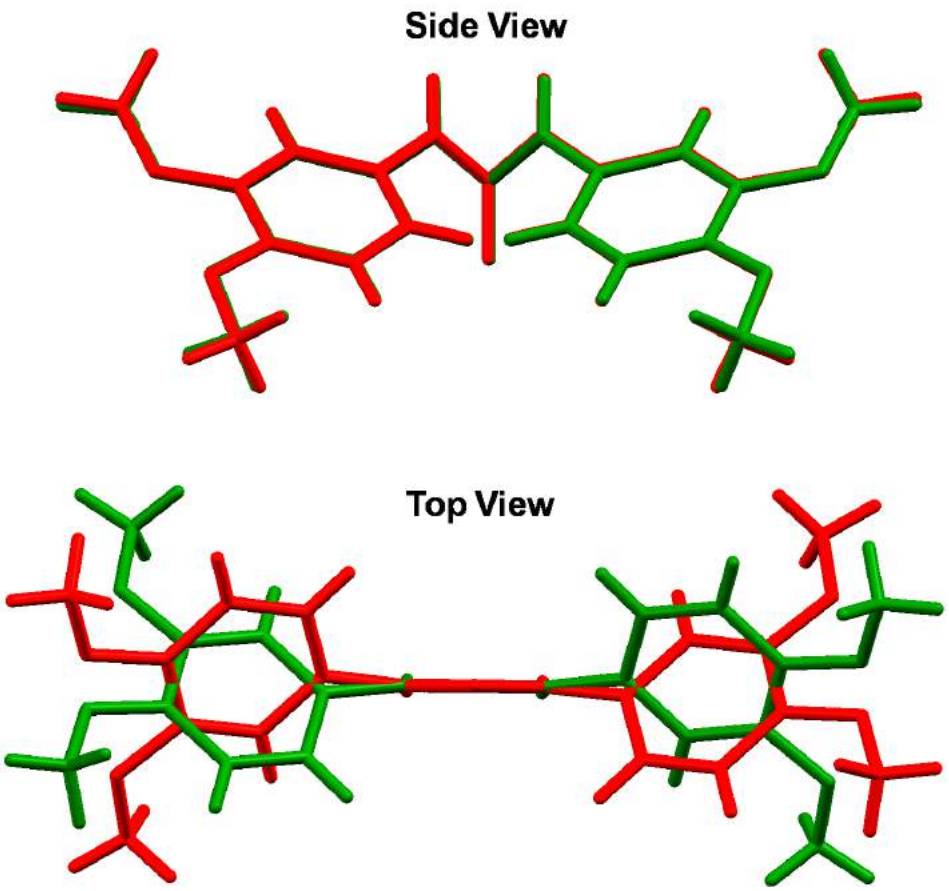

Fig. 7.13. Side and top views of the overlay of molecules in the polymorphic structures of **2c**. A molecule of phase I is shown in *green* and a corresponding molecule of phase II in *red*. Crystallographic details for both structures can be found in *Appendix F*.

Based on these results, we can propose potential relationships between the position of the methoxy functional group(s) on the aryl ring, and the resulting crystal packing and polymorphism in this system. The presence of methoxy substituents in the 2-position appears to cause orthogonal arrangement of alternating molecules in the hydrogen-bonded chains. Such structures did not exhibit any thermosalient behavior, possibly because the phase transformations always involve the twisting of alternating molecules around the supramolecular chain axis, leading to highly planar hydrogen-bonded chains. Such a large change in the molecular orientation within the unit cell apparently leads to the fragmentation of crystals, observed in **1a** and **2b**. On the other hand, having a methoxy-substituent in the 4-position of the aryl ring, a feature that is common to both **1c** and **2c**, might be supportive for achieving thermosalient behavior. In addition, the observed thermosalient effects in these two bis(aryl)urea systems suggests that thermal motion of bulk crystals might be "enhanced" by an additional methoxy-substituent in the 3-position of each aryl ring. This increases the

intermolecular hydrogen bond connectivity between neighboring urea chains in the crystal structure, which could presumably augment the accumulation of strain upon the system during the twisting of aryl groups.

7.7 Tri-substituted methoxy ureas

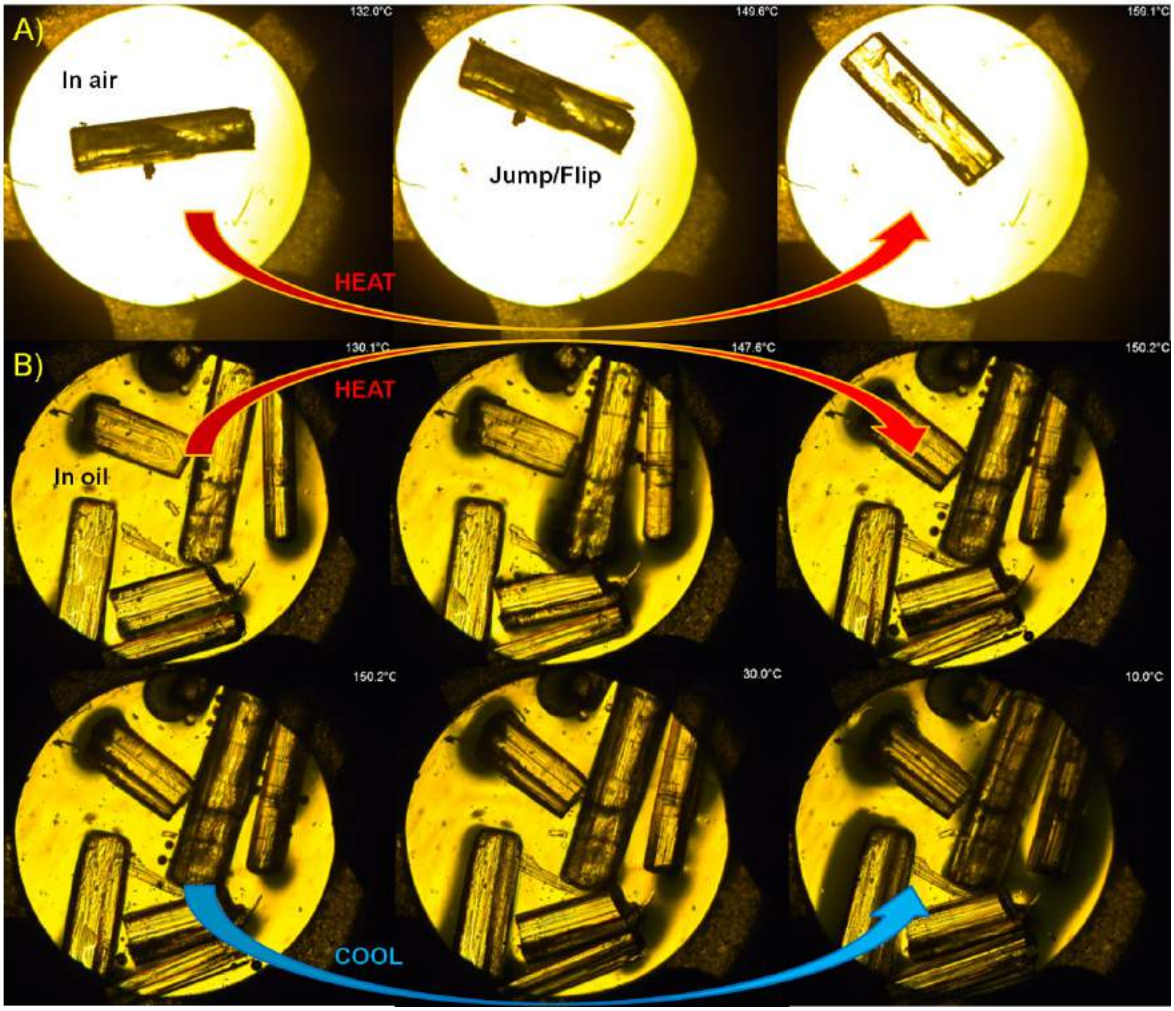

Fig. 7.14. Still images from hot-stage microscopy videos of crystals of **3a** upon heating and cooling. (a) Thermosalient behaviour of **3a** as it flips upon transforming from polymorph I to polymorph II upon heating to 146 °C, recorded in air. (b) Multiple crystals of **3a** covered in silicon oil: the crystals wiggle and move upon heating to 146 °C and upon subsequent cooling to 9 °C. Striated cracks can be seen forming on the block-shaped crystals upon multiple heating and cooling cycles.

Based on the so far described observations, made on mono- and di-methoxy arylureas, we speculated that another methoxy substituent on the 5-position, but not in the 2- or 6-positions, might further enhance thermosalient behaviour and perhaps even allow us to achieve a reversible thermosalient effect. With that in mind, we synthesized the compound

3a, containing two trimethoxy-substituted aryl rings. Single crystals of **3a** were obtained *via* slow evaporation of a solution of the compound in a mixture of acetone and methanol solvents. The HSM videos on these single crystals revealed notable, large-scale thermosalient behaviour upon heating of the crystals (Fig. 7.14a). The videos of the crystals moving, either in air or immersed in silicone oil to slow down their motion (Fig. 7.14b), revealed that movement takes place without any notable change in crystal appearance, indicating a SC-SC polymorphic transformation. The crystals, when heated in air, jump and flip at 146 °C, and then move again upon subsequent cooling to 9 °C. The cooling process is also accompanied by the formation of cracks within the crystals. High-quality X-ray diffraction data was obtained for both the room temperature phase I and the high temperature phase II of **3a**. In addition, SCXRD was also successfully performed on the same single crystal (phase II) after two cycles of polymorphic transitions (refer to *Appendix F*), further supporting the view that the transformation is of SC-SC type. Analysis of the cyclic DSC thermal data (Fig 7.15) revealed that the transformation in **3a** exhibited high reproducibility and reversibility, up to 15 times, albeit with diminishing intensity. The loss of intensity is probably due to the disintegration of the crystal into multiple fragments upon each heating/cooling cycle. Based on the DSC thermogram, there are two observed thermal events at 149.4 °C and 9.3 °C, associated with the polymorphic transformation from phase I to phase II (upon heating) and also from phase II to phase I (upon cooling), respectively.

Similar to polymorphs of **2c**, the unit cell volume and dimensions of the phase I and phase II structures of **3a** are very similar. Both phases adopt the same space group (*C*2/c) and only differ in the magnitude of the unit cell edge along the crystallographic *a*-axis dimension, the *β*-angle and the unit cell volume. Notably, as **3a** transformed from phase I to phase II there is contraction in the unit cell parameter along the *a*-axis of *ca.* 4.7%, a change of *ca.* 10.4% in the *β*-angle, and a change in unit cell volume of *ca.* 1.5%. An overlay of the molecular geometries in crystal structures of phase I and phase II of **3a** (Fig. 7.16) revealed a possible origin of the observed thermosalient effect. Similar to **2c**, from the top view (*i.e.* down the crystallographic *b*-axis), one can observe that both aryl rings of the molecule have been rotated along the respective C-N bonds into the opposite plane of the urea moiety through a twisting motion. This means that the entire molecule has been twisted in the crystallographic *ac*-plane during the phase transition, which is accompanied by the associated contraction in the unit cell edge. This contraction is also evident in the decrease in the N-H···O hydrogen bond lengths (N···O distances are 2.940(2) Å and 2.902(2) Å for phases I and II,

respectively). In addition, there is also an increase in the number of weak intermolecular C-H···O hydrogen bonds between neighbouring urea chains, from phase I to phase II (see *Appendix F* for further details). As the crystallographic *b*-axis contains the main strong intermolecular N-H···O motifs, motion along this direction is most likely restricted. Preferential anisotropic contraction along the crystallographic *a*-axis might be what triggers self-actuation and motility of crystals upon thermal treatment,[18] as the accumulated strain suddenly and rapidly dissipates, effectively translating into thermosalient behaviour. Subsequent fragmentation of the single crystal upon multiple heating-cooling cycles is attributed to the weaker intermolecular forces in the *ac*-plane *i.e.* cracks that form should be parallel to the crystallographic *b*-axis.

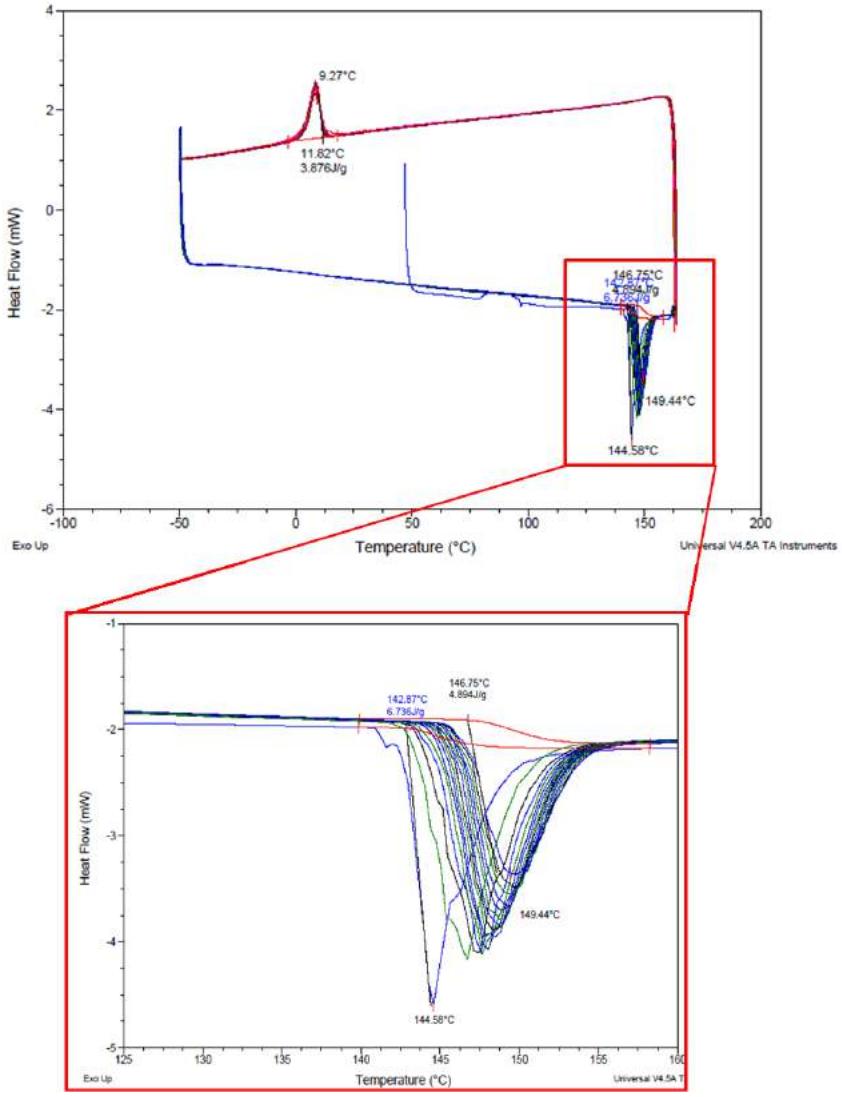

Fig. 7.15. A cyclic DSC thermogram (15 cycles of heating and cooling) recorded on crystals of **3a**. Zoom-in view of the transition from phase I to phase II shows reversibility between polymorphic forms, but with diminishing intensity of the thermal event.

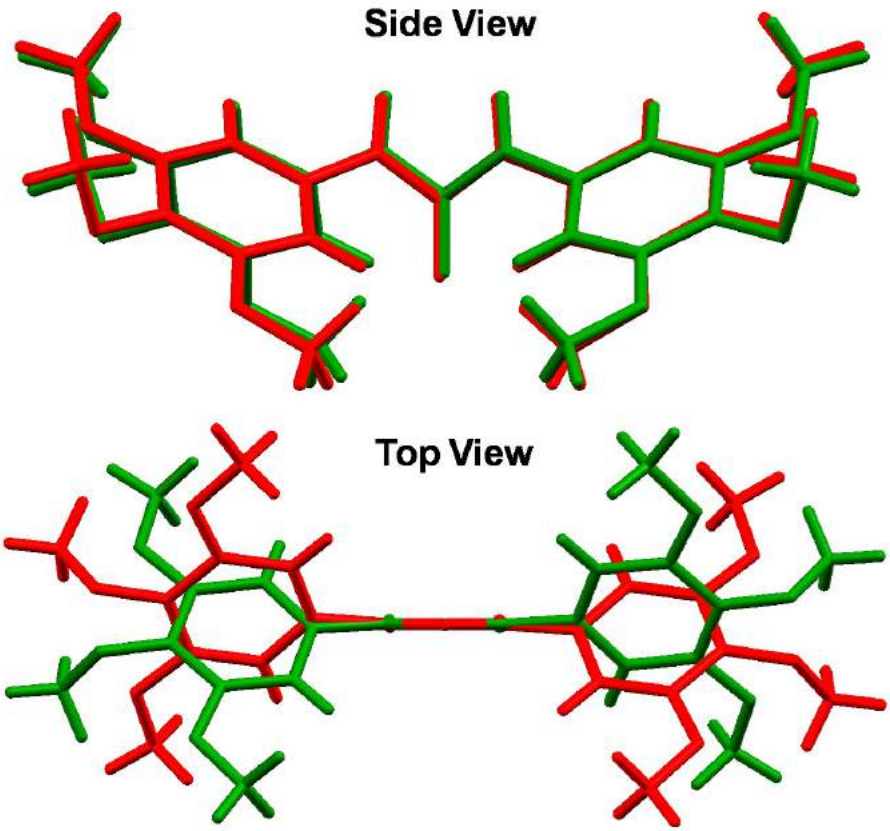

Fig. 7.16. Side and top views of the overlay of the molecular structures of both polymorphs of **3a**. A molecule of phase I is depicted in *green* and a molecule of phase II in *red*. Crystallographic information of both polymorphs can be found in *Appendix F*.

Table 7.1. SCXRD data of polymorphs of the thermosalient compounds **1c**, **2c** and **3a**.

	1c phase I	**1c phase II**	**2c phase I**	**2c phase II**	**3a phase I**	**3a phase II**
Molecular formula	$C_{15}H_{16}N_2O_3$	$C_{15}H_{16}N_2O_3$	$C_{17}H_{20}N_2O_5$	$C_{17}H_{20}N_2O_5$	$C_{19}H_{24}N_2O_7$	$C_{19}H_{24}N_2O_7$
M_r	272.30	272.30	332.35	332.35	392.40	392.40
Crystal System	Triclinic	Orthorhombic	Monoclinic	Monoclinic	Monoclinic	Monoclinic
Crystal colour	Colorless	Colorless	Colorless	Colorless	Colorless	Colorless
Space group	*P*-1	$P2_12_12_1$	*C*2/c	*C*2/c	*C*2/c	*C*2/c
Temperature (K)	100K	298K	100K	298K	298K	298K
Unit cell dimensions (Å,°)						
a	9.219(4)	4.6193(3)	30.04(3)	30.245(6)	31.255(15)	29.78(4)
b	11.935(5)	8.6489(6)	4.676(5)	4.6683(7)	4.705(2)	4.639(7)
c	13.464(5)	32.803(2)	12.433(13)	12.6148(19)	13.627(7)	13.66(2)
α	64.615(4)	90	90	90	90	90
β	87.716(4)	90	113.792(9)	114.574(2)	108.415(5)	97.152(18)
γ	76.698(4)	90	90	90	90	90
Volume (Å^3)	1299.7(9)	1310.56(15)	1598(3)	1619.8(5)	1901.2(16)	1872(5)
Z	4	4	4	4	4	4
D_{calc} (g cm^{-3})	1.392	1.380	1.382	1.363	1.371	1.393
μ (mm^{-1}) (abs coeff)	0.098	0.097	0.103	0.101	0.105	0.107
***F*(000)**	576	576	704	704	832	832
Refl. collected/independent	15419 / 6047	38693/5757	686 / 509	4571 / 935	9675 / 1963	3065 / 1142
No. observed refl. [$I>2\sigma(I)$]*	5144	4911	686	767	1656	738
No. restraints/No. parameters	0/ 361	0/184	0/ 112	0/ 110	0/ 128	0/ 128
R [all/gt]	0.0465/ 0.0383	0.0588/0.0446	0.0740/ 0.0511	0.0487/ 0.0374	0.0427/ 0.0365	0.0989/ 0.0644
wR [ref/gt]	0.1060/ 0.0998	0.1059/0.1001	0.1395/ 0.1265	0.1013/ 0.0956	0.1066/ 0.1006	0.1843/ 0.1606
Goodness-of-fit on F^2	1.014	1.046	1.019	1.046	1.028	1.083
Largest diff. peak, hole (*e* Å^{-3})	0.295, -0.227	0.437, -0.288	0.170, -0.230	0.085, -0.117	0.156, -0.177	0.415, -0.212

*$R = \sum||Fo|-|Fc||/\sum Fo, w = 1/[\sigma^2(F_o^2)+(g_1P)^2+ g_2P]$ where $P = (F_o^2+2F_c^2)/3$, $S = \Sigma[w(F_o^2 - F_c^2)^2/(N_{obs} - N_{param})]^{1/2}$.

7.8 Thiourea variants

Lastly, we investigated some thiourea variants of the bis(aryl)urea compounds that were found to undergo polymorphic transformations. As expected, molecules of these thiourea derivatives, such as **4c**, tend to arrange into hydrogen-bonded pairs, forming $R^2_2(8)$ homo-dimeric rings (Fig. 7.17). This type of self-assembly is common in thioureas with bulky substitutents, and prevents formation of linear hydrogen-bonded chains. Upon heating, crystals of these compounds did not exhibit any polymorphic change or thermosalient behaviour, unlike their urea counterparts. Crystal structures of **4a** and **4b** have already been reported[19] and their crystallographic data can be found in the Cambridge Crystal Structure Database (CCDC codes YAGGAQ and WEFQEE).

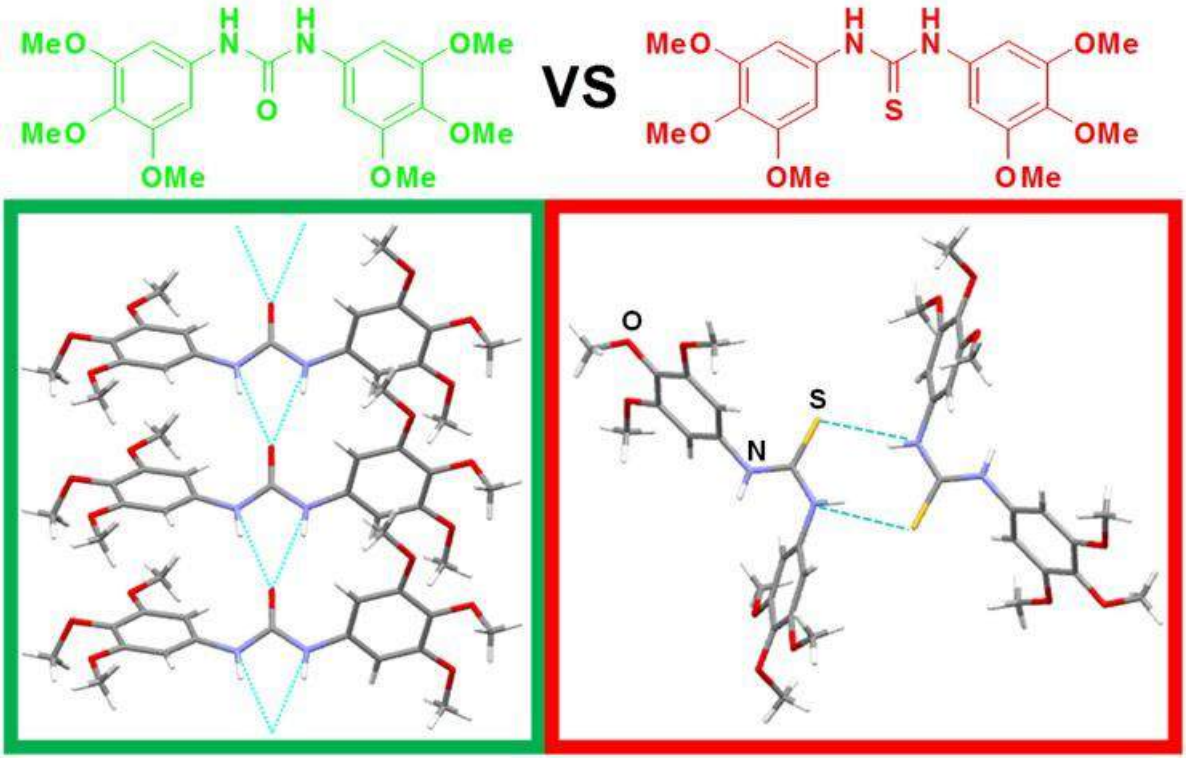

Fig. 7.17. Comparison of the fragments of crystal structures of **3a** (*green, left*) and its thiourea variant **4c** (*red, right*), illustrating the hydrogen-bonded chains in **3a** and the hydrogen-bonded dimer in **4c**.

7.9 Conclusion

Although the herein addressed bis(aryl)ureas were initially studied by Etter almost 25 years ago and some were found to exhibit polymorphism, their thermosalient behaviour and thermally-induced polymorphic interconversions have been very poorly studied or not at all. This chapter has discussed the polymorphic transformations and thermosalient effect in various symmetrical methoxy-substituted bis(aryl)ureas. We were able to methodically examine the relationship between the position of the methoxy-substituent on the aryl ring and the assembly of molecules in the crystal structure. This, in turn, affected how the atoms and molecules change their orientation and mutual arrangement during polymorphic transformation, thus influencing the thermosalient behavior observed in several members of this family of compounds. A total of 12 compounds were synthesized and seven new crystal structures (including previously not known polymorphs) were obtained. Of which, a total of three thermosalient crystals were developed, namely 4-methoxy- (**1c**), 3,4-dimethoxy- (**2c**) and 3,4,5-trimethoxy-bis(aryl)urea (**3a**). In particular, **3a** exhibited intense, readily observable thermosalient behaviour with high reversibility, as evidenced by HSM and cyclic DSC experiments. Analysis of the crystal structures of the polymorphs of all three thermosalient compounds, before and after their respective SC-SC polymorphic transformations, revealed a possible explanation for the origin of the occurrence of their thermosalient behavior. It is proposed that, upon heating, the aryl rings of each molecule twist into opposite directions around the urea moiety. Such twisting of the aryl rings could have caused a buildup, and subsequent release of strain along one direction in the crystal structure. This rapid anisotropic change in the unit cell then translates into an observable macro physical event: jumping/flipping motion of the crystal. As a continuation of this research program directed towards the discovery and, eventually, design of thermosalient molecular solids, I am planning to extend this investigation to other Etter-type ureas containing other functional groups (Fig. 7.18), such as halogens, extended π-systems and alkyl functionalities.

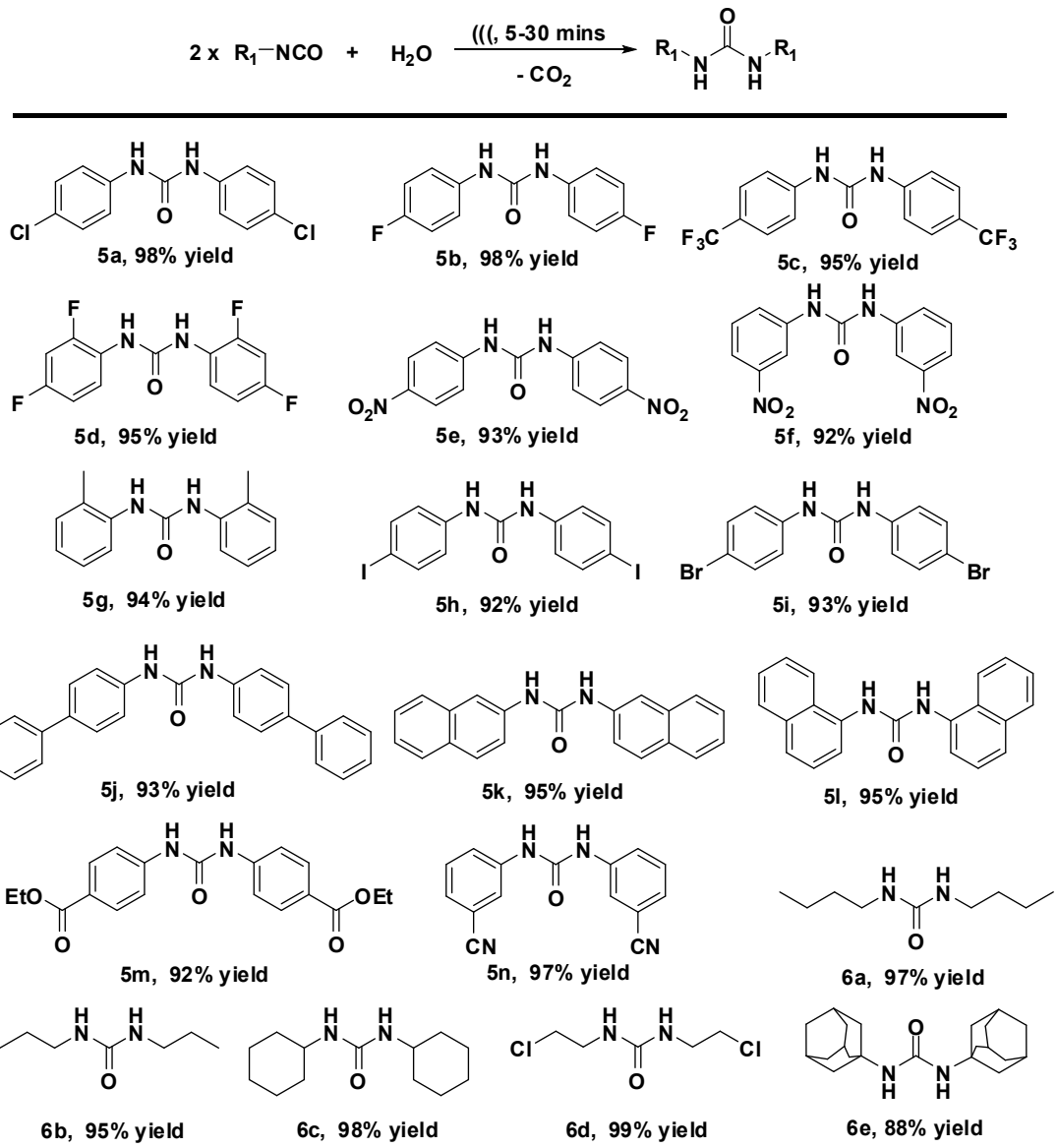

Fig. 7.18. Extended list of symmetrical *N,N'*-bis(aryl)ureas and *N,N'*-bis(alkyl)ureas that were synthesized and currently being investigated for thermosalient behaviour.

7.10 References

1 a) I. McConnell, G. Li, G. W. Brudvig, *Chem. Biol.*, **2010**, *17*, 434; b) P. Calvert, *Chem. Mater.*, **1996**, *8*, 1715; c) H. M.Wache, D. J. Tartakowska, A.Hentrich, M. H.Wagner, *J. Mater. Sci.: Mater. Med.*, **2003**, *14*, 109; d) I. Bellin, S. Kelch, R. Langer, A. Lendlein, *Proc. Natl. Acad. Sci. U. S. A.*, **2006**, *103*, 18043; e) A. Metcalfe, A.-C. Desfaits, I. Salazkin, L. Yahia, W. M. Sokolowski, J. Raymond, *Biomaterials*, **2003**, *24*, 491.

2 a) S. Juodkazis, N. Mukai, R. Wakaki, A. Yamaguchi, S. Matsuo, H. Misawa, *Nature*, **2000**, *408*, 178; b) Y. Yu, M. Nakano, T. Ikeda, *Nature*, **2003**, *425*, 145; c) H. Jiang, S.

Kelch, A. Lendlein, *Adv. Mater.*, **2006**, *18*, 1471; d) N. Spencer, J. F. Stoddart, *J. Am. Chem. Soc.*, **1991**, *113*, 5131; e) R. A. Bissell, E. Cordova, A. E. Kaifer, J. F. Stoddart, *Nature*, **1994**, *369*, 133; f) L. Fang, M. Hmadeh, J. Wu, M. A. Olson, J. M. Spruell, A. Trabolsi, Y.-W. Yang, M. Elhabiri, A.-M. Albrecht-Gary, J. F. Stoddart, *J. Am. Chem. Soc.*, **2009**, *131*, 7126; g) D. A. Leigh, J. K. Y. Wong, F. Dehez, F. Zerbetto, *Nature*, **2003**, *424*, 174.

3 a) N. K. Nath, M. K. Panda, S. C. Sahoo, P. Naumov, *CrystEngComm*, **2014**, *16*, 1850; b) P. Naumov, S. Chizik, M. K. Panda, N. K. Nath, E. Boldyreva, *Chem. Rev.*, **2015**, *115*, 12440; c) P. Commins, I. T. Desta, D. P. Karothu, M. K. Panda, P. Naumov, *Chem. Commun.*, **2016**, *52*, 13941.

4 a) O. S. Bushuyev, A. Tomberg, T. Friščić, C. J. Barrett, *J. Am. Chem. Soc.*, **2013**, *135*, 12556; b) G. Liu, J. Liu, Y. Liu, X. Tao, *J. Am. Chem. Soc*., **2014**, *136*, 590; c) S. C. Sahoo, N. K. Nath, L. Zhang, M. H. Semreen, T. H. Al-Tel, P. Naumov, *RSC Adv.*, **2014**, *4*, 7640; d) T. Kim, L. Zhu, L. J. Mueller, C. J. Bardeen, *CrystEngComm*, **2012**, *14*, 7792; e) M. K. Panda, S. Ghosh, N. Yasuda, T. Moriwaki, G. D. Mukherjee, C. M. Reddy, P. Naumov, *Nature Chem.*, **2015**, *7*, 65; f) R. M. Mohamed, M. J. Mishra, L. M. Al-Hari, M. S. Al-Ghamdi, U. Ramamurty, *RSC Adv.*, **2015**, *5*, 64156; g) T. Kim, L. Zhu, R. O. Al-Kaysi, C. J. Bardeen*, ChemPhysChem*, **2014**, *15*, 400; h) T. Kim, M. K. Al-Muhanna, S. D. Al-Suwaidan, R. O. Al-Kaysi, C. J. Bardeen, *Angew. Chem. Int. Ed.*, **2013**, *52*, 6889; M. Irie, *Chem. Rev.,* **2000,** *100*, 1685; i) J. Liu, G. Liu, Y. Liu, X. Zheng, Q. Han, X. Ye, X. Tao, *Chem. Asian J.*, **2016**, *11*, 1682; j) O. S. Bushuyev, A. Tomberg, J. R. Vinden, N. Moitessier, C. J. Barrett, T. Friščić, *Chem. Commun.,* **2016**, *52*, 2103; k) O. S. Bushuyev, T. Friščić, C. J. Barrett, *CrystEngComm*, **2016**, *18*, 7204; l) M. K. Kumar, U. Ramamurty, G. R. Desiraju, *Curr. Opin. Solid State Mat. Sci.*, **2016**, *20*, 361; m) S. Ghosh, M. K. Mishra, S. Ganguly, G. R. Desiraju*, J. Am. Chem. Soc.*, **2015**, *137*, 9912; n) R. M. Mohamed, M. K. Mishra, L. M. Al-Harbi, M. S. Al-Ghamdi, A. M. Asiri, C. M. Reddy, U. Ramamurty, *Cryst. Growth Des.*, **2015**, *15*, 2474; o) M. K. Mishra, G. R. Desiraju, U. Ramamurty, A. D. Bond, *Angew. Chem. Int. Ed.*, **2014**, *53*, 13102; p) D. P. Karothu, J. Weston, I. T. Desta, P. Naumov, *J. Am. Chem. Soc.*, **2016**, *138*, 13298; q) R. Medishetty, A. Husain, Z. Bai, T. Runčuvski, R. E. Dinnebier, P. Naumov, J. J. Vittal, *Angew. Chem. Int. Ed.*, **2014**, *53*, 5907; r) I.-H. Park, R. Medishetty, H.-H. Lee, C. E. Muljanto, H. S. Quah, S. S. Lee, J. J. Vittal, *Angew. Chem. Int. Ed.*, **2015**, *54*, 7313.

5 M. C. Etter, A. R. Siedle, *J. Am. Chem. Soc.*, **1983**, *105*, 641.

6 J. Gigg, R. Gigg, S. Payne, R. Conant, *J. Chem. Soc., Perkin Trans. 1*, **1987**, 2411.

7 a) M. –X. Zhang, P. M. Kelly, *Prog. Mater. Sci.*, **2009**, 54, 1101; b) C. M. Wayman, H. K. D. H. Bhadeshia, *Physical Metallurgy*, 4th ed.; Cahn, R. W., Haasen, P., Eds., Elsevier Science BV: New York, **1996**, 1507.

8 a) Ž. Skoko, S. Zamir, P. Naumov, J. Bernstein, *J. Am. Chem. Soc.,* **2010**, *132*, 14191; b) M. K. Panda, T. Runčevski, R. E. Dinnebier, P. Naumov, *J. Am. Chem. Soc.*, **2015**, *137*, 1895; c) S. C. Sahoo, M. K. Panda, N. K. Nath, P. Naumov, *J. Am. Chem. Soc.*, **2013**, *135*, 12241; d) M. K. Panda, R. Centore, M. Causá, A. Tuzi, F. Borbone, P. Naumov, *Sci. Rep.*, **2016**, *DOI: 10.1038/srep29610*; e) E. Nauha, P. Naumov, M. Lusi, *CrystEngComm*, **2016**, *18*, 4699; f) J.-H. Ko, K.-S. Lee, S. C. Sahoo, P. Naumov, *Solid-State Commun.*, **2013**, *173*, 46; g) T. Shima, T. Muraoka, N. Hoshino, T. Akutagawa, Y. Kobayashi, K. Kinbara, *Angew. Chem. Int. Ed.*, **2014**, *53*, 7173; h) O. Crottaz, F. Kubel, H. Schmid, *J. Mater. Chem.*, **1997**, *7*, 143; i) J. W., Edwards, G. L. Kington, R. Mason, *Trans. Faraday Soc.*, **1960**, *56*, 660; j) J. S. Bodenheimer, W. Low, *Phys. Lett. A*, **1971**, *36*, 253; k) C. Brandel, Y. Cartigny, N. Couvrat, M. E. S. Eusébio, J. Canotilho, S. Petit, G. Coquerel, *Chem. Mater.*, **2015**, *27*, 6360; l) S. C. Sahoo, S. B. Sinha, M. S. R. N. Kiran, U. Ramamurty, A. F. Dericioglu, C. M. Reddy, P. Naumov, *J. Am. Chem. Soc.*, **2013**, *135*, 13843; m) T. Takeda, T. Akutagawa, *Chem. Eur. J.*, **2016**, *22*, 7763; n) M. K.; Panda, T. Runćevski, S. C. Sahoo, A. A. Belik, N. K. Nath, R. E. Dinnebier, P. Naumov, *Nat. Commun.*, **2014**, *5*, 4811; o) T. Steiner, W. Hinrichs, W. Saenger, R. Gigg, *Acta Crystallogr. Sect. B: Struct. Sci.*, **1993**, *B49*, 708; p) B. Kohne, K. Praefcke, G. Mann, Perhydropyren, ein beim Phasenuebergang Huepfender Kohlenwasserstoff, *Chimia*, **1988**, *42*, 139; q) S. Zamir, J. Bernstein, D. J. A. Greenwood, *Mol. Cryst. Liq. Cryst. Sci. Technol., Sect. A*, **1994**, *242*, 193; r) J. Ding, R. Herbst, K. Praefcke, B. Kohne, W. Saenger, *Acta Crystallogr., Sect. B: Struct. Sci.*, **1991**, *47*, 739; s) C. J. Brown, *Acta Crystallogr., Sect. C: Cryst. Struct. Commun.*, **1984**, *40*, 1762; t) Z. A. Dreger, Y. Tao, Y. M. Gupta, *Chem. Phys. Lett.*, **2013**, *584*, 83; u) J. M. Corbett, M. H. Dickman, *Acta Crystallogr., Sect. C: Cryst. Struct. Commun.*, **1996**, *52*, 1851; v) H. Takemura, *Chemistry*, **2005**, 60, 46; w) R. Boese, J. K. Cammack, A. J. Matzger, K. Pflug, W. B. Tolman, K. P. C Vollhardt, T. W. Weidman*, J. Am. Chem. Soc.*, **1997**, *119*, 6757; x) M. A. Fernandes, D. C. Levendis, F. R. L. Schoening, *Acta Crystallogr., Sect. B: Struct. Sci.*, **2004**, *60*, 300; y) H. Wu, N. Reeves-McLaren, J. Pokorny, J. Yarwood, A. R. West, *Cryst. Growth Des.*, **2010**, *10*, 3141; z) R. Centore, M. Jazbinsek, A. Tuzi, A. Roviello, A. Capobianco, A. Peluso, *CrystEngComm*, **2012**, *14*, 2645.

9 V. I. Ovcharenko, S. V. Fokin, E. Yu, O. V. Kuznetsova, E. V. Tretyakov, G. V. Romanenko, A. S. Bogomyakov, *Inorg. Chem.*, **2011**, *50*, 4307.

10 a) G. R. Desiraju, *Angew. Chem. Int. Ed.*, **1995**, *34*, 2311; b) G. R. Desiraju, *Acc. Chem. Res.*, **2002**, *35*, 565.

11 a) M. C. Etter, Z. Urbańczyk-Lipkowska, M. Zia-Ebrahimi, T. W. Panunto, *J. Am. Chem. Soc.,* **1990**, *112*, 8415; b) K.-S. Huang, D. Britton, M. C. Etter, S. R. Byrn, *J. Mater. Chem.*, **1995**, *5*, 379.

12 W. H. Ojala, *Cryst. Growth Des.*, **2016**, *16*, 1144.

13 a) M. C. Etter, *Acc. Chem. Res.,* **1990**, *23*, 120; b) M. C. Etter, J. C. Macdonald, *Acta Crystallogr., Sect. B: Struct. Sci.*, **1990**, *46*, 256; c) J. Bernstein, R. E. Davis, L. Shimoni, N.-L. Chang, *Angew. Chem. Int. Ed.*, **1995**, *34*, 1555.

14 a) V. Štrukil, M. D. Igrc, L. Fábián, M. Eckert-Maksić, S. L. Childs, D. G. Reid, M. J. Duer, I. Halasz, C. Mottillo, T. Friščić, *Green Chem.*, **2012**, *14*, 2462; b) W.-D. Pfeiffer , K.-D. Ahlers , A. Falodun , A.Villinger, P. Langer, *Phosphorus Sulfur Silicon Relat. Elem.,* **2014**, *189*, 324.

15 a) K. S. Suslick, N. C. Eddingsaas, D. J. Flannigan, S. D. Hopkins, H. Xu, *Ultrasonics Sonochem.*, **2011**, *18*, 842; b) K. S. Suslick, *Faraday Discuss.*, **2014**, *170*, 411; c) G. Shkapenko, G. T. Gmitter, E. E. Gruber, *Ind. Eng. Chem.*, **1960**, *52*, 605.

16 I. Halasz, *Cryst. Growth Des.*, **2010**, *10*, 2817.

17 S. L. Huth, T. L. Threlfall, M. B. Hursthouse, *Univ. Southampton Crystal Structure Report Archive*, **2008**, *doi:10.5258/ecrystals/680*.

18 a) D. Das, T. Jacobs, L. J. Barbour, *Nat. Mater.*, **2010**, *9*, 36; b) H. Birkedal, D. Schwarzenbach, P. Pattison, *Angew. Chem., Int. Ed.*, **2002**, *41*, 754.

19 a) H. Khan, N. Daraz, M. N. Khan, M. Said, N. Akhtar, A. Badshah, A. S. Khan, M. Ali, *Bioinorg. Chem. Appl.*, **2014**, 1; b) J. van Rooyen, R. Betz, B. J. A. M. van Brecht, *Acta Crystallogr. Sect. E Struc. Rep.*, **2011**, *67*, 2889; c) Shashidhar, V. Thiruvenkatam, S. A. Shivashankar, M. B. Halli, T. N. G. Row, *Acta Crystallogr. Sect. E Struc. Rep.,* **2006**, *62*, 1518.

CHAPTER 8
EXPERIMENTAL DETAILS

This chapter outlines the synthetic and analytical methods used in all experiments discussed within this Dissertation. Synthetic details are divided by chapters, while detailed instrumental analysis has been generalized for all chapters in the interest of concision.

8.1 Experimental details for Chapter 2: Mechanosynthesis of pharmaceutically-relevant sulfonyl(thio)ureas.

8.1.1 Experimental section.

Syntheses of various sulfonyl(thio)urea compounds were carried out in a Retsch MM400 mill at a frequency of 30 Hz using a 10 mL stainless steel milling jar and a single ball made of the same material (diameter 10 mm). Gram scale synthesis reactions were carried out in a 25 mL stainless steel milling jar. ^{1}H- and ^{13}C-NMR spectra were recorded on a Varian MERCURY Plus-300 or Plus-400 spectrometer (300 or 400 MHz), and chemical shifts (δ) given in parts per million (ppm). The molecular weights of the pure products were determined using high-resolution mass spectra (HRMS). FTIR-ATR spectra were collected using a Fourier-transform infrared attenuated total reflection PerkinElmer Spectrum Two spectrometer in the range 400 cm^{-1} to 4000 cm^{-1}. Single crystal X-ray diffraction data was obtained on a Bruker VENTURE system using a MoKα or CuKα source.

8.1.2 Synthesis using copper catalyst

A mixture of 0.50 mmol of sulfonamide, 0.50 mmol of isocyanate (1 equiv.), 0.025 mmol (5% mol) of CuCl and nitromethane as the grinding liquid (η= 0.25 μL/mg) was milled at a frequency of 30 Hz for 2 hrs. After the reaction, 3mL of deionized water and 20 mg of $Na_2H_2EDTA{\cdot}2H_2O$ were added to the crude mixture, which was subsequently milled for 10 mins at a frequency of 25 Hz. The product was purified *via* vacuum filtration and dried.

For gram-scale synthesis, 5.0 mmol of sulfonamide, 5.0 mmol of isocyanate (1 equiv.), 0.25 mmol (5% mol) of CuCl and nitromethane as the grinding liquid (η= 0.25 μL/mg) were milled at a frequency of 30 Hz for 2 hrs. The reaction was carried out using two 10 mm diameter stainless steel balls in a 25 mL stainless steel jar. After the reaction, 15 mL of deionized water and 200 mg of $Na_2H_2EDTA{\cdot}2H_2O$ were added to the crude reaction mixture, which was subsequently milled for 10 mins at a frequency of 25 Hz. The product was purified *via* vacuum filtration and dried.

8.1.3 Base-assisted synthesis using K_2CO_3

A mixture of 0.50 mmol of sulfonamide and 0.50 mmol of K_2CO_3 (1 equiv.) was milled at a frequency of 30 Hz for 1hr. Then, 0.50 mmol isocyanate or isothiocyanate (1 equiv.) was added and the mixture subsequently milled for another 2 hrs at 30 Hz. Next, 20 mL of deionized water and dilute HCl were added to the crude reaction mixture. The pH of the resultant suspension was monitored using pH paper until pH= 3 was reached and then left to stir for 15 mins. The product was purified *via* vacuum filtration and dried.

For gram-scale synthesis, a mixture of 5.0 mmol of sulfonamide and 5.0 mmol of K_2CO_3 (1 equiv.) was milled at a frequency of 30 Hz for 1hr. Then, 5.0 mmol isocyanate or isothiocyanate (1 equiv.) was added and subsequently milled for another 2 hrs at 30 Hz. The reaction was carried out using two 10 mm diameter stainless steel balls in a 25 mL stainless steel jar. After the reaction, 20 mL of deionized water and dilute HCl were added to the crude reaction mixture. The pH of the resultant suspension was monitored using pH paper until pH= 3 was reached and then left to stir for another 15 mins. The product was purified *via* vacuum filtration and dried.

8.1.3 Pathway B for synthesis of tolbutamide 1a

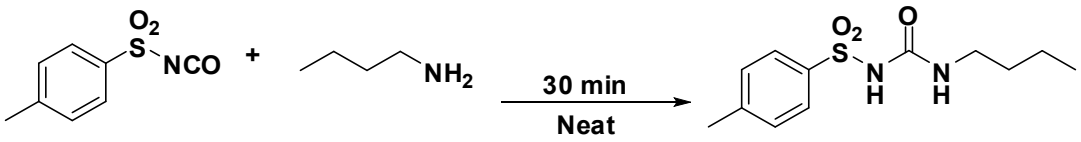

The mechanosynthesis of tolbutamide **1a** (93% yield) was also carried out between *p*-toluenesulfonyl-isocyanate and *n*-butyl-amine (retrosynthetic pathway B in the main paper). 0.50 mmol of *p*-toluenesulfonyl-isocyanate and 0.50 mmol of *n*-butyl-amine were added to a 25 mL stainless steel jar with one 10 mm diameter stainless steel ball. The mixture was milled at a frequency of 30 Hz for 30 min. Because of high reactivity of *p*-toluenesulfonyl-isocyanate, the reaction was prepared in a glovebox. The solid obtained after milling was then scrapped from the milling jar without further purification.

[1] D. Tan, V. Štrukil, C. Mottillo, T. Friščić, *Chem. Commun.,* **2014**, *50*, 5248.

8.2 Experimental details for Chapter 3: Development of C-N coupling using mechanochemistry: catalytic coupling of sulfonamides and carbodiimides

8.2.1 Experimental section.

Syntheses of various sulfonylguanidine compounds were carried out in a Retsch MM400 mill at a frequency of 30 Hz using a 10 mL stainless steel milling jar and a single ball made of the same material (diameter of 10 mm). Gram-scale synthesis reactions were carried out in a 25 mL stainless steel milling jar and two balls made of the same material. ^{1}H and ^{13}C-NMR spectra were recorded on a Varian MERCURY Plus-300 (300 MHz), spectrometer and chemical shifts (δ) given in parts per million (ppm). The molecular weights of the pure products were determined using high-resolution mass spectra (HRMS). FTIR-ATR spectra were collected using a Fourier-transform infrared attenuated total reflection PerkinElmer Spectrum Two spectrometer in the range 400 cm^{-1} to 4000 cm^{-1}. Single crystal X-ray diffraction data was obtained on a Bruker VENTURE system using a MoKα or CuKα source.

8.2.2 Synthesis by copper catalysis

A mixture of 0.50 mmol of sulfonamide, 0.50 mmol of carbodiimide (1 equiv.), 0.025-0.050 mmol (5-10% mol) of CuCl and nitromethane as the grinding liquid (η= 0.25 μL/mg) was milled at a frequency of 30 Hz for 2 hrs. After the reaction, 3 mL of deionized water and 20-40 mg of $Na_2H_2EDTA{\cdot}2H_2O$ were added to the crude reaction mixture, which was subsequently milled for 10 mins at a frequency of 25 Hz. The product was purified *via* vacuum filtration and dried.

For gram-scale syntheses, a mixture of the 5.0 mmol of sulfonamide, 5.0 mmol of carbodiimide (1 equiv.), 0.50 mmol (10% mol) of CuCl and nitromethane grinding liquid (η= 0. 25 μL/mg) was milled at a frequency of 30 Hz for 2 hrs. The reaction was carried out using three 10 mm diameter stainless steel balls in a 25 mL stainless steel jar. After the reaction, 15 mL of deionized water and 400 mg of $Na_2H_2EDTA{\cdot}2H_2O$ were added to the crude reaction mixture, and subsequently milled for 10 mins at a frequency of 25 Hz. The product was purified *via* vacuum filtration and dried.

8.2.3 Test reaction using di-o-tolyl-carbodiimide (DOTC)

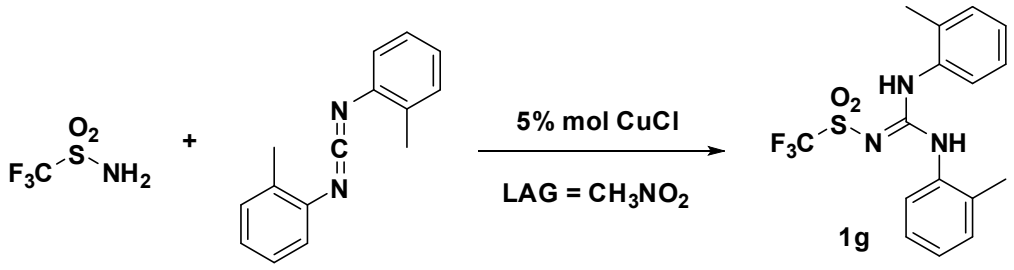

73% conversion by ^{1}H NMR.

The ability to conduct the synthesis of trifluoromethylsulfonylguanidine by a coupling reaction of di-(*o*-tolyl)carbodiimide (DOTC) was verified using only two experiments, due to the forbidding cost of this reagent. A mixture of 0.50 mmol of the sulfonamide, 0.50 mmol of the carbodiimide (1 equiv.), 0.025-0.050 mmol (5-10% mol) of CuCl and nitromethane as the grinding liquid (η= 0. 25 μL/mg) was milled at a frequency of 30 Hz for 2 hrs. After the reaction, 3 mL of deionized water and 20-40 mg of $Na_2H_2EDTA{\cdot}2H_2O$ was added to the crude reaction mixture, which was subsequently milled for 10 mins at a frequency of 25 Hz. The product was purified *via* vacuum filtration and dried. Based on NMR spectroscopy, the reaction proceeded to 73% conversion and, while no further purification was performed, the identity of the product was confirmed by MS. An analogous reaction was attempted without the addition of CuCl catalyst, without any success.

8.2.4 Test reaction using di-trimethylsilyl-carbodiimide (DTMSC)

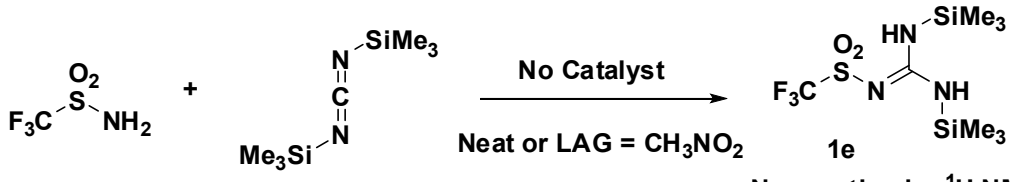

No reaction by ^{1}H NMR and IR

A mixture of 0.50 mmol of sulfonamide, 0.50 mmol carbodiimide (1 equiv.), and nitromethane as the grinding liquid (η= 0. 25 μL/mg) was milled at a frequency of 30 Hz for 2 hrs. After the reaction, the crude reaction was subjected to ^{1}H-NMR and FTIR-ATR spectroscopy. Based on botH-NMR and IR spectroscopy, the reaction did not take place at all, recovering back both starting materials. Similar spectra were also observed for the crude mixtures resulting from reactions with *p*-tolylsulfonamide and *p*-chlorophenylsulfonamide in attempts to form **2e** and **3e**, respectively. However, the absorption band at 2180cm^{-1} in the FTIR spectrum indicates the presence of unreacted DTMSC.

8.3 Experimental details for Chapter 4: Carbodiimide insertion into sulfonimides: one-step route to azepine derivatives by a two-atom saccharin ring expansion

8.3.1 Experimental section

Mechanosyntheses of various benzo[1,3]thiadiazepine compounds were carried out in a Retsch MM400 mill at a frequency of 30 Hz using a 10 mL stainless steel milling jar and a single ball made of the same material (diameter of 10 mm). Solution syntheses of the same compounds were performed using a 50 mL one-neck round bottom flask with a small magnetic stirrer bar. ^{1}H- and ^{13}C-NMR spectra were recorded on a Varian MERCURY Plus-300 (300 MHz) or Bruker AVANCE III (500 MHz) spectrometer and chemical shifts (δ) given in parts per million (ppm). The molecular weights of the pure products were determined using high-resolution mass spectra (HRMS). FTIR spectra were collected using a Fourier-transform infrared attenuated total reflection PerkinElmer Spectrum Two spectrometer in the range 400 cm^{-1} to 4000 cm^{-1}. Powder X-ray Diffraction data was obtained on a benchtop Bruker D2 Phaser using a Cu-source. Single crystal X-ray diffraction data was obtained on a Bruker VENTURE system using a MoKα or CuKα source.

8.3.2 Synthesis by ball milling

For compounds **1-4, 8-11**:

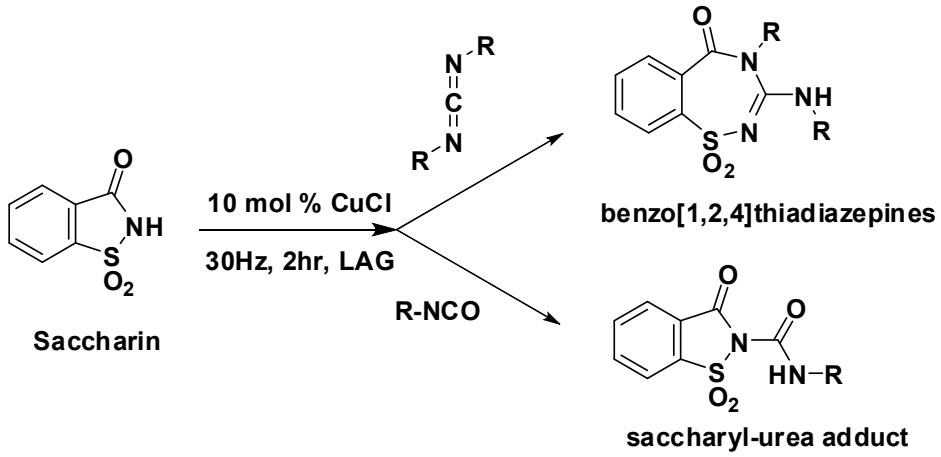

For milligram scale reactions: a mixture of 0.50 mmol of saccharin, 0.50 mmol of respective carbodiimide or isocyanate (1 equiv.), 0.025-0.050 mmol (5-10% mol) of CuCl and nitromethane or acetone as the grinding liquid (η= 0. 25 μL/mg) was milled in a 10mL stainless steel jar with one stainless steel ball of 10 mm diameter, at a frequency of 30 Hz for 2 hrs. After the reaction, 3 mL of deionized water and 20-40 mg of $Na_2H_2EDTA{\cdot}2H_2O$ was added to the crude mixture and subsequently milled for 10 mins at a frequency of 25 Hz. The product was purified *via* vacuum filtration and dried. The product can also be purified *via*

flash column chromatography using a mixture of ethyl acetate and hexane in a 1:2 respective ratio as the mobile phase.

For gram scale reactions: a mixture of 5 mmol of saccharin, 5 mmol of respective carbodiimide (1 equiv.), 0.25-0.50 mmol (5-10% mol) of CuCl and acetone as the grinding liquid liquid (η= 0. 25 μL/mg) was milled in a 25 mL stainless steel milling jar with two stainless steel balls of 10 mm diameter, at a frequency of 30 Hz for 2 hrs. After the reaction, 15mL of deionized water and 200-400 mg of $Na_2H_2EDTA{\cdot}2H_2O$ was added to the crude mixture and subsequently milled for 10 mins at a frequency of 25 Hz. The product was purified *via* vacuum filtration and dried.

8.3.3 Synthesis by solution method

For compounds **1**-**4**:

For milligram scale reactions: 1 mmol of saccharin, 1 mmol of respective carbodiimide (1 equiv.), were placed in a 20 mL (6 dram) vial with a stir bar using 10 mL of solvent (either acetone, ethyl acetate or acetonitrile). The solution mixtures were then heated to reflux temperatures for 2 hr. The solvent was then removed *in vacuo* and the product was purified using flash column chromatography, with a 1:2 ethyl acetate:hexane mixture as the mobile phase.

For gram scale reactions: a mixture of 5 mmol of saccharin and 5 mmol of respective carbodiimide (1 equiv.) was placed in a 50 mL round bottom flask with 25 mL of acetone as the solvent. The reaction was then stirred overnight at room temperature. The solvent was then removed *in vacuo* and extracted using ethyl acetate and an aqueous solution of $Na_2H_2EDTA{\cdot}2H_2O$. The combined organic layers were dried using $MgSO_4$, and the product was purified using silica column chromatography (ethyl acetate and hexane in a 1:1 ratio). Specifically for compound **4**, purification using column chromatography was performed using a gradient elution with mobile phase consisting of 1:5→1:3→1:1 ethyl acetate to hexane mixture.

8.3.3.1 Synthesis of N-methylsaccharin:

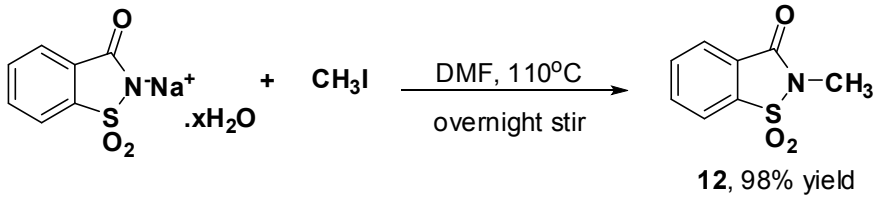

12, 98% yield

N-methylsaccharin **12** was synthesized using a modified protocol by Fernández-Tomé *et al.*[2] A solution mixture of 10 mmol hydrated sodium saccharinate and 10 mmol iodomethane (1 equiv.alent) in 100 mL of dimethylformamide (DMF) is heated to 110 °C and allowed to stir overnight in a 250 mL round bottom flask. Then, the reaction mixture is allowed to cool to ambient temperature and poured into a beaker containing 100 mL of deionized water. The resulting white precipitate is filtered and washed with water and recrystallized using a mixture of ethanol and water in a 2:1 ratio. Attempted reaction of **12** with DIC performed solvothermally in solution or mechanochemically (with and/or without CuCl catalyst added) did not show any reactivity.

*8.3.3.2 Synthesis of 4-methyl-N-tosylbenzamide **5**:*

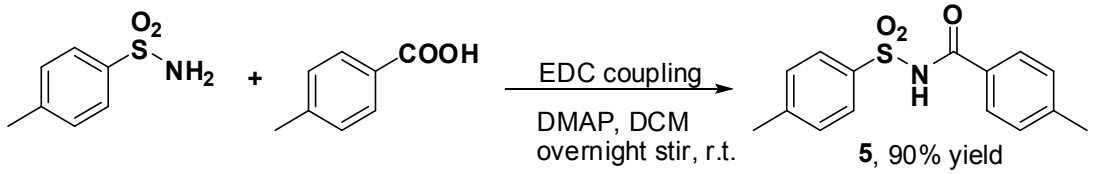

5, 90% yield

A solution of 10 mmol 4-tolylsulfonamide, 10 mmol 4-methylbenzoic acid (1 equiv.alent), 11 mmol 1-ethyl-3-(3-dimethylaminopropyl)-carbodiimide (1.1 equiv.), 10 mmol 4-dimethylamino-pyridine (1 equiv.alent) in 150 mL of dichloromethane was stirred overnight at room temperature in a 250 mL round bottom flask. The reaction mixture was then extracted exhaustively with 5 M sulfuric acid and the organic layer collected was removed *in vacuo*. The desired 4-methyl-*N*-tosylbenzamide product was purified *via* flash column chromatography using silica, with ethyl acetate as the eluting solvent.

*8.3.3.3 Synthesis of compound **6a**:*

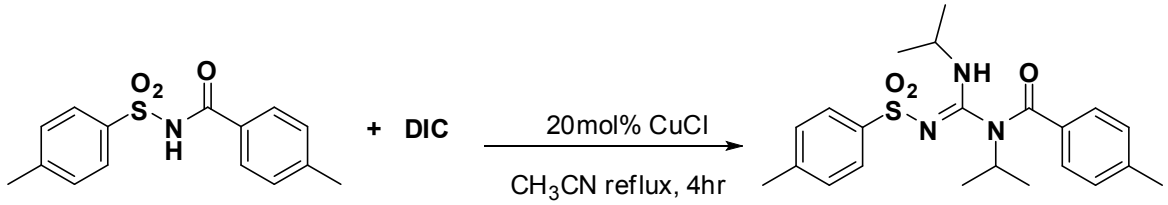

6, 99% conversion,
87% isolated yield

A solution of 2 mmol 4-dimethylamino-pyridine and 2 mmol diisopropylcarbodiimide was refluxed in 25 mL acetonitrile for 4 hr using 20mol% CuCl as the catalyst in a 50 mL round bottom flask. Alternatively, the reaction can be refluxed in acetone for 2 days. The reaction was monitored using thin layer chromatography, with a 1:1 ethyl acetate to hexane mixture as mobile phase (R_f value of product is 0.6 for neutral alumina or 0.1 for silica). After the reaction was complete, the solvent was removed *in vacuo* and the catalyst is removed by extraction using ethyl acetate and aqueous solution of $Na_2H_2EDTA{\cdot}2H_2O$. The product was purified by flash column chromatography using neutral alumina as the stationary phase, and a mixture of ethyl acetate and hexane in a 1:3 ratio as the mobile phase, followed by another column chromatography step using silica and gradient elution of ethyl acetate and hexane mixtures in 1:5→1:3→1:1 ratios.

*8.3.3.4 Synthesis of compound **6b**:*

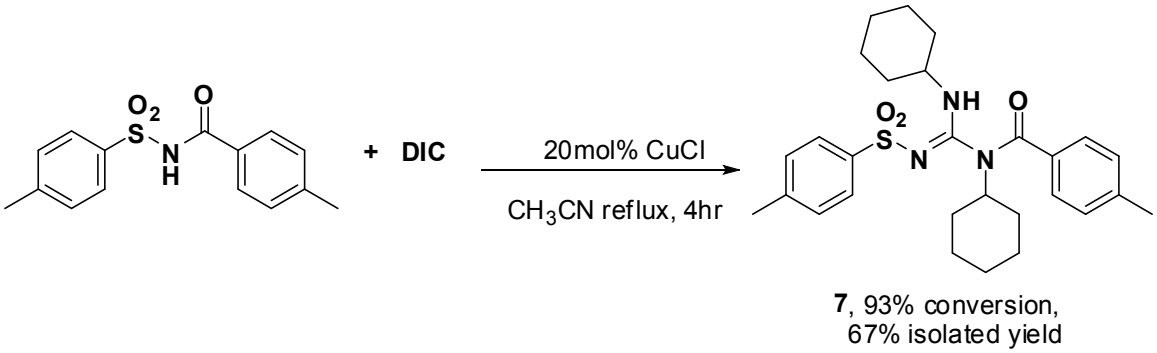

7, 93% conversion,
67% isolated yield

A solution of 2 mmol 4-dimethylamino-pyridine and 2 mmol diisopropylcarbodiimide was refluxed in 25 mL acetonitrile for 4hrs using 20mol% CuCl as the catalyst in a 50 mL round bottom flask. The solvent is removed *in vacuo* and the catalyst is removed by extraction using ethyl acetate and an aqueous solution of $Na_2H_2EDTA{\cdot}2H_2O$. Based on crude ^{1}H-NMR, the reaction achieved 93% conversion. The desired product was then recrystallized from acetone in 67% isolated yield.

[2] M. P. Fernández-Tomé, R. Madroñero, J. del Rio, S. Vega, *J. Med. Chem.*, **1972**, *15*, 887.

8.4 Experimental details for Chapter 5: Base-free mechanochemical copper-catalyzed amide coupling of isatins, benzamides and imides with isocyanates

8.4.1 Experimental section

Mechanosynthesis of various compounds were carried out in a Retsch MM400 mill at a frequency of 30 Hz using a 10 mL stainless steel milling jar and a single ball made of the same material (diameter of 10 mm). ^{1}H- and ^{13}C-NMR spectra were recorded on a Varian MERCURY Plus-300 (300 MHz) spectrometer and chemical shifts (δ) given in parts per million (ppm). The molecular weights of the pure products were determined using high-resolution mass spectra (HRMS). FTIR-ATR spectra were collected using a Fourier-transform infrared attenuated total reflection PerkinElmer Spectrum Two spectrometer in the range 400 cm^{-1} to 4000 cm^{-1}. Single crystal X-ray diffraction data was obtained on a Bruker VENTURE system using a MoKα or CuKα source.

8.4.2 Synthesis by ball milling

For milligram syntheses, a mixture of 0.50 mmol of isatin or benzamide or imide, 0.50-0.60 mmol of respective isocyanate (1-1.2 equiv), 0.025-0.050 mmol (5-10% mol) of CuCl, and nitromethane, ethyl-methyl-ketone or acetone as the grinding liquid (η = 0. 25 μL/mg) was milled at a frequency of 30 Hz for 2-4 hrs. After the reaction, 3 mL of deionized water and 20-40 mg of $Na_2H_2EDTA{\cdot}2H_2O$ were added to the crude reaction mixture and subsequently milled for 10 mins at a frequency of 25 Hz. For the synthesis of carbamoyl-isatin and carbamoyl-benzamide compounds, the products were purified by washing with warm distilled water and then dried *via* vacuum filtration. For carbamoyl-imide compounds, the products were purified by extraction with ethyl acetate and aqueous solution of $Na_2H_2EDTA{\cdot}2H_2O$, followed by flash column chromatography using a 1:1 mixture of hexane and ethyl acetate as the eluent.

8.5 Experimental details for Chapter 6: A family of isostructural crystals from conformationally flexible *ortho*-substituted *N*,*N*'-bis(cyclohexyl)-arylsulfonylguanidines

8.5.1 Experimental section.

Mechanosyntheses of various arylsulfonylguanidines were carried out in a Retsch MM400 mill at a frequency of 30 Hz using a 10 mL stainless steel milling jar and a single ball made of the same material (diameter of 10 mm). Solution syntheses of some of the compounds were performed in a 50 mL one-neck round bottom flask with a small magnetic stirrer bar. ^{1}H- and ^{13}C-NMR spectra were recorded on a Varian MERCURY Plus-300 (300 MHz) or Bruker AVANCE III (500 MHz) spectrometer with chemical shifts (δ) given in parts per million (ppm). The molecular weights of the pure products were determined using high-resolution mass spectra (HRMS). FTIR-ATR spectra were collected using a Fourier-transform infrared attenuated total reflection PerkinElmer Spectrum Two spectrometer in the range 400 cm^{-1} to 4000 cm^{-1}. Powder X-ray diffraction data was obtained on a benchtop Bruker D2 Phaser using a Cu-source. Single crystal X-ray diffraction data was obtained on a Bruker VENTURE system using a MoKα, GaKα or CuKα source.

8.5.2 Synthesis by ball milling

For milligram scale reactions: a mixture of 0.50 mmol of arylsulfonamide, 0.50 mmol of respective carbodiimide (1 equiv.), 0.025-0.050 mmol (5-10% mol) of CuCl and nitromethane or acetone as the grinding liquid (η= 0. 25 μL/mg) was milled in a 10 mL stainless steel jar with one stainless steel ball of 10 mm diameter, at a frequency of 30 Hz for 2 hrs. After the reaction, 3 mL of deionized water and 20-40 mg of $Na_2H_2EDTA{\cdot}2H_2O$ were added to the crude reaction mixture, which was subsequently milled for 10 mins at a frequency of 25 Hz. The product was purified *via* vacuum filtration and dried. The product can also be purified *via* extraction using ethyl acetate and aqueous solution of $Na_2H_2EDTA{\cdot}2H_2O$.

For gram scale reactions: a mixture of 5 mmol of arylsulfonamide, 5 mmol of respective carbodiimide (1 equiv.), 0.25-0.50 mmol (5-10% mol) of CuCl and acetone as the grinding liquid liquid (η= 0. 25 μL/mg) was milled in a 25 mL stainless steel milling jar with two stainless steel balls of 10 mm diameter, at a frequency of 30 Hz for 2 hrs. After the reaction, 15 mL of deionized water and 200-400 mg of $Na_2H_2EDTA{\cdot}2H_2O$ were added to the crude reaction mixture and subsequently milled for 10 mins at a frequency of 25 Hz. The product was purified *via* vacuum filtration and dried. The product can also be purified *via* extraction using ethyl acetate and aqueous solution of $Na_2H_2EDTA{\cdot}2H_2O$.

8.5.3 Synthesis by solution method

A mixture of 5 mmol of arylsulfonamide, 5 mmol of respective carbodiimide (1 equiv.), were placed in a 50 mL round bottom flask using 25 mL of either toluene or a mixture of xylenes as the solvent. The reaction was then refluxed for 3 days. The solvent was then removed *in vacuo* and extracted using ethyl acetate and aqueous solution of $Na_2H_2EDTA{\cdot}2H_2O$.

8.5.4 Growing of single crystals

For growing single-component crystals, 50 mg of purified compound was dissolved in a 25 mL (6 dram) vial using either acetone or methanol, or a mixture of both in a 1:1 ratio, as the solvent. The obtained solution was then filtered through a short silica/cotton plug and subsequently placed on the benchtop or in a vacuum dissicator, until small crystals appeared. For compound **12**, toluene was used for crystal growing as other solvents did not yield diffraction-quality crystals.

For multi-component crystals, 0.25 mmol of each individual components were dissolved in a 25 mL (6 dram) vial using either acetone or methanol, or a mixture of both in a 1:1 ratio, as the solvent. The obtained solution was then filtered through a short silica/cotton plug and subsequently placed on the benchtop or in a vacuum dissicator, until small crystals appeared.

8.6 Experimental details for Chapter 7: Evolution through design: a serendipitous discovery, systematic investigation and design of a new thermosalient crystal based on Etter-type *N*,*N*'-bis(aryl)ureas

8.6.1 Experimental section.

Mechanosyntheses of various thiourea compounds were carried out in a Retsch MM400 mill at a frequency of 30 Hz using a 10 mL stainless steel milling jar and a single ball made of the same material (diameter of 10 mm). Sonochemical syntheses of the various urea compounds were performed in 50 mL round bottom flask or 25mL (6 dram) vials in a Fisherbrand FB11207 ultrasonic bath. ^{1}H- and ^{13}C-NMR spectra were recorded on a Varian MERCURY Plus-300 (300 MHz) with chemical shifts (δ) given in parts per million (ppm). The molecular weights of the pure products were determined using high-resolution mass spectra (HRMS). Infra-red spectrums of the compounds were taken using Bruker Vertex 70 ATR-FTIR, in the range 400 cm^{-1} to 4000 cm^{-1}. Powder X-ray diffraction data was obtained on a benchtop Bruker D2 Phaser using a Cu-source. Single crystal X-ray diffraction data was obtained on a Bruker VENTURE system using a MoKα or CuKα source. TGA and DSC data were obtained on TA Instrument Q2000 Differential Scanning Calorimeter or Mettler Toledo Simultaneous Thermal Analysis TGA/DSC system. Hot-stage microscopy videos were taken using a Leica Polarized Optical Microscope equipped with a Mettler Toledo FP84 HT Heating Stage, a FP90 Central Processor and an Infinity 1 Camera.

8.6.2 Synthesis by ball milling

For synthesis of substituted bis(aryl)thiourea:

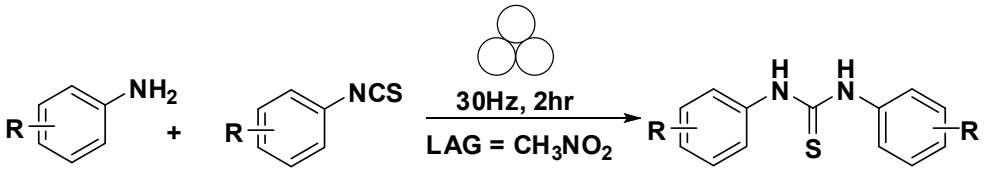

For gram scale reactions: a mixture of 5 mmol of substituted aniline, 5 mmol of respective substituted phenylisothiocyanate (1 equiv.) and nitromethane as the grinding liquid (η= 0. 25 μL/mg) was milled in a 25 mL stainless steel milling jar with two 10 mm stainless steel balls of 10 mm diameter, at a frequency of 30 Hz for 2 hrs. After the reaction, 15 mL of deionized water was added to the crude mixture and subsequently milled for 10 mins at a frequency of 25 Hz. The product was purified *via* vacuum filtration and dried.

8.6.3 Synthesis by sonochemistry

For synthesis of substituted bis(alkyl)urea and bis(aryl)ureas:

For solid isocyanates: 3-5 mmol of isocyanate was dissolved in 10 mL of acetone in a 50 mL round bottom flask. Approximately 25-30 mL of deionized water was added and the mixture was sonicated using a common laboratory sonic bath at room temperature for 30-60 min. The reaction gives off CO_2 gas, so either a balloon trap is used or the reaction vessel is open to atmosphere. After the reaction is complete *i.e.* once effervescence has stopped, the acetone/water azeotropic solvent mixture was removed *in vacuo* using a rotatory evaporator and the solid product was purified by filtration and washing with copious amounts of deionized water.

For liquid isocyanates: 3-5 mmol of isocyanate was placed in a 50 mL round bottom flask with 30-40mL of water. The reaction mixture was sonicated using a common laboratory sonic bath at room temperature for 5-30 min. The reaction gives off CO_2 gas, so either a balloon trap is used or the reaction vessel is open to atmosphere. After the reaction is complete *i.e.* once effervescence has stopped, the solid product was filtered and washed with deionized water.

8.6.4 Growing of single crystals

For growing of diffraction-quality single crystals, 100 mg of each compound was dissolved in a variety of different solvents, and crystals were obtained by slow evaporation on the benchtop for several days or weeks, or by placing in a vacuum dessicator for overnight or several days. These solvents include acetone, methanol, ethyl acetate, dimethylsulfoxide, chloroform, acetonitrile, water and dichloromethane, or a combination of several solvent mixtures.

CONCLUSION AND CONTRIBUTION TO KNOWLEDGE

In this Dissertation, mechanochemistry has been demonstrated to be a green, efficient and rapid method for the synthesis of diverse organic molecules, including biologically-active, pharmaceutically-relevant compounds. In comparison to solution-based methodologies, performing mechanochemical reactions eliminated the need for bulk solvents and thus can be considered to be more environmentally-friendly by generating less solvent waste. Without the need for bulk solvents, the issues of solubility of the starting reactants can be avoided, removing the need to find suitable but often toxic organic solvents. Such mechanochemical reactivity that is independent of solubility enables the use of alternative starting materials that can be available to synthetic chemists. As discussed in this Dissertation, mechanochemistry can not only be used to improve existing synthetic protocols, it can also be used as a powerful tool for the discovery of new reactions that were previously inaccessible using conventional solution methods.

The field of medicinal mechanochemistry, whose development was proposed in *Chapters 1* and *2*, combines mechanochemistry with the synthesis of active pharmaceutical ingredients (APIs). Although mechanochemistry has previously enabled chemists to selectively synthesize new forms of pharmaceutical solids, such as cocrystals, salts and polymorphs, recently, there has been a shift in research interests towards the use of mechanochemistry in making API molecules instead. This is an emergent area of mechanochemistry research that has recently started to gain momentum. The work presented in this Dissertation has contributed to this budding field of research by demonstrating the mechanochemical coupling of sulfonamides with isocyanates to furnish anti-diabetic sulfonylurea compounds, specifically first generation API drugs Tolubutamide® and Chlorpropamide®, and second generation drug Glibenclamide®. These mechanosyntheses were performed by using either a base-mediated one-pot two-step method, or using a new much more atom-economic one-step copper-catalyzed direct coupling reaction, in this case, without the extensive use of solvents. This is highly aligned with the demands from pharmaceutical industries to develop cleaner and more efficient synthetic methodologies. In addition, it is not unreasonable to fathom the concept of combining the two areas of medicinal mechanochemistry: combining the synthesis of an API molecule, and its cocrystallization into a one-pot two-step mechanochemical process. To the best of our knowledge, this concept has not yet been reported and could represent a new milestone in simultaneously making and fine-tuning pharmaceuticals. Preliminary results have already

shown that base-mediated synthesis of sulfonylthioureas yielded the inorganic salt of the API as final mechanochemical reaction product. Thus, the idea of synthesizing API cocrystals or salts in a one-pot manner from precursor molecular fragements using mechanochemistry is plausible and should be explored.

Parallel to the formation of APIs by mechanochemical methods is the use of mechanochemistry to discover new reactions. It must be reiterated that mechanochemistry can be utilized for reaction discovery and this has been exemplified by novel coupling reactions developed and discussed in this Dissertation. In particular, the synthesis of pharmaceutically-relevant arylsulfonylguanidine molecules from sulfonamides and carbodiimides *via* a direct copper-catalyzed mechanochemical coupling reaction has been discussed. Importantly, it was also demonstrated that this coupling reaction worked poorly when using traditional solvent-based methods, but afforded the target products in good to excellent yields at room temperature when using mechanochemistry. In addition, gram-scale sulfonamide-isocyanate/carbodiimide reactions have been performed, demonstrating the scalability of these milling processes. These multi-gram syntheses also allowed for high quality single crystals to be grown, and thus structural crystallographic characterization of the reaction products. Such crystallographic analysis revealed that several bis(cyclohexyl)-arylsulfonylguanidines crystallize in a highly unique manner, possibly caused by the presence of highly polar sulfonylguanidine units and very non-polar cyclohexyl rings. Specifically, eight of these achiral molecules formed an unprecedented family of isostructural crystals, characterized by helical self-assembly in a chiral space group. These eight compounds all shared similar molecular structures, varying only in the *ortho*-substituent functional group on the aryl ring. Additionally, other arylsulfonylguanidines were also found to exhibit unique self-assembly motifs in the solid state, such as forming hexamers (for the 4-methoxy variant) and π-stacked systems (for the 2-naphthyl variant). Currently, Hirschfeld surface calculations are being performed on these crystal structures to elucidate the relevance and distribution of intermolecular interactions between the molecules of these compounds in the solid state, and this should be completed, and reported in a form of a publication in due course.

An extensive investigation of creating C-N bonds by coupling other poorly nucleophilic substrates, such as sulfonimides, benzamides, isatins, imides *etc*, with electrophiles, such as isocyanates and carbodiimides, was performed using mechanochemical methods. This mechanochemical screening led to the discovery of a new two-atom insertion reaction involving saccharin, a cyclic sulfonimide, and carbodiimides. Structural characterization by SCXRD was vital for the correct determination of the product, which

revealed the expansion of the saccharin 5-membered ring to form a 7-membered benzo[1,2,4]thiadiazepine system. This unique insertion reaction can either be performed mechanochemically, using a copper-based catalyst, or in solution by heating. In addition, an acyclic linear variant of saccharin was synthesized, which also underwent this type of two-atom chain extension, demonstrating that ring strain was not a factor for this unique C-N insertion. The SCXRD structural data for all two-atom insertion products have been obtained and were consistent with results of other characterization techniques (NMR, FTIR-ATR and MS). Currently, density functional theory calculations are being performed to elucidate the mechanism of these insertion reactions and will be reported soon.

Although mechanochemical synthesis of amides has been reported in the literature, the functionalization of amido groups with isocyanates has not been explored. As a part of this Dissertation, the mechanochemical coupling of isatin, benzamides and imides with isocyanates to furnish their respective carbamoyl compounds, was demonstrated using new base-free and solvent-free methodology. This is part of an ongoing research program to discover and develop new coupling reactions using mechanochemistry. The resulting carbamoyl-benzamide and -isatin functional groups can be found in many biologically-active compounds, such as insecticides and pharmaceutical drug molecules. This work opens up a new opportunity to explore other type C-N coupling reactions using mechanochemistry, and thus initiated the exploration of the selective functionalization of zwitterionic reagents using mechanochemistry. Specifically, the base-free chemoselective mechanochemical C-N coupling of amino-acids, such as glycine and L-proline, with isothiocyanates, forming chiral thioureido and bicyclic thiohydantoin compounds, respectively, is currently being investigated by Dr. Dayaker Gandrath, a post-doctoral fellow in our group. This is by far the first direct route to form these functional groups by selective C-N bond formation at the positively charged nitrogen atom of zwitterionic amino-acid molecules, without the use of auxiliary bases.

Last, but not least, sonochemistry, which is a part of mechanochemistry, was used for the synthesis of symmetrical Etter-type ureas. In particular, the reaction involved the use of ultrasonic irradiation for the sonochemical blowing reaction between arylisocyanates and water, to form *N*,*N*'-bis(aryl)ureas. The ease of this synthetic methodology enabled the multi-gram scale synthesis of these molecular targets. Subsequently, it was discovered that single crystals of some of these compounds underwent thermally-induced polymorphic transformation. In particular, some of these compounds exhibited a "jumping" motion upon heating, which is also known as the thermosalient effect. This discovery prompted a

systematic investigation and development of a series of related thermosalient crystals. Although over twenty thermosalient compounds have been discovered and studied in the last few decades, these reported molecules are completely unrelated, in terms of both composition and molecular strcutres. This Dissertation has presented a so far unique, systematic study of the relationship between the positioning of functional groups on the aryl ring and the thermosalient behaviour in a family of methoxy-substituted *N*,*N*'-bis(aryl)ureas. This study utilized a diversity of solid-state characterization techniques, such as XRD, HSM and DSC. This extensive study led to the discovery of *N*,*N*'-bis(3,4,5-trimethoxyaryl)urea, a compound exhibiting pronounced thermosalient behaviour which was highly reversible. In addition, preliminary screening of other members of this unique family of compounds, revealed that *N*,*N*'-bis(2,4-difluoroaryl)urea also exhibits thermosalient behaviour. Future work should certainly include a thorough investigation of thermosalient behaviour in this compound, and also possibly having it modified by halogen bond-driven cocrystal formation.

APPENDIX A

SPECTROSCOPIC AND X-RAY DIFFRACTION DATA FOR COMPOUNDS IN CHAPTER 2

***N*-(butylcarbamoyl)-4-methylbenzenesulfonamide 1a**

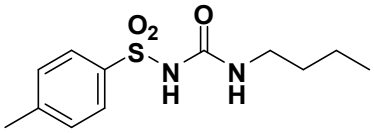

White Powder (92% yield); **^{1}H-NMR** (400 MHz, DMSO-*d6*) δ 0.79 (t, *J* = 7.20Hz, 3H), δ 1.11-1.18 (m, 2H), δ 1.23-1.30 (m, 2H), δ 2.37 (s, 3H), δ 2.88-2.93 (m, 2H), δ 6.41 (t, *J* = 5.80Hz, 1H), δ 7.38 (d, *J* = 8.00Hz, 2H), 7.75 (d, *J* = 7.6Hz, 2H), δ 10.45 (s, 1H); **^{13}C-NMR** (300 MHz, DMSO-*d6*) δ 14.0, 19.7, 21.5, 31.7, 39.2, 127.6, 129.8, 137.9, 143.9, 151.7. **HRMS**: Calculated for $C_{12}H_{18}N_2NaO_3S$ [M+Na]: 293.0930; measured: 293.0925.

4-methyl-*N*-(phenylcarbamothioyl)benzenesulfonamide 1b

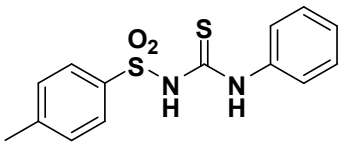

White powder (91% yield); **^{1}H-NMR** (400 MHz, DMSO-*d6*) δ 2.38 (s, 3H), δ 7.16 (t, *J* = 7.26Hz, 1H), δ 7.39-7.43 (m, 4H), δ 7.28-7.36 (m, 2H), δ 7.81 (d, *J* = 8.37Hz, 2H), δ 10.14 (s, 1H); **^{13}C-NMR** (300 MHz, DMSO-*d6*) δ 21.5, 119.4, 124.5, 126.2, 128.2, 129.0, 129.9, 138.5, 144.3, 178.0; **HRMS**: Calculated for $C_{14}H_{14}N_2NaO_2S_2$ [M+Na]: 329.0389; measured: 329.0390.

4-methyl-*N*-(4-nitrophenylcarbamothioyl)benzenesulfonamide 1c

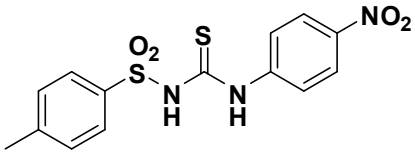

Yellow powder (80% yield); **^{1}H-NMR** (400 MHz, DMSO-*d6*) δ 2.31 (s, 3H), δ 7.18 (d, *J* = 8.12Hz, 2H), δ 7.63 (d, *J* = 8.40Hz, 2H),7.95-8.04 (m, 4H), δ 9.66 (s, 1H); **^{13}C-NMR** (300 MHz, DMSO-*d6*) δ 21.1, 118.6, 124.9, 127.9, 128.3, 140.0, 142.1, 147.8, 183.0; **HRMS**: Calculated for $C_{14}H_{12}N_3O_4S_2$ [M+Na]: 350.0275; measured: 350.0272.

4-methyl-*N*-(phenylcarbamoyl)benzenesulfonamide 1d

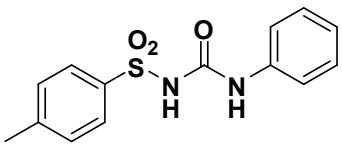

^{1}H-NMR (400 MHz, DMSO-*d6*) δ 2.37, δ 6.99 (t, *J* = 4.00 Hz, 1H), δ 2.37 δ 2.37 δ 7.37-7.41 (m, 4H), δ 7.20-7.33 (m, 2H), δ 7.82 (d, *J* = 7.84Hz, 2H), δ 8.78 (s, 1H), δ 10.63 (s, 1H); **^{13}C-NMR** (300 MHz, DMSO-*d6*) δ 21.5, 119.3, 123.5, 126.1, 127.9, 129.9, 137.7, 138.6, 144.1, 150.0 ppm. HRMS: Calculated for $C_{14}H_{14}N_2NaO_3S$ [M+Na]: 313.0617; measured: 313.0614.

***N*-(cyclohexylcarbamoyl)-4-methylbenzenesulfonamide 1e**

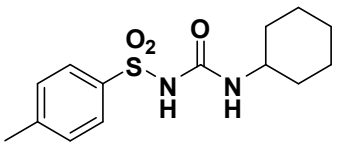

White powder (88% yield); **^{1}H-NMR** (400 MHz, DMSO-*d6*) δ 1.02-1.25 (m, 5H), δ 1.22-1.66 (m, 5H), δ 2.37 (s, 3H), δ 3.25 (d, *J* = 7.28Hz, 1H), δ 6.30 (d, *J* = 8.40Hz, 1H) δ 7.38 (d, *J* = 8.00Hz, 2H), 7.75 (d, *J* = 7.60Hz, 2H), δ 10.26 (s, 1H); **^{13}C-NMR** (300 MHz, DMSO-*d6*) δ 21.5, 24.6, 25.4, 32.7, 48.5, 127.6, 129.9, 137.9, 144.0, 150.9. **HRMS**: Calculated for $C_{14}H_{20}N_2NaO_3S$ [M+Na]: 319.1087; measured: 319.1082.

4-methyl-*N*-(propylcarbamoyl)benzenesulfonamide 1f

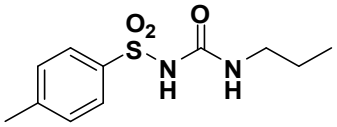

White powder (86% yield) **^{1}H-NMR** (400 MHz, DMSO-*d6*) δ 0.73 (t, *J* = 7.00Hz, 3H), δ 1.28-1.32 (m, 2H), δ 2.37 (s, 3H), δ 2.84-2.91 (m, 2H), δ 6.42 (t, *J* = 5.80Hz, 1H), δ 7.38 (d, *J* = 8.00Hz, 2H), 7.75 (d, *J* = 7.6Hz, 2H), δ 10.46 (s, 1H); **^{13}C-NMR** (300 MHz, DMSO-*d6*) δ 11.4, 21.4, 23.0, 41.2, 127.6, 129.7, 137.7, 143.7, 151.7; **HRMS**: Calculated for $C_{11}H_{16}N_2NaO_3S$ [M+Na]: 279.0774; measured: 279.0764.

4-chloro-*N*-(propylcarbamoyl)benzenesulfonamide 2a

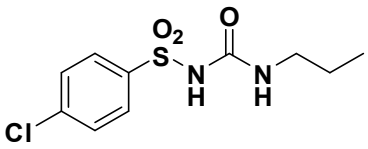

White powder (92% yield); **^{1}H-NMR** (400 MHz, DMSO-*d6*) δ 0.73 (t, *J* = 7.48Hz, 3H), δ 1.26-1.35 (m, 2H) δ 2.85-2.89 (m, 3H), δ 6.51 (t, *J* = 5.80Hz, 1H), δ 7.67 (d, *J* = 8.36Hz, 2H), δ 7.88 (d, *J* = 7.96Hz, 2H), δ 10.66 (s, 1H); **^{13}C-NMR** (300 MHz, DMSO-*d6*) δ 11.5, 22.9, 41.4, 129.6, 129.7, 138.5; **HRMS**: Calculated for $C_{10}H_{13}ClN_2NaO_3S$ [M+Na]: 299.0228; measured: 299.0229.

***N*-(butylcarbamoyl)-4-chlorobenzenesulfonamide 2b**

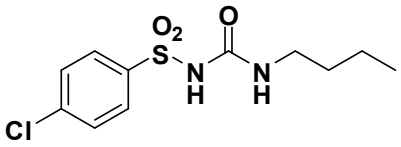

Off-white Powder (92% yield); **^{1}H-NMR** (400 MHz, DMSO-*d6*) δ 0.79 (t, *J* = 7.20Hz, 3H), δ 1.10-1.18 (m, 2H), δ 1.22-1.30 (m, 2H), δ 2.88-2.93 (m, 2H), δ 6.50 (t, *J* = 5.80Hz, 1H), δ 7.67 (d, *J* = 8.00Hz, 2H), 7.88 (d, *J* = 7.6Hz, 2H), δ 10.64 (s, 1H); **^{13}C-NMR** (300 MHz, DMSO-*d6*) δ 13.9, 19.7, 31.1, 31.7, 129.6, 129.7, 138.4, 139.6, 151.7; **HRMS**: Calculated for $C_{11}H_{15}ClN_2NaO_3S$ [M+Na]: 313.0384; measured: 313.0376.

4-chloro-*N*-(cyclohexylcarbamoyl)benzenesulfonamide 2c

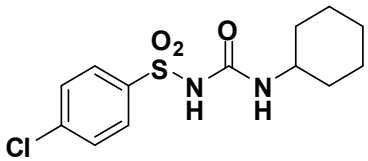

White powder (91% yield); **^{1}H-NMR** (400 MHz, DMSO-*d6*) δ 1.03-1.22 (m, 5H), δ 1.46-1.66 (m, 5H), δ 3.26 (d, *J* = 7.28Hz, 1H), δ 6.39 (d, *J* = 8.40Hz, 1H) δ 7.66 (d, *J* = 8.28Hz, 2H), 7.88 (d, *J* = 8.64Hz, 2H), δ 10.44 (s, 1H)**^{13}C-NMR** (300 MHz, DMSO-*d6*) δ 24.6, 25.4, 32.7, 48.6, 129.6, 129.7, 138.4; **HRMS**: Calculated for $C_{13}H_{17}ClN_2NaO_3S$ [M+Na]: 339.0541; measured: 339.0541.

5-chloro-2-methoxy-*N*-(4-sulfamoylphenethyl)benzamide 3a

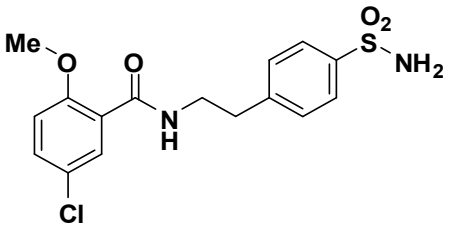

White powder (74% yield); **^{1}H-NMR** (400 MHz, DMSO-*d6*) δ 2.89 (t, *J* = 7.04Hz, 2H), δ 3.48-3.53 (m, 2H), δ 3.79 (s, 3H) δ 7.14 (d, *J* = 8.96Hz, 2H), δ 7.29 (s, 2H), δ 7.43 (d, *J* = 8.24Hz, 2H), δ 7.47-7.50 (m, 1H), δ 7.62 (d, *J* = 2.84Hz, 1H), δ 7.74 (d, *J* = 8.12Hz, 2H), δ 8.25 (t, *J* = 5.52Hz, 1H); **^{13}C-NMR** (300 MHz, DMSO-*d6*) δ 35.1, 56.7, 114.6, 124.8, 125.3, 126.1, 129.6, 130.0, 131.2, 142.5, 144.1, 156.1, 164.0. **HRMS**: Calculated for $C_{16}H_{17}ClN_2NaO_4S$ [M+Na]: 391.0490; measured: 391.0478.

5-chloro-*N*-(4-(*N*-(cyclohexylcarbamoyl)sulfamoyl)phenethyl)-2-methoxybenzamide 3b

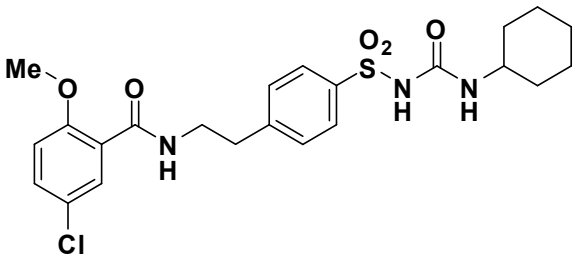

White powder; **^{1}H-NMR** (400 MHz, DMSO-*d6*) δ 1.03-1.22 (m, 5H), δ 1.46-1.66 (m, 5H), 2.89 (t, *J* = 7.04Hz, 2H),), δ 3.26 (d, *J* = 7.28Hz, 1H), δ 3.48-3.53 (m, 2H), δ 3.79 (s, 3H) δ 7.14 (d, *J* = 8.96Hz, 2H), δ 7.43 (d, *J* = 8.24Hz, 2H), δ 7.47-7.50 (m, 1H), δ 7.62 (d, *J* = 2.84Hz, 1H), δ 7.74 (d, *J* = 8.12Hz, 2H), δ 8.25 (t, *J* = 5.52Hz, 1H); **^{13}C-NMR** (300 MHz, DMSO-*d6*) δ 24.6, 25.4, 31.2, 32.7, 35.1, 48.5, 56.7, 114.6, 124.7, 125.3, 127.7, 129.8, 129.9, 131.9, 138.6, 145.7, 150.8, 156.1, 164.0; **HRMS**: Calculated for $C_{23}H_{28}ClN_3NaO_5S$ [M+Na]: 516.1330; measured: 516.1331.

FTIR-ATR spectrum of the crude mixture shows the absence of the characteristic peak of iso(thio)cyanates (C=N stretching bands between 2000-2200 cm^{-1}), which indicates that all the iso(thio)cyanates has been completely consumed and that the reaction has reached completion during milling, *i.e.* the product has formed during ball milling and not during workup. Similarly, FTIR-ATR spectra revealed that in the absence of the catalyst the reactions did not take place, as indicated by a strong residual iso(thio)cyanate peak.

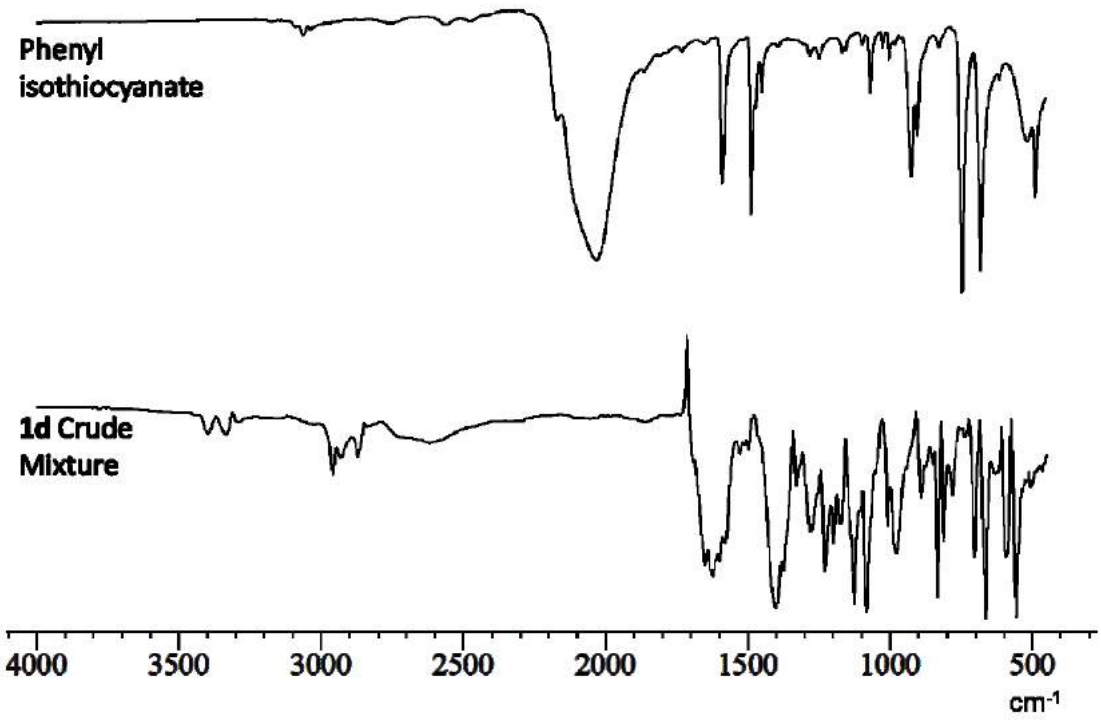

Fig. A1. Comparison of the FTIR-ATR spectra of mechanochemical crude reaction for the synthesis of **1d** and the phenylisothiocyanate starting material. The spectra clearly shows the disappearance of the C=N stretching bands in the 2000-2200 cm^{-1} region, which clearly denotes that all of the isothiocyanates has reacted.

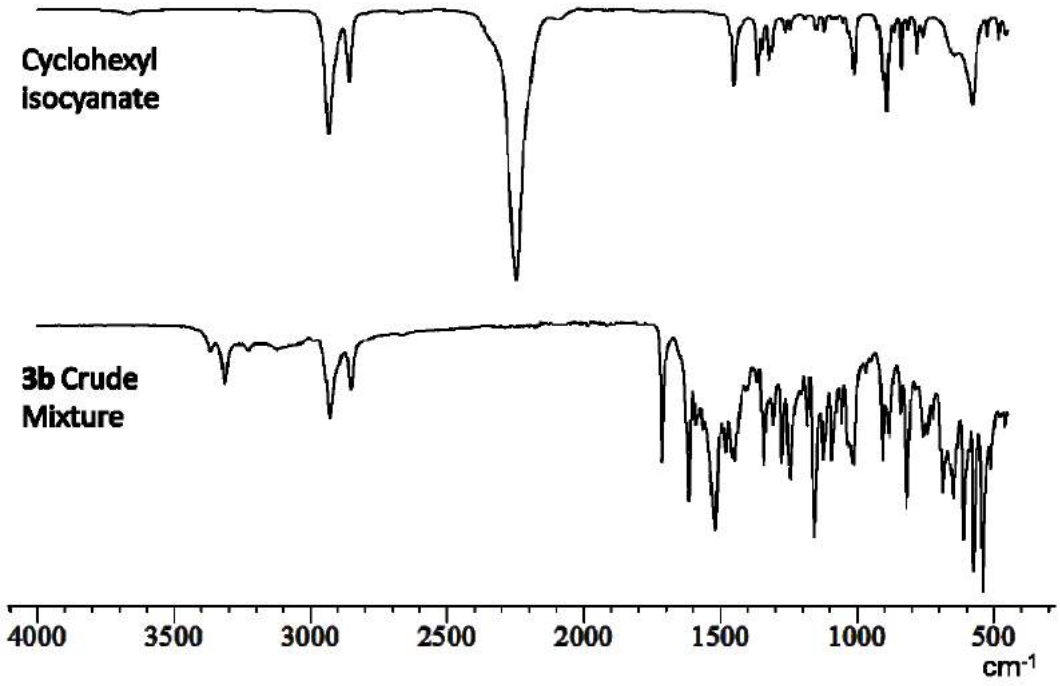

Fig. A2. Comparison of the FTIR-ATR spectra of mechanochemical crude reaction for the synthesis of **3b** and the cyclohexylisocyanate starting material. The spectra clearly shows the disappearance of the C=N stretching bands in the 2000-2200 cm^{-1} region, which clearly denotes that all of the isothiocyanates has reacted.

Detailed FTIR-ATR and NMR spectra for all compounds have been published and can be found in the supporting information of this article: *Chem. Commun.*, **2014**, *50*, 5248.

Table A1. SCXRD data of various sulfonyl(thio)urea compounds.

	1b	**1c**	**2c**	**3a**
Molecular formula	$C_{14}H_{14}N_2O_2S_2$	$C_{13}H_{13}N_3O_4S_2K$	$C_{13}H_{17}N_2O_3SCl$	$C_{16}H_{17}ClN_2O_4S$
M_r	306.41	389.49	316.80	368.84
Crystal System	Triclinic	Triclinic	Monoclinic	Triclinic
Crystal colour	Colourless	Yellow	Colourless	Colourless
Space group	$P\bar{1}$	$P\bar{1}$	$P2_1/c$	$P\bar{1}$
Temperature (K)	293	293	293	293
Unit cell dimensions (Å,°)				
a	7.557(4)	7.3664(12)	9.3333(8)	9.634(2)
b	9.922(5)	16.466(3)	16.0646(14)	10.046(2)
c	11.266(6)	18.699(3)	19.6441(17)	10.667(2)
α	106.421(6)	107.650(2)	90	64.209(3)
β	103.828(6)	93.736(2)	97.580(1)	69.198(2)
γ	98.312(6)	96.762(2)	90	72.313(2)
Volume (Å^3)	766.1(7)	2134.07	2919.6(4)	855.2(3)
Z	2	1	8	2
D_{calc} (g cm^{-3})	1.328	1.406	1.437	1.432
μ (mm^{-1})	0.349	0.478	0.413	0.368
***F*(000)**	320	936	1320	384
Refl. collected/independent	5487/1876	15038/ 5047	32712/6633	15990/5640
No. observed refl. [$I>2\sigma(I)$]*	1381	3324	5453	2129
No. restraints/No. parameters	1876/189	5047/525	6633/361	5640/145
***R/wR* [all data]**	0.0462/ 0.1402	0.0631/0.2110	0.0370/0.1087	0.9612/ 0.9992
Goodness-of-fit on F^2	0.93	0.99	0.79	12.13
Largest diff. peak and hole (*e* Å^{-3})	-0.33, 0.23	-0.34, 1.21	-0.47, 1.01	-1.42, 4.92

	1d
Molecular formula	$C_{14}H_{20}N_2O_3S$
M_r	296.38
Crystal System	Orthorhombic
Crystal colour	Colorless
Space group	*P*bca
Temperature (K)	298K
Unit cell dimensions (Å,°)	
a	10.776(2)
b	9.1377(19)
c	32.025(6)
α	90
β	90
γ	90
Volume (Å^3)	3153.4(11)
Z	8
D_{calc} (g cm^{-3})	1.249
μ (mm^{-1}) (abs coeff)	0.214
***F*(000)**	1264
Refl. collected/independent	32556 / 3395
No. observed refl. [$I>2\sigma(I)$]*	3006
No. restraints/No. parameters	0/229
R [all/gt]	0.1039 / 0.0974
wR [ref/gt]	0.2898 / 0.2863
Goodness-of-fit on F^2	1.241
Largest diff. peak and hole (*e* Å^{-3})	0.330, -0.468

*$R = \sum||Fo|-|Fc||/\sum Fo, w = 1/[\sigma^2(F_o^2)+(g_1P)^2+ g_2P]$ where $P = (F_o^2+2F_c^2)/3$, $S = \Sigma[w(F_o^2 - F_c^2)^2/(N_{obs} - N_{param})]^{1/2}$.

APPENDIX B

SPECTROSCOPIC AND X-RAY DIFFRACTION DATA FOR COMPOUNDS IN CHAPTER 3

***N*-(bis(cyclohexylamino)methylene)-1,1,1-trifluoromethanesulfonamide 1a**

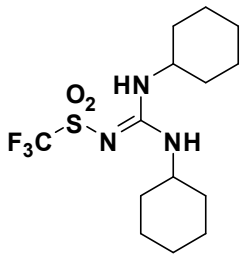

White powder (98% yield); **^{1}H-NMR** (300 MHz, DMSO-*d6*) δ 1.01-1.39 (m, 10H), δ 1.44-1.88 (m, 10H), δ 3.52-3.70 (m, 2H),), δ 7.22 (d, *J* = 11.45Hz, 2H); **^{13}C-NMR** (300 MHz, DMSO-*d6*) δ 25.3, 32.3, 50.3, 153.9; **HRMS**: Calculated for $C_{14}H_{24}O_2N_3F_3S$ [M+H]: 356.16141; measured: 356.16098.

***N*-(bis(isopropylamino)methylene)-1,1,1-trifluoromethanesulfonamide 1b**

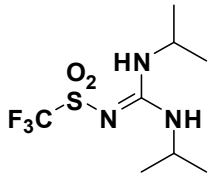

White powder (96% yield); **^{1}H-NMR** (300 MHz, DMSO-*d6*) δ 1.10 (d, *J* = 1.21Hz, 6H), δ 1.12 (d, *J* = 1.20Hz, 6H), δ 3.81-4.03 (m, 2H), δ 6.94-7.48 (s, 2H); **^{13}C-NMR** (300 MHz, DMSO-*d6*) δ 22.4, 43.8, 118.6, 154.0; **HRMS**: Calculated for $C_8H_{16}F_3N_3NaO_2S$ [M+Na]: 298.0808; measured: 298.0804.

***N*-(bis(tert-butylamino)methylene)-1,1,1-trifluoromethanesulfonamide 1c**

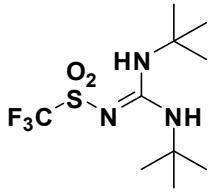

White powder (92% yield); **^{1}H-NMR** (300 MHz, DMSO-*d6*) δ 1.34 (s, 18H), δ 6.24 (s, 2H); **^{13}C-NMR** (300 MHz, DMSO-*d6*) δ 29.2, 53.1, 75.4; **HRMS**: Calculated for $C_{10}H_{20}F_3N_3NaO_2S$ [M+Na]: 326.1121; measured: 326.1118.

(*Z*)-*N*-((tert-butylamino)(ethylamino)methylene)-1,1,1-trifluoromethanesulfonamide 1d

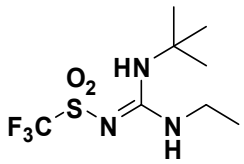

White powder (99% yield); **^{1}H-NMR** (300 MHz, DMSO-*d6*) δ 1.05 (t, *J* = 6.57Hz, 3H), δ 1.33 (s, 9H), δ 3.27 (m, 2H), δ 6.76 (s, 1H), δ 7.14 (s, 1H); **^{13}C-NMR** (300 MHz, DMSO-*d6*) δ 14.5, 29.1, 36.9, 52.7, 122.6, 155.1; **HRMS**: Calculated for $C_8H_{16}F_3N_3NaO_2S$ [M+Na]: 298.0808; measured: 298.0804.

***N*-(bis(p-tolylamino)methylene)-1,1,1-trifluoromethanesulfonamide 1f**

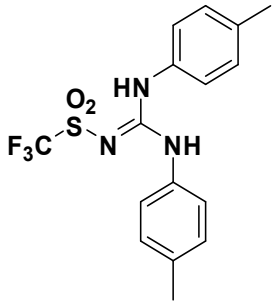

Grey powder (95% yield); **^{1}H-NMR** (300 MHz, DMSO-*d6*) δ 2.28 (s, 6H), δ 7.00-7.35 (m, 8H), δ 9.52 (s, 2H); **^{13}C-NMR** (300 MHz, DMSO-*d6*) δ 20.7, 125.0, 129.5, 134.3, 135.7, 154.3; **HRMS**: Calculated for $C_{16}H_{17}F_3N_3O_2S$ [M+H]: 372.0988; measured: 372.0991.

***N*-(bis(*o*-tolylamino)methylene)-1,1,1-trifluoromethanesulfonamide 1g**

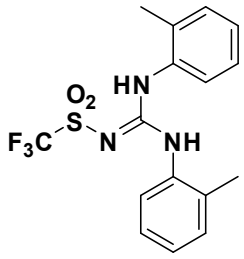

Orange solid (73% conversion); **^{1}H-NMR** (300 MHz, DMSO-*d6*) δ 2.21 (s, 6H), δ 7.08-7.21 (m, 8H), δ 9.09 (s, 2H); **HRMS**: Calculated for $C_{16}H_{17}F_3N_3O_2S$ [M+H]: 372.0988; measured: 372.0992.

***N*-(bis(cyclohexylamino)methylene)-4-methylbenzenesulfonamide 2a**

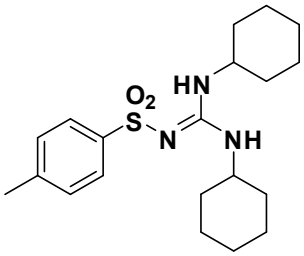

White Powder (98% yield); **^{1}H-NMR** (300 MHz, DMSO-*d6*) δ 1.02-1.29 (m, 10H), δ 1.22-1.66 (m, 10H), δ 2.32 (s, 3H), δ 3.43-3.66 (m, 2H), δ 6.84 (s, 2H), δ 7.28 (d, *J* = 8.19Hz, 2H), δ 7.57 (d, *J* = 7.80Hz, 2H); **^{13}C-NMR** (300 MHz, DMSO-*d6*) δ 21.3, 24.9, 25.4, 25.7, 75.3, 33.8, 125.9, 129.4, 141.5, 141.9, 153.8; **HRMS**: Calculated for $C_{20}H_{31}N_3NaO_2S$ [M+Na]: 400.2029; measured: 400.2026.

***N*-(bis(isopropylamino)methylene)-4-methylbenzenesulfonamide 2b**

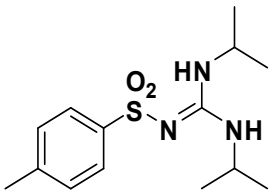

White powder (99% yield); **^{1}H-NMR** (300 MHz, DMSO-*d6*) δ 0.99 (d, *J* = 1.21Hz, 6H), δ 1.02 (d, *J* = 1.25Hz, 6H), δ 2.32, (s, 3H), δ 3.72-3.92 (m, 2H), δ 6.75 (d, *J* = 7.56Hz, 2H), δ 7.27 (d, *J* = 7.98Hz, 2H), 7.58 (d, *J* = 8.28Hz, 2H); **^{13}C-NMR** (300 MHz, DMSO-*d6*) δ 21.3, 22.8, 43.0, 125.9, 129.5, 141.5, 142.0, 153.9; **HRMS**: Calculated for $C_{14}H_{24}O_2N_3S$ [M+H]: 298.15972; measured: 298.15837.

***N*-(bis(p-tolylamino)methylene)-4-methylbenzenesulfonamide 2c**

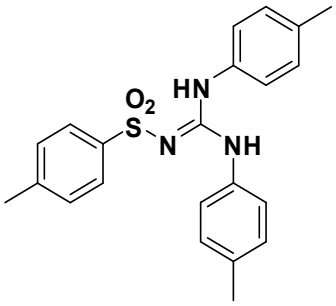

White powder (98% yield); **^{1}H-NMR** (300 MHz, DMSO-*d6*) δ 2.24 (s, 6H), δ 2.35 (s, 3H), δ 7.00 (d, *J* = 8.46Hz, 4H), δ 7.08 (d, *J* = 8.49Hz, 4H), δ 7.33 (d, *J* = 7.92Hz, 4H), δ 7.67 (d, *J* = 8.49Hz, 4H), δ 8.91 (s, 2H); **^{13}C-NMR** (300 MHz, DMSO-*d6*) δ 20.9, 21.4, 118.6, 124.1, 126.1, 129.7, 134.8, 135.0, 141.3, 142.2, 152.9; **HRMS**: Calculated for $C_{22}H_{23}N_3NaO_2S$ [M+Na]: 416.1403; measured: 416.1400.

***N*-(bis(cyclohexylamino)methylene)-4-chlorobenzenesulfonamide 3a**

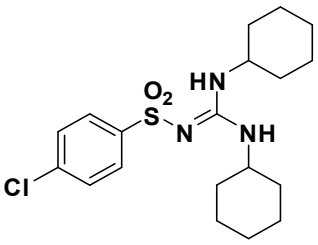

White powder (91% yield); **^{1}H-NMR** (300 MHz, DMSO-*d6*) δ 1.02-1.30 (m, 10H), δ 1.46-1.72 (m, 10H), δ 3.45-3.61 (m, 2H), δ 6.84 (d, *J* = 7.41Hz, 2H), δ 7.56 (d, *J* = 8.49Hz, 2H) δ 7.69 (d, *J* = 9.00Hz, 2H) ; **^{13}C-NMR** (300 MHz, DMSO-*d6*) δ 24.9, 25.4, 25.7, 32.6, 33.8, 127.8, 129.3, 136.3, 143.6, 153.7; **HRMS**: Calculated for $C_{19}H_{28}ClN_3NaO_2S$ [M+Na]: 420.1483; measured: 420.1485.

***N*-(bis(isopropylamino)methylene)-4-chlorobenzenesulfonamide 3b**

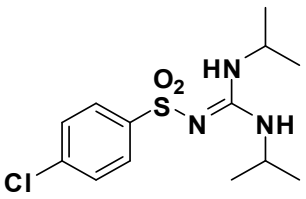

White powder (95% yield); **^{1}H-NMR** (300 MHz, DMSO-*d6*) δ 1.00 (d, *J* = 1.21Hz, 6H), δ 1.03 (d, *J* = 1.21Hz, 6H), δ 3.74-3.98 (m, 2H), δ 6.80 (d, *J* = 7.89Hz, 2H), δ 7.56 (d, *J* = 8.55Hz, 2H), δ 7.71 (d, *J* = 8.46Hz, 2H); **^{13}C-NMR** (300 MHz, DMSO-*d6*) **^{13}C-NMR** (300 MHz, DMSO-*d6*) δ 27.5, 47.9, 132.6, 133.9, 141.1, 148.4, 158.6; **HRMS**: Calculated for $C_{13}H_{21}O_2N_3ClS$ [M+H]: 318.10375; measured: 318.10506.

***N*-(bis(p-tolylamino)methylene)-4-chlorobenzenesulfonamide 3c**

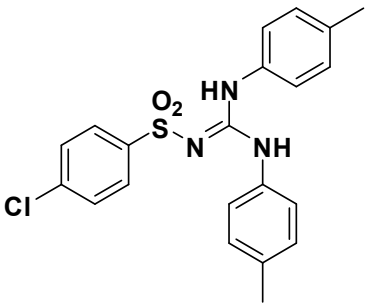

White powder (88% yield) **^{1}H-NMR** (300 MHz, DMSO-*d6*) δ 2.24 (s, 6H), δ 7.01 (d, *J* = 8.31Hz, 4H), δ 7.09 (d, *J* = 8.37Hz, 4H), δ 7.61 (d, *J* = 8.49Hz, 2H) δ 7.79 (d, *J* = 8.49Hz, 2H), δ 8.95 (s, 2H); **^{13}C-NMR** (300 MHz, DMSO-*d6*) δ 20.9, 124.4, 128.1, 129.7, 135.1; **HRMS**: Calculated for $C_{21}H_{20}ClN_3NaO_2S$ [M+Na]: 436.0857; measured: 436.0852.

***N*-(bis(cyclohexylamino)methylene)-2-chlorobenzenesulfonamide 4a**

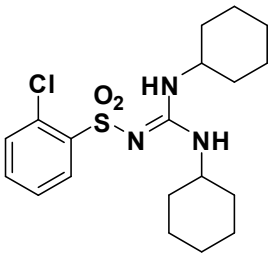

White powder (94% yield); **^{1}H-NMR** (300 MHz, DMSO-*d6*) δ 0.94-1.30 (m, 10H), δ 1.45-1.77 (m, 10H), δ 3.47-3.68 (m, 2H), δ 6.88 (m, 2H), δ 7.40-7.65 (m, 3H), δ 7.88-8.01 (m, 1H); **^{13}C-NMR** (300 MHz, DMSO-*d6*) δ 24.8, 25.3, 25.7, 32.7, 33.8, 127.4, 129.4, 131.1, 132.0, 133.1, 141.6, 153.5; **HRMS**: Calculated for $C_{19}H_{29}O_2N_3ClS$ [M+H]: 398.16635; measured: 398.16581.

***N*-(bis(isopropylamino)methylene)-2-chlorobenzenesulfonamide 4b**

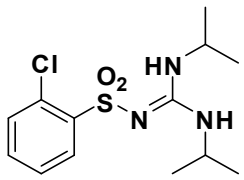

White Powder (97% yield); **^{1}H-NMR** (300 MHz, DMSO-*d6*) δ 1.01 (d, *J* = 1.21Hz, 6H), δ 1.03 (d, *J* = 1.20Hz, 6H), δ 3.77-3.94 (m, 2H), δ 6.81 (d, *J* = 8.31Hz, 2H), δ 7.41-7.61 (m, 3H), δ 7.93-7.98 (m, 1H); **^{13}C-NMR** (300 MHz, DMSO-*d6*) δ22.9, 42.9, 127.5, 129.3, 131.9, 133.1, 141.7, 154.0; **HRMS**: Calculated for $C_{13}H_{21}O_2N_3ClS$ [M+H]: 318.10375; measured: 318.10320.

***N*-(bis(p-tolylamino)methylene)-2-chlorobenzenesulfonamide 4c**

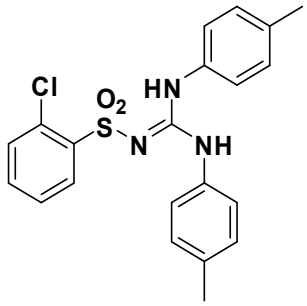

White powder (99% yield); **^{1}H-NMR** (300 MHz, DMSO-*d6*) δ 2.22 (s, 6H), δ 7.07 (s, 8H), δ 7.44-7.66 (m, 3H), δ 7.98-8.02 (m, 1H), δ 9.03 (s, 2H); **^{13}C-NMR** (300 MHz, DMSO-*d6*) δ 20.9, 124.0, 127.9, 129.8, 131.0, 132.0, 133.7, 134.8, 135.1, 141.1, 153.1; **HRMS**: Calculated for $C_{13}H_{17}ClN_2NaO_3S$ [M+Na]: 436.08570; measured: 436.08516.

***N*-(bis(cyclohexylamino)methylene)naphthalene-2-sulfonamide 5a**

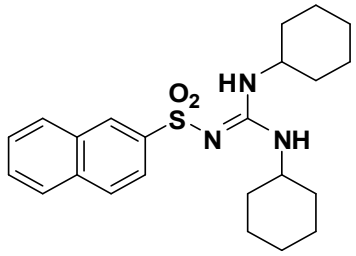

Greenish-white powder (92% yield); **^{1}H-NMR** (300 MHz, DMSO-*d6*) δ 0.98-1.29 (m, 10H), δ 1.41-1.75 (m, 10H), δ 3.48-3.69 (m, 2H), δ 6.86 (m, 2H), δ 7.58-7.74 (m, 3H), δ 7.94-8.11 (m, 3H), δ 8.32 (s, 1H); **^{13}C-NMR** (300 MHz, DMSO-*d6*) δ 24.9, 25.4, 32.7, 33.8, 122.8, 125.8, 127.8, 128.1, 128.5, 129.2, 129.4, 132.1, 134.1, 141.7, 153.8; **HRMS**: Calculated for $C_{23}H_{32}N_3O_2S$ [M+H]: 414.22097; measured: 414.22060.

***N*-(bis(isopropylamino)methylene)naphthalene-2-sulfonamide 5b**

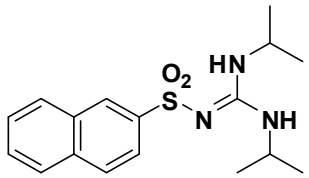

White powder (99% yield); **^{1}H-NMR** (300 MHz, DMSO-*d6*) δ 0.98 (d, *J* = 1.21Hz, 6H), δ 1.00 (d, *J* = 1.25Hz, 6H), δ 3.71-4.00 (m, 2H), δ 6.81 (d, *J* = 7.32Hz, 2H), δ 7.61 (m, 2H), δ 7.73 (d, *J* = 7.74Hz, 1H), δ 7.92-8.13 (m, 3H), δ 8.34 (s, 1H); **^{13}C-NMR** (300 MHz, DMSO-*d6*) δ 22.7, 43.0, 122.7, 125.7, 127.6, 128.0, 128.4, 129.1, 129.4, 132.1, 134.0, 141.6, 153.9. **HRMS**: Calculated for $C_{17}H_{24}O_2N_3S$ [M+Na]: 334.158374; measured: 334.15785.

***N*-(bis(cyclohexylamino)methylene)-4-methoxybenzenesulfonamide 6a**

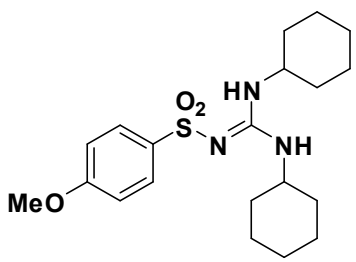

White powder (87% yield); **^{1}H-NMR** (300 MHz, DMSO-*d6*) δ 0.91-1.31 (m, 10H), δ 1.43-1.76 (m, 10H), δ 3.43-3.62 (m, 2H),), δ 3.77 (s, 3H), 6.78 (d, *J* = 7.41Hz, 2H), δ 6.99 (d, *J* = 8.85Hz, 2H), δ 7.60 (d, *J* = 8.43Hz, 2H); **^{13}C-NMR** (300 MHz, DMSO-*d6*) δ 24.9, 25.4, 25.7, 32.7, 33.8, 55.9, 114.2, 127.6,

136.7, 153.6, 161.8; **HRMS**: Calculated for $C_{20}H_{32}O_3N_3S$ [M+H]: 394.21589; measured: 394.21525.

***N*-(bis(isopropylamino)methylene)-4-methoxybenzenesulfonamide 6b**

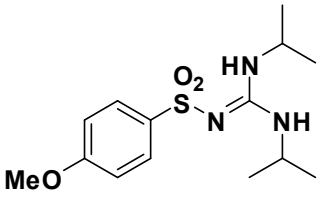

White powder (89% yield); **^{1}H-NMR** (300 MHz, DMSO-*d6*) δ 1.00 (d, *J* = 1.21Hz, 6H), δ 1.02 (d, *J* = 1.20Hz, 6H), δ 3.77 (s, 3H), δ 3.79-3.88 (m, 2H), δ 6.73 (d, *J* = 7.29Hz, 2H), δ 6.99 (d, *J* = 8.73Hz, 2H), δ 7.63 (d, *J* = 9.12, 2H); **^{13}C-NMR** (300 MHz, DMSO-*d6*) 22.7, 43.1, 55.7, 114.2, 127.8, 136.8, 153.7, 161.4; **HRMS**: Calculated for $C_{14}H_{24}O_3N_3S$ [M+H]: 314.15329; measured: 314.15270.

***N*-(bis(p-tolylamino)methylene)-4-methoxybenzenesulfonamide 6c**

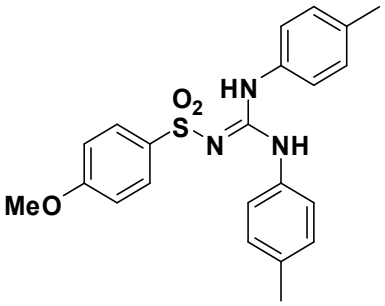

Off-white solid (99% yield); **^{1}H-NMR** (300 MHz, DMSO-*d6*) δ 2.24 (s, 6H), δ 3.80 (s, 3H), δ 6.99-7.13 (m, 10H), δ 7.73 (d, *J* = 8.85Hz, 3H), δ 8.90 (s, 2H); **^{13}C-NMR** (300 MHz, DMSO-*d6*) δ 20.4, 31.0, 56.2, 114.6, 124.2, 128.1, 129.8, 134.8, 135.2, 136.1, 152.9, 162.0; **HRMS**: Calculated for $C_{22}H_{24}N_3O_3S$ [M+H]: 410.15329; measured: 410.15265.

***N*-(bis(isopropylamino)methylene)-4-nitrobenzenesulfonamide 7b**

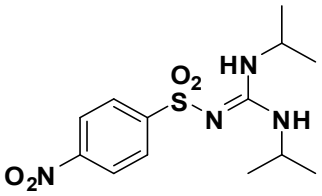

Orange solid (59% yield); **^{1}H-NMR** (300 MHz, DMSO-*d6*) δ 1.05 (s, 12H), δ 3.86 (m, 2H), δ 6.90 (s, 2H), δ 7.98 (s, 2H), δ 8.35 (s, 2H); **^{13}C-NMR** (300 MHz, DMSO-*d6*) δ 22.5, 42.9, 124.4, 127.2, 149.1, 150.1, 153.5; **HRMS**: Calculated for $C_{13}H_{19}N_4O_4S$ [M-H]: 327.11325; measured: 327.11320.

All detailed FTIR-ATR and NMR spectra for all compounds has been published and can be found in the supporting information of this article: *Angew. Chem. Int. Ed.*, **2014**, *53*, 9321.

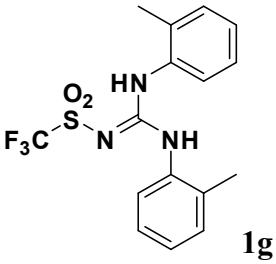

1g

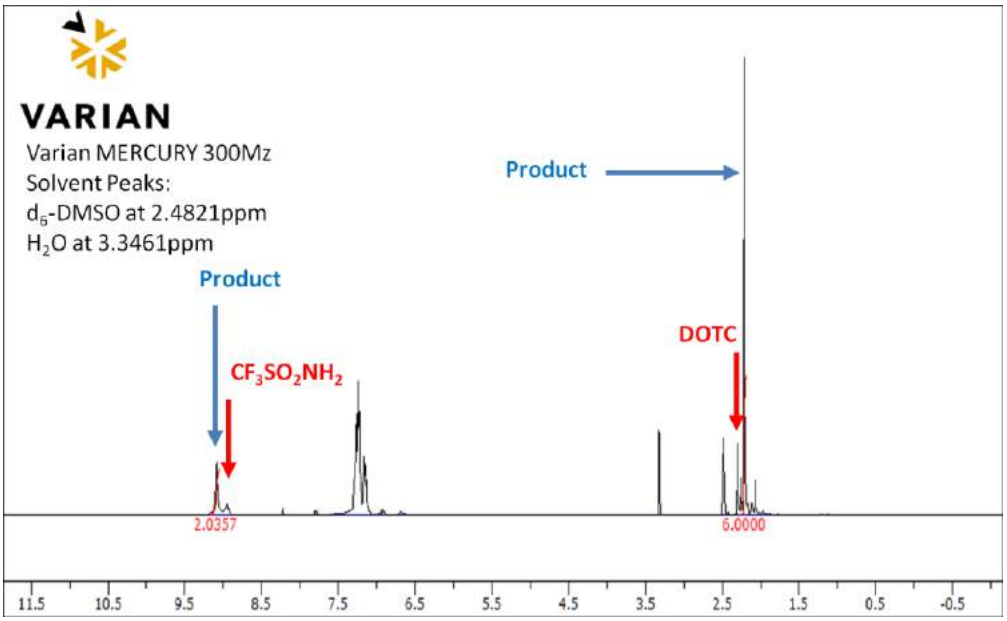

Fig. B1. ^{1}HNMR spectrum of the crude reaction mixture for the mechanochemical synthesis of **1g**. The spectrum shows incomplete conversion and presence of signals corresponding to both the starting materials and product.

Table B1. SCXRD data of various sulfonylguanidine compounds.

	2a	**3a**	**4b**	**5b**
Molecular formula	$C_{20}H_{31}N_3O_2$	$C_{19}H_{28}ClN_3O_2S$	$C_{13}H_{20}ClN_3O_2S$	$C_{17}H_{23}N_3O_2S$
M_r	377.54	397.95	317.83	333.44
Crystal System	Triclinic	Monoclinic	Monoclinic	Monoclinic
Crystal colour	Colorless	Colorless	Colorless	Colorless
Space group	*P*-1	$P2_1/c$	$P2_1$	$C2/c$
Temperature (K)	293	293	293	293
Unit cell dimensions (Å,°)				
a	12.075(3)	6.750(1)	7.655(1)	23.382(7)
b	12.703(3)	23.343(3)	10.363(2)	13.003(4)
c	15.167(4)	13.358(2)	10.668(2)	15.039(4)
α	92.220(3)	90	90	90
β	109.140(3)	100.640(2)	95.138(2)	126.614(3)
γ	106.008(3)	90	90	90
Volume (Å^3)	2091.2(9)	2068.8(5)	842.9(2)	3670(2)
Z	4	4	2	8
D_{calc} (g cm^{-3})	1.199	1.278	1.252	1.207
μ (mm^{-1})	0.173	0.304	0.355	0.189
***F*(000)**	816	848.0	336.0	1424.0
Refl. collected/independent	7325/5001	5283/4944	7362/1972	3869/3036
No. observed refl. [$I>2\sigma(I)$]*	7231	3881	3434	3844
No. restraints/No. parameters	0/475	0/235	1/188	22/255
***R*/*wR* [all data]**	0.0432/0.0971	0.0523/0.1551	0.0517/0.1405	0.0915/0.2891
Goodness-of-fit on F^2	1.049	0.981	1.013	1.118
Largest diff. peak and hole (*e* Å^{-3})	0.549/-0.360	0.545/-0.619	0.215/-0.226	1.001/-0.658

Table B1. (Cont'd)

	1c	1d
Molecular formula	$C_8H_{16}N_3O_2SF_3$	$C_{21}H_{33}N_3O_4S$
M_r	275.30	423.56
Crystal System	Monoclinic	Monoclinic
Crystal colour	Colorless	Colorless
Space group	$P2_1/c$	Cc
Temperature (K)	298K	298K
Unit cell dimensions (Å,°)		
a	9.057(15)	16.939(11)
b	14.15(2)	6.073(4)
c	11.267(18)	16.398(16)
α	90	90
β	108.341(19)	118.437(5)
γ	90	90
Volume (Å^3)	1370(4)	1483.4(19)
Z	4	4
D_{calc} (g cm^{-3})	1.334	1.358
μ (mm^{-1}) (abs coeff)	0.266	0.253
F(000)	576	640
Refl. collected/independent	14414/ 2844	5271 / 2440
No. observed refl. [I>2σ(I)]*	1900	2374
No. restraints/No. parameters	0/ 208	2/179
R [all/gt]	0.0737/ 0.0464	0.0915/ 0.0871
wR [ref/gt]	0.1605/0.1377	0.2426/ 0.2365
Goodness-of-fit on F^2	1.021	1.196
Largest diff. peak and hole (e Å^{-3})	0.234, -0.262	0.965, -0.770

	5a	6a	3a	7a
Molecular formula	$C_{23}H_{31}N_3O_2S$	$C_{20}H_{31}N_3O_3S$	$C_{13}H_{20}ClN_3O_2S$	$C_{17}H_{23}N_3O_2S$
M_r	377.54	393.54	317.83	408.51
Crystal System	Monoclinic	Monoclinic	Monoclinic	Monoclinic
Crystal colour	Colorless	Colorless	Colorless	Colorless
Space group	$C2/c$	$P2_1/c$	$P2_1/c$	$P2_1/n$
Temperature (K)	298	298	100	298
Unit cell dimensions (Å,°)				
a	16.2221(15)	14.754(2)	6.7504(10)	7.8053(13)
b	18.9120(18)	14.991(2)	23.343(3)	24.822(4)
c	14.8480(14)	15.194(2)	13.3584(19)	10.5234(17)
α	90	102.280(2)	90	90
β	92.8580(10)	97.275(2)	100.640(2)	101.961(2)
γ	90	100.716(2)	90	90
Volume (Å^3)	2091.2(9)	3177.7(7)	842.9(2)	1994.6(6)
Z	8	6	4	4
D_{calc} (g cm^{-3})	1.208	1.234	1.278	1.360
μ (mm^{-1})	0.165	0.177	0.304	0.196
F(000)	1776	1272	848	872
Refl. collected/independent	26082/5147	34258/12674	24007/4944	21997/4166
No. observed refl. [I>2σ(I)]*	3609	6637	3881	2233
No. restraints/No. parameters	0/262	0/730	0/235	0/253
R [all/gt]	0.0811/0.0560	0.1354/0.0618	0.0670/0.0523	0.1239/0.0559
wR [ref/gt]	0.1804/0.1585	0.1670/0.1381	0.1445/0.1333	0.1484/0.1182
Goodness-of-fit on F^2	1.025	1.018	1.018	0.988
Largest diff. peak and hole (e Å^{-3})	0.607/-0.314	0.254/-0.285	0.527/-0.624	0.239/-0.290

*$R = \sum||Fo|-|Fc||/\sum Fo, w = 1/[\sigma^2(F_o^2)+(g_1P)^2+ g_2P]$ where $P = (F_o^2+2F_c^2)/3$, $S = \Sigma[w(F_o^2 - F_c^2)^2/(N_{obs} - N_{param})]^{1/2}$.

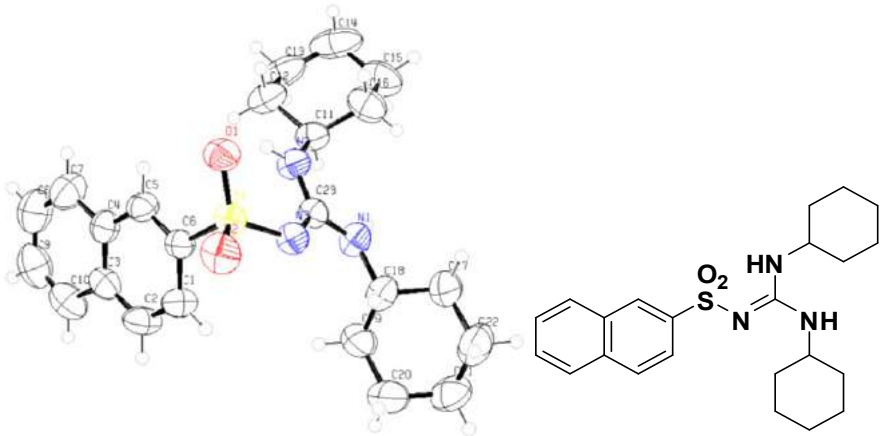

Fig. B2. Molecular structure visualized using ORTEP-3 of **5a** with thermal ellipsoids at 50% probability level as determined by SCXRD, along with a schematic representation of the molecule.

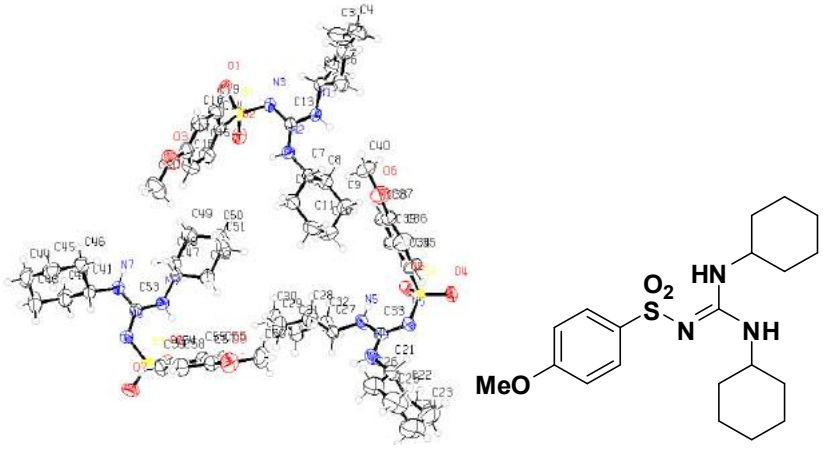

Fig. B3. Molecular structure visualized using ORTEP-3 of **6a** with thermal ellipsoids at 50% probability level as determined by SCXRD, along with a schematic representation of the molecule. Structure shows three molecules packed differently in the asymmetric unit.

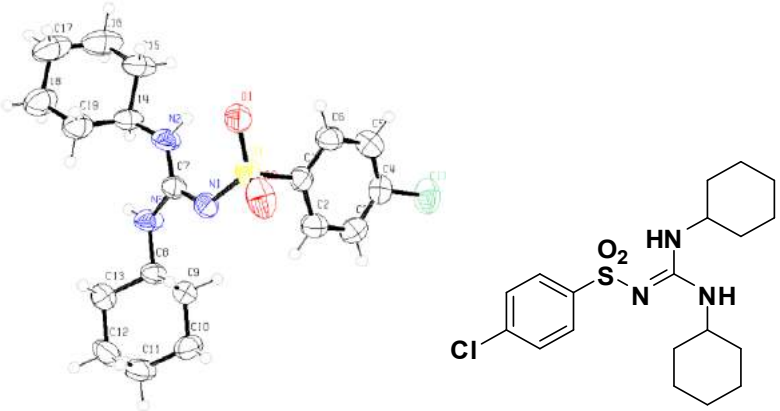

Fig. B4. Molecular structure visualized using ORTEP-3 of **3a** with thermal ellipsoids at 50% probability level as determined by SCXRD, along with a schematic representation of the molecule.

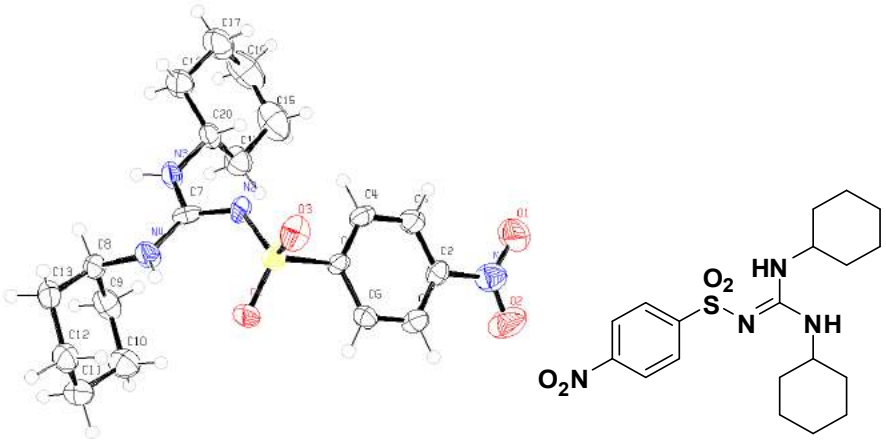

Fig. B5. Molecular structure visualized using ORTEP-3 of **7a** with thermal ellipsoids at 50% probability as determined by SCXRD, along with a schematic representation of the molecule.

APPENDIX C

SPECTROSCOPIC AND X-RAY DIFFRACTION DATA FOR COMPOUNDS IN CHAPTER 4

_N,N'_-dicyclohexyl-benzo[1,3]thiadiazepine 1

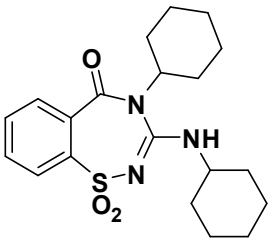

White Powder (95% yield); **^{1}H-NMR** (300 MHz, DMSO-*d6*) δ 0.98-1.86 (m, 20H), δ 3.54 (m, 1H), δ 4.12 (m, 1H), δ 7.67-7.81 (m, 4H) δ 8.23 (d, *J* = 7.26Hz, 1H); **^{13}C-NMR** (300 MHz, DMSO-*d6*) δ 24.8, 25.3, 25.6, 26.1, 52.7, 60.8, 123.4, 130.7, 131.8, 132.4, 132.8, 143.9, 153.9, 165.8; **HRMS**: Calculated for $C_{20}H_{27}N_3O_3S$ [M+H]: 388.17004; measured: 388.17065.

_N,N'_-diisopropyl-benzo[1,3]thiadiazepine 2

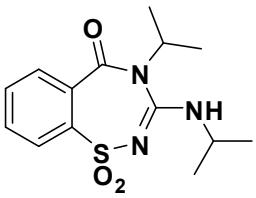

White powder (91% yield); **^{1}H-NMR** (300 MHz, DMSO-*d6*) δ 0.96-1.11 (m, 6H), δ 1.14 (d, *J* = 6.20 Hz 6H), δ 3.80-3.92 (m, 1H), δ 4.40-4.50 (m, 1H), δ 7.68-7.96 (m, 4H) δ 8.12 (d, *J* = 7.26Hz, 1H) ; **^{13}C-NMR** (300 MHz, DMSO-*d6*) δ 21.4, 23.7, 41.1, 45.7, 53.4, 123.5, 130.7, 132.0, 132.5, 133.1, 143.9, 154.2, 165.8; **HRMS**: Calculated for $C_{14}H_{20}N_3O_3S$ [M+H]: 310.1220; measured: 310.1219.

***N*-ethyl-*N'*-tertbutyl-benzo[1,3]thiadiazepine 3**

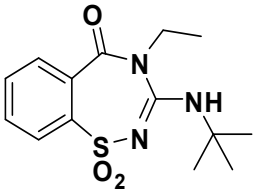

White powder (90% yield); **^{1}H-NMR** (300 MHz, DMSO-*d6*) δ 1.00 (t, *J* = 7.11 Hz, 3H), δ 1.56 (s, 9H), δ 3.08-3.29 (m, 2H), δ 7.66-7.88 (m, 4H), δ 8.75 (t, *J* = 6.12 Hz, 1H); **^{13}C-NMR** (300 MHz, DMSO-*d6*) δ 13.1, 27.8, 38.2, 62.3, 123.6, 130.9, 132.4, 132.6, 132.7, 144.3, 155.4, 164.2 ; **HRMS**: Calculated for $C_{14}H_{18}O_3N_3S$ [M+H]: 308.10744; measured: 308.10802.

_N,N'_-di-p-tolyl-benzo[1,3]thiadiazepine 4

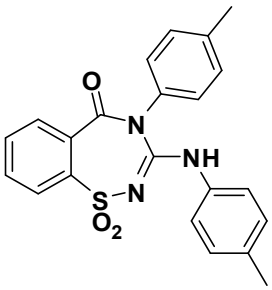

White powder (98% yield); **^{1}H-NMR** (300 MHz, DMSO-*d6*) δ 2.22 (s, 3H), δ 2.35 (s, 3H), δ 7.09-7.17 (m, 4H), δ 7.31-7.46 (m, 4H), δ 7.77-7.84 (m, 3H), δ 7.93-8.00 (m, 1H), δ 9.63 (s, 1H); **^{13}C-NMR** (300 MHz, DMSO-*d6*) δ 20.9, 21.2, 123.4, 123.8, 128.2, 129.7, 130.1, 130.6, 132.4, 133.1, 133.5, 134.5, 135.9, 136.7, 138.6, 142.5, 153.5, 166.6; **HRMS**: Calculated for $C_{22}H_{20}N_3O_3S$ [M+H]: 406.12199; measured: 406.12195.

4-methyl-*N*-tosylbenzamide 5

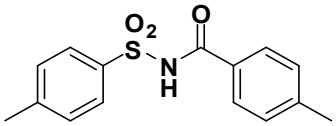

White powder (90% yield); **^{1}H-NMR** (300 MHz, DMSO-*d6*) δ 2.32 (s, 3H), δ 2.36 (s, 3H), δ 7.26 (d, *J* = 8.16 Hz, 2H), δ 7.41 (d, *J* = 8.00 Hz, 2H), δ 7.74 (d, *J* = 7.80 Hz, 2H), δ 7.87 (d, *J* = 8.05 Hz, 2H), δ 12.36 (s, 1H); **^{13}C-NMR** (300 MHz, DMSO-*d6*) δ 12.5, 126.1, 128.2, 128.9, 129.1, 129.5, 129.9, 137.1, 144.1, 144.6, 165.4. **HRMS**: Calculated for $C_{15}H_{15}O_3N_1S$ [M-H]: 288.06999; measured: 288.07024.

(E)-*N*-isopropyl-*N*-(*N*-isopropyl-*N*'-tosylcarbamimidoyl)-4-methylbenzamide 6

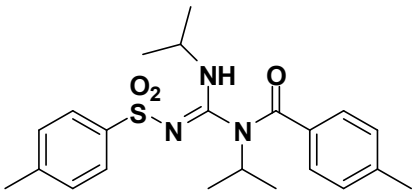

White powder (87% yield); **^{1}H-NMR** (300 MHz, DMSO-*d6*) δ 0.72-0.89 (m, 6H), δ 1.35 (d, *J* = 6.60 Hz 6H), δ 2.27 (s, 3H), δ 2.33 (s, 3H), δ 3.47-3.57 (m, 1H), δ 3.47-3.57 (m, 1H), δ 4.29-4.41 (m, 1H), δ 7.10 (d, *J* = 7.98 Hz, 2H), δ7.26 (d, *J* = 8.10 Hz, 2H), δ 7.46-7.53 (m, 4H), δ 8.59 (d, *J* = 8.43 Hz, 1H); **^{13}C-NMR** (300 MHz, DMSO-*d6*) δ 14.5, 20.5, 20.9, 21.2, 21.3, 21.7, 22.5, 23.7, 25.2, 31.4, 45.0, 51.1, 60.2, 125.8, 126.1, 128.1, 128.5, 128.7, 129.3, 129.5, 134.2, 140.6, 141.6, 142.0, 151.9, 168.9, 170.8. **HRMS**: Calculated for $C_{22}H_{29}O_3N_3S$ [M+H]: 416.20024; measured: 416.20036.

(E)-*N*-cyclohexyl-*N*-(*N*- cyclohexyl -*N*'-tosylcarbamimidoyl)-4-methylbenzamide 7

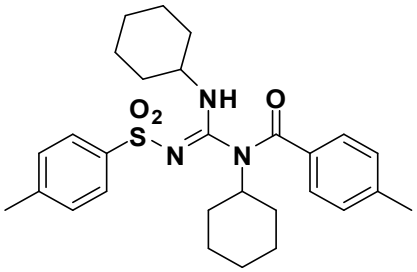

Colorless crystals (67% yield); **^{1}H-NMR** (300 MHz, DMSO-*d6*) δ 0.92-1.80 (m, 20H), δ 2.29 (s, 3H) δ 2.35 (s, 3H), 3.29-3.33 (m, 1H), δ 4.02 (m, 1H), δ 7.10 (d, *J* = 8.02 Hz, 2H), δ 7.26 (d, *J* = 8.10 Hz, 2H), δ 7.43 (d, *J* = 7.96 Hz, 2H), δ 7.51 (d, *J* = 7.89 Hz, 2H), δ 7.88 (d, *J* = 8.52 Hz, 1H). **^{13}C-NMR** (300 MHz, DMSO-*d6*) δ 21.3, 21.4, 24.6, 25.4, 25.7, 26.1, 30.3, 31.0, 33.8, 52.1, 58.3, 125.7, 128.2, 128.6, 129.4, 134.1, 140.5, 141.6, 141.9, 151.4, 168.5. **HRMS**: Calculated for $C_{28}H_{37}O_3N_3S$ [M+H]: 496.26284; measured: 496.26271.

***N*-cyclohexyl-carbamoyl-saccharin 8**

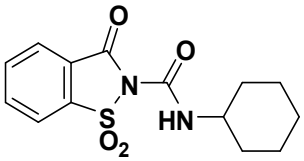

White powder (95% yield); **^{1}H-NMR** (300 MHz, DMSO-*d6*) δ 0.91-1.31 (m, 10H), δ 1.02-2.02 (m, 10H), δ 3.44-3.87 (m, 1H),), δ 7.63-8.40 (m, 5H); **^{13}C-NMR** (300 MHz, DMSO-*d6*) δ 24.4, 25.3, 32.2, 49.2, 121.9, 124.9, 126.3, 133.4, 135.8, 137.5, 147.2, 159.6; **HRMS**: Calculated for $C_{14}H_{16}O_3N_2SNa$ [M+Na]: 311.0723; measured: 311.0725.

***N*-butyl-carbamoyl-saccharin 9**

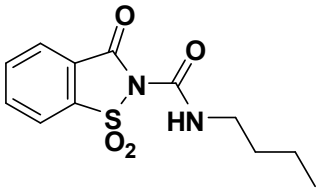

White powder (71% yield); **^{1}H-NMR** (300 MHz, DMSO-*d6*) δ 0.87 (s, 3H), δ 1.18-1.39 (m, 2H), δ 1.39-1.56 (m, 2H), δ 3.12-3.27 (m, 2H), δ 7.91-8.41 (m, 5H); **^{13}C-NMR** (300 MHz, DMSO-*d6*) **^{13}C-NMR** (300 MHz, DMSO-*d6*) δ 14.0, 19.8, 31.4, 121.9, 124.8, 126.2, 135.9, 137.4, 137.6, 147.0, 159.4; **HRMS**: Calculated for $C_{12}H_{14}N_2NaO_4S$ [M+Na]: 305.0566; measured: 305.0566.

***N*-(2-chloroethyl)-carbamoyl-saccharin 10**

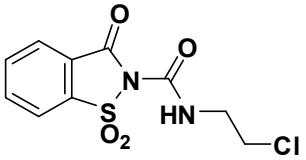

White powder (80% yield); **^{1}H-NMR** (300 MHz, DMSO-*d6*) δ 3.18 (t, *J* = 4.56Hz, 2H), δ 3.79 (t, *J* = 4.75Hz, 2H), δ 7.56-7.73 (m, 3H), δ 6.81 (m, 2H), δ 7.87-8.14 (m, 2H); **^{13}C-NMR** (300 MHz, DMSO-*d6*) δ 41.1, 41.9, 119.9, 123.3, 132.1, 132.6, 167.6. **HRMS**: Calculated for $C_{10}H_{10}O_4N_2SCl$ [M+H]: 289.00443; measured: 289.00411.

***N*-phenyl-carbamoyl-saccharin 11**

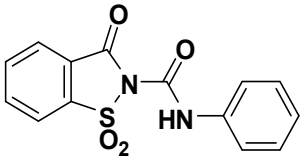

White powder (99% conversion); **^{1}H-NMR** (300 MHz, DMSO-*d6*) δ 6.62-6.72 (m, 3H), δ 7.08-7.17 (m, 2H), δ 7.66-7.77 (m, 4H), δ 7.82-7.88 (s, 1H); **^{13}C-NMR** (300 MHz, DMSO-*d6*) δ 120.4, 121.8, 123.9, 129.8, 132.0, 133.4, 143.0, 165.3, 171.1. **HRMS**: Calculated for $C_{15}H_{11}O_4N_2S$ [M+H]: 303.04340; measured: 303.04234.

***N*-methyl-saccharin 12**

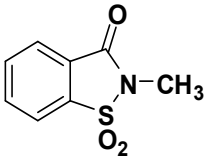

White powder (98% yield); **^{1}H-NMR** (300 MHz, DMSO-*d6*) δ 3.15 (s, 3H), δ 7.94-8.12 (m, 3H), δ 8.28-8.33 (m, 1H); **^{13}C-NMR** (300 MHz, DMSO-*d6*) δ 23.3, 121.9, 125.4, 127.0, 135.6, 136.0, 137.1, 158.9.

Detailed FTIR-ATR and NMR spectra for all compounds have been published and can be found in the supporting information of this article: *Chem. Commun.*, **2017**, *53*, 901.

2D NMR: ^{1}H-^{15}N HMBC

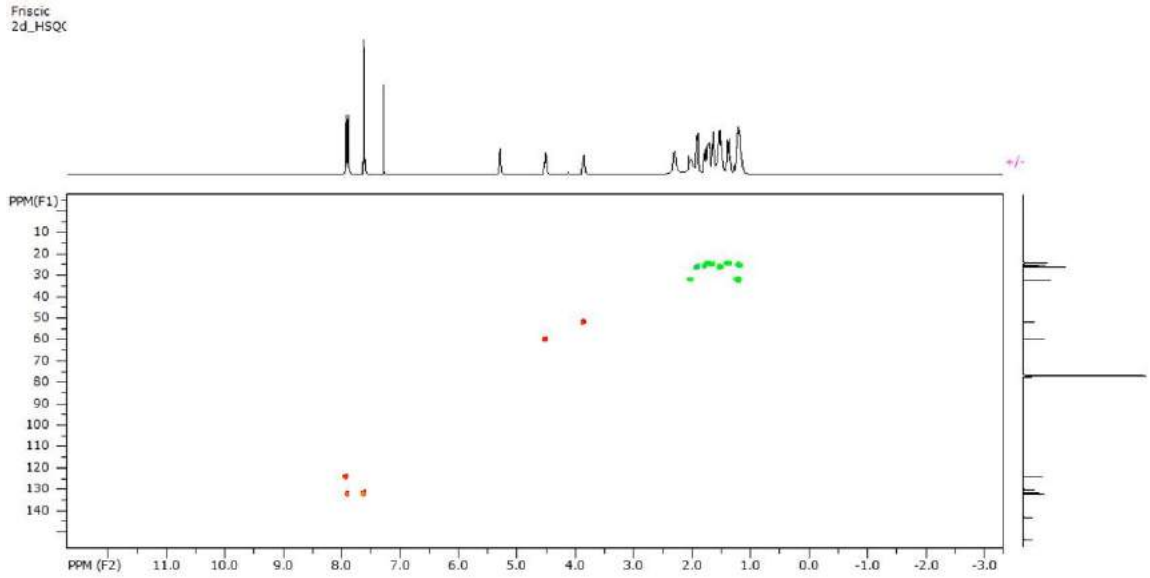

2D NMR: ^{1}H-^{13}C HSQC

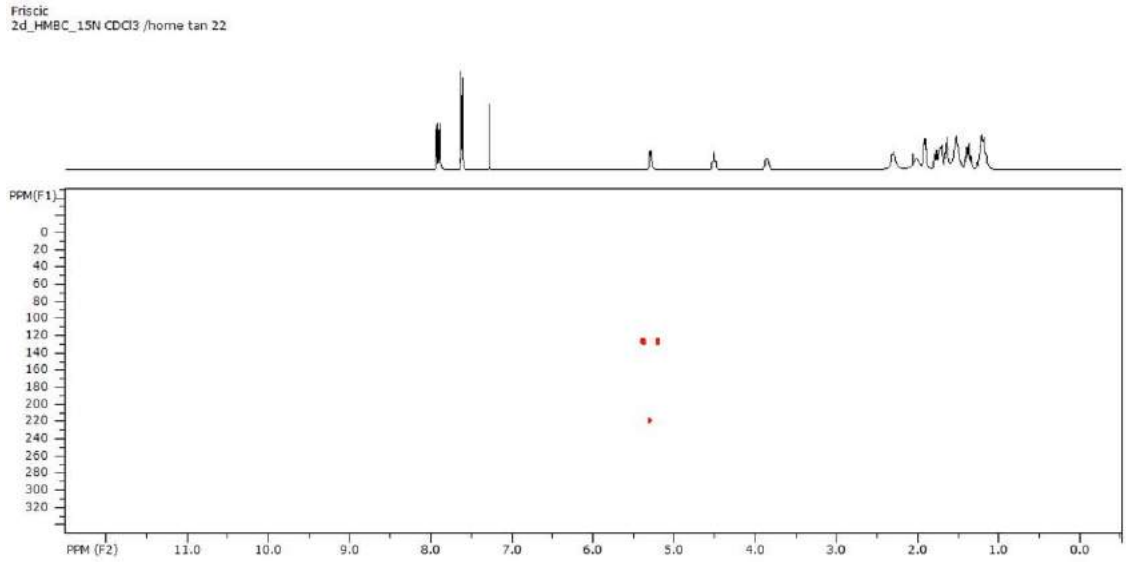

Fig. C1. Two-dimensional NMR, ^{1}H-^{15}N HMBC (top) and ^{1}H-^{13}C HSQC (bottom) spectra performed on the product of the solution reaction as reported by Moffatt and Lerch (JOC 1971). Based on 2D NMR analysis (and XRD data), identity of the product obtained from reaction is not the saccharin adduct as reported but is the ring expanded *N,N'*-dicyclohexyl-benzo[1,3]thiadiazepine **1.**

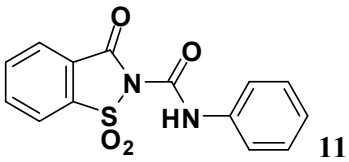

11

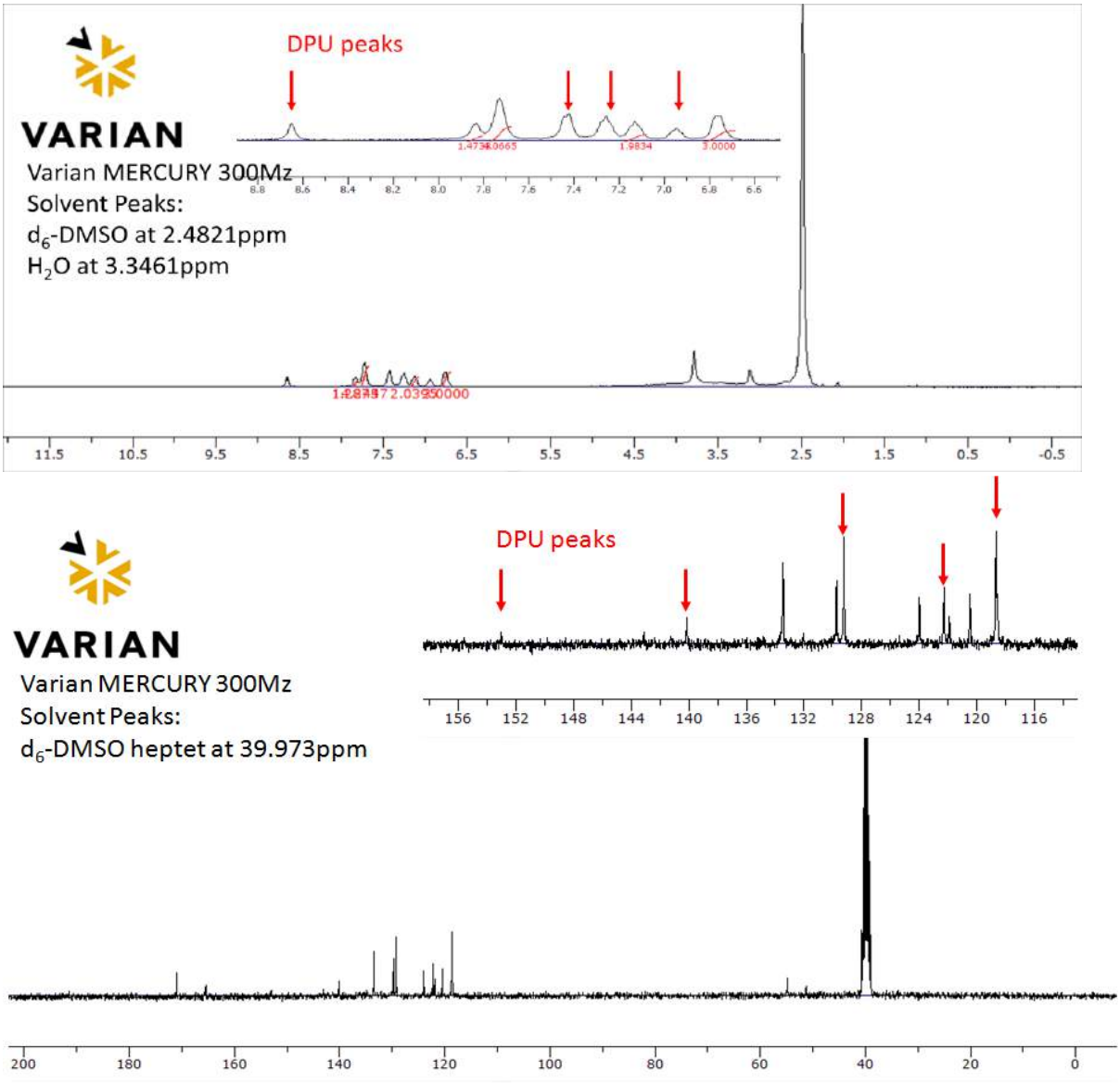

Fig. C2. [1]HNMR spectrum of the crude mixture for the mechanochemical synthesis of *N*-phenyl-carbamoyl-saccharin **11**. Based on NMR, there is 9% conversion, full consumption of the saccharin starting material (absence of saccharin peaks). However, there are significant *N*,*N*'-diphenylurea (DPU) signals observed. Isolated yield for **11** was not obtained.

Table C1. SCXRD data of various two-atom insertion products.

	1	2	3	4
Molecular formula	$C_{20}H_{27}N_3O_3S$	$C_{14}H_{19}N_3O_3S$	$C_{14}H_{19}N_3O_3S$	$C_{24}H_{25}N_3O_4S_2$
M_r	389.18	309.11	309.11	483.13
Crystal System	Orthorombic	Orthorhombic	Monoclinic	Orthorhombic
Crystal colour	Colorless	Colorless	Colorless	Colorless
Space group	*P*bca	*P*bca	$P2_1/c$	$Pna2_1$
Temperature (K)	100K	298K	100K	100K
Unit cell dimensions (Å,°)				
a	12.474(6)	11.1910(9)	11.537(7)	26.324(2)
b	11.835(5)	11.3302(9)	14.933(9)	14.6841(11)
c	26.509(12)	25.142(2)	9.438(6)	5.8835(4)
α	90	90	90	90
β	90	90	112.304(7)	90
γ	90	90	90	90
Volume (Å^3)	3912.52	3188.0(4)	1504.35	2274.23
Z	8	8	4	4
D_{calc} (g cm^{-3})	1.441	1.289	1.366	1.412
μ (mm^{-1}) (abs coeff)	0.300	0.216	0.229	0.272
***F*(000)**	1816	1312	656	1016
Refl. collected/independent	3464/ 2283	3959/ 2255	2686/ 1804	3896 / 3310
No. observed refl. [$I>2\sigma(I)$]*	35897	35978	13409	31390
No. restraints/No. parameters	0/ 244	6/ 223	0/194	1/ 302
R [all/gt]	0.0950/ 0.0517	0.0958/ 0.0439	0.0841/ 0.0550	0.0568 / 0.0403
wR [ref/gt]	0.1382/ 0.1148	0.1226/ 0.1008	0.1833/ 0.1630	0.0848 / 0.0789
Goodness-of-fit on F^2	1.018	1.026	1.030	1.053
Largest diff. peak and hole (*e* Å^{-3})	0.297, -0.487	0.165, -0.300	0.249, -0.396	0.270, -0.350

	6	7
Molecular formula	$C_{22}H_{29}N_3O_3S$	$C_{28}H_{37}N_3O_3S$
M_r	415.19	495.26
Crystal System	Monoclinic	Monoclinic
Crystal colour	Colorless	Colorless
Space group	$P2_1/n$	$P2_1$
Temperature (K)	100K	100K
Unit cell dimensions (Å,°)		
a	10.0595(10)	12.0370(3)
b	20.175(2)	35.2714(10)
c	11.1108(11)	12.5698(3)
α	90	90
β	107.837(4)	96.9780(10)
γ	90	90
Volume (Å^3)	2146.55	5297.1(2)
Z	4	8
D_{calc} (g cm^{-3})	1.286	1.243
μ (mm^{-1})	0.179	1.351
***F*(000)**	888	2128
Refl. collected/independent	4971/ 4458	20864/14988
No. observed refl. [$I>2\sigma(I)$]*	65819	20864
No. restraints/No. parameters	0/ 268	1/1270
R [all/gt]	0.0454/0.0373	0.1019/0.0637
wR [ref/gt]	0.1087/0.0993	0.1531/0.1357
Goodness-of-fit on F^2	1.117	1.010
Largest diff. peak and hole (*e* Å^{-3})	0.365, -0.623	0.567, -0.424

*$R = \sum||Fo|-|Fc||/\sum Fo, w = 1/[\sigma^2(F_o^2)+(g_1P)^2+ g_2P]$ where $P = (F_o^2+2F_c^2)/3$, $S = \Sigma[w(F_o^2 - F_c^2)^2/(N_{obs} - N_{param})]^{1/2}$.

Table C2. SCXRD data of various saccharin-isocyanate adducts.

	8	**10**	**11**
Molecular formula	$C_{15}H_{20}N_2O_5S$	$C_{10}H_9ClN_2O_4S$	$C_{14}H_{10}N_2O_4S$
M_r	340.11	288.00	302.04
Crystal System	Orthorhombic	Monoclinic	Monoclinic
Crystal colour	Colorless	Colorless	Colorless
Space group	$P2_12_12_1$	$P2_1/c$	$P2_1/c$
Temperature (K)	100K	150K	100K
Unit cell dimensions (Å,°)			
a	6.7492(7)	11.8316(16)	6.4988(6)
b	7.2139(7)	14.0713(19)	15.6631(14)
c	31.441(3)	7.0351(10)	12.8234(14)
α	90	90	90
β	90	96.718(2)	100.670(4)
γ	90	90	90
Volume (Å^3)	1530.8(3)	1163.2	1282.74
Z	4	4	4
D_{calc} (g cm^{-3})	1.477	1.649	1.669
μ (mm^{-1})	0.240	0.516	0.274
***F*(000)**	720	592	660
Refl. collected/independent	60042	2137/ 1808	2262/ 1842
No. observed refl. [$I>2\sigma(I)$]*	8232/ 7166	11594	18893
No. restraints/No. parameters	0/211	0/ 163	0/190
R [all/gt]	0.0529/ 0.0405	0.0425/ 0.0341	0.0471/ 0.0338
wR [ref/gt]	0.1032 / 0.0983	0.0893/ 0.0839	0.0849/ 0.0796
Goodness-of-fit on F^2	1.098	1.064	1.054
Largest diff. peak and hole (*e* Å^{-3})	0.503, -0.568	0.337, -0.366	0.213, -0.392

*$R = \sum||Fo|-|Fc||/\sum Fo, w = 1/[\sigma^2(F_o^2)+(g_1P)^2+ g_2P]$ where $P = (F_o^2+2F_c^2)/3$, $S = \Sigma[w(F_o^2 - F_c^2)^2/(N_{obs} - N_{param})]^{1/2}$.

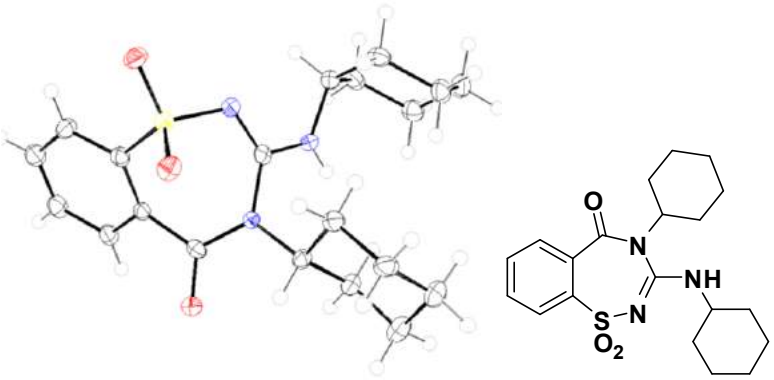

Fig. C3. Molecular structure visualized using ORTEP-3 with thermal ellipsoids at 50% probability level of N,N'-dicyclohexyl-benzo[1,3]thiadiazepine **1** as determined by SCXRD, along with a schematic representation of the molecule.

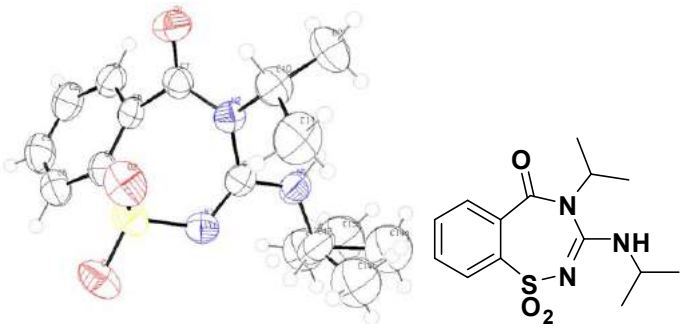

Fig. C4. Molecular structure visualized using ORTEP-3 with thermal ellipsoids at 50% probability of N,N'-diisopropyl-benzo[1,3]thiadiazepine **2** as determined by SCXRD, along with a schematic representation of the molecule.

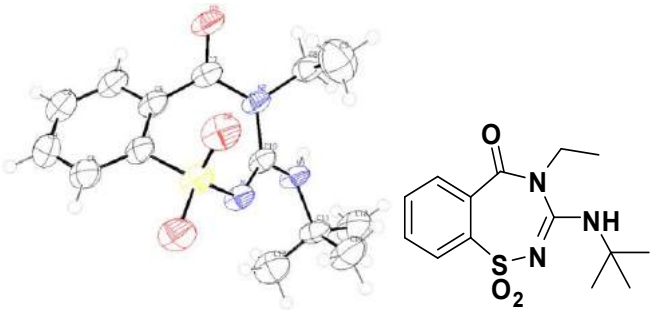

Fig. C5. Molecular structure visualized using ORTEP-3 with thermal ellipsoids at 50% probability level of N-ethyl-N'-tertbutyl-benzo[1,3]thiadiazepine **3** as determined by determined by SCXRD, along with a schematic representation of the molecule.

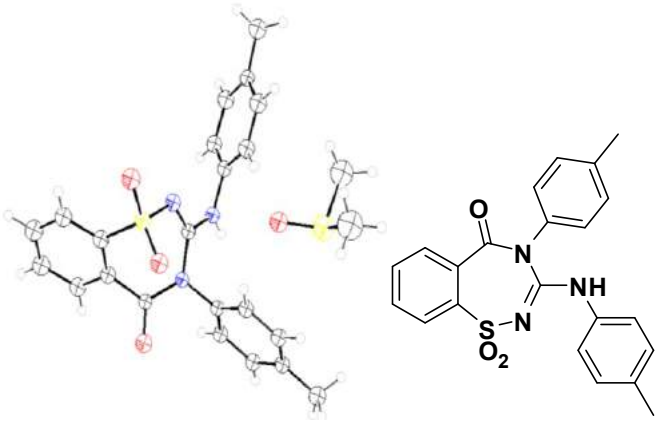

Fig. C6. Molecular structure visualized using ORTEP-3 with thermal ellipsoids at 50% probability level of N,N'-diisopropyl-benzo[1,3]thiadiazepine **2** as determined by SCXRD, along with a schematic representation of the molecule.

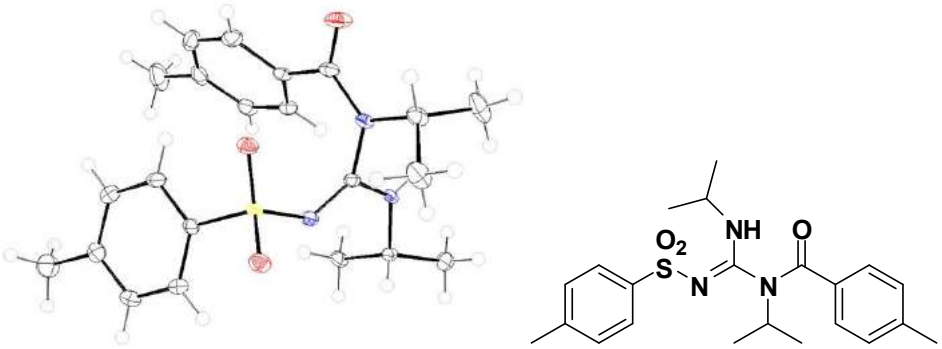

Fig. C7. Molecular structure visualized using ORTEP-3 with thermal ellipsoids at 50% probability level of (*E*)-*N*-isopropyl-*N*-(*N*-isopropyl-*N*'-tosylcarbamimidoyl)-4-methylbenzamide **6** as determined by SCXRD, along with a schematic representation of the molecule.

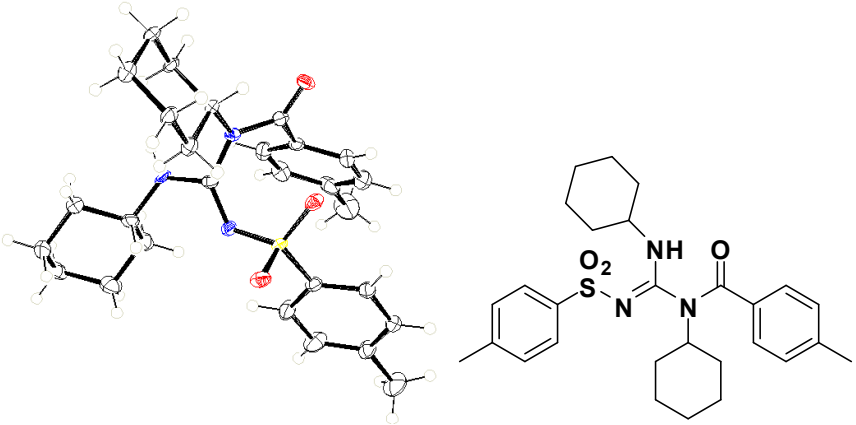

Fig. C8. Molecular structure visualized using ORTEP-3 with thermal ellipsoids at 50% probability level of (*E*)-*N*-cyclohexyl-*N*-(*N*-cyclohexyl -*N*'-tosylcarbamimidoyl)-4-methylbenzamide **7** as determined by SCXRD, along with a schematic representation of the molecule.

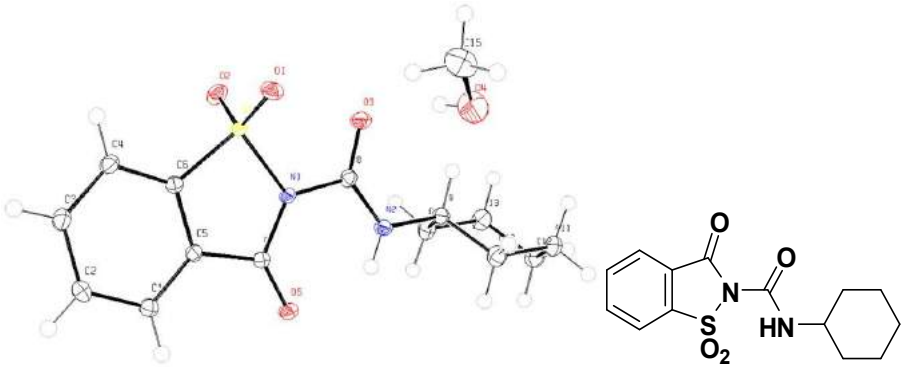

Fig. C9. Molecular structure visualized using ORTEP-3 with thermal ellipsoids at 50% probability level of (E)-N-isopropyl-N-(N-isopropyl-N'-tosylcarbamimidoyl)-4-methylbenzamide **8** with a methanol solvate as determined by SCXRD, along with a schematic representation of the molecule.

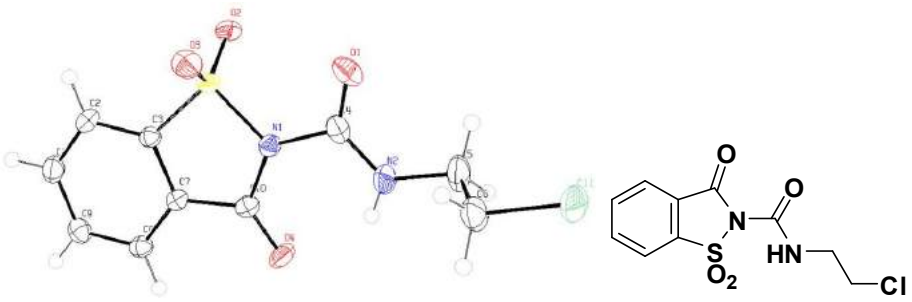

Fig. C10. Molecular structure visualized using ORTEP-3 with thermal ellipsoids at 50% probability level of N-(2-chloroethyl)-carbamoyl-saccharin **10** as determined by SCXRD, along with a schematic representation of the molecule.

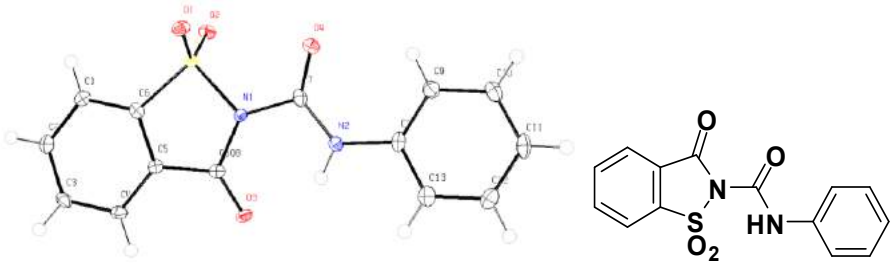

Fig. C11. Molecular structure visualized using ORTEP-3 with thermal ellipsoids at 50% probability level of N-phenyl-carbamoyl-saccharin **11** as determined by SCXRD, along with a schematic representation of the molecule.

APPENDIX D

SPECTROSCOPIC AND X-RAY DIFFRACTION DATA FOR COMPOUNDS IN CHAPTER 5

_N_-cyclohexyl-2,3-dioxoindoline-1-carboxamide 1a

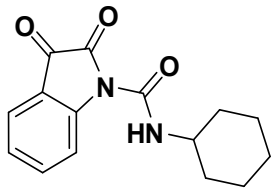

Yellow Powder (95% yield); **^{1}H-NMR** (300 MHz, DMSO-*d6*) δ 1.16-1.89 (m, 10H), δ 3.63-3.79 (m, 1H), δ 7.23-7.30 (m, 1H), δ 7.63-7.75 (m, 2H) δ 8.05-8.19 (m, 2H); **^{13}C-NMR** (300 MHz, DMSO-*d6*) δ 24.5, 25.4, 32.5, 48.7, 116.9, 119.4, 124.8, 125.2, 137.9, 148.6, 150.2, 159.8, 180.7; **HRMS**: Calculated for $C_{15}H_{16}N_2O_3$ [M^{-}•]: 272.11664; measured: 272.11691.

_N_-cyclohexyl-5-methoxy-2,3-dioxoindoline-1-carboxamide 1b

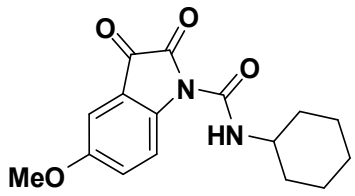

Brown powder (99% yield); **^{1}H-NMR** (300 MHz, DMSO-*d6*) δ 1.15-1.90 (m, 10H), δ 3.61-3.73 (m, 1H), δ 3.78 (s, 3H), δ 7.19 (s, 1H), δ 7.27 (d, *J* = 7.50Hz, 2H) δ 7.98-8.13 (m, 2H) ; **^{13}C-NMR** (300 MHz, DMSO-*d6*) δ 24.5, 25.4, 32.5, 48.7, 56.3, 108.4, 118.4, 120.2, 124.4, 142.2, 150.5, 156.5, 159.8, 180.8; **HRMS**: Calculated for $C_{16}H18N_2O_4$ [M^{-}•]: 302.12721; measured: 302.12735.

5-chloro-_N_-cyclohexyl-2,3-dioxoindoline-1-carboxamide 1e

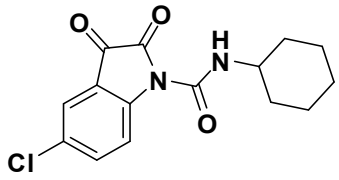

Orange powder (99% yield); **^{1}H-NMR** (300 MHz, DMSO-*d6*) δ 1.09-1.91 (m, 10H), δ 3.62-3.80 (m, 1H), δ 7.47-7.82 (m, 2H), δ 7.94-8.27 (m, 2H); **^{13}C-NMR** (300 MHz, DMSO-*d6*) δ 24.5, 25.4, 32.4, 48.8, 118.5, 121.0, 124.2, 129.6, 136.9, 147.0, 150.1, 159.4, 179.6 ; **HRMS**: Calculated for $C_{15}H_{15}O_3N_2Cl$ [M^{-}•]: 306.07767; measured: 306.07776.

_N_-cyclohexyl-5-fluoro-2,3-dioxoindoline-1-carboxamide 1f

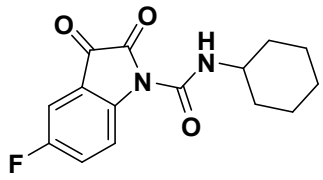

Orange powder (99% yield); **^{1}H-NMR** (300 MHz, DMSO-*d6*) δ 1.09-1.95 (m, 10H), δ 3.60-3.76 (m, 1H), δ 7.47-7.67 (m, 2H), δ 7.97-8.26 (m, 2H); **^{13}C-NMR** (300 MHz, DMSO-*d6*) δ 24.5, 25.4, 32.4, 48.7, 111.2, 111.5, 118.6, 118.7, 120.8, 120.9, 123.9, 124.2, 144.7, 150.2, 157.8, 159.7, 161.1, 179.9; **^{19}F-NMR** (300 MHz, DMSO-*d6*): δ –117.7; **HRMS**: Calculated for $C_{15}H15N_2O_3F$ [M^{-}•]: 290.10722; measured: 290.10722.

***N*-cyclohexyl-5-nitro-2,3-dioxoindoline-1-carboxamide 1g**

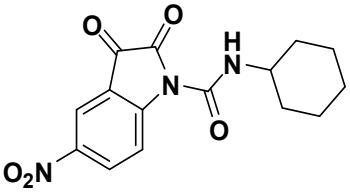

Yellow powder (97% yield); **^{1}H-NMR** (300 MHz, DMSO-*d6*) δ 1.09-1.98 (m, 10H), δ 3.60-3.76 (m, 1H), δ 7.93-8.26 (m, 2H),), δ 8.27-8.65 (m, 2H); **^{13}C-NMR** (300 MHz, DMSO-*d6*) δ 24.2, 25.0, 32.2, 33.9, 42.1, 117.2, 119.0, 120.0, 132.5, 144.5, 149.7, 153.1, 159.6, 178.8; **HRMS**: Calculated for $C_{15}H_{15}O_5N_2$ [M^{-}•]: 317.10172; measured: 317.10175.

***N*-cyclohexyl-2,3-dioxo-5-(trifluoromethoxy)indoline-1-carboxamide 1h**

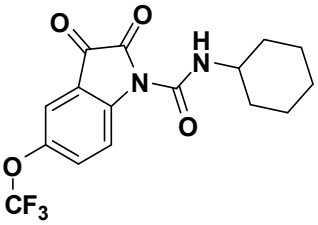

Orange powder (91% yield); **^{1}H-NMR** (300 MHz, DMSO-*d6*) δ 1.15-19.6 (m, 10H), δ 3.59-3.79 (m, 1H), δ 7.61-7.72 (m, 2H), δ 7.96-8.36 (m, 2H); **^{13}C-NMR** (300 MHz, DMSO-*d6*) **^{13}C-NMR** (300 MHz, DMSO-*d6*) δ 24.5, 25.4, 32.4, 48.8, 117.5, 118.7, 120.9, 130.2, 145.1, 146.9, 150.2, 159.6, 179.6; **^{19}F-NMR** (300 MHz, DMSO-*d6*): δ –57.4; **HRMS**: Calculated for $C_{16}H_{15}N_2F_3O_4$ [M^{-}•]: 356.09894; measured: 356.09838.

(*Z*)-3-(cyclohexylcarbamoyloxyimino)indolin-2-one 1i

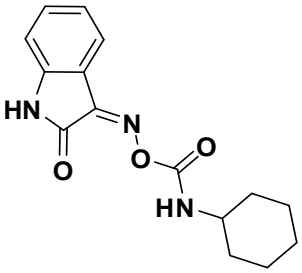

Yellow (95% yield); **^{1}H-NMR** (300 MHz, DMSO-*d6*) δ 1.08-1.92 (m, 10H), δ 3.34-3.47 (m, 1H), δ 6.80-7.11 (m, 2H), δ 7.43 (t, d, *J* = 7.65Hz, 1H), δ 7.81-8.22 (m, 2H) δ 10.85 (s, 1H); **^{13}C-NMR** (300 MHz, DMSO-*d6*) δ 25.1, 25.5, 32.6, 50.6, 111.0, 115.4, 122.4, 129.7, 134.7, 144.3, 147.1, 152.7, 163.9; **HRMS**: Calculated for $C_{15}H_{16}O_3N_3$ [M-H]: 286.11971; measured: 286.11985.

(*Z*)-N-cyclohexyl-3-(cyclohexylcarbamoyloxyimino)-2-oxoindoline-1-carboxamide 1j

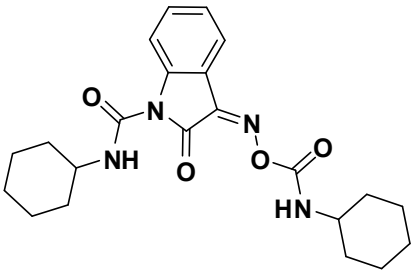

Orange powder (68% yield); **^{1}H-NMR** (300 MHz, DMSO-*d6*) δ 1.11-19.2 (m, 20H), δ 3.34-3.50 (m, 1H), δ 3.61-3.73 (m, 1H), δ 7.17-7.34 (m, 1H), δ 7.99-8.52 (m, 4H);; **^{13}C-NMR** (300 MHz, DMSO-*d6*) δ 24.5, 24.8, 25.1, 25.5, 25.8, 32.4, 32.8, 33.7, 34.4, 48.8, 50.7, 115.6, 115.9, 125.0, 126.8, 129.0, 134.4, 142.4, 146.0, 150.0, 152.5, 164.4. **HRMS**: Calculated for $C_{22}H_{28}O_4N_4$ [M+H]: 361.12165; measured: 361.12105.

2,3-dioxo-N-phenylindoline-1-carboxamide 2a

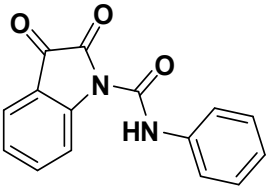

Green powder (95% conversion by NMR); **^{1}H-NMR** (300 MHz, DMSO-*d6*) δ 7.11-7.20 (m, 1H), δ 7.30-7.39 (m, 2H), δ 7.53-7.88 (m, 5H), δ 8.08-8.24 (m, 1H), δ 10.18 (s, 1H); **HRMS**: Calculated for $C_{15}H_{10}O_3N_2$ [M-]: 266.06997; measured: 266.06983.

***N*-(biphenyl-4-yl)-2,3-dioxoindoline-1-carboxamide 2d**

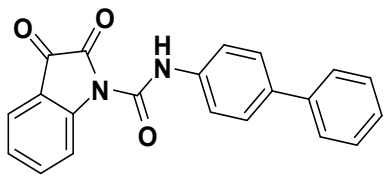

Green powder (83% yield); **^{1}H-NMR** (300 MHz, DMSO-*d6*) δ 7.26-7.94 (m, 12H), δ 8.08-8.29 (m, 1H), δ 10.2 (s, 1H);; **^{13}C-NMR** (300 MHz, DMSO-*d6*) δ 116.9, 119.0, 119.6, 120.9, 125.0, 125.6, 126.5, 126.9, 127.4, 127.8, 129.3, 136.9, 138.3. **HRMS**: Calculated for $C_{21}H_{14}O_3N_2$ [M^{-}•]: 342.10099; measured: 342.10093.

***N*-(4-fluorophenyl)-2,3-dioxoindoline-1-carboxamide 2h**

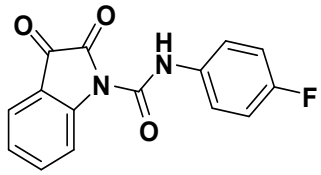

Green powder (58% yield); **^{1}H-NMR** (300 MHz, DMSO-*d6*) δ 7.03-7.87 (m, 7H), δ 8.04-8.17 (m, 1H), δ 10.2 (s, 1H); **^{13}C-NMR** (300 MHz, DMSO-*d6*) δ 115.6, 116.0, 117.0, 119.6, 120.4, 122.8, 124.8, 126.0, 138.1, 147.9, 148.5, 159.6, 180.6; **^{19}F-NMR** -118.5 (300 MHz, DMSO-*d6*): δ ; **HRMS**: Calculated for $C_{15}H_9O_3N_2F$ [M^{-}•]: 248.06027; measured: 248.06031.

***N*-(4-bromophenyl)-2,3-dioxoindoline-1-carboxamide 2j**

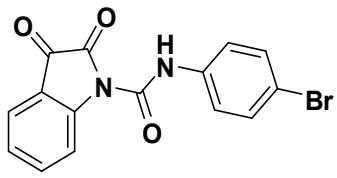

Green powder (83% yield); **^{1}H-NMR** (300 MHz, DMSO-*d6*) δ 7.04-7.89 (m, 7H), δ 8.03-8.16 (m, 1H), δ 10.2 (s, 1H);; **^{13}C-NMR** (300 MHz, DMSO-*d6*) δ 115.6, 116.0, 117.0, 119.6, 120.4, 122.8, 124.8, 126.0, 138.1, 147.9, 148.5, 159.6, 180.6. **HRMS**: Calculated for $C_{15}H_9O_3N_2Br$ [M^{-}•]:343.98020; measured: 343.98007.

***N*-butyl-2,3-dioxoindoline-1-carboxamide 2k**

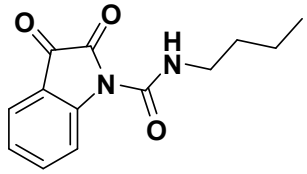

Yellow powder (56% yield); **^{1}H-NMR** (300 MHz, DMSO-*d6*) δ 0.93 (s, 3H), δ 1.18-1.61 (m, 4H), δ 3.12-3.29 (m, 2H)), δ 7.19-7.34 (m, 1H)), δ 7.58-7.77 (m, 2H)), δ 8.07-8.33 (m, 2H); **^{13}C-NMR** (300 MHz, DMSO-*d6*) δ 14.4, 19.9, 31.6, 39.5, 116.8, 119.4, 124.8, 125.2, 138.1, 147.7, 151.0, 159.6, 180.6; **HRMS**: Calculated for $C_{13}H_{14}O_3N_2Na$ [M+Na]: 269.0897; measured: 269.0889.

***N*-(2-chloroethyl)-2,3-dioxoindoline-1-carboxamide 2l**

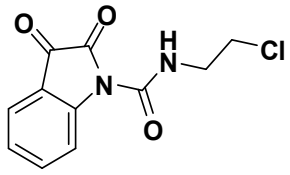

Yellow powder (83% yield); **^{1}H-NMR** (300 MHz, DMSO-*d6*) δ 3.60-3.69 (m, 2H), δ 3.72-3.79 (m, 2H), δ 7.24-7.32 (m, 1H), δ 7.64-7.74 (m, 2H), δ 8.10 (d, *J* = 8.01Hz, 1H), δ 8.48 (t, *J* = 6.30Hz, 1H); **^{13}C-NMR** (300 MHz, DMSO-*d6*) δ 41.7, 43.5, 117.0, 119.4, 124.8, 125.2, 138.0, 148.3, 151.3, 159.7, 180.4. **HRMS**: Calculated for $C_{11}H_9O_3N_2Cl$ [M^{-}•]: 252.03072; measured: 252.03053.

***N*-(cyclohexylcarbamoyl)benzamide 3a**

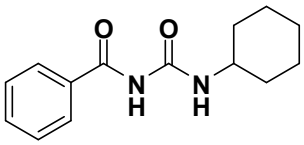

White powder (98% yield); **^{1}H-NMR** (300 MHz, DMSO-*d6*) δ 1.16-1.91 (m, 10H), δ 3.53-3.67 (m, 1H), δ 7.41-7.64 (m, 3H), δ 7.94 (d, *J* = 7.94Hz, 2H), δ 8.65 (d, *J* = 6.52Hz, 3H), δ 10.7 (s, 1H) ;**^{13}C-NMR** (300 MHz, DMSO-*d6*) δ 24.5, 25.5, 32.7, 48.2, 128.4, 128.9, 132.9, 133.2, 153.0, 168.9. **HRMS**: Calculated for $C_{14}H_{18}O_2N_2$ [M^{-}•]: 245.12955; measured: 245.12940.

***N*-(cyclohexylcarbamoyl)-2,4-bis(trifluoromethyl)benzamide 3b**

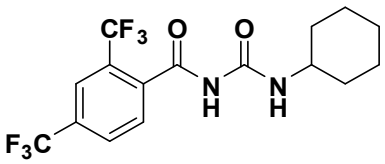

White powder (87% yield); **^{1}H-NMR** (300 MHz, DMSO-*d6*) δ 0.99-1.89 (m, 10H), δ 3.49-3.65 (m, 1H), δ δ 7.73-8.33 (m, 4H), δ 11.07 (s, 1H); **^{13}C-NMR** (300 MHz, DMSO-*d6*) δ 24.5, 25.5, 32.7, 48.2, 123.8, 130.1, 130.4, 151.7, 168.4; **^{19}F-NMR** (300 MHz, DMSO-*d6*): δ –58.2, -61.5; **HRMS**: Calculated for $C_{16}H_{15}O_2N_2F_6$ [M-H]: 381.10432; measured: 381.10439.

***N*-(cyclohexylcarbamoyl)-3,5-bis(trifluoromethyl)benzamide 3c**

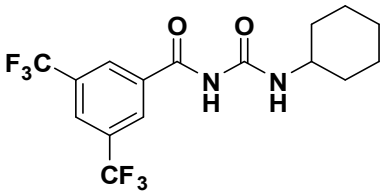

White powder (88% yield); **^{1}H-NMR** (300 MHz, DMSO-*d6*) δ 0.89-1.91 (m, 10H), δ 3.54-3.66 (m, 1H), δ 7.76-8.00 (m, 1H), δ 8.27-8.75 (m, 3H), δ 11.1 (s, 1H); **^{13}C-NMR** (300 MHz, DMSO-*d6*) δ 24.5, 24.9, 25.5, 32.6, 33.7, 48.2, 125.4, 128.7, 130.7, 136.9, 152.5, 165.2, **^{19}F-NMR** (300 MHz, DMSO-*d6*): δ -61.3; **HRMS**: Calculated for $C_{16}H_{15}O_2N_2F_6$ [M+H]: 383.11887; measured: 383.11939.

***N*-(cyclohexylcarbamoyl)-4-nitrobenzamide 3d**

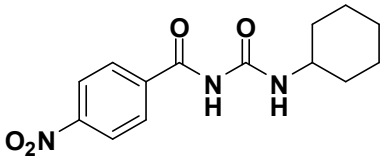

Yellow powder (35% conversion); **^{1}H-NMR** (300 MHz, DMSO-*d6*) δ 0.89-1.918 (m, 10H), δ 3.54-3.66 (m, 1H), δ 8.11-8.17 (m, 3H), δ 8.48 (d, *J* = 7.96Hz, 2H), δ 11.00 (s, 1H).

***N*-(cyclohexylcarbamoyl)-4-methylbenzamide 3e**

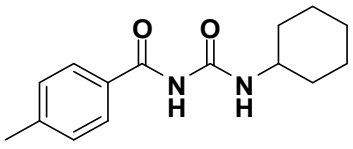

White powder (65% yield); **^{1}H-NMR** (300 MHz, DMSO-*d6*) δ 1.07-1.83 (m, 10H), δ 2.35 (s, 3H), δ 3.48-3.76 (m, 1H), δ 7.27 (s, 2H), δ 7.82 (s, 2H), δ 8.65 (s, 1H), δ 10.53 (s, 1H); **^{13}C-NMR** (300 MHz, DMSO-*d6*) δ 21.3, 24.5, 25.5, 32.7, 33.7, 48.2, 128.5, 129.5, 152.9, 168.6; **HRMS**: Calculated for $C_{15}H_{19}O_2N_2$ [M-H]: 259.14520; measured: 259.14515.

***N*-(cyclohexylcarbamoyl)-4-methoxybenzamide 3f**

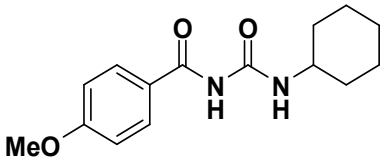

White powder (73% yield); **^{1}H-NMR** (300 MHz, DMSO-*d6*) δ 0.99-1.85 (m, 10H), δ 3.38-3.69 (m, 1H), δ 3.81 (s, 3H), δ 6.99 (s, 2H), δ 7.96 (s, 2H), δ 8.70 (s, 1H), δ 10.50 (s, 1H); **^{13}C-NMR** (300 MHz, DMSO-*d6*) δ 24.5, 25.5, 32.7, 33.6, 48.2, 55.6, 114.0, 124.8, 130.6, 153.2, 163.2, 168.3; **HRMS**: Calculated for $C_{15}H_{19}O_3N_2$ [M-H]: 275.14012; measured: 275.14030.

***N*-(cyclohexylcarbamoyl)-N-methylbenzamide 3g**

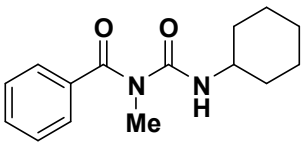

White powder (76% yield); **^{1}H-NMR** (300 MHz, DMSO-*d6*) δ 0.89-1.87(m, 10H), δ 3.07 (s, 3H), δ 3.18-3.47 (m, 1H), δ 7.11-7.68 (m, 4H), δ 8.11-8.54 (m, 1H); **^{13}C-NMR** (300 MHz, DMSO-*d6*) δ 24.5, 25.5, 32.6, 34.2, 49.2, 127.4128.9, 130.7, 136.9, 155.1, 172.4; **HRMS**: Calculated for $C_{16}H_{15}O_2N_2$ [M+H]: 261.15975; measured: 261.15935.

***N*-cyclohexyl-1,3-dioxoisoindoline-2-carboxamide 4**

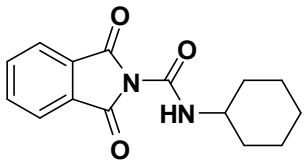

White powder (60% yield); **^{1}H-NMR** (300 MHz, DMSO-*d6*) δ 1.18-1.36 (m, 5H), δ 1.47-1.86 (m, 5H), δ 3.52-3.60 (m, 1H), δ 7.87-8.02 (m, 4H), δ 8.38 (d, *J* = 8.31Hz, 1H); **^{13}C-NMR** (300 MHz, DMSO-*d6*) δ 24.3, 25.3, 32.2, 49.6, 124.4, 131.5, 146.9, 166.0; **HRMS**: Calculated for $C_{15}H_{16}O_3N_2$ [M+H]: 273.12337; measured: 273.12264.

***N*-cyclohexyl-2-oxooxazolidine-3-carboxamide**

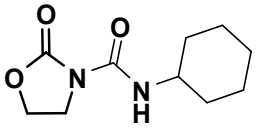

White powder (92% yield); **^{1}H-NMR** (300 MHz, DMSO-*d6*) δ 1.11-1.38 (m, 5H), δ 1.45-1.82 (m, 5H), δ 3.48-3.58 (m, 1H), δ 3.86 (t, *J* = 8.10 Hz, 2H), δ 4.34 (t, *J* = 8.00 Hz, 2H), δ 7.67 (d, *J* = 7.89 Hz, 1H); **^{13}C-NMR** (300 MHz, DMSO-*d6*) δ 24.6, 25.4, 32.6, 42.7, 48.6, 62.9, 150.8, 156.2; **HRMS**: Calculated for $C_{10}H_{16}O_3N_2$ [M+H]: 213.12337; measured: 213.12329.

FTIR-ATR Spectra for all mechanosynthesized compounds

Comparison of the FTIR-ATR spectrum of the crude mixture shows the absence of the characteristic peak of isocyanates (C=N stretching bands between 2000-2200 cm^{-1}), which indicates that all the isocyanates has been completely consumed and that the reaction has reached completion during milling, *i.e.* the product has formed during ball milling and not during workup.

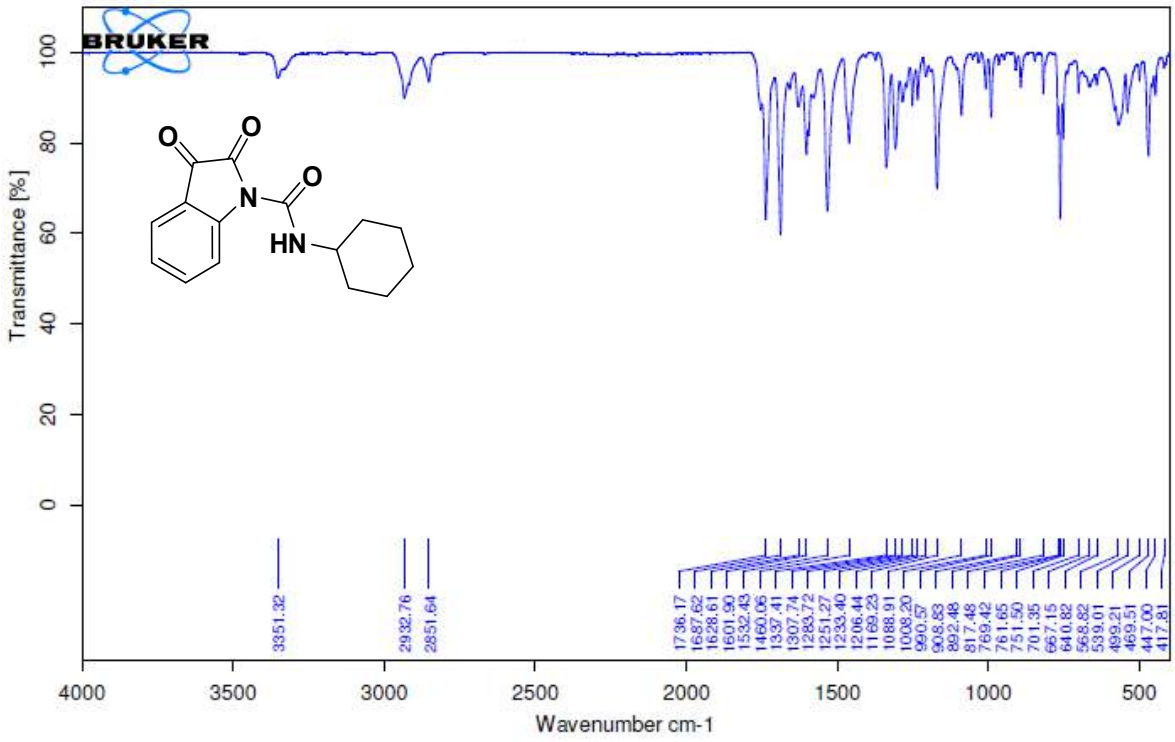

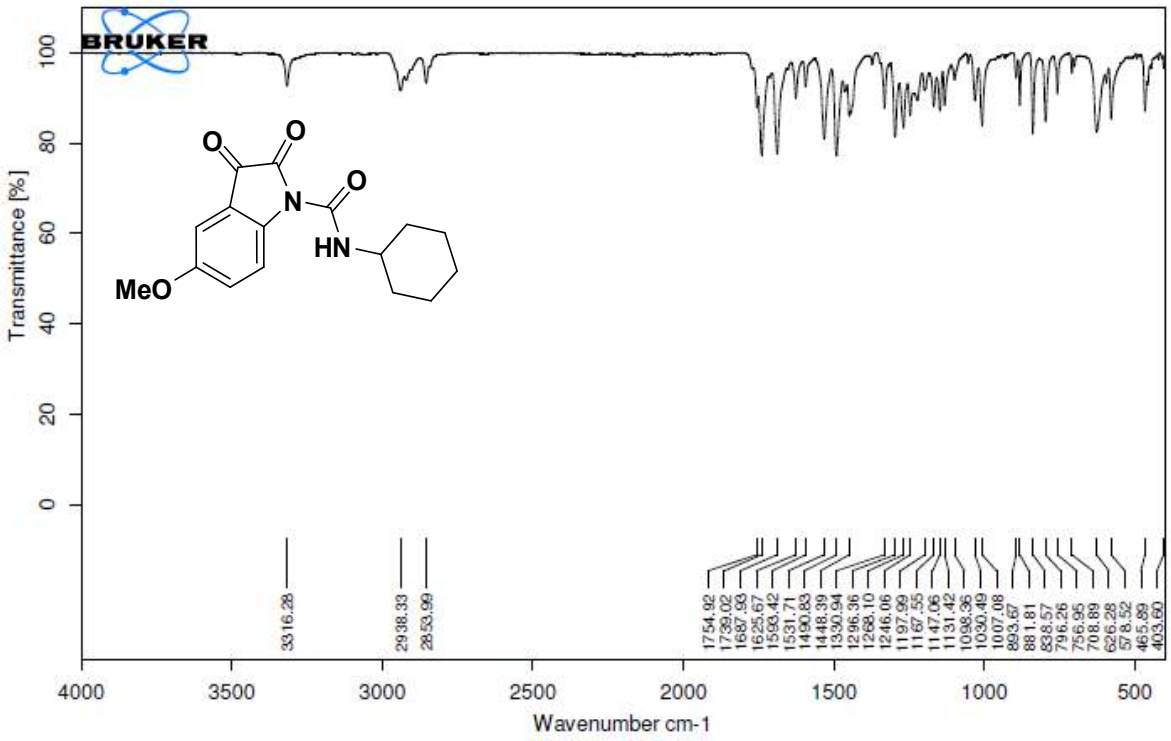
BRUKER
O
O
N
O
HN
MeO
Transmittance [%]
100
80
60
40
20
0
3316.28
2938.33
2853.99
1754.92
1739.02
1687.99
1625.67
1593.42
1531.71
1490.83
1448.39
1330.94
1296.36
1268.10
1246.06
1197.99
1167.55
1147.06
1131.42
1098.36
1030.49
1007.08
893.67
881.81
838.57
796.25
756.95
708.89
626.28
578.52
465.89
403.60
4000
3500
3000
2500
2000
1500
1000
500
Wavenumber cm-1

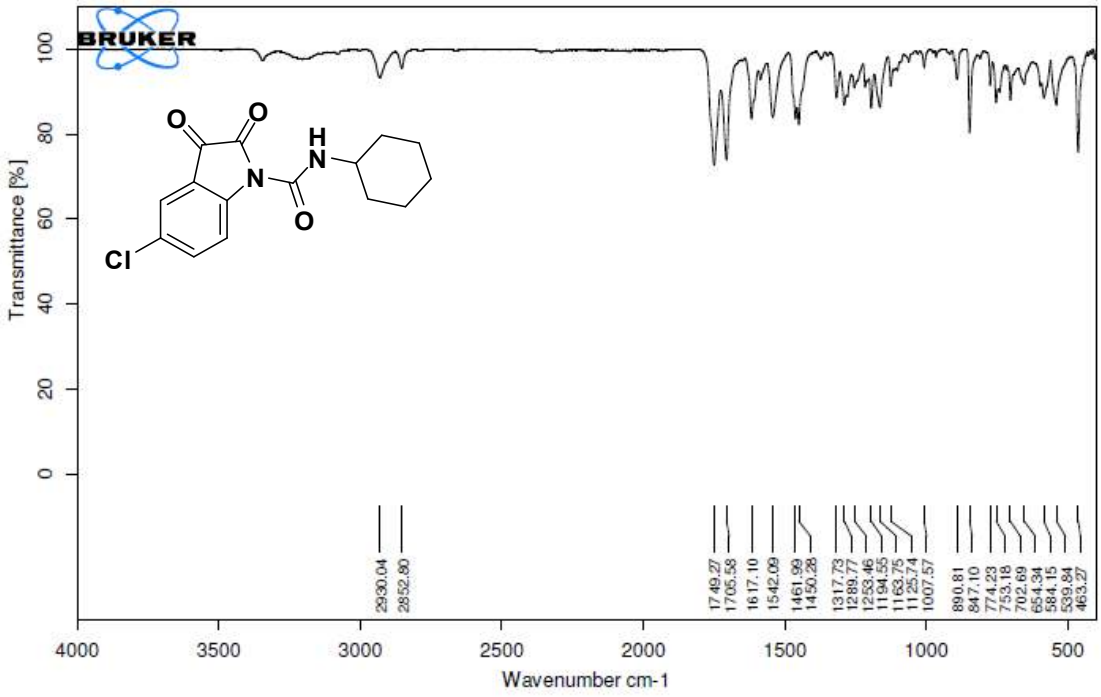
BRUKER
O
O
N
H
N
O
Cl
Transmittance [%]
100
80
60
40
20
0
2930.04
2852.90
1749.27
1705.58
1617.10
1542.09
1461.99
1450.28
1317.73
1289.77
1253.46
1194.55
1163.75
1125.74
1007.57
890.81
847.10
774.23
753.18
702.69
654.34
584.15
539.84
463.27
4000
3500
3000
2500
2000
1500
1000
500
Wavenumber cm-1

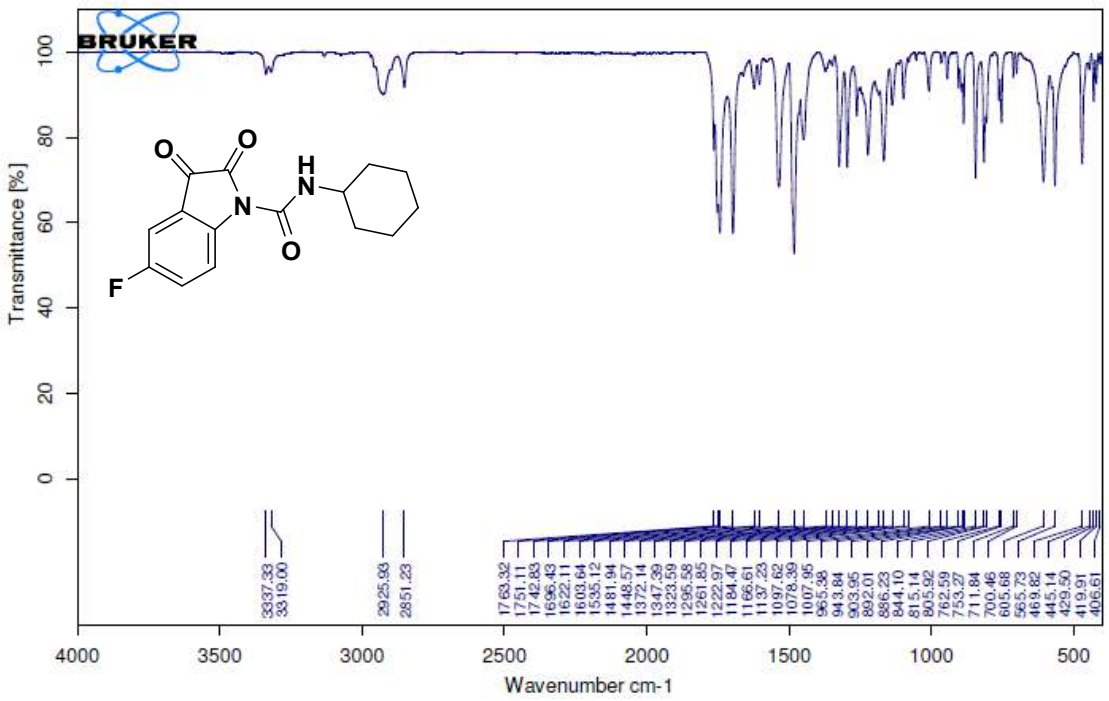
BRUKER
Transmittance [%]
Wavenumber cm-1
3337.33
3319.00
2925.93
2851.23
1763.32
1751.11
1742.83
1696.43
1622.11
1603.64
1535.12
1481.94
1448.57
1372.14
1347.39
1323.59
1296.58
1261.85
1222.97
1184.47
1166.61
1137.23
1097.62
1078.39
1007.95
965.38
943.84
903.95
892.01
886.23
844.10
815.14
805.92
762.59
753.27
711.84
700.46
605.68
565.73
469.82
445.14
429.50
419.91
406.61

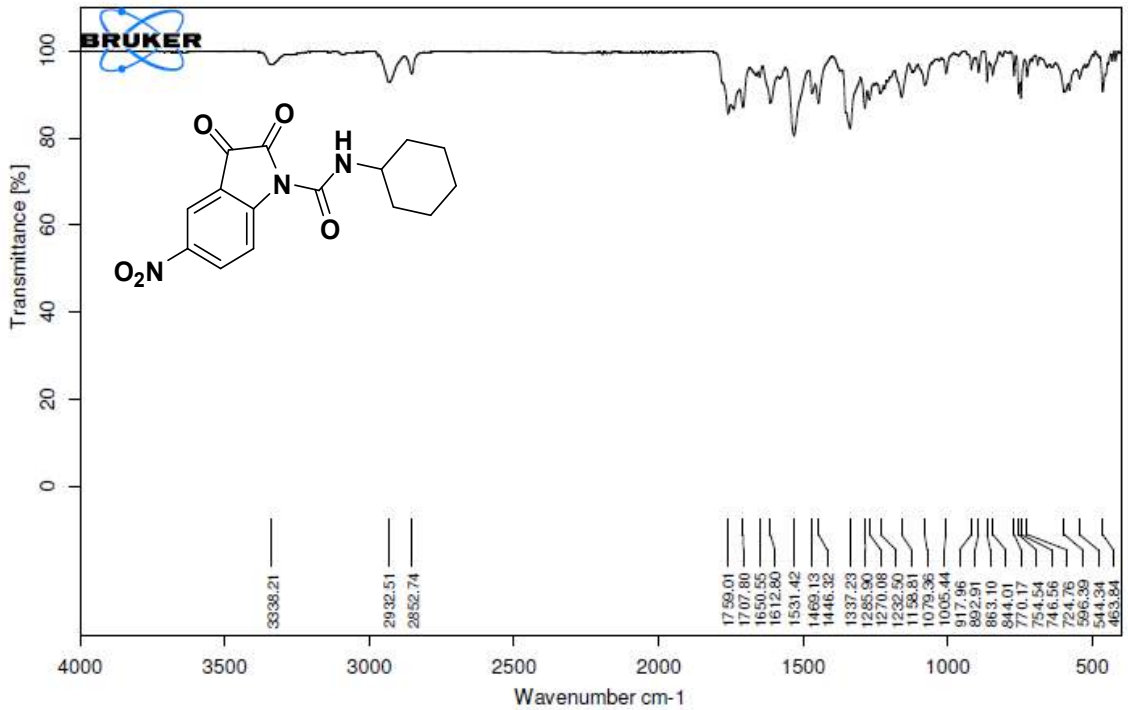
BRUKER
Transmittance [%]
Wavenumber cm-1
3338.21
2932.51
2852.74
1759.01
1707.80
1650.55
1612.80
1531.42
1469.13
1446.32
1397.23
1285.90
1270.08
1232.50
1158.81
1079.36
1005.44
917.96
892.91
863.10
844.01
770.17
754.54
746.56
724.76
596.39
544.34
463.84

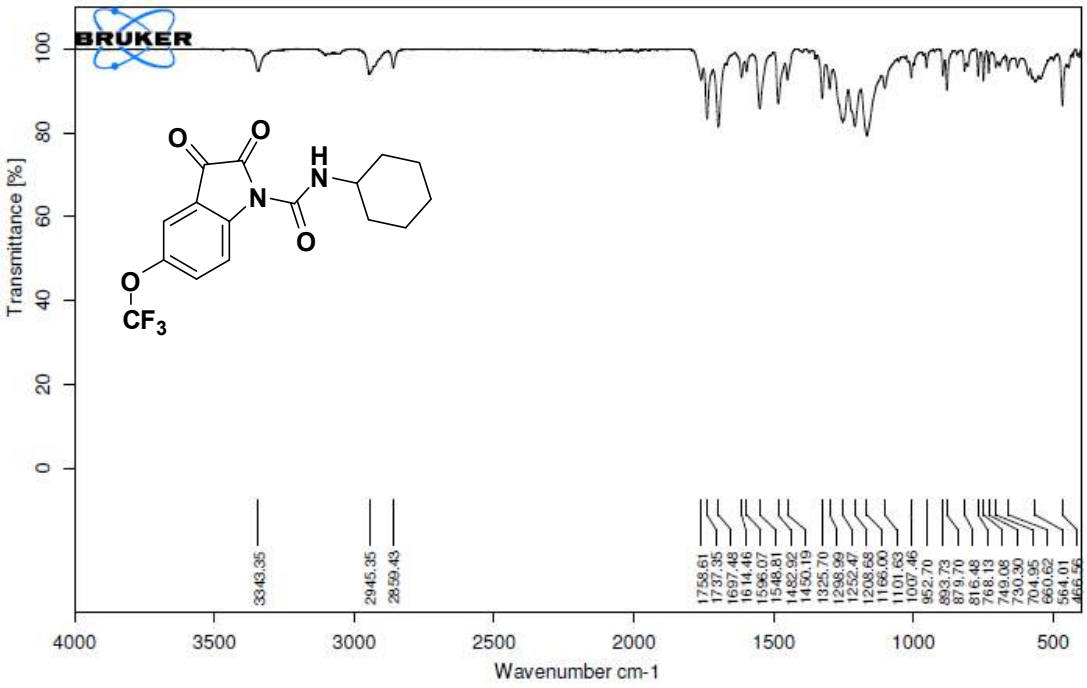
BRUKER
Transmittance [%]
Wavenumber cm-1
3343.35
2945.35
2859.43
1758.61
1737.35
1697.48
1614.46
1596.07
1548.81
1482.92
1450.19
1325.70
1298.99
1252.47
1208.68
1166.00
1101.63
1007.46
952.70
893.73
879.70
816.48
768.13
749.08
730.30
704.95
660.62
564.01
466.56

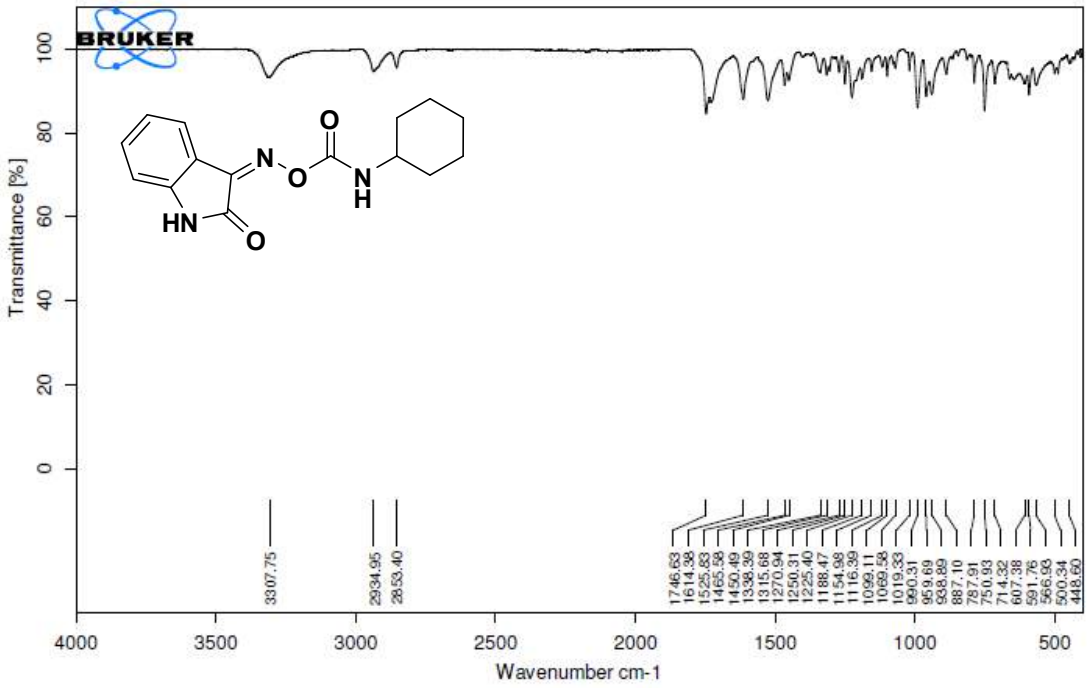
BRUKER
Transmittance [%]
Wavenumber cm-1
3307.75
2934.95
2853.40
1746.63
1614.38
1525.83
1465.56
1450.49
1338.39
1315.68
1270.94
1250.31
1225.40
1188.47
1154.98
1116.39
1099.11
1069.58
1019.33
990.31
959.69
938.89
887.10
787.91
750.93
714.32
607.38
591.76
566.93
500.34
448.60

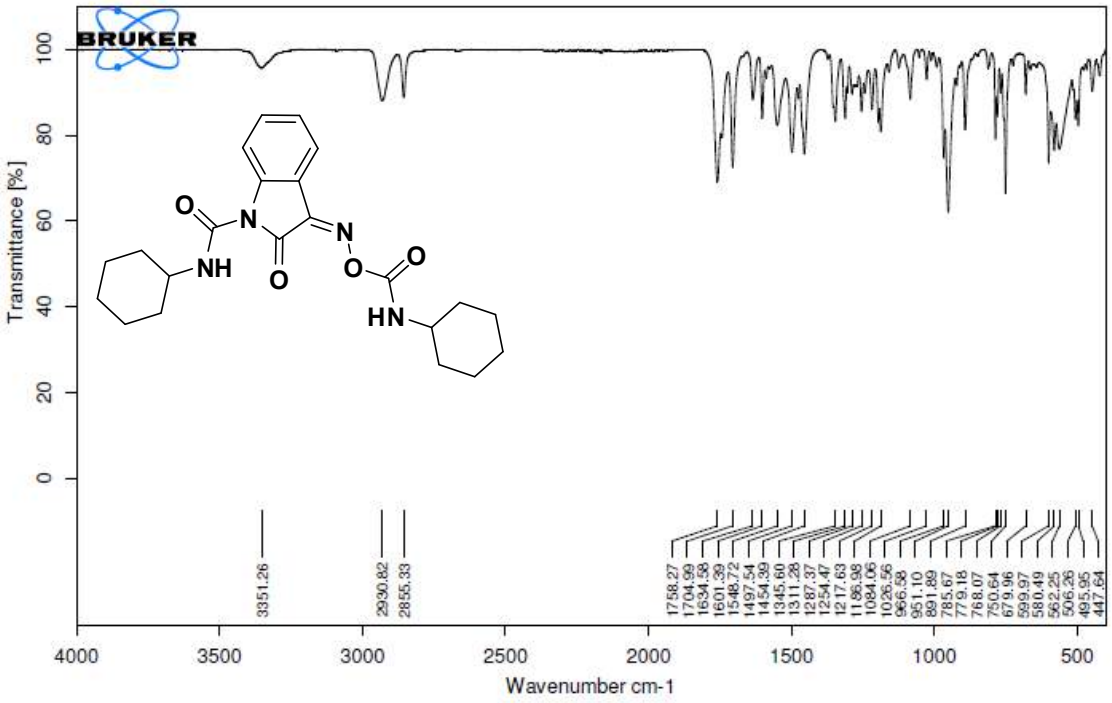
BRUKER
Transmittance [%]
Wavenumber cm-1
3351.26
2930.82
2855.33
1758.27
1704.99
1634.58
1601.39
1548.72
1497.54
1454.39
1345.60
1311.28
1287.37
1254.47
1217.63
1186.98
1084.06
1026.56
966.38
951.10
891.89
785.67
779.18
768.07
750.64
679.96
599.97
580.49
562.25
506.26
495.95
447.64

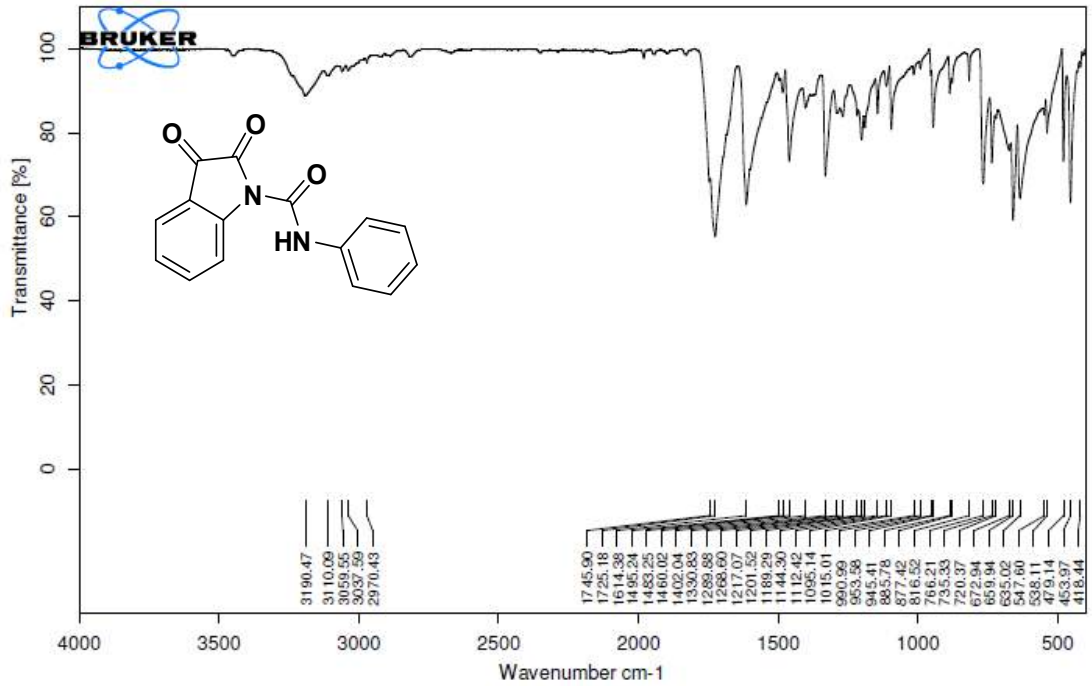
BRUKER
Transmittance [%]
Wavenumber cm-1
3190.47
3110.09
3059.55
3037.59
2970.43
1745.90
1725.18
1614.38
1495.24
1483.25
1460.02
1402.04
1330.83
1289.88
1268.60
1217.07
1201.52
1189.29
1144.30
1112.42
1095.14
1015.01
990.99
953.38
945.41
885.78
877.42
816.52
766.21
735.33
720.37
672.94
659.94
635.02
547.60
538.11
479.14
453.97
418.44

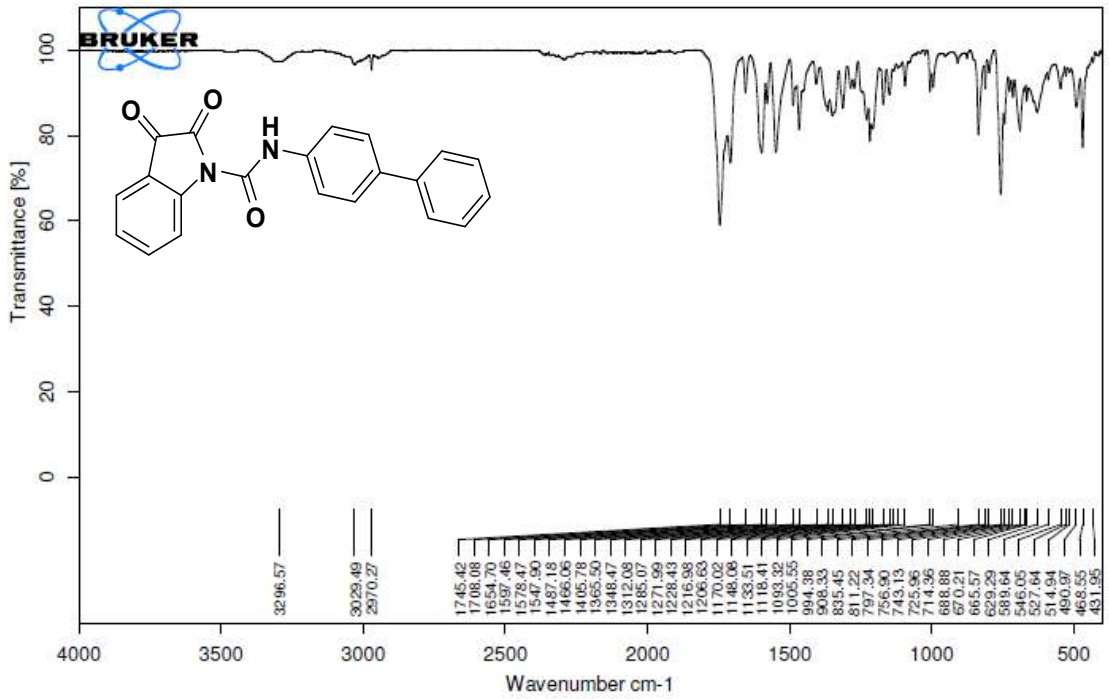
BRUKER
Transmittance [%]
Wavenumber cm-1
3296.57
3029.49
2970.27

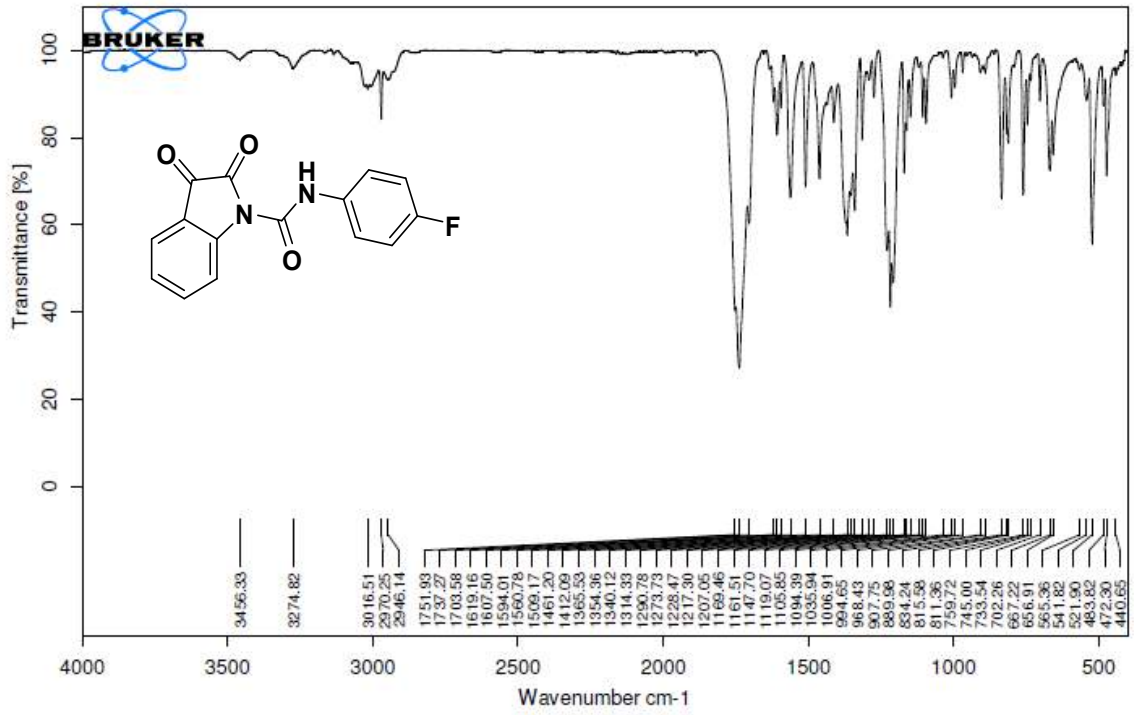
BRUKER
Transmittance [%]
Wavenumber cm-1
F
3456.33
3274.82
3016.51
2970.25
2946.14

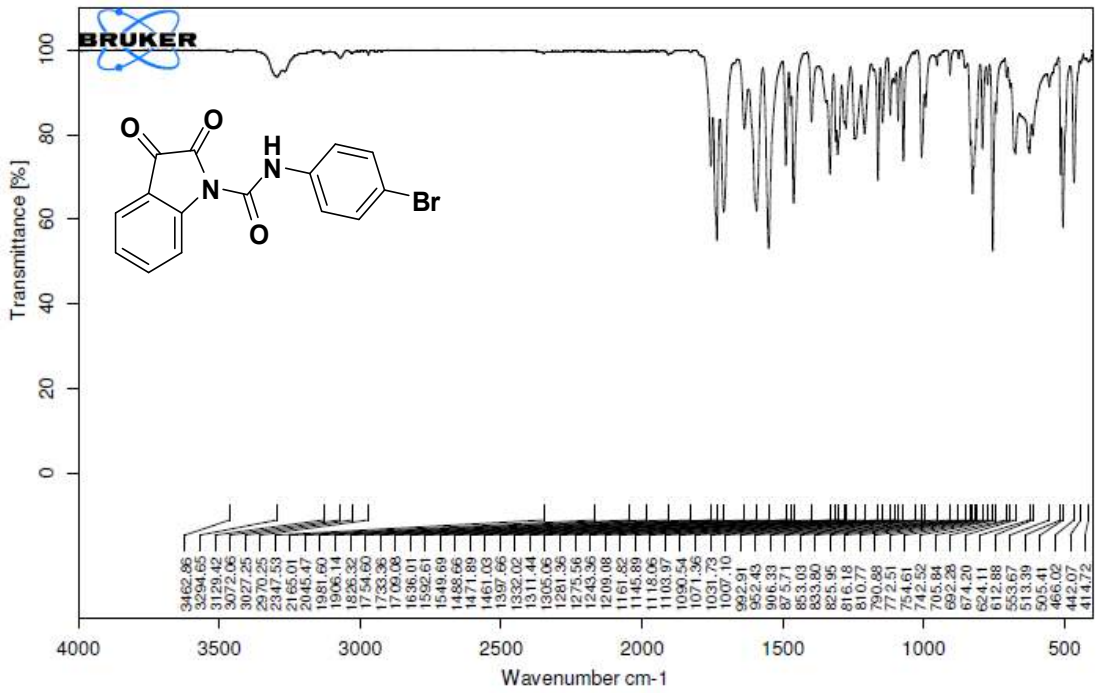
BRUKER
Transmittance [%]
Wavenumber cm-1
Br

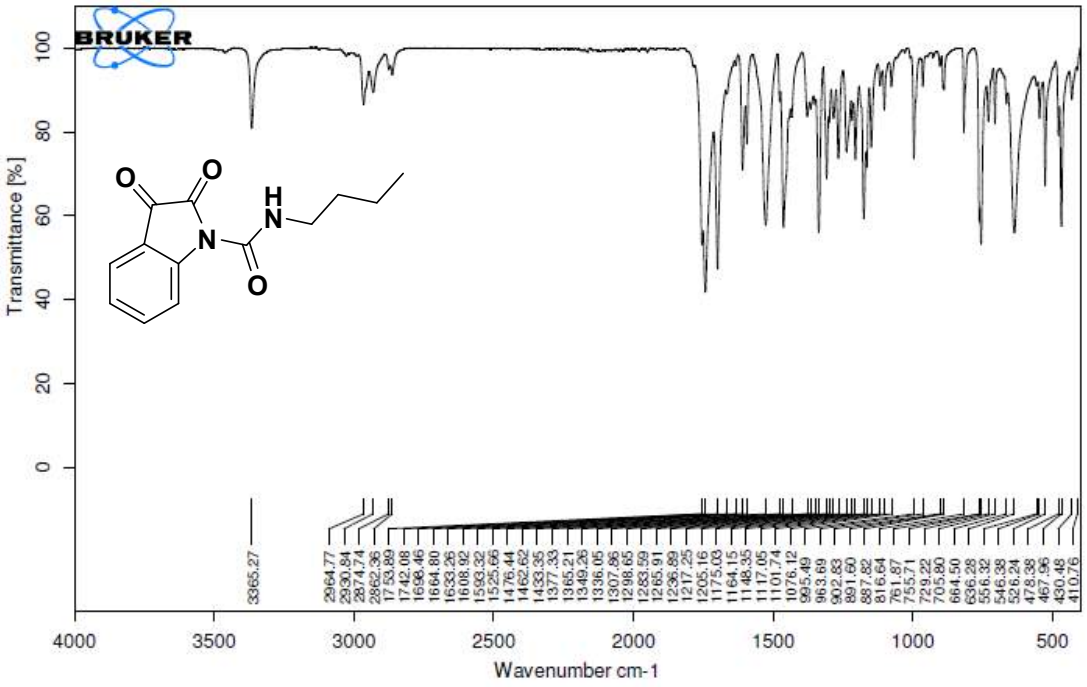
BRUKER
Transmittance [%]
Wavenumber cm-1

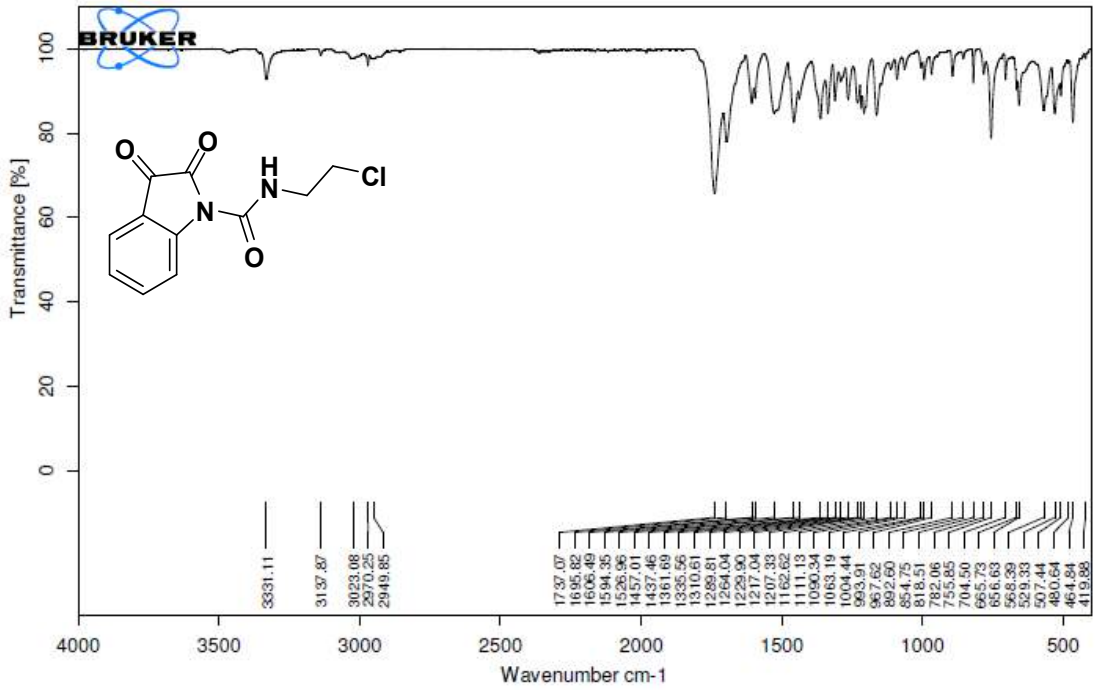
BRUKER
Transmittance [%]
Wavenumber cm-1
3331.11
3137.87
3023.08
2970.25
2949.85

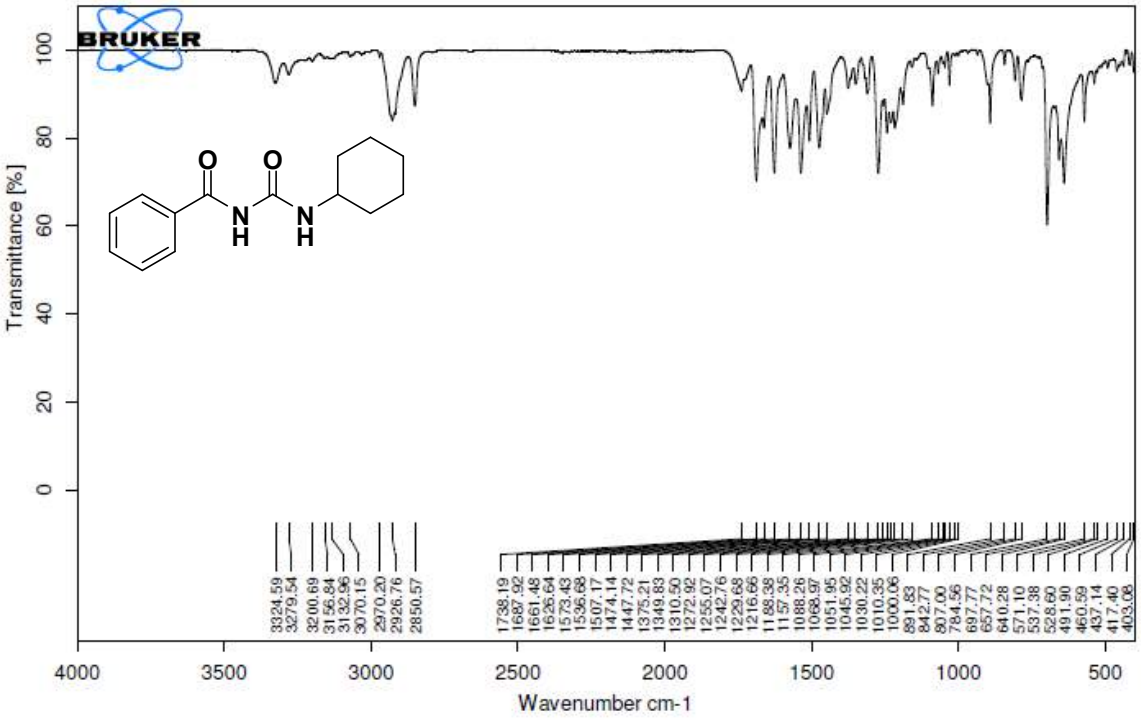
BRUKER
Transmittance [%]
Wavenumber cm-1
3324.59
3279.54
3200.69
3156.84
3132.96
3070.15
2970.20
2926.76
2850.57

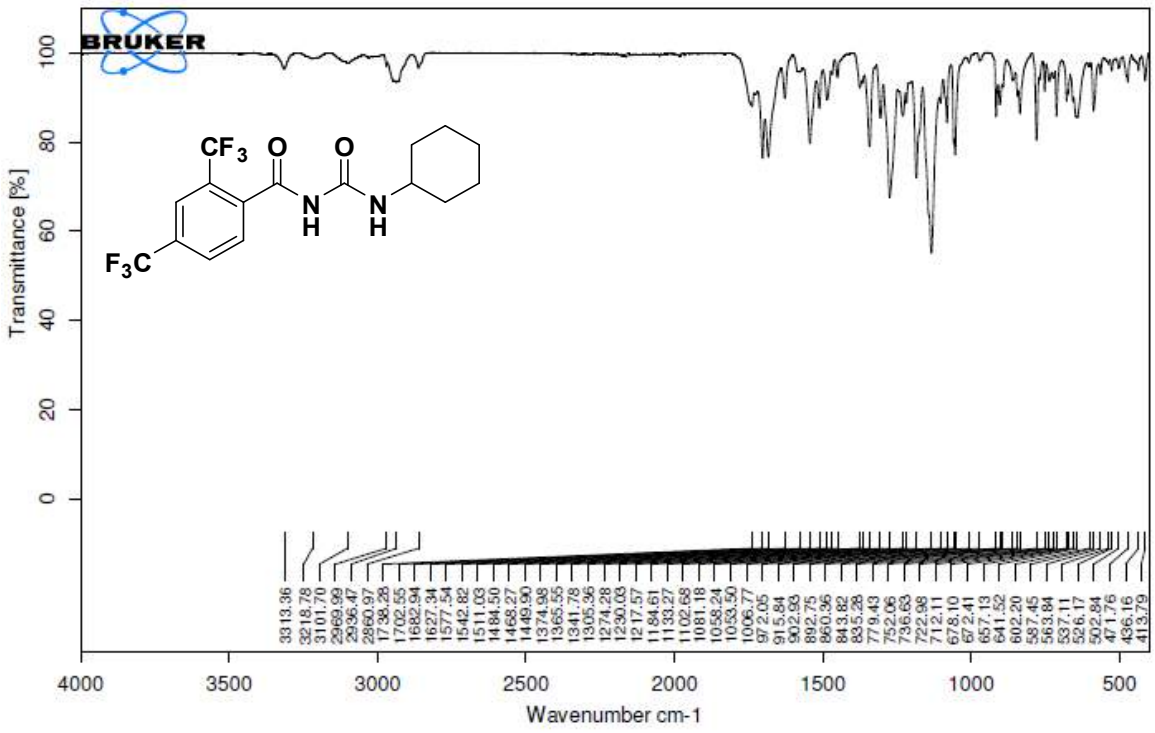
BRUKER
Transmittance [%]
Wavenumber cm-1
4000
3500
3000
2500
2000
1500
1000
500
0
20
40
60
80
100
3313.36
3218.78
3101.70
2969.99
2936.47
2860.97
1738.28
1702.55
1682.94
1627.34
1577.54
1542.82
1511.03
1484.50
1468.27
1449.90
1374.98
1365.55
1341.78
1305.96
1274.28
1290.03
1217.57
1184.61
1133.27
1102.68
1081.18
1058.24
1033.50
1006.77
972.05
915.84
902.93
892.75
860.36
843.82
835.28
779.43
752.06
736.63
722.98
712.11
678.10
672.41
657.13
641.52
602.20
587.45
563.84
537.11
526.17
502.84
471.76
436.16
413.79

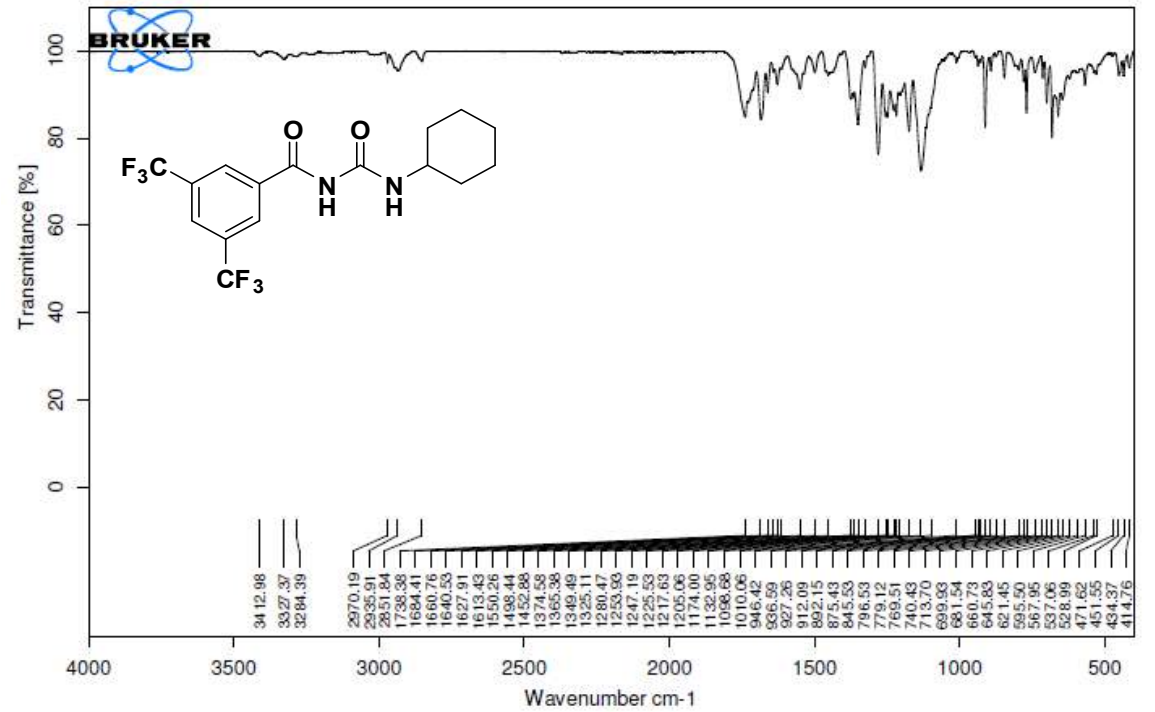
BRUKER
Transmittance [%]
Wavenumber cm-1
4000
3500
3000
2500
2000
1500
1000
500
0
20
40
60
80
100
3412.98
3327.37
3284.39
2970.19
2935.91
2851.84
1738.38
1684.41
1660.76
1640.53
1627.91
1613.43
1550.26
1498.44
1452.88
1374.58
1365.38
1349.49
1325.11
1280.47
1253.93
1247.19
1225.53
1217.63
1205.06
1174.00
1132.95
1098.68
1010.06
946.42
936.59
927.26
912.09
892.15
875.43
845.53
796.53
779.12
769.51
740.43
713.70
699.93
681.54
660.73
645.83
621.45
595.50
567.95
537.06
528.99
471.62
451.55
434.37
414.76

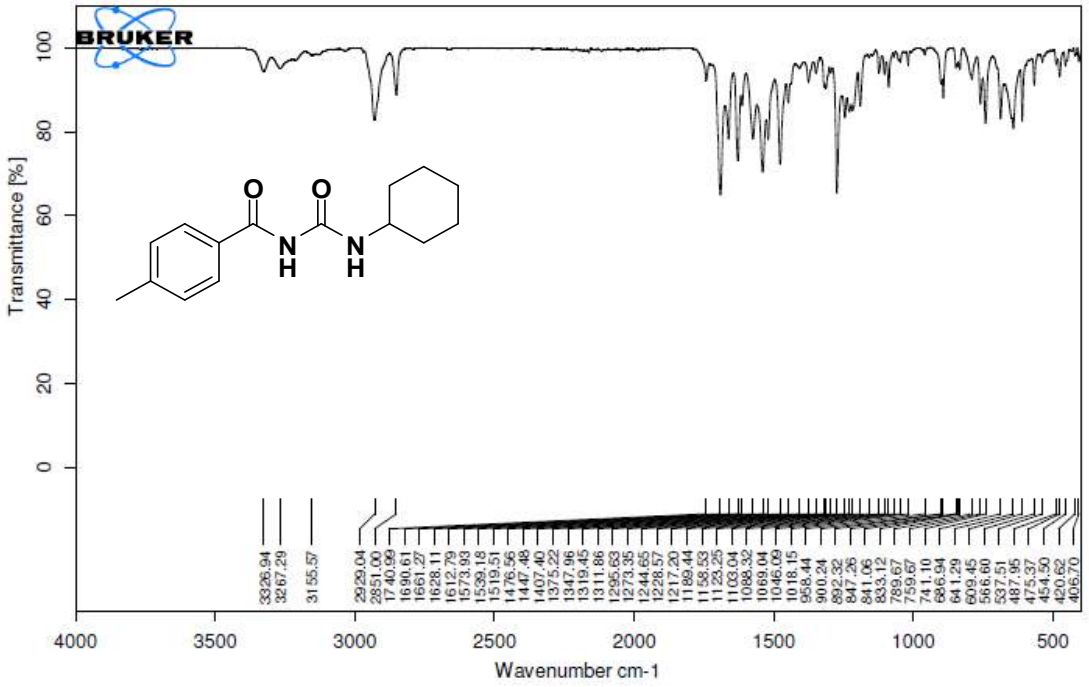
BRUKER
Transmittance [%]
Wavenumber cm-1
O
O
N
H
N
H
3326.94
3267.29
3155.57
2929.04
2851.00
1740.99
1690.61
1661.27
1628.11
1612.79
1573.93
1539.18
1519.51
1476.56
1447.48
1407.40
1375.22
1347.96
1319.45
1311.86
1295.63
1273.35
1244.65
1228.57
1217.20
1189.44
1158.53
1123.25
1103.04
1088.32
1069.04
1046.09
1018.15
958.44
900.24
892.32
847.26
841.06
833.12
789.67
759.67
741.10
686.94
641.29
609.45
566.60
537.51
487.95
475.37
454.50
420.62
406.70

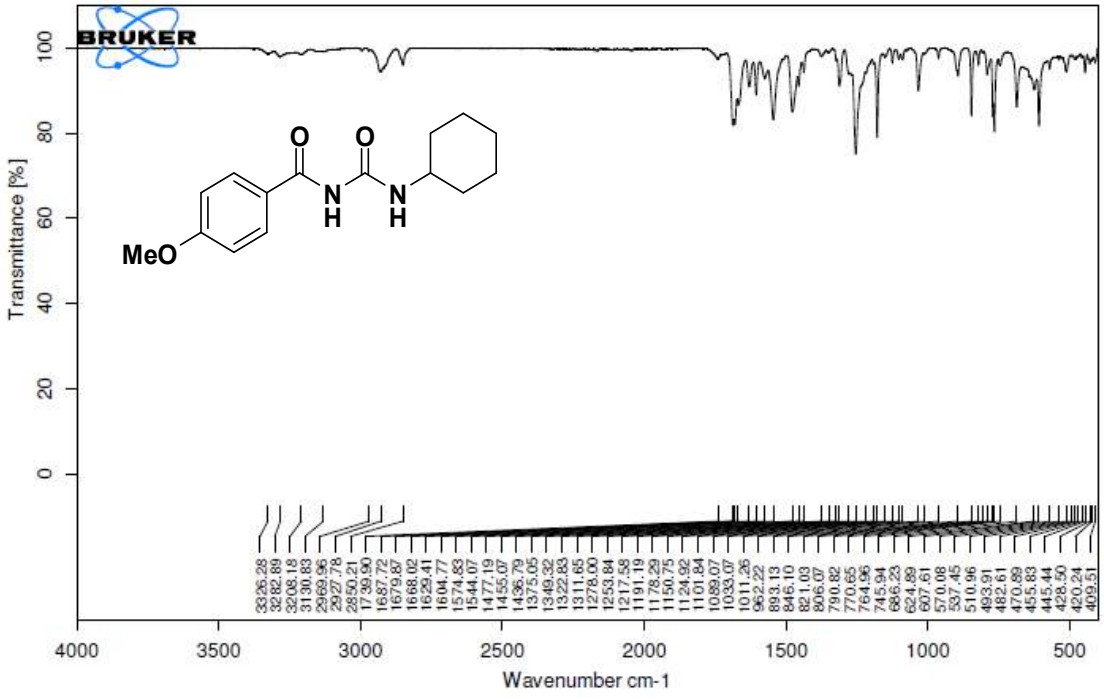
BRUKER
Transmittance [%]
Wavenumber cm-1
O
O
N
H
N
H
MeO
3326.28
3262.89
3206.18
3130.83
2969.96
2927.78
2850.21
1739.90
1687.72
1679.87
1668.02
1629.41
1604.77
1574.83
1544.07
1477.19
1455.07
1436.79
1375.05
1349.32
1322.83
1311.65
1278.00
1253.84
1217.58
1191.19
1178.29
1150.75
1124.92
1101.84
1089.07
1033.07
1011.25
962.22
893.13
846.10
821.03
806.07
790.82
770.65
764.96
745.94
686.23
624.89
607.61
570.08
537.45
510.96
493.91
482.61
470.89
455.83
445.44
428.50
420.24
409.51

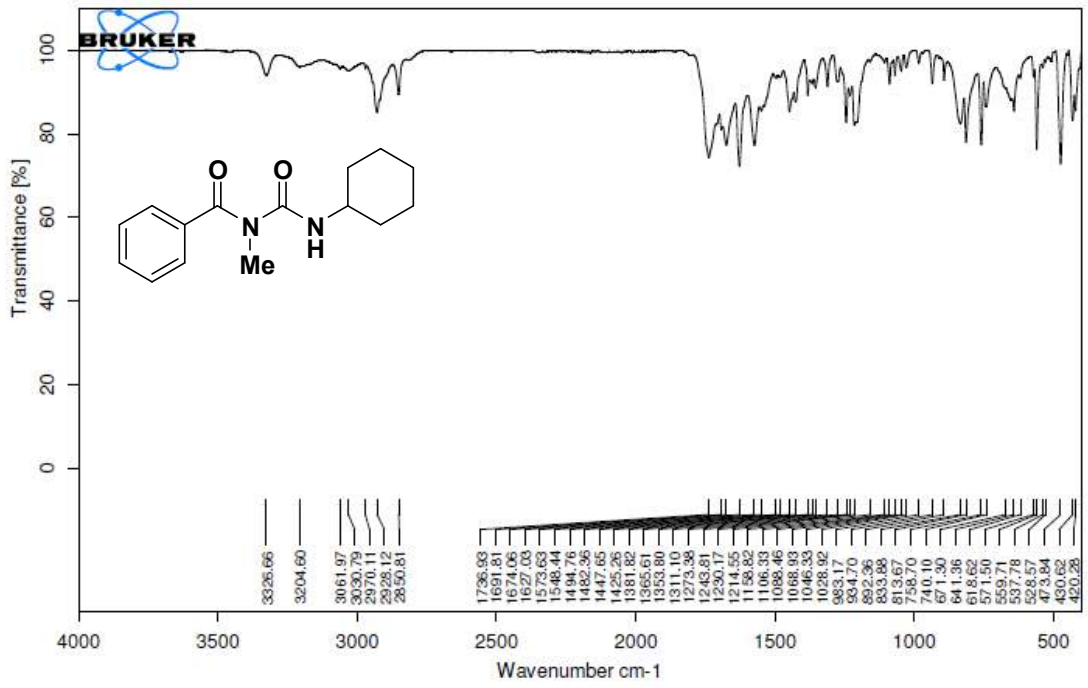
BRUKER
O
O
N
Me
N
H
Transmittance [%]
0
20
40
60
80
100
3326.66
3204.60
3061.97
3030.79
2970.11
2928.12
2850.81
1736.93
1691.81
1674.06
1627.03
1573.63
1548.44
1494.76
1482.36
1447.65
1425.26
1381.82
1365.61
1353.80
1311.10
1273.38
1243.81
1230.17
1214.55
1188.82
1106.33
1088.46
1068.93
1046.33
1028.92
983.17
934.70
892.36
833.88
813.67
758.70
740.10
671.30
641.36
618.62
571.50
559.71
537.78
528.57
473.84
430.62
420.28
4000
3500
3000
2500
2000
1500
1000
500
Wavenumber cm-1

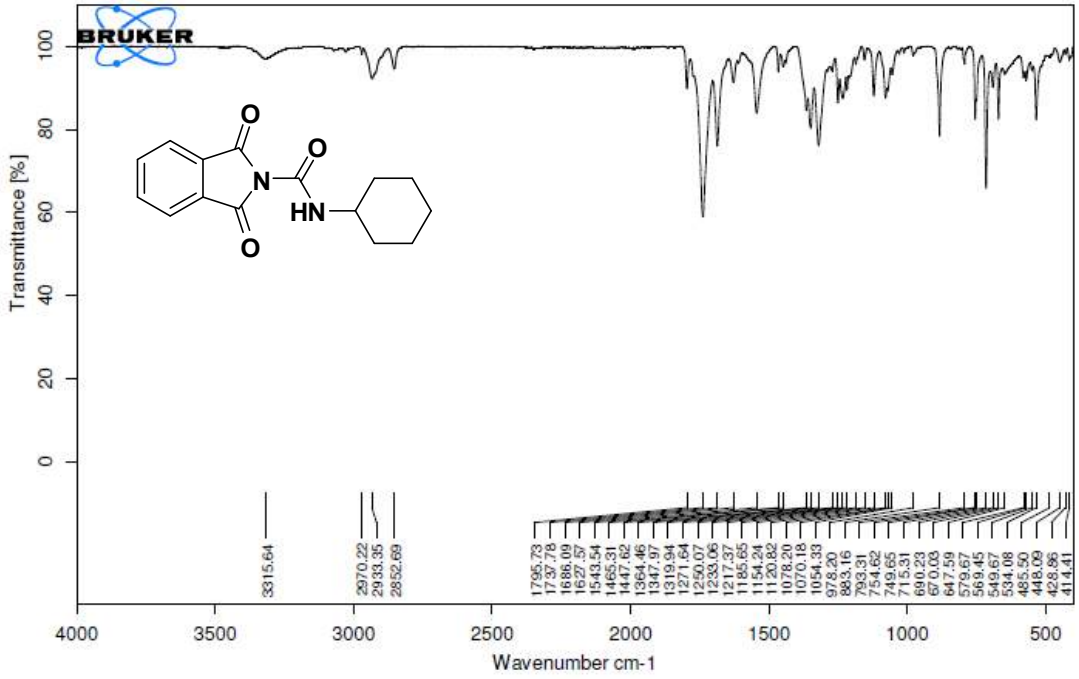
BRUKER
O
O
N
HN
O
Transmittance [%]
0
20
40
60
80
100
3315.64
2970.22
2933.35
2852.69
1795.73
1737.78
1686.09
1627.57
1543.54
1465.31
1447.62
1364.46
1347.97
1319.94
1271.64
1250.07
1233.06
1217.37
1185.65
1154.24
1120.82
1078.20
1070.18
1054.33
978.20
883.16
793.31
754.62
749.65
715.31
690.23
670.03
647.59
579.67
569.45
549.67
534.08
485.50
448.09
428.96
414.41
4000
3500
3000
2500
2000
1500
1000
500
Wavenumber cm-1

NMR Spectra for all mechanosynthesized compounds

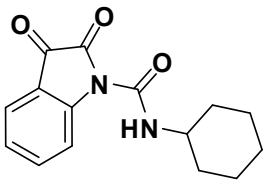

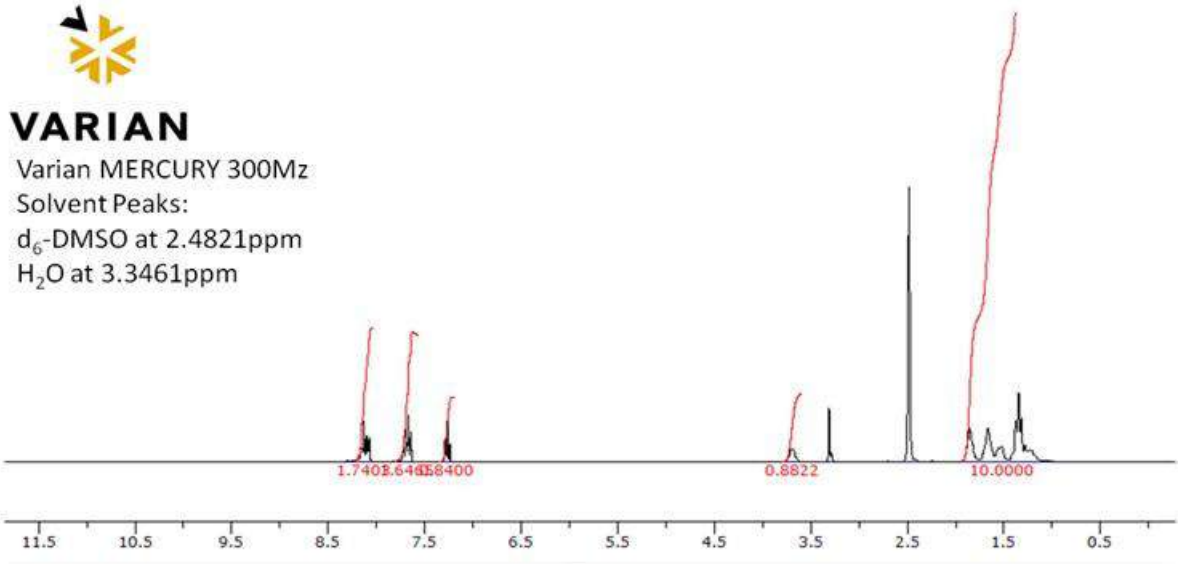

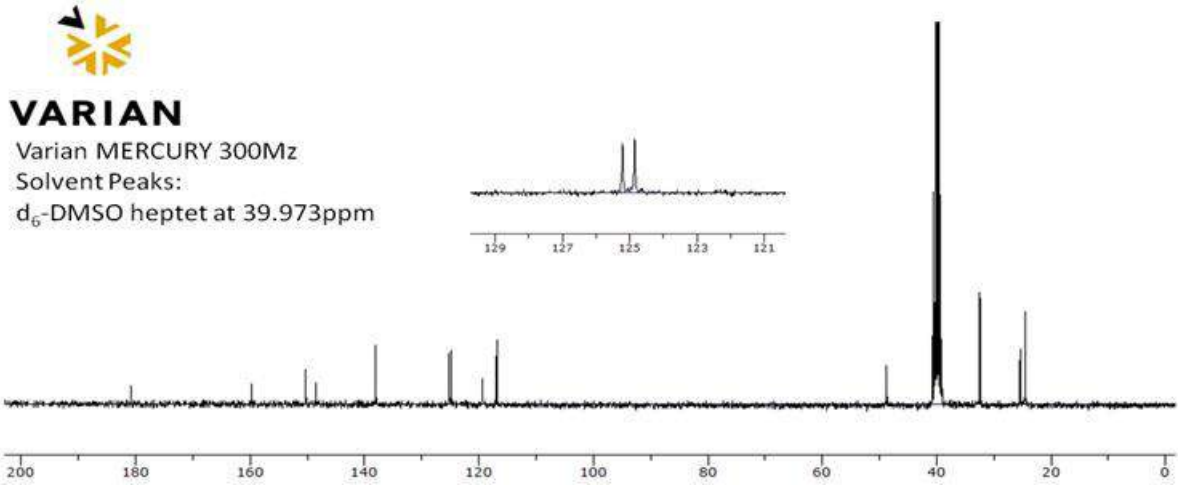

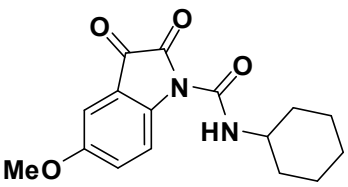
O
O
N
O
HN
MeO

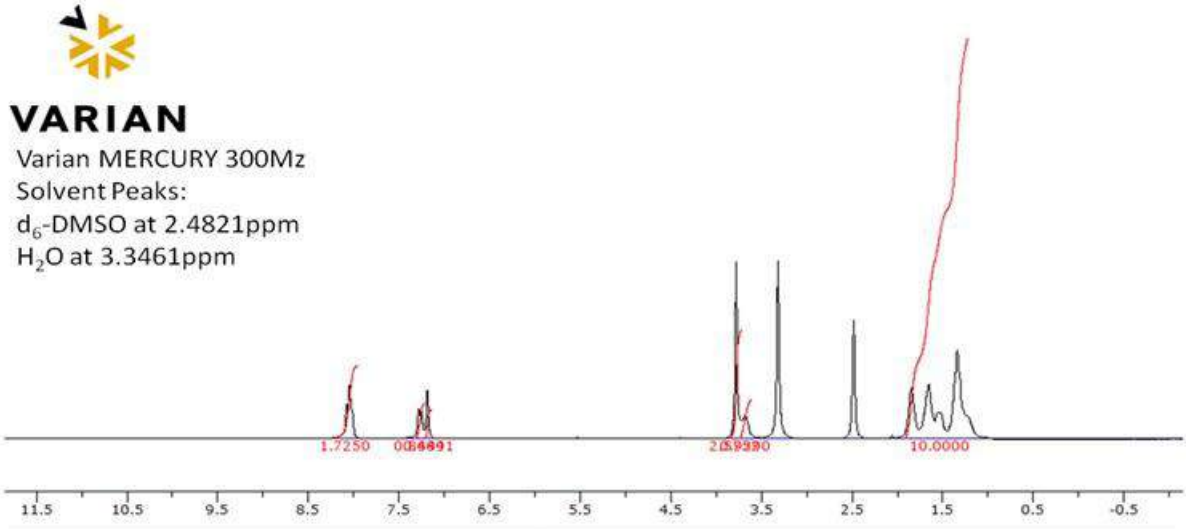
VARIAN
Varian MERCURY 300Mz
Solvent Peaks:
d6-DMSO at 2.4821ppm
H2O at 3.3461ppm
1.7250
10.0000
11.5
10.5
9.5
8.5
7.5
6.5
5.5
4.5
3.5
2.5
1.5
0.5
-0.5

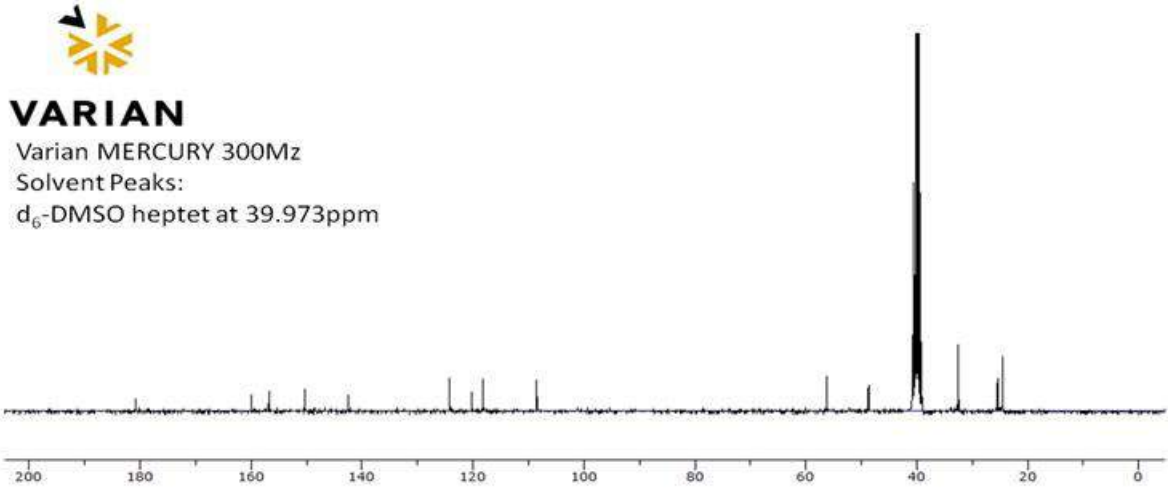
VARIAN
Varian MERCURY 300Mz
Solvent Peaks:
d6-DMSO heptet at 39.973ppm
200
180
160
140
120
100
80
60
40
20
0

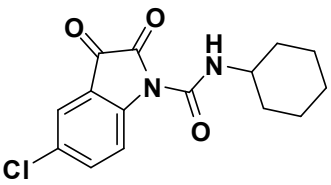
O
O
H
N
N
O
Cl

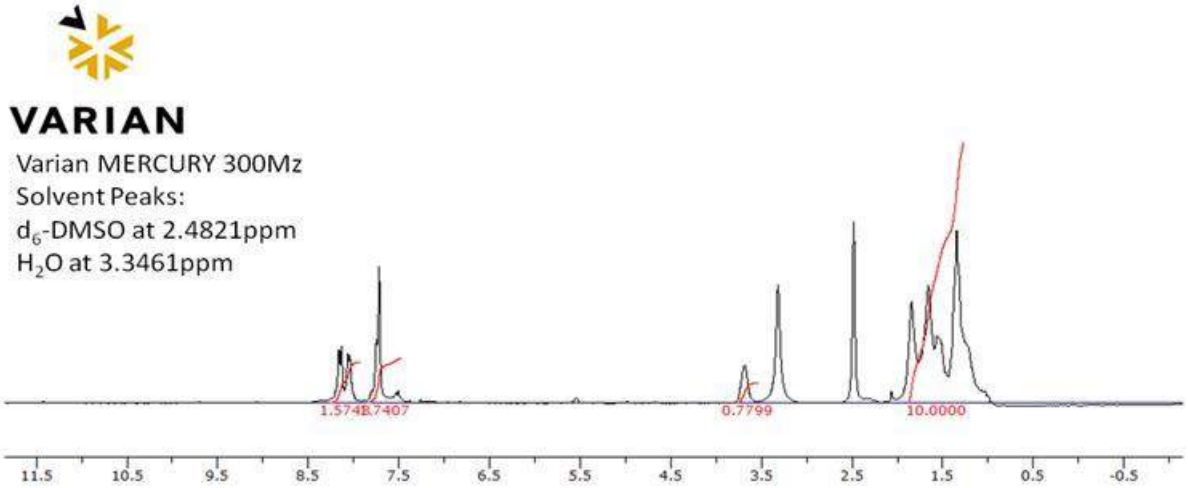
VARIAN
Varian MERCURY 300Mz
Solvent Peaks:
d6-DMSO at 2.4821ppm
H2O at 3.3461ppm
1.5748
7.7407
0.7799
10.0000
11.5
10.5
9.5
8.5
7.5
6.5
5.5
4.5
3.5
2.5
1.5
0.5
-0.5

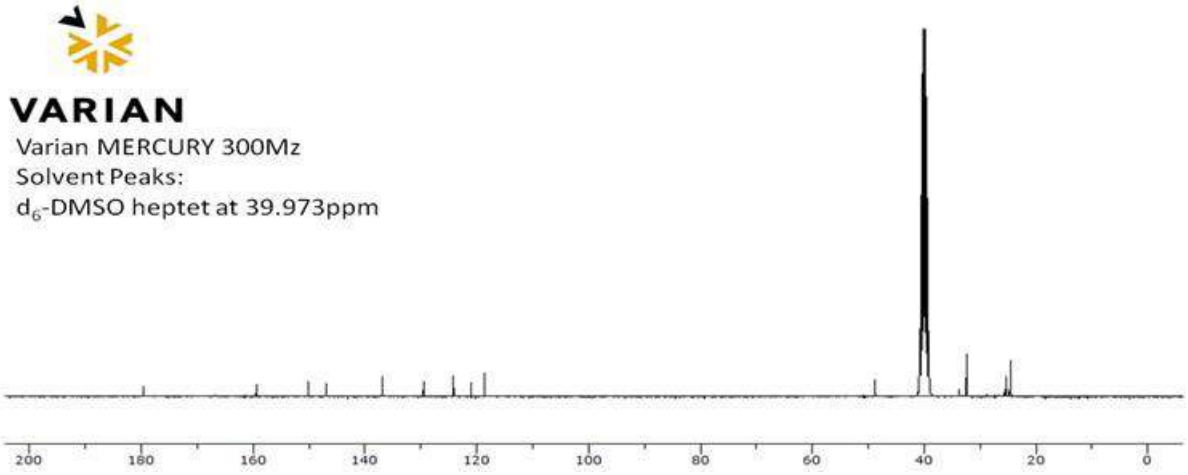
VARIAN
Varian MERCURY 300Mz
Solvent Peaks:
d6-DMSO heptet at 39.973ppm
200
180
160
140
120
100
80
60
40
20
0

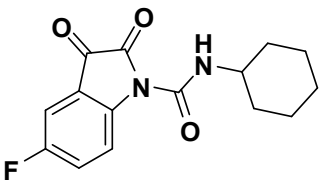
O
O
H
N
N
O
F

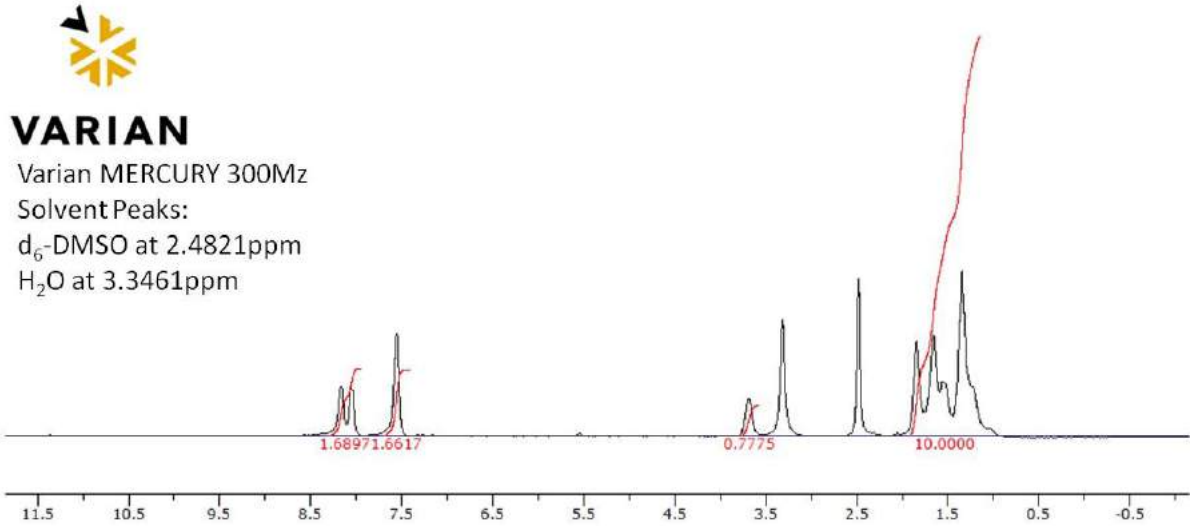
VARIAN
Varian MERCURY 300Mz
Solvent Peaks:
d6-DMSO at 2.4821ppm
H2O at 3.3461ppm
1.68971.6617
0.7775
10.0000
11.5
10.5
9.5
8.5
7.5
6.5
5.5
4.5
3.5
2.5
1.5
0.5
-0.5

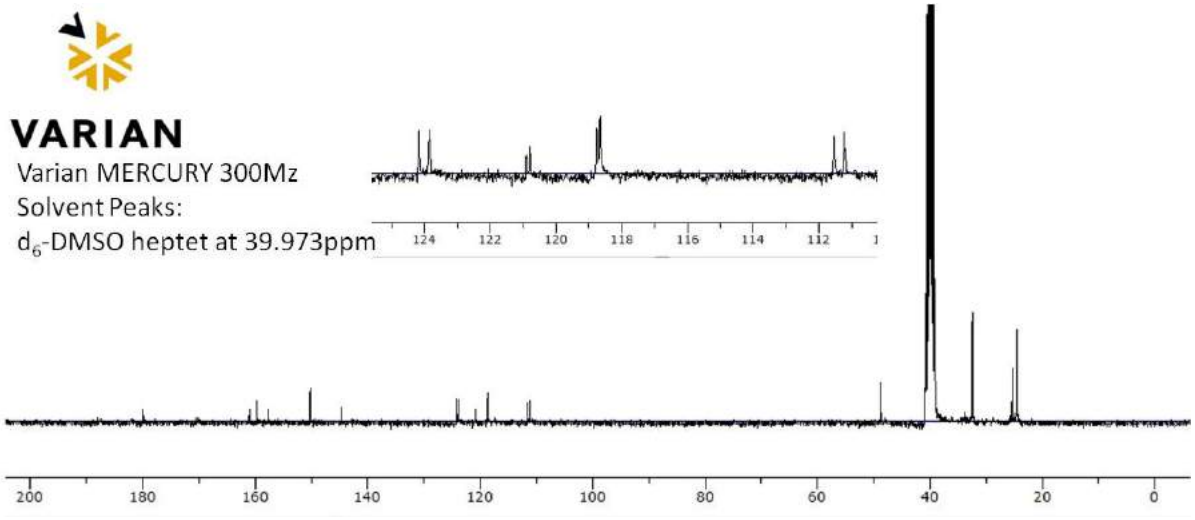
VARIAN
Varian MERCURY 300Mz
Solvent Peaks:
d6-DMSO heptet at 39.973ppm
124
122
120
118
116
114
112
200
180
160
140
120
100
80
60
40
20
0

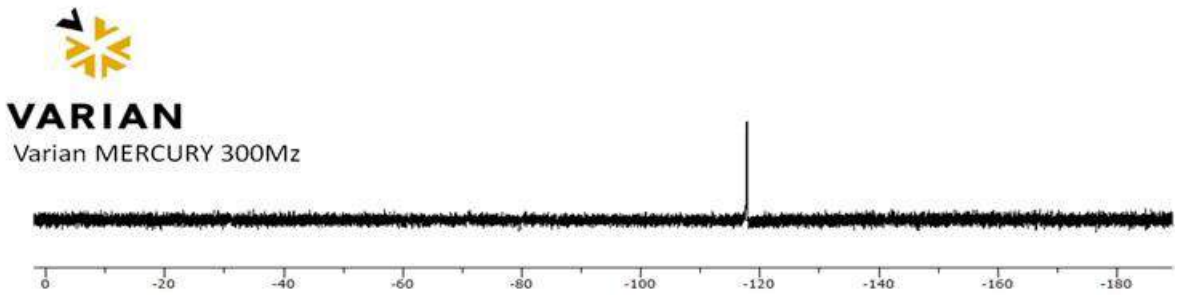
VARIAN
Varian MERCURY 300Mz
0
-20
-40
-60
-80
-100
-120
-140
-160
-180

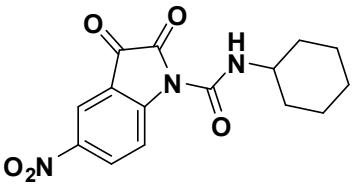
O
O
H
N
N
O
O2N

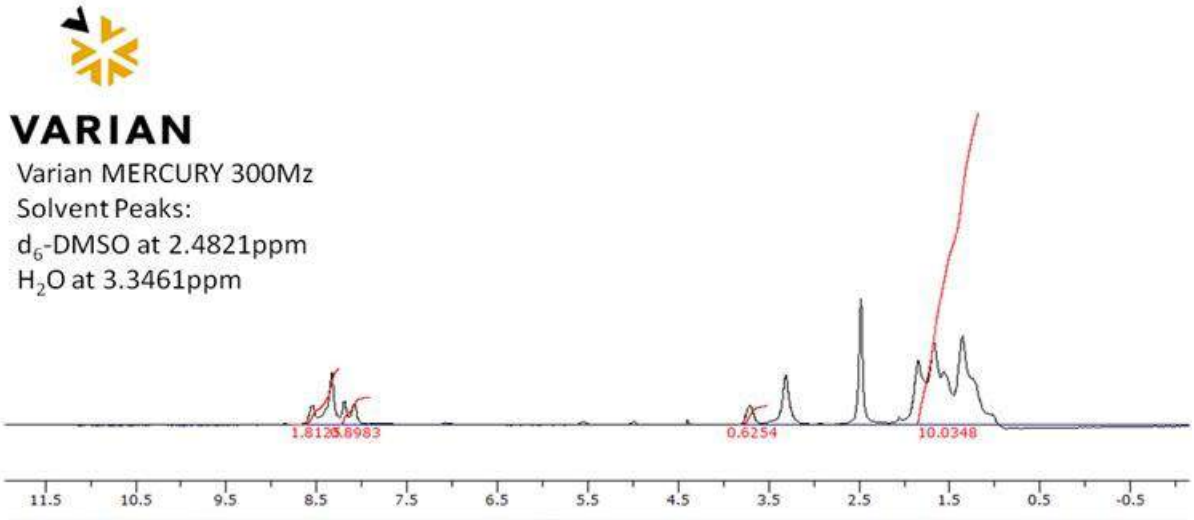
VARIAN
Varian MERCURY 300Mz
Solvent Peaks:
d6-DMSO at 2.4821ppm
H2O at 3.3461ppm
1.8125
5.8983
0.6254
10.0348
11.5
10.5
9.5
8.5
7.5
6.5
5.5
4.5
3.5
2.5
1.5
0.5
-0.5

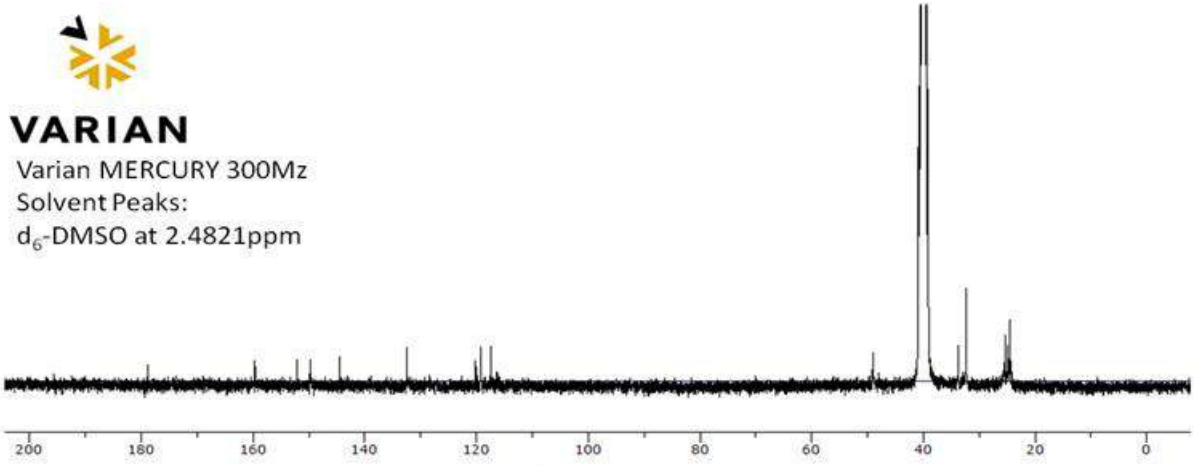
VARIAN
Varian MERCURY 300Mz
Solvent Peaks:
d6-DMSO at 2.4821ppm
200
180
160
140
120
100
80
60
40
20
0

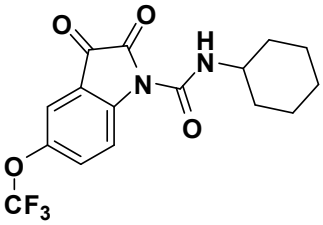
O
O
H
N
N
O
O
CF3

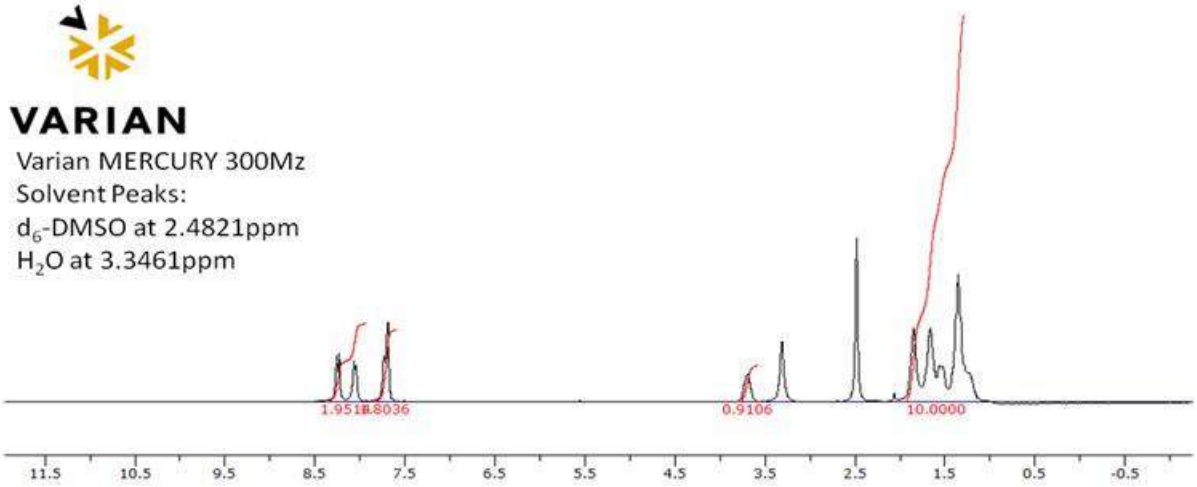
VARIAN
Varian MERCURY 300Mz
Solvent Peaks:
d6-DMSO at 2.4821ppm
H2O at 3.3461ppm
1.9518
1.8036
0.9106
10.0000
11.5
10.5
9.5
8.5
7.5
6.5
5.5
4.5
3.5
2.5
1.5
0.5
-0.5

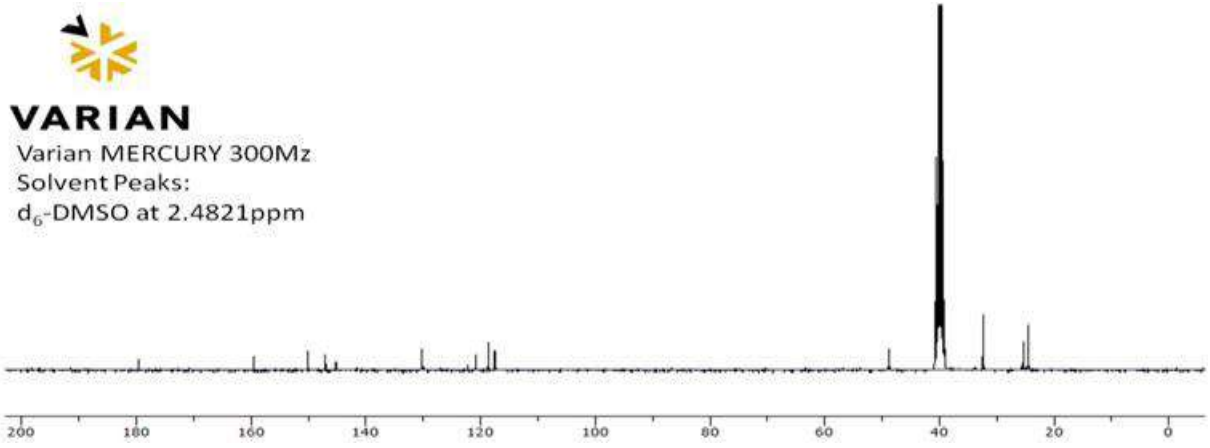
VARIAN
Varian MERCURY 300Mz
Solvent Peaks:
d6-DMSO at 2.4821ppm
200
180
160
140
120
100
80
60
40
20
0

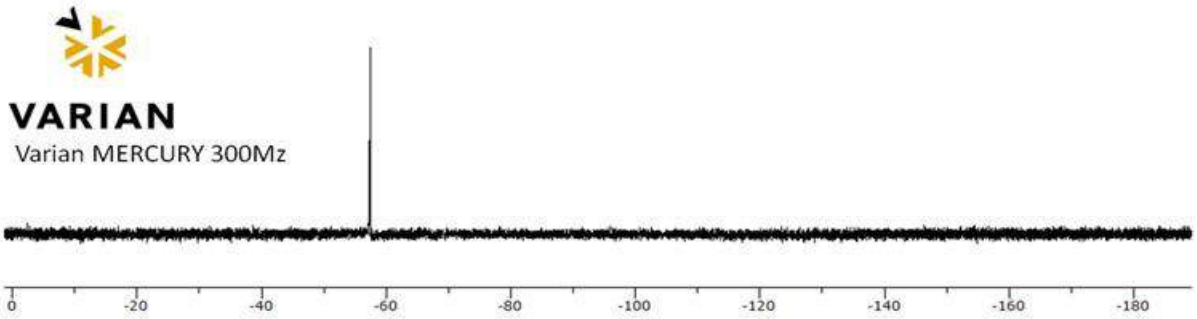
VARIAN
Varian MERCURY 300Mz
0
-20
-40
-60
-80
-100
-120
-140
-160
-180

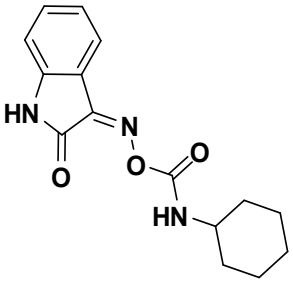
HN
N
O
O
O
HN

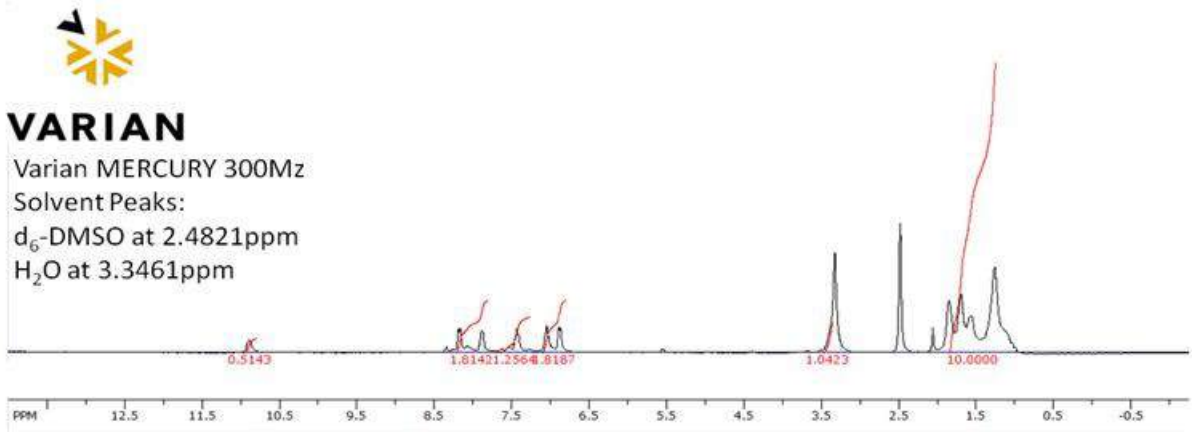
VARIAN
Varian MERCURY 300Mz
Solvent Peaks:
d6-DMSO at 2.4821ppm
H2O at 3.3461ppm
0.5143
1.8142
1.2564
1.8187
1.0423
10.0000
PPM
12.5
11.5
10.5
9.5
8.5
7.5
6.5
5.5
4.5
3.5
2.5
1.5
0.5
-0.5

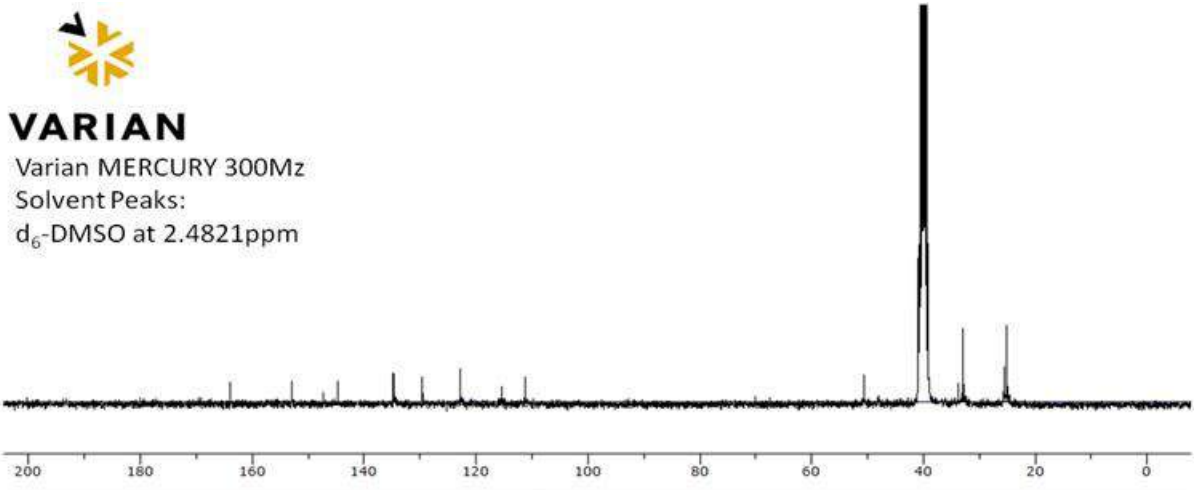
VARIAN
Varian MERCURY 300Mz
Solvent Peaks:
d6-DMSO at 2.4821ppm
200
180
160
140
120
100
80
60
40
20
0

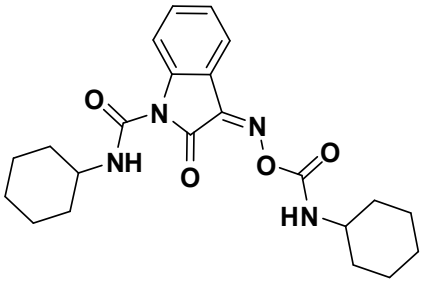
O
N
NH
O
N
O
O
HN

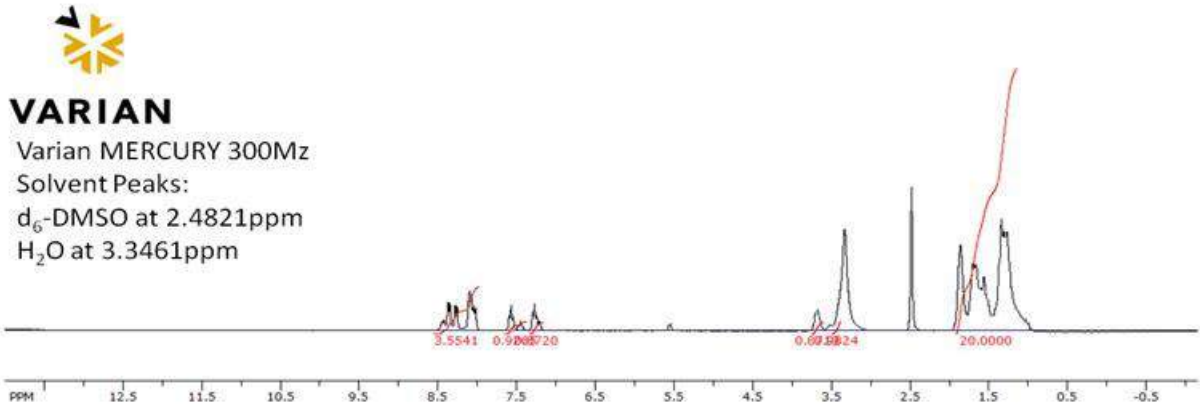
VARIAN
Varian MERCURY 300Mz
Solvent Peaks:
d6-DMSO at 2.4821ppm
H2O at 3.3461ppm
3.5541
20.0000
PPM
12.5
11.5
10.5
9.5
8.5
7.5
6.5
5.5
4.5
3.5
2.5
1.5
0.5
-0.5

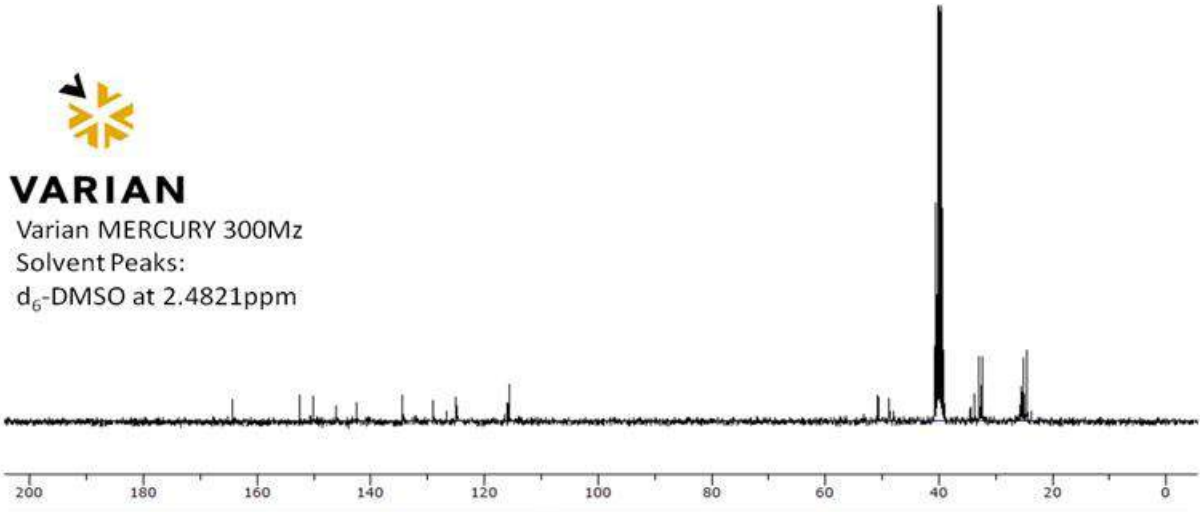
VARIAN
Varian MERCURY 300Mz
Solvent Peaks:
d6-DMSO at 2.4821ppm
200
180
160
140
120
100
80
60
40
20
0

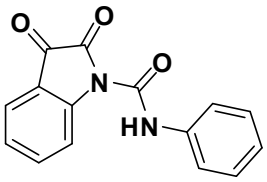
O
O
N
O
HN

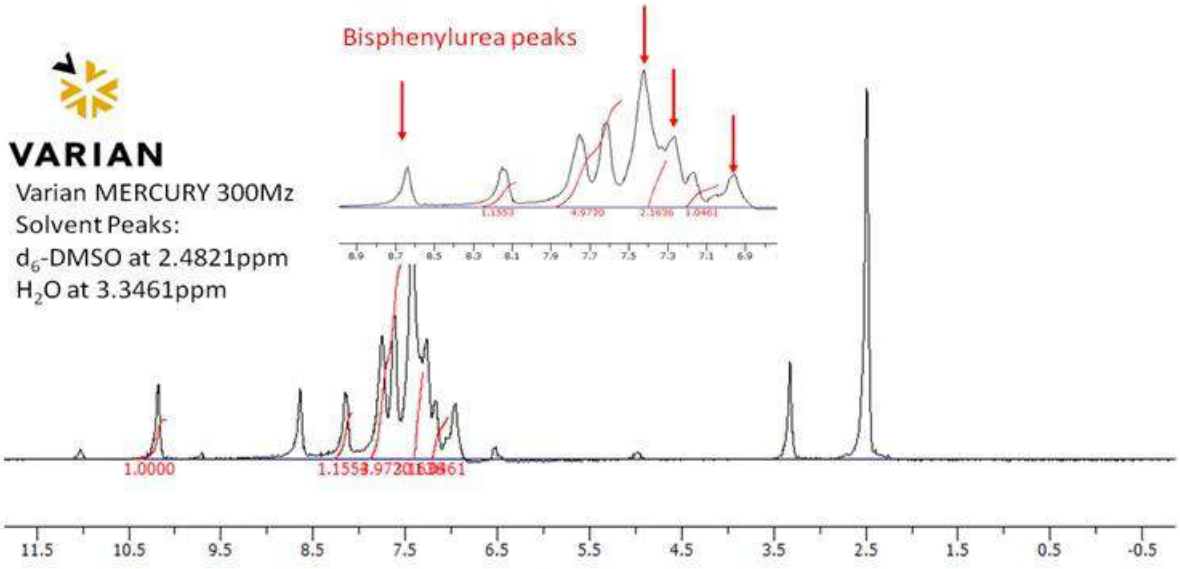
Bisphenylurea peaks
VARIAN
Varian MERCURY 300Mz
Solvent Peaks:
d6-DMSO at 2.4821ppm
H2O at 3.3461ppm
1.0000
11.5
10.5
9.5
8.5
7.5
6.5
5.5
4.5
3.5
2.5
1.5
0.5
-0.5

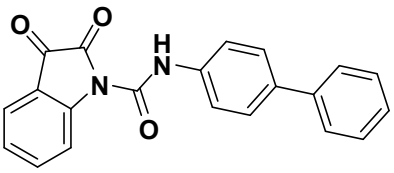
O
O
H
N
N
O

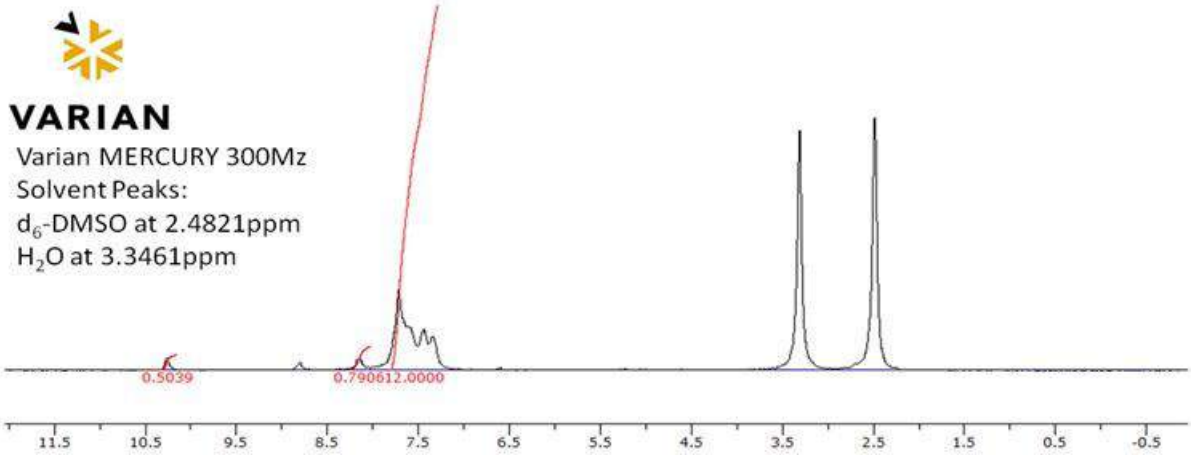
VARIAN
Varian MERCURY 300Mz
Solvent Peaks:
d6-DMSO at 2.4821ppm
H2O at 3.3461ppm
0.5039
0.790612.0000
11.5
10.5
9.5
8.5
7.5
6.5
5.5
4.5
3.5
2.5
1.5
0.5
-0.5

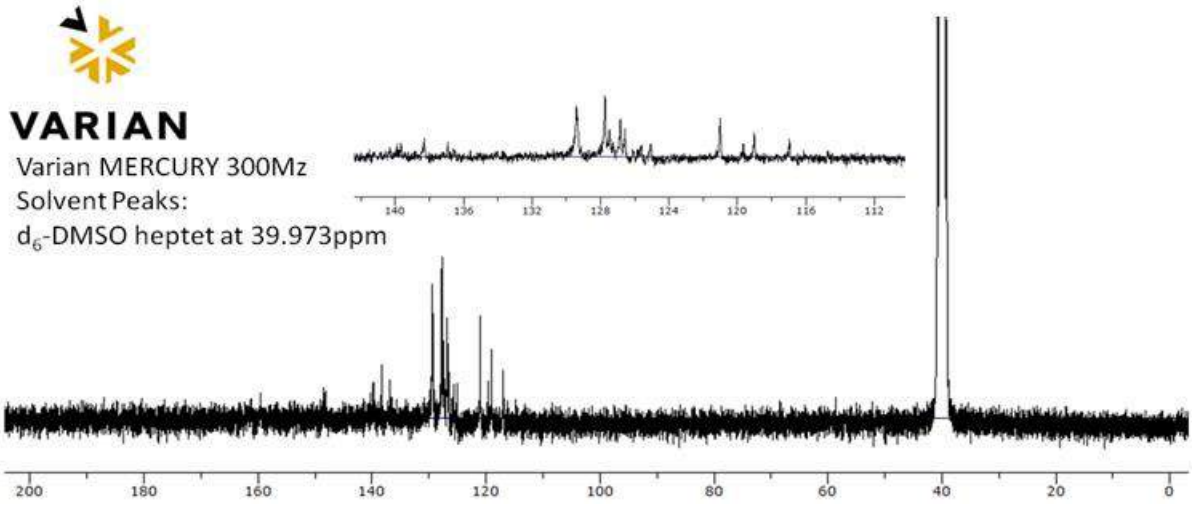
VARIAN
Varian MERCURY 300Mz
Solvent Peaks:
d6-DMSO heptet at 39.973ppm
140
136
132
128
124
120
116
112
200
180
160
140
120
100
80
60
40
20
0

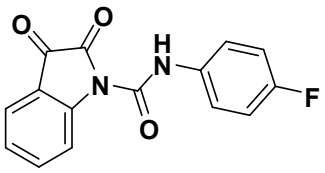
O
O
H
N
N
O
F

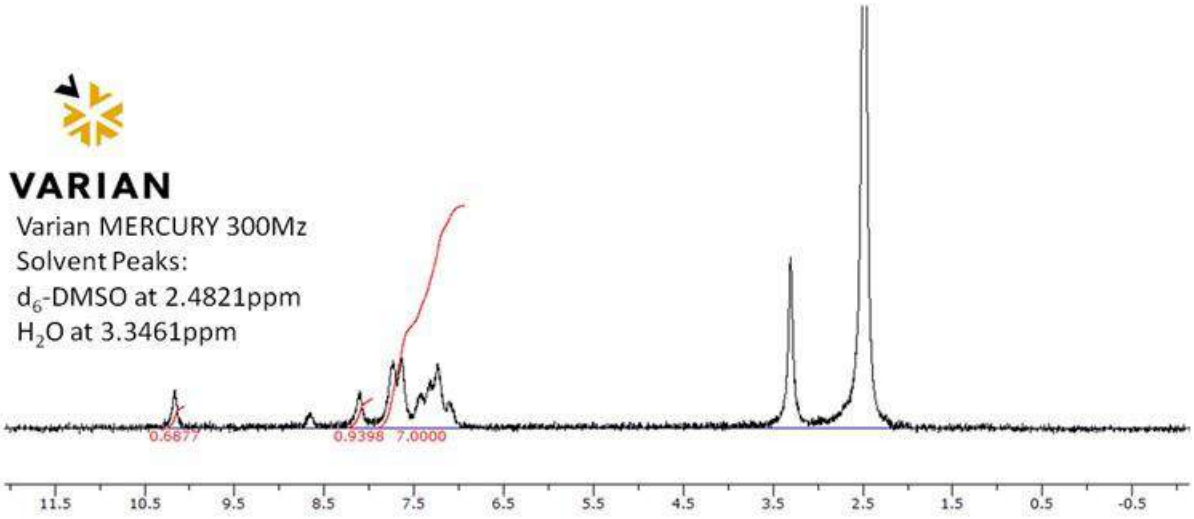
VARIAN
Varian MERCURY 300Mz
Solvent Peaks:
d6-DMSO at 2.4821ppm
H2O at 3.3461ppm
0.6877
0.9398
7.0000
11.5
10.5
9.5
8.5
7.5
6.5
5.5
4.5
3.5
2.5
1.5
0.5
-0.5

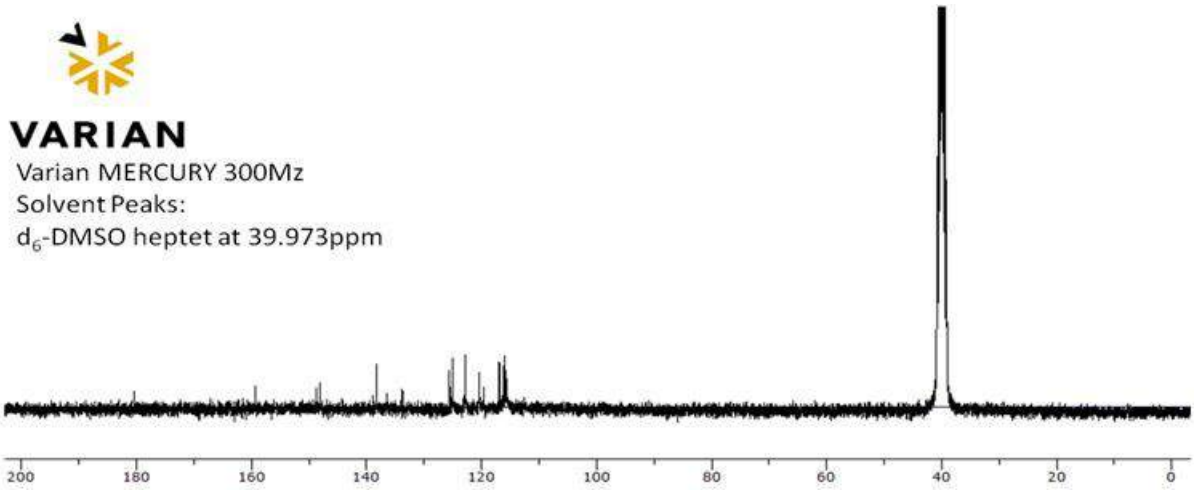
VARIAN
Varian MERCURY 300Mz
Solvent Peaks:
d6-DMSO heptet at 39.973ppm
200
180
160
140
120
100
80
60
40
20
0

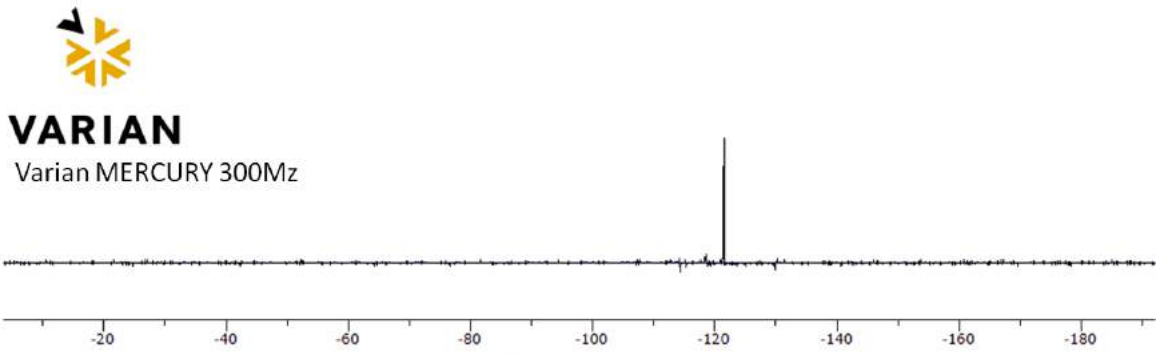
VARIAN
Varian MERCURY 300Mz
-20
-40
-60
-80
-100
-120
-140
-160
-180

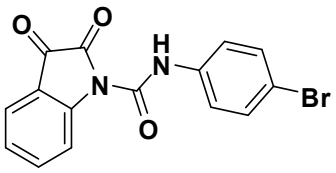
O
O
N
H
N
O
Br

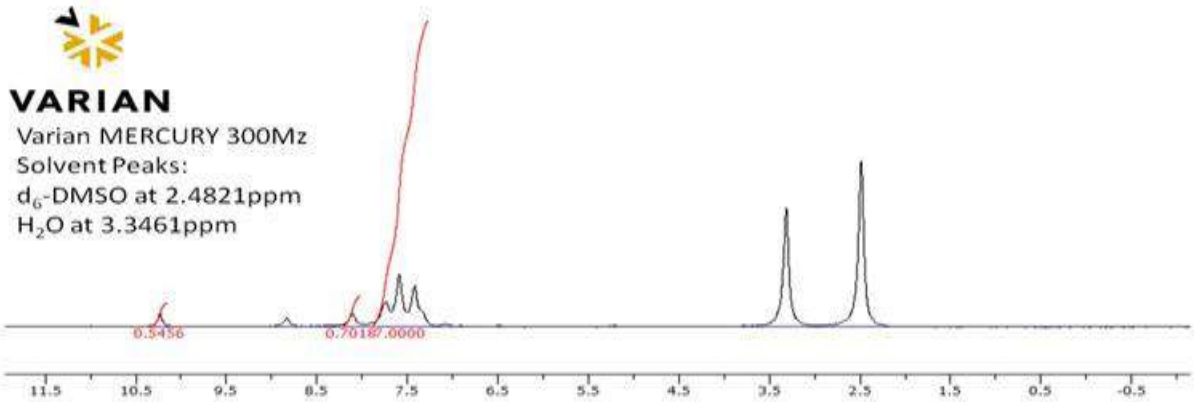
VARIAN
Varian MERCURY 300Mz
Solvent Peaks:
d6-DMSO at 2.4821ppm
H2O at 3.3461ppm
0.5456
0.7018
7.0000
11.5
10.5
9.5
8.5
7.5
6.5
5.5
4.5
3.5
2.5
1.5
0.5
-0.5

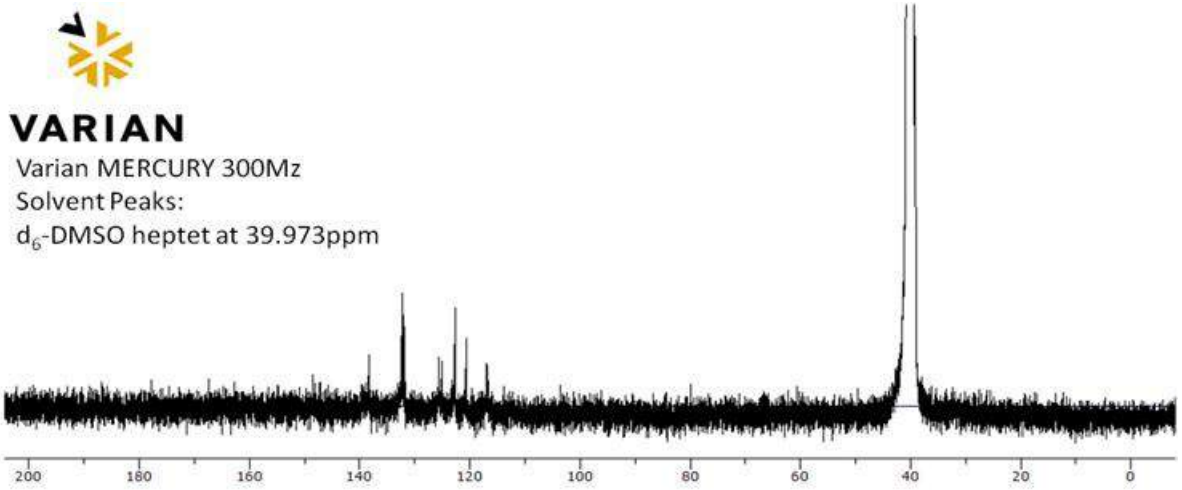
VARIAN
Varian MERCURY 300Mz
Solvent Peaks:
d6-DMSO heptet at 39.973ppm
200
180
160
140
120
100
80
60
40
20
0

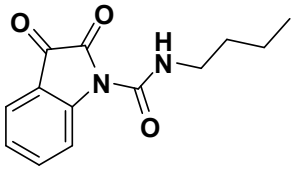
O
O
H
N
N
O

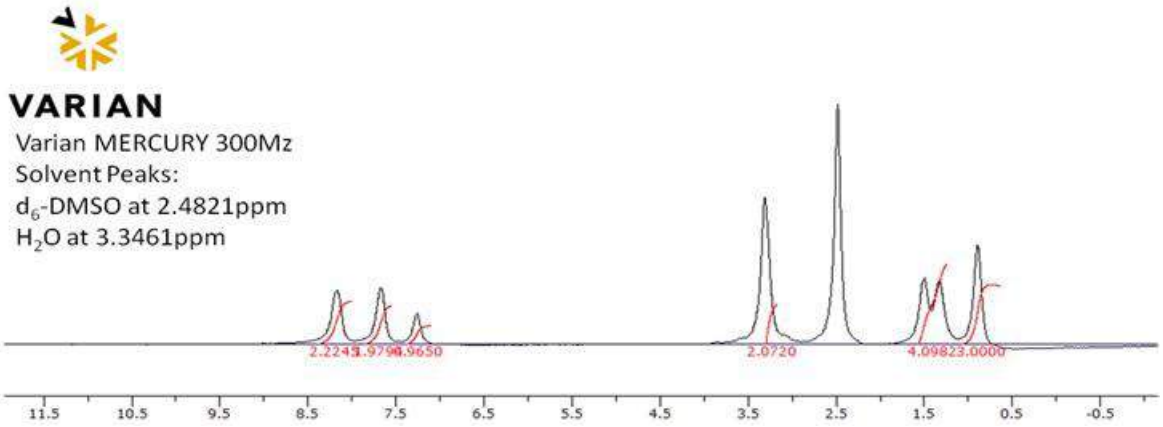
VARIAN
Varian MERCURY 300Mz
Solvent Peaks:
d6-DMSO at 2.4821ppm
H2O at 3.3461ppm
2.0720
4.09823.0000
11.5
10.5
9.5
8.5
7.5
6.5
5.5
4.5
3.5
2.5
1.5
0.5
-0.5

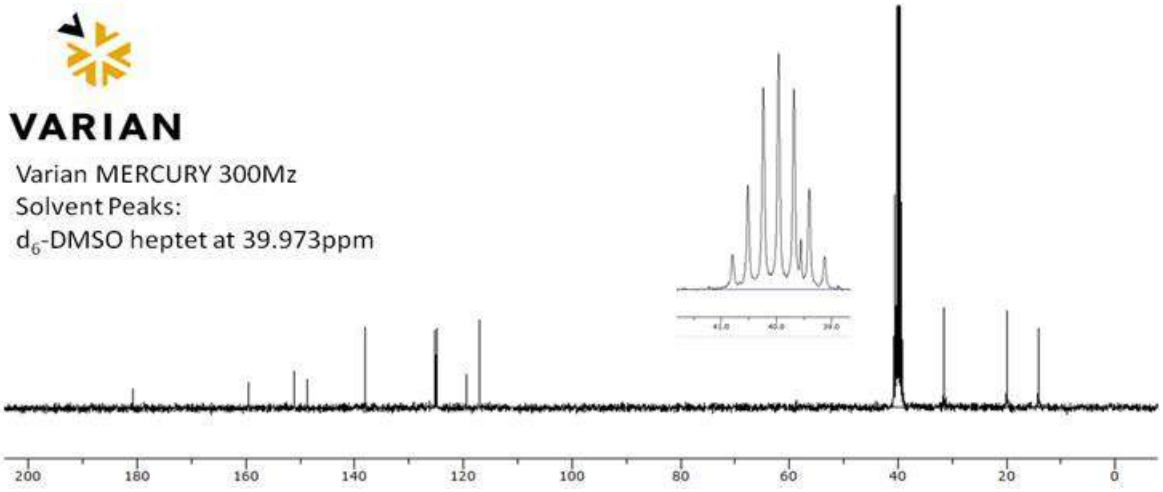
VARIAN
Varian MERCURY 300Mz
Solvent Peaks:
d6-DMSO heptet at 39.973ppm
200
180
160
140
120
100
80
60
40
20
0

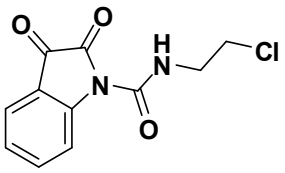
O
O
H
N
Cl
N
O

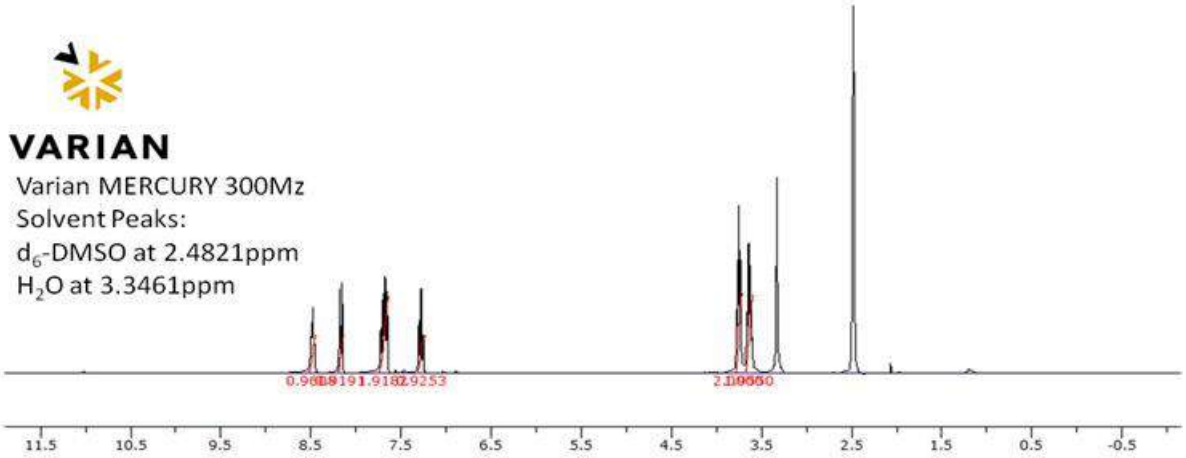
VARIAN
Varian MERCURY 300Mz
Solvent Peaks:
d6-DMSO at 2.4821ppm
H2O at 3.3461ppm
11.5
10.5
9.5
8.5
7.5
6.5
5.5
4.5
3.5
2.5
1.5
0.5
-0.5

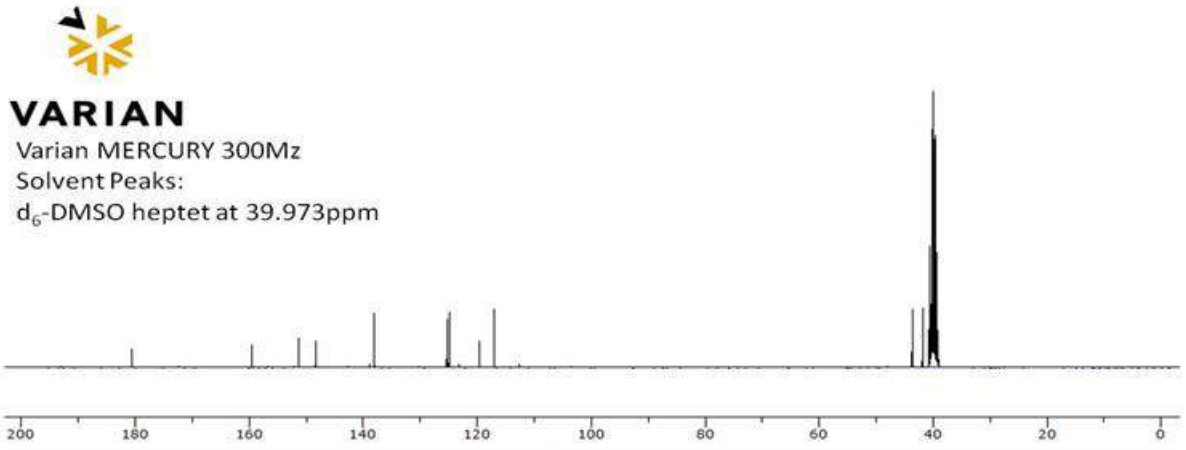
VARIAN
Varian MERCURY 300Mz
Solvent Peaks:
d6-DMSO heptet at 39.973ppm
200
180
160
140
120
100
80
60
40
20
0

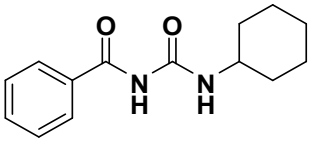
O
O
N
H
N
H

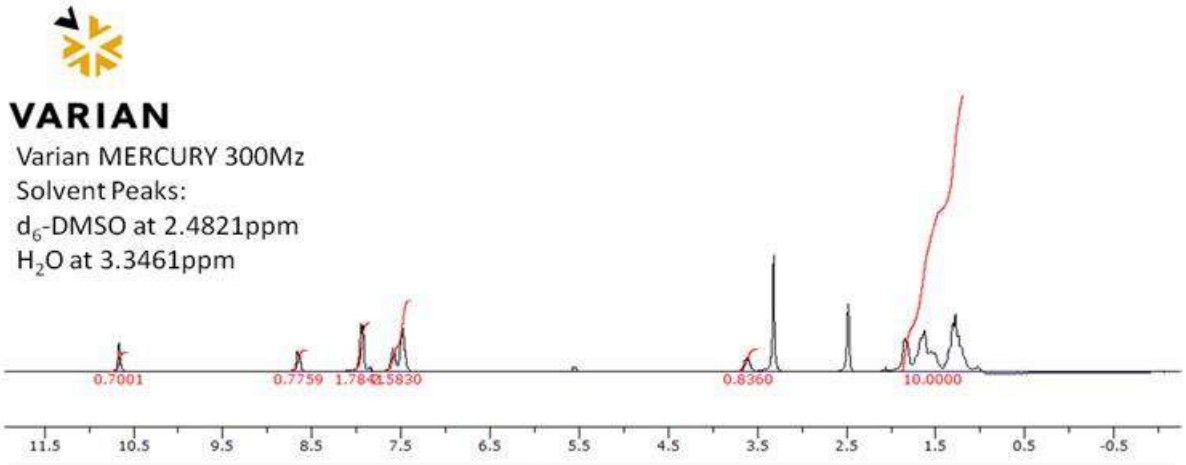
VARIAN
Varian MERCURY 300Mz
Solvent Peaks:
d6-DMSO at 2.4821ppm
H2O at 3.3461ppm
0.7001
0.7759
1.7841
1.5830
0.8360
10.0000
11.5
10.5
9.5
8.5
7.5
6.5
5.5
4.5
3.5
2.5
1.5
0.5
-0.5

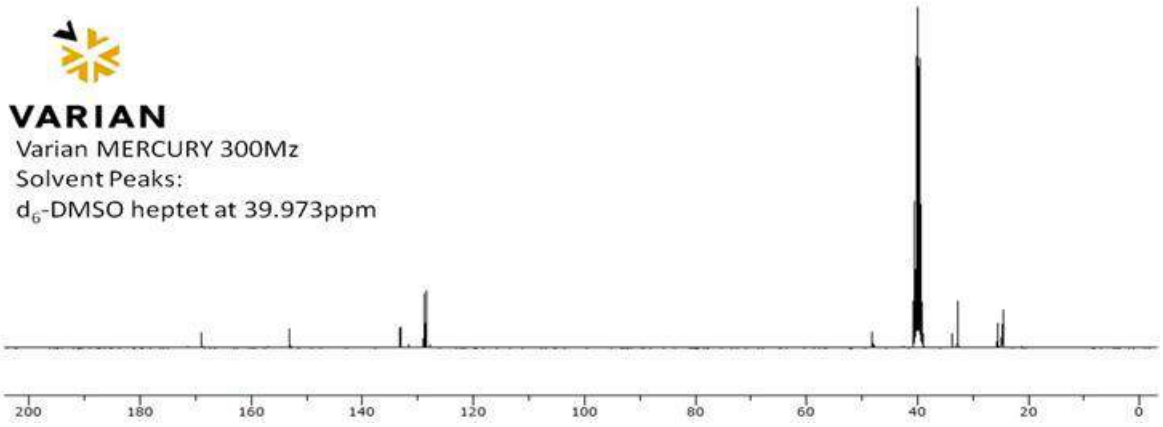
VARIAN
Varian MERCURY 300Mz
Solvent Peaks:
d6-DMSO heptet at 39.973ppm
200
180
160
140
120
100
80
60
40
20
0

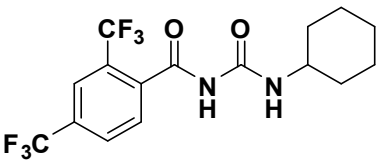
CF3
O
O
N
H
N
H
F3C

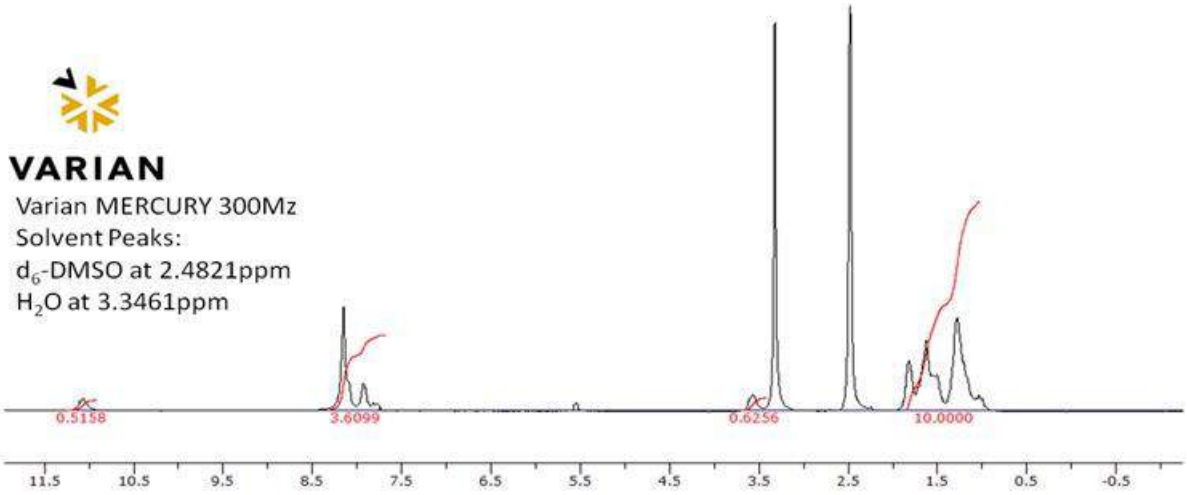
VARIAN
Varian MERCURY 300Mz
Solvent Peaks:
d6-DMSO at 2.4821ppm
H2O at 3.3461ppm
0.5158
3.6099
0.6256
10.0000
11.5
10.5
9.5
8.5
7.5
6.5
5.5
4.5
3.5
2.5
1.5
0.5
-0.5

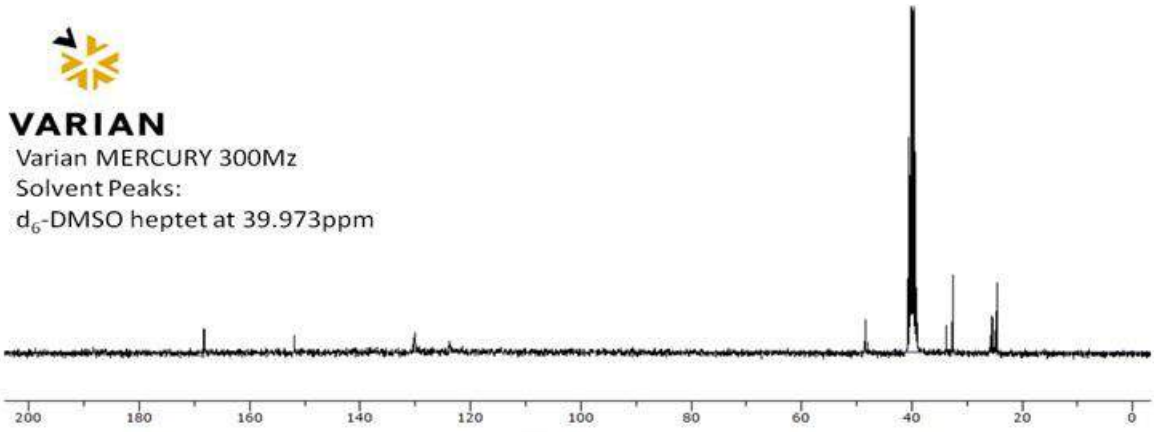
VARIAN
Varian MERCURY 300Mz
Solvent Peaks:
d6-DMSO heptet at 39.973ppm
200
180
160
140
120
100
80
60
40
20
0

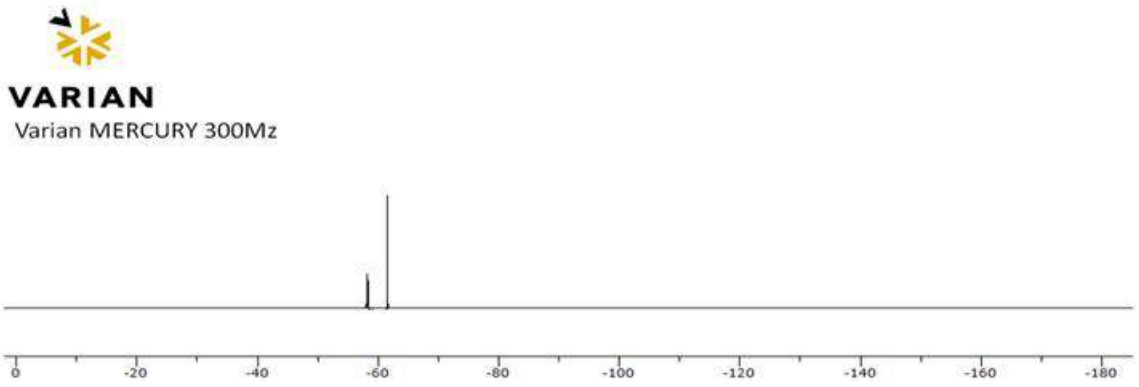
VARIAN
Varian MERCURY 300Mz
0
-20
-40
-60
-80
-100
-120
-140
-160
-180

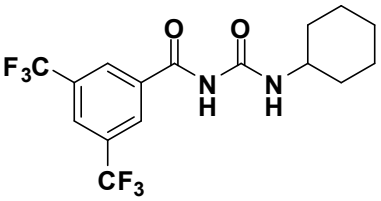
O
O
F3C
N
H
N
H
CF3

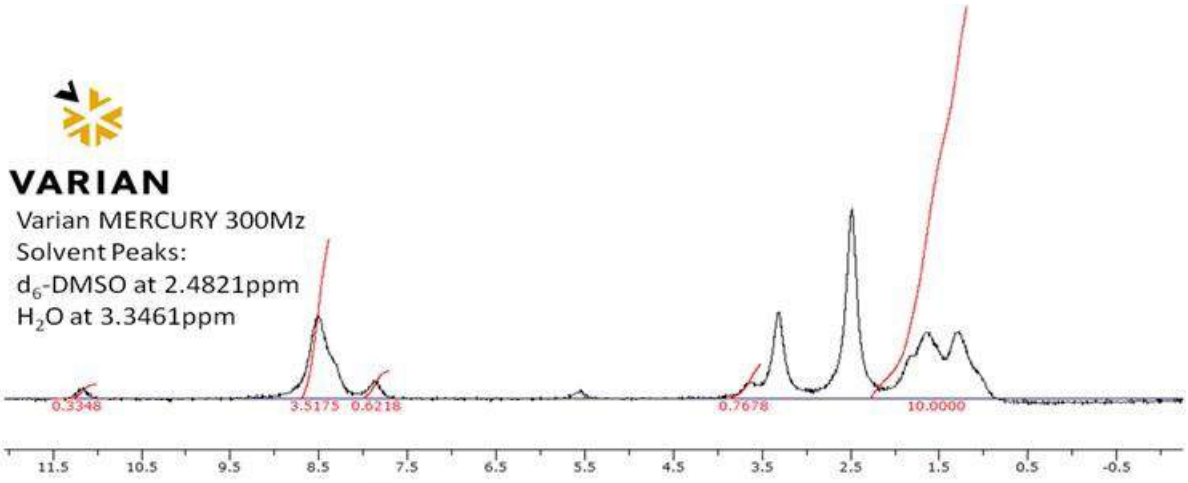
VARIAN
Varian MERCURY 300Mz
Solvent Peaks:
d6-DMSO at 2.4821ppm
H2O at 3.3461ppm
0.3348
3.5175
0.6218
0.7678
10.0000
11.5
10.5
9.5
8.5
7.5
6.5
5.5
4.5
3.5
2.5
1.5
0.5
-0.5

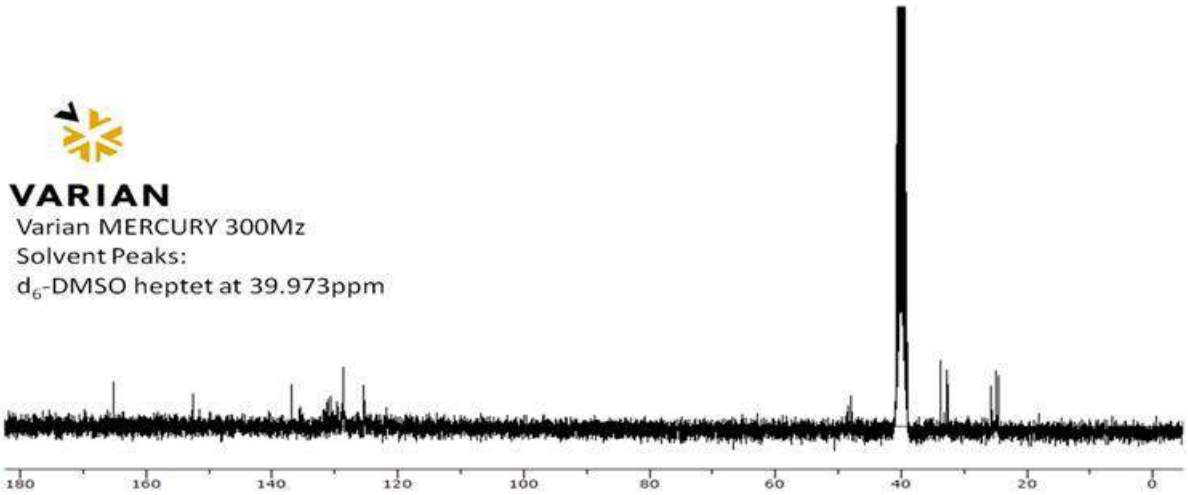
VARIAN
Varian MERCURY 300Mz
Solvent Peaks:
d6-DMSO heptet at 39.973ppm
180
160
140
120
100
80
60
40
20
0

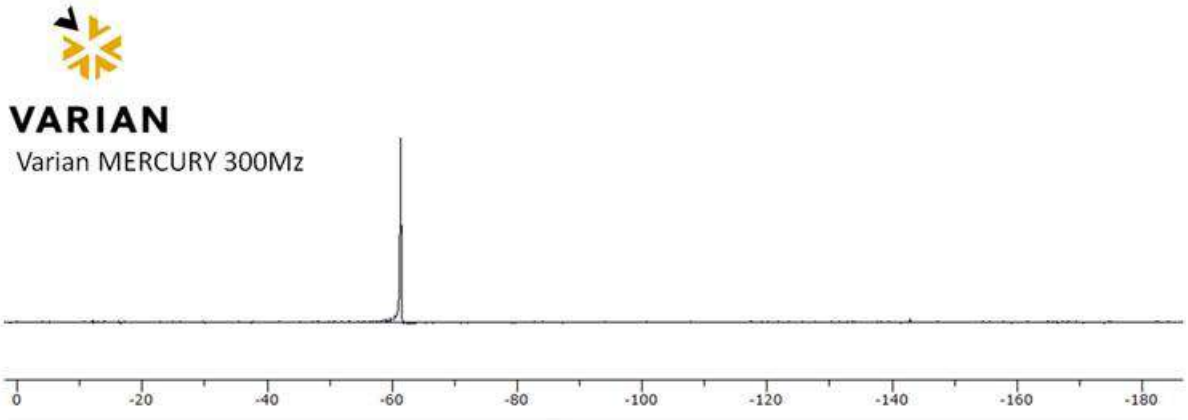
VARIAN
Varian MERCURY 300Mz
0
-20
-40
-60
-80
-100
-120
-140
-160
-180

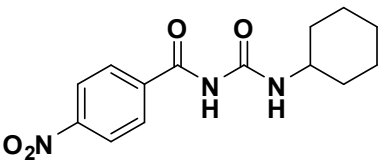

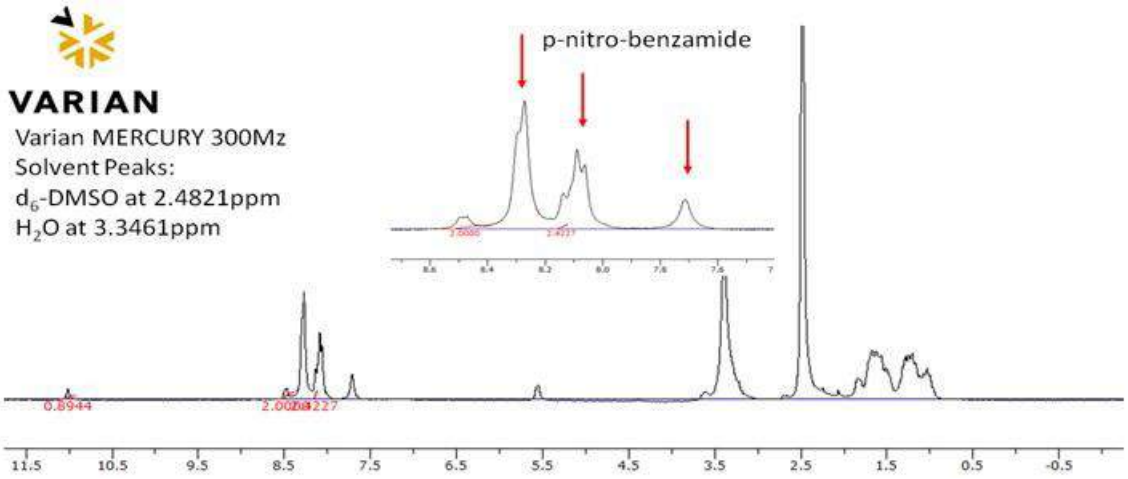
p-nitro-benzamide
VARIAN
Varian MERCURY 300Mz
Solvent Peaks:
d6-DMSO at 2.4821ppm
H2O at 3.3461ppm
0.8944
2.0000
11.5
10.5
9.5
8.5
7.5
6.5
5.5
4.5
3.5
2.5
1.5
0.5
-0.5

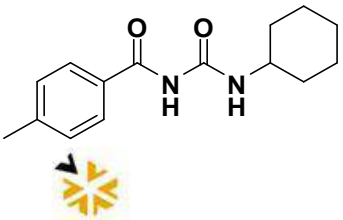

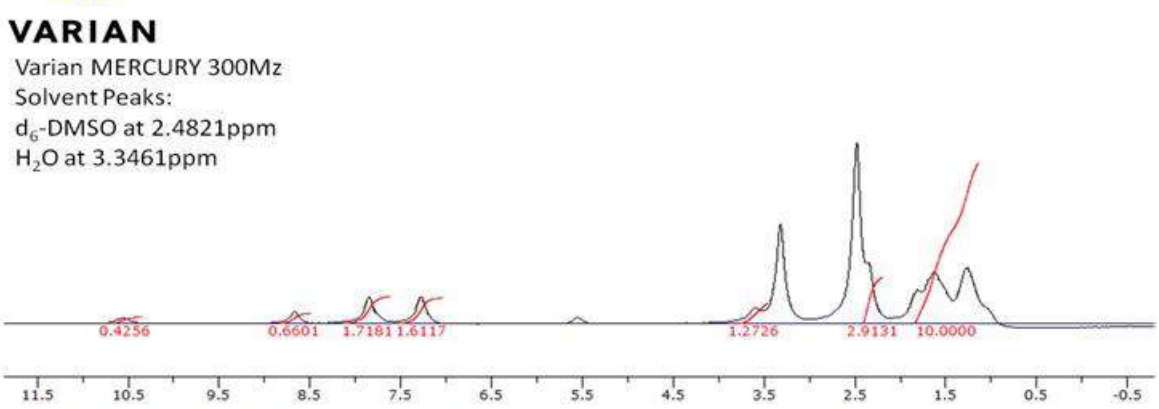
VARIAN
Varian MERCURY 300Mz
Solvent Peaks:
d6-DMSO at 2.4821ppm
H2O at 3.3461ppm
0.4256
0.6601
1.7181
1.6117
1.2726
2.9131
10.0000
11.5
10.5
9.5
8.5
7.5
6.5
5.5
4.5
3.5
2.5
1.5
0.5
-0.5

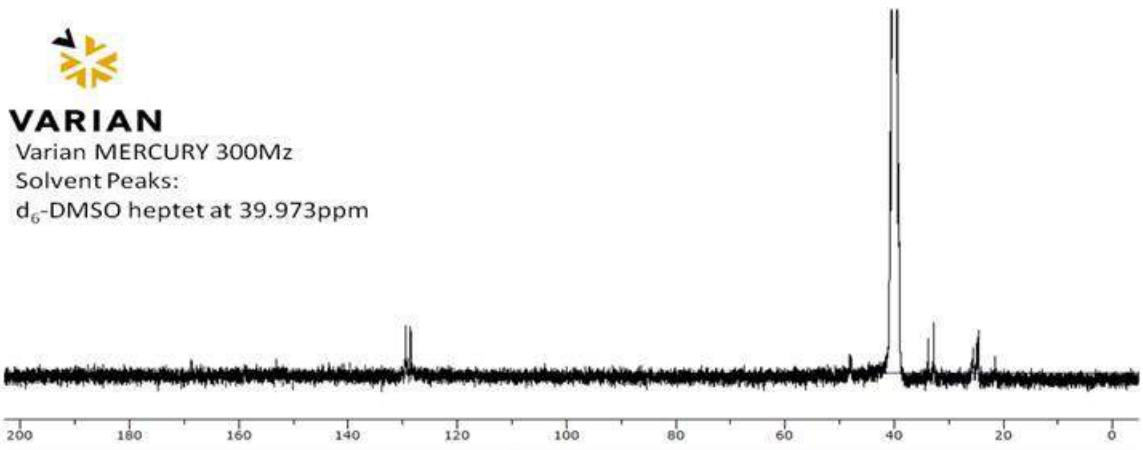
VARIAN
Varian MERCURY 300Mz
Solvent Peaks:
d6-DMSO heptet at 39.973ppm
200
180
160
140
120
100
80
60
40
20
0

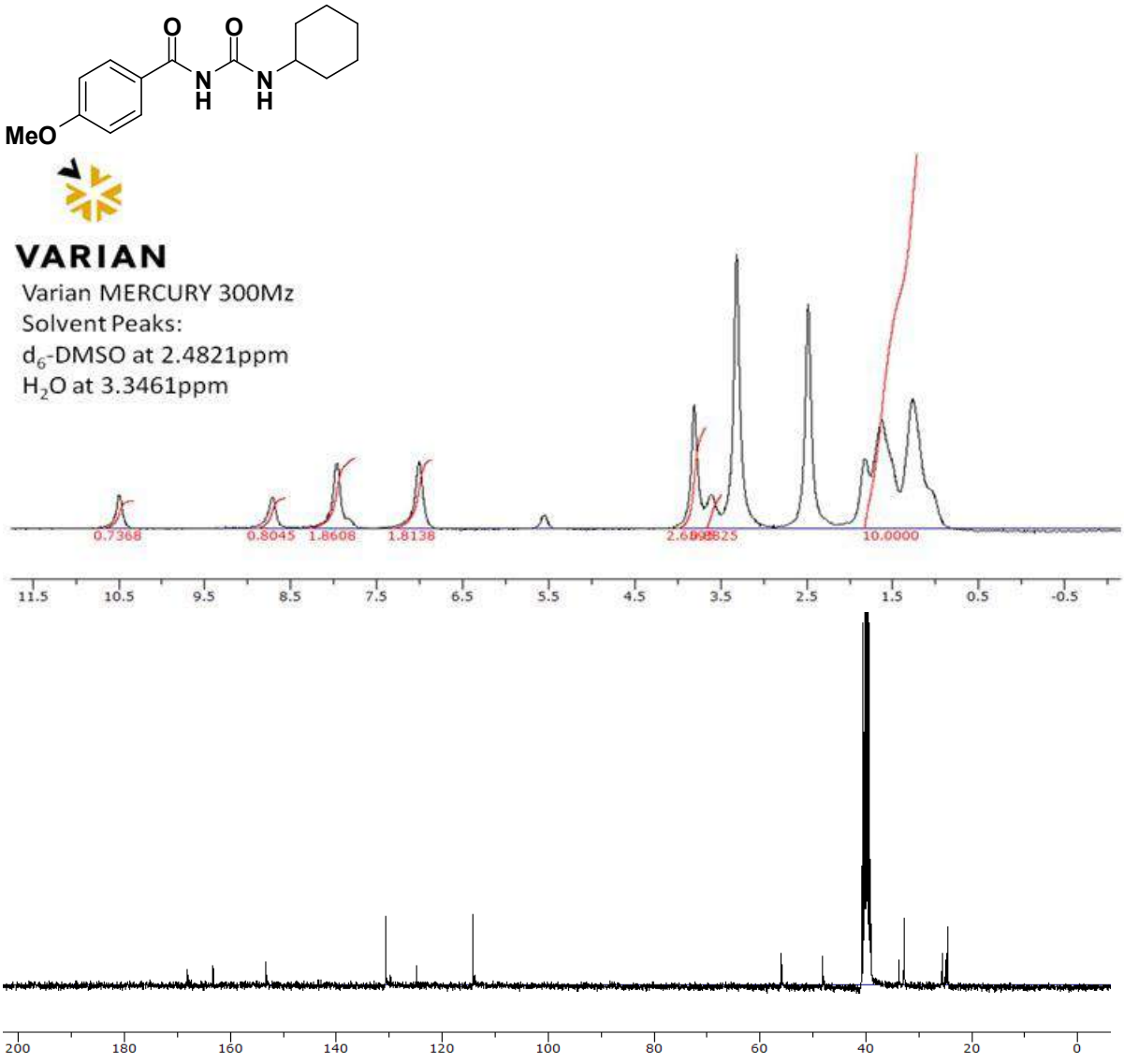
MeO
O
O
N
H
N
H
VARIAN
Varian MERCURY 300Mz
Solvent Peaks:
d6-DMSO at 2.4821ppm
H2O at 3.3461ppm
0.7368
0.8045
1.8608
1.8138
10.0000
11.5
10.5
9.5
8.5
7.5
6.5
5.5
4.5
3.5
2.5
1.5
0.5
-0.5
200
180
160
140
120
100
80
60
40
20
0

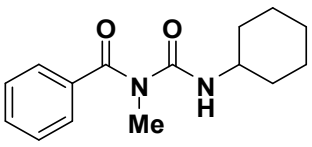
O
O
N
Me
N
H

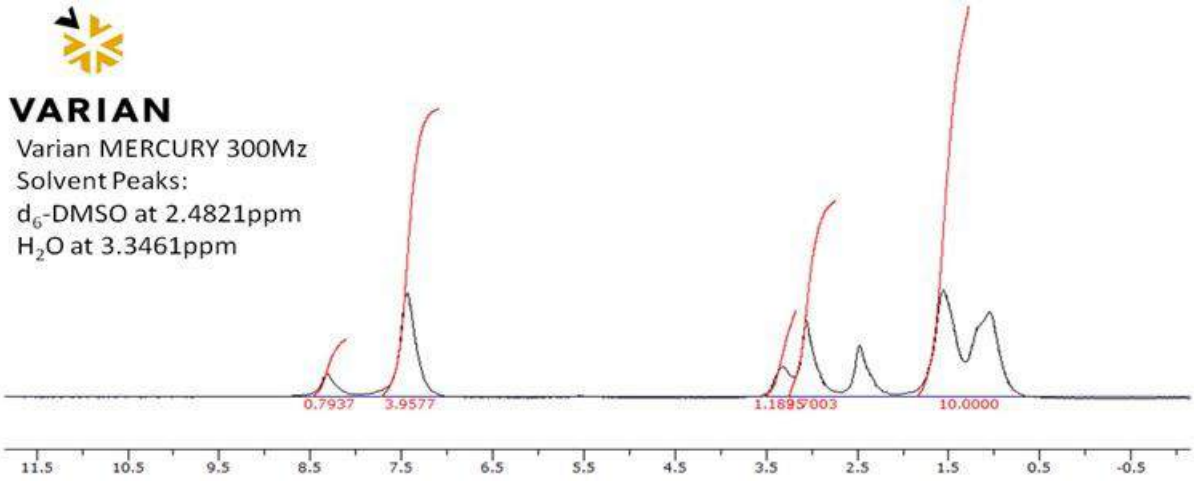
VARIAN
Varian MERCURY 300Mz
Solvent Peaks:
d6-DMSO at 2.4821ppm
H2O at 3.3461ppm
0.7937
3.9577
1.1895
3.0003
10.0000
11.5
10.5
9.5
8.5
7.5
6.5
5.5
4.5
3.5
2.5
1.5
0.5
-0.5

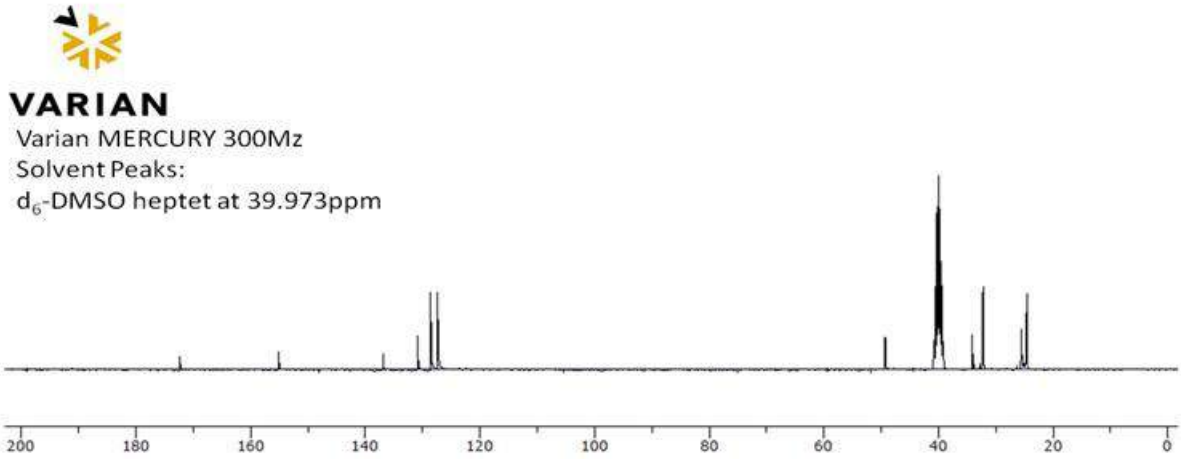
VARIAN
Varian MERCURY 300Mz
Solvent Peaks:
d6-DMSO heptet at 39.973ppm
200
180
160
140
120
100
80
60
40
20
0

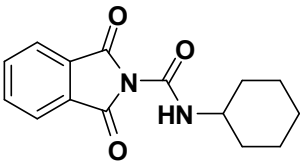

VARIAN

Varian MERCURY 300Mz
Solvent Peaks:
d_6-DMSO at 2.4821ppm
H_2O at 3.3461ppm
Ethyl Acetate at 1.17, 1.99, 4.03ppm.
Hexane at 0.86, 1.25ppm

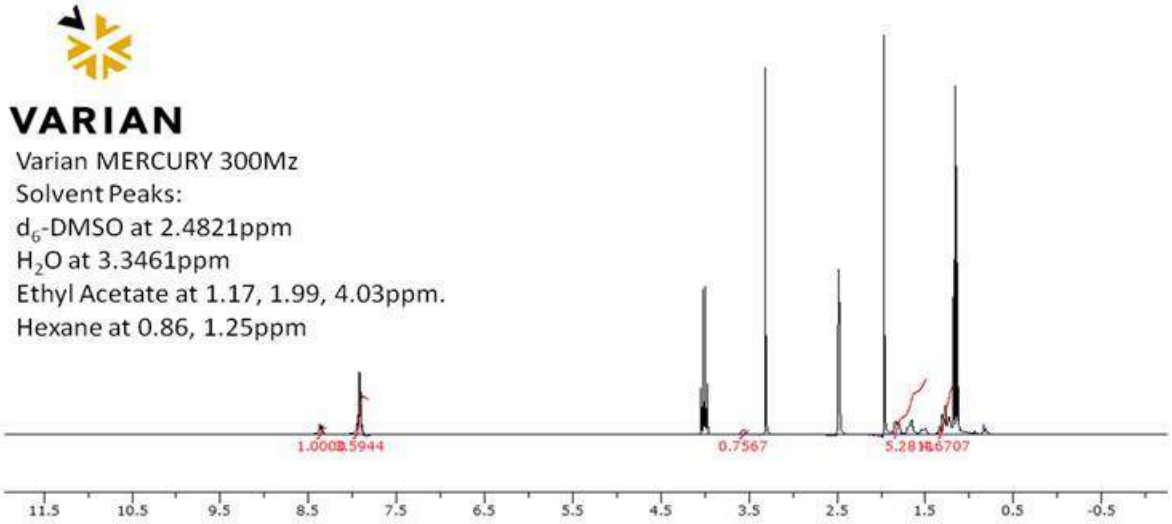

VARIAN

Varian MERCURY 300Mz
Solvent Peaks:
d_6-DMSO heptet at 39.973ppm
Ethyl acetate at 14.40, 20.68, 59.74, 170.31ppm

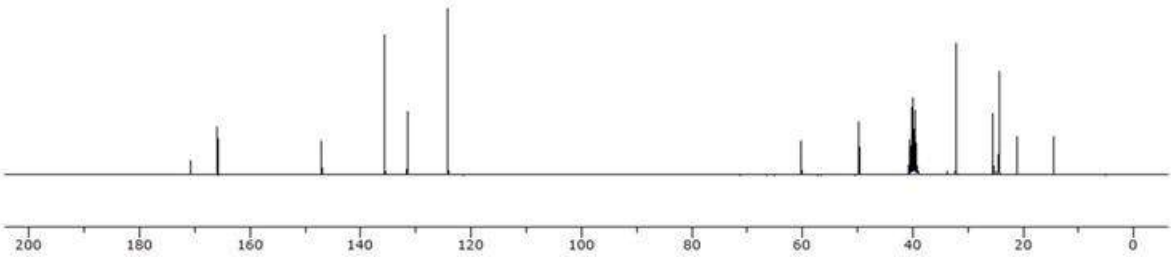

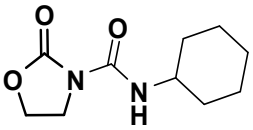

VARIAN

Varian MERCURY 300Mz

Solvent Peaks:

d_6-DMSO at 2.4821ppm

H_2O at 3.3461ppm

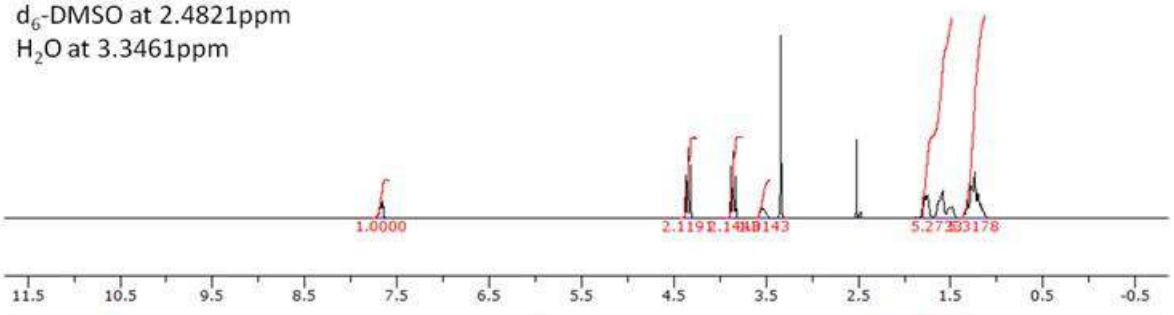

VARIAN

Varian MERCURY 300Mz

Solvent Peaks:

d_6-DMSO heptet at 39.973ppm

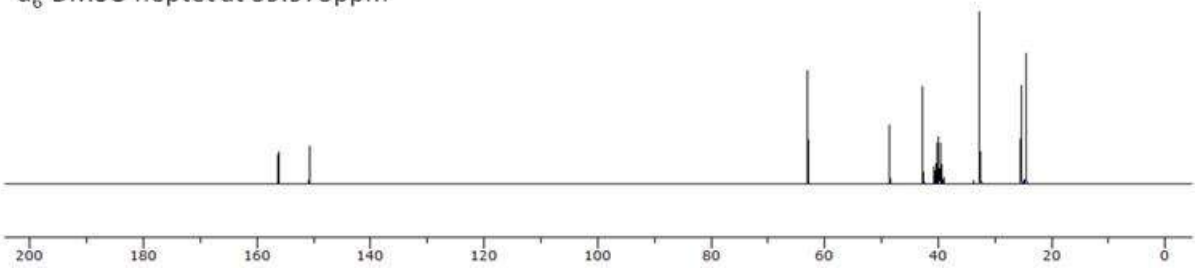

Table C2. Crystallographic data of compounds **1b** and **3c**.

	1b	**3c**
Molecular formula	$C_{16}H_{18}N_2O4$	$C_{16}H_{16}N_2O_2F_6$
M_r	302.32	382.31
Crystal System	Triclinic	Triclinic
Crystal colour	Orange	Colorless
Space group	*P*-1	*P*-1
Temperature (K)	100K	150K
Unit cell dimensions (Å,°)		
a	5.281(2)	7.507(10)
b	11.095(5)	10.293(14)
c	13.812(7)	11.327(16)
α	110.463(5)	91.737(15)
β	95.078(7)	99.457(15)
γ	95.905(6)	94.131(15)
Volume (Å^3)	747.4(6)	860(2)
Z	2	2
D_{calc} (g cm^{-3})	1.343	1.243
μ (mm^{-1})	0.098	0.141
***F*(000)**	320	392
Refl. collected/independent	3718/ 2495	1964/1179
No. observed refl. [$I>2\sigma(I)$]*	1992	1141
No. restraints/No. parameters	0/ 200	0/235
R [all/gt]	0.0579/0.0471	0.1426/0.0991
wR [ref/gt]	0.1337/0.1224	0.3041/0.2668
Goodness-of-fit on F^2	1.045	1.075
Largest diff. peak and hole (*e* Å^{-3})	0.160, -0.332	0.360, -0.524

*$R = \sum||Fo|-|Fc||/\sum Fo, w = 1/[\sigma^2(F_o^2)+(g_1P)^2+ g_2P]$ where $P = (F_o^2+2F_c^2)/3$, $S = \Sigma[w(F_o^2 - F_c^2)^2/(N_{obs} - N_{param})]^{1/2}$.

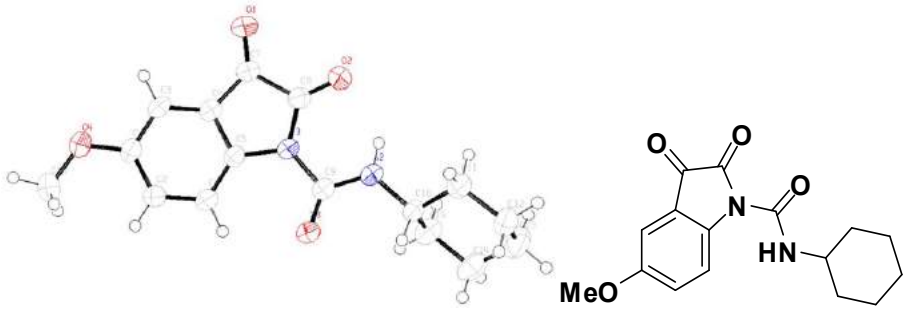

Molecular structure visualized using ORTEP-3 with thermal ellipsoids at 50% probability of *N*-cyclohexyl-5-methoxy-2,3-dioxoindoline-1-carboxamide **1b** as determined by SCXRD, along with a schematic representation of the molecule. CCDC code 1503019.

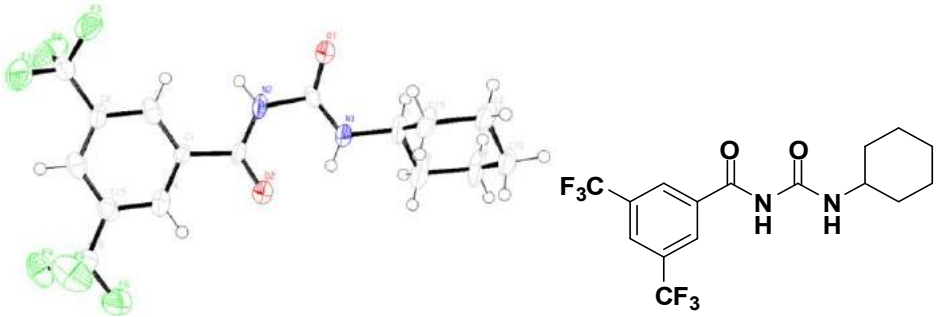

Molecular structure visualized using ORTEP-3 with thermal ellipsoids at 50% probability of *N*-(cyclohexylcarbamoyl)-3,5-bis(trifluoromethyl)benzamide **3c** as determined by SCXRD, along with a schematic representation of the molecule. CCDC code 1503020.

APPENDIX E

SPECTROSCOPIC AND X-RAY DIFFRACTION DATA FOR COMPOUNDS IN CHAPTER 6

***N*-(bis(cyclohexylamino)methylene)-2-methylbenzenesulfonamide**

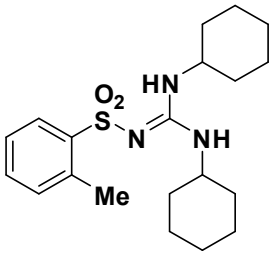

White powder (96% yield); **^{1}H-NMR** (300 MHz, DMSO-*d6*) δ 0.94-1.30 (m, 10H), δ 1.45-1.77 (m, 10H), δ 2.55 (s, 3H), δ 3.47-3.68 (m, 2H), δ 6.79 (m, 2H), δ 7.39-7.63 (m, 3H), δ 7.65-7.84 (m, 1H); **^{13}C-NMR** (300 MHz, DMSO-*d6*) δ 24.8, 25.3, 25.7, 32.7, 33.8, 125.9, 127.1, 131.7, 132.3, 136.5, 142.6, 153.6; **HRMS**: Calculated for $C_{20}H_{31}O_2N_3S$ [M+H]: 378.22097; measured: 378.22057.

***N*-(bis(cyclohexylamino)methylene)-2-fluorobenzenesulfonamide**

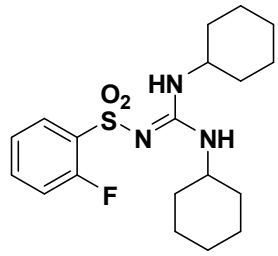

White powder (98% yield); **^{1}H-NMR** (300 MHz, DMSO-*d6*) δ 0.76-1.33 (m, 10H), δ 1.34-1.87 (m, 10H), δ 3.47-3.68 (m, 2H), δ 6.66-7.91 (m, 6H); **^{13}C-NMR** (300 MHz, DMSO-*d6*) δ 24.8, 25.3, 25.7, 32.7, 33.8, 117.1, 124.6, 129.0, 134.1, 153.3; **^{19}F-NMR** (300 MHz, DMSO-*d6*) δ -110.9; **HRMS**: Calculated for $C_{19}H_{28}O_2N_3SF$ [M+H]: 382.19590; measured:

***N*-(bis(cyclohexylamino)methylene)-2-bromobenzenesulfonamide**

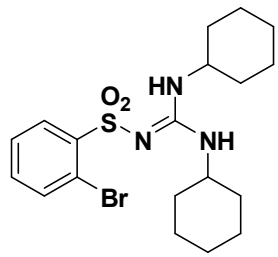

White powder (90% yield); **^{1}H-NMR** (300 MHz, DMSO-*d6*) δ 0.83-1.95 (m, 20H), δ 2.94-3.27 (m, 2H), δ 7.21-8.07 (m, 6H); **^{13}C-NMR** (300 MHz, DMSO-*d6*) δ 24.8, 25.4, 34.0, 55.0, 119.3, 128.4, 129.6, 133.8, 135.4, 139.4, 143.1; **HRMS**: Calculated for $C_{19}H_{28}O_2N_3BrS$ [M+H]: 442.11584; measured: 442.11481.

***N*-(bis(cyclohexylamino)methylene)-benzenesulfonamide**

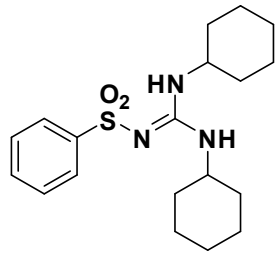

White powder (99% yield); **^{1}H-NMR** (300 MHz, DMSO-*d6*) δ 0.94-1.26 (m, 10H), δ 1.45-1.70 (m, 10H), δ 3.43-3.69 (m, 2H), δ 6.83-6.94 (m, 2H), δ 7.42-7.54 (m, 3H), δ 7.62-7.72 (m, 2H); **^{13}C-NMR** (300 MHz, DMSO-*d6*) δ 24.8, 25.3, 25.7, 32.7, 33.8, 126.0, 129.1, 131.5, 144.5, 154.1; **HRMS**: Calculated for $C_{19}H_{29}O_2N_3S$ [M+H]: 364.20532; measured: 364.20493.

***N*-(bis(cyclohexylamino)methylene)-2-nitrobenzenesulfonamide**

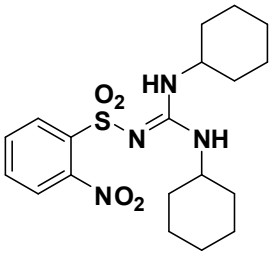

Pale yellow powder (98% yield); **^{1}H-NMR** (300 MHz, DMSO-*d6*) δ 0.97-1.32 (m, 10H), δ 1.42-1.73 (m, 10H), δ 3.43-3.68 (m, 2H), δ 6.72-6.96 (m, 2H), δ 7.66-7.97 (m, 4H); **^{13}C-NMR** (300 MHz, DMSO-*d6*) δ 24.9, 25.4, 25.7, 32.7, 33.8, 125.8, 129.2, 131.7, 144.7, 153.9; **HRMS**: Calculated for $C_{19}H_{28}O_4N_4S$ [M+H]: 409.19040; measured: 409.18966.

***N*-(bis(cyclohexylamino)methylene)-2,6-difluorobenzenesulfonamide**

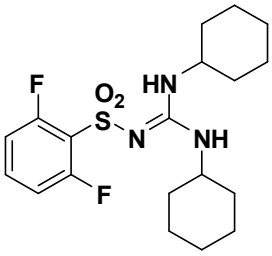

White powder (96% yield); **^{1}H-NMR** (500 MHz, DMSO-*d6*) δ 0.93-1.32 (m, 10H), δ 1.44-1.75 (m, 10H), δ 3.43-3.672 (m, 2H), δ 6.94 (m, 2H), δ 7.14-7.28 (m, 2H), δ 7.52-7.75 (m, 1H); **^{13}C-NMR** (500 MHz, DMSO-*d6*) δ 24.8, 25.3, 25.7, 32.7, 33.8, 115.3, 115.5, 119.1, 119.4, 120.5, 120.7, 153.9; **^{19}F-NMR** (500 MHz, DMSO-*d6*) δ -108.5; **HRMS**: Calculated for $C_{19}H_{29}O_2N_3ClS$ [M+H]: 400.18648; measured: 400.18563.

***N*-(bis(cyclohexylamino)methylene)-2,5-difluorobenzenesulfonamide**

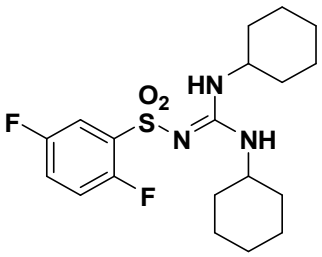

White powder (97% yield); **^{1}H-NMR** (500 MHz, DMSO-*d6*) δ 1.03-1.31 (m, 10H), δ 1.46-1.75 (m, 10H), δ 3.47-3.69 (m, 2H), δ 6.88 (m, 2H), δ 7.39-7.61 (m, 3H); **^{13}C-NMR** (500 MHz, DMSO-*d6*) δ 24.8, 25.3, 25.7, 32.7, 33.8, 115.3, 119.3, 120.5, 153.5; **^{19}F-NMR** (500 MHz, DMSO-*d6*) δ -117.3, -116.7; **HRMS**: Calculated for $C_{19}H_{28}O_2N_3SF_2$ [M+H]: 400.18648; measured: 400.18559.

***N*-(bis(isopropylamino)methylene)-2-chlorobenzenesulfonamide**

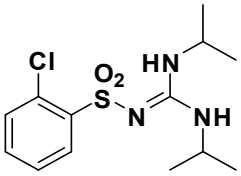

White Powder (97% yield); **^{1}H-NMR** (500 MHz, DMSO-*d6*) δ 1.01 (d, *J* = 1.21Hz, 6H), δ 1.03 (d, *J* = 1.20Hz, 6H), δ 3.77-3.94 (m, 2H), δ 6.81 (d, *J* = 8.31Hz, 2H), δ 7.41-7.61 (m, 3H), δ 7.93-7.98 (m, 1H); **^{13}C-NMR** (500 MHz, DMSO-*d6*) δ22.9, 42.9, 127.5, 129.3, 131.9, 133.1, 141.7, 154.0; **HRMS**: Calculated for $C_{13}H_{21}O_2N_3ClS$ [M+H]: 318.10375; measured: 318.10320.

***N*-(bis(cyclohexylamino)methylene)-2,5-dimethoxybenzenesulfonamide**

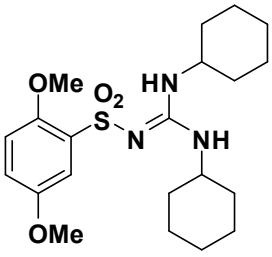

White powder (91% yield); **^{1}H-NMR** (300 MHz, DMSO-*d6*) δ 0.99-1.28 (m, 10H), δ 1.45-1.74 (m, 10H), δ 3.42-3.59 (m, 2H), δ 3.70 (s, 6H), δ 6.53-6.82 (m, 2H), δ 7.00-7.07 (m, 2H), δ 7.23 (s, 1H); **^{13}C-NMR** (300 MHz, DMSO-*d6*) δ 24.8, 25.3, 32.7, 56.1, 56.7, 113.6, 114.2, 118.2, 133.1, 150.7, 152.5, 153.7; **HRMS**: Calculated for $C_{21}H_{33}O_4N_3S$ [M+H]: 424.22645; measured: 424.22566.

***N*-(bis(cyclohexylamino)methylene)-2,4-dimethoxybenzenesulfonamide**

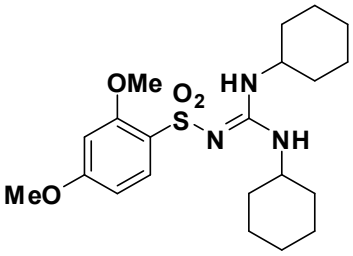

White powder (90% yield); **^{1}H-NMR** (300 MHz, DMSO-*d6*) δ 0.95-1.23 (m, 10H), δ 1.42-1.57 (m, 10H), δ 3.40-3.63 (m, 2H), δ 3.76 (s, 6H), δ 6.40-6.65 (m, 2H), δ 6.78-7.14 (m, 2H), δ 7.51-7.67 (m, 1H); **^{13}C-NMR** (300 MHz, DMSO-*d6*) δ 24.8, 25.3, 32.9, 56.1, 56.2, 99.4, 104.4, 124.8, 130.1, 153.7, 158.3, 163.2 ; **HRMS**: Calculated for $C_{21}H_{33}O_4N_3S$ [M+H]: 424.22645; measured: 424.22531.

***N*-(bis(cyclohexylamino)methylene)-3,5-difluorobenzenesulfonamide**

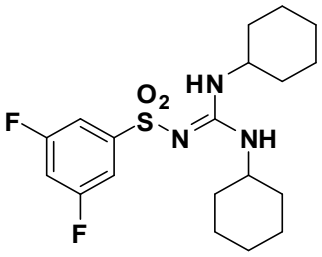

Beige solid (90% yield); **^{1}H-NMR** (300 MHz, DMSO-*d6*) δ 1.03-1.34 (m, 10H), δ 1.48-1.73(m, 10H), δ 3.47-3.66 (m, 2H), δ 6.91 (d, *J* = 7.4Hz, 2H), δ 7.33-7.40 (m, 2H), δ 7.47-7.53 (m, 1H); **^{13}C-NMR** (300 MHz, DMSO-*d6*) δ 24.5, 25.3, 32.6, 107.1, 109.4, 109.5, 148.3, 153.8, 1261.4, 163.5; **HRMS**: Calculated for $C_{19}H_{27}O_2N_3F_2SNa$ [M+Na]: 422.1684; measured: 422.1686.

***N*-(bis(cyclohexylamino)methylene)-3,5-difluorobenzenesulfonamide**

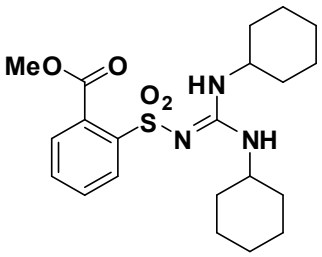

Beige solid (90% yield); **^{1}H-NMR** (300 MHz, DMSO-*d6*) δ 1.03-1.32 (m, 10H), δ 1.48-1.76 (m, 10H), δ 3.46-3.67 (m, 2H), δ 3.80 (s, 3H), δ 6.74 (m, *J* = 7.2Hz, 2H), δ 7.47-7.51 (m, 1H), δ 7.56-7.83 (m, 3H); **^{13}C-NMR** (300 MHz, DMSO-*d6*) δ 24.8, 25.3, 53.0, 127.7, 128.2, 130.6, 131.6, 132.2, 141.6, 153.6, 168.7; **HRMS**: Calculated for $C_{21}H_{31}O_4N_3S$ [M+H]: 422.21080; measured: 422.21028.

FTIR-ATR Spectra for all arylsulfonylguanidine compounds

FTIR-ATR spectrum of the crude mixture shows the absence of the characteristic peak of carbodiimides (C=N stretching bands between 2000-2200 cm^{-1}), which indicates that all the carbodiimide has been completely consumed and that the reaction has reached completion during milling, *i.e.* the product has formed during ball milling and not during workup. Similarly, FTIR-ATR spectra revealed that in the absence of the catalyst the reactions did not take place, as indicated by a strong residual carbodiimide peak.

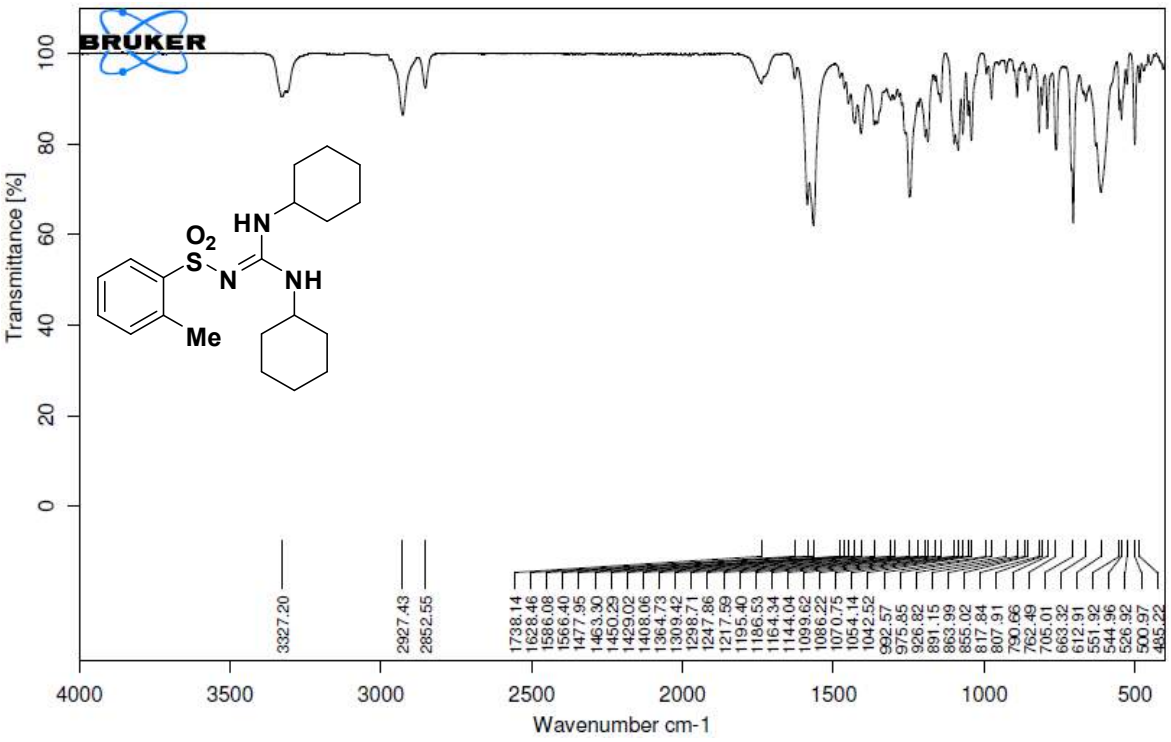
BRUKER
Transmittance [%]
Wavenumber cm-1
HN
O2
S
N
NH
Me
3327.20
2927.43
2852.55

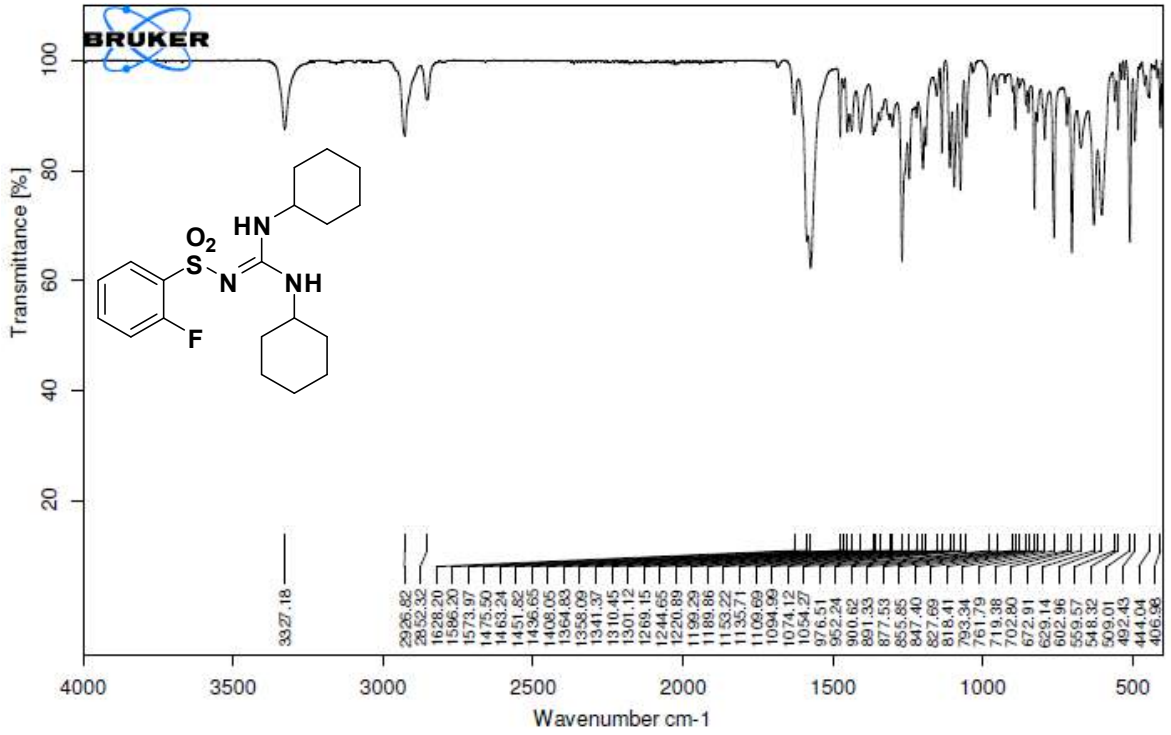
BRUKER
Transmittance [%]
Wavenumber cm-1
HN
O2
S
N
NH
F
3327.18

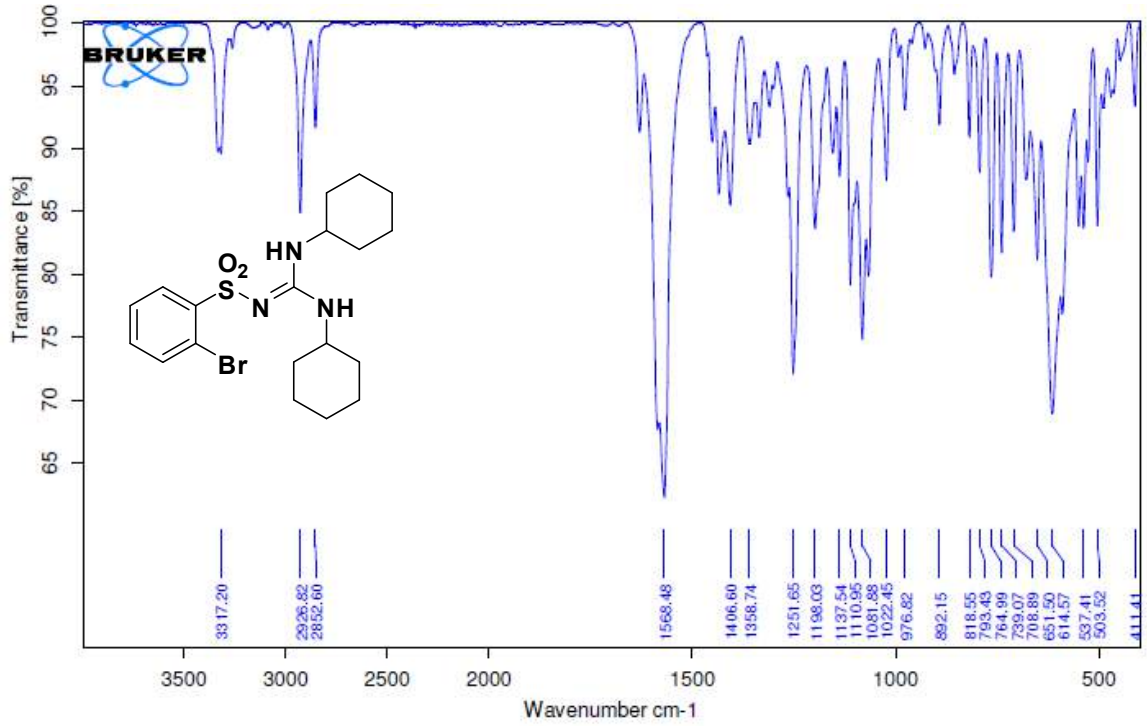
BRUKER
Transmittance [%]
100
95
90
85
80
75
70
65
HN
O2
S
N
NH
Br
3317.20
2926.82
2852.60
1568.48
1406.60
1358.74
1251.65
1198.03
1137.54
1110.95
1081.88
1022.45
976.82
892.15
818.55
793.43
764.99
739.07
708.89
651.50
614.57
537.41
503.52
411.41
3500
3000
2500
2000
1500
1000
500
Wavenumber cm-1

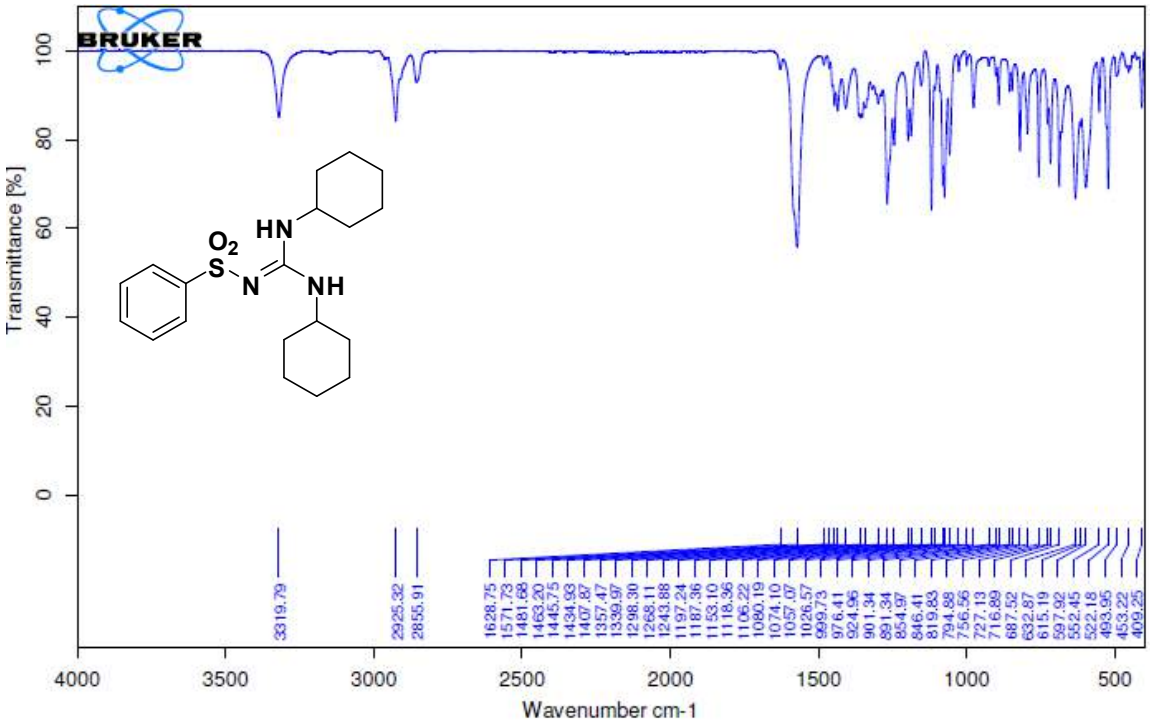
BRUKER
Transmittance [%]
100
80
60
40
20
0
HN
O2
S
N
NH
3319.79
2925.32
2855.91
1628.75
1571.73
1481.68
1463.20
1445.75
1434.93
1407.87
1357.47
1339.97
1298.30
1268.11
1243.88
1197.24
1187.36
1153.10
1118.36
1106.22
1080.19
1074.10
1057.07
1026.57
999.73
976.41
924.96
901.34
891.34
854.97
846.41
819.83
794.88
756.56
727.13
716.89
687.52
632.87
615.19
597.92
552.45
522.18
493.95
453.22
409.25
4000
3500
3000
2500
2000
1500
1000
500
Wavenumber cm-1

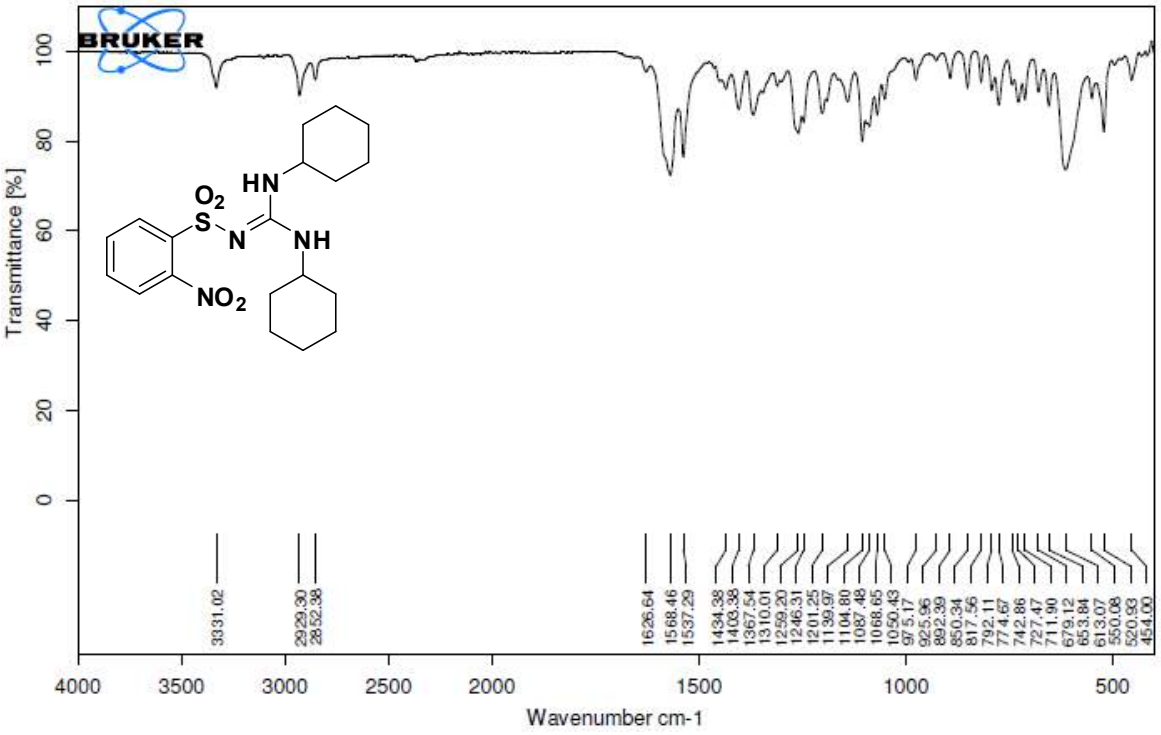
BRUKER
Transmittance [%]
Wavenumber cm-1
HN
O2
S
N
NH
NO2
3331.02
2929.30
2852.38
1626.64
1568.46
1537.29
1434.38
1408.38
1367.54
1310.01
1259.20
1246.31
1201.25
1139.97
1104.80
1087.48
1068.65
1050.43
975.17
925.96
892.39
850.34
817.56
792.11
774.67
742.86
727.47
711.90
679.12
653.84
613.07
550.08
520.93
454.09

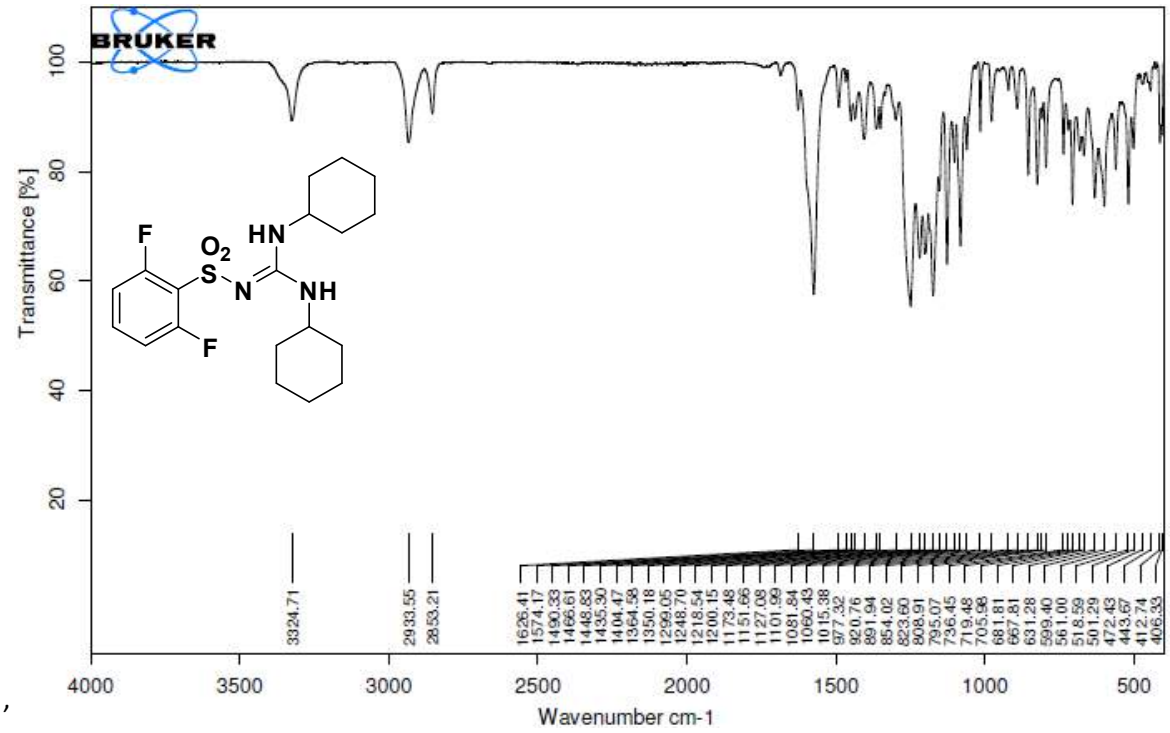
BRUKER
Transmittance [%]
Wavenumber cm-1
F
HN
O2
S
N
NH
F
3324.71
2933.55
2853.21
1626.41
1574.17
1490.33
1466.61
1448.83
1435.30
1404.47
1364.99
1350.18
1299.05
1248.70
1218.54
1200.15
1173.48
1151.66
1127.09
1101.99
1081.84
1060.43
1015.38
977.32
920.76
891.94
854.02
823.60
808.91
795.07
736.45
719.48
705.98
681.81
667.81
631.28
599.40
561.00
518.59
501.29
472.43
443.67
412.74
406.33

,

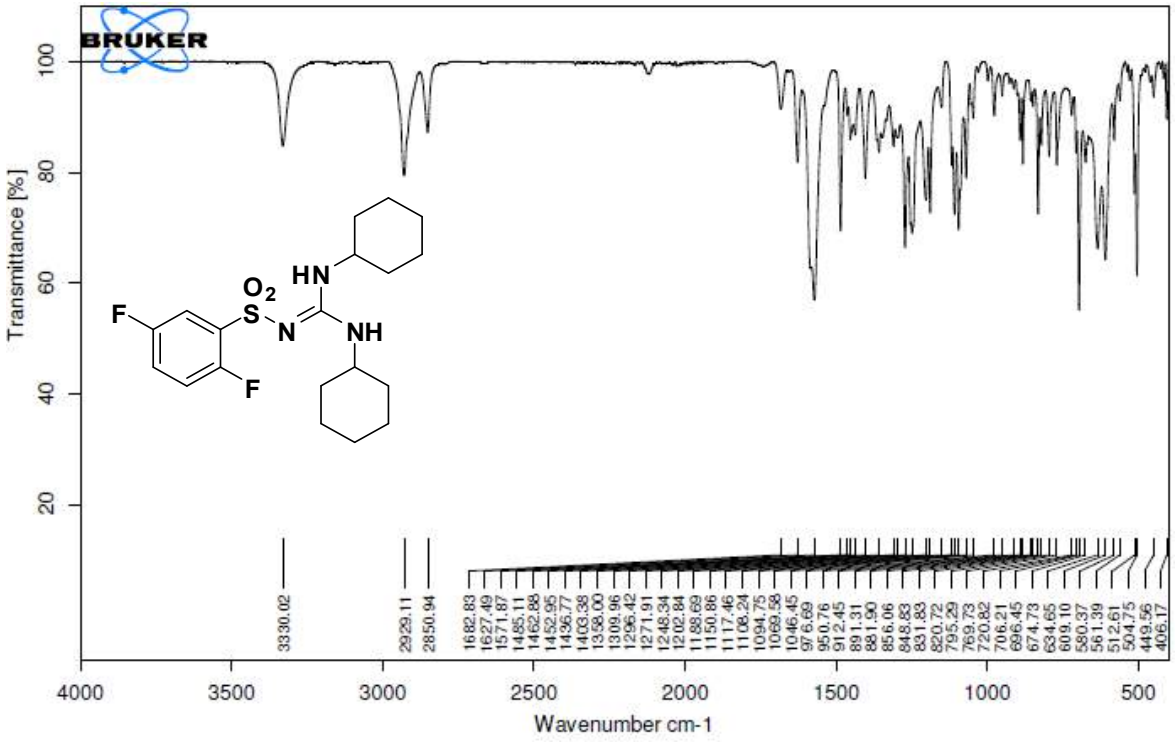
BRUKER
Transmittance [%]
Wavenumber cm-1
F
F
O2
S
N
HN
NH
3330.02
2929.11
2850.94

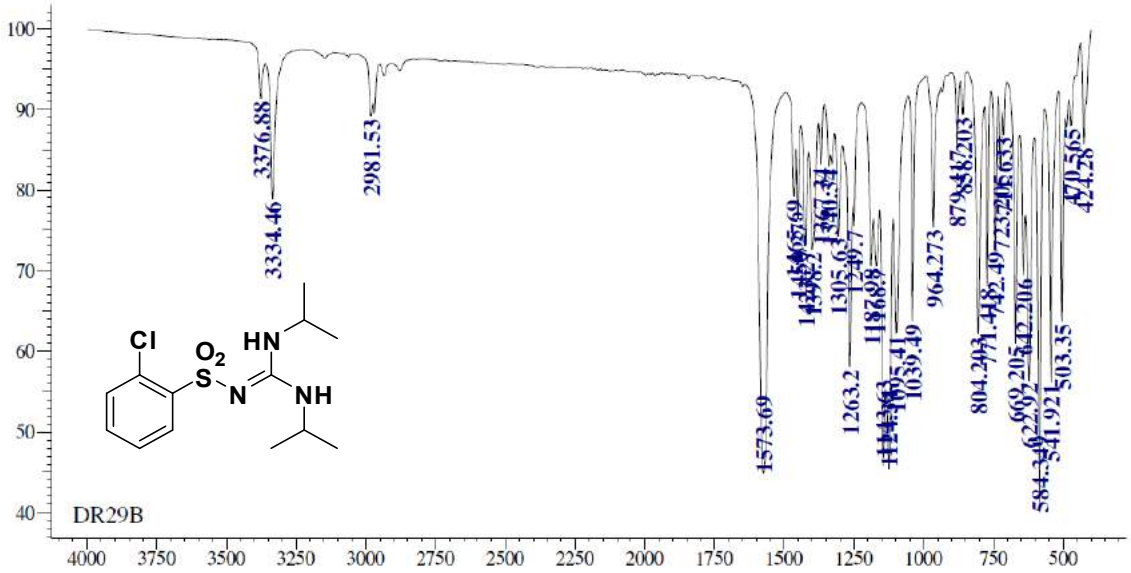
3376.88
3334.46
2981.53
1573.69
1263.2
964.273
DR29B
Cl
O2
S
N
HN
NH

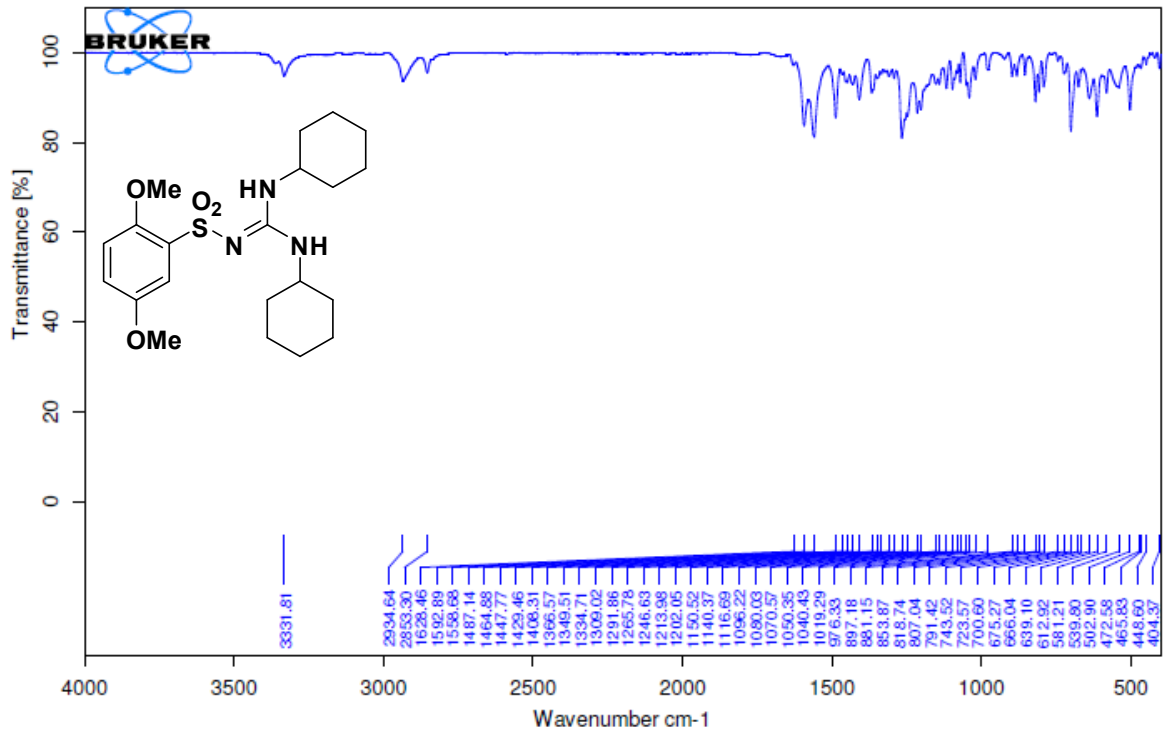
BRUKER
OMe
O2
S
N
HN
NH
OMe
Transmittance [%]
Wavenumber cm-1
3331.81
2934.64
2853.30
1628.46
1592.89
1558.68
1487.14
1464.88
1447.77
1429.46
1408.31
1366.57
1349.51
1334.71
1309.02
1291.86
1265.78
1246.63
1213.98
1202.05
1150.52
1140.37
1116.69
1096.22
1080.03
1070.57
1050.35
1040.43
1019.29
976.33
897.18
881.15
853.87
818.74
807.04
791.42
743.52
723.57
700.60
675.27
666.04
639.10
612.92
581.21
539.80
502.90
472.58
465.83
448.60
404.37

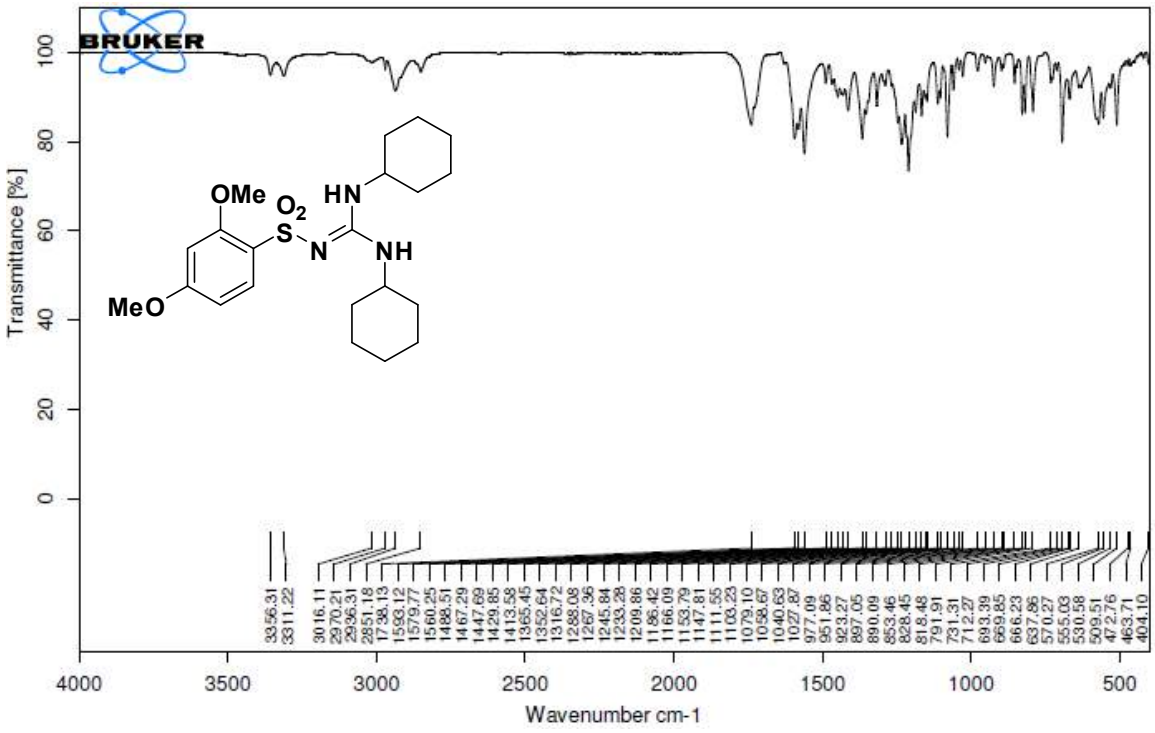
BRUKER
OMe
O2
S
N
HN
NH
MeO
Transmittance [%]
Wavenumber cm-1
3356.31
3311.22
3016.11
2970.21
2936.31
2851.18
1738.13
1593.12
1579.77
1560.25
1488.51
1467.29
1447.69
1429.85
1413.58
1365.45
1352.64
1316.72
1288.08
1267.36
1245.84
1233.28
1209.86
1186.42
1166.09
1153.79
1147.81
1111.55
1103.23
1079.10
1038.67
1010.63
1027.87
977.09
951.86
923.27
897.05
890.09
853.46
828.45
818.48
791.91
731.31
712.27
693.39
669.85
666.23
637.86
570.27
555.03
530.58
509.51
472.76
463.71
404.10

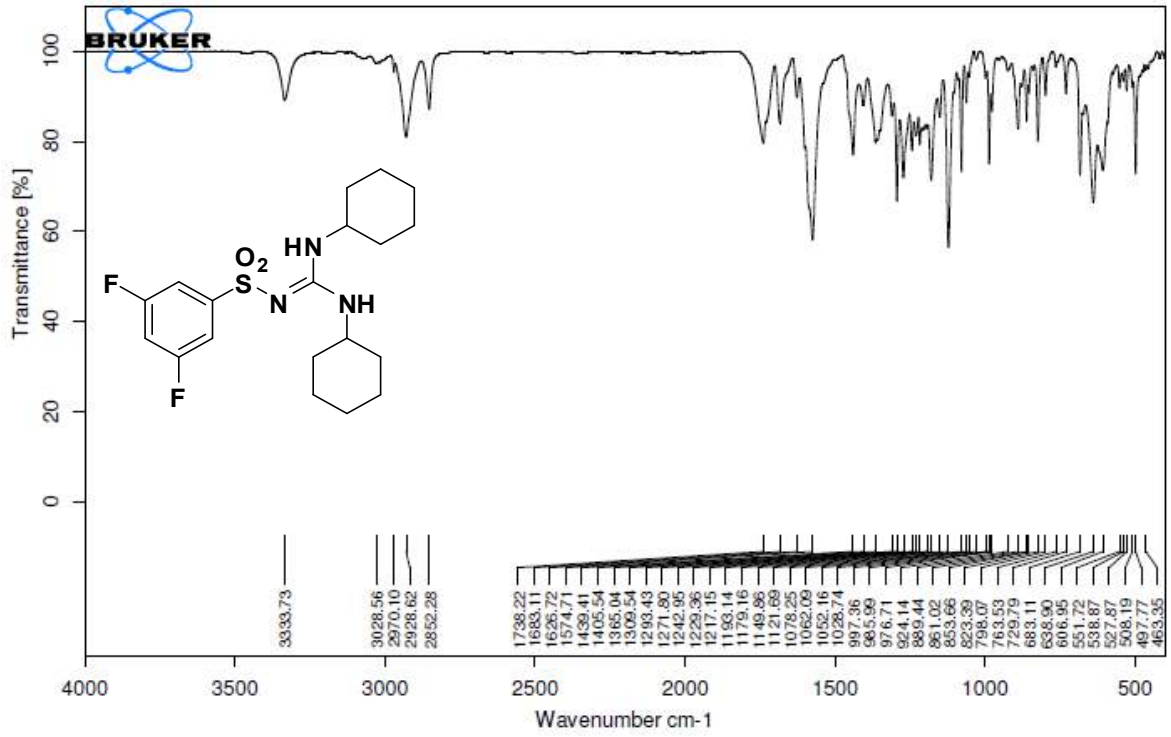
BRUKER
Transmittance [%]
Wavenumber cm-1
F
F
O2
S
N
HN
NH
3333.73
3028.56
2970.10
2928.62
2852.28
1738.22
1683.11
1626.72
1574.71
1439.41
1405.54
1365.04
1309.54
1293.43
1271.80
1242.95
1229.36
1217.15
1193.14
1179.16
1149.86
1121.69
1078.25
1062.09
1052.16
1028.74
997.36
985.99
976.71
924.14
889.44
861.02
853.66
823.39
798.07
763.53
729.79
683.11
638.90
606.95
551.72
538.87
527.87
508.19
497.77
463.35

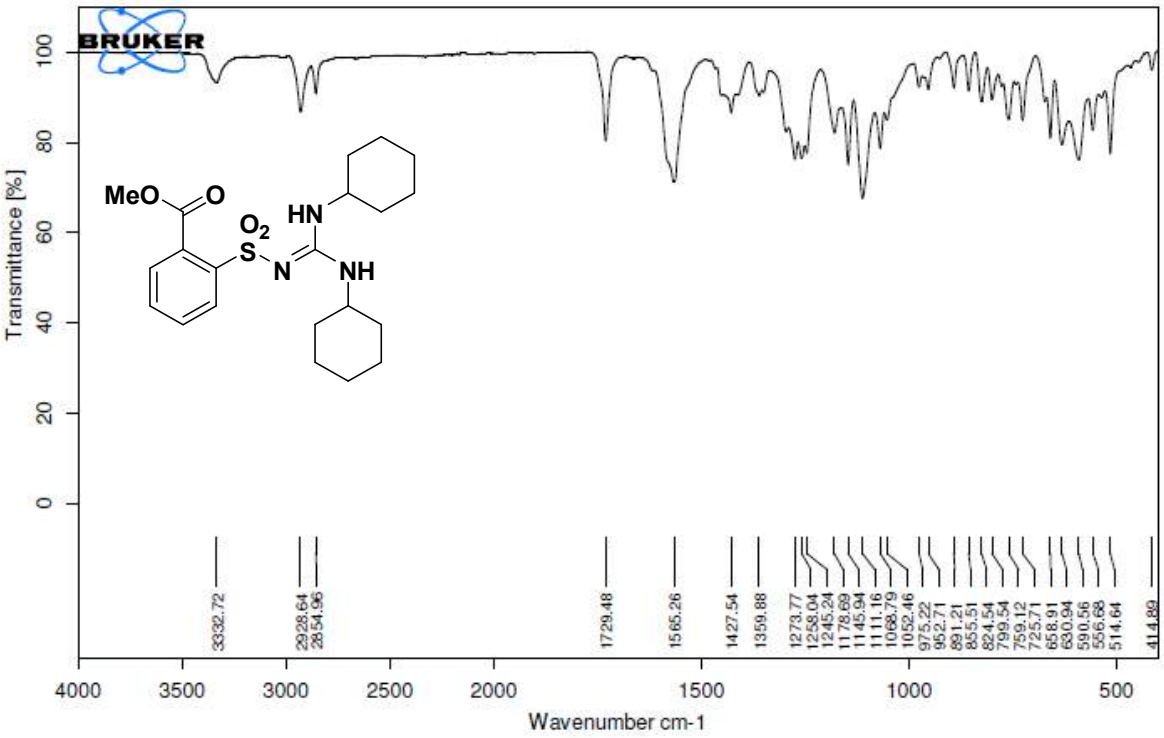
BRUKER
Transmittance [%]
Wavenumber cm-1
MeO
O
O2
S
N
HN
NH
3332.72
2928.64
2854.95
1729.48
1565.26
1427.54
1359.88
1273.77
1258.04
1245.24
1178.69
1145.94
1111.16
1068.79
1052.46
975.22
952.71
891.21
855.51
824.54
799.54
759.12
725.71
658.91
630.94
590.56
556.68
514.64
414.89

NMR Spectra for all arylsulfonylguanidine compounds

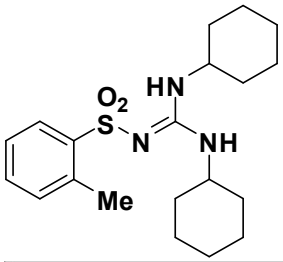

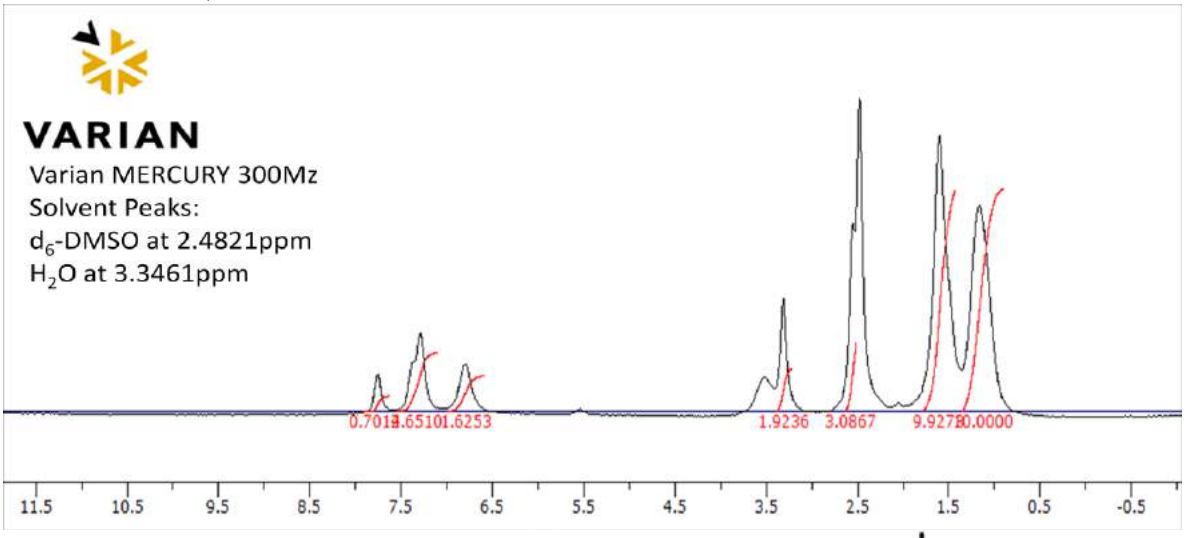

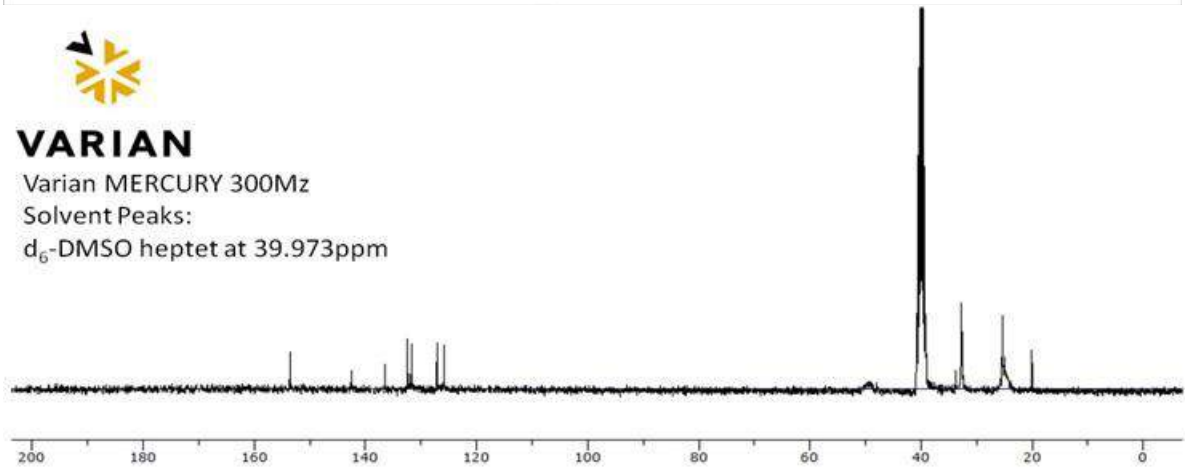

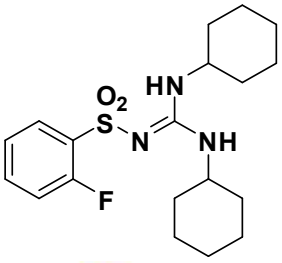
O2
S
HN
N
NH
F

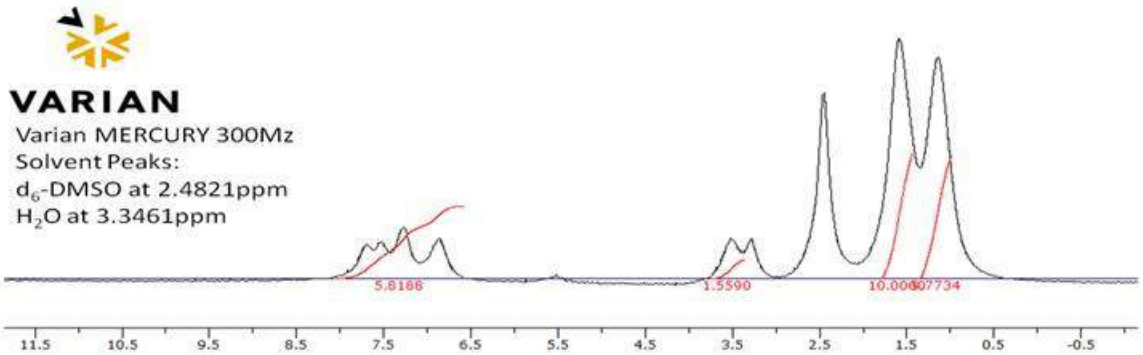
VARIAN
Varian MERCURY 300Mz
Solvent Peaks:
d6-DMSO at 2.4821ppm
H2O at 3.3461ppm
5.8186
1.5590
11.5
10.5
9.5
8.5
7.5
6.5
5.5
4.5
3.5
2.5
1.5
0.5
-0.5

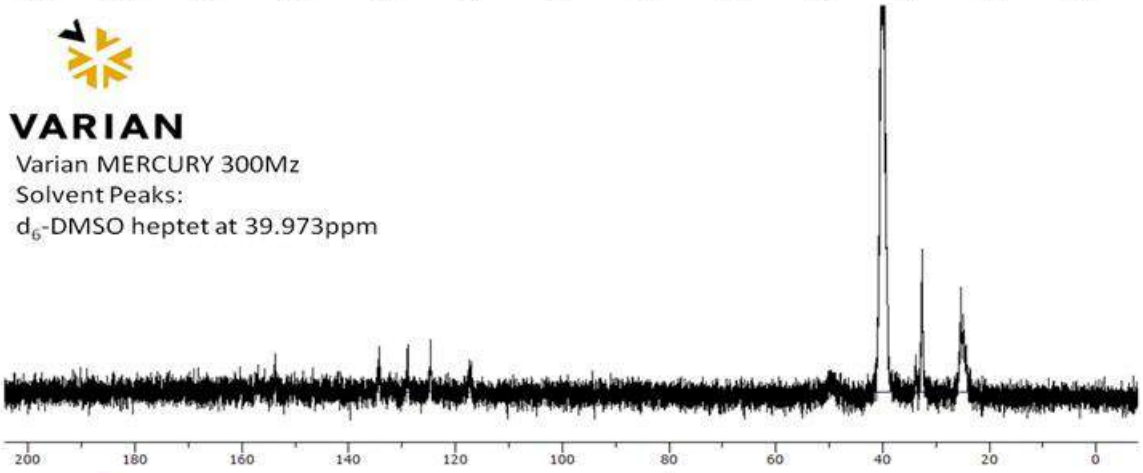
VARIAN
Varian MERCURY 300Mz
Solvent Peaks:
d6-DMSO heptet at 39.973ppm
200
180
160
140
120
100
80
60
40
20
0

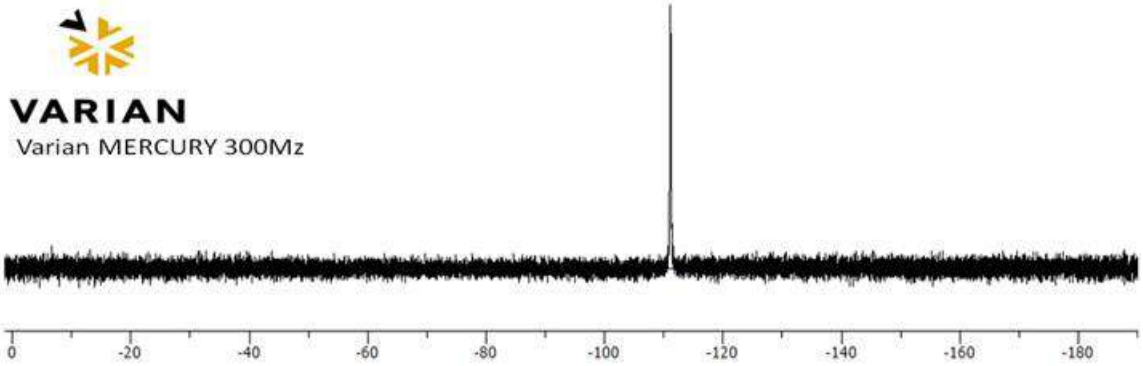
VARIAN
Varian MERCURY 300Mz
0
-20
-40
-60
-80
-100
-120
-140
-160
-180

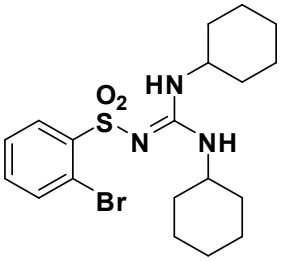
O2
S
HN
N
NH
Br

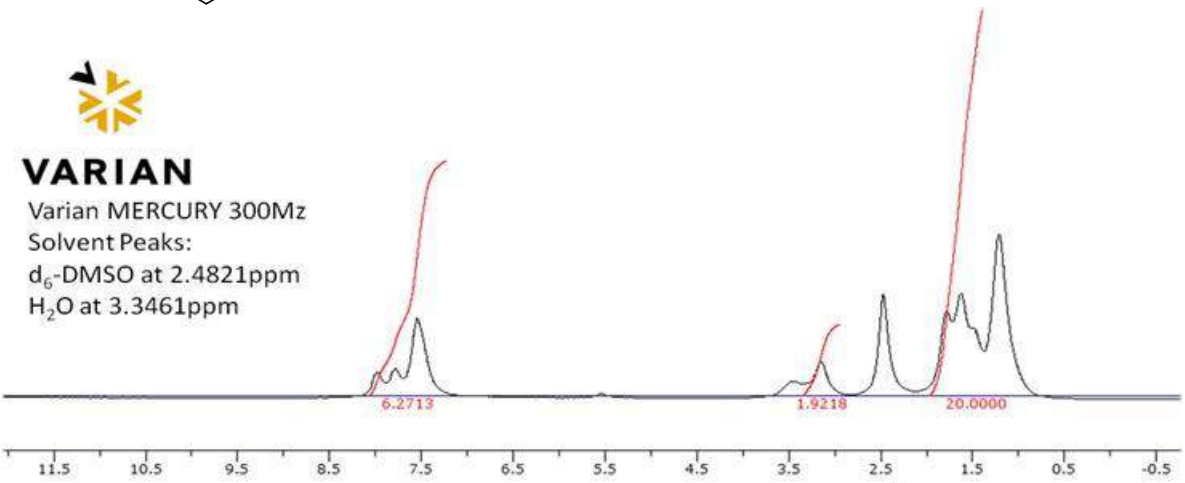
VARIAN
Varian MERCURY 300Mz
Solvent Peaks:
d6-DMSO at 2.4821ppm
H2O at 3.3461ppm
6.2713
1.9218
20.0000
11.5
10.5
9.5
8.5
7.5
6.5
5.5
4.5
3.5
2.5
1.5
0.5
-0.5

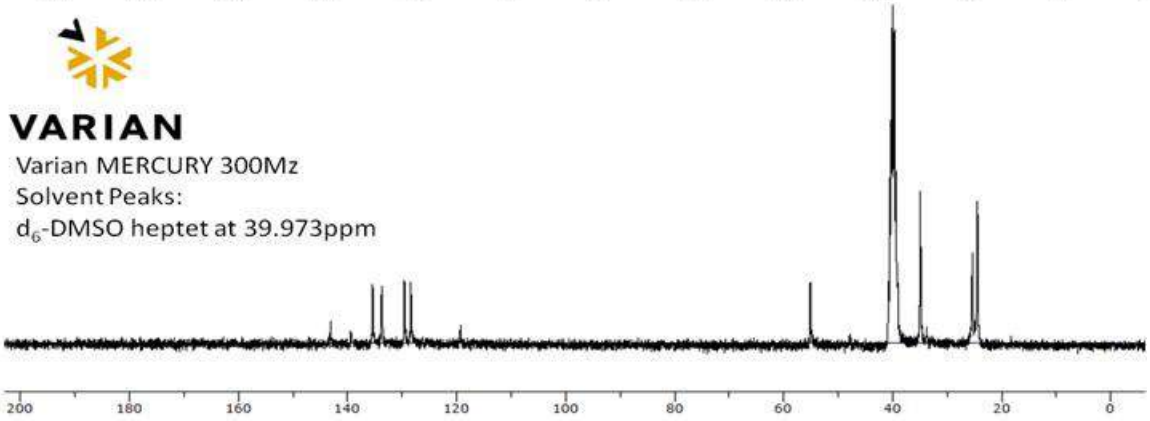
VARIAN
Varian MERCURY 300Mz
Solvent Peaks:
d6-DMSO heptet at 39.973ppm
200
180
160
140
120
100
80
60
40
20
0

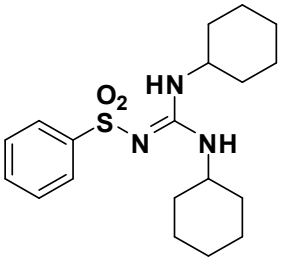
O2
S
HN
N
NH

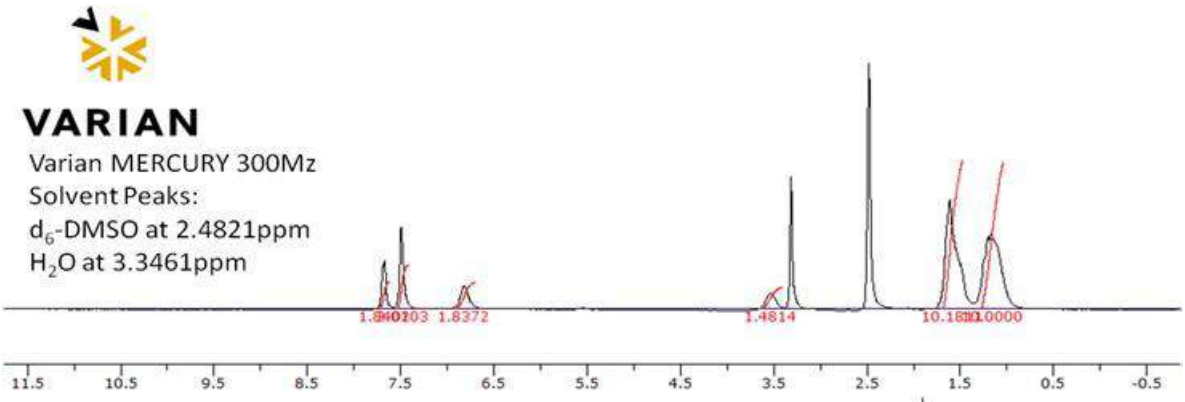
VARIAN
Varian MERCURY 300Mz
Solvent Peaks:
d6-DMSO at 2.4821ppm
H2O at 3.3461ppm
1.8372
1.4814
11.5
10.5
9.5
8.5
7.5
6.5
5.5
4.5
3.5
2.5
1.5
0.5
-0.5

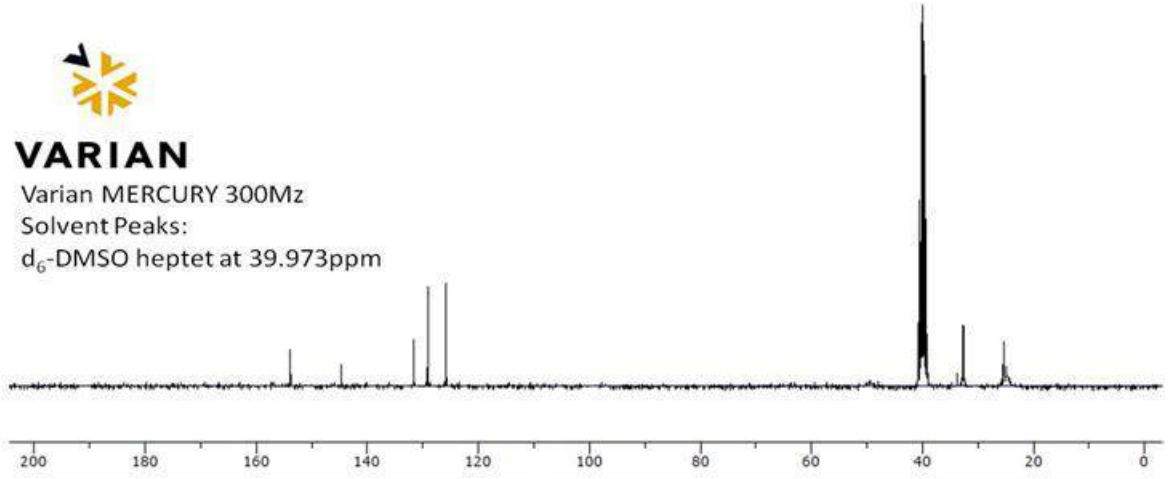
VARIAN
Varian MERCURY 300Mz
Solvent Peaks:
d6-DMSO heptet at 39.973ppm
200
180
160
140
120
100
80
60
40
20
0

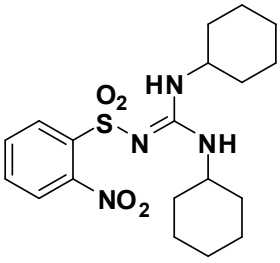
O2
S
N
HN
NH
NO2

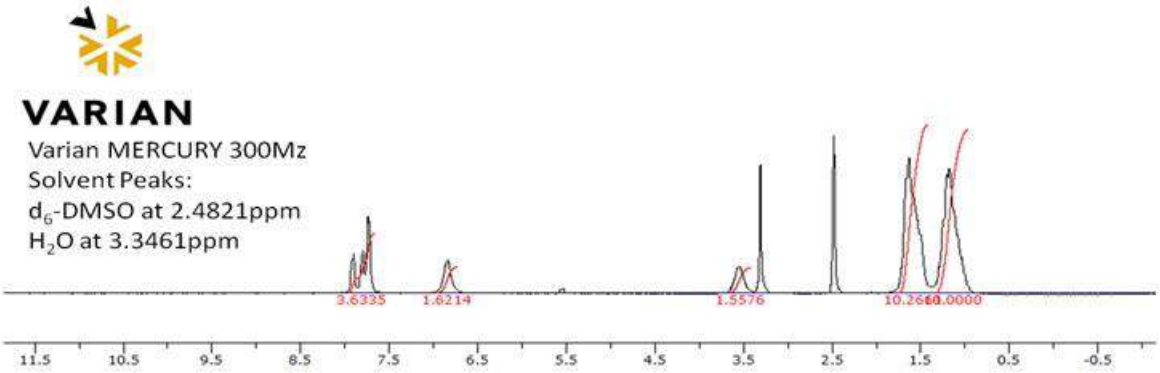
VARIAN
Varian MERCURY 300Mz
Solvent Peaks:
d6-DMSO at 2.4821ppm
H2O at 3.3461ppm
3.6335
1.6214
1.5576
10.2664
11.5
10.5
9.5
8.5
7.5
6.5
5.5
4.5
3.5
2.5
1.5
0.5
-0.5

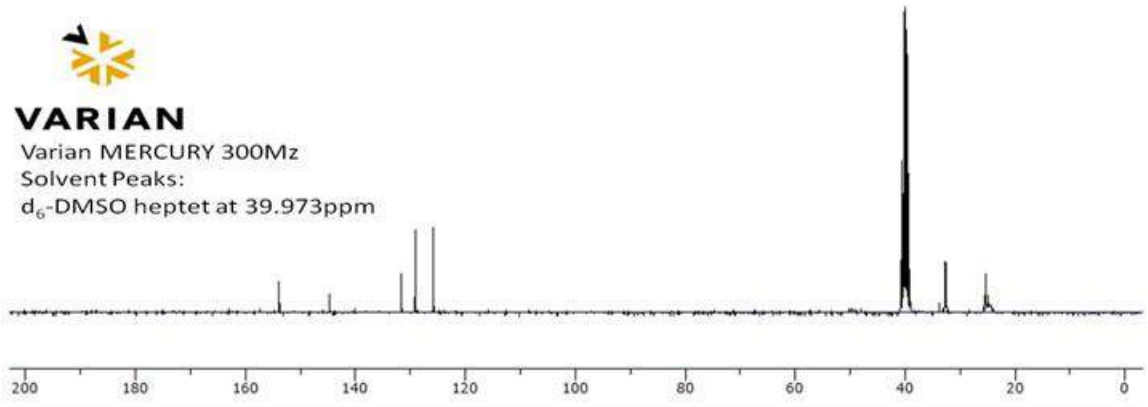
VARIAN
Varian MERCURY 300Mz
Solvent Peaks:
d6-DMSO heptet at 39.973ppm
200
180
160
140
120
100
80
60
40
20
0

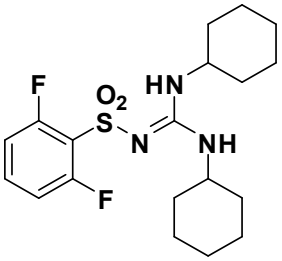
F
O2
S
HN
N
NH
F

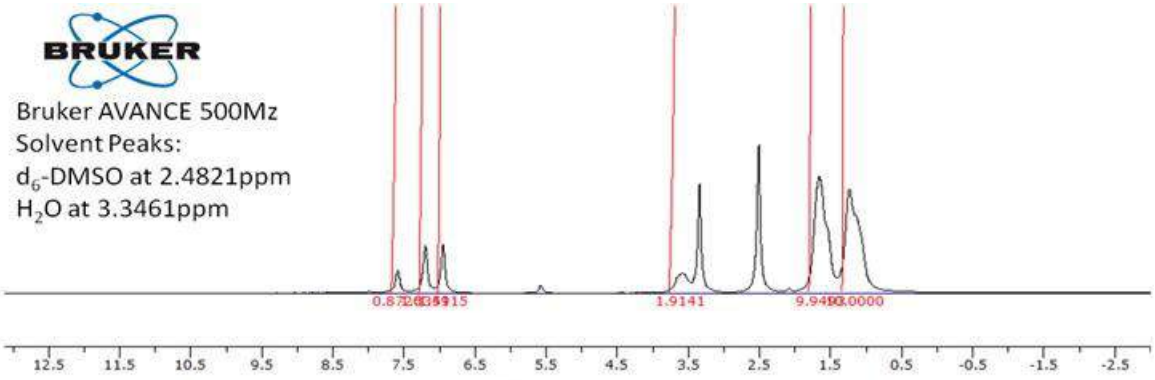
Bruker AVANCE 500Mz
Solvent Peaks:
d6-DMSO at 2.4821ppm
H2O at 3.3461ppm
1.9141
12.5
11.5
10.5
9.5
8.5
7.5
6.5
5.5
4.5
3.5
2.5
1.5
0.5
-0.5
-1.5
-2.5

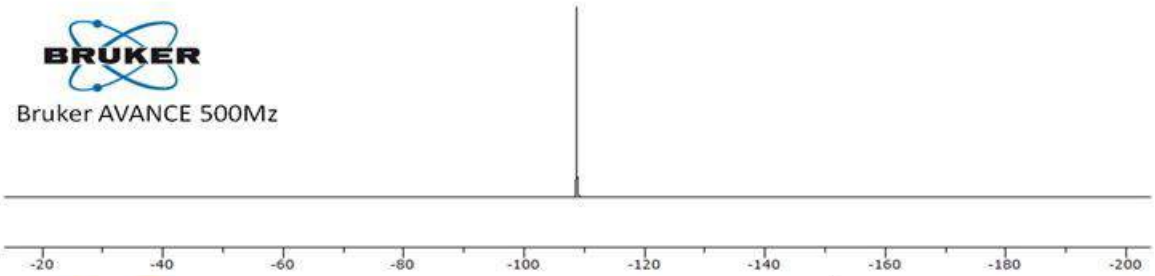
Bruker AVANCE 500Mz
-20
-40
-60
-80
-100
-120
-140
-160
-180
-200

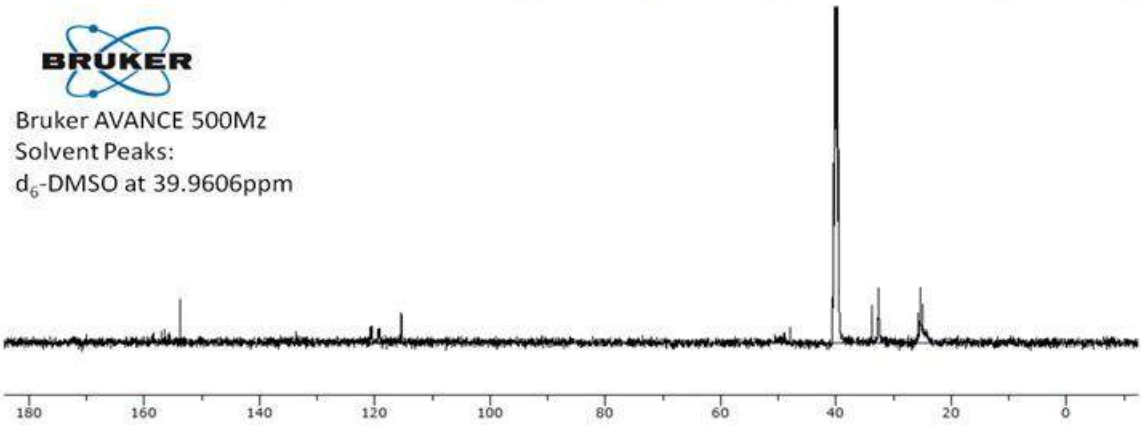
Bruker AVANCE 500Mz
Solvent Peaks:
d6-DMSO at 39.9606ppm
180
160
140
120
100
80
60
40
20
0

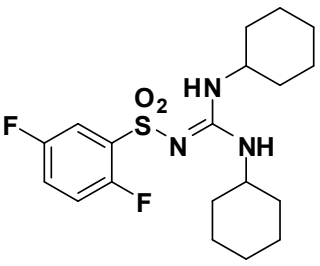
F
O2
S
N
HN
NH
F

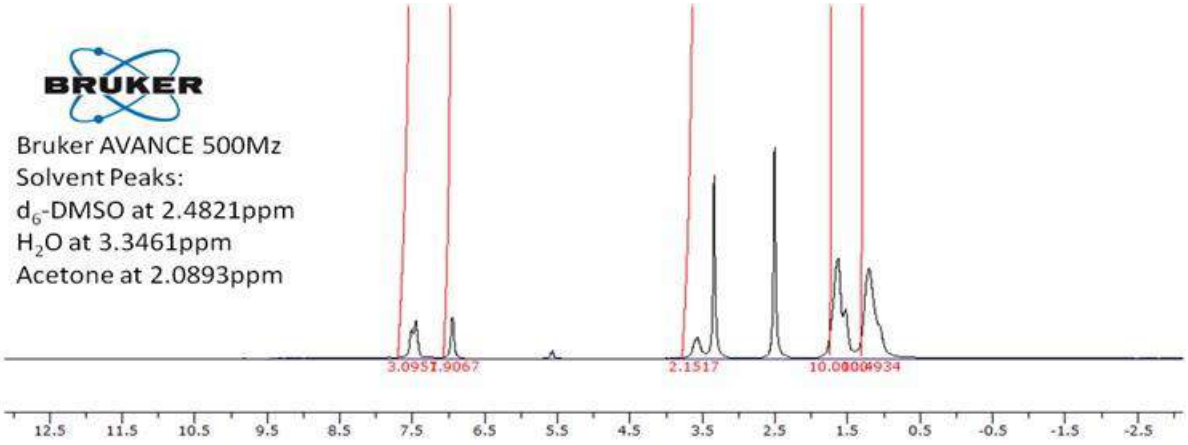
Bruker AVANCE 500Mz
Solvent Peaks:
d6-DMSO at 2.4821ppm
H2O at 3.3461ppm
Acetone at 2.0893ppm
3.0951
1.9067
2.1517
10.0000
4.9934
12.5
11.5
10.5
9.5
8.5
7.5
6.5
5.5
4.5
3.5
2.5
1.5
0.5
-0.5
-1.5
-2.5

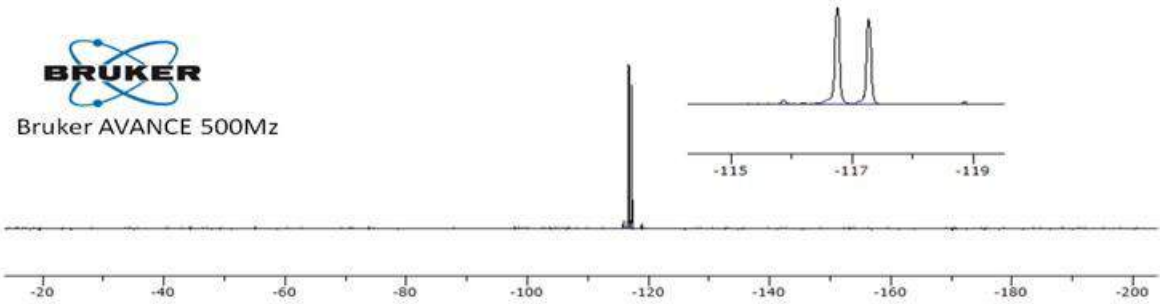
Bruker AVANCE 500Mz
-115
-117
-119
-20
-40
-60
-80
-100
-120
-140
-160
-180
-200

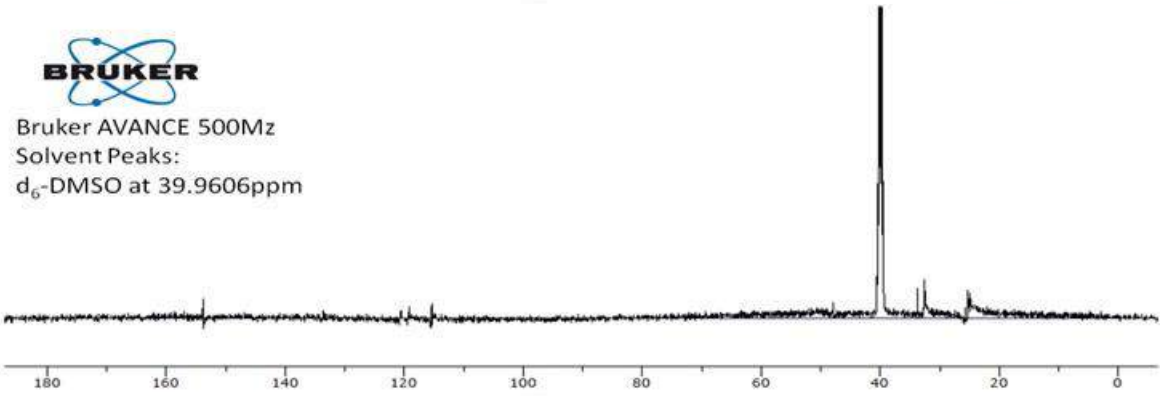
Bruker AVANCE 500Mz
Solvent Peaks:
d6-DMSO at 39.9606ppm
180
160
140
120
100
80
60
40
20
0

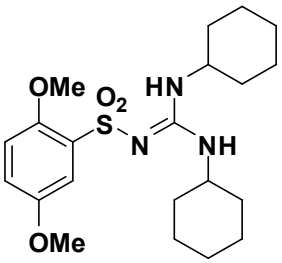
OMe
O2
S
HN
N
NH
OMe

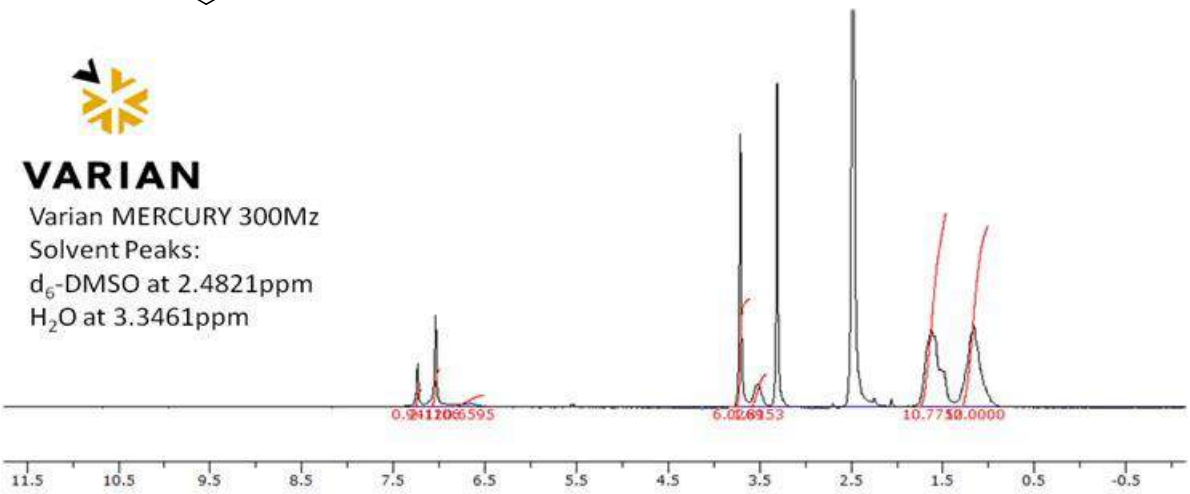
VARIAN
Varian MERCURY 300Mz
Solvent Peaks:
d6-DMSO at 2.4821ppm
H2O at 3.3461ppm
11.5
10.5
9.5
8.5
7.5
6.5
5.5
4.5
3.5
2.5
1.5
0.5
-0.5

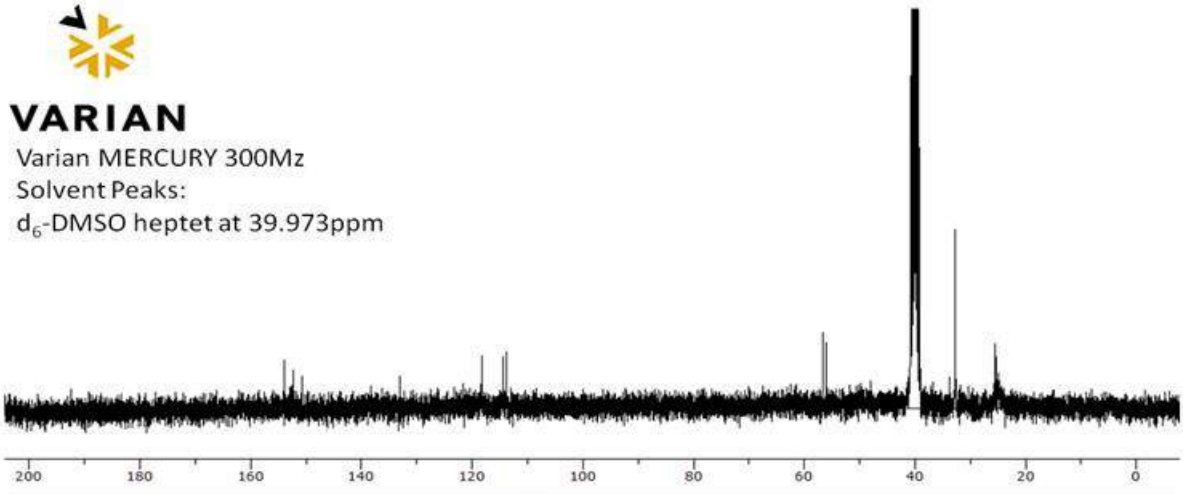
VARIAN
Varian MERCURY 300Mz
Solvent Peaks:
d6-DMSO heptet at 39.973ppm
200
180
160
140
120
100
80
60
40
20
0

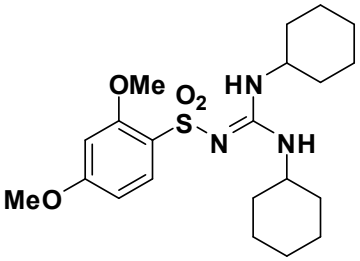
OMe
O2
S
HN
N
NH
MeO

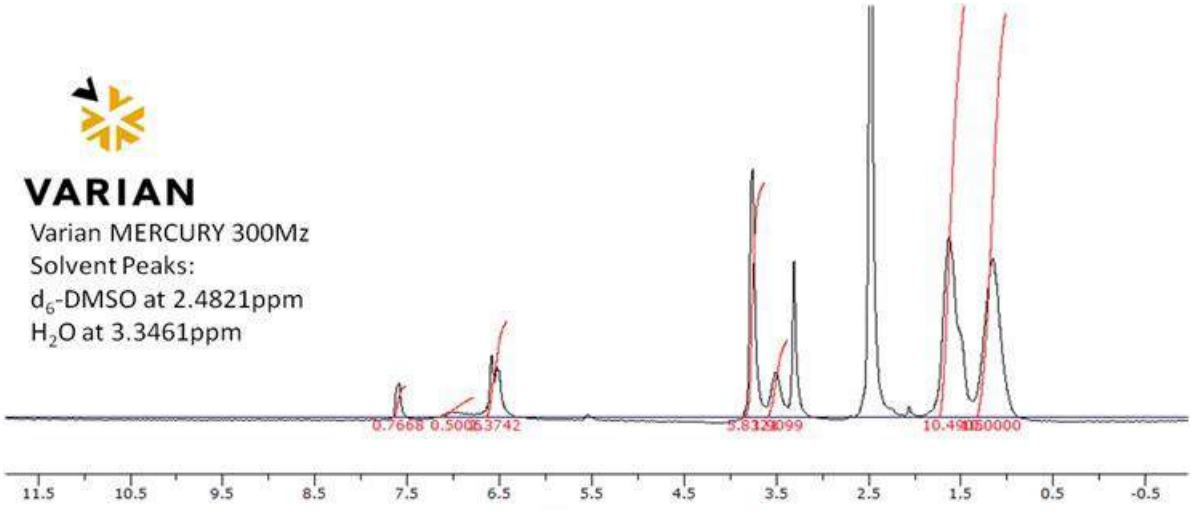
VARIAN
Varian MERCURY 300Mz
Solvent Peaks:
d6-DMSO at 2.4821ppm
H2O at 3.3461ppm
11.5
10.5
9.5
8.5
7.5
6.5
5.5
4.5
3.5
2.5
1.5
0.5
-0.5

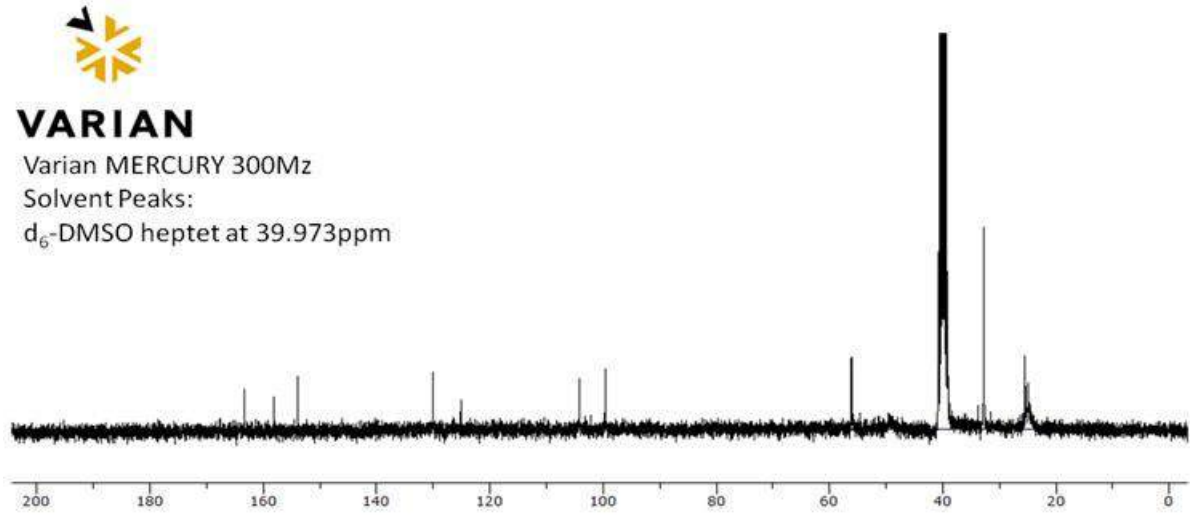
VARIAN
Varian MERCURY 300Mz
Solvent Peaks:
d6-DMSO heptet at 39.973ppm
200
180
160
140
120
100
80
60
40
20
0

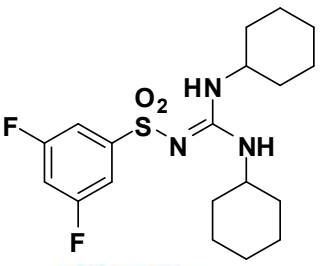
F
O2
S
N
HN
NH
F

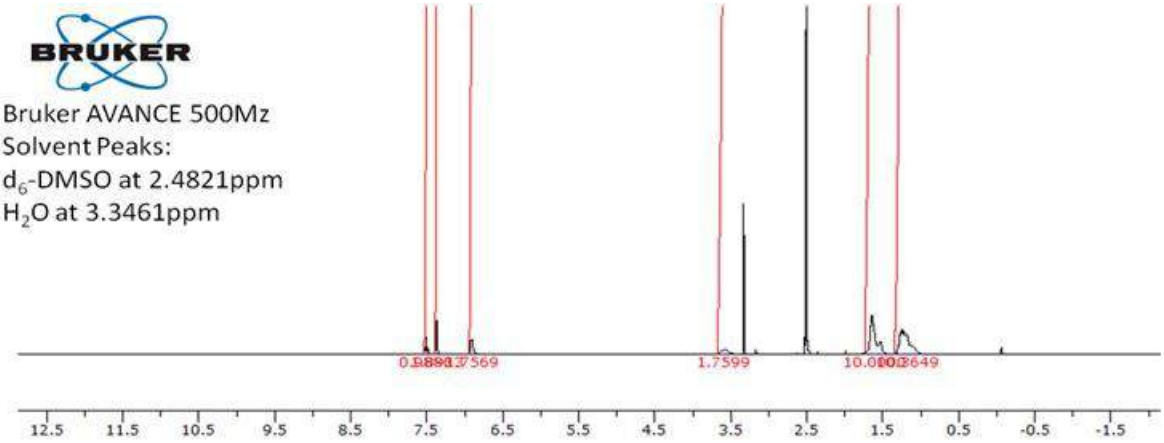
Bruker AVANCE 500Mz
Solvent Peaks:
d6-DMSO at 2.4821ppm
H2O at 3.3461ppm
1.7599
12.5
11.5
10.5
9.5
8.5
7.5
6.5
5.5
4.5
3.5
2.5
1.5
0.5
-0.5
-1.5

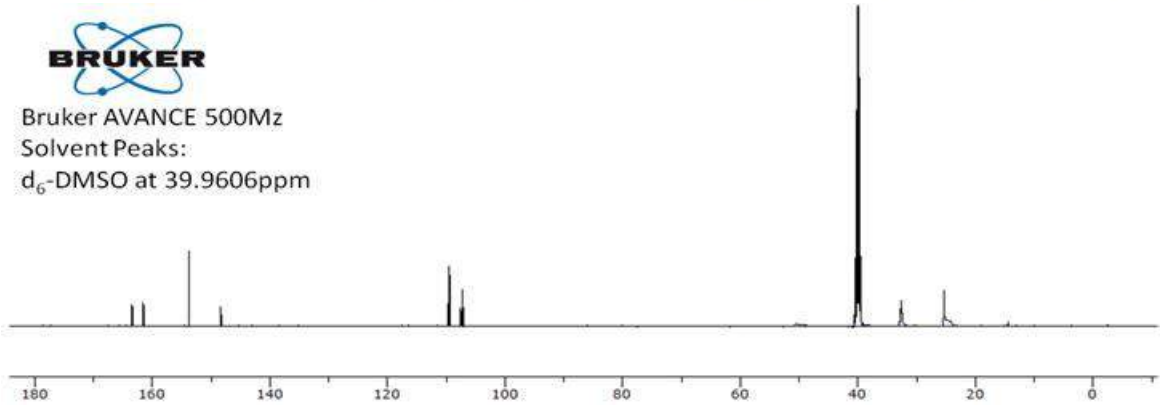
Bruker AVANCE 500Mz
Solvent Peaks:
d6-DMSO at 39.9606ppm
180
160
140
120
100
80
60
40
20
0

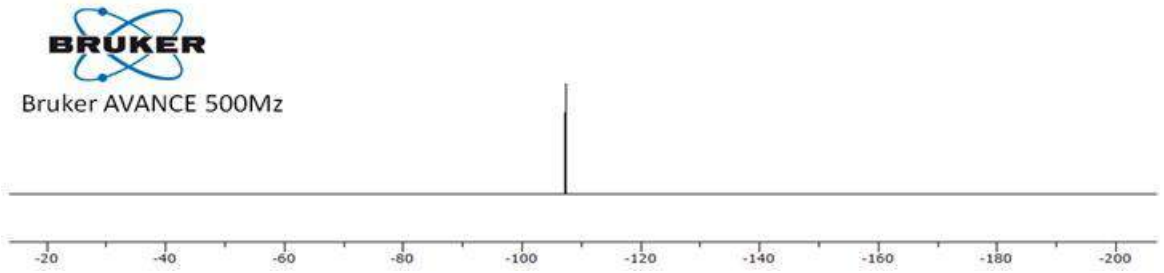
Bruker AVANCE 500Mz
-20
-40
-60
-80
-100
-120
-140
-160
-180
-200

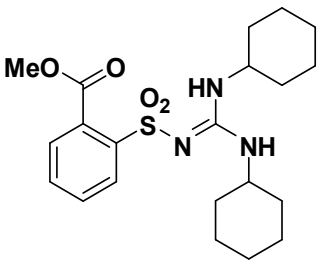
MeO
O
O2
S
N
HN
NH

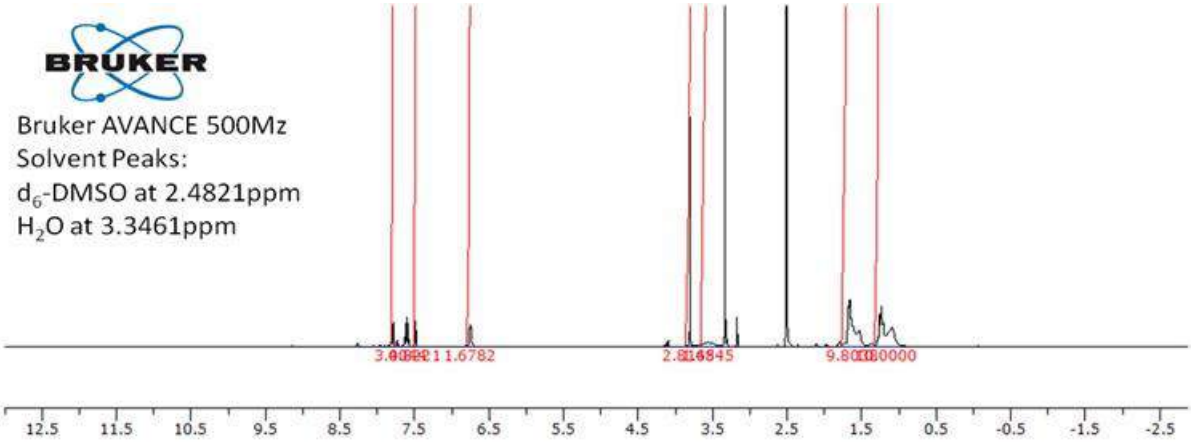
Bruker AVANCE 500Mz
Solvent Peaks:
d6-DMSO at 2.4821ppm
H2O at 3.3461ppm
12.5
11.5
10.5
9.5
8.5
7.5
6.5
5.5
4.5
3.5
2.5
1.5
0.5
-0.5
-1.5
-2.5

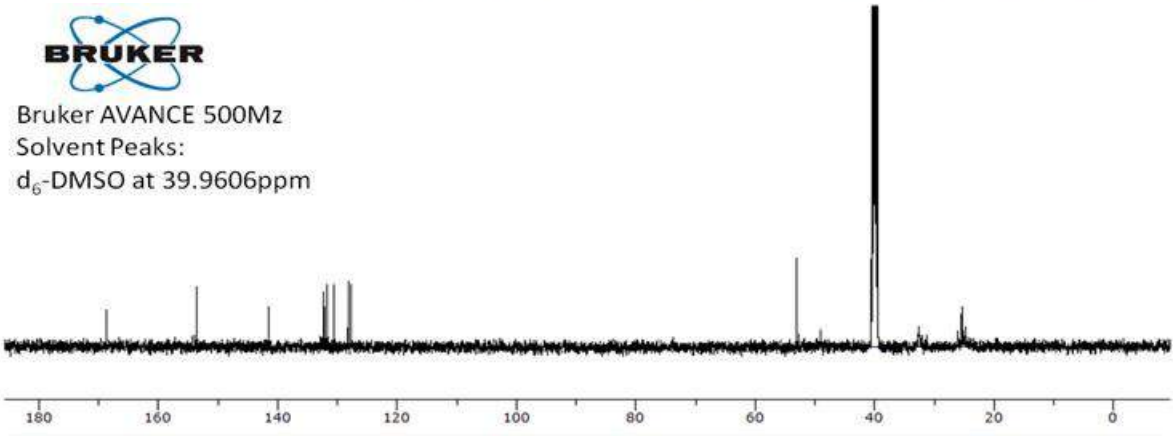
Bruker AVANCE 500Mz
Solvent Peaks:
d6-DMSO at 39.9606ppm
180
160
140
120
100
80
60
40
20
0

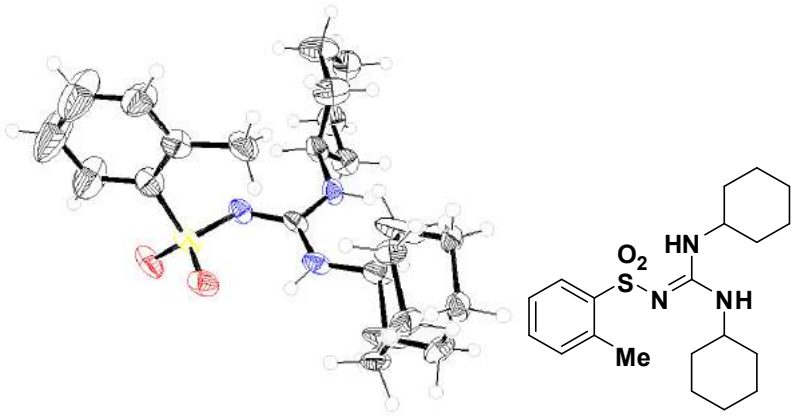

Fig. E1. Molecular structure visualized using ORTEP-3 with thermal ellipsoids at 50% probability level of *N*-(bis(cyclohexylamino)methylene)-2-methylbenzenesulfonamide **2** as determined by SCXRD, along with a schematic representation of the molecule.

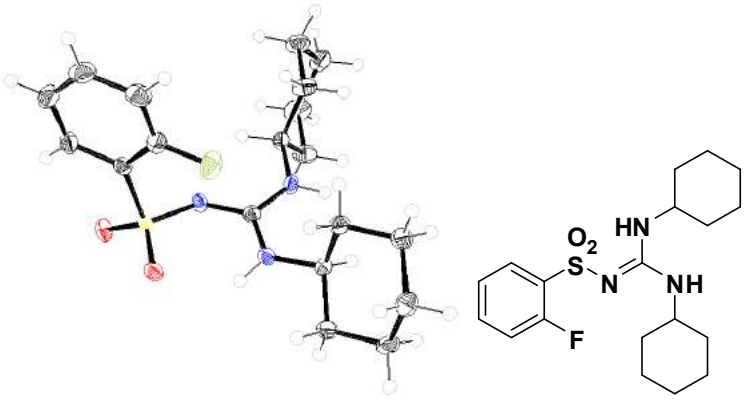

Fig. E2. Molecular structure visualized using ORTEP-3 with thermal ellipsoids at 50% probability level of *N*-(bis(cyclohexylamino)methylene)-2-fluorobenzenesulfonamide **3** as determined by SCXRD, along with a schematic representation of the molecule.

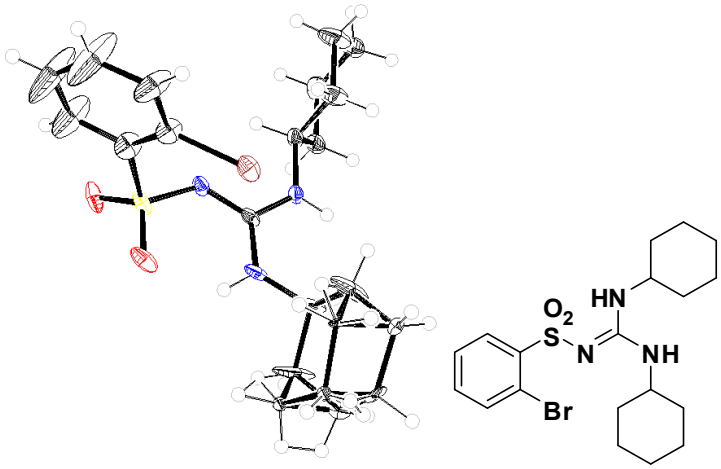

Fig. E3. Molecular structure visualized using ORTEP-3 with thermal ellipsoids at 50% probability level of *N*-(bis(cyclohexylamino)methylene)-2-bromobenzenesulfonamide **4** as determined by SCXRD, along with a schematic representation of the molecule.

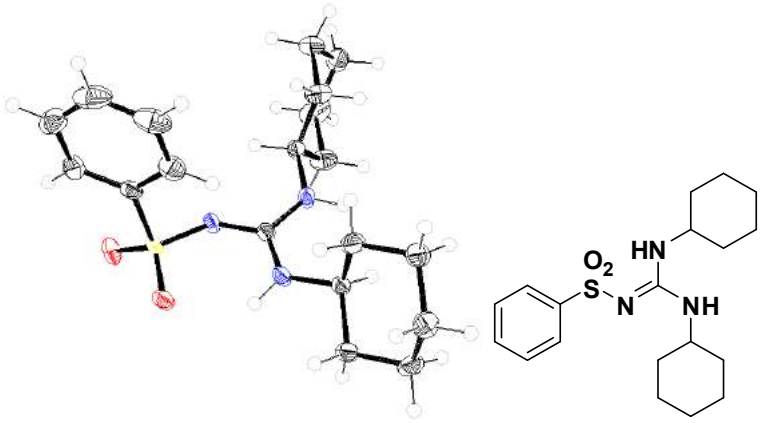

Fig. E4. Molecular structure visualized using ORTEP-3 with thermal ellipsoids at 50% probability level of *N*-(bis(cyclohexylamino)methylene)-benzenesulfonamide **6** as determined by SCXRD, along with a schematic representation of the molecule.

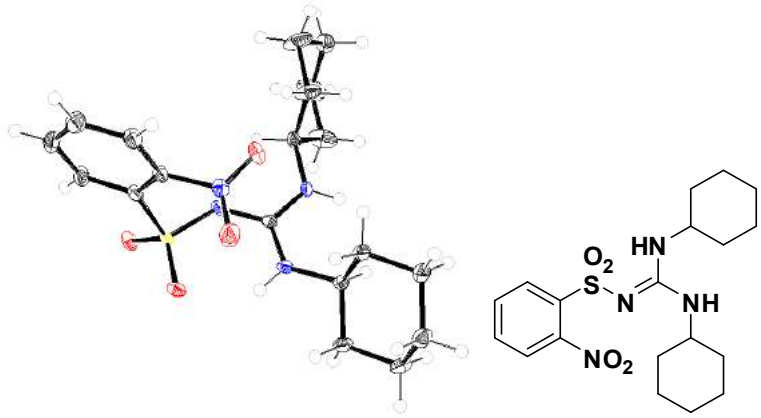

Fig. E5. Molecular structure visualized using ORTEP-3 with thermal ellipsoids at 50% probability level of *N*-(bis(cyclohexylamino)methylene)-2-nitrobenzenesulfonamide **5** as determined by SCXRD, along with a schematic representation of the molecule.

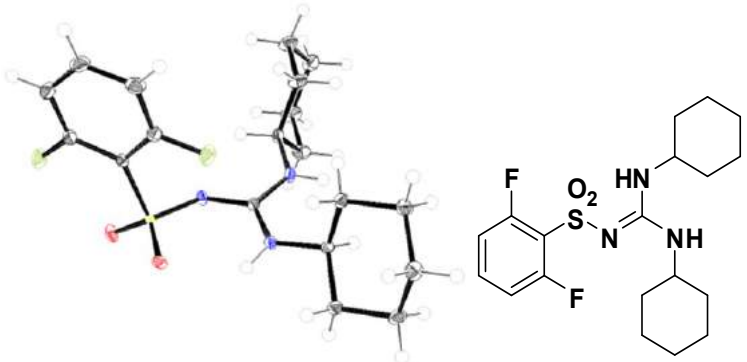

Fig. E6. Molecular structure visualized using ORTEP-3 with thermal ellipsoids at 50% probability of *N*-(bis(cyclohexylamino)methylene)-2,6-difluorobenzenesulfonamide **7** as determined by SCXRD, along with a schematic representation of the molecule.

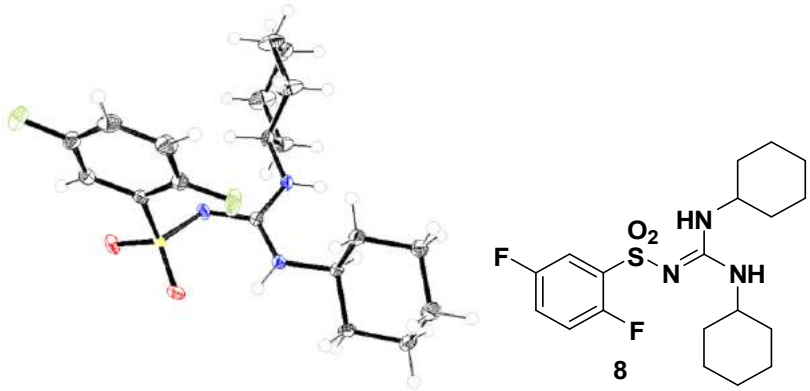

Fig. E7. Molecular structure visualized using ORTEP-3 with thermal ellipsoids at 50% probability of *N*-(bis(cyclohexylamino)methylene)-2,5-difluorobenzenesulfonamide **8** as determined by SCXRD, along with a schematic representation of the molecule.

Table E1. SCXRD data of various arylsulfonylguanidine compounds.

	2,5-diMeO-DCC	**2,4-diMeO-DCC**	**3,5-diF-DCC**
Molecular formula	$C_{21}H_{33}N_3O_4S$	$C_{21}H_{33}N_3O_4S$	$C_{19}H_{27}N_3O_2SF_2$
M_r	423.56	423.56	399.49
Crystal System	Monoclinic	Orthorhombic	Tetragonal
Crystal colour	Colorless	Colorless	Colorless
Space group	*P*21/c	*P*bcn	$I4_1/a$
Temperature (K)	150K	150K	100K
Unit cell dimensions (Å,°)			
a	12.038(3)	16.8586(19)	16.8011(14)
b	15.429(4)	12.5071(14)	16.8011(14)
c	13.101(4)	20.380(2)	30.403(2)
α	90	90	90
β	115.403(3)	90	90
γ	90	90	90
Volume (Å^3)	2197.9(10)	4297.2(8)	8582.2(16)
Z	4	8	16
***D*$_{calc}$ (g cm^{-3})**	1.280	1.309	1.237
***μ* (mm^{-1}) (abs coeff)**	0.179	0.183	0.185
***F*(000)**	912	1824	3392
Refl. collected/independent	25999/ 5464	49959 / 5496	110126 / 5383
No. observed refl. [*I*>2σ(*I*)]*	3856	3896	3400
No. restraints/No. parameters	0/ 264	0/264	0/244
R [all/gt]	0.0809/ 0.0536	0.0739 / 0.0460	0.1265 / 0.0746
wR [ref/gt]	0.1522/0.1347	0.1203 / 0.1070	0.2139 / 0.1827
Goodness-of-fit on F^2	1.043	1.034	1.070
Largest diff. peak and hole (*e* Å^{-3})	0.758, -0.885	0.363, -0.450	0.483, -0.562

*$R = \sum||Fo|-|Fc||/\sum Fo, w = 1/[\sigma^2(F_o^2)+(g_1P)^2+ g_2P]$ where $P = (F_o^2+2F_c^2)/3$, $S = \Sigma[w(F_o^2 - F_c^2)^2/(N_{obs} - N_{param})]^{1/2}$.

Table E1. (Cont'd)

	2-COOMe-DCC	2-Cl-DIC
Molecular formula	$C_{22.74}H_{32.99}N_3O_4S$	$C_{13}H_{20}N_3O_2SCl$
M_r	444.45	309.11
Crystal System	Monoclinic	Orthorhombic
Crystal colour	Colorless	Colorless
Space group	$P2_1/c$	$Pbca$
Temperature (K)	100K	150K
Unit cell dimensions (Å,°)		
a	13.9027(13)	11.1910(9)
b	12.7754(12)	11.3302(9)
c	26.400(2)	25.142(2)
α	90	90
β	92.574(4)	90
γ	90	90
Volume (Å^3)	4684.2(7)	3188.0(4)
Z	8	8
D_{calc} (g cm^{-3})	1.260	1.289
μ (mm^{-1}) (abs coeff)	0.171	0.216
F(000)	1907	1312
Refl. collected/independent	146185/ 12205	3959/ 2255
No. observed refl. [I>2σ(I)]*	8993	35978
No. restraints/No. parameters	0/ 570	6/ 223
R [all/gt]	0.0794/ 0.0484	0.0958/ 0.0439
wR [ref/gt]	0.1206/0.1042	0.1226/ 0.1008
Goodness-of-fit on F^2	1.071	1.026
Largest diff. peak and hole (e Å^{-3})	0.378, -0.548	0.165, -0.300

*$R = \sum||Fo|-|Fc||/\sum Fo, w = 1/[\sigma^2(F_o^2)+(g_1P)^2+ g_2P]$ where $P = (F_o^2+2F_c^2)/3$, $S = \Sigma[w(F_o^2 - F_c^2)^2/(N_{obs} - N_{param})]^{1/2}$.

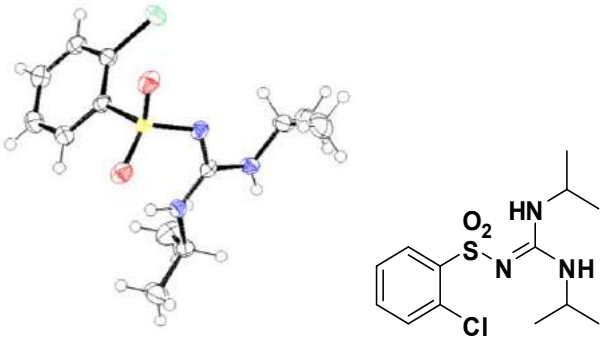

Fig. E8. Molecular structure visualized using ORTEP-3 with thermal ellipsoids at 50% probability level of *N*-(bis(isopropylamino)methylene)-2chlorobenzenesulfonamide **13** as determined by SCXRD, along with a schematic representation of the molecule.

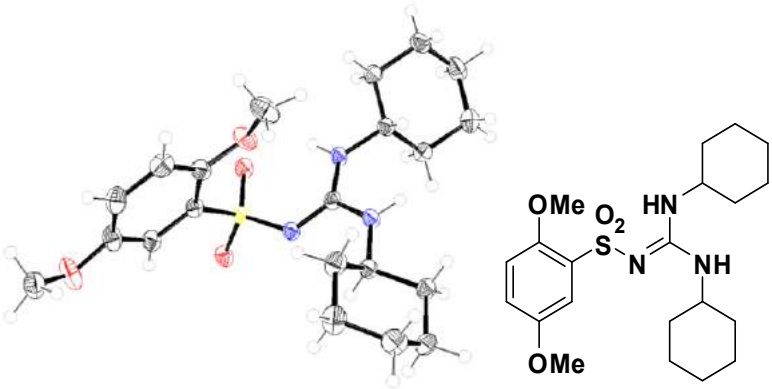

Fig. E9. Molecular structure visualized using ORTEP-3 with thermal ellipsoids at 50% probability level of *N*-(bis(cyclohexylamino)methylene)-2,5-dimethoxybenzenesulfonamide **10** as determined by SCXRD, along with a schematic representation of the molecule.

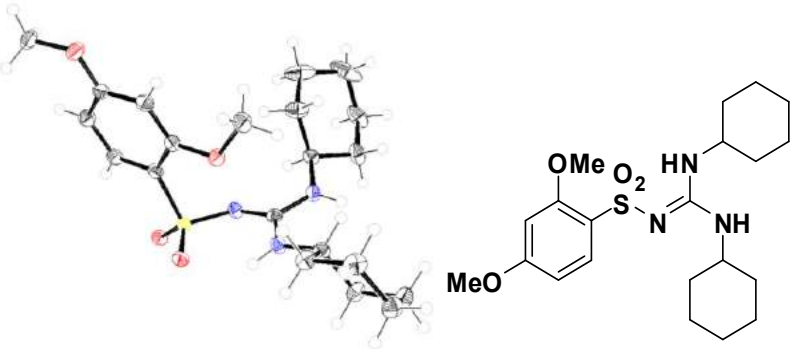

Fig. E10. Molecular structure visualized using ORTEP-3 with thermal ellipsoids at 50% probability level of *N*-(bis(cyclohexylamino)methylene)-2,4-dimethoxybenzenesulfonamide **11** as determined by SCXRD, along with a schematic representation of the molecule.

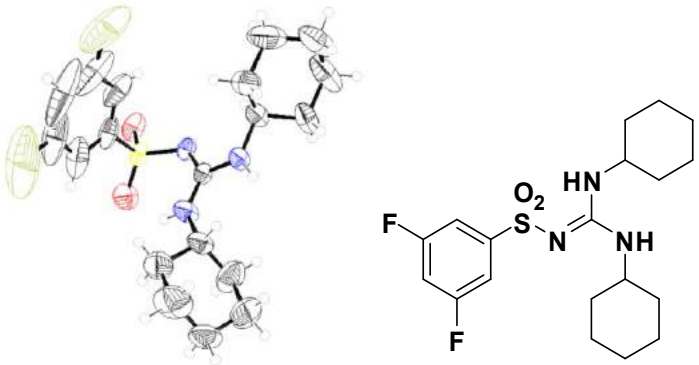

Fig. E11. Molecular structure visualized using ORTEP-3 with thermal ellipsoids at 50% probability level of *N*-(bis(cyclohexylamino)methylene)-3,5-difluorobenzenesulfonamide **9** as determined by SCXRD, along with a schematic representation of the molecule.

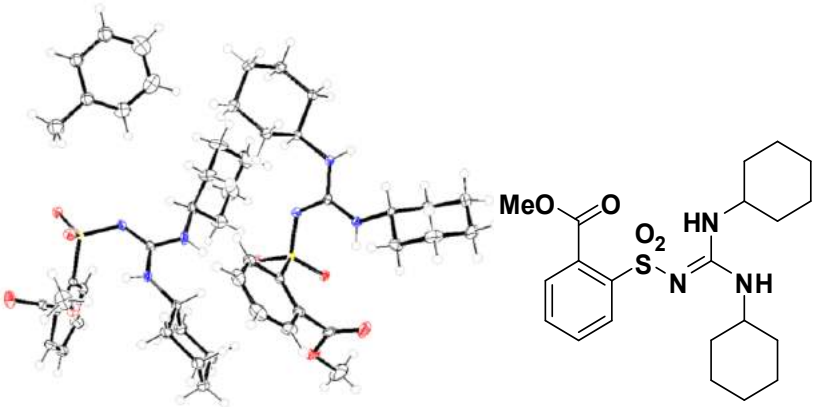

Fig. E12. Molecular structure visualized using ORTEP-3 with thermal ellipsoids at 50% probability level of *N*-(bis(cyclohexylamino)methylene)-2-methoxycarbonylbenzenesulfonamide **13** as determined by SCXRD, along with a schematic representation of the molecule. Each asymmetric unit consists of two molecules of **12** and one molecule of toluene that is disordered i.e. $(\mathbf{12})_2$.(toluene).

Table E2. Multi-component crystals and the *sof* values of their individual components.

Sample	Bz (A)	2-Br (A)	2,5 F (B)	2-NO2 (C)	2,6 F (D)	Me (E)	Formula
3CC-II	0.299(8)		0.356(6)			0.394(6)	$C_{19.69}H_{29.32}F_{0.71}N_3O_2S$
3CC-I		0.332(5)	0.311(6)			0.381(1)	$C_{19.52}H_{28.93}Br_{0.33}F_{0.62}N_3O2S$
4CC-II		0.170(3)	0.265(4)	0.150(5)		0.457(9)	$C_{19.70}H_{29.27}Br_{0.17}F_{0.53}N_{3.15}O_{2.30}S$
4CC-I		0.316(3)	0.256(5)	0.178(4)	0.245(5)		$C_{18.97}H_{27.48}Br_{0.32}FN_{3.18}O_{2.36}S$

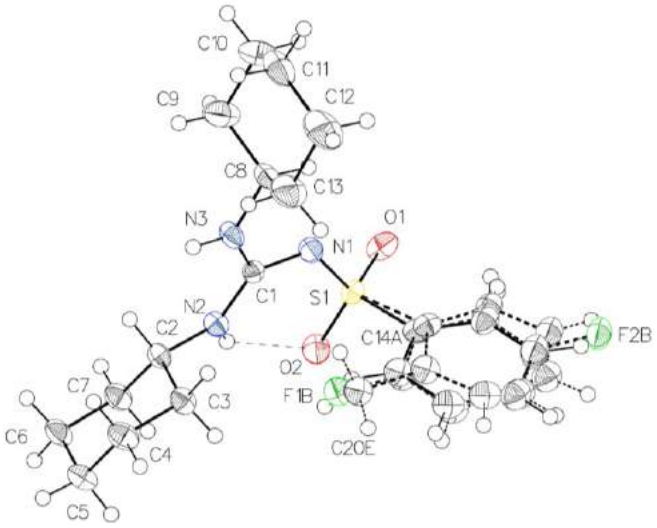

Fig. E13. Molecular structure and overlay of the individual components visualized using ORTEP-3 with thermal ellipsoids at 50% probability level of **3CC-II** as determined by SCXRD.

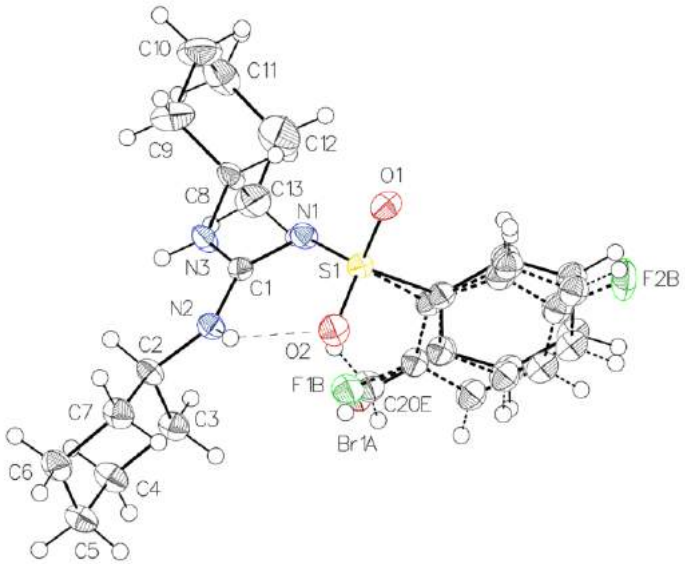

Fig. E14. Molecular structure and overlay of the individual components visualized using ORTEP-3 with thermal ellipsoids at 50% probability level of **3CC-I** as determined by SCXRD.

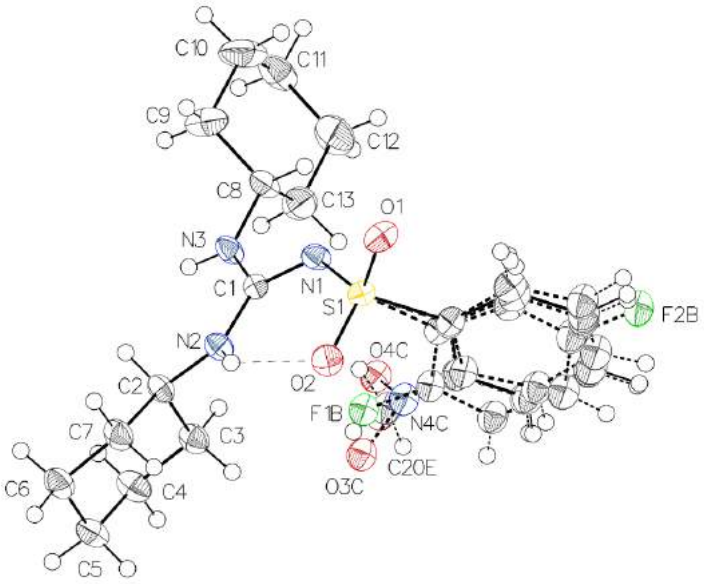

Fig. E15. Molecular structure and overlay of the individual components visualized using ORTEP-3 with thermal ellipsoids at 50% probability level of **4CC-II** as determined by SCXRD.

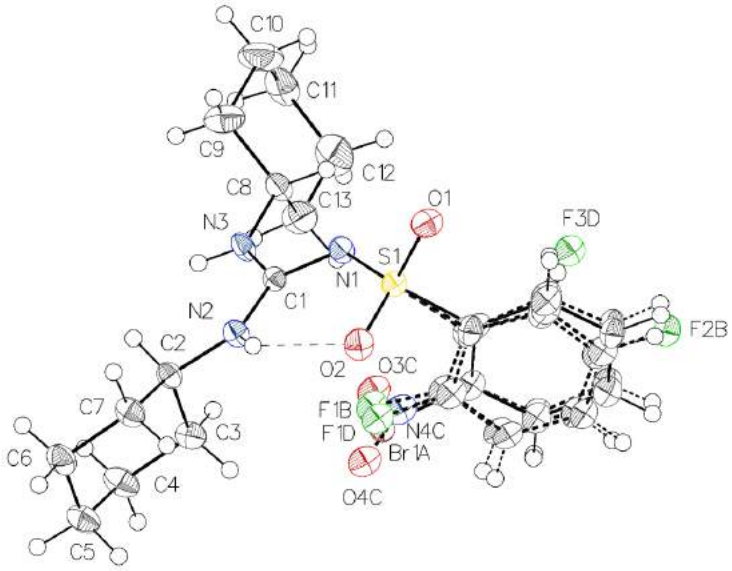

Fig. E16. Molecular structure and overlay of the individual components visualized using ORTEP-3 with thermal ellipsoids at 50% probability level of **4CC-I** as determined by SCXRD.

APPENDIX F

SPECTROSCOPIC AND X-RAY DIFFRACTION DATA FOR COMPOUNDS IN CHAPTER 7

1,3-bis(4-methoxyphenyl)urea

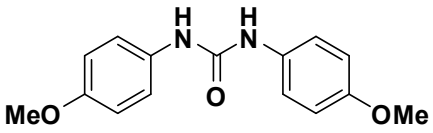

White powder (98% yield); **^{1}H-NMR** (300 MHz, DMSO-*d6*) δ 3.69 (s, 6H), δ 6.84 (d, *J* = 7.42Hz, 4H), δ 7.32 (m, *J* = 7.12Hz, 4H), δ 8.35 (m, 2H); **^{13}C-NMR** (300 MHz, DMSO-*d6*) δ 55.6, 114.2, 120.4, 133.6, 153.3, 154.3.

1,3-bis(4-methoxyphenyl)thiourea

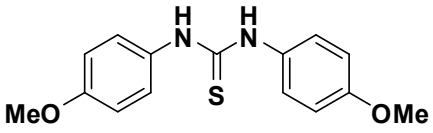

White powder (95% yield); **^{1}H-NMR** (300 MHz, DMSO-*d6*) δ 3.72 (s, 6H), δ 6.88 (d, *J* = 7.42Hz, 4H), δ 7.29 (d, *J* = 7.32Hz, 4H), δ 9.40 (s, 2H); **^{13}C-NMR** (300 MHz, DMSO-*d6*) δ 55.6, 113.8, 126.4, 132.9, 156.7, 180.4.

1,3-bis(3-methoxyphenyl)urea

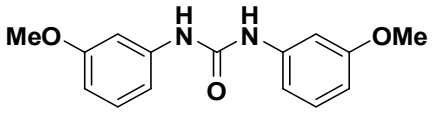

White powder (98% yield); **^{1}H-NMR** (300 MHz, DMSO-*d6*) δ 3.70 (s, 6H), δ 6.50-6.56 (m, 2H), δ 6.88-6.92 (m, 2H), δ 7.12-7.20 (m, 4H), δ 8.62 (s, 2H); **^{13}C-NMR** (300 MHz, DMSO-*d6*) δ 55.6, 104.2, 107.5, 111.0, 130.3, 141.3, 152.9, 160.2. **HRMS**: Calculated for $C_{15}H_{16}O_3N_2Na$ [M+Na]: 295.10531, measured: 295.10594.

1,3-bis(3,5-dimethoxyphenyl)urea

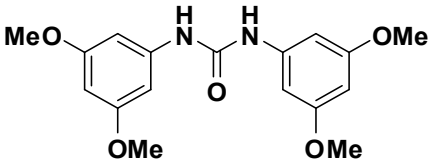

White powder (98% yield); **^{1}H-NMR** (300 MHz, DMSO-*d6*) δ 3.71 (s, 12H), δ 6.10 (s, 2H), δ 6.64 (s, 4H), δ 8.60 (s, 2H); **^{13}C-NMR** (300 MHz, DMSO-*d6*) δ 55.2, 94.3, 96.9, 141.6, 152.5, 161.4. **HRMS**: Calculated for $C_{17}H_{20}O_5N_2Na$ [M+Na]: 355.12644; measured: 355.12710.

1,3-bis(3,4-dimethoxyphenyl)urea

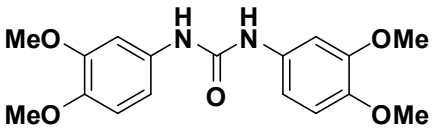

White powder (97% yield); **^{1}H-NMR** (300 MHz, DMSO-*d6*) δ 3.71 (s, 12H), δ 3.72 (s, 6H), δ 6.82-6.86 (m, 4H), δ 7.17 (s, 2H), δ 8.38 (s, 2H); **^{13}C-NMR** (300 MHz, DMSO-*d6*) δ 55.8, 56.2, 104.3, 110.5, 112.8, 133.9, 144.3, 149.3, 153.2. **HRMS**: Calculated for $C_{17}H_{20}O_5N_2Na$ [M+Na]: 355.12754; measured: 355.12723.

1,3-bis(2-methoxyphenyl)urea

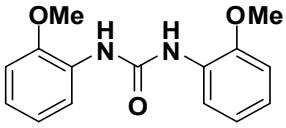

White powder (97% yield); **^{1}H-NMR** (300 MHz, DMSO-*d6*) δ 3.84 (s, 6H), δ 6.82-7.02 (m, 6H), δ 8.07 (d, *J* = 7.20Hz, 2H), δ 8.85 (s, 2H); **^{13}C-NMR** (300 MHz, DMSO-*d6*) δ 56.0, 111.2, 119.6, 120.8, 122.0, 129.2, 148.7, 152.9. **HRMS**: Calculated for $C_{15}H_{16}O_3N_2Na$ [M+Na]: 295.10531, measured: 295.10610.

1,3-bis(2,5-dimethoxyphenyl)urea

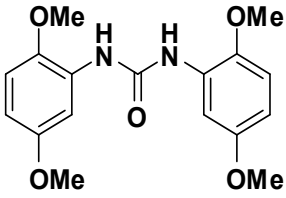

White powder (98% yield); **^{1}H-NMR** (300 MHz, DMSO-*d6*) δ 3.66 (s, 6H), δ 3.78 (s, 6H), δ 6.43-6.51 (m, 2H), δ 6.88 (d, *J* = 7.14Hz, 2H), δ 7.80 (s, 2H), δ 6.94 (s, 2H); **^{13}C-NMR** (300 MHz, DMSO-*d6*) δ 55.7, 56.7, 105.9, 106.4, 111.9, 130.1, 142.9, 152.9, 153.6. **HRMS**: Calculated for $C_{17}H_{20}O_5N_2Na$ [M+Na]: 355.12644; measured: 355.12693.

1,3-bis(2-methoxyphenyl)thiourea

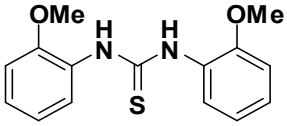

White powder (94% yield); **^{1}H-NMR** (300 MHz, DMSO-*d6*) δ 4.09 (s, 6H), δ 6.81-7.72 (m, 6H), δ 7.88-8.58 (m, 2H), δ 9.67 (s, 2H); **^{13}C-NMR** (300 MHz, DMSO-*d6*) δ 57.4, 112.9, 121.4, 127.3, 129.1, 153.2, 181.0; **HRMS**: Calculated for $C_{15}H_{16}S_1N_2O_2Na$ [M+Na]: 311.0825; measured: 311.0835.

1,3-bis(2,4-dimethoxyphenyl)urea

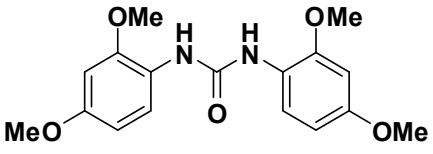

White powder (99% yield); **^{1}H-NMR** (300 MHz, DMSO-*d6*) δ 3.71 (s, 6H), δ 3.81 (s, 6H), δ 6.40 (d, *J* = 7.04Hz, 2H), δ 6.57 (s, 2H), δ 7.84 (d, *J* =7.34Hz, 2H), δ 8.44 (s, 2H); **^{13}C-NMR** (300 MHz, DMSO-*d6*) δ 55.4, 56.2, 98.9, 104.6, 120.8, 122.8, 150.1, 153.3, 155.3; **HRMS**: Calculated for $C_{17}H_{20}O_5N_2Na$ [M+Na]: 355.12644; measured: 355.12704.

1,3-bis(3,4,5-trimethoxyphenyl)urea

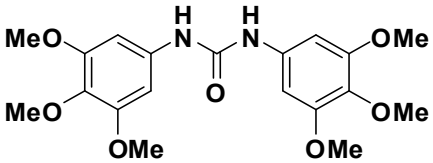

White powder (98% yield); **^{1}H-NMR** (300 MHz, DMSO-*d6*) δ 3.58 (s, 6H), δ 3.72 (s, 12H), δ 6.74 (s, 4H), δ 8.51 (s, 2H); **^{13}C-NMR** (300 MHz, DMSO-*d6*) δ 56.1, 60.5, 96.4, 132.9, 136.2, 152.9, 153.3 ; **HRMS**: Calculated for $C_{20}H_{28}O7N_2Na$ [M+Na]: 415.1484; measured: 415.1491.

1,3-bis(3,4,5-trimethoxyphenyl)thiourea

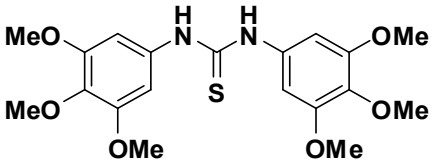

White powder (96% yield); **^{1}H-NMR** (300 MHz, DMSO-*d6*) δ 3.62 (s, 6H), δ 3.72 (s, 12H), δ 6.78 (s, 4H), δ 9.59 (m, 2H); **^{13}C-NMR** (300 MHz, DMSO-*d6*) δ 56.4, 60.4, 102.4, 135.0, 135.4, 152.8, 179.5; **HRMS**: Calculated for $C_{19}H_{25}O_6N_2S$[M+H]: 409.14278; measured: 409.14121.

1,3-diphenylurea

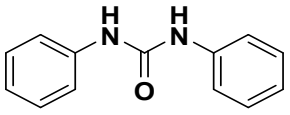

White Powder (98% yield); **^{1}H-NMR** (300 MHz, DMSO-*d6*) δ 6.94 (t, , *J* = 7.14Hz, 2H), δ 7.20-7.30 (m, 4H), δ 9.63 (s, 2H); **^{13}C-NMR** (300 MHz, DMSO-*d6*) δ 118.6, 122.2, 129.3, 140.2, 152.9; **HRMS**: Calculated for $C_{13}H_{12}N_2O_1Na$ [M+Na]: 235.0842; measured: 235.0845.

1,3-bis(4-fluorophenyl)urea

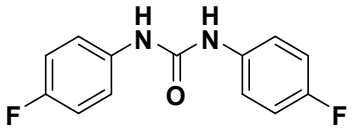

White powder (98% yield); **^{1}H-NMR** (300 MHz, DMSO-*d6*) δ 7.03-7.16 (m, 4H), δ 7.38-7.46 (m, 4H), δ 8.66 (s, 2H), δ 8.63 (s, 2H) ; **^{13}C-NMR** (300 MHz, DMSO-*d6*) δ 115.6, 120.2, 136.4, 153.1, 155.9, 159.4; **HRMS**: Calculated for $C_{13}H_{11}N_2O_1$ [M+H]: 249.08340; measured: 249.08312.

1,3-bis(4-(trifluoromethyl)phenyl)urea

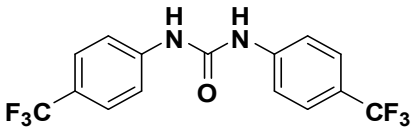

White powder (95% yield); **^{1}H-NMR** (300 MHz, DMSO-*d6*) δ 7.60-7.68 (m, 8H), δ 9.22 (s, 2H); **^{13}C-NMR** (300 MHz, DMSO-*d6*) δ 118.2, 126.5, 126.6, 143.5, 152.5 ; **HRMS**: Calculated for $C_{15}H_{10}O_1N_2F_6Na$ [M+Na]: 371.0601; measured: 371.0597.

1,3-bis(2,4-difluorophenyl)urea

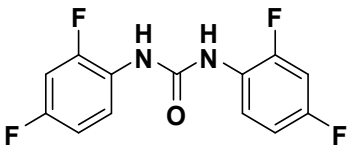

White powder (95% yield); **^{1}H-NMR** (300 MHz, DMSO-*d6*) δ 6.99-7.05 (m, 1H), δ 7.26-7.35 (m, 1H), δ 8.02-8.12 (m, 1H), δ 8.90 (m, 1H); **^{19}F-NMR** (300MHz, DMSO-d6) -124.93, -117.90; **^{13}C-NMR** (300 MHz, DMSO-*d6*) δ 103.8, 104.2, 104.6, 111.4, 111.6, 122.1, 122.2. 124.2, 124.3, 150.8, 152.6, 154.1, 155.5, 158.9; HRMS: Calculated for $C_{13}H_9ON_2F_4$ [M+Na]: 283.04862; measured: 283.04903.

1,3-bis(4-nitrophenyl)urea

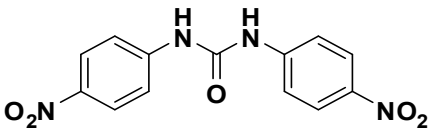

Yellow powder (93% yield); **^{1}H-NMR** (300 MHz, DMSO-*d6*) δ 7.69 (d, *J* = 7.4Hz, 2H), δ 8.19 (d, *J* = 7.2Hz, 2H); **^{13}C-NMR** (300 MHz, DMSO-*d6*) δ 112.8, 118.4, 125.6, 126.8, 141.9, 146.1, 152.0; **HRMS**: Calculated for $C_{13}H_{10}O_5N_4Na$ [M+Na]: 325.0543; measured: 325.0548.

1,3-bis(3-nitrophenyl)urea

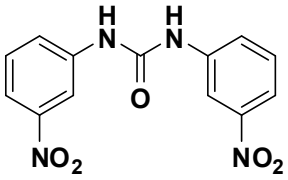

Yellow powder (92% yield); **^{1}H-NMR** (300 MHz, DMSO-*d6*) δ 7.50-7.86 (m, 6H), δ 8.54 (s, 2H), δ 9.39 (s, 2H); **^{13}C-NMR** (300 MHz, DMSO-*d6*) δ 112.9, 117.1, 125.2, 130.4, 141.2, 148.5, 152.9 ; **HRMS**: Calculated for $C_{13}H_9O_5N_4$ [M-H]: 301.0578; measured: 301.0573.

1,3-di(*o*-tolyl)urea

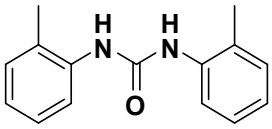

White powder (94% yield); **^{1}H-NMR** (300 MHz, DMSO-*d6*) δ 2.24 (s, 6H), δ 6.84-6.98 (m, 2H), δ 7.05, 7.21 (m, 4H), δ 7.69-7.81 (m, 2H), δ 8.21(s, 2H); **^{13}C-NMR** (300 MHz, DMSO-*d6*) δ 18.3, 121.9, 123.1, 126.5, 128.2, 130.6, 137.8, 153.4; **HRMS**: Calculated for $C_{15}H_{16}O_1N_2$ [M+H]: 241.13354; measured: 241.13343.

1,3-di(naphthalen-2-yl)urea

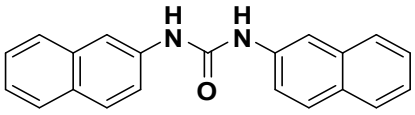

White powder (95% yield); **^{1}H-NMR** (300 MHz, DMSO-*d6*) δ 7.45-8.37 (m, 14H), δ 9.17 (s, 1H); **^{13}C-NMR** (300 MHz, DMSO-*d6*) δ 118.0, 121.8, 123.1, 123.4, 126.2, 126.3, 126.4, 128.5, 128.9, 134.2, 134.7; **HRMS**: Calculated for $C_{21}H_{16}O_1N_2Na$ [M+Na]: 335.1155; measured: 335.1149.

1,3-di(naphthalen-1-yl)urea

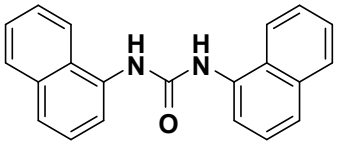

White powder (95% yield); **^{1}H-NMR** (300 MHz, DMSO-*d6*) δ 5.56 (s, 1H), δ 6.55-7.74 (m, 9H), δ 7.86-8.36 (m, 5H), δ 9.18 (s, 1H); **^{13}C-NMR** (300 MHz, DMSO-*d6*) δ 117.8, 121.8, 123.4, 126.2, 126.4, 128.9, 134.2, 134.8, 153.7; **HRMS**: Calculated for $C_{21}H_{16}O_1N_2Na$ [M+Na]: 335.1155; measured: 335.1157.

1,3-di(biphenyl-4-yl)urea

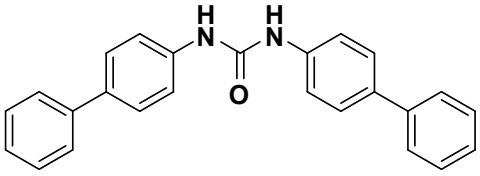

White powder (93% yield); **^{1}H-NMR** (300 MHz, DMSO-*d6*) δ 7.19-7.86 (m, 20H), δ 8.81 (s, 2H); **^{13}C-NMR** (300 MHz, DMSO-*d6*) δ 119.0, 126.6, 127.1, 127.4, 129.3, 134.0, 139.6, 140.2, 152.8; **HRMS**: Calculated for $C_{25}H_{20}O_1N_2Na$ [M+Na]: 387.1468; measured: 387.1474.

1,3-di(*n*-butyl)urea

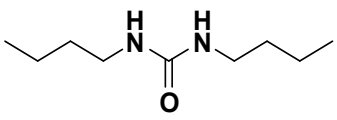

White powder (97% yield); **^{1}H-NMR** (300 MHz, DMSO-*d6*) δ 0.84 (t, *J* = 6.25Hz, 6H), δ 1.14-1.35 (m, 8H), δ 2.80-2.98 (m, 4H), δ 5.69 (t, *J* = 6.82Hz, 2H); **^{13}C-NMR** (300 MHz, DMSO-*d6*) δ 14.2, 19.9, 32.6, 39.3, 158.5 ; **HRMS**: Calculated for $C_9H_{20}O_1N_2Na$ [M+Na]: 195.1468; measured: 195.1474.

1,3-dipropylurea

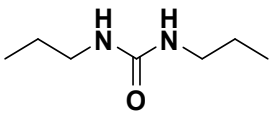

White powder (95% yield); **^{1}H-NMR** (300 MHz, DMSO-*d6*)) δ 0.79 (t, *J* = 6.4Hz, 6H), δ 1.26-1.40 (m, 4H), δ 2.83-2.96 (m, 4H), δ 5.74 (t, *J* = 6.52Hz, 2H); **^{13}C-NMR** (300 MHz, DMSO-*d6*) δ 11.7, 23.4, 41.4, 158.3 ; **HRMS**: Calculated for $C_7H_{16}O_1N_2Na$ [M+Na]: 167.1155; measured: 167.1159.

1,3-dicyclohexylurea

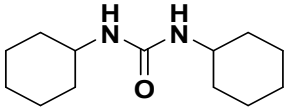

White powder (98% yield); **^{1}H-NMR** (300 MHz, DMSO-*d6*) δ 0.96-1.28 (m, 10H), δ 1.44-1.74 (m, 10H), δ 5.55 (d, *J* = 6.8Hz, 2H); **^{13}C-NMR** (300 MHz, DMSO-*d6*) δ 24.8, 25.8, 33.7, 47.9 ; **HRMS**: Calculated for $C_{13}H_{24}O_1N_2Na$ [M+Na]: 247.1781; measured: 247.1789.

1,3-bis(2-chloroethyl)urea

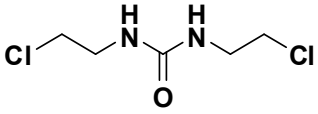

White powder (99% yield); **^{1}H-NMR** (300 MHz, DMSO-*d6*) δ 3.29 (t, *J* = 6.27Hz, 4H), δ 3.54 (t, *J* = 6.42Hz, 2H), δ 6.31 (t, *J* = 7.02 Hz, 2H); **^{13}C-NMR** (300 MHz, DMSO-*d6*) δ 41.8, 44.9, 157.9 ; **HRMS**: Calculated for $C_{13}H_{24}O_1N_2Na$ [M+Na]: 247.1781; measured: 247.1789.

1,3-bis(3-cyanophenyl)urea

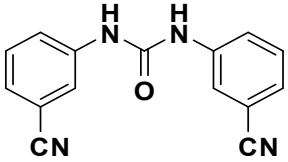

White powder (97% yield); **^{1}H-NMR** (300 MHz, DMSO-*d6*) δ 7.39-7.52 (m, 4H), δ 7.63-7.69 (m, 2H), δ 7.93-7.96 (m, 2H), δ 9.15 (s, 2H); **^{13}C-NMR** (300 MHz, DMSO-*d6*) δ 112.0, 119.2, 121.5, 123.4, 126.0, 130.6, 140.7, 152.6 ; **HRMS**: Calculated for $C_{15}H_{11}O_5N_4$ [M+H]: 263.09274; measured: 263.09315.

diethyl 4,4'-carbonylbis(azanediyl)dibenzoate

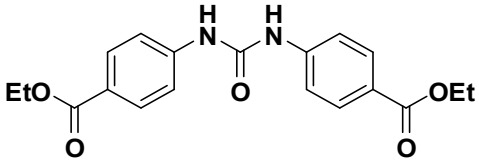

White powder (92% yield); **^{1}H-NMR** (300 MHz, DMSO-*d6*) δ 1.28 (t, *J* = 6.28Hz, 6H), δ 4.26 (q, *J* = 6.86Hz, 4H), δ 7.58 (d, *J* = 7.32Hz, 4H), δ 7.88 (d, *J* = 7.04Hz, 4H), δ 9.16(s, 2H); **^{13}C-NMR** (300 MHz, DMSO-*d6*) δ 14.7, 60.8, 117.8, 123.2, 130.8, 144.3, 152.3, 165.8 . **HRMS**: Calculated for $C_{19}H_{21}O_5N_2$ [M+H]: 357.14450; measured: 357.14366.

1,3-bisadamantylurea

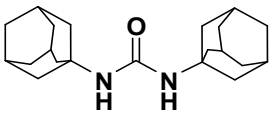

White powder (88% yield); **^{1}H-NMR** (300 MHz, DMSO-*d6*) δ 1.40-1.49 (m, 4H), δ 1.53-1.62 (m, 10H), δ 1.73-1.84 (m, 10H), δ 1.89-2.00 (m, 6H), δ 5.30 (s, 2H); **^{13}C-NMR** (300 MHz, DMSO-*d6*) δ 29.4, 36.4, 36.6, 42.5 ; **HRMS**: Calculated for $C_{21}H_{33}O_1N_2$ [M+H]: 329.2587; measured: 329.2588.

1,3-bis(4-chlorophenyl)urea

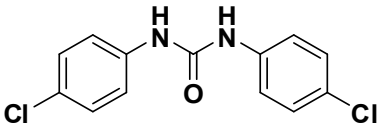

White powder (98% yield); **^{1}H-NMR** (300 MHz, DMSO-*d6*) δ 7.30 (d, *J* = 7.26Hz, 4H), δ 7.46 (d, *J* = 7.38, 4H), δ 8.82 (s, 2H); **^{13}C-NMR** (300 MHz, DMSO-*d6*) δ 120.4, 125.9, 129.0, 138.9, 152.8; **HRMS**: Calculated for $C_{13}H_9ON_2Cl_2$[M+H]: 279.00974; measured: 279.01041.

1,3-bis(4-bromophenyl)urea

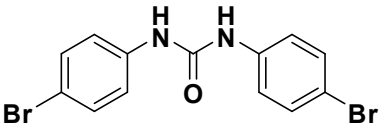

White powder (93% yield); **^{1}H-NMR** (300 MHz, DMSO-*d6*) δ 7.37-7.46 (m, 10H), δ 8.83 (s, 2H); **^{13}C-NMR** (500 MHz, DMSO-*d6*) δ 113.9, 120.7, 132.0, 139.4, 152.4. **HRMS**: Calculated for $C_{13}H_9ON_2Br_2$[M+H]: 366.90871; measured: 366.90934.

1,3-bis(4-iodophenyl)urea

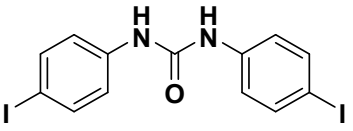

White powder (92% yield); **^{1}H-NMR** (300 MHz, DMSO-*d6*) δ 7.27 (d, *J* = 7.40Hz, 4H), δ 7.58 (d, *J* = 7.14Hz, 4H), δ 8.79 (s, 2H). **^{13}C-NMR** (500 MHz, DMSO-*d6*) δ 85.3, 120.9, 137.9, 140.1, 152.7. **HRMS**: Calculated for $C_{13}H_9ON_2I_2$[M+H]: 462.88097; measured: 462.88179.

1,3-bis(2,4,5-trifluorophenyl)urea

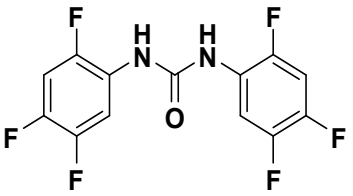

White powder (95% yield); **^{1}H-NMR** (300 MHz, DMSO-*d6*) δ 7.58-7.72 (m, 2H), δ 8.11-8.24 (m, 2H), δ 9.20 (s, 2H); **^{13}C-NMR** (500 MHz, DMSO-*d6*) δ 106.1, 108.9, 152.1; **^{19}F-NMR** (500 MHz, DMSO-*d6*) δ -130.8, -141.7, -143.0; **HRMS**: Calculated for $C_{13}H_5ON_2F_6$ [M+H]: 319.03116; measured: 319.03184.

1,3-bis(2,4-dichlorophenyl)urea

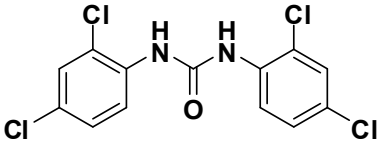

White powder (96% yield); **^{1}H-NMR** (300 MHz, DMSO-*d6*) δ 7.37 (d, *J* = 7.06Hz, 2H), δ 7.62 (s, 2H), δ 8.08 (d, *J* = 7.64Hz, 2H), δ 9.14 (s, 2H); **^{13}C-NMR** (300 MHz, DMSO-*d6*) δ 123.8, 124.0, 127.2, 127.9, 129.1, 135.3, 152.4. **HRMS**: Calculated for $C_{13}H_7ON_2Cl_4$[M+H]: 346.93180; measured: 346.93270.

1,3-bis(2,4-difluorophenyl)thiourea

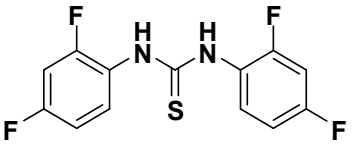

White powder (96% yield); **^{1}H-NMR** (300 MHz, DMSO-*d6*) δ 7.00-7.13 (m, 2H), δ 7.24-7.36 (m, 2H), δ 7.47-7.57 (m, 2H), δ 9.56 (s, 2H); **^{13}C-NMR** (300 MHz, DMSO-*d6*) δ 104.5, 104.8, 105.1, 111.4, 111.8, 123.7, 124.0, 130.8, 130.9, 155.6, 155.8,

159.0, 159.1, 162.2, 162.4, 182.6; **HRMS**: Calculated for $C_{13}H_7N_2SF_4$[M-H]: 299.02716; measured: 299.02756.

Table F1. Crystallographic data of the various methoxy-substituted bis(aryl)ureas and bis(aryl)thioureas.

	3,4,5-triMeO- (I→II→I)	**3,4,5-triMeO-TU**	**4-MeO-Urea (I→II→I)**	**4-MeO-heat 220°C**
Molecular formula	$C_{19}H_{24}N_2O_7$	$C_{19}H_{24}N_2O_6S$	$C_{15}H_{16}N_2O_3$	$C_{15}H_{16}N_2O_3$
M_r	392.40	408.46	272.30	272.30
Crystal System	Monoclinic	Orthorhombic	Triclinic	Triclinic
Crystal colour	Colorless	Colorless	Colorless	Colorless
Space group	*C*2/c	*P*bca	*P*-1	*P*-1
Temperature (K)	298K	150K	298K	298
Unit cell dimensions (Å,°)				
a	31.058(17)	14.331(7)	9.222(5)	9.265(4)
b	4.673(3)	11.126(6)	11.948(7)	12.013(5)
c	13.543(8)	24.936(15)	13.455(7)	13.648(6)
α	90	90	64.656(7)	65.164(15)
β	108.474(6)	90	87.690(7)	88.703(18)
γ	90	90	76.743(6)	77.667(18)
Volume (Å^3)	1864.2(18)	3976(4)	1301.3(12)	1342.8(10)
Z	4	8	4	4
***D*$_{calc}$ (g cm^{-3})**	1.398	1.365	1.390	1.327
μ (mm^{-1}) (abs coeff)	0.107	0.201	0.098	0.087
***F*(000)**	832	1728	576	568
Refl. collected/independent	7252 / 1392	44572 / 4619	13232 / 5840	29263 /4701
No. observed refl. [*I*>2σ(*I*)]*	1121	2558	3382	2297
No. restraints/No. parameters	0/128	0/ 259	0/ 361	0/365
R [all/gt]	0.0498 / 0.0387	0.1280/ 0.0589	0.1210/ 0.0806	0.2454/ 0.1467
wR [ref/gt]	0.1351 / 0.1231	0.1561/ 0.1226	0.2839/ 0.2638	0.4418/ 0.3941
Goodness-of-fit on F^2	1.027	1.015	1.032	1.389
Largest diff. peak and hole (*e* Å^{-3})	0.136, -0.176	0.342, -0.357	1.006, -0.434	0.672, -0.534

*$R = \sum||Fo|-|Fc||/\sum Fo, w = 1/[\sigma^2(F_o^2)+(g_1P)^2+ g_2P]$ where $P = (F_o^2+2F_c^2)/3$, $S = \Sigma[w(F_o^2 - F_c^2)^2/(N_{obs} - N_{param})]^{1/2}$.

	4-MeO-TU	**3,5-diMeO-Urea**	**2,5-diMeO-Urea**	**2,5-diMeO-Urea**
Molecular formula	$C_{15}H_{16}N_2O_7S$	$C_{17}H_{20}N_2O_5$	$C_{8.5}H_{10}N_1O_{2.5}$	$C_{8.5}H_{10}N_1O_{2.5}$
M_r	288.36	332.35	166.17	166.17
Crystal System	Orthorhombic	Orthorhombic	Tetragonal	Tetragonal
Crystal colour	Colorless	Colorless	Colorless	Colorless
Space group	*P*nma	*P*ccn	*I*4	*I*4
Temperature (K)	100K	100K	100K	298K
Unit cell dimensions (Å,°)				
a	8.206(9)	13.402(3)	13.282(2)	13.4536(14)
b	31.61(3)	13.461(3)	13.282(2)	13.4536(14)
c	5.328(6)	9.128(2)	9.434(2)	9.4600(10)
α	90	90	90	90
β	90	90	90	90
γ	90	90	90	90
Volume (Å^3)	1382(3)	1646.6(7)	1664.3(7)	1712.3(4)
Z	4	4	4	4
***D*$_{calc}$ (g cm^{-3})**	1.386	1.341	1.326	1.289
μ (mm^{-1}) (abs coeff)	0.237	0.100	0.098	0.096
***F*(000)**	608	704	704	704
Refl. collected/independent	5574 /1191	17647 / 1860	5093 / 1051	7117 / 1183
No. observed refl. [*I*>2σ(*I*)]*	1127	950	797	1136
No. restraints/No. parameters	0/94	0/ 100	1/111	1/113
R [all/gt]	0.0430 / 0.0400	0.1355/ 0.0637	0.0618 / 0.0447	0.0283/ 0.0268
wR [ref/gt]	0.1229 / 0.1197	0.1825/ 0.1433	0.0933 / 0.0879	0.0666/ 0.0654
Goodness-of-fit on F^2	1.225	1.003	0.848	1.130
Largest diff. peak and hole (*e* Å^{-3})	0.136, -0.176	0.249, -0.311	0.172, -0.152	0.078, -0.127

*$R = \sum||Fo|-|Fc||/\sum Fo, w = 1/[\sigma^2(F_o^2)+(g_1P)^2+ g_2P]$ where $P = (F_o^2+2F_c^2)/3$, $S = \Sigma[w(F_o^2 - F_c^2)^2/(N_{obs} - N_{param})]^{1/2}$.

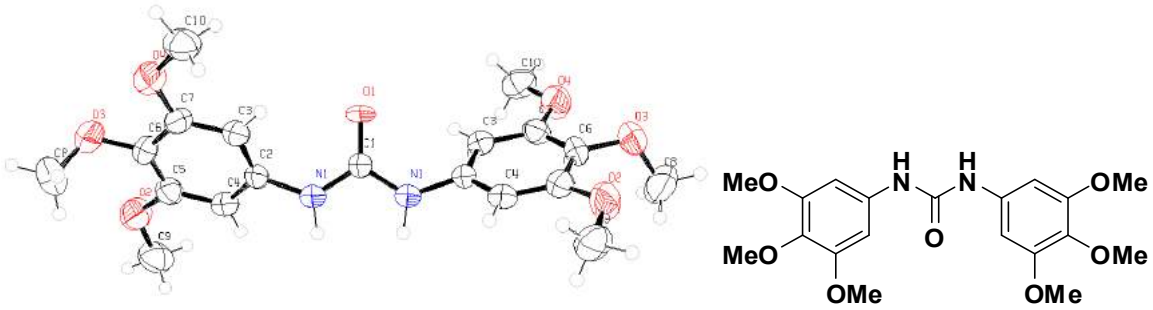

Fig. F1. Molecular structure visualized using ORTEP-3 with thermal ellipsoids at 50% probability level of 1,3-bis(3,4,5-trimethoxyphenyl)urea as determined by SCXRD, along with a schematic representation of the molecule.

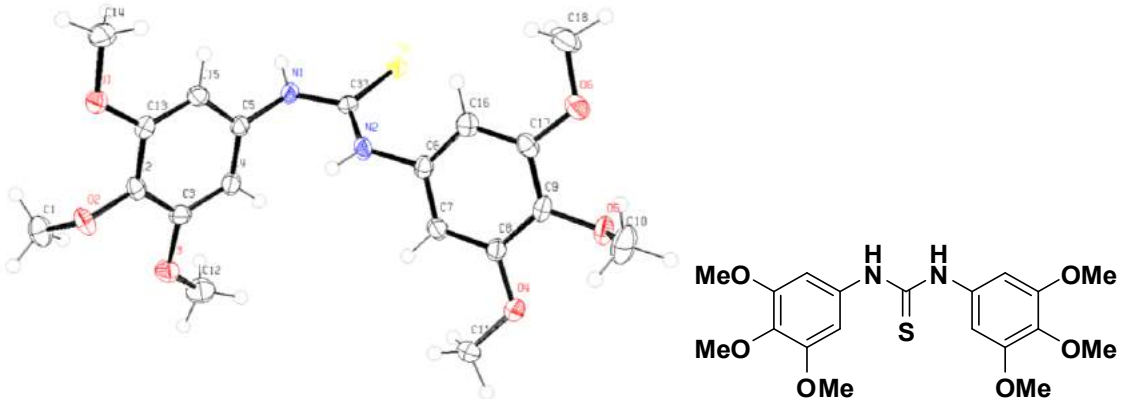

Fig. F2. Molecular structure visualized using ORTEP-3 with thermal ellipsoids at 50% probability level of 1,3-bis(3,4,5-trimethoxyphenyl)urea as determined by SCXRD, along with a schematic representation of the molecule.

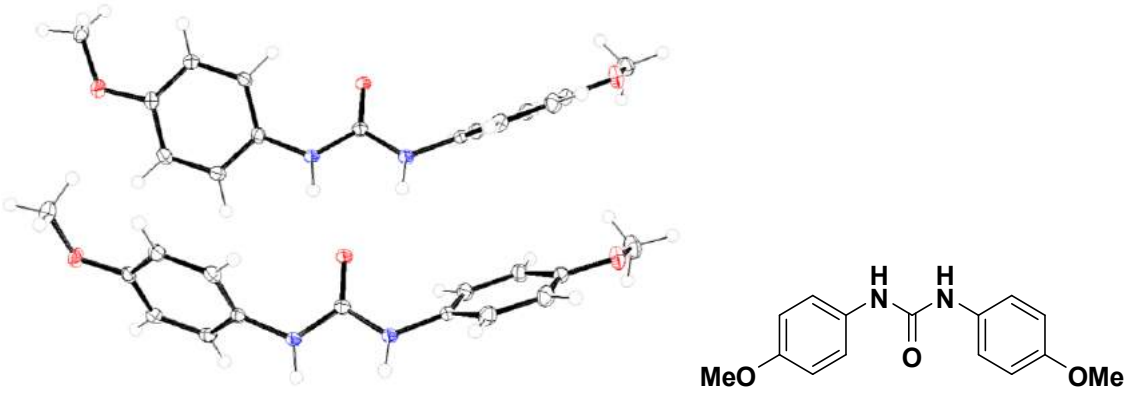

Fig. F3. Molecular structure visualized using ORTEP-3 with thermal ellipsoids at 50% probability level of 1,3-bis(4-methoxyphenyl)urea as determined by SCXRD, along with a schematic representation of the molecule. Each asymmetric unit consists of two molecules.

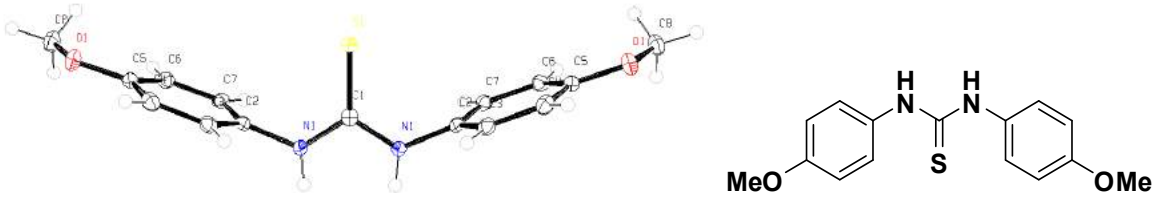

Fig. F4. Molecular structure visualized using ORTEP-3 with thermal ellipsoids at 50% probability level of 1,3-bis(4-methoxyphenyl)thiourea as determined by single-crystal X-ray diffraction.

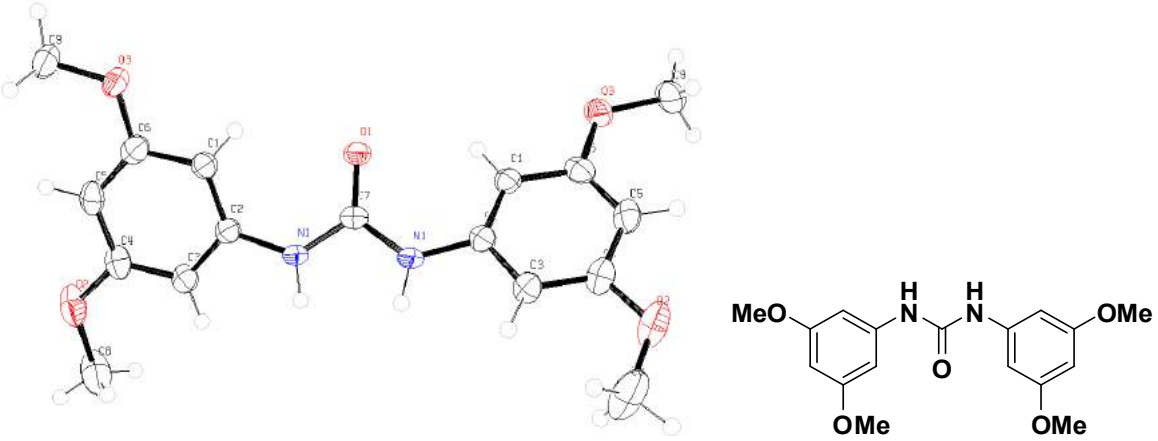

Fig. F5. Molecular structure visualized using ORTEP-3 with thermal ellipsoids at 50% probability level of 1,3-bis(3,5-dimethoxyphenyl)urea as determined by SCXRD, along with a schematic representation of the molecule.

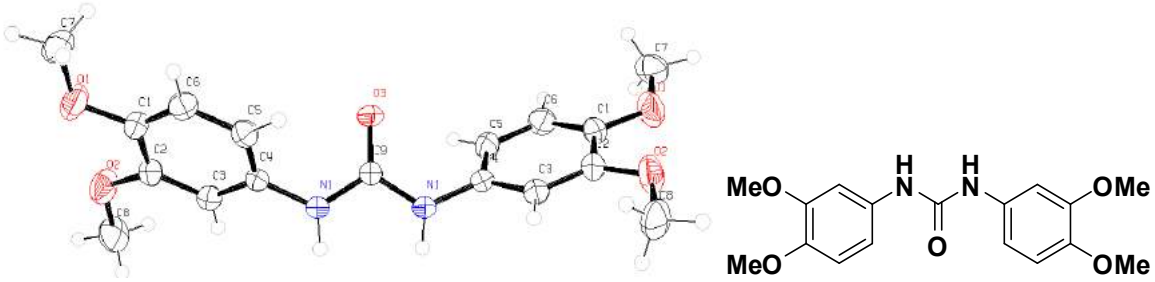

Fig. F6. Molecular structure visualized using ORTEP-3 with thermal ellipsoids at 50% probability level of 1,3-bis(3,4-dimethoxyphenyl)urea as determined by SCXRD, along with a schematic representation of the molecule.

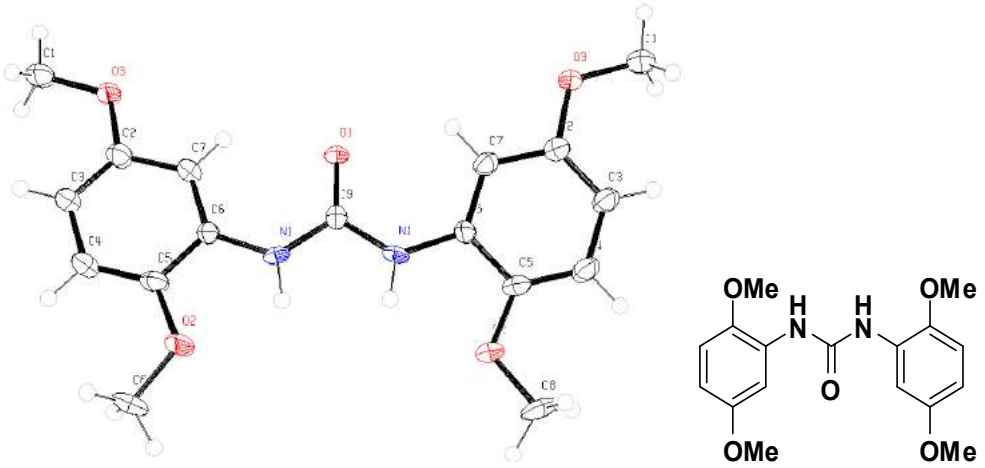

Fig. F7. Molecular structure visualized using ORTEP-3 with thermal ellipsoids at 50% probability level of 1,3-bis(2,5-dimethoxyphenyl)urea as determined by SCXRD, along with a schematic representation of the molecule.

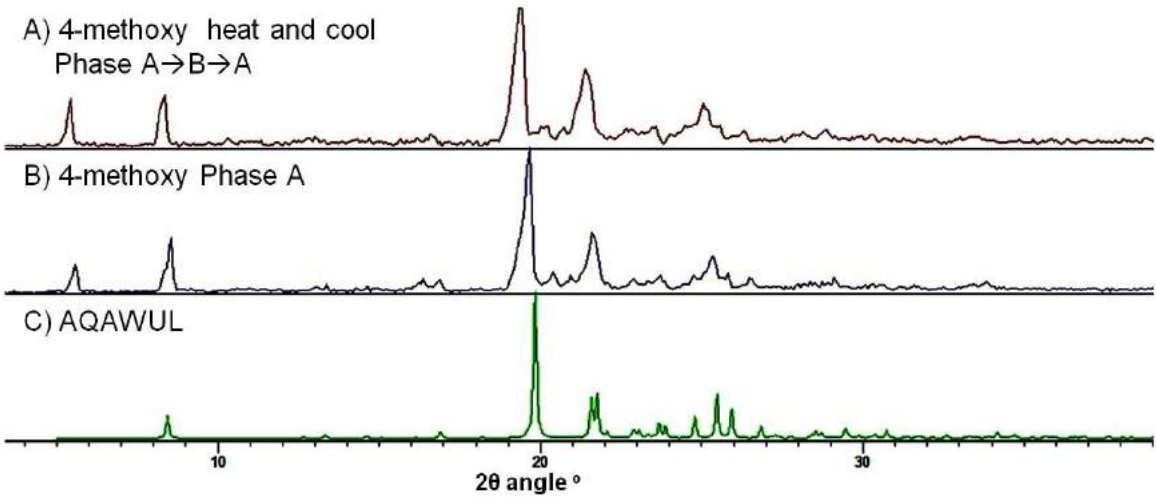

Fig. F8. Comparison of the PXRD patterns of powder of 4-methoxyphenylurea A) after heating and cooling, B) before heating and C) from pattern simulated from single crystal data.

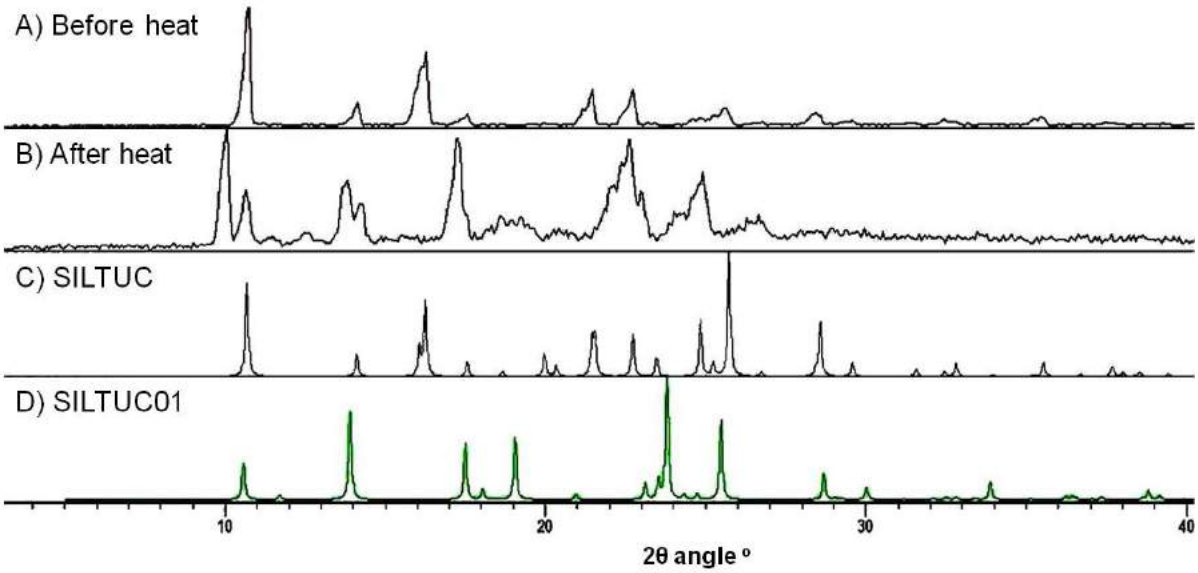

Fig. F9. Comparison of the PXRD patterns of powder of 2-methoxyphenylurea A) before heating, B) after heating and C) and D) are patterns simulated from single crystal data of the two known polymorphs SILTUC and SILTUC01.

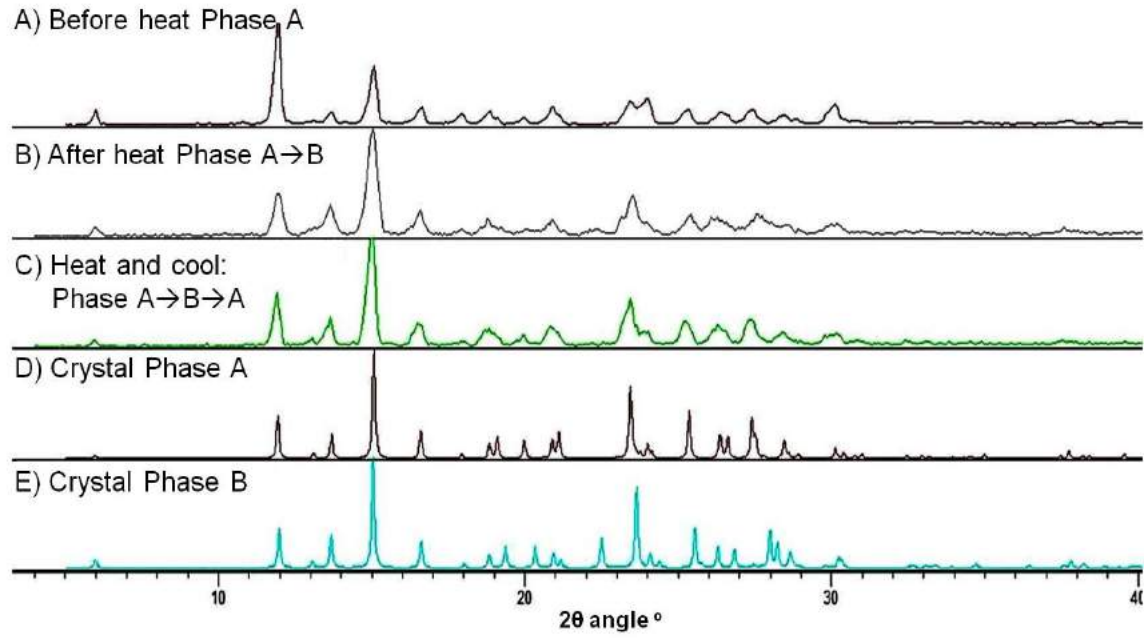

Fig. F10. Comparison of the PXRD patterns of powder of 3,4,5-trimethoxyphenylurea A) phase A before heating, B) phase B after heating, C) phase A after heating and cooling, C) and D) are patterns simulated from single crystal data obtained experimentally of phase A and B respectively.

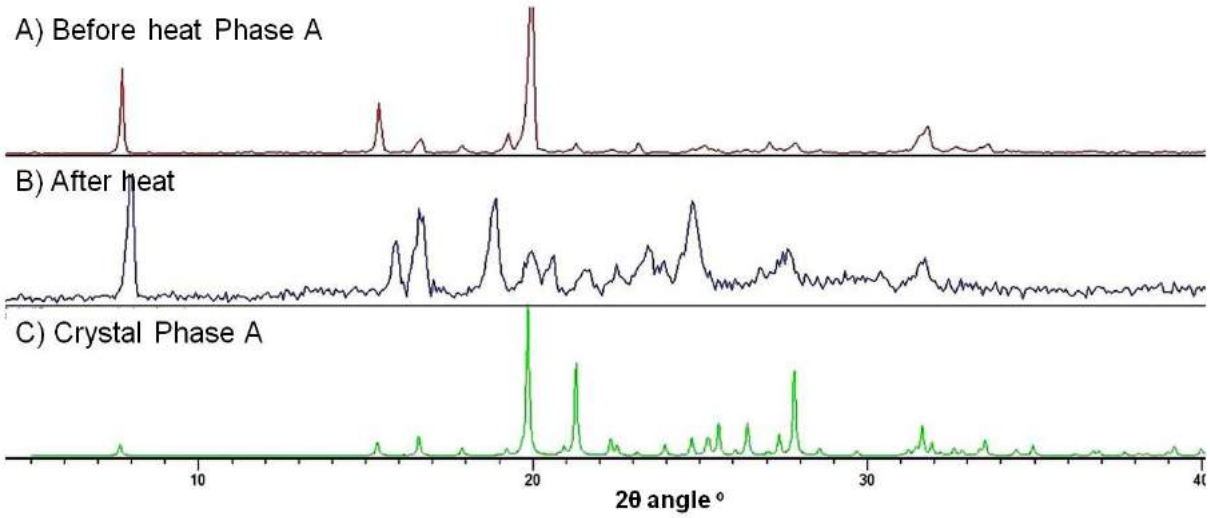

Fig. F11. Comparison of the PXRD patterns of powder of 2,4-difluorophenylurea A) phase A before heating, B) after heating and C) pattern simulated from single crystal data obtained experimentally of phase A.

Table F2. Comparison of intermolecular hydrogen bond lengths for compounds that underwent polymorphic transformation.

Compound	Substituent	CCSD Code	Polymorph	N···O (Å)	C-H···O (Å)
1a	2-methoxy	SILTUC01	I	3.144	-
1a	2-methoxy	SILTUC	II	2.996	-
1c	4-methoxy	AQAWUL	I	2.890, 2.861, 2.975, 2.810	3.366
1c	4-methoxy	-	II	2.961(2), 2.824(2)	3.383(3)
2b	2,5-dimethoxy	-	I	2.955(2)	3.266(3), 3.458(3), 3.266(4)
2b	2,5-dimethoxy	-	II	-	-
2c	3,4-dimethoxy	-	I	2.929(2)	3.470(4), 3.487(4)
2c	3,4-dimethoxy	-	II	2.935(2)	3.438(4), 3.461(4)
3a	3,4,5-trimethoxy	-	I	2.940(2)	3.353(3), 3.084(3), 3.451(3)
3a	3,4,5-trimethoxy	-	II	2.902(2)	3.328(4), 3.402(4), 3.071(4), 3.465(4)

Table F3. Crystallographic data of other symmetrical bis(alkyl)ureas and bis(aryl)ureas.

	4-CF3-urea	2-Cl-ethyl-urea	2-F-urea+TBD	Adamantly-urea
Molecular formula	$C_{15}H_{10}N_2O_1F_{5.96}$	$C_5H_{10}N_2O_3Cl$	$C_{28}H_{38}N_8O_4F2$	$C_{21}H_{32}N_2O$
M_r	347.51	185.05	588.66	328.48
Crystal System	Orthorombic	Orthorhombic	Triclinic	Monoclinic
Crystal colour	Colorless	Colorless	Colorless	Colorless
Space group	*F*dd2	$P2_12_12$	*P*-1	*C*2/c
Temperature (K)	298K	100K	100K	150K
Unit cell dimensions (Å,°)				
a	13.854(6)	8.4221(12)	9.198(4)	21.66(6)
b	44.45(2)	10.5040(15)	12.198(6)	9.26(2)
c	4.748(2)	4.6192(7)	13.245(6)	20.89(5)
α	90	90	107.579(6)	90
β	90	90	95.474(7)	118.40(11)
γ	90	90	101.043(6)	90
Volume (Å^3)	2924(2)	408.64(10)	1371.7(11)	3686(16)
Z	8	2	2	8
D_{calc} (g cm^{-3})	1.579	1.504	1.425	1.184
μ (mm^{-1}) (abs coeff)	0.152	0.730	0.107	0.072
***F*(000)**	1405	192	624	1440
Refl. collected/independent	3464/ 2283	4616/ 948	16188/ 6338	3896 / 3310
No. observed refl. [$I>2\sigma(I)$]*	35897	938	3714	31390
No. restraints/No. parameters	0/ 244	0/ 47	0/380	1/ 302
R [all/gt]	0.0950/ 0.0517	0.0335/ 0.0332	0.1436/ 0.0976	0.0568 / 0.0403
wR [ref/gt]	0.1382/ 0.1148	0.0878/ 0.0874	0.2892/ 0.2518	0.0848 / 0.0789
Goodness-of-fit on F^2	1.018	1.203	1.013	1.053
Largest diff. peak and hole (*e* Å^{-3})	0.297, -0.487	0.272, -0.509	0.624, -0.588	0.270, -0.350

*$R = \sum||Fo|-|Fc||/\sum Fo,w = 1/[\sigma^2(F_o^2)+(g_1P)^2+ g_2P]$ where $P = (F_o^2+2F_c^2)/3$, $S = \Sigma[w(F_o^2 - F_c^2)^2/(N_{obs} - N_{param})]^{1/2}$.

	4-COOEt-urea
Molecular formula	$C_{19}H_{20}N_2O_5$
M_r	356.37
Crystal System	Monoclinic
Crystal colour	Colorless
Space group	*C*2/c
Temperature (K)	100K
Unit cell dimensions (Å,°)	
a	12.896(6)
b	10.532(5)
c	14.069(9)
α	90
β	108.300(7)
γ	90
Volume (Å^3)	1814.2(17)
Z	4
D_{calc} (g cm^{-3})	1.305
μ (mm^{-1})	0.095
***F*(000)**	752
Refl. collected/independent	4220/ 1604
No. observed refl. [$I>2\sigma(I)$]*	1080
No. restraints/No. parameters	0/ 120
R [all/gt]	0.1105/ 0.0920
wR [ref/gt]	0.2370/ 0.2209
Goodness-of-fit on F^2	1.130
Largest diff. peak and hole (*e* Å^{-3})	0.538, -0.580

*$R = \sum||Fo|-|Fc||/\sum Fo,w = 1/[\sigma^2(F_o^2)+(g_1P)^2+ g_2P]$ where $P = (F_o^2+2F_c^2)/3$, $S = \Sigma[w(F_o^2 - F_c^2)^2/(N_{obs} - N_{param})]^{1/2}$.

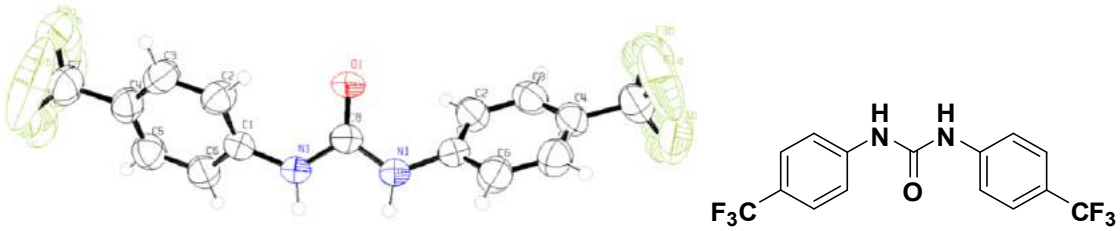

Fig. F12. Molecular structure visualized using ORTEP-3 with thermal ellipsoids at 50% probability level of 1,3-bis(4-(trifluoromethyl)phenyl)urea as determined by SCXRD, along with a schematic representation of the molecule.

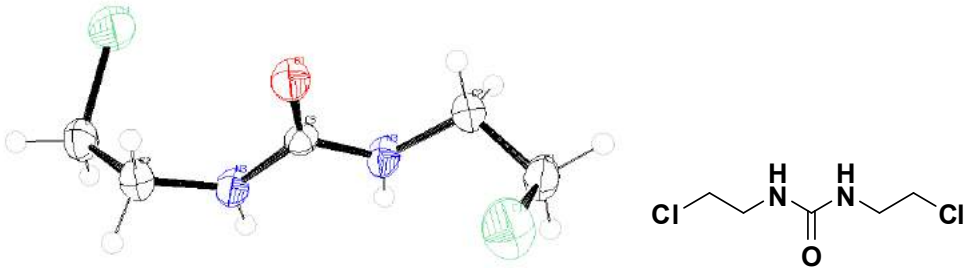

Fig. F13. Molecular structure visualized using ORTEP-3 with thermal ellipsoids at 50% probability level of 1,3-bis(2-chloroethyl)urea as determined by SCXRD, along with a schematic representation of the molecule.

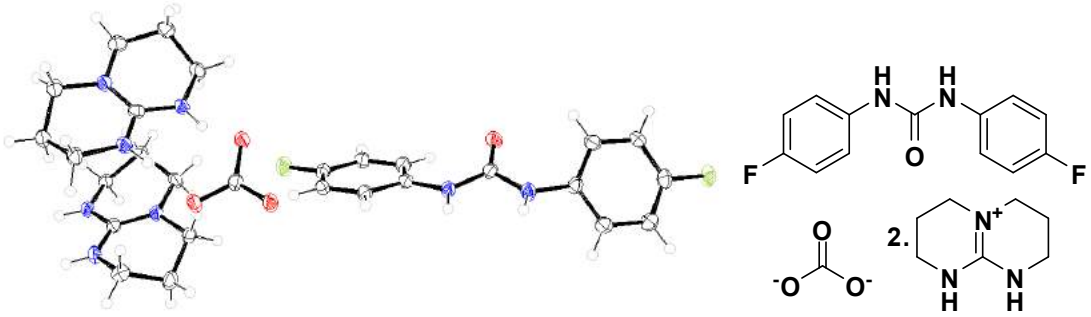

Fig. F14. Molecular structure visualized using ORTEP-3 with thermal ellipsoids at 50% probability level of 1,3-bis(4-fluorophenyl)urea.$(TBDH)_2$-carbonate as determined by SCXRD, along with a Chemdraw image of the molecules.

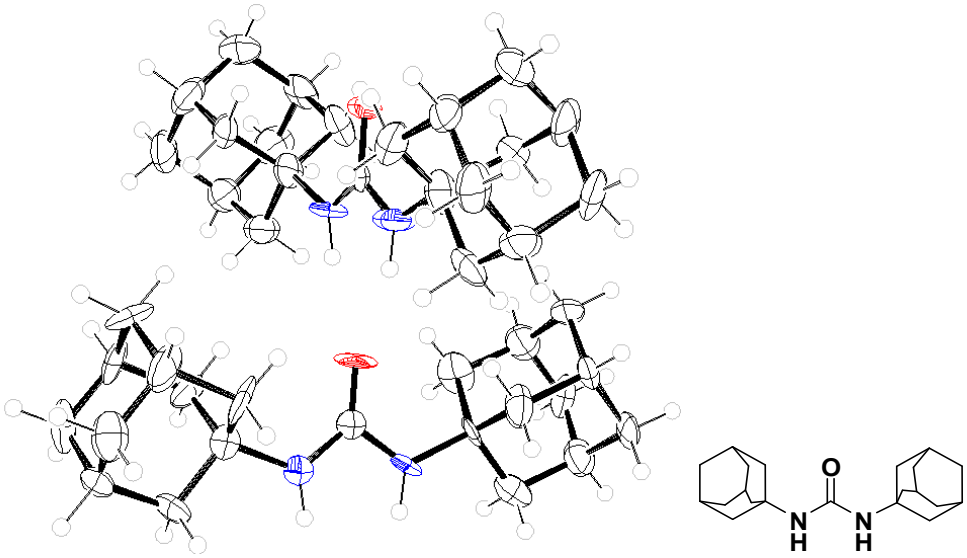

Fig. F15. Molecular structure visualized using ORTEP-3 with thermal ellipsoids at 50% probability level of 1,3-adamantylurea as determined by SCXRD, along with a schematic representation of the molecule. Each asymmetric unit consists of two molecules.

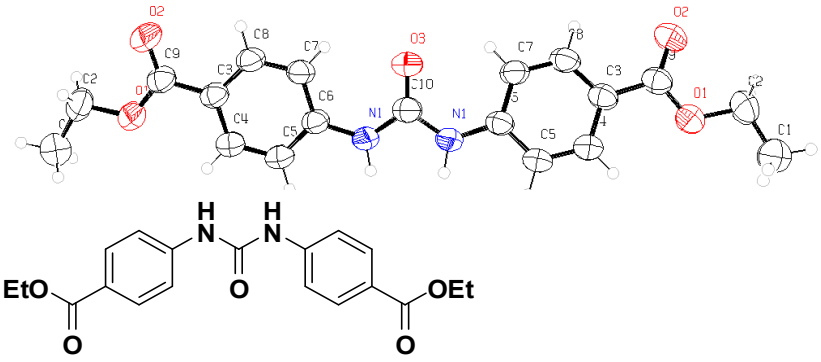

Fig. F16. Molecular structure visualized using ORTEP-3 with thermal ellipsoids at 50% probability level of diethyl 4,4'-carbonylbis(azanediyl)dibenzoate as determined by SCXRD, along with a schematic representation of the molecule.

Table F4. SCXRD data of other symmetrical halogenated bis(aryl)ureas.

	2,4-difluoro-urea	**2,4-difluoroTU**	**2,4,5-trifluoro-urea**	**2,4-dichloro-urea**
Molecular formula	$C_{13}H_8N_2O_1F_4$	$C_5H_{10}N_2O_3Cl$	$C_{16}H_{12}N_2O_2F_6$	$C_{13}H_8N_2OCl_4$
M_r	347.51	185.05	378.28	350.01
Crystal System	Monoclinic	Orthorhombic	Monoclinic	Triclinic
Crystal colour	Colorless	Colorless	Colorless	Colorless
Space group	$P2_1/c$	$P2_12_12$	$C2/c$	P-1
Temperature (K)	100K	100K	100K	150K
Unit cell dimensions (Å,°)				
a	22.793(5)	8.4221(12)	18.464(10)	4.615(6)
b	4.5866(8)	10.5040(15)	9.922(6)	12.277(15)
c	10.811(2)	4.6192(7)	8.408(5)	13.374(17)
α	90	90	90	70.302(13)
β	91.954(7)	90	91.398(7)	89.267(13)
γ	90	90	90	89.025(12)
Volume (Å^3)	1129.5(4)	408.64(10)	1539.9(15)	713.3(15)
Z	4	2	4	2
D_{calc} (g cm^{-3})	1.671	1.504	1.632	1.630
μ (mm^{-1}) (abs coeff)	0.153	0.730	0.157	0.824
F(000)	576	192	768	352
Refl. collected/independent	11371/ 1654	4616/ 948	8383/ 1815	3822/ 2432
No. observed refl. [$I>2\sigma(I)$]*	1137	938	1285	1625
No. restraints/No. parameters	0/ 244	0/ 47	0/120	0/ 181
R [all/gt]	0.0988/ 0.0628	0.0335/ 0.0332	0.0915/ 0.0636	0.1038/ 0.0665
wR [ref/gt]	0.1728/ 0.1509	0.0878/ 0.0874	0.1700/ 0.1567	0.1672/ 0.1514
Goodness-of-fit on F^2	1.008	1.203	1.055	1.050
Largest diff. peak and hole (e Å^{-3})	0.948, -0.527	0.272, -0.509	0.526, -0.500	0.680, -0.382

*$R = \sum||Fo|-|Fc||/\sum Fo, w = 1/[\sigma^2(F_o^2)+(g_1P)^2+ g_2P]$ where $P = (F_o^2+2F_c^2)/3$, $S = \Sigma[w(F_o^2 - F_c^2)^2/(N_{obs} - N_{param})]^{1/2}$

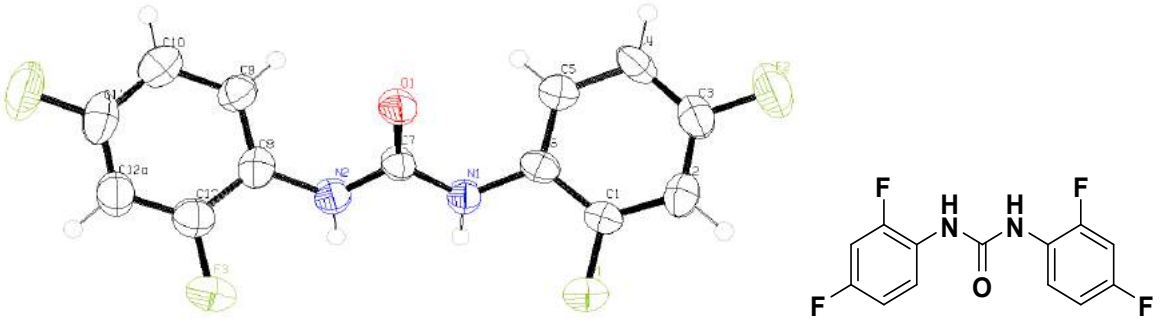

Fig. F17. Molecular structure visualized using ORTEP-3 with thermal ellipsoids at 50% probability level of 1,3-bis(2,4-difluorophenyl)urea as determined by SCXRD, along with a schematic representation of the molecule.

.

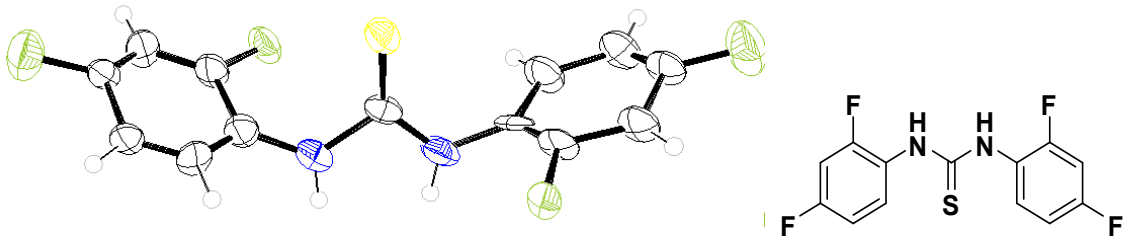

Fig. F18. Molecular structure visualized using ORTEP-3 with thermal ellipsoids at 50% probability level of 1,3-bis(2,4-difluorophenyl)thiourea as determined by SCXRD, along with a schematic representation of the molecule.

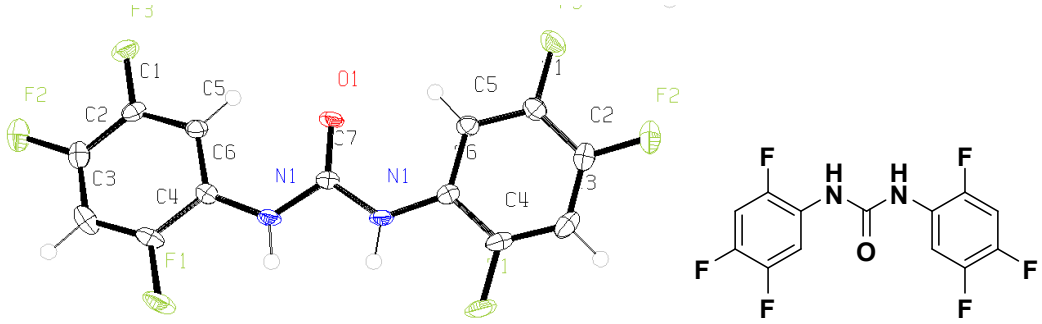

Fig. F19. Molecular structure visualized using ORTEP-3 with thermal ellipsoids at 50% probability level of 1,3-bis(2,4,5-trifluorophenyl)urea as determined by SCXRD, along with a schematic representation of the molecule.

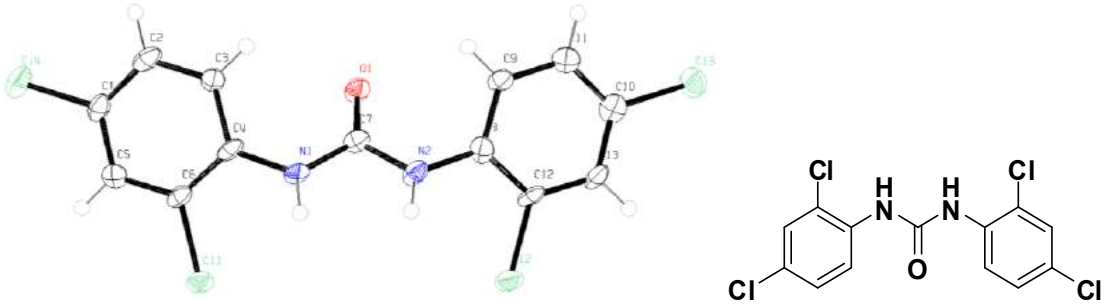

Fig. F20. Molecular structure visualized using ORTEP-3 with thermal ellipsoids at 50% probability level of 1,3-bis(2,4-dichlorophenyl)urea as determined by SCXRD, along with a schematic representation of the molecule.

Differential scanning calorimetry data and hot-stage microscopy images

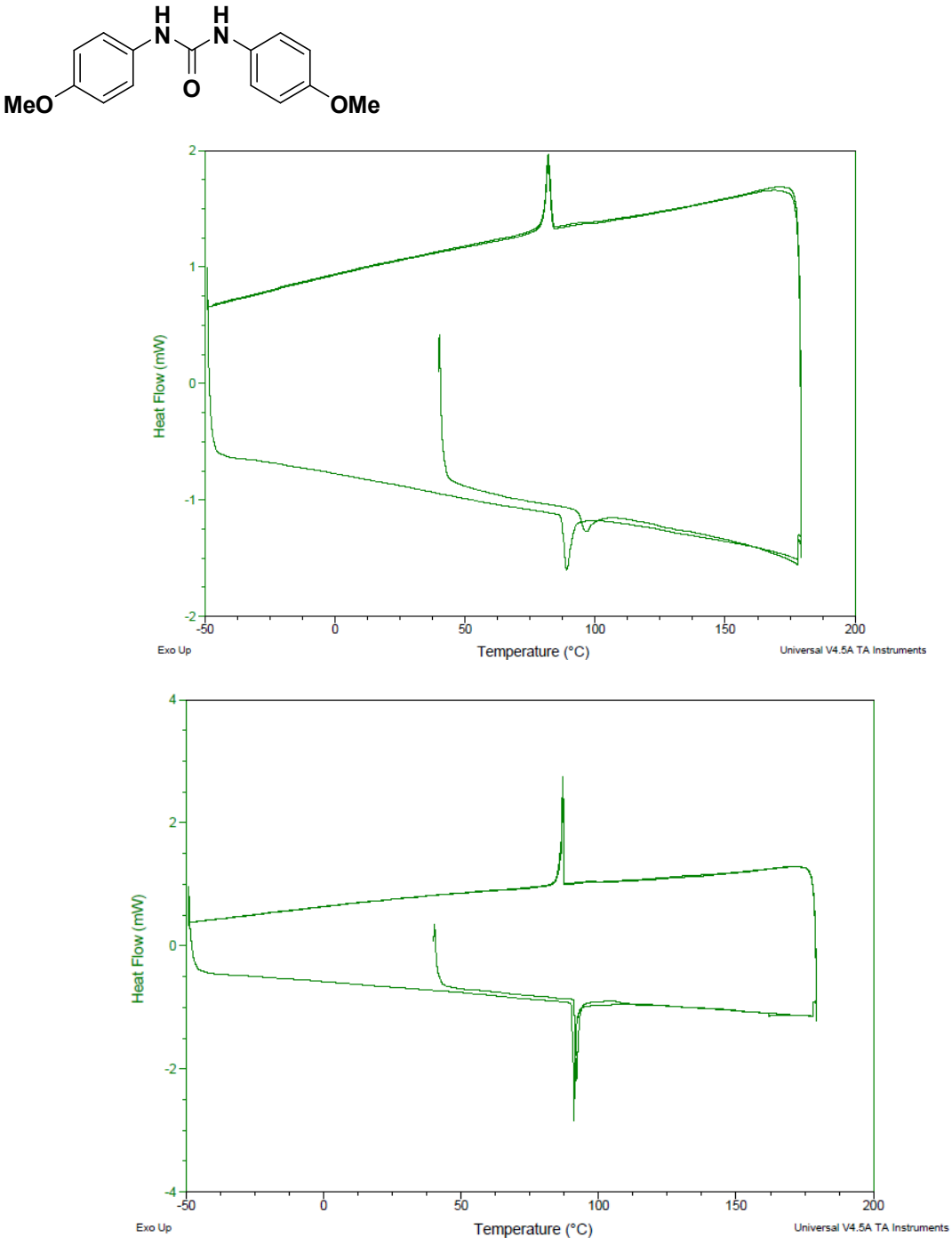

Fig. F21. Cyclic DSC thermograms (two cycles of heating and cooling) of **1c**. Based on cyclic DSC analysis, a reversible phase transition was observed for both powder (top) and crystal (bottom) samples.

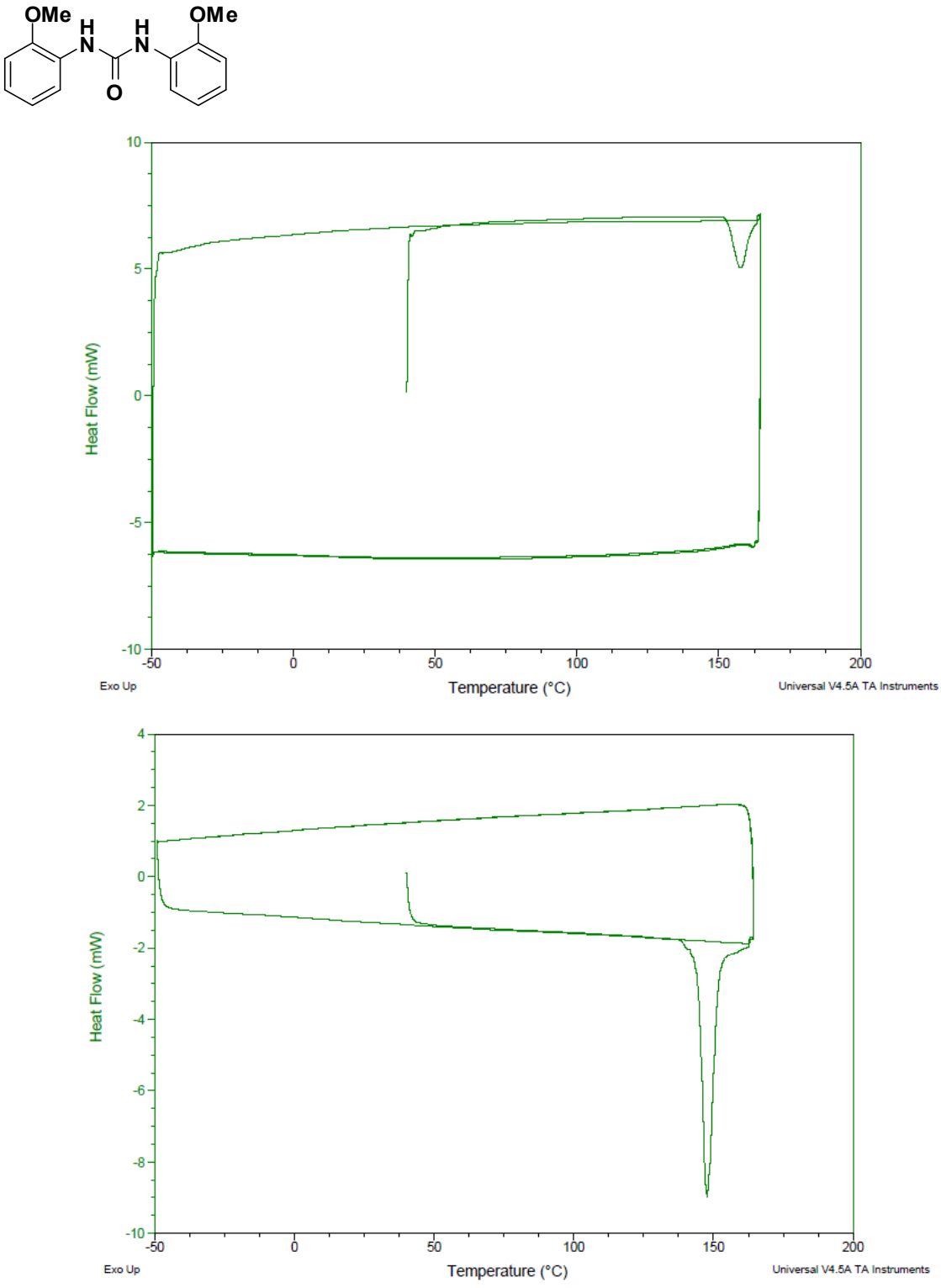

Fig. F21. Cyclic DSC thermograms of (two cycles of heating and cooling) **1a**. Based on cyclic DSC analysis, an irreversible phase transition was observed for both powder (top) and crystal (bottom) samples.

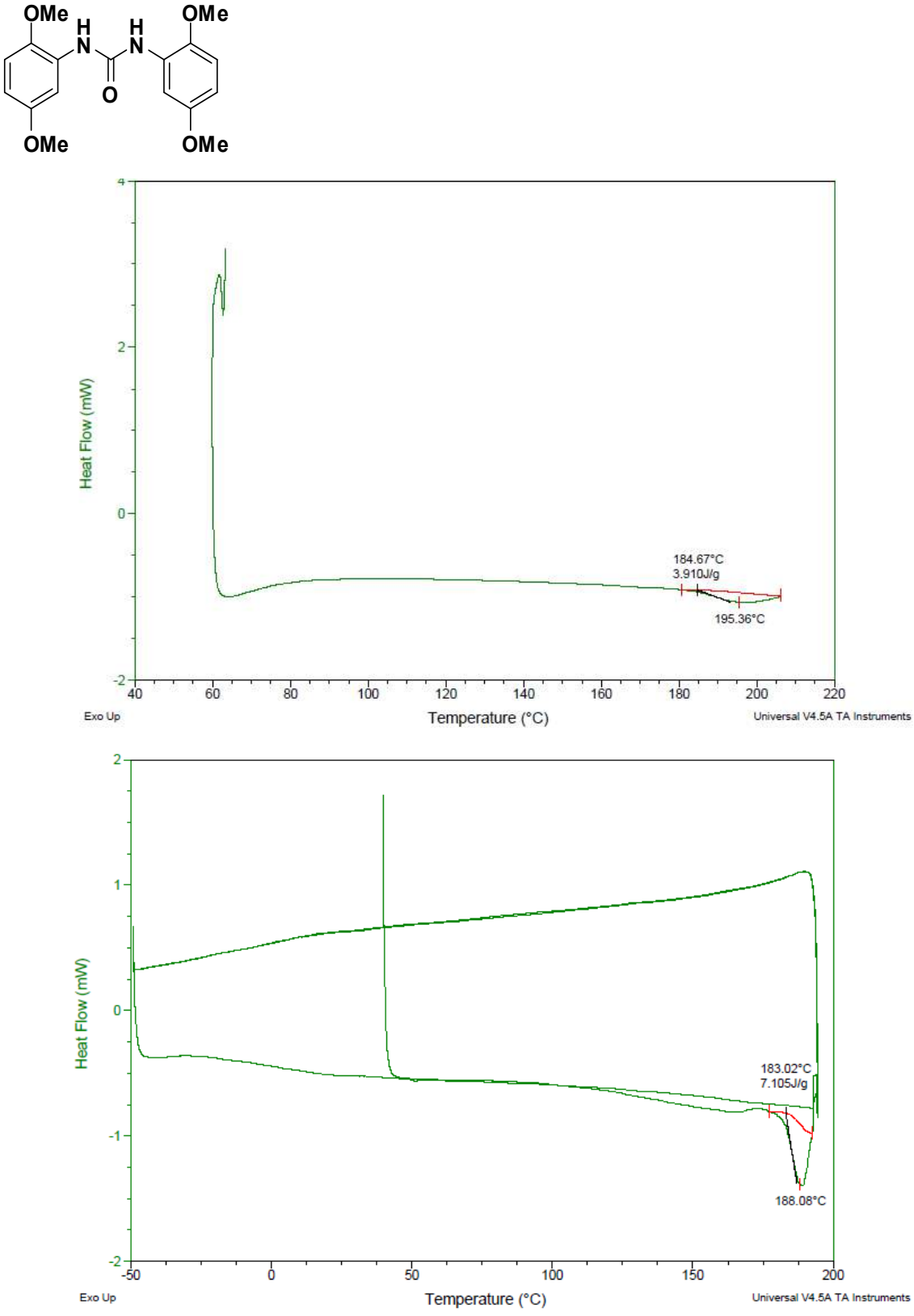

Fig. F22. Cyclic DSC thermograms of (two cycles of heating and cooling) **2b**. Based on cyclic DSC analysis, an irreversible phase transition was observed for both powder (top) and crystal (bottom) samples.

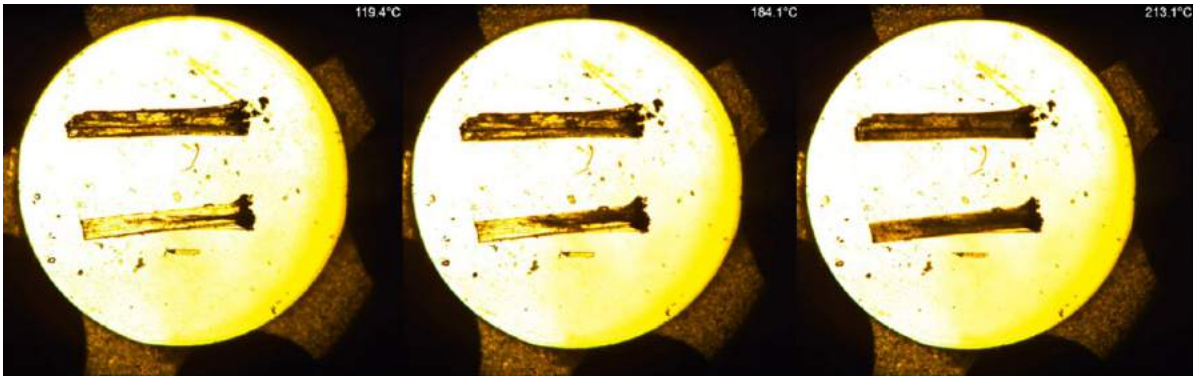

Fig. F23. Still images taken from the hot-stage microscopy video of the heating of crystals of **2b**.

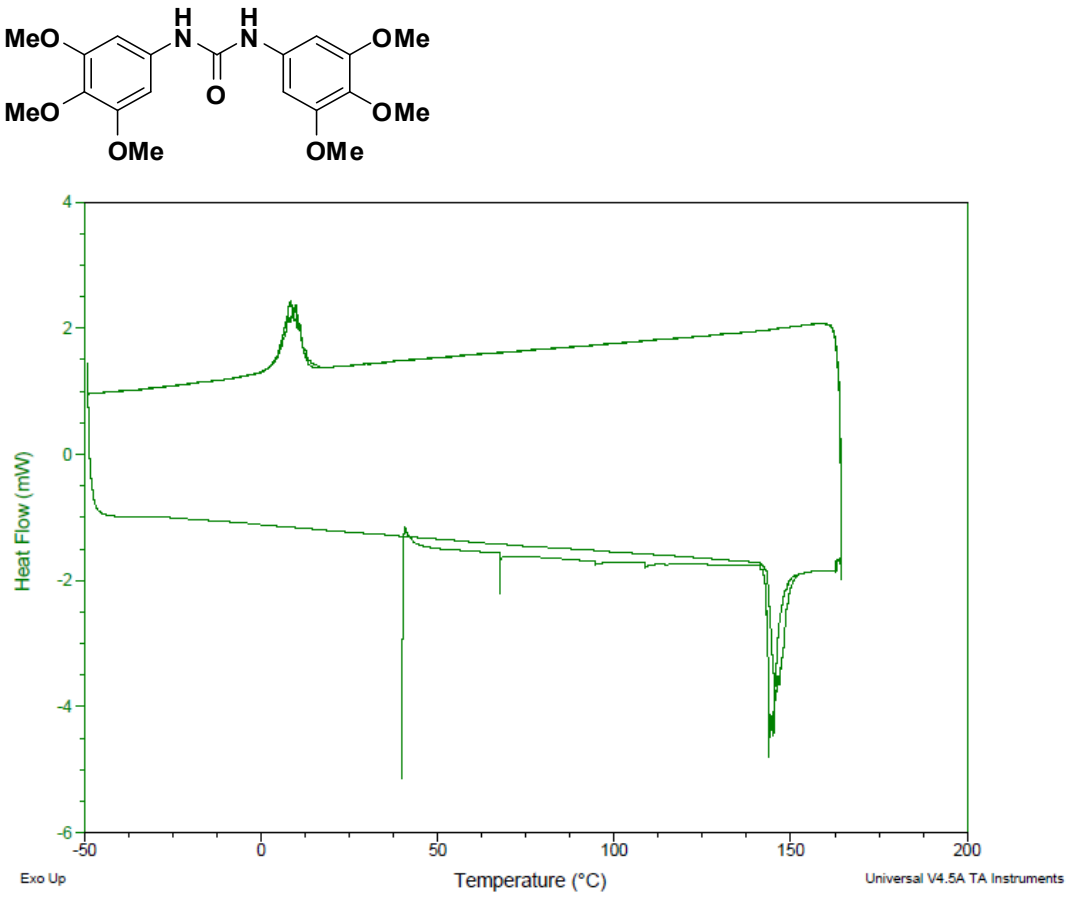

Fig. F24. Cyclic DSC thermograms of (two cycles of heating and cooling) powder of **3a**. Based on cyclic DSC analysis, a reversible phase transition was observed.

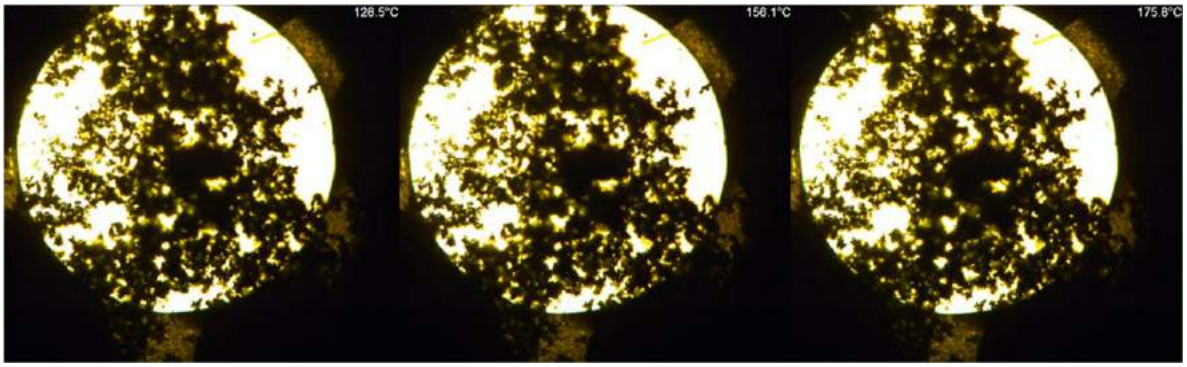

Fig. F25. Still images taken from the hot-stage microscopy video of the heating of powders of **3a**.

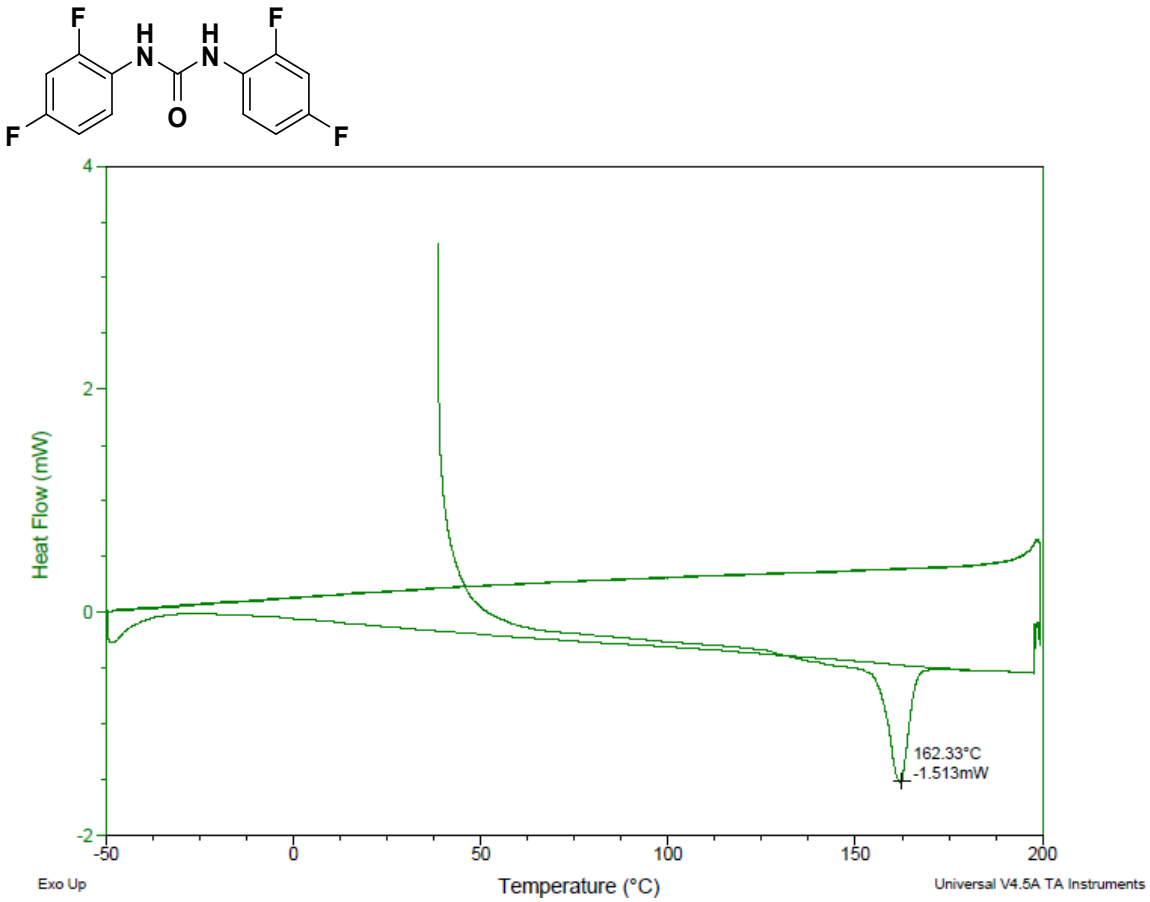

Fig. F26. Cyclic DSC thermograms of (two cycles of heating and cooling) 1,3-bis(2,4-difluorophenyl)urea. Based on cyclic DSC analysis, an irreversible phase transition was observed upon heating.

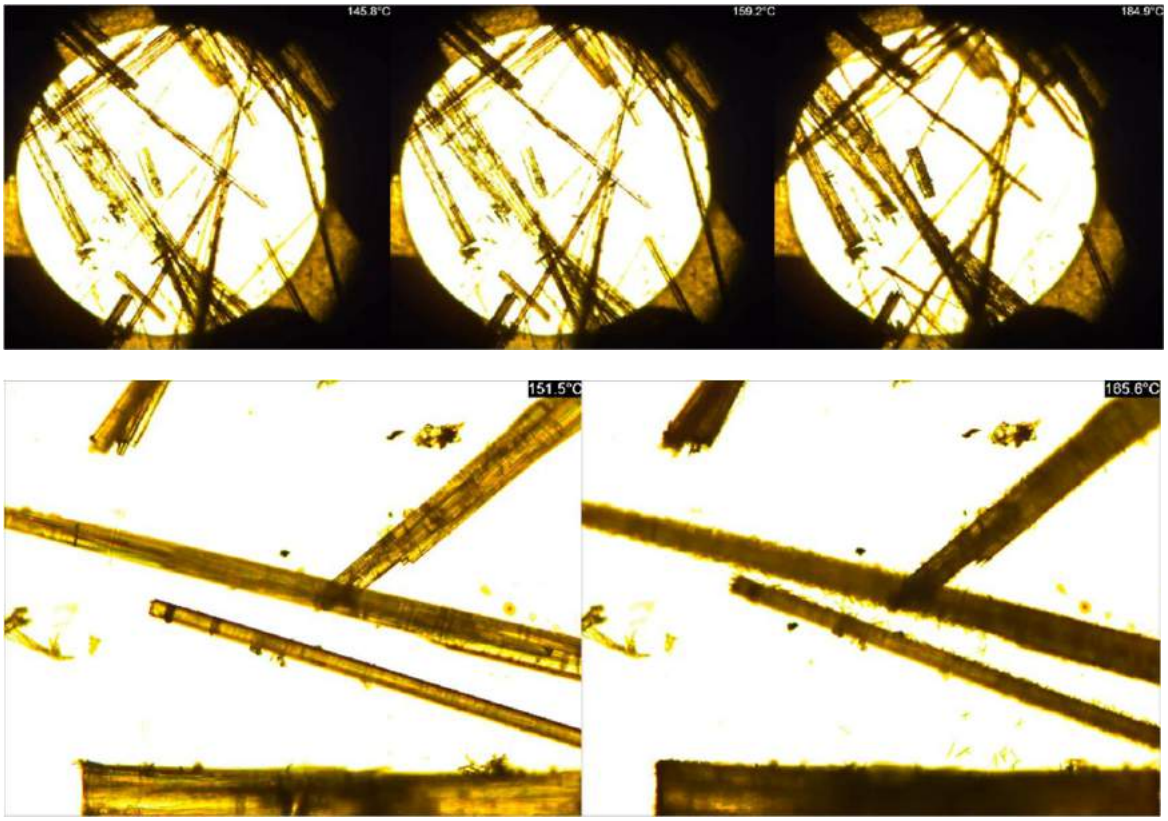

Fig. F27. Still images taken from the hot-stage microscopy video of the heating of crystals of 1,3-bis(2,4-difluorophenyl)urea. The crystals wiggle and become opaque upon heating during the polymorphic transformation.

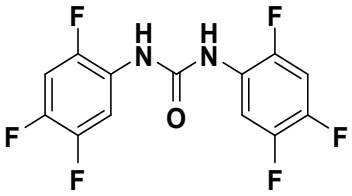

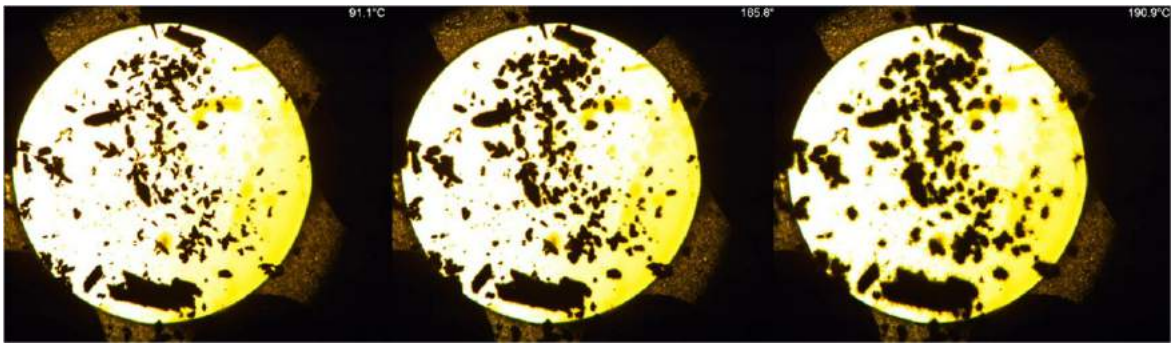

Fig. F28. Still images taken from the hot-stage microscopy video of the heating of small crystals of 1,3-bis(2,4,5-trifluorophenyl)urea. The crystals seem to be growing and getting slightly bigger upon heating.

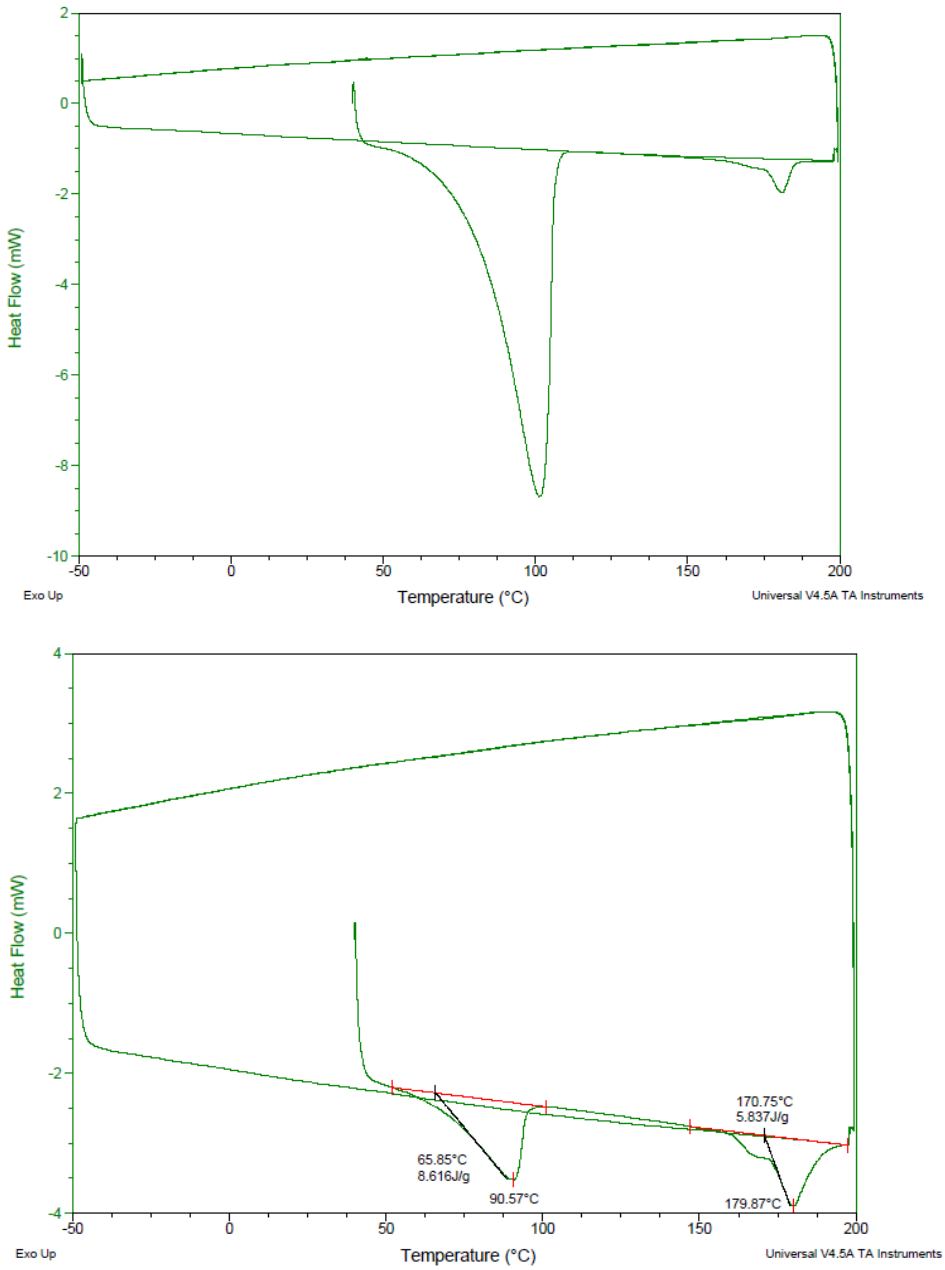

Fig. F29. Cyclic DSC thermograms of (two cycles of heating and cooling) 1,3-bis(2,4,5-trifluorophenyl)urea. Based on cyclic DSC analysis, an irreversible phase transition was observed for both powder (top) and crystal (bottom) samples.